Exploring the substrate scope of the fluorinase from *Streptomyces cattleya* for applications to positron emission tomography

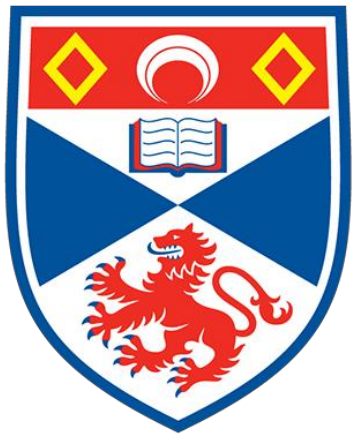

University of
St Andrews

Stephen Thompson

Supervisor: Prof. David O'Hagan

This thesis is submitted in partial fulfilment for the degree of Doctor of Philosophy at the University of St Andrews

September 2015

Declarations

1. Candidate's declarations:

I, Stephen Thompson, hereby certify that this thesis, which is approximately 71 000 words in length, has been written by me, and that it is the record of work carried out by me, or principally by myself in collaboration with others as acknowledged, and that it has not been submitted in any previous application for a higher degree.

I was admitted as a research student in September 2011 and as a candidate for the degree of Doctor of Philosophy in September 2012; the higher study for which this is a record was carried out in the University of St Andrews between 2011 and 2015.

Date _____ Signature of candidate _____

2. Supervisor's declaration:

I hereby certify that the candidate has fulfilled the conditions of the Resolution and Regulations appropriate for the degree of Doctor of Philosophy in the University of St Andrews and that the candidate is qualified to submit this thesis in application for that degree.

Date _____ Signature of supervisor _____

3. Permission for publication:

In submitting this thesis to the University of St Andrews I understand that I am giving permission for it to be made available for use in accordance with the regulations of the University Library for the time being in force, subject to any copyright vested in the work not being affected thereby. I also understand that the title and the abstract will be published, and that a copy of the work may be made and supplied to any bona fide library or research worker, that my thesis will be electronically accessible for personal or research use unless exempt by award of an embargo as requested below, and that the library has the right to migrate my thesis into new electronic forms as required to ensure continued access to the thesis. I have obtained any third-party copyright permissions that may be required in order to allow such access and migration, or have requested the appropriate embargo below.

The following is an agreed request by candidate and supervisor regarding the publication of this thesis: Access to all of printed copy, but embargo on all electronic copy for a period of 2 years on the following ground: publication would preclude future publication.

Date _____ Signature of candidate _____

Signature of supervisor _____

Abstract

The fluorinase enzyme, originally isolated from *Streptomyces cattleya*, has the unique ability to generate a C–F bond from aqueous fluoride ion and *S*-adenosylmethionine, making the fluorinase an attractive biochemical tool for radiolabelling biomolecules with fluorine-18 for application to positron emission tomography (PET). The inherent substrate specificity of the enzyme is, however, limiting, as only small modifications to the natural nucleoside substrate were known to be tolerated. This thesis describes an exploration and expansion of the substrate scope of the fluorinase enzyme, and its application to radiolabelling biomolecules for PET.

The design and synthesis of a novel acetylene bearing substrate for the fluorinase, 5'-chloro-5'-deoxy-2-ethynyladenosine (ClDEA) is described. ClDEA proved an excellent substrate for the fluorinase, and the kinetics of the transformation and binding affinities of the new substrate and product were investigated. The fluorinated acetylenic product was demonstrated to undergo a copper-catalysed azide-alkyne cycloaddition (CuAAC) reaction with an azide bearing RGD peptide, and this methodology was investigated for the synthesis of a novel fluorine-18-bearing prosthetic group for the synthesis of a radiolabelled RGD peptide, which was assessed *in vivo* in a rat.

After the demonstration that the fluorinase can be used for "last step" radiolabelling of bioactive peptides, the synthesis of dimeric and tetrameric RGD-bearing substrates for the fluorinase was investigated. These large constructs underwent efficient enzymatic fluorination, and the fluorinated products showed increased binding affinity to their targets, compared to monomeric analogues. The challenges encountered during radiolabelling of these multimers with fluorine-18 using the fluorinase are discussed.

A difluoromethyl-bearing nucleoside substrate (F_2DA) was synthesised as a potential substrate in the reverse direction for the fluorinase, to further probe the substrate specificity if the fluorinase. Upon incubation with the enzyme, F_2DA did not appear to undergo reaction, despite the demonstration that F_2DA binds to the enzyme.

Finally, the optimisation of a fluorinase-based protocol for the synthesis of the PET radiotracer [^{18}F]fluoroacetate is described. The enzymatic method proved unsuitable for a small animal study due to contamination of the final product, and a chemical method was investigated and optimised as an alternative approach. [^{18}F]Fluoroacetate synthesised using the developed chemical method was employed in an *in vivo* evaluation of acetyl CoA synthetase (ACSS2) activity in healthy and tumour-bearing mouse models, in an study to assess the activity of ACSS2 in breast and colon cancer models in mice.

Acknowledgements

The work that has gone into this thesis, and the entire PhD experience more generally, is anything but just my own. Countless people have contributed to what fills these pages, some in a big way, others through passing comments. I wish I could remember each and every little contribution, and pay each person their acknowledgements by name, but unfortunately my memory is not good enough for that. So first, a general thank you to everyone who has been a part of this journey. Without you, this piece of work would not be what it is.

Thank you to the many people and organisations that have funded the work in this project. Thank you to the John and Kathleen Watson Scholarship, the Scottish Imaging Network SINAPSE and the School of Chemistry at the University of St Andrews for giving me the opportunity to pursue this PhD.

To Prof. David O'Hagan, who supervised the work described herein. I am immensely grateful for the opportunities that were offered during my time as a PhD student. Your enthusiasm and passion for science (and everything fluorinated) has been contagious, and will be something that I take on with me long into the future. Your encouragement when experiments looked like they weren't working out was invaluable. The diverse projects that you challenged me with allowed me to gain experience and insight into areas of science I had never come across before, and I will forever be grateful for this.

One of the biggest contributions to this work has come from past and present members of the DOH and NPB groups. When I arrived 4 years ago, I knew a bit of chemistry, and almost no biology. But with your help, I now know a bit more chemistry, and maybe a little biology too. A few members of the group have made much this time easier than it otherwise would have been. I owe huge thanks to Dr Neil Keddie, for all the proof reading and advice, chemistry and otherwise, he has offered over the last 4 years. Nouchali Bandaranayaka and Dr Jason Chan, thank you for your patience with me in the Biolab, between the two of you, you have taught me all the practical biology I know. I would also like to thank Dr Gavin Milne, Dr Alistair Durie, Dr Qingzhi Zhang, and Dr Andy Nortcliffe and Axel Bartholome for the many fruitful discussions about chemistry. To Rudy, Rodrigo, Ricardo, Davide, Phill, Tanya, Nawaf, Flavio, Leonardo, Tony, Christina, Michael, Mohammed, Andrea, Tomoya, Gosia, Saki, Danny, Fatah, Ming Yang, Bouchra and Yi, thank you all for being such excellent lab mates.

I am also eternally grateful to Dr Stephen McMahon and Prof. Jim Naismith for always being willing assist with protein crystallography. I would also like to thank many other dedicated people at St Andrews, including Prof. Alex Slawin for carrying out crystallography, Dr Tomas Lebl and Melanja Smith for their help with NMR, and Caroline Horsburgh, Dr Sally Shirran and Dr Catherine Botting for their assistance with mass spectrometry.

Starting out this journey, I knew almost nothing about PET. I am indebted to Dr Mayca Onega and Dr Jan Passchier at Imanova Ltd for being willing to host and introduce me to radiochemistry. I owe much of my hands on experience to Dr Sally Pimlott, thank you for

being willing to teach someone so inexperienced. I also thank Dr Sue Champion, Dr Gaurav Malviya and Agata Mrowinska for all their help with the fluoroacetate project. Thank you too to Dr Ian Fleming for always being willing to run ELISA assays within days of getting the samples.

I owe special thanks to Tamara Kosikova, for proof reading this work (I'll never start a sentence with "This" again), and also for being an incredibly generous friend. To Dr Maciej Skibinski, thank you for being an excellent housemate and a wonderful friend. To Stefan Borsley, thanks for all the delicious meals and interesting conversations, and to Frida Michailidou, I will always miss your enthusiasm and laugh in the corridor. You all made up the Lunch Club, kept me sustained (both with food and company) throughout a large part of this work. Tamara, Maciek, Stefan and Frida, thank you for many, many interesting meals!

I am especially grateful for the love from my friends and family back in South Africa. Mom, Dad, Richard, Simone, Amber, and Abbey, thank you for always being there for me. You have given me tremendous support throughout this process, and I will forever be grateful for the love, support and opportunities that you have given me over the last 4 years.

Silvie, I don't know how I would have made it through the last 2 and a half years if I hadn't had you by my side, constantly supporting me. We got through your PhD together, and now thankfully, mine too. Thank you for keeping me sane, especially over the last few months of stress, anxiety and late nights at the office. So much of this experience has been shaped by you, often by reminding me to listen to you, because you already have a PhD. It's been wonderful my bub, and your love is what has got me through. I can't wait to start the next exciting adventure together.

Abbreviations

Ac	acetyl
acetyl coA	acetyl coenzyme A
ACN	acetonitrile
ACP	acyl carrier protein
ACSS	acetyl coenzyme A synthetase
ACSS1	acetyl coenzyme A synthetase 2
ACSS2	acetyl coenzyme A synthetase 2
ACSS3	acetyl coenzyme A synthetase 3
ADA	adenosine deaminase
ADIBO	aza-dibenzocyclooctyne
ADP	adenosine diphosphate
AgOTf	silver triflate
AMP	adenosine monophosphate
ATCC	American Type Culture Collection
ATP	adenosine triphosphate
b.p.	boiling point
Bn	benzyl
Boc	*tert*-butyloxycarbonyl
br	broad
BrDA	5'-bromo-5'-deoxyadenosine
Bz	benzoyl
BzCl	benzoyl chloride
c	concentration
calc.	calculated
ClDA	5'-chloro-5'-deoxyadenosine
ClDEA	5'-chloro-2-ethynyl-5'-deoxyadenosine
CLS	chronological lifespan
CoA	coenzyme A
CoASH	coenzyme A
COD	cyclooctadiene
cRGD	cyclic Arg-Gly-Asp-bearing peptides
CSA	camphorsulfonic acid
CT	computerised tomography
CuAAC	copper catalysed alkyne-azide cycloaddition
d	deuteron, or doublet
Da	dalton
DAST	(diethylamino)sulfur trifluoride
dba	dibenzylideneacetone
DCC	dicyclohexylcarbodiimide
DCM	dichloromethane
dd	doublet of doublets
ddd	doublet of doublets of doublets
Deoxofluor®	bis(2-methoxyethyl)aminosulfur trifluoride
DFT	density functional theory
DIPEA	diisopropylethylamine
DMA	dimethylaniline
DMAPP	dimethylallyl pyrophosphate
DMF	dimethylformamide
DMP	2,2-dimethoxypropane
DMSO	dimethyl sulfoxide
DMTr	dimethoxytrityl
DNA	deoxyribonucleic acid
DOX	doxycycline
dt	doublet of triplets
EDCI	1-ethyl-3-(3-dimethylaminopropyl)carbodiimide
EDTA	ethylenediaminetetraacetic acid
ee	enantiomeric excess
ELISA	enzyme-linked immunosorbant assay
eq.	equivalents

ES	electrospray
ESI	electrospray ionisation
F_2DA	5',5'-difluoro-5'-deoxyadensine
FAc	fluoroacetate
FAcCoA	fluoroacetyl coenzyme A
FAcOH	fluoroacetic acid
FAD	flavin adenine dinucleotide, oxidised form
$FADH_2$	flavin adenine dinucleotide, reduced form
FAS	fatty acid synthase
FBA	*p*-fluorobenzoic acid
FBAld	*p*-fluorobenzaldehyde
FDA	5'-fluoro-5'-deoxyadenosine
FDAS	5'-fluoro-5'-deoxyadenosine synthase
FDEA	5'-fluoro-2-ethynyl-5'-deoxyadenosine
FDG	2-deoxy-2-[^{18}F]fluoro-D -glucose
FDI	5'-fluoro-5'-deoxyinosine
FDOPA	6-fluoro-L-3,4-dihydroxyphenylalanine
FDR	5-fluoro-5-deoxyribose
FDRP	5-fluoro-5-deoxyribose-1-phosphate
FDRulP	5-fluoro-5-deoxyribulose-1-phosphate
FLT	fluorothymidine
FMISO	fluoromisonidazole
FPA	2-fluoropropionic acid
FPP	farnesyl pyrophosphate
FSAM	*S*-(5'-fluoroadenosyl)-L-methionine
FSeSAM	*Se*-(5'-fluoroadenosyl)-L-selenomethionine
GLUT	glucose transporter
GPP	geranyl pyrophosphate
h	hours
H-bond	hydrogen bond
HILIC	hydrophilic interaction liquid chromatography
HMGCoA	3-hydroxy-3-methylglutaryl coenzyme A
HOMO	highest occupied molecular orbital
HPLC	high performance liquid chromatography
HRMS	high resolution mass spectrometry
HYNIC	hydrazinonicotinic acid
IBX	2-iodoxybenzoic acid
IC_{50}	half maximal inhibitory concentration
IPP	isopentenyl-5-pyrophosphate
IPTG	isopropyl β-D-1-thiogalactopyranoside
IR	infrared
ITC	isothermal titration calorimetry
J	coupling constant
K_a	association constant
k_{cat}	turnover number
K_d	dissociation constant
K_i	inhibitory constant
K_M	Michaelis Menten constant
krypto222	4,7,13,16,21,24-hexaoxa-1,10-diazabicyclo-(8.8.8)-hexacosane
Kryptofix 222	4,7,13,16,21,24-hexaoxa-1,10-diazabicyclo-(8.8.8)-hexacosane
L-AAO	L-amino acid oxidase
LB	Luria broth
LC-MS	liquid chromatography-mass spectrometry
LD_{50}	half maximal lethal dose
LDA	lithium diisopropylaminde
LI	large intestine
L-Met	L-methionine
L-SeMet	L-selenomethionine
LUMO	lowest unoccupied molecular orbital
M	molecular ion
m	multiplet

m/z	mass to charge ratio
MALDI-TOF MS	matrix-assisted laser desorption ionization time of flight mass spectrometry
Max.	maximum
min	minutes
MME	monomethyl ether
MOPS	3-(*N*-morpholino)propanesulfonic acid
mp	melting point
MRI	magnetic resonance imaging
Ms	methanesulfonyl
MS	mass spectrometry
MTBE	methyl *t*-butyl ether
MTRP	5-*S*-methyl-5-thioribose-1-phosphate
n	neutron
NAD^+	nicotinamide adenine dinucleotide, oxidised form
NADH	nicotinamide adenine dinucleotide, reduced form
$NADP^+$	nicotinamide adenine dinucleotide phosphate, oxidised form
NADPH	nicotinamide adenine dinucleotide phosphate, reduced from
NAG	*N*-acetylglucosamine
NAM	*N*-acetylmuramic acid
NFP	2-fluoropropionate
NFSI	*N*-fluorobenzenesulfonimide
NMR	nuclear magnetic resonance
NODA	1,4,7-triazacyclononane-1,4-diacetate
NOTA	1,4,7-triazacyclononane-1,4,7-trisacetate
NRRL	ARS Culture Collection
OD	optical density
p	proton
PAMAM	polyamidoamine
PBS	phosphate buffered saline
PCK	phosphoenolpyruvate carboxykinase
PEG	polyethyleneglycol
PET	positron emission tomography
Piv	pivaloyl
PKS	polyketide synthase
PLP	pyridoxal phosphate
PPARγ	peroxisome proliferator-activated receptor-γ
PP_i	pyrophosphate
ppm	parts per million
py	pyridine
Q	normalised activity
q	quartet
QM/MM	quantum mechanics/molecular mechanics
RCP	radiochemical purity
RCY	radiochemical incorporation
R_f	retention factor
RGD	arginyl-glycinyl-aspartyl
RNA	ribonucleic acid
RNAi	ribonucleic acid interference
rpm	revolutions per minute
rt	room temperature
s	singlet
s.e.	standard error
SAGA	Spt-Ada-Gcn5 acetyltransferase
SAH	*S*-adenosyl-L-homocysteine
salen	*N*,*N*'-ethylenebis(salicylimine)
SAM	*S*-adenosyl-L-methionine
sat.	saturated
SDS PAGE	sodium dodecylsulfate polyacrylamide gel electrophoresis
SEC	size exclusion chromatography
SeEAM	*Se*-(2-ethynyladenosyl)-L-selenomethionine
Selectfluor	1-chloromethyl-4-fluoro-1,4-diazoniabicyclo[2.2.2]octane

SeSAM	*Se*-adenosyl-L-selenomethionine
SFB	*N*-succinimidyl 4-fluorobenzoate
SI	small intestine
SiFA	silicon-based fluoride acceptor
siRNA	small interfering ribonucleic acid
SPECT	single photon emission computerised tomography
SREBP	sterol regulatory element-binding protein
SUV	standardised uptake value
SUV_{max}	maximal standardised uptake value
t	triplet
$t_{1/2}$	half life
TBAF	tetrabutylammonium fluoride
TBTA	tris[(1-benzyl-1H-1,2,3-triazol-4-yl)methyl]amine
^{t}BuOH	*tert*-butanol
TCO	*trans*-cyclooctene
TEG	tetraethyleneglycol
TEMPO	(2,2,6,6-tetramethylpiperidin-1-yl)oxidanyl
Tf	trifluoromethanesulfonyl
TFA	trifluoroacetate
THF	tetrahydrofuran
TIC	total ion chromatogram
TLC	thin layer chromatography
TMEDA	tetramethylethylenediamine
TMS	trimethylsilyl
$TMSCF_2H$	(difluoromethyl)trimethylsilane
$TMSCF_3$	(trifluoromethyl)trimethylsilane
TMSCl	trimethylsilyl chloride
t_R	retention time
TRIS	tris(hydroxymethyl)aminomethane
Ts	toluenesulfonyl
TsCl	*p*-toluenesulfonyl chloride
TsF	p-toluenesulfonyl fluoride
TsOH	*p*-toluenesulfonic acid
UV	ultraviolet
v/v	volume per volume
ν_{max}	maximal absorption
w/v	weight per volume
WT	wild type
XRD	X-ray diffraction
α	alpha particle
β^-	electron
β^+	positron
μW	microwave

Contents

Declaration ii

Abstract iii

Acknowledgements iv

Abbreviations vi

Contents x

1. Introduction 1

1.1. Fluorine and the fluorinase 1

1.1.1. Fluorine in nature 1

1.1.2. Biological halogenation 5

1.1.3. The fluorinase 8

1.1.4. Mechanism of enzymatic fluorination 10

1.1.5. Fluorometabolite biosynthesis 14

1.1.6. Fluorinases and analogues from other species 17

1.2. Positron emission tomography (PET) 21

1.2.1. PET for molecular imaging 21

1.2.2. Sources of ^{18}F for radiotracer synthesis 25

1.2.3. Synthesis of ^{18}F-bearing radiotracers by nucleophilic substitution 28

1.2.4. Late-stage fluorinations for PET 29

1.3. Protein and peptide labelling strategies for PET 37

1.3.1. Prosthetic groups 37

1.3.2. “Last step” radiolabelling of peptides 43

1.4. Fluorinase and PET 43

1.4.1. Applying the fluorinase to PET 49

1.4.2. Base swaps 49

1.4.3. Fluoroacetate 50

1.4.4. Fluorodeoxyribose 51

1.5. Conclusions 52

1.6. References 53

2. Synthesis and evaluation of an alkynyl-bearing substrate for the fluorinase 67

2.1. Modified fluorinase substrates 67

2.2. Aims 71

2.3. Synthesis of an ethynyl substrate for the fluorinase 72

2.3.1. Synthesis of 5'-chloro-2-ethynyl-5'-deoxyadenosine (ClDEA) **174** 73

2.3.2. 5'-fluoro-2-ethynyl-5'-deoxyadenosine (FDEA) **176** 76

2.4. Over-expression and purification of recombinant fluorinase 78

2.4.1. Fluorinase over-expression 78

2.4.2. Removal of adenosine from the fluorinase 80

2.4.3. Cleavage of His-Tag for protein crystallisation 83

2.5. Evaluation of ClDEA 174 as a substrate for the fluorinase 84

2.5.1. Evaluation of ClDEA **174** as a substrate for the fluorinase 84

2.5.2. Comparison of rate of transhalogenation for ClDEA **174** and ClDA **23** 88

2.5.3. Michaelis-Menten kinetic evaluation of ClDEA **174** as a fluorinase substrate 90

2.5.4. Competition experiment with ClDEA **174** and ClDA **23** 92

2.5.5. Thermodynamic characterisation of ClDEA **174** and FDEA **176** as ligands 93

2.5.6. Crystallographic study of FDEA **176** as a ligand 97

2.6. Bioconjugation of FDEA 176 to a peptide 100

2.6.1. Preparation of synthetic samples of ClDEA-RGD **200** and FDEA-RGD **201** 101

2.6.2. Coupling the enzymatic transhalogenation with the CuAAC reaction 102

2.6.3. Binding assay of FDEA-RGD **201** to $\alpha_V\beta_3$ integrin 105

2.7. Radiosynthetic evaluation of ClDEA-fluorinase system for PET 106

2.7.1. Fluorinase mediated [^{19}F]fluoride labelling *vs* [^{18}F]fluoride labelling 106

2.7.2. Synthesis of [^{18}F]FDEA-RGD [^{18}F]-**201** 107

2.7.3. *In vivo* evaluation of [^{18}F]FDEA-RGD **201** 110

2.8. Conclusions 113

2.9. References 115

3. Synthesis and evaluation of multimeric RGD substrates for the fluorinase 118

3.1. Extension of the fluorinase system to "last step" labelling for PET 118

3.1.1. Development of a peptide-bearing substrate for the fluorinase 119

3.1.2. "Last step" radiolabelling of a peptide with fluorine-18 121

3.2. RGD multimers in molecular imaging 122

3.2.1. Multimeric RGD peptides based on amides 124

3.2.2. Multimeric RGD peptides based on triazoles 128

3.3. Aims 130

3.4. Synthesis of di- and tetra-alkynes and for a CuAAC reaction 133

3.4.1. Synthesis of the alkyne fragments for Sonogashira couplings 133

3.4.2. Synthesis of the iodinated fragments for Sonogashira couplings 135

3.4.3. Sonogashira couplings towards multimeric alkynes 137

3.4.4. Assessment of ClDEA-PEG-$(C{\equiv}CH)_2$ **219** as a fluorinase substrate 140

3.5. CuAAC reaction with c(RGDfK[N_3]) 199 141

3.5.1. Investigation of the CuAAC reaction under microwave heating 142

3.5.2. Synthesis of ClDEA-PEG-$(RGD)_2$ **224** and FDEA-PEG-$(RGD)_2$ **248** 144

3.5.3. Synthesis of ClDEA-PEG-$(RGD)_4$ **225** and FDEA-PEG-$(RGD)_4$ **249** 145

3.6. Evaluation of multimeric RGDs as substrates for the fluorinase 148

3.6.1. Evaluation of ClDEA-PEG-$(RGD)_2$ **224** as a substrate for the fluorinase 148

3.6.2. Evaluation of ClDEA-PEG-$(RGD)_4$ **225** as a substrate for the fluorinase 151

3.7. Binding assay of denrimeric RGDs to $\alpha_V\beta_3$ integrin 155

3.8. Radiosynthetic evaluation of multimeric RGDs 157

3.8.1. Initial radiolabelling experiments with ClDEA-PEG-$(RGD)_2$ **224** 157

3.8.2. Optimisation of radiolabelling conditions with ClDA **23** as a substrate 160

3.8.3. Radiolabelling of ClDEA-PEG-$(RGD)_2$ **224** under optimised conditions 161

3.8.4. Radiolabelling of ClDEA-PEG-$(RGD)_4$ **225** under optimised conditions 164

3.9. Conclusions 168

3.10. References 170

4. A difluoromethyl-bearing nucleoside substrate for the fluorinase 174

4.1. The difluoromethyl group 174

4.1.1. Applications of the difluoromethyl group 174

4.1.2. Synthesis of the difluoromethyl group 176

4.2. Aims 178

4.3. Synthesis of 5',5'-difluoro-5'-deoxyadensine 276 (F_2DA) 180

4.3.1. Synthesis of an adenosine-5'-aldehyde 180

4.3.2. Difluorination of adenosine-5'-aldehyde **283** 182

4.4. Investigation of F_2DA 276 binding to the fluorinase 187

4.5. Evaluation of F_2DA 276 as a substrate 189

4.5.1. Evaluation of F_2DA **276** with L-Met **21** as a co-substrate 189

4.5.2. Evaluation of F_2DA **276** with L-SeMet **161** as a co-substrate 191

4.6. Crystallography of F_2DA 276 bound to the fluorinase 193

4.7. Conclusions 196

4.8. References 197

5. Synthesis of [^{18}F]fluoroacetate for assessment of acetyl CoA synthetase 2 activity *in vivo* 201

5.1. Acetyl coenzyme A 201

5.1.1. Sources of acetyl CoA 202

5.1.2. Acetyl CoA as a metabolic building block 204

5.1.3. Acetyl CoA as a source of acetyl units 206

5.1.4. Other functions of acetyl CoA 208

5.2. Acetyl CoA Synthetase 208

5.2.1. Acetyl CoA synthetase genes and proteins 208

5.2.2. The role of ACSS2 in cancer 209

5.3. Fluoroacetate 212

5.3.1. Fluoroacetate as a metabolic toxin 212
5.3.2. Synthesis and applications of [^{18}F]fluoroacetate [^{18}F]-**1** 213
5.4. Aims 214
5.5. Method development 215
5.5.1. Kuhn-Roth oxidation investigation 215
5.5.2. Enzymatic synthesis of [^{18}F]fluoroacetate [^{18}F]-**1** 217
5.5.3. Chemical synthesis of [^{18}F]fluoroacetate [^{18}F]-**1** 221
5.6. Imaging of ACSS mouse model 225
5.6.1. Assessment of [18F]fluoroacetate [^{18}F]-**1** in healthy and ApcMin/+ models 226
5.6.2. Xenograft breast cancer model 230
5.7. Conclusions 234
5.8. References 235

6. Experimental 239
6.1. General Experimental 239
6.2. Compound preparation for Chapter 2 242
6.2.1. 2′,3′,5′-Tri-*O*-acetylguanosine **184** 242
6.2.2. 2-Amino-6-chloro-9β-(2′,3′,5′-tri-*O*-acetyl-D-ribofuranosyl)-purine **185** 243
6.2.3. 6-Chloro-2-iodo-9β-(2′,3′,5′-tri-*O*-acetyl-D-ribofuranosyl)-purine **186** 244
6.2.4. 2-Iodoadenosine **179** 245
6.2.5. 2-(Trimethylsilylethynyl)adenosine **187** 246
6.2.6. 2-Ethynyladenosine **180** 247
6.2.7. 5′-Chloro-5′-deoxy-2-ethynyladenosine (ClDEA) **174** 248
6.2.8. 2',3'-*O*-Isopropylidene-2-(trimethylsilylethynyl) adenosine **191** 249
6.2.9. 5′-Deoxy-5'-fluoro-2',3'-*O*-isopropylidene-2-ethynyladenosine **192** 250
6.2.10. 5′-Deoxy-5'-fluoro-2-ethynyladenosine (FDEA) **176** 251
6.2.11. 5′-Chloro-5′-deoxyadenosine **23** 252
6.2.12. ClDEA-RGD **200** 253
6.2.13. FDEA-RGD **201** 254
6.3. Compound preparation for Chapter 3 255
6.3.1. Methyl 3,5-bis(prop-2-yn-1-yloxy)benzoate **227** 255

6.3.2. Methyl 3,5-bis((3-(trimethylsilyl)prop-2-yn-1-yl)oxy) benzoate **228** 256

6.3.3. 3,5-Bis((3-(trimethylsilyl)prop-2-yn-1-yl)oxy)benzyl alcohol **229** 257

6.3.4. 3,5-Bis((3-(trimethylsilyl)prop-2-yn-1-yl)oxy) benzaldehyde **223** 258

6.3.5. 3,6,9,12-Tetraoxapentadec-14-yn-1-ol **231** 259

6.3.6. 3,6,9,12-Tetraoxapentadec-14-yn-1-yl tosylate **232** 260

6.3.7. 1-Azido-3,6,9,12-tetraoxapentadec-14-yne **233** 261

6.3.8. 1-Amino-3,6,9,12-tetraoxapentadec-14-yne **222** 262

6.3.9. *N*-(3',5'-bis((3-(trimethylsilyl)prop-2-yn-1-yl)oxy)benzyl)-3,6,9,12-tetraoxapentadec-14-yn-1-amine **234** 263

6.3.10. *N,N*-bis(3',5'-bis((3-(trimethylsilyl)prop-2-yn-1-yl)oxy) benzyl)-3,6,9,12-tetraoxapentadec-14-yn-1-amine **235** 264

6.3.11. 5'-Chloro-5'-deoxy-2-iodoadenosine **238** 265

6.3.12. 2',3'-*O*-Isopropylidene-2-iodoadenosine **239** 266

6.3.13. 5'-Fluoro-5'-deoxy-2',3'-*O*-isopropylidene-2-iodoadenosine **240** 267

6.3.14. 5'-Fluoro-5'-deoxy-2-iodoadenosine **241** 268

6.3.15. ClDEA-PEG-$(C\equiv CH)_2$ **219** 269

6.3.16. ClDEA-PEG-$(C\equiv CH)_4$ **220** 261

6.3.17. FDEA-PEG-$(C\equiv CH)_2$ **245** 273

6.3.18. FDEA-PEG-$(C\equiv CH)_4$ **247** 275

6.3.19. ClDEA-PEG-$(RGD)_2$ **224** 287

6.3.20. ClDEA-PEG-$(RGD)_4$ **225** 279

6.3.21. FDEA-PEG-$(RGD)_2$ **248** 281

6.3.22. FDEA-PEG-$(RGD)_4$ **249** 282

6.4. Compound preparation for Chapter 4 284

6.4.1. 2',3'-*O*-Isopropylideneadenosine **285** 284

6.4.2. *N*-Benzoyl-2',3'-*O*-isopropylideneadenosine **280** 285

6.4.1. *N*-Benzoyl-5'-deoxy-2',3'-*O*-isopropylidene-5',5'-(*N′,N″*- diphenylethylenediamino)adenosine **282** 286

6.4.2. *N,N*-Dibenzoyl-2',3'-*O*-isopropylideneadenosine **287** 287

6.4.3. *N,N*-Dibenzoyl-2',3'-*O*-isopropylideneadenosine-5'-aldehyde **283** 288

6.4.4. *N,N*-Dibenzoyl-5',5'-difluoro-5'-deoxy-2',3'-*O*-isopropylideneadenosine **284** 289

6.4.5. 5',5'-Difluoro-5'-deoxy-2',3'-*O*-isopropylideneadenosine **288** 290

6.4.6. 5',5'-Difluoro-5'-deoxyadenosine (F_2DA) **276** 291

6.5. Compound preparation for Chapter 5 **292**
6.5.1. 5'-Fluoro-5'-deoxy-2',3'-*O*-isopropylideneadenosine **325** 292
6.5.2. 5'-Fluoro-5'-deoxyadenosine **22** 293
6.5.3. Ethyl *O*-mesylglycolate **49** 294
6.6. Fluorinase overexpression and purification **295**
6.7. Enzymatic Assays for Chapter 2 **296**
6.7.1. ClDEA **174** to FDEA **176** 296
6.7.2. ClDEA **174** and ClDA **23** rate comparison experiments 297
6.7.3. Michaelis-Menten investigation of ClDEA **174** 297
6.7.4. ClDEA **174** and ClDA **23** competition experiments 298
6.7.5. Enzymatic production and click reaction of FDEA **174** with c(RGDfK[N_3]) **199** 298
6.7.6. LCMS of Click Reaction with 0.5 eq. of c(RGDfK[N_3]) **199** 299
6.7.7. Synthesis of [^{18}F]FDEA [^{18}F]-**176** and [^{18}F]FDEA-RGD [^{18}F]-**201** 299
6.7.8. *In vivo* evaluation of [^{18}F]FDEA-RGD [^{18}F]-**201** 300
6.8. Enzymatic experiments for Chapter 3 **300**
6.8.1. ClDEA-PEG-(C≡CH)$_2$ **219** to FDEA-PEG-(C≡CH)$_2$ **245** 300
6.8.2. ClDEA-PEG-(RGD)$_2$ **224** to FDEA-PEG-(RGD)$_2$ **248** 300
6.8.3. ClDEA-PEG-(RGD)$_4$ **225** to FDEA-PEG-(RGD)$_4$ **249** 301
6.8.4. ClDA **23** to [^{18}F]FDA [^{18}F]-**22** 301
6.8.5. ClDEA-PEG-(RGD)$_2$ **224** to [^{18}F]FDEA-PEG-(RGD)$_2$ [^{18}F]-**248** 302
6.8.6. ClDEA-PEG-(RGD)$_4$ **225** to [^{18}F]FDEA-PEG-(RGD)$_4$ [^{18}F]-**249** 303
6.9. Enzymatic Experiments for Chapter 4 **304**
6.9.1. F_2DA **276** with L-Met **21** 304
6.9.2. F_2DA **276** with L-SeMet **161** 304
6.10. Synthesis of [^{18}F]FAc [^{18}F]-1 for Chapter 5 **304**
6.10.1. Enzymatic synthesis of [^{18}F]FAc [^{18}F]-**1** 304
6.10.2. Chemical synthesis of [^{18}F]FAc [^{18}F]-**1** 305
6.10.3. *In vivo* evaluation of [^{18}F]FAc [^{18}F]-**1** 306
6.11. Miscellaneous **306**
6.11.1. Preparation of 10 mM $CuSO_4$.TBTA (55% DMSO solution) 306
6.11.2. Isothermal titration calorimetry 306
6.11.3. X-Ray crystallography of the fluorinase and FDEA **176** and F_2DA **276** 307
6.11.4. Evaluation of RGD compound affinity to $\alpha_V\beta_3$ 307

6.12. References 308

1. Introduction

1.1. Fluorine and the fluorinase

1.1.1. Fluorine in nature

Fluorine is the 13th most abundant element in the earth's crust, existing predominantly in the form of insoluble fluorous minerals such as fluorite. Elemental fluorine, first prepared by Moissan in 1886, has recently (2012) been confirmed to exist in minute quantities in nature, in inclusions within the mineral antozonite.[1] Antozonite releases a pungent odour when crushed and many possible causes for this odour, including ozone, fluorine gas, acyl fluorides and oxyfluorides have been proposed as the causative agent. Fluorine gas was confirmed to be responsible for the odour when elemental fluorine was detected in samples of antozonite using solid state ^{19}F NMR spectroscopy.[1] Radioactive decay of uranium within the calcium fluoride-based mineral leads to breakdown of calcium fluoride into small calcium inclusions, responsible for the dark colour of the mineral. Fluorine radicals generated in this process combine to form fluorine gas, responsible for the mineral's pungent odour.

In contrast to the other halogens, chlorine, bromine and iodine, fluorine serves no role in regular metabolism. The limited biological role of fluorine is reflective of the low water solubility of fluorous minerals and the high solvation energy of aqueous fluoride ion. In addition, the oxidation of fluoride ion by mechanisms used in most other biohalogenations, where oxidation of the halide ion is coupled to reduction of peroxide, is not available for fluoride. The oxidation potential of fluoride (+2.87 V) is higher than that of peroxide (+2.07 V), and cannot be reduced *via* the haloperoxidase mechanism. Despite the abundance of fluorous minerals, fluorine has limited presence in the biosphere and is known to occur in only about 20 natural products.

Fluoroacetate **1** (**Figure 1**), first isolated from the plant *Dichapetalum cymosum* in 1943,[2,3] is a potent metabolic toxin produced by a number *Dichapetalum* and other plant species, and also by several bacteria.[4] The toxicity of fluoroacetate **1** arises from its incorporation in the citric acid cycle. Fluoroacetate **1** is first condensed with coenzyme A to give fluoroacetyl coenzyme A (fluoroacetyl CoA). Fluoroacetyl CoA reacts with a unit of oxaloacetate, catalysed by citrate synthase, to give

(2*R*,3*R*)-fluorocitrate **2**.[5] The (2*R*,3*R*)-fluorocitrate **2** is then converted, by aconitase, to 4-hydroxy-*trans*-aconitate, a potent inhibitor of aconitase. The process was termed "lethal synthesis" by Peters, as inhibition of aconitase severely reduces energy production within the cell, which is a potentially lethal effect.[5]

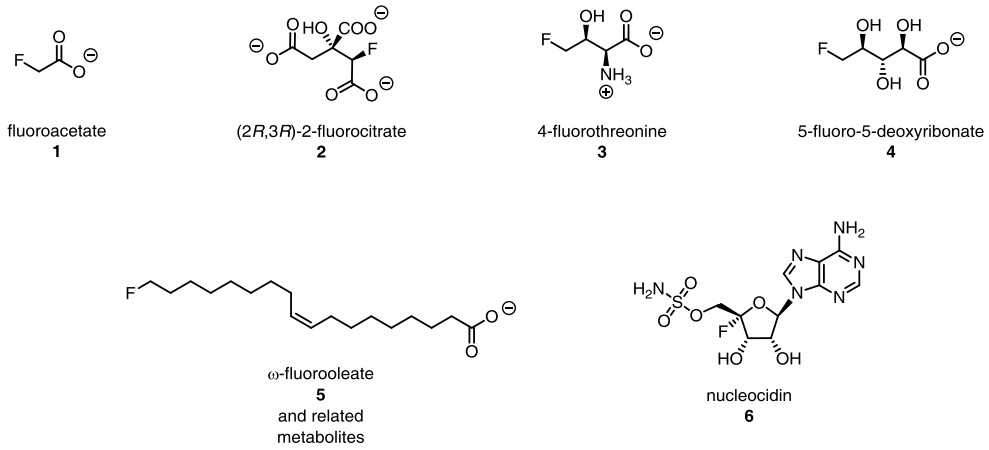

Figure 1. Fluorinated natural products.

The β-lactam producer *Streptomyces cattleya* (NRRL 8057) was known to produce an unidentified anti-metabolite when grown in selected media. After extensive chromatographic fractionation of cell culture extracts, the unknown anti-metabolite was identified as 4-fluorothreonine **3**.[6] 4-Fluorothreonine **3** showed weak antibacterial activity, proposed to be a result of its structural similarity to threonine. In addition to 4-fluorothreonine **3**, ^{19}F NMR spectroscopy of *S. cattleya* extracts revealed that the organism also produced fluoroacetate **1** in millimolar concentrations when the growth media was supplemented with inorganic fluoride.

In addition to accumulating fluoroacetate **1** in the leaves, the plant species *Dichapetalum toxicarium* also accumulates significant organofluorine in its seeds, however, not as fluoroacetate **1**.[7] Peters *et al*.[8] identified the principal entity of this organofluorine accumulation to be ω-fluorooleic acid **5**, shown in **Figure 1**. A number of additional ω-fluoro fatty acids have also been identified as minor components of the seed oil. These products include arachidic- ($C_{20:0}$), eicosenoic- ($C_{20:1}$), linoleic- ($C_{18:2}$), palmitic- ($C_{16:0}$), palmitoleic- ($C_{16:1}$), myristic- ($C_{14:0}$) and capric- ($C_{10:0}$) ω-fluoro-derivatives.[4,9] A dihydroxylated fluorooleic acid derivative has also been identified in the *D. toxicarium* seed extracts, hypothesised to arise *via* an epoxide intermediate.[10]

Fluorinated fatty acids are proposed to arise from use of fluoroacetyl CoA as a starter unit during fatty acid biosynthesis.[11] Fluorine is only ever observed at the terminal

position of the fatty acid, indicating acetyl CoA producing enzymes, such as acetyl CoA carboxylase, do not utilise fluoroacetate **1** as a substrate. It is also possible that fluoromalonyl CoA is not a substrate for the fatty acid synthase complex.[4]

More recently, engineered polyketide synthases (PKSs) have been coaxed to use fluoroacetyl CoA **7** or 2-fluoromalonyl CoA **9** and incorporate terminal or mid-chain fluorine substituents into polyketide architectures, as shown in **Scheme 1**. Spencer *et al.*[12] showed that fluoroacetyl CoA **7** was incorporated into octaketide **8** (**Scheme 1 A**) by an overexpressed minimal PKS. Chang *et al.*[13] showed incorporation of 2-fluoromalonyl CoA **9** into **10** and **11** also using an engineered PKS (**Scheme 1 B**). These strategies illustrate the possibility of applying the well understood polyketide biosynthetic pathways for the production of fluorinated analogues using this biocatalytic approach. Engineering PKSs to have the ability to incorporate fluorinated precursors has the potential to generate motifs that would otherwise be challenging to access by traditional organic chemistry.

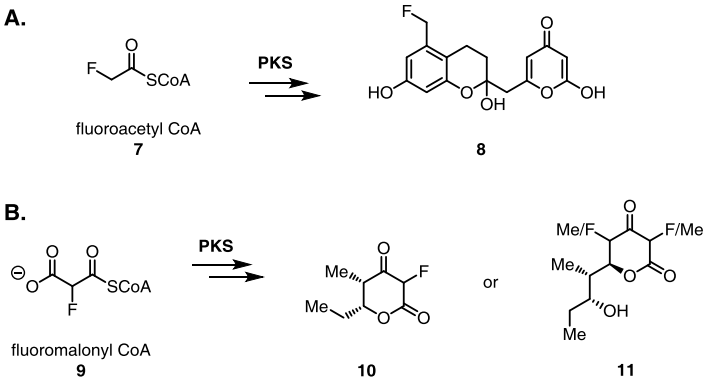

Scheme 1. Incorporation of **A.** fluoroacetyl CoA[12] and **B.** 2-fluoromalonyl CoA[13] into polyketides by engineered PKSs.

5-Fluoro-5-deoxyribonic acid **4** was identified in fermentation broths of the soil bacterium *Streptomyces* sp. MA37, isolated from soil samples from Ghana.[14] When incubated in fluoride supplemented culture media, ^{19}F NMR spectroscopy of cell free extracts from this organism showed the production of fluoroacetate **1** and 4-fluorothreonine **3**, along with 5-fluoro-5-deoxyribonic acid **4**.[14] Total synthesis of 5-fluoro-5-deoxyribonic acid **4**, and spiking extracts with the reference material confirmed the identity of this new fluorinated natural product. Additionally, a series of unidentified fluorometabolites were observed in these culture broths.

The most unusual of the fluorinated natural products discovered to date is nucleocidin **6**, a trypanosome active antibiotic isolated from *Streptomyces calvus*.[15]

Other fluorinated natural products all bear a conserved -CH_2F moiety and are all related to fluoroacetate **1** (except fluorocitrate **2**, but this is known to derive from fluoroacetate **1**). Nucleocidin **6**, however, contains a quaternary fluorinated centre, which bears no obvious relationship to a fluoroacetate origin.

Nucleocidin **6** was first isolated from the soil bacterium *S. calvus* in 1957.[15] Initially misidentified and thought not to contain fluorine, the correct, fluorinated structure of this natural product was proposed in 1969.[16] Doubled signals in the ^{1}H NMR spectrum of the compound were suggested to be a result of coupling to a fluorine atom rather than the presence of rotamers.[17,18] The correct stereochemical assignment and fluorine-containing structure of nucleocidin **6** was confirmed in 1976 by total synthesis.[19]

Recent efforts to induce nucleocidin **6** production in a number of commercial and proprietary strains of *S. calvus* have shown limited success.[20] The lack of production is suggested to be due to loss of the appropriate biosynthetic genes upon freezing of cultures for storage.[21] The lack of a producing strain of *S. calvus* has frustrated investigation of what would be an unusual biosynthetic pathway for the activation and incorporation of fluoride into biomolecules.

Three other classes of molecules have been proposed as fluorinated natural products, but have been misidentified, or are unlikely to be of biological origin. Fluoroacetone **12**, **Figure 2**, was proposed as a volatile fluorinated intermediate in fluoride metabolism from *Acacia georginae*, however, it is more likely that the volatile carbonyl compound detected was fluoroacetaldehyde, now known as an intermediate in the biosynthetic pathway of 4-fluorothreonine **3** and fluoroacetate **1**.

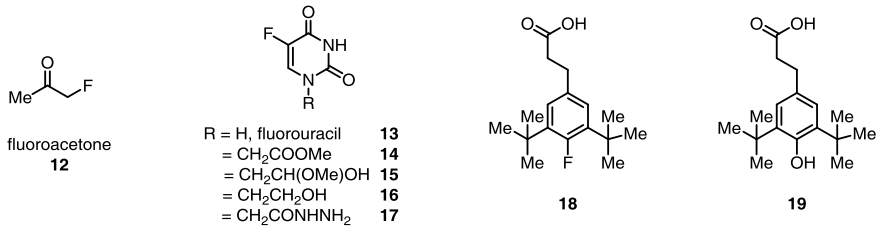

Figure 2. Compounds proposed as fluorinated natural products.

5-Fluorouracil **13** and a number of derivatives thereof (**14** to **17**) have been isolated from the marine sponge *Phakellia fusca*.[22] 5-Fluorouracil **13** is an anticancer agent, produced and used on an industrial scale. Rather than the sponge synthesising these compounds, 5-fluorouracil **13** is suggested to bio-accumulate in the sponge,

sequestered either from industrial or domestic effluent.[23] Metabolic action on the 5-fluorouracil **13** core is proposed to give rise to derivatives **14** to **17**.

In 2014, fluoroarene **18** (**Figure 2**) was proposed as the structure of a compound isolated from *Streptomyces* sp. TC1 broths.[24] Arene **18** was prepared synthetically and found to have distinctly different spectroscopic properties to the isolated product.[25] Specifically, a sharp peak in the ^{19}F NMR spectrum at –110.1 ppm was observed, in contrast to the broad "peak" (−140 ppm to −180 ppm) observed for the compound isolated from *S.* sp. TC1. Further investigations showed that the isolated compound was in fact the 4-hydroxy-derivative **19**, and did not contain a fluorine atom.[26]

1.1.2. Biological halogenation

There are over 4000 natural products containing halogens described.[27] The majority of these are chlorinated (approx. 2300) or brominated (approx. 2100). Fewer than 150 natural products containing iodine are known, but only about 20 natural products containing fluorine have been isolated and described, as discussed above.[27] Most biological halogenations utilise oxidative or radical reactions to generate formal electrophilic "X^+"[28–31] or radical "$X^\bullet$"[32,33] equivalents respectively from the corresponding bioavailable chloride, bromide or iodide ions. An additional class of halogenating enzymes has more recently been described, capable of catalysing the formation of C–X bonds directly from either fluoride or chloride ion by nucleophilic substitution.[34,35]

A haem-containing chloroperoxidase from *Caldariomyces fumago* was the first described halogenase. This enzyme is responsible for the chlorination event in the biosynthetic pathway of caldariomycin.[36] In this class of enzymes, a haem-Fe(III) species is oxidised by H_2O_2 to form an Fe(IV) species. The Fe(IV) species performs a 2-electron oxidation of chloride ion to produce iron-bound hypochlorite, the active chlorinating agent, as shown in **Scheme 2 A**.[28,29]

A. Haem Iron-Peroxide Electrophilic Halogenation

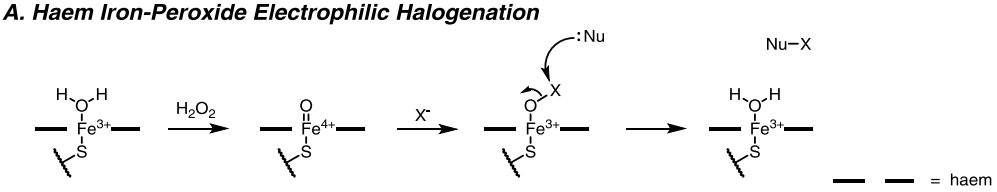

B. Vanadium-Peroxide Electrophilic Halogenation

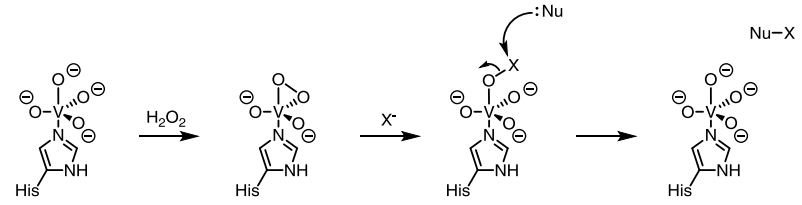

C. Flavin Catalysed Halogenation

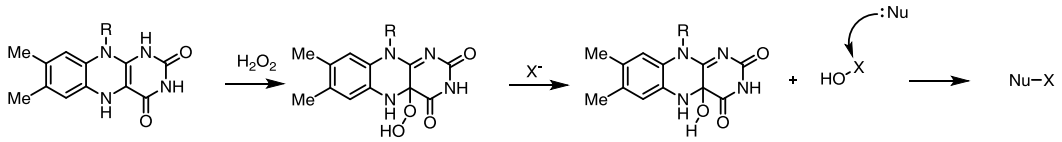

D. Non-Haem Iron Radical Halogenation

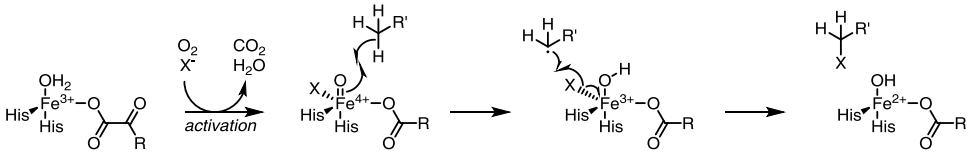

Scheme 2. Mechanisms of oxidative halogenation of natural products catalysed by **A.** haem-iron, **B.** vanadium or **C.** flavin mediated generation of an electrophilic halogenating agent and its reaction with the appropriate nucleophile. **D.** Radical halogenation by non-haem iron species of unactivated centres.

Similar electrophilic halogenases operating through vanadium-oxo species are also known. The vanadium centre co-ordinates a peroxide ion to give an oxo-peroxo-V(V) species (**Scheme 2 B**), which reacts with halide ion to form a hypohalite ion. Hypohalite then reacts with the appropriate substrate to produce a halogenated product.[30,31]

Flavin also acts as a source of hypohalite in some enzymes. $FADH_2$ reacts with peroxide to generate an oxidised flavin intermediate. The peroxo-intermediate oxidises halide ions to generate hypohalous acid (**Scheme 2 C**), which diffuses through the enzyme to halogenate the substrate.[37]

A number of non-haem-iron halogenases are known to catalyse radical halogenation.[32] These iron-containing enzymes are dependent on molecular oxygen and α-ketoglutarate, which in the presence of chloride or bromide ion, react to give a halo-Fe(IV)-oxo species. This species abstracts a hydrogen radical from the

appropriate enzyme-bound substrate, forming an Fe(III) species. The C-centred radical is then quenched by forming a bond to the halogen, restoring the iron centre to the ferrous oxidation state, as shown in **Scheme 2 D**.[33]

Of particular interest to this thesis are the halogenases catalysing reactions through nucleophilic substitution. The first enzyme described in this class was the fluorinase, isolated from *Streptomyces cattleya* in 2002, which catalyses the formation of a C–F bond from fluoride and SAM **20**, to generate FDA **22**.[34] This enzyme is responsible for the first committed step of biosynthetic pathway of fluoroacetate **1** and 4-fluorothreonine **3**, shown in **Scheme 3**. Subsequently, a chlorinase operating through the same mechanism was discovered in the marine bacterium *Salinospora tropica*. The chlorinase forms part of the biosynthetic pathway of salinosporamide A **24**, and is responsible for generating ClDA **23**, the first committed product in the biosynthetic pathway. Salinosporamide A **24** is currently in clinical trials as an anticancer agent.[35]

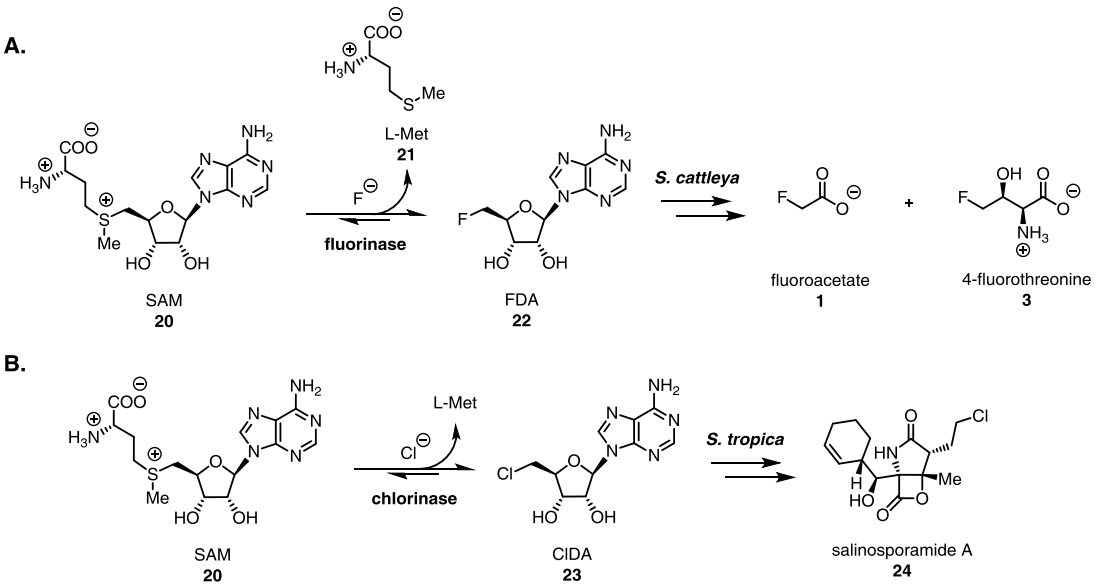

Scheme 3. Nucleophilic biohalogenation by **A.** the fluorinase enzyme, in the biosynthetic pathway towards fluoroacetate **1** and 4-fluorthreonine **3** and **B.** the chlorinase enzyme, in the biosynthetic pathway of salinosporamide A **24**.

The chlorinase and fluorinase activate halide ion by replacing hydrogen bonds (H-bonds) to solvent with H-bonds to amino acid residues in the active site. The enzyme then presents this activated nucleophile to *S*-adenosylmethionine **20** (SAM). The desolvated halide attacks the C-5' of the sulfonium centre, displacing methionine **21** as a leaving group and generating a 5'-halo-5'-deoxyadenosine (**22** or **23**). More detail regarding this mode of halogenation will be provided below.

1.1.3. The fluorinase

Enzymatic synthesis of a C–F bond was first reported in mutant glycosidases under high fluoride ion concentration. Fluoride was able to intercept highly electrophilic glycosyl donors, producing fluorinated sugars.[38,39] This activity was not native to the glycosidases, and provided no information about the origin of fluorinated natural products.

Investigation into the biochemistry of fluorine metabolism in *Streptomyces cattleya* (NRL 8057) led to the isolation of 5'-fluoro-5'-deoxyadenosine synthase (FDAS, more commonly termed "fluorinase") in 2002.[34] Addition of adenosine triphosphate (ATP) and methionine to fluoride-containing cell free extracts of *S. cattlyea* led to enhanced fluorometabolite production. This pointed to *S*-adenosylmethioinine **20** (SAM) as the immediate biosynthetic precursor to the observed fluorometabolites. A partially purified protein preparation from *S. cattleya* was able to convert SAM **20** and inorganic fluoride to 5'-fluoro-5'-deoxyadenosine **22** (FDA) shown in **Scheme 4**, the first committed step in the fluorometabolite biosynthetic pathway. The fluorinase was also found to operate in the reverse direction, and upon incubation of the fluorinase with FDA **22** and L-methionine **21**, SAM **20** was produced as a product.

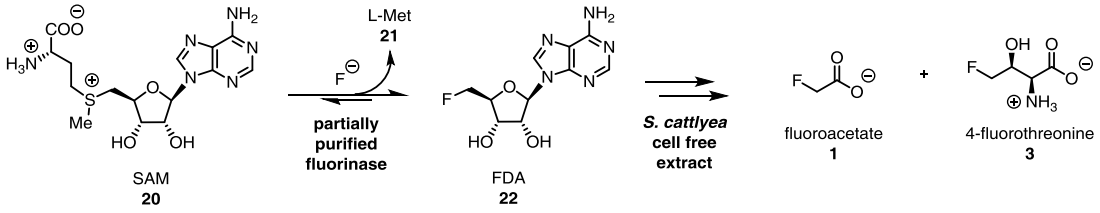

Scheme 4. The first step in the fluorometabolite pathway in *S. cattleya* is catalysed by the fluorinase to give FDA **22**. Cell free extracts from the organism were capable of transforming SAM **20** and inorganic fluoride to fluoroacetate **1** and 4-fluorothreonine **3**.

Crude cell free extracts from *S. cattleya* were capable of converting SAM **20** and inorganic fluoride to fluoroacetate **1** and 4-fluorothrenonine **3**,[40] showing that all the necessary biosynthetic enzymes for fluoroacetate **1** and 4-fluorothreonine **3** production were expressed in *S. cattleya*.

The fluorinase (E.C. 2.5.1.63) was further purified from cell homogenates using a combination of ammonium sulfate precipitation, hydrophobic interaction, size exclusion and anion exchange chromatography.[41] Sodium dodecylsulfate polyacrylamide gel electrophoresis (SDS PAGE) and mass spectrometry revealed that the monomer of the fluorinase had a molecular weight of 32.2 kDa. Size exclusion chromatography showed

that the intact protein had a mass of approximately 196 kDa, suggesting that the enzyme organised as a hexamer in solution.[41]

Subsequent crystallisation of both native and recombinant variants of the fluorinase[42,43] allowed the structure of the enzyme bound to substrate to be solved to 1.9 Å, revealing the fluorinase to be a dimer of trimers. A single trimer is shown in **Figure 3 A**. The monomer (**Figure 3 B**) consists of distinct *N*-terminal and *C*-terminal domains linked by a short polypeptide chain. The enzyme also has a distinctive 21 amino acid loop in the *N*-terminal domain, which contacts the *C*-terminal domain and makes up a part of the active site. The structural fold of the fluorinase places the enzyme in a superfamily of proteins which, up to that point, had no known function. Other members of the family lack the flexible loop in the *N*-terminal domain of the fluorinase, suggesting that the loop may play a critical role in the function of the enzyme. The organisation of three monomers into a trimer gives the minimal functional unit of the fluorinase, as the active site of the enzyme (**Figure 3 C**) is located at the interface of the *N*-terminal domain of one monomer and the *C*-terminal domain of another. Two trimers interact through the *C*-terminal domains to form the hexamer in solution.

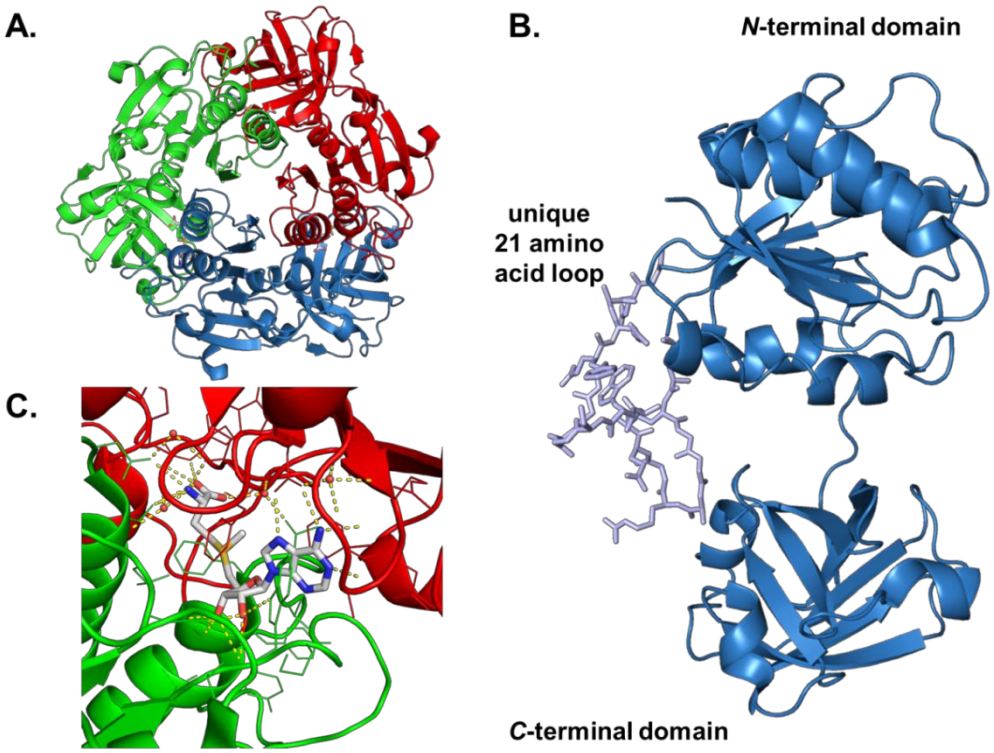

Figure 3. Crystal structure of the fluorinase with SAM **20** bound in the active site. **A.** Top view of the fluorinase trimer. **B.** Single fluorinase monomer showing the *N*- and *C*-terminal domains, with the characteristic loop highlighted in light blue. **C.** SAM **20** in the active site, which lies between two monomers.

1.1.4. Mechanism of enzymatic fluorination

The location of the sulfonium centre in the substrate:enzyme complex and the fluorine atom in the product:enzyme complex suggested that the fluorinase enzyme operated through an S_N2-like mechanism. The position of these atoms suggested that desolvated fluoride ion acts as a nucleophile, attacking the sulfonium centre of SAM **20**, displacing methionine as a leaving group and generating FDA **22** Feeding experiments with chiral deuterated glycerols had previously suggested that the fluorination reaction proceeded with an inversion of configuration at C-5'.[44] This was confirmed by the synthesis of a chiral deuterated SAM **20** derivative, (5'*S*)-[5'-$^2H_1$]-SAM, and the stereochemical outcome of a fluorinase catalysed reaction was explored.[45] The resultant chiral FDA **22** was purified by reverse phase chromatography and subjected to ^2H NMR spectroscopy in a chiral liquid-crystalline solvent. The NMR experiment revealed that the reaction had proceeded with inversion of configuration at C-5', implying an S_N2 process.

Comparison of the enzyme-substrate and enzyme-product complexes reveals that the C–S bond is oriented at 164° compared to the C–F bond in the product. This orientation agrees with the interpretation that the reaction occurs through an S_N2 process. Distinguishing water from fluoride in the active site proved difficult due to their similar size and electron count, however crystal structures of S159A mutants with *S*-adenosylhomocysteine (SAH, a high affinity inhibitor) and SAM **20** were solved where chloride ion was distinguishable in the active site. In these cases, a water molecule fulfilled the role of the hydroxyl group of Ser-158, participating in hydrogen bonding contacts with the halide ion. In this structure, the halide ion was oriented at approximately 130° to the C–S bond rather than the optimal 180° required for an S_N2 substitution, but this may be due to the shifting of residues in the active site to accommodate the larger chloride, rather than fluoride ion.

The native fluorinase isolated from *S. cattleya* was found to co-crystallise with SAM **20** bound within the active site. The crystal structure revealed extensive interactions between SAM **20** and residues in the active site. The active site itself is buried within the enzyme, suggesting that the enzyme also exists in an open conformation, capable of binding the substrate.

Fluoride ion appears to bind in a 1.4–1.6 Å pocket in the active site, optimally sized to bind fluoride (1.3 Å ionic radius) rather than chloride (1.81 Å ionic radius) or the other larger halide ions. HOLE[46] analysis showed no obvious ion channel through which

fluoride ion could enter the active site after the binding of SAM **20**. Fluoride therefore enters the active site first, and is forced into its binding pocket upon the binding of SAM **20**. This process is consistent with a model where fluoride ion exchanges H-bonds with water to residues within the active site.

Incubating SAM **20** and fluoride with the fluorinase prior to crystallisation afforded a second X-ray structure with FDA **22** and L-methionine **21** bound to the active site. The location of FDA **22** revealed that the fluoromethyl group makes contacts with a number of residues in a hydrophobic pocket defined by Phe-156, Tyr-77 and Thr-80, as illustrated in **Figure 4**. In addition, the fluorine atom itself makes two contacts with the amide hydrogen and hydroxyl hydrogen of Ser-158, and possibly Thr-80.[47]

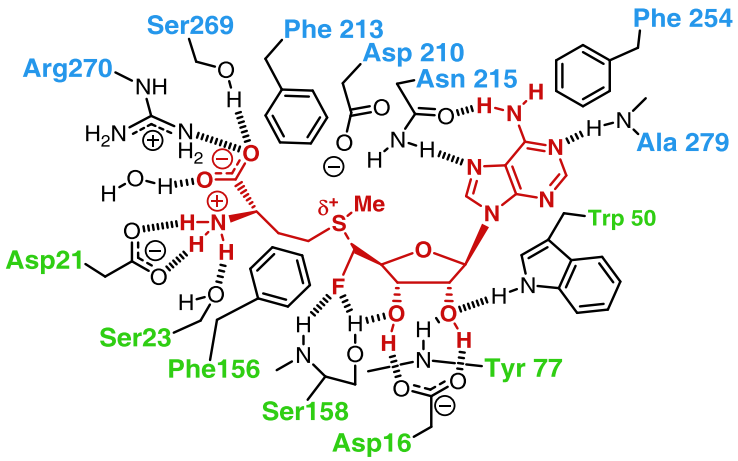

Figure 4. Fluorinase (black) interactions with FDA **22** and L-Met **21** (red). Residues belonging to the individual monomers making up the active site are shown in green and blue. Adapted with permission from Naismith *et.al.*[43]

Ser-158 and Asp-16 were suggested to be critical residues which formed H-bonds to incoming fluoride ion in an otherwise hydrophobic environment formed partly by Phe-156. To probe the importance of these residues, mutants at these positions were investigated. In the S158A mutant, catalytic activity was reduced due to the loss of H-bond donors for fluoride in the active site.[48] Similarly, little activity was observed in an F156A mutant, while a F156V mutant led to the restoration of some catalytic activity. The loss of activity suggested that the hydrophobic pocket was involved in increasing the reactivity of fluoride ion. D16A, D16S and D16N mutants were also found to have little activity, suggesting that the aspartate residue that interacts with the 2',3'-diol of the ribose ring plays a key role in organising the substrate for catalysis.

The mechanism of the fluorination reaction was further investigated using isothermal titration calorimetry (ITC) in order to deduce the order in which each of the components

necessary for reaction bound into the active site of the enzyme.[48] Fluoride showed no detectable binding by ITC, and steady state kinetic measurements suggested that fluoride had a low affinity (K_M > 5 mM).

SAM **20** was found to bind with high affinity to the fluorinase (K_d = 1.3 μM) in a highly thermodynamically favoured process. The high affinity for SAM **20** may contribute to securing the fluoride in the active site, promoting its desolvation and activation. Binding is further favoured by the formation of multiple hydrogen bonding and π-π stacking interactions between the adenine base and the enzyme. The high affinity of the fluorinase for the adenosyl fragment of the substrate is illustrated in the binding affinities of both adenosine (K_d = 0.82 μM) and the product of the reaction, FDA **22** (K_d = 0.22 μM), both higher than that of the substrate SAM **20**.

In the reverse direction, L-methionine showed no appreciable binding to the apo-fluorinase. Binding affinity was restored upon incubation of the fluorinase with either FDA **22** or adenosine, suggesting that in the reverse direction, the binding of the nucleoside organises the binding site for L-methionine.

Density functional theory (DFT) and quantum mechanics/molecular mechanics (QM/MM) calculations were used to further investigate the fluorinase reaction.[47] A number of reaction pathways were explored in terms of their thermodynamic feasibility. Formation of a sulfur ylide by deprotonation at one of the four acidic sites (the three positions alpha to the sulfonium, or at C-4') followed by HF addition was found to be either highly endothermic or kinetically prohibitive and, therefore, improbable as viable reaction pathways. Alternatively, all three positions alpha to the sulfonium centre offer potential electrophilic sites for nucleophilic attack of fluoride ion. Calculating the reaction energies of attack at the three positions showed all three to be similarly exothermic. The regioselectivity observed was concluded to result from the organisation of the nucleophile and electrophile within the active site of the enzyme, rather than from an intrinsic thermodynamic driving force for reaction at a specific site of SAM **20**.

The fluorinase was found to lower the activation energy barrier for the formation of the transition state complex. Activation energy for the reaction between the free species in solution was found to be 93 kJ.mol^{-1}, while this was reduced to 53 kJ.mol^{-1} in the active site. This reduction in activation energy represents a rate acceleration of 10^6 to 10^8 times for the enzyme catalysed reaction *versus* the reaction in solution. This rate acceleration was determined to largely result from pre-organisation of the substrates

within the active site, rather than from other factors intrinsic to the protein environment. There was also a small contribution to rate acceleration from lowering the HOMO-LUMO gap by substrate distortion and the electric field within the active site.

The steady state kinetics of the enzymatic transformation were also investigated, revealing that the fluorinase has a K_M for SAM **20** of between 6.5 μM and 29 μM.[48,49] The high affinity observed in the kinetic experiments was in agreement with the affinity previously determined by ITC. More interestingly, the fluorinase enzyme was found to exhibit very low turnover numbers, with a k_{cat} value of 0.06 min^{-1}. Considering that the enzyme enhances the rate of catalysis by a factor as high as 2×10^{15} times,[50] this low turnover number illustrates the difficulty in the formation of a C–F bond under aqueous conditions, even in specially evolved enzymatic systems.

When the fluorinase was originally isolated and characterised, its selectivity for halide ion was investigated and the enzyme was found to react only with fluoride.[34,43] When incubated with chloride ion, no conversion to the analogous chlorinated product, 5'-chloro-5'-deoxy-adenosine **23** (ClDA) was observed. The enzyme-catalysed reaction was, however, found to be reversible and able to catalyse the cleavage of the C–F bond when incubated with FDA **22** and L-methionine (or its selenium analogue), to generate SAM **20** (or its selenium analogue) and fluoride ion.[51] The equilibrium for this reaction was found to lie in favour of FDA **22**, by a factor of three.

The reversibility of the transformation led to the discovery that the fluorinase could utilise chloride ion and synthesise ClDA **23** from SAM **20** in the presence of an L-amino acid oxidase (L-AAO). The equilibrium for this transformation lies heavily in favour of SAM **20** and chloride ion, in contrast to reaction with fluoride (**Scheme 5**). Addition of an L-AAO to the reaction drives the forward reaction by removing L-methionine **21** from solution by its irreversible conversion to the corresponding oxo-acid **25**.

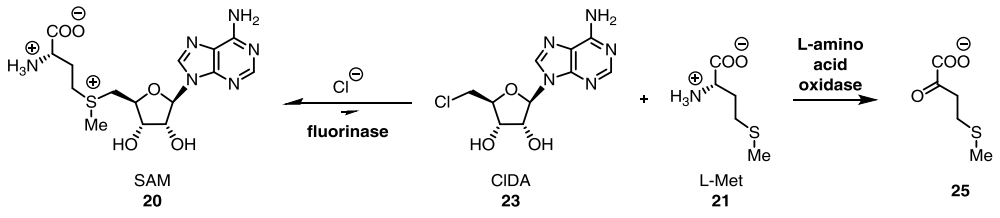

Scheme 5. Chlorinase activity was observed with the fluorinase when reactions were carried out coupled to the action of L-AAO, which removes L-methionine **21** from the medium and drives the synthesis of ClDA **23**.

The reversibility of the reaction coupled to the ability to use chlorinated substrates led to the demonstration of a fluorinase catalysed transhalogenation. In this reaction, the

chlorinated nucleoside **23** was fed to the enzyme which catalysed reaction to produce the seleno-SAM intermediate **26**. The equilibrium for this reaction favours production of SeSAM **26**, which then acts as a substrate for a subseqent fluorination reaction, to generate FDA **22**, driven by the enzyme equilibrium lying towards the products as shown in **Scheme 6**.[51]

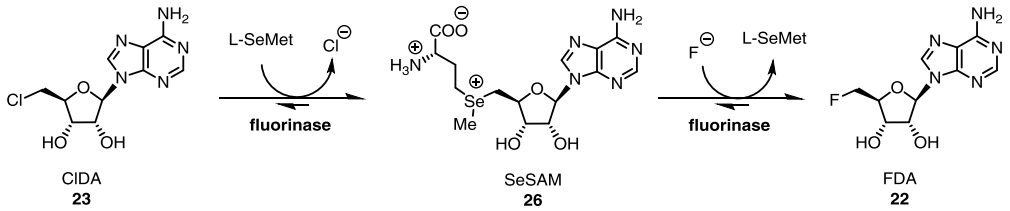

Scheme 6. Fluorinase–catalysed transhalogenation of chloro-nucleosides to fluoro-nucleosides though a SeSAM **26** intermediate.

This process is a useful alternative route towards fluorinated products from chlorinated starting materials. This transformation has allowed the discovery of new substrates for the fluorinase, as SAM **20** analogues are difficult to prepare synthetically. More detailed discussion of these non-natural substrates will be provided in **Chapter 2**.

1.1.5. Fluorometabolite biosynthesis

S. cattleya was known to produce millimolar quantities of fluoroacetate **1** and 4-fluorothreonine **3** when grown in fluoride supplemented media. Most work towards the elucidation of fluorometabolite biosynthetic pathway (**Scheme 7**) has therefore been undertaken in the organism.

Feeding experiments with ^{13}C- and ^{2}H- labelled metabolic precursors, including acetate, glycine and serine, suggested that there was a single fluorination enzyme present in *S. cattleya*, as both fluorinated products showed similar incorporations of the heavy isotopes.[52–54] Fluoroacetaldehyde **29** subsequently emerged as the key branching point in the biosynthetic pathway to fluoroacetate **1** and 4-fluorothreonine **3.**[55] Feeding of fluoroacetaldehyde **29** to cultures of *S. catteya* was found to increase the production of both fluoroacetate **1** and 4-fluorothreonine **3**.

A 55 kDa aldehyde dehydrogenase was purified from *S. cattlyea* homogenates which oxidises fluoroacetaldehyde **29** to fluoroacetate **1**.[56] This NAD^{+}-dependent enzyme was non-specific, and oxidised glycolaldehyde (150% activity compared to fluoroacetaldehyde **29**) and chloroacetaldehyde (80%) as well as some other short chain aldehydes to a lower degree.

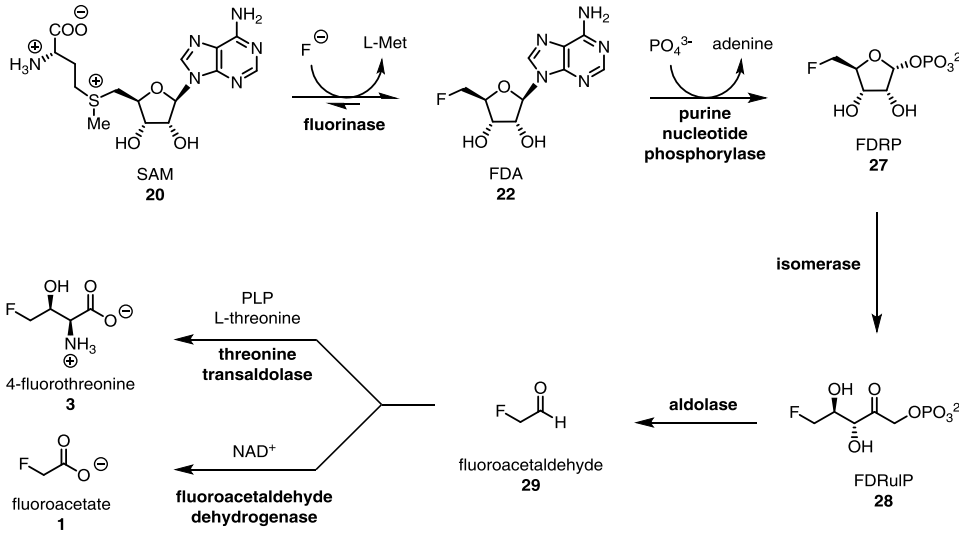

Scheme 7. Biosynthesis of 4-fluorothreonine **3** and fluoroacetate **1** in *S. cattleya*.

4-Fluorothreonine **3** production was enhanced upon incubation of threonine, fluoroacetaldehyde **29** and pyridoxal phosphate (PLP) with cell free extracts of *S. cattleya*.[57] These experiments led to the isolation of a 60 kDa PLP-dependent fluorothreonine transaldolase from *S. cattleya* homogenates. Threonine transaldolase was suggested to catalyse a novel reaction between PLP and threonine to form a PLP-bound glyoxylic acid Schiff base, releasing an equivalent of acetaldehyde. The Schiff base was proposed to react with fluoroacetaldehyde **29** in an aldol-type reaction to generate 4-fluorothreonine **3**.[57]

The fluorinase enzyme itself was identified from *S. cattleya* homogenates,[34] and a genomic library from *S cattleya* was sequenced,[58] accelerating the elucidation of the remainder of the biosynthetic pathway. The fluorinase gene, *flA*, was identified at the centre of a gene cluster, known as the Spencer cluster, illustrated in **Figure 5**.[58] Based on the location of the fluorinase gene, the genes flanking the *flA* gene were hypothesised to be involved in fluorometabolite biosynthesis.

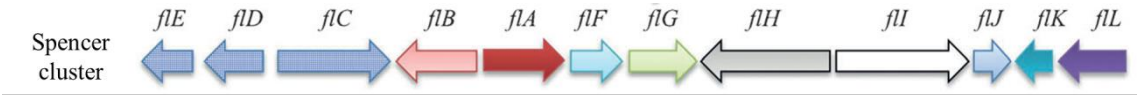

Figure 5. The fluorinase gene in *S. cattleya* determined from a cosmid library, showing the open reading frames surrounding the gene responsible for the first step in the pathway, *flA*. Image reproduced and modified with permission from O'Hagan *et al.*[49]

Directly adjacent to the fluorinase gene, an open reading frame was identified and named *flB*, which showed high homology to known purine nucleotide phosphorylases. 5-Fluoro-5-deoxyribose-1-phosphate **27** (FDRP) was previously shown to be an

intermediate in the biosynthetic pathway,[59] and the identification of the gene suggested that FDA **22** was phosphorylated by this enzyme to release FDRP **27** and adenine. Overexpression of this 299 amino acid protein proved challenging as the recombinant protein was largely insoluble, however, sufficient protein was obtained to confirm its role in the transformation of FDA **22** to FDRP **27**, as illustrated in **Scheme 7**.[58]

After the identification of FRDP **27** as an intermediate, it remained to be determined how FDRP **27** was transformed to fluoroacetaldehyde **29**. An analogous ribose phosphate, 5-*S*-methyl-5-thioribose-1-phosphate **30** (MTRP), is a known intermediate of the methionine salvage pathway. MTRP **30** (**Scheme 8**) is known to undergo transformation to the corresponding ribulose phosphate derivative **31**, under the action of an MTRP isomerase.[60] The ribulose phosphate products of such isomerisations, are well characterised substrates for aldolase enzymes, generating aldehyde intermediates through a retro-aldol reaction. It was hypothesised that a similar isomerase possibly played a role in metabolism of FDRP **27** to 5-fluoro-5-deoxyribulose-1-phosphate **28** (FDRulP). Under the action of such an aldolase, FDRulP **28** may be converted to fluoroacetaldehyde **29**, they key intermediate in the fluorometabolite biosynthetic pathway.

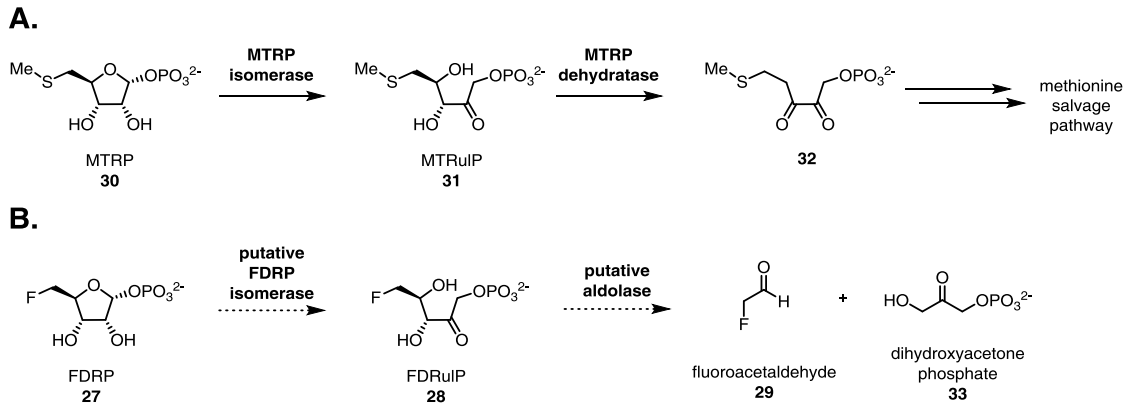

Scheme 8. **A.** MTRP isomerase involved in the methionine salvage pathway, generating a ribulose phosphate **31**. **B**. Proposed biosynthetic pathway to fluoroacetaldehyde **29** involving an isomerase and aldolase, *via* an intermediate ribulose phosphate **28**.

Incubation of FDRP **27** with *S. cattlyea* cell free extracts led to the production of FDRulP **28**, identified by GCMS after derivatisation.[61] Comparison of ^{19}F NMR chemical shifts to those of a standard confirmed the identity of the product as FDRulP **28**. These experiments provided evidence that FDRulP **28** was a biosynthetic intermediate, though the enzyme responsible for its biosynthesis remained to be isolated and identified. Incubation of FDRP **27** with an MTRP isomerase cloned from *S. coelicolor*

generated FDRulP **28**, providing further support for the hypothesis that a similar homologue in *S cattleya* may be responsible for the generation for FDRulP **28**.[62]

PCR amplification of genomic DNA from *S. cattleya* using primers generated from conserved regions of two *Streptomyces* MTRP isomerases led to the discovery of a similar gene in *S. cattleya*. This gene was amplified and cloned into and overexpressed in *E. coli*. The resultant 80 kDa dimer was able to transform FDRP **27** to FDRulP **28**,[62] though this activity was proposed to be secondary to its role in the methionine salvage pathway, as this gene was not located in the Spencer cluster.

Isolation of the aldolase responsible for the cleavage of FDRubP **28** to fluoroacetaldehyde **29** and dihydroxyacetone phosphate **33** has proved challenging. Aldolase activity has been isolated from cell free extracts from *S. cattleya*, but found to convert fluoroacetaldehyde **29** and dihydroxyacetone phosphate **33** to a stereoisomer of FDRubP **28** when the reaction was explored in the reverse direction. The aldolase responsible for cleavage of FDRubP **28** to fluoroacetaldehyde **29** remains to be definitively identified.[62]

Substitution of this aldolase with a putative fuculose aldolase from *S. coelicolor* in an *in vitro* reconstitution of fluorometabolite biosynthesis, using overexpressed variants of the other enzymes in the pathway, led to the production of fluoroacetate **1** and 4-fluorothreonine **3** in cultures, detected by ^{19}F NMR spectroscopy.[62] This result provided strong evidence that an aldolase is responsible for the generation of fluoroacetaldehyde **29** in the fluorometabolite biosynthetic pathway, but this enzyme remains to be isolated and characterised.

1.1.6. Fluorinases and analogues from other species

In 2008, salL, a chlorinase enzyme with moderate homology (30%) to the fluorinase was found to be responsible for a chlorination reaction during the biosynthesis of the anticancer agent salinosporamide A **24** (**Scheme 9 A**) from the marine organism *Salinospora tropica*.[35] The enzyme was unable to utilise fluoride ion as a substrate and selected for larger halide ions, specifically chloride. Comparison of the amino acid sequences of these two related enzymes revealed that the chlorinase lacked the distinctive 21 amino acid loop identified in the fluorinase, further suggesting that the loop may be essential for the selectivity of the fluorinase for fluoride ion over other halides.

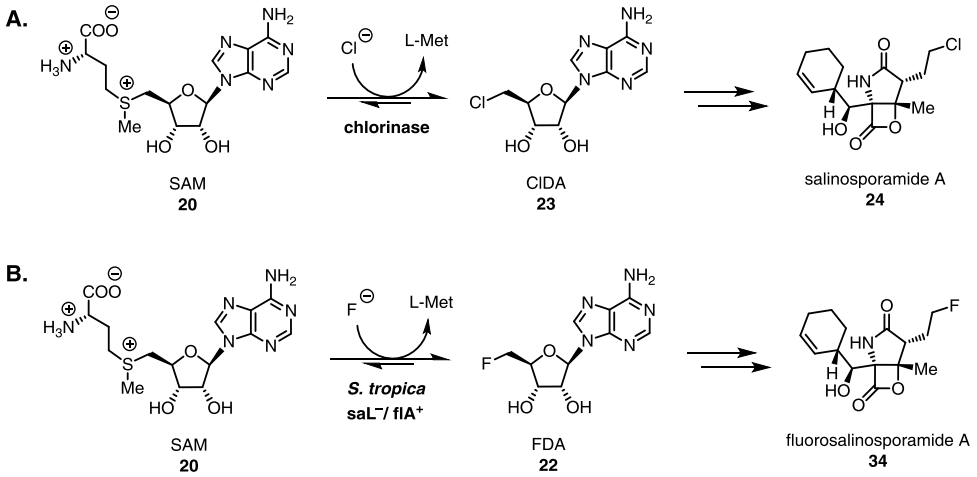

Scheme 9. **A.** Biosynthesis of salinosporamide A **24** by the chlorinase enzyme. **B.** Engineered production of fluorosalinosporamide A **34** by a mutant *S. tropica* strain containing the fluorinase gene from *S. cattleya*.

While salL, the enzyme responsible for the biohalogenation step, was found to be halide ion selective, fluorinated substrates were well tolerated by the downstream biosynthetic machinery. In *salL* knockouts, the organism was found able to synthesise fluorosalinosporamide A **34** when the medium was supplemented with FDA **22**.[63] In knockouts where the *salL* gene was replaced with the *flA* gene, production of fluorosalinosporamide A **34** was detected when the medium was supplemented with fluoride ion near the end of the exponential growth phase, as high fluoride ion concentration was toxic to the organism.[64]

Until 2014, the fluorinase from *Streptomyces cattleya* was the only known enzyme able to synthesise a C–F bond. Gene mining of publically available databases revealed two genes in bacterial species that shared high homology to the fluorinase from *S. cattleya*. The first gene was identified from the genome of *Nocardia brasiliensis* HUJEG-1 (ATCC 700358), a hospital pathogen.[49] The predicted amino acid sequence showed 81% similarity to the fluorinase from *S. cattleya*. The second was identified in an *Actinoplanes* sp. N902-109 and showed 80% similarity to the known fluorinase.[49,65] A third gene with 87% similarity to the *S. cattleya* was identified after sequencing of *Streptomyces sp*. MA37, an organism isolated from a Ghanaian soil sample.[49] Sequence analysis revealed that, unlike the chlorinase from *S. tropica*, these proteins contained the unique fluorinase *N*-terminal domain 21 amino acid loop.[43] The amino acid sequences of these proteins showed that all active site residues were highly conserved.

The three proteins were overexpressed in *E. coli* and found to be able to catalyse the reaction of fluoride ion with SAM **20** to generate 5'-fluoro-5'-deoxyadenosine **22**. Steady state kinetic characterisation of these three new fluorinases showed them to have similar k_{cat} values (0.122 to 0.262 min^{-1}) to the *S. cattleya* fluorinase (0.082 min^{-1}), confirming that the enzymatic fluorination reaction is inherently slow and this was not a feature unique to the *S. cattleya* fluorinase. The K_M values for SAM **20** for these three fluorinases were all similar to that for *S. cattleya*.

The identification of fluorinases in these organisms opened up the possibility for the discovery of new fluorometabolites. The genomes of all three organisms (**Figure 6 B**, **C** and **D**) bore homologues to fluorometabolite biosynthetic genes identified in *S. cattleya* (**Figure 6 A**), suggesting that all three have latent capacity for fluoroacetate **1** and 4-fluorothreonine **3** biosynthesis.

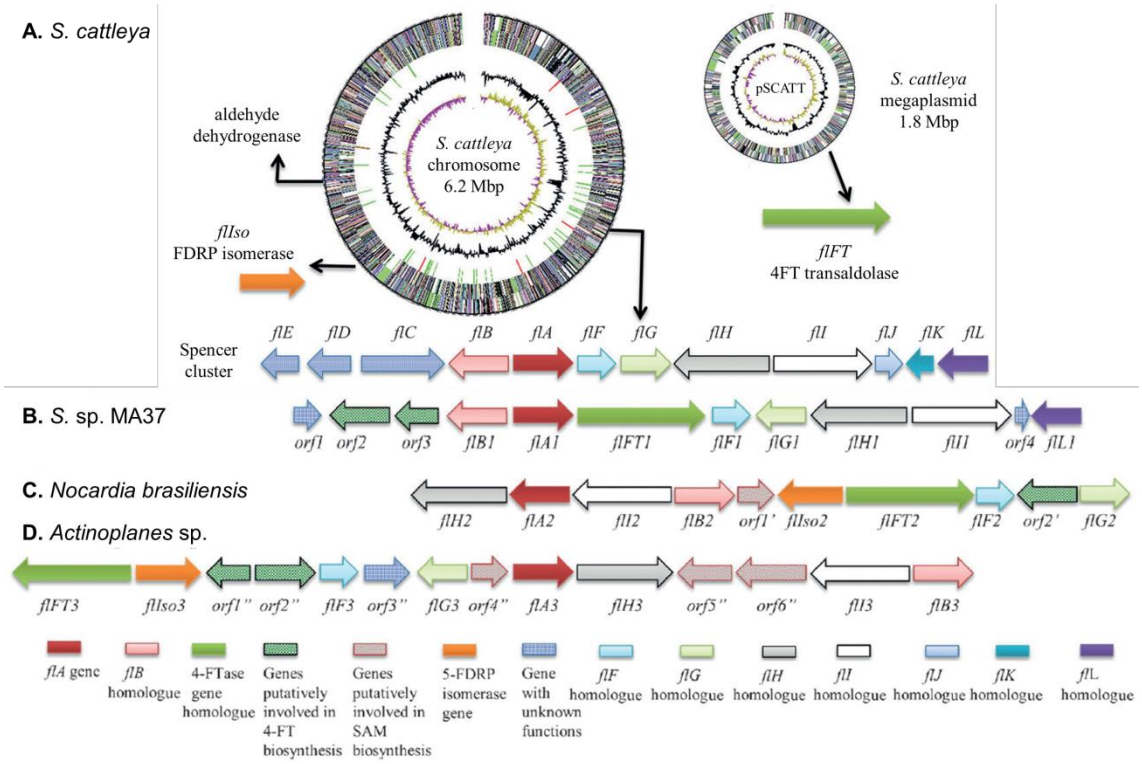

Figure 6. Fluorometablite biosynthesis gene organisation in **A.** *S. cattlyea*,[66] **B.** *S.* sp. MA37,[49] **C.** *N. brasiliensis*[67,68] and **D.** *Actinoplanes* sp. **D**[69] contain genes for functional fluorinases. Gene maps are centred around the fluorinase gene, *flA*, shown in red. Image reproduced and modified with permission from O'Hagan *et al.*[49]

The organisation of the biosynthetic genes within the four species was of interest. In *S. cattleya*, the genes encoding for 4-fluorthreonine transaldolase and FDRP isomerase were both located external to the Spencer cluster which contains the fluorinase gene. In the genomes of the three new species, these two genes were found

clustered near to *flA* as shown in **Figure 6.** This further confirmed their involvement in the fluorometabolite biosynthetic pathway in *S. cattleya* and suggested greater evolutionary regulation of fluorometabolite biosynthesis in the newly discovered organisms.

The *N. brasiliensis* strain was successfully cultured but found not to produce detectable quantities of fluorometabolites, using ^{19}F NMR spectroscopy.[49] This result suggested that the fluorometaboilte genes, while present, were not active in the organism. The *Actinoplanes* sp. strain is not publically available and it remains to be determined whether the organism has the capacity for fluorometabolite biosynthesis.

Streptoymyces sp. MA37 was successfully cultured and found to produce fluoroacetate **1** and 4-fluorothreonine **3** in culture broths, similar to *S. cattleya*.[49] An ^{19}F NMR profile of culture broths also revealed the presence of at least seven new, unidentified, fluorometabolites. One of these was successfully identified as 5-fluoro-5-deoxyribonic acid **4** by total synthesis, as discussed in **Section 1.1.1**.[14]

The only remaining fluorometabolite biosynthetic genes in the *S. cattleya* Spencer cluster with known functions are *flK*, coding for a thioesterase, and *flI*, coding for a *S*-adenosylhomocysteine (SAH) hydrolase. SAH is a potent inhibitor of the fluorinase, and flI is thought to relieve this inhibition.[58] The flK protein was hypothesised to confer resistance to fluoroacetate **1** to *S. cattleya*. The 18 kDa enzyme was overexpressed in *E. coli* and found to selectively hydrolyse fluoroacetyl CoA, while showing no activity towards acetyl CoA.[58] Hydrolysis of fluoroacetyl CoA prevents its entry into the citric acid cycle, and the formation of *trans*-4-hydroxyaconitate, the potent inhibitor of aconitase responsible for the toxicity of fluoroacetate **1**. Chang *et al.*[70] recently showed that hydrolysis of fluoroacetyl CoA proceeds through a ketene intermediate, and that the enzyme specifically recognises the fluorine atom of fluoroacetyl CoA. The residues in the active site recognise the fluorine atom of a mixed anhydride, orienting the substrate for selective abstraction of the *pro-R* proton by His-76. This fluorine recognition mechanism offers an explanation for the selectivity of flK for fluoroacetyl CoA over acetyl CoA.

1.2. Positron emission tomography (PET)

Introduction of C–F bonds into organic molecules remains an active area of research,[71] and the fluorinase enzyme offers a complimentary method to accomplish such a transformation. In contrast to the many other fluorination methods, the enzymatic reaction takes place in water, under mild conditions (neutral pH, ambient temperature). As the enzyme utilises fluoride ion as a fluorine source, the methodology is particularly applicable to labelling molecules with fluorine-18 for positon emission tomography (PET).

1.2.1. PET for molecular imaging

Molecular imaging techniques have emerged in the clinic as a means to supplement more common structural imaging techniques such as CT (computerised tomography) and MRI (magnetic resonance imaging).[72] Two of the most widely used molecular imaging techniques are SPECT (single photon emission computerised tomography), with technicium-99m, and PET (positron emission tomography) with isotopes such as fluorine-18 and carbon-11. Molecular imaging provides access to images of dynamic metabolic events and has provided new methods to investigate complex biological processes. PET has found application predominantly for imaging of cancer and neurodegenerative disorders and compliments the anatomical information obtained from structural imaging modalities.

PET imaging makes use of drug-like molecules known as radiotracers that bear unstable isotopes that decay through the emission of a positron (β^+). The emitted positrons undergo annihilation upon meeting their anti-particle, the electron (β^-), and this process emits two co-linear 511 keV γ-rays, as illustrated in **Figure 7**. These two γ-rays are registered by γ-cameras, usually arranged in a ring around the patient. Detection of the annihilation events and processing these to form an image, allows localisation of the radiotracer within the body.

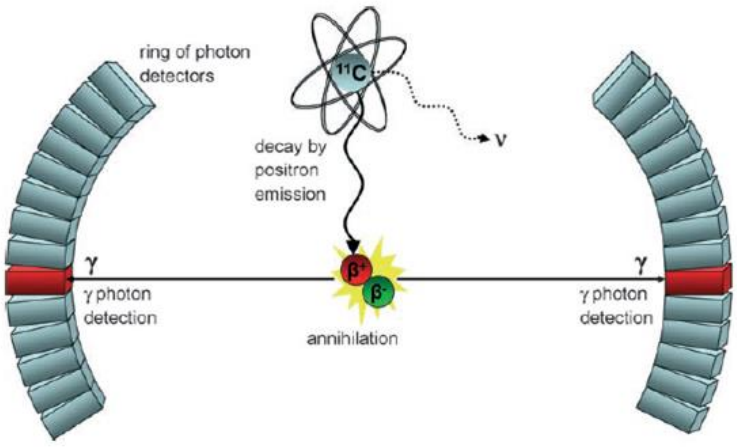

Figure 7. Decay of the ^{11}C nucleus and annihilation of a positron (β^+) by an electron (β^-). The γ-photons are detected by the circular ring of gamma cameras. Image used with permission from Gee *et al.* [73]

The most commonly used radioisotopes used for PET, shown below in **Table 1**, include both metals and non-metals. Isotopes such as carbon-11, nitrogen-13 and oxygen-15 are attractive as PET radioisotopes as they are elements which form the natural building blocks of biological molecules. Replacement of stable nuclei in such molecules with positron emitting isotopomers offers a route for imaging the distribution of these biological molecules within the body. The synthesis of radiotracers containing PET radioisotopes is restricted by the nuclear synthetic methods available for the production of such isotopes. These methods usually involve a range of accelerator-based technologies and provide a limited range of radioactive staring materials, as shown in **Table 1**.

Table 1. Radioisotopes commonly used in PET imaging applications, their energy of emission and their maximum range in water. Table adapted from Frey.[74]

Isotope	*Half-life*	*Form available for synthesis*	*Max. energy (MeV)*	*Max. range (mm in H_2O)*
^{11}C	20.4 min	$[^{11}C]CH_4$ $[^{11}C]CO$ $[^{11}C]CO_2$	0.97	4
^{13}N	9.97 min	$[^{13}N]NO_x$ $[^{13}N]NH_3$	1.20	5
^{15}O	2.04 min	$[^{15}O]O_2$	1.74	8
^{18}F	109.8 min	$[^{18}F]F_2$ $[^{18}F]F^-$	0.64	2
^{68}Ga	68.1 min	$[^{68}Ga]Ga^{3+}$	1.90	9
^{89}Zr	78 h	$[^{89}Zr]Zr^{4+}$	0.987	-

Nitrogen-13 and oxygen-15 have synthetically-limiting half-lives and it is often not practical to synthesise complex molecules bearing these isotopes. Their application has therefore been mostly limited to simple derivatives such as [^{15}O]H_2O and [^{13}N]NH_3, which have been used for imaging processes such as cerebral[75] and myocardial blood[76] flow respectively.

The longer half-life of carbon-11 ($t_{1/2}$ = 20.4 min) allows a greater freedom in the synthetic transformations available for incorporation of this isotope into biological or drug molecules.[73] Incorporation is generally accomplished using one of three strategies. The first transforms [^{11}C]CH_4 into either [^{11}C]CH_3I or [^{11}C]CH_3OTf, powerful electrophiles for methylation of nucleophilic sites of target molecules.[77] These electrophiles are also suited for use in metal-catalysed cross couplings, such as Suzuki[78] or Stille[79] couplings. [^{11}C]CO_2 can be used directly in Grignard reactions where quenching an alkyl or aryl magnesium halide species generates the corresponding [^{11}C]carboxylate.[80,81] [^{11}C]CO_2 can also be reduced to [^{11}C]CO which is suited for a variety of metal-catalysed carbonylation reactions, providing access to carbonates, amides, ketones, esters and acids.[82]

Gallium-68 and zirconium-89 are radiometal-type isotopes used primarily for the synthesis of radiolabelled chelates. These agents can also be deployed as biometal mimics.[83] Zirconium-89 in particular finds increasing application for PET due to its extended half-life of 78 hours. Zirconium-89 is employed for radiolabelling large molecules which are particularly slow to distribute through the body, requiring several hours or days before they reach a representative distribution equilibrium. These large molecules include biologics, such as antibodies, and more novel approaches to imaging, such as nanoparticles.[84,85]

Despite the utility of these other radioisotopes, fluorine-18 remains the most popular radionuclide for the majority of clinical applications of PET. Fluorine-18 is particularly suitable due to its relatively long half-life (109.8 min) and the low energy of the positon emitted by the decaying nucleus (see **Table 1**).

The longer half-life of fluorine-18 enables off-site production of isotope or radiotracers, as well as their transport to imaging locations. In addition, longer and more complex synthetic procedures are available as decay of the isotope is less of a concern than with shorter lived isotopes such as carbon-11. The low energy of the positron emitted results in the positron having a short mean free path (2 mm) in aqueous biological tissue. This mean free path approximates the theoretical maximum resolution of a PET

image, and therefore use of nuclides with low energy positrons, such as fluorine-18, is often preferred.[86]

Although fluorine does not feature in mammalian metabolism, fluorine substitution of bioactive molecules has found wide application in PET. The widespread use of fluorine-18 has arisen in part due to an understanding of the effects of fluorine substitution that has emerged from the field of medicinal chemistry.[87] Fluorine substitution is often employed during the development process to modify the pharmacokinetic and pharmacodynamic properties of candidate drug molecules.[88] In this setting, fluorine can act as a bioisostere for hydrogen or oxygen.[89] Fluorine has a van der Waals radius (1.47 Å) in-between those of hydrogen (1.2 Å) and oxygen (1.52 Å).[90] Fluorine substitution is also employed to reduce metabolic processing at specific sites due to the high bond dissociation energy of the C–F bond (105.4 kcal.mol^{-1}) compared to other bonds found commonly in organic molecules (e.g. 98.8 kcal.mol^{-1} for C–H).[90]

Over 90% of clinical PET applications utilise a single [^{18}F]-radiotracer, namely 2-deoxy-2-[^{18}F]fluoro-D-glucose [^{18}F]-**35** ([^{18}F]FDG).[91,92] [^{18}F]FDG [^{18}F]-**35** has emerged as an ubiquitous PET radiotracer as it is an excellent glucose mimic, leading to high uptake *via* GLUT transporters into metabolically active cells.[93] Following uptake, [^{18}F]FGD [^{18}F]-**35** is phosphorylated at C-6 by hexose kinase, illustrated in **Scheme 10**.

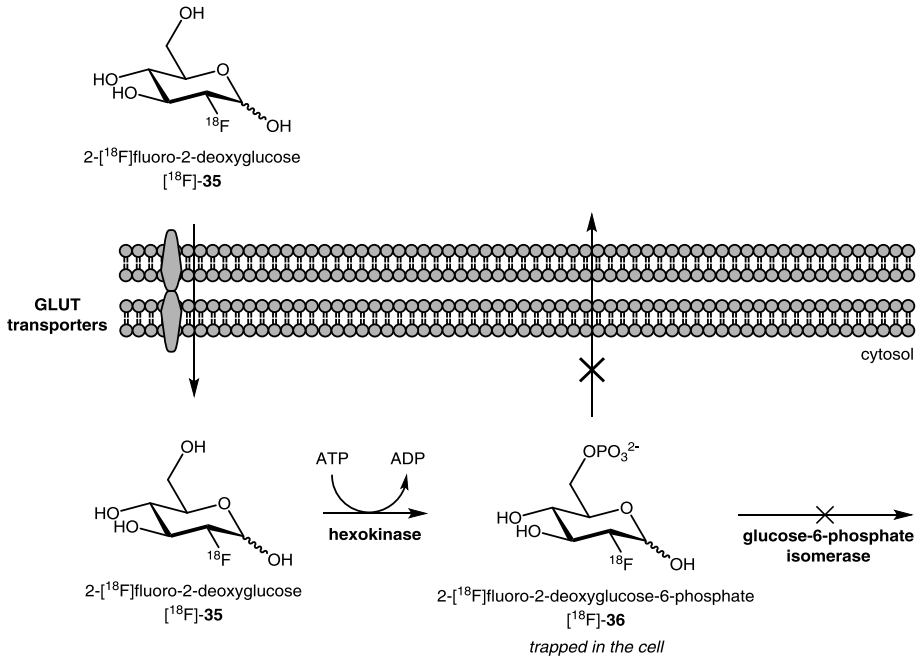

Scheme 10. Phosphorylation of [^{18}F]FDG [^{18}F]-**35** by hexokinase leads to trapping of the radiotracer in the cell as [^{18}F]-**36**.

However, unlike glucose-6-phosphate, [^{18}F]-**36** is not a substrate for the next enzyme in the glycolytic pathway (glucose-6-phosphate isomerase) due to the lack of a hydroxyl group at C-2. The phosphorylated derivative [^{18}F]-**36** remains trapped in the cell, allowing for imaging of glucose uptake (**Figure 8**) as a proxy for metabolic activity, until the radioactive nucleus decays.[93]

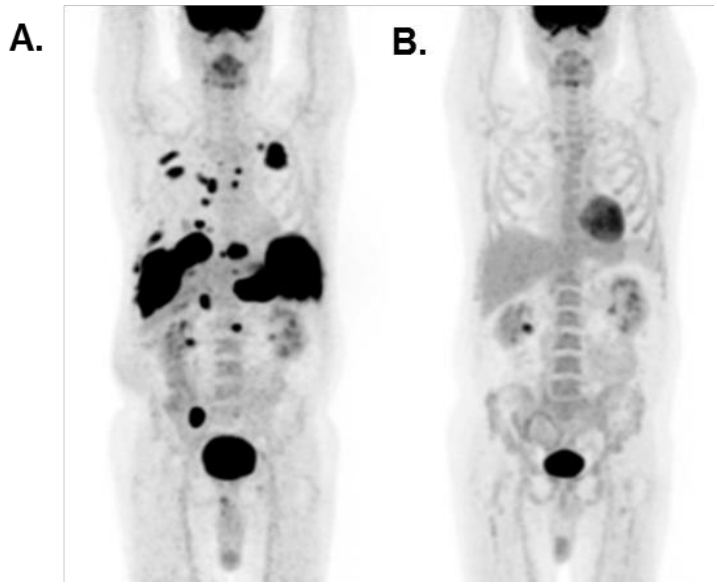

Figure 8. Patient with diffuse large B-cell lymphoma imaged with [^{18}F]FDG [^{18}F]-**35** **A**. before treatment and **B**. after treatment. Image used with permission from Mankoff *et al.*[94]

The favourable metabolic profile of [^{18}F]FDG [^{18}F]-**35**, coupled with large infrastructure and research investment into this tracer has led to the monopolisation of FDG [^{18}F]-**35** as the primary radiotracer in the clinic. This situation is changing however, as research into new labelling methods and applications of new and old tracers continues to emerge, particularly in cases where PET imaging with [^{18}F]FGD [^{18}F]-**35** has proved inefficient.[72]

1.2.2. Sources of ^{18}F for radiotracer synthesis

Fluorine-18 is available for use in synthetic chemistry in two forms, either as [^{18}F]fluoride or [^{18}F]fluorine gas. These two preparations of fluorine-18 can be used to introduce fluorine-18 into organic molecules using either nucleophilic or electrophilic approaches respectively.

[^{18}F]Fluorine gas is obtained through the ^{20}Ne(d,α)^{18}F nuclear reaction, where a neon target is bombarded with deuterons accelerated in a cyclotron, to release an α-particle and a fluorine-18 nucleus.[95] As these reactions usually produce only traces

(nM or pM amounts) of the radioactive nucleus, $[^{19}F]F_2$ gas is added as a carrier, to ensure efficient transfer of $[^{18}F]F_2$ from the production site to the reaction vessel.[96]

The necessity of using $[^{19}F]F_2$ as a carrier gas results in dilution of fluorine-18 with fluorine-19 in the final product. This ratio is measured as "specific activity", and tracers synthesised using this carrier-added approach have low specific activity (1-55 GBq.μmol^{-1}).[97] Low specific activity is an undesirable property for clinical tracers, as the unlabelled compound, present in larger amounts, competes with its labelled analogue for binding to the appropriate receptor, leading to receptor saturation with the competitor and increased background uptake of the label. Despite these limitations, $[^{18}F]F_2$ is employed for the synthesis of 6-[^{18}F]fluoro-L-3,4-dihydroxyphenylalanine [^{18}F]-**39** ([^{18}F]FDOPA, **Scheme 11**) using a stannylated precuror,[98,99] used for routine clinical imaging the dopaminergic pathways.

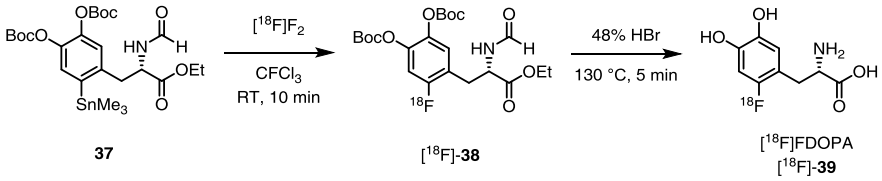

Scheme 11. Synthesis of [^{18}F]FDOPA [^{18}F]-**39** using a fluorodestannylation approach with $[^{18}F]F_2$ gas.[97]

$[^{18}F]F_2$ gas is also used for the synthesis of other electrophilic fluorination reagents (**Figure 9**), including [^{18}F]acetyl hypofluorite [^{18}F]-**40** and [^{18}F]perchloryl fluoride [^{18}F]-**41**. These reagents suffer from the drawback of being difficult to handle due to their high reactivity and produce products with low specific activity. Milder N–F based electrophilic fluorination reagents, including [^{18}F]-*N*-fluoropyridinium triflate [^{18}F]-**42**, [^{18}F]Selectfluor™ bistriflate [^{18}F]-**43**,[100] and [^{18}F]NFSI (*N*-fluorobenzenesulfonimide) [^{18}F]-**44**[101] have been developed to overcome handling difficulties, but these too are synthesised from $[^{18}F]F_2$ and share similar drawbacks, giving access to ^{18}F-labelled products with low specific activity.[102]

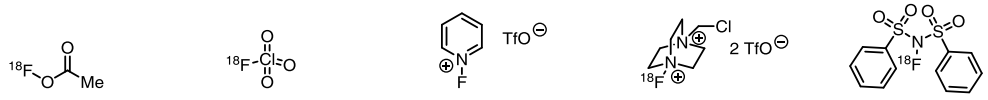

acetyl [^{18}F]hypofluorite [^{18}F]-**40**

perchloryl [^{18}F]fluoride [^{18}F]-**41**

N-[^{18}F]fluoropyridinium triflate [^{18}F]-**42**

[^{18}F]Selectfluor bistriflate [^{18}F]-**43**

[^{18}F]NFSI [^{18}F]-**44**

Figure 9. Electrophilic fluorinating reagents derived from $[^{18}F]F_2$.[97]

[^{18}F]Fluoride is most commonly produced by the $^{18}O(p,n)^{18}F$ nuclear reaction, where a metallic target containing $[^{18}O]H_2O$ is bombarded with protons accelerated using a

cyclotron.[73] This process generates a dilute solution of [^{18}F]fluoride in [^{18}O]H_2O. Under these conditions, [^{18}F]fluoride is strongly hydrated, and requires drying before use as a nucleophile.[103]

The most common method for the preparation and activation of [^{18}F]fluoride ion involves passing the dilute [^{18}F]fluoride solution though a quaternary ammonium resin, which traps [^{18}F]fluoride ion, separating it from adventitious metal ions that are produced during target bombardment. This procedure also allows for the recovery and recycling of [^{18}O]H_2O, if required. [^{18}F]Fluoride is eluted from the anion exchange column using an aqueous solution of potassium carbonate containing Kryptofix 222, an aminopolyether cryptand with high affinity for potassium ions. The addition of Kryptofix 222 serves to complex potassium ions, leaving charge separated [^{18}F]fluoride ion with increased nucleophilicity. Water is then removed by azeotropic distillation under a stream of inert gas, following the addition of anhydrous acetonitrile. This azeotropic drying procedure is repeated two or three times, as required by the synthetic procedure. The drying procedure provides a potassium-kryptofix 222 salt of the fluoride ion, [K•Kryptofix222][^{18}F]F [^{18}F]-**45**, as illustrated in **Scheme 12**.

Most infrastructure surrounding the generation of PET radiotracers is geared towards the delivery of [^{18}F]fluoride for the preparation of [^{18}F]FDG [^{18}F]-**35**. [^{18}F]FDG [^{18}F]-**35** is synthesised by nucleophilic substitution of the corresponding protected mannosyl triflate derivative **46** by [^{18}F]fluoride complex [^{18}F]-**45** (**Scheme 12**). As [^{18}F]FDG [^{18}F]-**35** remains the most commonly used radiotracer, most research into new methodologies for the synthesis of PET radiotracers utilises [^{18}F]fluoride as the source of the radioactive isotope.

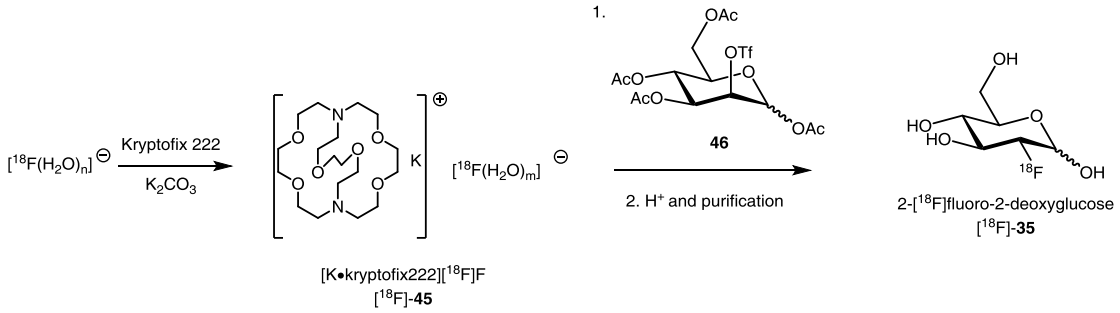

Scheme 12. Preparation of [^{18}F]fluoride ion as the potassium-kryptofix 222 salt [^{18}F]-**45**, where m<n, and reaction with a protected mannose triflate **46**, which after protecting group cleavage gives [^{18}F]FDG [^{18}F]-**35**.[103,104]

1.2.3. Synthesis of ^{18}F-bearing radiotracers by nucleophilic substitution

The widespread availability of nucleophilic [^{18}F]fluoride ion has meant that most radiolabelling methodology employs this source of isotope as a means to label appropriate tracers. The most common approaches for radiolabelling with [^{18}F]fluoride can be divided into those using S_N2 reactions and those using S_NAr reactions. More recently, a number of novel approaches using heavy atom carriers or heavy atom catalysis have also been developed.[103]

Aliphatic substrates with appropriate leaving groups, including sulfonate esters, bromide, iodide and cyclic precursors have been successfully employed as methods for introduction of fluorine-18 into molecules. Reactions work best with leaving groups at primary centres, as competing elimination reactions lower yields on substitutions performed at secondary centres.[102] This method generally uses polar aprotic solvents, including acetonitrile, DMSO or DMF and involves heating of the appropriate precursor in the solvent with the prepared [^{18}F]fluoride salt [^{18}F]-**45** and a non-nucleophilic base.[105] The desire for reduced synthesis times means that such reactions are heated strongly so that synthetic reactions are complete within minutes.

[^{18}F]FDG [^{18}F]-**35** is synthesised using this approach, as shown in **Scheme 12**. Other commonly used tracers synthesised in this manner include 3'-deoxy-3'-[^{18}F]fluorothymidine [^{18}F]-**48** ([^{18}F]-FLT)[106] and [^{18}F]fluoroacetate [^{18}F]-**1**,[107] as illustrated in **Scheme 13**. In some cases, addition of small amounts of protic solvents (such as ^{t}BuOH) to such reactions leads to higher incorporation and radiochemical yields (RCY).[108,109] Protic solvents are thought to both increase the nucleophilicity of [^{18}F]fluoride and promote the departure of the leaving group through hydrogen bonding interactions.[110]

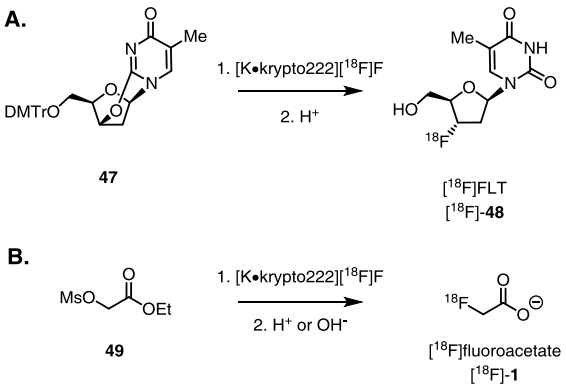

Scheme 13. S_N2 reactions for the synthesis of radiotracers including **A.** [^{18}F]FLT [^{18}F]-**48**[106] and **B.** [^{18}F]fluoroacetate [^{18}F]-**1**.[107] DMTr = dimethoxytrityl.

Substitutions on aromatic rings[97] through S_NAr reactions are confined to substrates bearing a good leaving group (such as $–N^+Me_3$, –F, –Cl, –Br, –OTf, –OMs and $–NO_2$),[105] and an electron withdrawing substituent *ortho* or *para* to the leaving group. The reaction conditions for these substitutions are similar to those employed for S_N2 reactions, using high temperatures (120–180 °C) and polar aprotic solvents. These conditions have proved successful for the synthesis of many tracers, including [^{18}F]haloperidol [^{18}F]-**51** in **Scheme 14**, a brain imaging agent.[111,112]

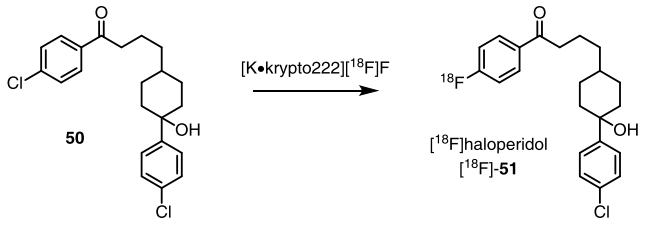

Scheme 14. Synthesis of [^{18}F]haloperodol [^{18}F]-**51**[112] using an S_NAr approach.

1.2.4. Late-stage fluorinations for PET

In addition to these common modes of reactivity for the introduction of fluorine-18, metal-catalysed fluorinations have recently emerged as an alternative to the harsh conditions usually employed in the reactions described above. Metal-catalysed reactions tend to offer milder reaction conditions and high selectivity.[113,114]

Substitution of electron rich arenes is challenging, and fluorination of such motifs was previously accessible through the use of electrophilic fluorinating reagents such as [^{18}F]F_2. Oxidative [^{18}F]-fluorination of electron rich phenols has been reported,[115] but a more common and versatile approach utilises unsymmetrically substituted diaryl iodonium salts.[116] Unsymmetrical 2-thienyl aryl iodonium salts favour substitution at the less electron rich aryl ring, provided no ortho-substituent is present, giving access to electron rich [^{18}F]fluorinated aromatics using more accessible and easier to handle [^{18}F]fluoride as the source of radioactivity.[117] Peroxisome proliferator-activated receptor-γ (PPARγ) ligands, such as [^{18}F]-**53** in **Scheme 15 A**, for investigating lipid metabolism in metastatic cancers, has been synthesised using a 2-thienyl aryl iodonium precursor **52**.[118] 2-Thienyl aryl iodinium salts suffer from moderate selectivity and poor tolerance to functional groups and mixtures of products are sometimes observed.[113] Spirocyclic [119] or Meldrum's acid [120] derived iodonium ylides, **54** and **56** respectively, shown in **Scheme 15 B** and **C**, offer increased precursor stability while retaining reactivity towards [^{18}F]fluoride.

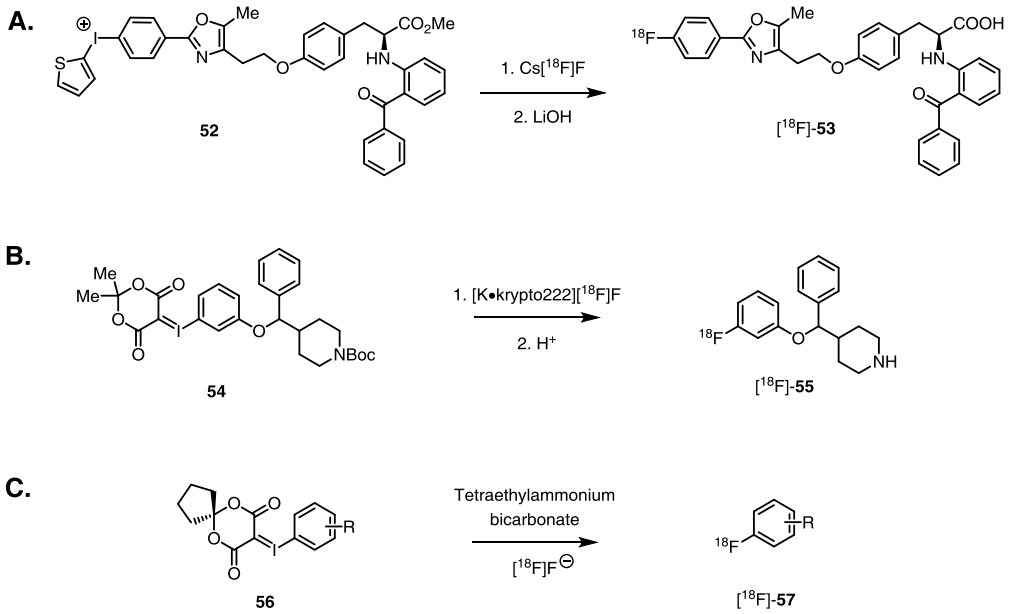

Scheme 15. S_NAr reactions for the synthesis of **A.** [^{18}F]-**53** using the diaryliodonium approach,[118] **B.** [^{18}F]-**55** using the Meldrum's acid iodonium ylide approach,[120] and **C.** [^{18}F]-**57** using the spirocyclic iodonium ylide approach.[119]

Ritter *et al.*[121] have developed a palladium catalysed electrophilic fluorination methodology that uses [^{18}F]fluoride as a source of radioactivity, as shown in **Scheme 16 A**. High-valent palladium(IV) complex **58** has the ability to sequester azeotropically-dried [^{18}F]fluoride from an acetone solution to generate an electrophilic complex [^{18}F]-**59**. This electrophilic palladium(IV) [^{18}F]fluoride complex [^{18}F]-**59** transfers the fluorine-18 centre to a nucleophilic aryl palladium(II) complex **60** through a series of single electron transfer events to generate an aryl [^{18}F]fluoride palladium(IV) species. This palladium(IV) intermediate undergoes reductive elimination to give [^{18}F]-labelled arenes, such as [^{18}F]-**61**, in high radiochemical yield.[122] This method requires azeotropically dried sources of [^{18}F]fluoride, as the palladium(IV) [^{18}F]fluoride complex [^{18}F]-**59** is sensitive to traces of air and moisture.

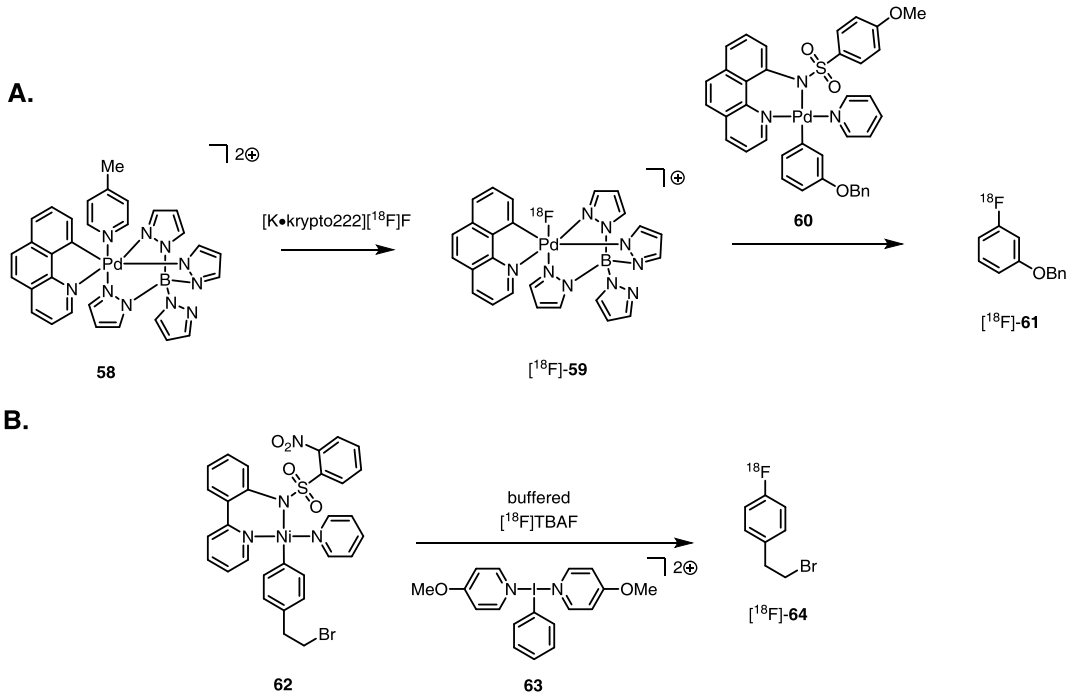

Scheme 16. **A.** High valent palladium(IV) complex **58** sequesters [^{18}F]fluoride from solution, and reacts with nucleophilic Pd(II) complex **60**, effectively acting as a source of electrophilic fluorine-18.[121] **B.** Oxidative nickel-catalysed fluorination of arenes that does not require stringently dry conditions.[123]

To circumvent this air and moisture sensitivity, Ritter and Hooker *et al.*[123] developed an analogous Ni(II)-based oxidative ^{18}F-fluorination of arenes and alkenes utilising pre-prepared nickel complexes of the arene/alkene as shown in **Scheme 16 B**. Addition of aqueous [^{18}F]fluoride to a solution of Ni(II) complex **62** and oxidant **63** in acetonitrile at room temperature generated the corresponding aryl [^{18}F]fluoride [^{18}F]-**64** rapidly and in high radiochemical yields. This procedure utilises aqueous [^{18}F]fluoride, without the need for exhaustive pre-drying and securing as the potassium-kyrptofix-222 salt, offering a mild and selective route to radiolabelled arenes and alkenes.

Gouverneur *et al.*[124] have reported an allylic ^{18}F-fluorination of cinnamyl methyl carbonates, such as **66**, using $Pd(dba)_2$ as catalyst (**Scheme 17 A**), in combination with tetrabutylammonium [^{18}F]fluoride in acetonitrile. In addition to carbamates, other leaving groups, including bromide and chloride were tolerated in this substitution reaction. The halides however required more forcing conditions (110 °C) to give good radiochemical yields. Similarly, Nguyen *et al.*[125] reported ^{18}F-fluorination of secondary and tertiary allyl trichloroacetimidates such as **68** using $(Ir(COD)Cl)_2$ as a catalyst and potassium-kryptofix [^{18}F]fluoride as fluoride source, to give access to branched allyl [^{18}F]fluorides, such as [^{18}F]-**69** shown in **Scheme 17 B**. Using the same iridium catalyst,

Gouverneur *et al*.[126] reported the transformation of linear and substituted *cis* and *trans* allyl carbonates to their analogous allyl [^{18}F]fluorides, with good retention of double bond geometry (**Scheme 17 C**). Allyl fluorides, such as [^{18}F]-**71** are not common motifs in drug molecules, however they could provide access to useful [^{18}F]fluorinated building blocks.[114]

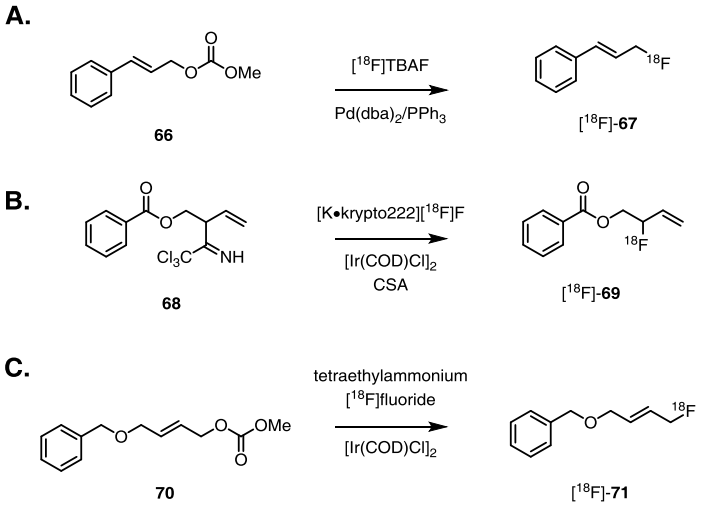

Scheme 17. A. ^{18}F-Fluorination of cinnamyl carbonates under Pd(II) catalysis.[124] **B.** Reaction of allyl trichloroacetimidates to give allyl [^{18}F]fluorides under iridium catalysis.[125] **C.** Extension of iridium catalysis for ^{18}F-fluorination of allyl carbonates, with good control of alkene geometry.[126]

The first enantioselective synthesis of a C–^{18}F bond was reported by Doyle *et al*.[127] who utilised a Co(salen)-mediated opening of racemic epoxides to generate enantioenriched [^{18}F]fluorohydrins, such as [^{18}F]-**73**. The [^{18}F]fluoro-Co(salen) complex is generated by elution of [^{18}F]fluoride from a quaternary ammonium resin with a solution of Co(salen)OTs pre-catalyst. The catalyst is added to the racemic epoxide in methyl *t*-butyl ether (MTBE) at 50 °C to generate fluorohydrins in greater than 95% enantiomeric access (ee), as shown in **Scheme 18 A**. The use of a dimeric Co(salen) species allowed fluorination of substrates that are Lewis basic, which had been challenging using the mononuclear cobalt complexes. This procedure was used for the synthesis of a number of validated radiotracers, including [^{18}F]FMISO [^{18}F]-**73**, used for imaging and detection of hypoxia.[128]

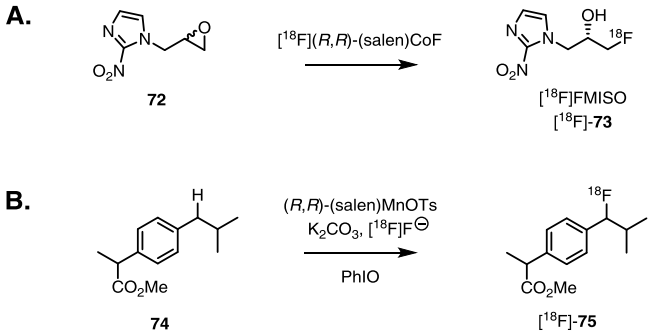

Scheme 18. A. Stereoselective epoxide opening using a [^{18}F](salen)CoF complex, generated from [^{18}F]fluoride.[127] **B.** Synthesis of an ibuprofen [^{18}F]-analogue [^{18}F]-**75**, using a Mn-catalysed C–H activation approach.[129]

Using a similar Mn(salen) complex, Hooker and Groves *et al.*[129] have demonstrated a radical C–H activation approach to ^{18}F-fluorination at substituted benzylic positions, as illustrated in **Scheme 18 B**. This methodology is attractive as it does not require pre-functionalisation of substrates, but the substrate scope remains limited. The reaction proceeds through the generation of Mn(III)(salen) [^{18}F]fluoride, which is oxidised by iodosylbenzene to generate a Mn(V)(salen) [^{18}F]fluoride complex. This complex is reduced by hydrogen abstraction from the benzylic substrate to give Mn(IV)(salen) [^{18}F]fluoride and a benzylic radical. Radical transfer of the radioligand to the benzylic substrate generates a radiolabelled product and reforms the catalyst. The utility of this approach was demonstrated by synthesis of a number of fluorinated analogues of common drugs, including ibuprofen methyl ester **74**, cinnacalcet, and celecoxib.

Copper catalysis has found widespread application for the synthesis of [^{18}F]-bearing radiotracers. Copper catalysis has been used for the direct synthesis of aryl fluorides from boronic esters[130] and iodonium salts.[131] Gouverneur *et al.*[130] have shown that a range of electron rich, neutral and deficient (hetero)aryl pinacol boronic esters are efficiently fluorinated using potassium-kryptofix [^{18}F]fluoride and [Cu(OTf)$_2$(py)$_4$]. The utility of this approach was illustrated by preparation of [^{18}F]FDOPA [^{18}F]-**39**, a neuroimaging agent, as shown in **Scheme 19 A**.

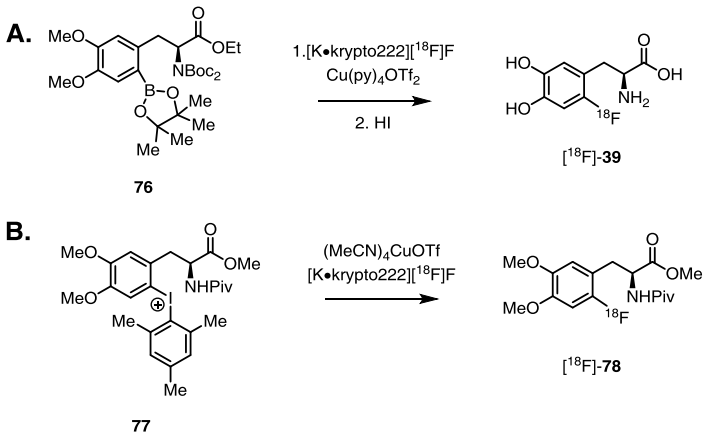

Scheme 19. A. Copper-catalysed ^{18}F-fluorination of boronic acids using [^{18}F]fluoride.[130] **B.** Copper catalysis also proves useful for the ^{18}F-fluorination of mesityl aryl iodonium salts.[131]

Scott and Sanford *et al.*[131] have illustrated a similar reaction using mesityl aryl iodonium salts and the copper (I) catalyst $(MeCN)_4CuOTf$. In contrast to the previously described 2-thienyl iodonium salt approach, the copper(I)-mediated protocol offers high selectivity and radiochemical yield, with the added advantage of proceeding at lower temperatures (85°C *vs* 150 °C). The authors showed that this method had similar substrate scope to the boronic ester method reported by Gouverneur *et al.*,[130] and also illustrated its utility by applying the approach to the synthesis of a protected [^{18}F]FDOPA [^{18}F]-**78**, as shown in **Scheme 19 B**.

Copper (I) salts of the trifluoromethyl anion ($[Cu]CF_3$) have emerged as powerful reagents for the introduction of [^{18}F]-labelled trifluoromethyl groups onto arenes. These reactions are predicated on the generation of difluorocarbene **80** from an appropriate precursor, which is then intercepted by [^{18}F]fluoride to generate [^{18}F]CF_3^- anion [^{18}F]-**81**, stabilised by a Cu(I) counterion. Gouverneur *et al.*[132] have reported the synthesis of a reagent for iodoarene [^{18}F]trifluoromethylation. Their method uses a methyl chlorodifluoroacetate **79**, which decomposes to difluorocarbene **80** which is intercepted by a TMEDA complex of Cu(I)I (**Scheme 20 A**) to generate the active $[Cu][^{18}F]CF_3$ [^{18}F]-**81** reagent. Riss *et al.*[133] have reported a similar [^{18}F]trifluoromethylation of iodoarenes using difluoromethyl iodide **84** in the presence of bicarbonate, diisopropylethylamine and copper (I) bromide to accomplish a similar transformation, as illustrated in **Scheme 20 B**.

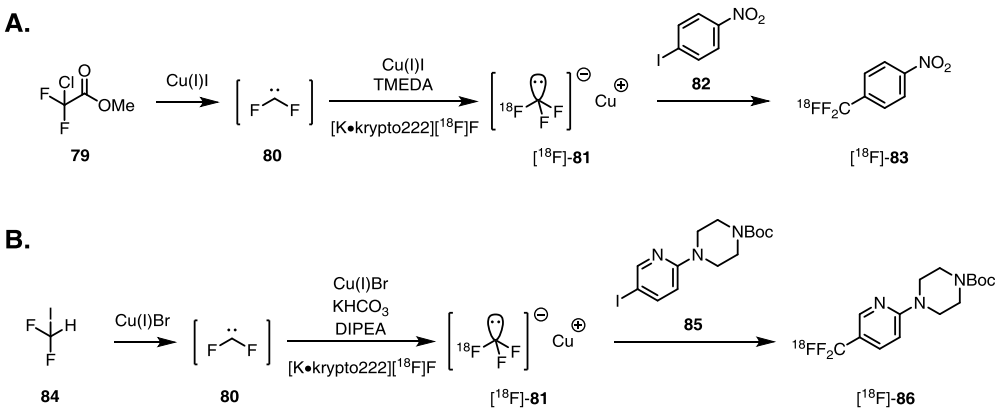

Scheme 20. **A.** Generation of difluorocarbene **80** under copper catalysis, and trapping by [^{18}F]fluoride to generate Cu[^{18}F]CF_3 [^{18}F]-**81**,[132] which reacts efficiently with aryl iodides to give aryl [^{18}F]trifluoromethyl compounds, such as [^{18}F]-**83**. **B.** Similarly, difluoroiodomethane **84** can be used as a source of difluorocarbene **80**.[133]

Alternatively, [^{18}F]trifluoromethyl anion can be synthesised directly from [^{18}F]CF_3H [^{18}F]-**88**. Labar and Jubault *et al.*[134] have reported the use of a dimethylsulfonium tetra-arylborate **87** as an efficient source of *in situ* [^{18}F]trifluoromethane [^{18}F]-**88**, upon treatment with potassium-kryptofix [^{18}F]fluoride, as shown in **Scheme 21 A**. [^{18}F]Trifluoromethane [^{18}F]-**88** is deprotonated by the addition of a potassium cuprate salt to generate [^{18}F][Cu]CF_3 [^{18}F]-**81** directly, rather than through the generation of difluorocarbene. Reaction of [^{18}F][Cu]CF_3 [^{18}F]-**81** with either aryl iodides or boronic esters generated the corresponding [^{18}F]trifluoromethylated products. Vugts *et al.*[135] have reported the use of difluoromethyl iodide **84** to generate [^{18}F]trifluoromethane [^{18}F]-**88** *in situ*, as shown in **Scheme 21 B**. Under the action of a copper (I) salt, base and 3HF.Et_3N, [^{18}F]trifluoromethane [^{18}F]-**88** generates [^{18}F][Cu]CF_3 [^{18}F]-**81** with high specific activity, which they showed reacts with aryliodides and arylboronic acids to give [^{18}F]trifluoromethylarenes. [136]

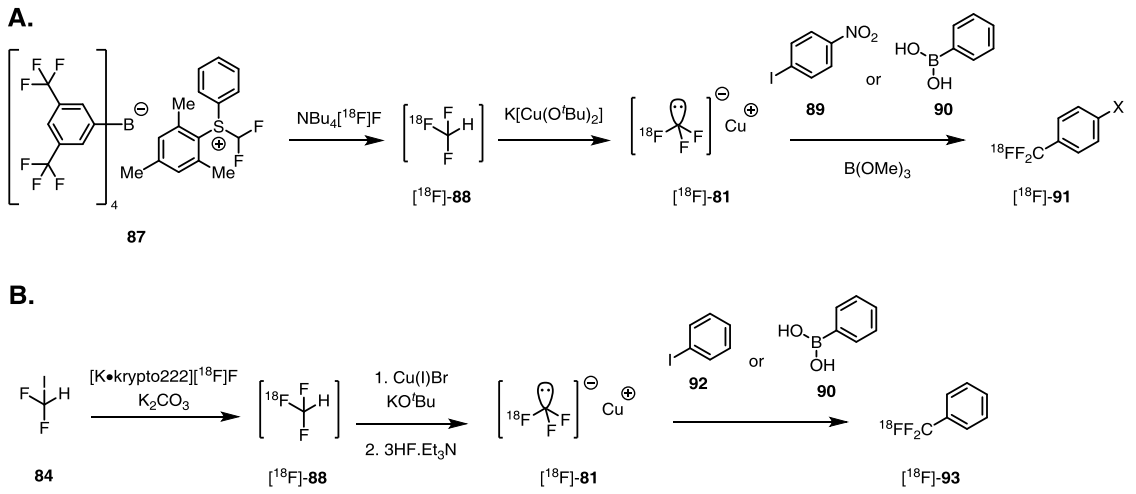

Scheme 21. Generation of [^{18}F]trifluoromethane [^{18}F]-**88** from **A.** sulfonium salt **87**[134] and **B.** difluoroiodomethane **84** to generate Cu[^{18}F]CF_3 [^{18}F]-**81**, which reacts with aryl iodides and aryl boronic acids.[135]

Most recently, silver(I) catalysis has been employed to extend the scope of [^{18}F]trifluoromethylation beyond that of simple aryl substrates to aryl [^{18}F]trifluoromethyl ethers, [^{18}F]trifluorothiomethyl ethers, and aryl [^{18}F]difluoromethyl ethers as shown in **Scheme 22**.[137] The corresponding alkyl halides **94**, **96** and **98** were found to react with silver(I) triflate and potassium-kryptofix [^{18}F]fluoride in dichloromethane or dichloroethane to give radiolabelled products in moderate to good radiochemical yields. This approach compliments a previously reported procedure where difluoroenol ethers were utilised as electrophilic traps for [^{18}F]fluoride, generating aryl [^{18}F]trifluoroeethyl ethers.[138–140]

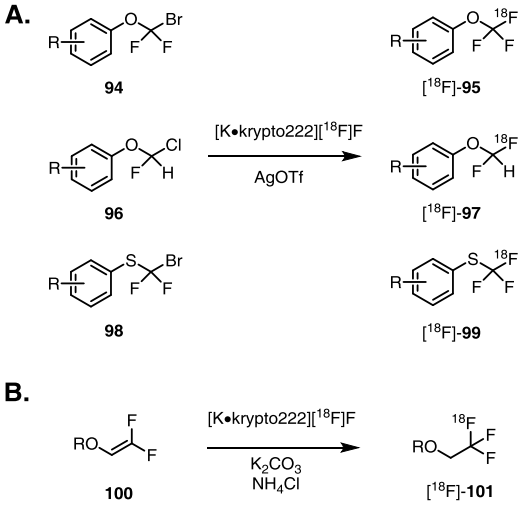

Scheme 22. **A.** Synthesis of fluorinated aryl [^{18}F]trifluoromethyl ethers and thioethers under silver (I) catalysis. **B.** Difluoroenol ethers as electrophilic traps for [^{18}F]fluoride ion also generate [^{18}F]trifluoroethyl ethers.[137]

Clearly, metal catalysis will continue to play an innovative role in [^{18}F]fluorinations, as many reactions, including the generation of simple alkyl [^{18}F]fluorides by such mild and selective processes, remain to be discovered.

1.3. Protein and peptide labelling strategies for PET

1.3.1. Prosthetic groups

Labelling of large peptides with PET isotopes has attracted increasing attention as this technique allows imaging of protein or peptides and their targets in the body.[141] Labelling of such molecules for PET allows more rapid development and better understanding of a new generation of diagnostic and therapeutic agents.[142] Biomolecules are attractive labelling targets compared to small molecules as they tend to higher specificty for receptors. Better radioligands lead to increased image quality and reduced background uptake, both desirable qualities for PET imaging. PET labelling with ^{18}F is especially suited for biomolecule labelling as it offers higher sensitivity and lower radiation dose compared to SPECT or CT.[142]

The ^{18}F-labelling methods discussed in the previous sections generally make use of organic solvents, heating and strongly acidic or basic reaction conditions to incorporate [^{18}F]fluoride. While small molecules are usually tolerant to such conditions, direct labelling of biomolecules requires milder conditions, such as lower temperatures, aqueous solvents and neutral pH conditions, all in an effort to maintain the structural integrity of the biomolecule.

A two-step “prosthetic group” approach is most commonly used for labelling biomolecules. A prosthetic group is a bifunctional molecule, such as [^{18}F]SFB [^{18}F]-**103** shown in **Scheme 23**. One site bears the fluorine-18 atom, while the second, in this case an *N*-hydroxysuccinimide activated ester, is available for coupling to a biomolecule of interest. Fluorine-18 labelling of the prosthetic group (**102** to [^{18}F]-**103**) is accomplished using one of the radiolabelling methods described above, before the ^{18}F-labelled tag is conjugated to the biomolecule. This second step is usually carried out in water or buffer to ensure stability and structural integrity of the biomolecule.

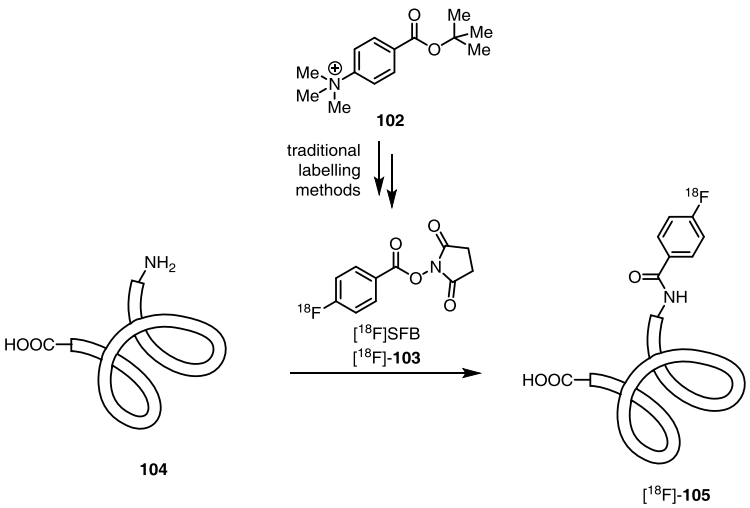

Scheme 23. Prosthetic group approach for labelling peptide **104** with fluorine-18, using [^{18}F]SFB [^{18}F]-**103**.

Labelling strategies can either use reactive groups naturally present in a peptide, most often free amines or thiols, or alternatively, biomolecules can be chemically or biologically modified to introduce biorthogonal reactive sites.[141] Free thiols are usually conjugated to maleimides or sulfides, while amines are conjugated to activated esters or acids.

Amine bioconjugation strategies target the *N*-terminus or amines of lysine residues in peptides or proteins. An abundance of free amine residues can affect the homogeneity of the product, as labelling may occur at multiple sites. This can be advantageous as it increases the likelihood of successful labelling.[142]

The two best characterised amine-reactive prosthetic groups are *N*-succinimydyl-4-[^{18}F]fluorobenzoate [^{18}F]-**103** ([^{18}F]SFB)[135] and *p*-nitrophenyl 2-[^{18}F]fluoropropionate [^{18}F]-**106 (**[^{18}F]NFP).[145] [^{18}F]NFP [^{18}F]-**106** has been used for labelling of integrin-targeting cyclic RGD peptides for imaging of angiogenesis in cancers.[145] [^{18}F]SFB [^{18}F]-**103** has been used for labelling many proteins and peptides,[146,147] including antibody fragments to image colorectal cancer in xenograft tumour mice.[148]

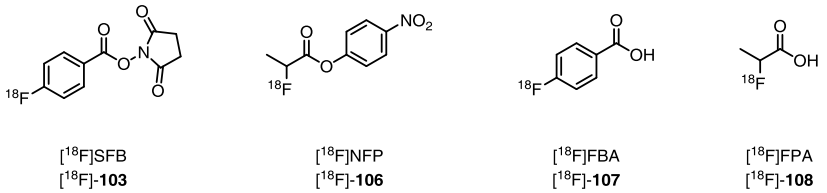

Figure 10. Amine-reactive prosthetic groups for ^{18}F-labelling of peptides and protein.

To overcome problems with selectivity and the difficulty in preparing these activated esters, the acid derivatives *p*-[^{18}F]fluorobenzoic acid [^{18}F]-**107** ([^{18}F]FBA)[149] and 2-[^{18}F]fluoropropionic acid [^{18}F]-**108** ([^{18}F]FPA),[150] have been developed. These two reagents have been used for automated solid phase synthesis of radiolabelled peptides. [^{18}F]FPA [^{18}F]-**108** offers advantages over [^{18}F]FBA [^{18}F]-**107** as it does not significantly alter the lipophilicity of peptides.[151]

Amine groups on peptides and proteins can also be modified to contain more reactive groups such as hydrazines **109** or hydroxylamines **112**, as shown in **Scheme 24**. These two functional groups react rapidly and selectively with aldehydes, such as *p*-[^{18}F]fluorobenzaldehyde [^{18}F]-**110** ([^{18}F]FBAld),[142] to give radiolabelled hydrazones[152] [^{18}F]-**111** or oximes[153] [^{18}F]-**113** respectively.

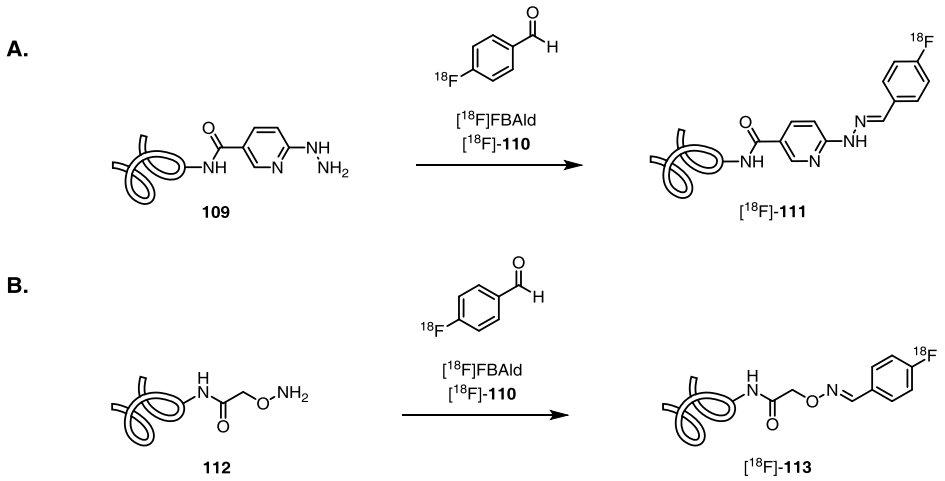

Scheme 24. Coupling of amines to groups containing either **A.** hydrazine **109** or **B.** hydroxylamine **112** react with labelled aldehydes to give hydrazone [^{18}F]-**111** or oxime [^{18}F]-**13** labelled peptides.

Thiols have also been used extensively for conjugate addition with maleimides.[73,141] This approach has the advantage of being highly selective, as maleimides react only with thiols at physiological pH, as illustrated in **Scheme 25**. In addition, most proteins and peptides bear one or two free cysteine residues, and multiple labelling events are rarely observed.[154]

Maleimide prosthetic groups (**Scheme 25**) have been prepared by reaction of a maleimide with [^{18}F]FBAld [^{18}F]-**110**, [^{18}F]FBA [^{18}F]-**107**,[155] or [^{18}F]FDG [^{18}F]-**35** to give [^{18}F]-**116** to [^{18}F]-**118**.[156] The maleimide functionality can also be introduced after [^{18}F]fluorination, as in the case for [^{18}F]-**119**.[157]

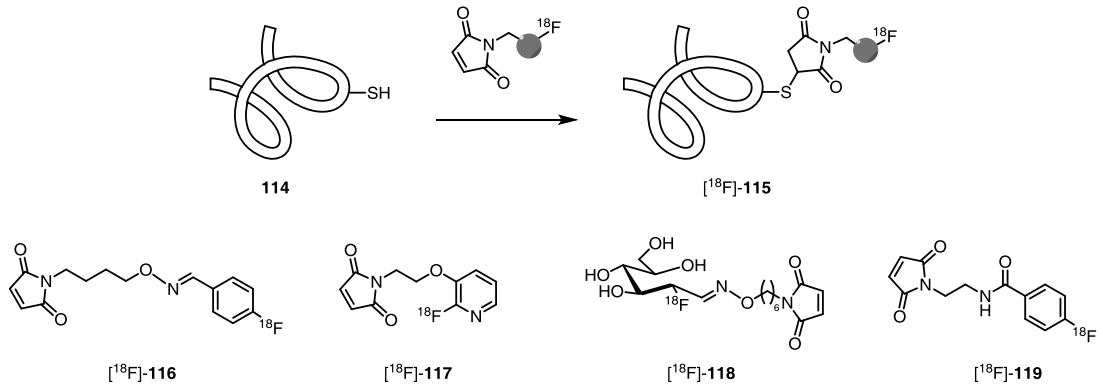

Scheme 25. Maleimide derivatives used for protein and peptide labelling.

The benzenethiosulfonate [^{18}F]FDG conjugate [^{18}F]-**121** is a useful reagent for labelling thiols on proteins.[158] Thiosulfonate [^{18}F]-**121** is prepared from a protected [^{18}F]FDG [^{18}F]-**35** and is accessible by routine automated synthesis. This reagent reacts with thiols such as **120** as shown in **Scheme 26**, to give disulfide [^{18}F]-**122** to provide access to radiolabelled peptides.

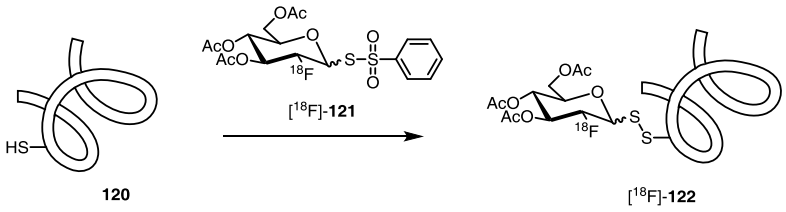

Scheme 26. Reaction of thiols with [^{18}F]FDG derivatives to give ^{18}F-radiolabelled disulfide [^{18}F]-**122**.

The Cu-catalysed and strain-promoted variants of the Huisgen 1,3-dipolar cycloaddition between alkynes and azides have emerged as powerful tools for PET radiochemistry.[159] The reactions proceed rapidly in water and are chemoselective. The reactions give access to triazoles which are stable under physiological conditions.[141] These features are desirable for PET radiolabelling reactions where biomolecules need to be rapidly and selectively labelled with short-lived radioisotopes under mild conditions.

The general strategy for labelling of proteins or peptides using copper-catalysed alkyne-azide coupling (CuAAC) involves the synthesis of a small, minimally functionalised alkyne- or azide-bearing [^{18}F]-labelled prosthetic group, which is then coupled to a pre-functionalised protein or peptide. This strategy avoids the sometimes lengthy radiochemical synthesis of more complex prosthetic groups (such as the maleimides or *N*-hydroxysuccinimides described above).

The first application of the CuAAC reaction for ^{18}F-radiolabelling involved the reaction between ω-[^{18}F]fluoroalkynes, such as [^{18}F]-**124** with peptides, functionalised at the *N*-terminus with an azide, as shown in **Scheme 27 A**.[160] Alkyne [^{18}F]-**124** was synthesised by S_N2 methods, similar to those described above. Primary alkyl [^{18}F]fluorides usually suffer from poor *in vivo* stability, and azide-labelled [^{18}F]fluorobenzenes have been utilised to circumvent this problem.[161]

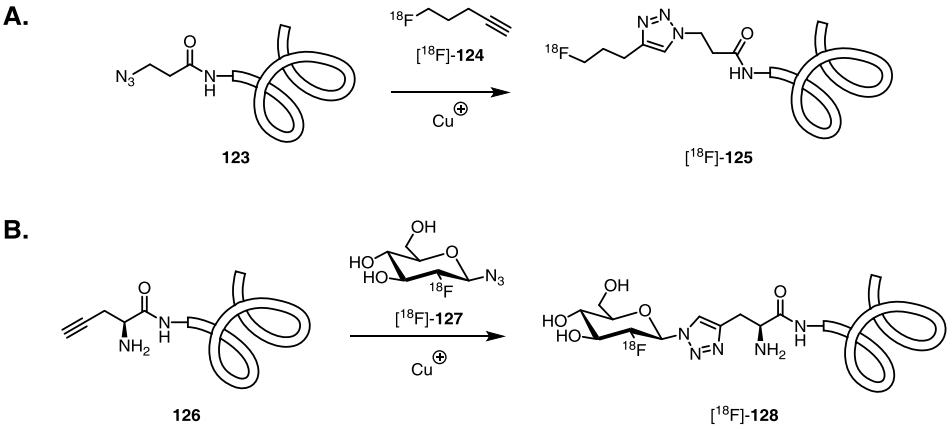

Scheme 27. 'Click' chemistry for PET labelling, showing the two possible modes of reaction: **A.** A peptide bearing azide **123** and **B.** a peptide bearing alkyne **126**.

N-Terminal propargylglycinic peptides, such as **126**, have been reacted with ^{18}F-labelled azides, reversing the reactivity, to generate ^{18}F-labelled peptides such as [^{18}F]-**128**, as shown in **Scheme 27 B,** in a similar Cu(I)-based protocol.[162] Based on this strategy, a glycosylation approach was reported using an azido-[^{18}F]FDG prosthetic group [^{18}F]-**127**, as glycosylation of proteins and peptides had been shown to improve pharmacokinetic properties.[163] This approach was used to label a variety of peptides and the triazole products of these reactions, such as [^{18}F]-**128** in **Scheme 27,** were found to be stable and effective imaging agents *in vivo*.[162]

The use of copper salts to catalyse the CuAAC reaction had led to difficulties in translating this methodology into the clinic. Copper salts show toxicity even at low levels,[164] and ensuring complete copper removal from radiolabelled products has proved challenging.[165] The utility of this reaction for live cell labelling and the desire for a biocompatible reaction, led to the development of copper-free, strain-promoted variant of the (3+2) cycloadditon by Bertozzi *et al.*[166,167] The reaction takes advantage of the strain energy of cyclooctynes (19.9 kcal.mol^{-1}),[168] which promotes their cycloaddition to azides to give fused triazoles, as a mixture of regioisomers. Shortly after the reaction was reported, variants using both [^{18}F]-labelled cyclooctynes with

azides[169] and [^{18}F]-labelled azides with cyclooctynes[165] were reported. This reaction had been applied to ^{18}F-labelling of aza-dibenzocyclooctyne (ADIBO)[170] labelled peptides including the lysine-modified bombesin **129** shown in **Scheme 28**, where a strain-prompted cycloaddition with *p*-[^{18}F]fluorobenzyl azide [^{18}F]-**130** gave radiolabelled peptide [^{18}F]-**131**.[171] A number of peptides synthesised using this methodology have since been assessed in small animal models.[172,173]

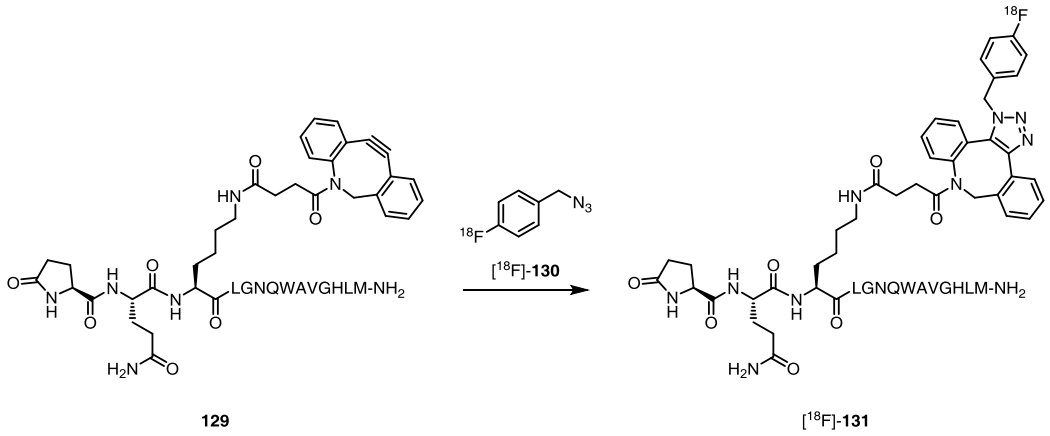

129 [^{18}F]-131

Scheme 28. Strain-promoted alkyne-azide cycloaddition to generate ^{18}F-labelled bombesin analogue [^{18}F]-**131**.

Further exploration of copper free bioconjugations for PET led to inverse electron demand Diels Alder reactions between tetrazines and *trans* cyclooctenes,[174] norbornenes,[175] or cyclooctynes[176] as reactions suitable for rapid PET labelling.

Generally, a low concentration of one reaction partner, such as an ^{18}F-labelled prosthetic group, leads to long reaction times for complete conversion. Using reactions which show remarkably fast kinetics allows such reactions to proceed to completion, even when the concentration of one of the reaction partners is extremely low. The reaction of *trans*-cyclooctenes is an order of magnitude faster (k_2 > 2000 $M^{-1}.s^{-1}$)[174] than similar reaction with other alkenes due to the release of the large strain energy (17.9 $kcal.mol^{-1}$)[168] in the *trans*-cyclooctene system. This rapid reaction is especially suited to PET labelling as the concentration of the reaction partner bearing the fluorine-18 radiolabel is very low.

The first PET imaging experiments using this tetrazine/*trans*-cyclooctene (TCO) approach were reported by Fox *et. al.*[177,178] When heated or treated with strong bases, the tetrazines proved unstable to radiolabelling with fluorine-18, giving only 1% radiochemical yield. In response, they developed a synthesis of [^{18}F]TCO [^{18}F]-**136**, a radiolabelled *trans*-cyclooctene, in 71% radiochemical yield, which reacted efficiently

with tetrazine-conjugated RGD peptide **135**, as illustrated in **Scheme 29**. This gave radiolabelled RGD-peptide [^{18}F]-**137** as a mixture of regioisomers in 90% radiochemical yield, in only 5 minutes.

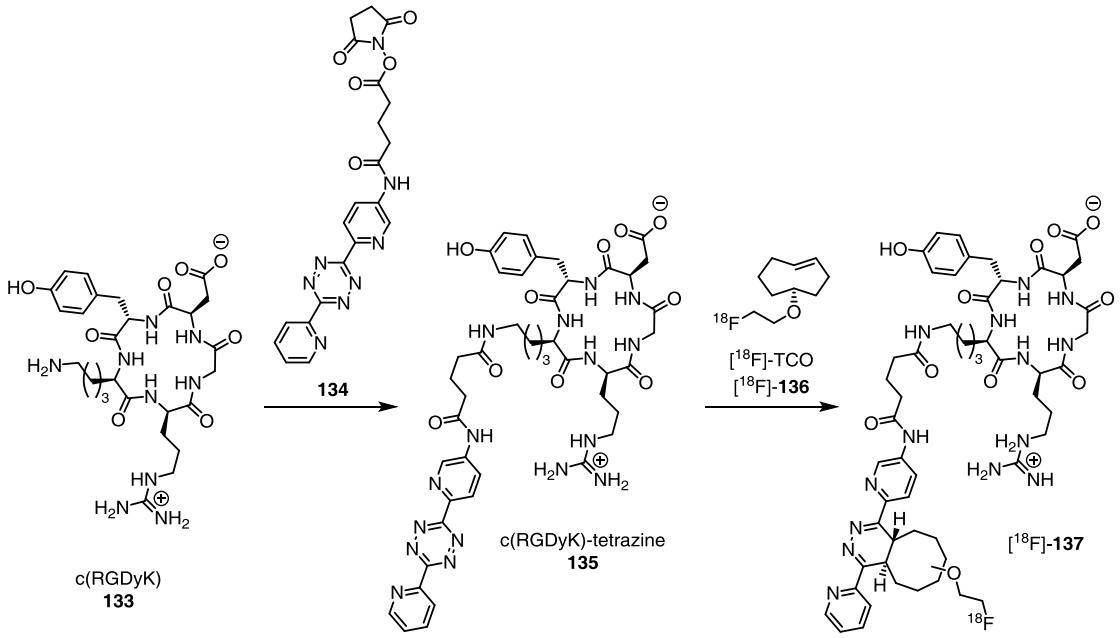

Scheme 29. Radiolabelling of an RGD peptide by conjugation to a tetrazine prosthetic group to give **135**, which reacts rapidly with [^{18}F]-TCO [^{18}F]-**136** to give peptide [^{18}F]-**137**.

The rapid kinetics of this ligation makes it attractive as a PET labelling protocol for peptides for small animal imaging using traditional nucleophilic fluorination chemistry.[179] Neither of the reaction partners are naturally present in biological systems and there is interest in using this methodology for pre-targeted PET imaging.[87] Pre-targeting would involve prior administration of a biomolecule (such as an antibody) bearing either a tetrazine or *trans*-cyclooctene, allowing distribution through the body hours or days, before the radiolabelled coupling partner is administered. The two coupling partners would react *in vivo*, and allow PET imaging of the localised biomolecule of interest.[180] Physiologically stable tetrazines have been developed,[181] and the first *in vivo* antibody-fragment labelling experiments with ^{18}F-labelled tetrazine-containing dextrans, has recently been reported.[182]

1.3.2. "Last step" radiolabelling of peptides

All of the above prosthetic group approaches for fluorine-18 labelling rely upon a fluorination event on a small molecule, which is then subsequently coupled to a biomolecule. "Last step" fluorination protocols of peptides are less well developed due to the incompatibility of peptides with non-aqueous solvents and heating, conditions

which are usually required to carry out nucleophilic [^{18}F]fluoride chemistry. In addition, such peptides bear multiple functional groups, which would lead to side reactions and lower yields if such reactions were employed.

Last step fluorination protocols are, however, desirable in PET radiochemistry due to the short half-life of fluorine-18. Such protocols reduce handling time and the number of purification steps required. The main challenge for "last step" radiolabeling is need for reactions to be carried out in aqueous, biocompatible solvents, however, the strong hydration of fluoride ion severely reduces its nucleophilicity in these solvents.

Small peptides, such as *p*-trimethylammonium amide **138**,[183] aziridine-bearing **140**,[184] and *p*-nitroamide **142**[185] in **Scheme 30** have been labelled in a single step from [^{18}F]fluoride. These methods use [^{18}F]fluoride which is azeotropically dried in the presence of Kryptofix 222, and the peptides heated in organic solvents to accomplish [^{18}F]fluorination. The use of these harsh conditions is similar to those used for labelling prosthetic groups, and precludes use of similar methodology for labelling larger, more sensitive biomolecules.

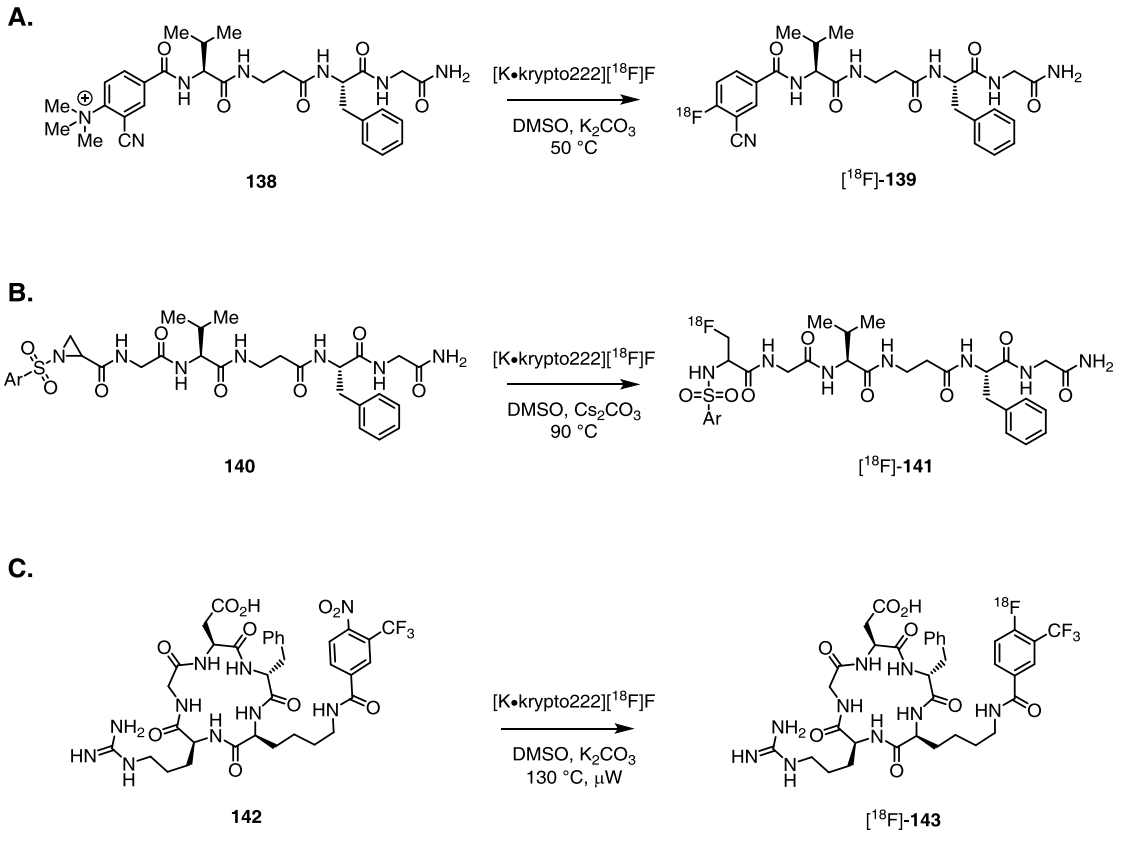

Scheme 30. Direct labelling of peptides under standard nucleophilic conditions using **A.** trimethylammonium-**138**,[183] **B.** aziridine-**140**[184] and **C.** nitro-**142** precursors.[185]

The desire for last step labelling strategies has led to the development of inorganic species, including boron,[186] silicon[187] and aluminium-derived[188] complexes which have high affinity for fluoride ion and have the ability to sequester fluoride from the solvent.

Silicon fluorides are well characterised species, and the strength of the Si–F bond has been exploited for silicon-based protecting group chemistry. Schirrmacher *et al.*[187] have developed a fluorine isotope exchange reaction at silicon (SiFA) in DMSO at room temperature (**Scheme 31 A**) as a means of radiolabeling biological molecules, such as **144**, in a single step.[189–191] While this method proves operationally simple, the isotopic dilution inherent to the process lowers specific activity of the final ^{18}F-labelled products. While suitable for rapidly labeling peptides, the isotope exchange reaction requires dry [^{18}F]fluoride and the reaction is performed in DMSO, and thus not compatible with biomolecules that are not stable in organic solvents.

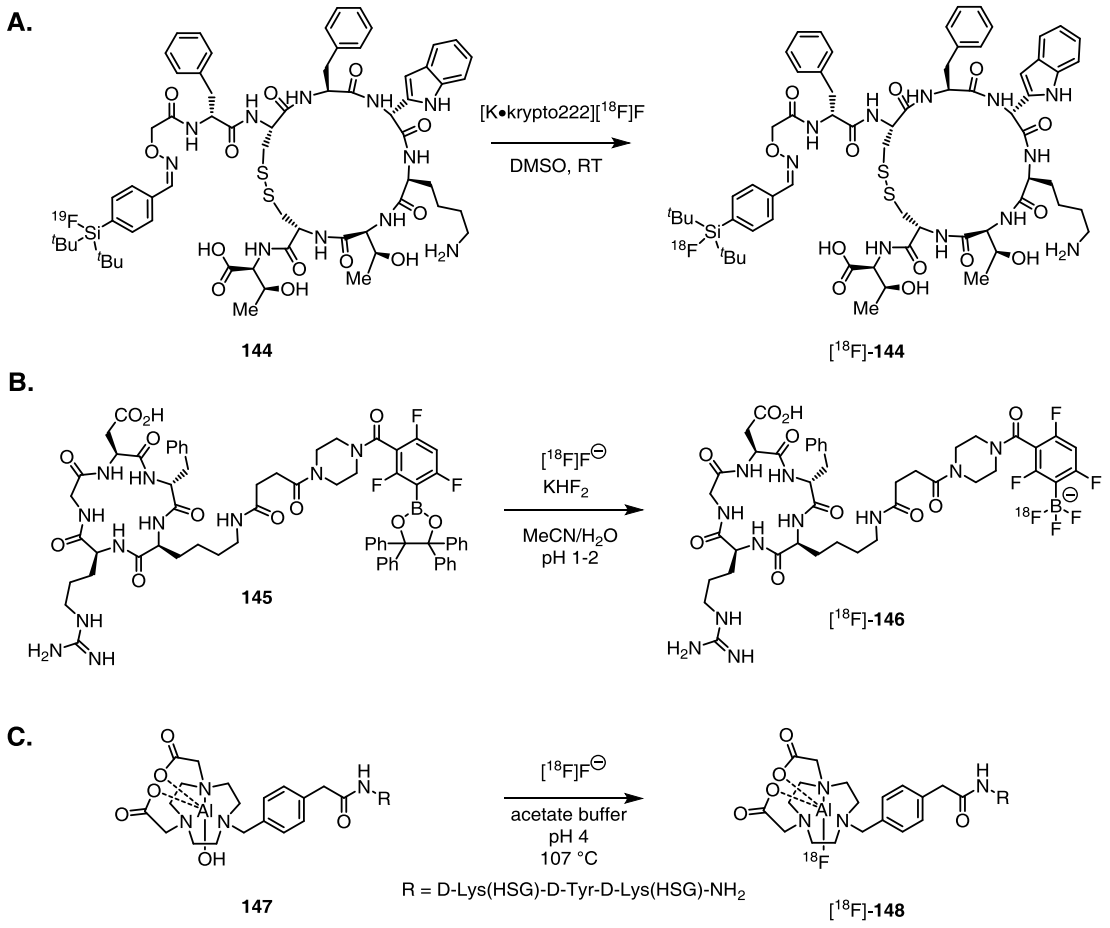

Scheme 31. "Last step" peptide labelling strategies using [^{18}F]fluoride. **A.** SiFA (silicon-based fluoride acceptor) direct labelling approach using isotope exchange of ^{19}F for ^{18}F in DMSO.[187] **B.** Borate ester based labelling strategy gives [^{18}F]-trifluoroborate-labelled products under carrier added conditions at pH 2.[192] **C.** Aluminium 1,4,7-triazacyclononane-1,4-diacetate (NODA) complex labelling of linear peptides at high temperatures in water. HSG = histamine-glycinyl-serine.[193]

Perrin *et al.*[192] have developed a last-step labelling strategy based on the formation of a B–F bond under aqueous conditions. The method uses acid-catalyzed fluorolysis of a diaryl boronate ester **145** by potassium bifluoride/potassium [^{18}F]fluoride solution in water at pH 2, generating a [^{18}F]trifluoroborate species such as [^{18}F]-**146**. The resultant [^{18}F]trifluoroborates were found to be stable *in vivo* and did not eliminate [^{18}F]fluoride ion.[194] This labelling methodology was subsequently used for last step labelling of a RGD peptide with fluorine-18, as illustrated in **Scheme 31 B**.[195] While labelling is efficient, the method is not suitable for use with acid sensitive biomolecules.

Goldenberg *et al.*[193] have developed a fluoride-capture strategy using pre-formed aluminium hydroxide NODA- or NOTA-chelates, such as **147** shown in **Scheme 31 C**.[196] When reacted with [^{18}F]fluoride in an ethanol/saline mixture and heated to 100 °C, these complexes sequester fluoride ion to give the [^{18}F]fluoro complex [^{18}F]-**148** in good radiochemical yields.[197] This methodology has been transferred to kit form for ease of use,[198] and a ^{18}F-labelled dimeric RGD peptide synthesised using this protocol has been investigated in human patients for imaging of angiogenesis associated with lung cancer.[199]

1.4. Fluorinase and PET

The direct aryl labelling at carbon and SiFA exchange process both require the use of azeotropically dried [^{18}F]fluoride ion and are consequently not compatible with aqueous reaction conditions. [^{18}F]Fluoride capture by boronic esters or aluminium chelates are also not suitable, as they use low pH and high temperature labelling conditions respectively for efficient labelling.

In this context, the fluorinase enzyme and its ability to catalyse C–F bond formation under mild aqueous conditions is immediately attractive for synthesis of either prosthetic groups or direct labelling of biomolecules for PET. The fluorinase reaction takes place at 37 °C in aqueous buffer at near neutral pH, ideal conditions for carrying out ^{18}F-fluorinations of sensitive biomolecules.

There is precedent for the application of enzymes for PET radiotracer synthesis for nitrogen-13-,[200,201] carbon-11-[202–206] and fluorine-18-based[207] tracers. Two examples where enzymatic syntheses of radiotracers had advantages over chemical syntheses are discussed below.

Daunorubicin **151** (**Scheme 32 A**) is a potent anti-cancer agent, derived enzymatically from carubicin **150**, its desmethyl analogue. *O*-Methylation of carubicin **150** with [^{11}C]methyl iodide gave many radiolabelled products, but not [^{11}C]daunorubicin [^{11}C]-**151**. Carubicin **150** bears four hydroxyl groups and a primary amine, all reactive towards methylation by [^{11}C]MeI. As an alternative approach, SAM synthetase was used to synthesise *S*-adenosyl-L-[^{11}C]methionine [^{11}C]-**20** ([^{11}C]SAM) from L-[^{11}C]methionine [^{11}C]-**21** and ATP **149**.[206] The enzymatically synthesised [^{11}C]SAM [^{11}C]-**20** was used for *O*-[^{11}C]methylation of carubicin **150** under the action of carubicin *O*-methyl transferase to give [^{11}C]daunorubicin [^{11}C]-**151** in good yield. In this case, enzymatic control of regiochemistry gave access to the desired compound through a biomimetic approach, without resorting to complex protecting group chemistry.

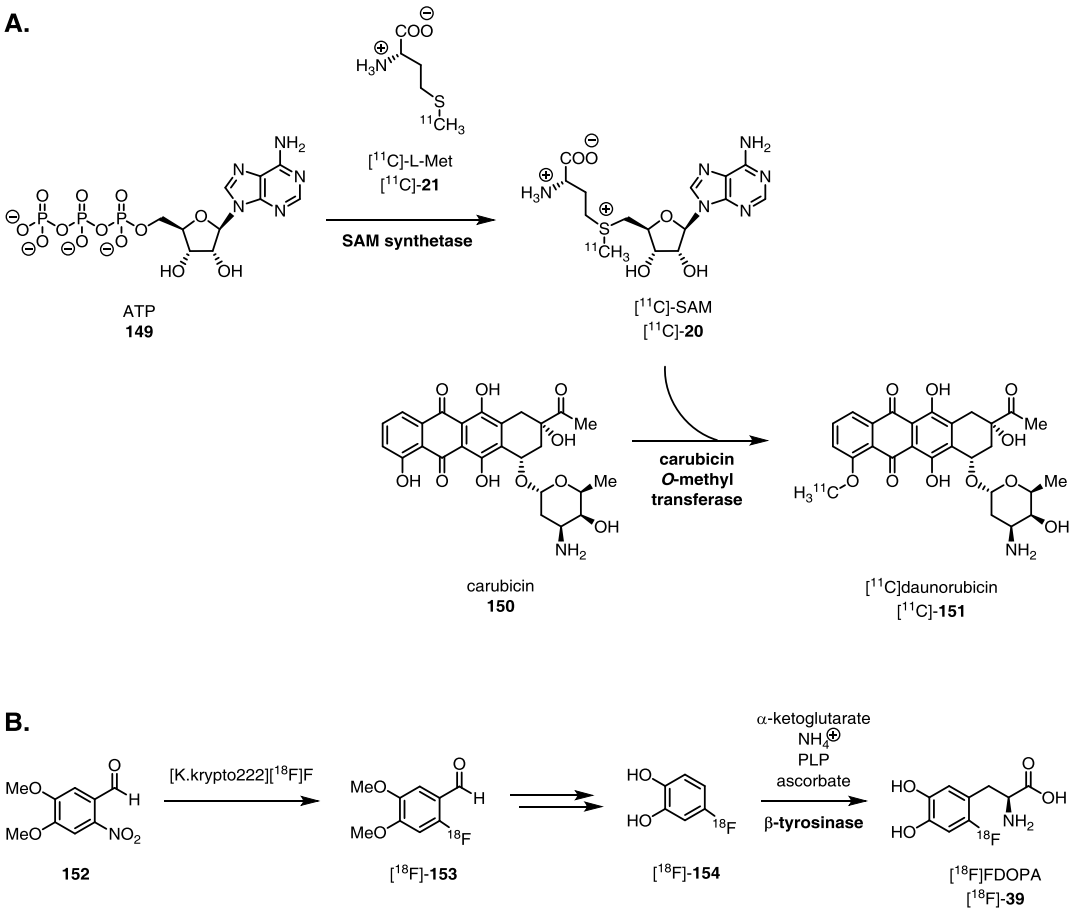

Scheme 32. Enzymatic synthesis of **A.** [^{11}C]daunorubicin [^{11}C]-**151**[206] and **B.** [^{18}F]-FDOPA [^{18}F]-**39**[207] for use as PET tracers.

In addition to the regioselectivity of enzymes, their stereoselectivity has also been exploited for the synthesis of radiotracers. [^{18}F]FDOPA [^{18}F]-**39** (**Scheme 32 B**), an

imaging agent for neurodegenerative disorders, has also been synthesised enzymatically using β-tyrosinase.[207] Catechol [^{18}F]-**154** was prepared chemically, using an S_NAr reaction with [^{18}F]fluoride in a the key step. The catechol [^{18}F]-**154** was reacted with an ammonium salt and α-ketoglutarate under the action of β-tyrosinase to give [^{18}F]FDOPA [^{18}F]-**39**. This methodology allowed for the synthesis of [^{18}F]-**39** from [^{18}F]fluoride rather than [^{18}F]F_2, offering higher specific activities and better control of regioselectivity compared to electrophilic fluorination routes. In addition, the enzymatic transformation allows complete control of the stereochemistry of the product, which had proved difficult with previous syntheses.

1.4.1. Applying the fluorinase to PET

After discovery of the fluorinase in 2002, it was immediately attractive to explore application of the enzyme for the synthesis of PET radiotracers. Initial incubations of partially purified fluorinase fractions from *S. cattleya* with [^{18}F]fluoride and SAM **20** at 40 °C led to the production of 5'-[^{18}F]fluoro-5'-deoxyadenosine [^{18}F]-**22** ([^{18}F]FDA), shown in **Scheme 33**. Conversions for this enzymatic transformation were very low (approx. 1%) and the synthesis took approximately 5 hours, conditions not suitable for synthesis of PET radiotracers. The observation that the enzyme-catalysed reaction was reversible[51] led to coupling of the fluorinase reaction to a second enzyme, an L-amino acid oxidase, driving the reaction in the forward direction. Under similar radiolabelling conditions to those previously reported, but with the addition of an L-amino acid oxidase, the reaction proceeded to greater than 90% conversion to [^{18}F]-**22** within 2 hours, when high enzyme concentrations (24 mg.mL^{-1}) were utilised.[208]

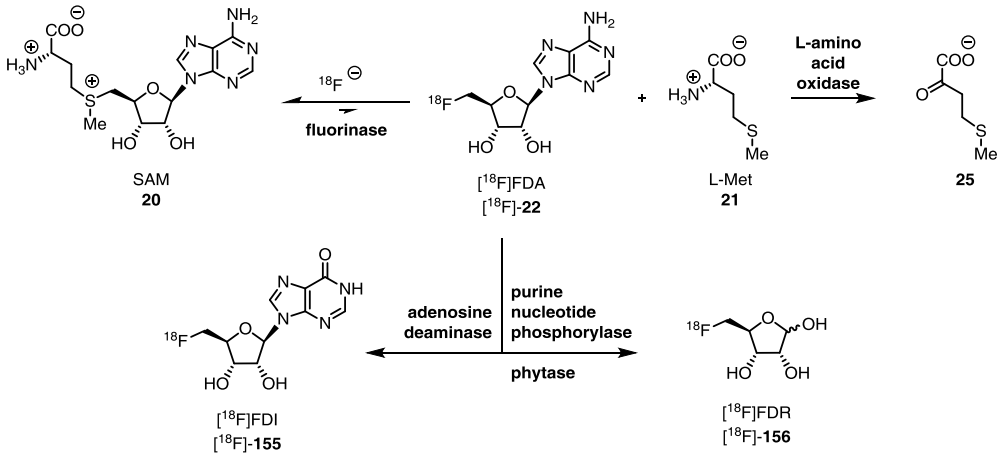

Scheme 33. Synthesis of C–^{18}F bonds using the fluorinase coupled to an L-amino acid oxidase. Coupling the transformation to other enzymes gives access to novel potential radiotracers.

High conversions with relatively short reaction times meant that the fluorinase enzyme compared well to the more traditional methods as a means for the synthesis of C–^{18}F bonds for PET. [^{18}F]FDA [^{18}F]-**22**, however, proved to be a poor radiotracer, undergoing rapid defluorination to release [^{18}F]fluoride ion *in vivo*.[209] While [^{18}F]FDA [^{18}F]-**22** is a poor tracer, the radiolabelled compound was used as a substrate for further enzymatic transformations, showing that fluorinase-derived [^{18}F]FDA [^{18}F]-**22** could act as a source of novel radiotracers. Coupling the enzymatic ^{18}F-fluorination to an adenosine deaminase gave 5'-[^{18}F]fluoro-5'-deoxyinosine [^{18}F]-**155** ([^{18}F]FDI), while coupling to a purine nucleotide phosphorylase and phytase gave 5-[^{18}F]fluoro-5'-deoxyribose [^{18}F]-**156** ([^{18}F]FDR), as shown in **Scheme 33 A**.[208]

1.4.2. Base swaps

Nucleosides are an attractive prospect for radiolabelling due to their role in DNA and RNA synthesis during cell proliferation in cancers.[210] In this context, the fluorinase offers access to a range of 5'-[^{18}F]-fluorinated nucleosides, as shown in **Scheme 34**, which have traditionally been difficult tracers to access through chemical synthesis.[211,212] Coupling of a fluorinase-catalysed synthesis of [^{18}F]FDA [^{18}F]-**22** to a purine nucleotide phosphorylase generated 5-[^{18}F]fluoro-5-deoxyribose-1-phosphate [^{18}F]-**27** ([^{18}F]FDRP).[213] [^{18}F]FDRP [^{18}F]-**27** was used as a substrate for a thymidine phosphorylase and a range of uracils to generate a series of 5'-[^{18}F]fluoro-5'-deoxyuridine analogues [^{18}F]-**157** to [^{18}F]-**159** in **Scheme 34**. The analogues were not used in imaging experiments, but these experiments illustrate the utility of the fluorinase enzyme for the synthesis of a fluorinated nucleoside analogues.

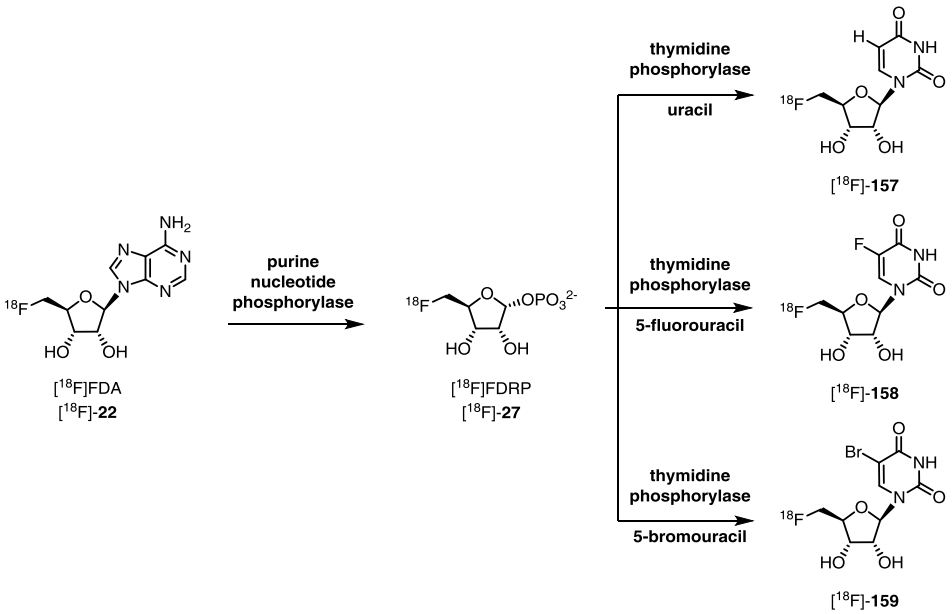

Scheme 34. Synthesis of a range of thymidine analogues from [^{18}F]FDA [^{18}F]-**22** though an [^{18}F]FDRP [^{18}F]-**27** intermediate in a series of one-pot transformations.[213]

1.4.3. Fluoroacetate

[^{18}F]Fluoroacetate [^{18}F]-**1** ([^{18}F]FAc) has found application in PET imaging, primarily as an acetate surrogate for investigating metabolic changes associated with disease, and is discussed further in **Chapter 5**.[214–217] In this context, it became desirable to develop a synthesis of [^{18}F]FAc [^{18}F]-**1** using the fluorinase, to complement existing methods for its synthesis, which traditionally use S_N2 substitution with [^{18}F]fluoride on an appropriate substrate.[217,218] The Kuhn-Roth oxidation[219,220] is a reaction used to oxidise pendant methyl groups in organic compounds to carve out acetate, and has found application in determining the number of such groups in ^{14}C- and ^{3}H- labelled natural products. A similar transformation could be used with [^{18}F]FDA [^{18}F]-**22**, where the [^{18}F]fluoromethyl group would be oxidised using a mixture of CrO_3 and H_2SO_4 to generate [^{18}F]FAc [^{18}F]-**1**, as shown in **Scheme 35**.

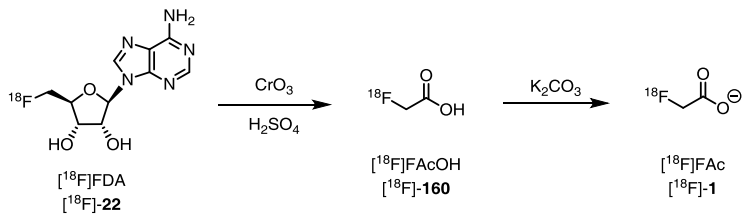

Scheme 35. Synthesis of [^{18}F]fluoroacetate [^{18}F]FAc [^{18}F]-**1** from [^{18}F]FDA [^{18}F]-**22** using strongly oxidising conditions.

This oxidation was trialled using [^{18}F]FDA [^{18}F]-**22** derived from reaction of SAM **20** with [^{18}F]fluoride, coupled to L-amino acid oxidase.[221] The reaction was found to produce [^{18}F]FAcOH [^{18}F]-**160**, very efficiently, and was successfully extracted as the carboxylic acid from the reaction mixture using diethyl ether. Extraction into aqueous potassium carbonate gave [^{18}F]FAc [^{18}F]-**1** in a 36% decay corrected radiochemical yield. More detail about [^{18}F]FAc [^{18}F]-**1** will be discussed in **Chapter 5**.

1.4.4. Fluorodeoxyribose

2-[^{18}F]Fluoro-2-deoxyglucose [^{18}F]-**35** ([^{18}F]FDG) is used in over 90% of clinical PET applications.[91,92] A fluorinase-catalysed transformation of SAM **20** to [^{18}F]FDA [^{18}F]-**22** could provide access to a similar [^{18}F]fluoro-deoxy sugar by cleavage of the adenine base from the nucleoside. As stated, the fluorinase transformation could be coupled to a PNP and a phytase to generate [^{18}F]FDR [^{18}F]-**156**,[208] however, a single step transformation using a nucleoside hydrolase *Trypanosoma vivax* was reported in an effort to remove a synthetic step and improve the efficiency of this synthesis, as shown in **Scheme 36**.[222] This route offered significantly shorter reaction times and radiochemical incorporations of 80%, excellent for the synthesis of PET radio tracers.

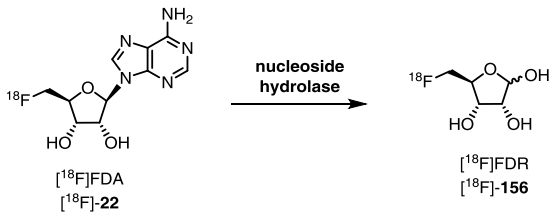

[^{18}F]FDA
[^{18}F]-**22**

[^{18}F]FDR
[^{18}F]-**156**

Scheme 36. Synthesis of 5-[^{18}F]fluoro-5-deoxyribose [^{18}F]-**156** ([^{18}F]FDR) from [^{18}F]FDA [^{18}F]-**22** derived from a fluorinase reaction.

[^{18}F]FDR [^{18}F]-**156** was compared with [^{18}F]FDG [^{18}F]-**35** as a radiotracer in mice bearing human epithelial cell carcinoma xenograft tumours, as shown in **Figure 11**.[223] This represented the first reported *in vivo* use of a radiotracer prepared using the fluorinase enzyme. In this experiment, it was found that [^{18}F]FDR [^{18}F]-**156** behaved similarly to the gold standard for PET imaging, [^{18}F]FDG [^{18}F]-**35**, and was concentrated in the tumours, as shown in **Figure 11**. Additionally, [^{18}F]FDR [^{18}F]-**156** appeared metabolically stable to [^{18}F]fluoride ion elimination as no accumulation of radioactivity was seen in the bone. The new radiotracer was however cleared from the tumours more rapidly, predominantly *via* the urinary system. These experiments illustrate the compatibility of the fluorinase enzyme with small animal PET imaging, and open the possibility for exploration of novel fluorinase-synthesised radiotracers in *in vivo* models.

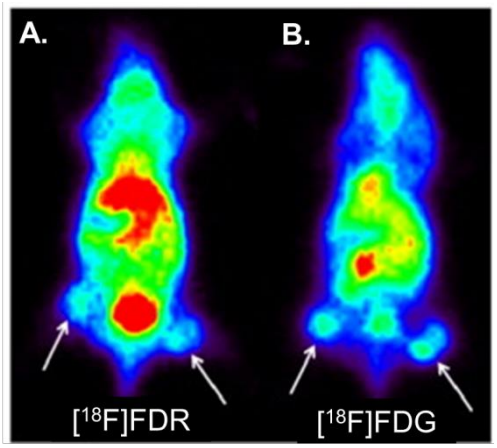

Figure 11. PET images of mice bearing tumours (white arrows) imaged with **A.** [^{18}F]FDR [^{18}F]-**156** and **B.** [^{18}F]FDG [^{18}F]-**35**. Image reproduced with permission from O'Hagan *et al.*[223]

1.5. Conclusions

The isolation and characterisation of a fluorinating enzyme form *S. cattleya* provided insight into the biosynthesis of rare fluorinated natural products. The enzyme was found capable of sequestering fluoride anion from aqueous solution, and activating this anion for reaction with *S*-adenosylmethionine **20**. Under non-enzymatic conditions in the context of PET, the activation of fluoride from aqueous solutions is accomplished by azeotropic dying in the presence of cryptands. A potential advantage of coupling the fluorinase to traditional PET radiotracer synthetic methodology is to circumvent pre-drying required to activate the nucleophile.

Fluorination methodology for PET is an area of growing interest. There is a major effort to develop mild and selective transformations to introduce [^{18}F]fluoride ion into organic molecules, either for use as radiotracers themselves, or for the development of novel prosthetic groups for labelling of biomolecules. In addition, last-step labelling protocols continue to receive attention in an effort to reduce synthesis times and improve labelling efficiency for biomolecules.

The fluorinase occupies a unique position in this regard, in that it represents the only method capable of catalysing the formation of C–F bonds under neutral pH and ambient conditions in water. The utility of the fluorinase has been explored, generating a range of novel radiotracers. However, all potential radiotracers developed thus far, including 5'-[^{18}F]fluorouridine nucleosides **157**, **158** and **159**, [^{18}F]fluoroacetate [^{18}F]-**1**

and 5-[^{18}F]fluororibose [^{18}F]-**156**, have used [^{18}F]FDA [^{18}F]-**22** as an intermediate in their synthesis.

In order to further capitalise on the mild conditions offered by fluorinase catalysis, we were interested in exploring the use of the fluorinase for the synthesis of a novel prosthetic group, with the possibility of extending this methodology for "last step" labelling of biomolecules with fluorine-18. Application of the fluorinase to such labelling approaches required the development of novel substrates that bore either reactive sites for reaction with biomolecules, or more ambitiously, already conjugated to biomolecules.

One foreseeable limitation of such an approach is the inherent substrate specificity usually exhibited by enzymes, especially near the site of reactivity. This may limit the choice of sites for modification of the fluorinase substrate. The substrate specificity of the fluorinase has previously been explored to some degree, and will be discussed in **Chapter 2**. In addition, a strategy for exploiting the fluorinase for the synthesis of a novel prosthetic group is explored.

1.6. References

1. J. Schmedt Auf Der Günne, M. Mangstl, and F. Kraus, *Angew. Chem. Int. Ed.*, 2012, **51**, 7847–7849.

2. J. Marais, *Onderstepoort J. Vet. Sci. Anim. Ind.*, 1943, **18**, 203.

3. J. Marais, *Onderstepoort J. Vet. Sci. Anim. Ind.*, 1944, **20**, 67.

4. D. B. Harper and D. O'Hagan, *Nat. Prod. Rep.*, 1994, **11**, 123–133.

5. R. A. Peters, R. W. Wakelin, P. Buffa, and L. C. Thomas, *Proc. Roy. Soc. B*, 1953, **140**, 497– 507.

6. M. Sanada, T. Miyano, S. Iwadare, J. M. Williamson, B. H. Arison, J. L. Smith, A. W. Douglas, J. M. Liesch, and E. Inamine, *J. Antibiot. (Tokyo).*, 1986, **39**, 259–265.

7. R. Peters and R. J. Hall, *Biochem. Pharmacol.*, 1959, **2**, 25–36.

8. P. F. V. Ward, R. J. Hall, and R. A. Peters, *Nature*, 1964, **201**, 611– 612.

9. J. T. G. Hamilton, Queens University, Belfast, *Unpublished Results*.

10. D. B. Harper, D. O'Hagan, and J. T. G. Hamilton, *Tetrahedron Lett.*, 1990, **31**, 1776.

11. M. Walsh, W. Klopfenstein, and J. Harwood, *Phytochemistry*, 1990, **29**, 3797.

12. H. Hong, D. Spiteller, and J. B. Spencer, *Angew. Chem. Int. Ed.*, 2008, **47**, 6028–6032.

13. M. C. Walker, B. W. Thuronyi, L. K. Charkoudian, B. Lowry, C. Khosla, and M. C. Y. Chang, *Science*, 2013, **341**, 1089–1094.

14. L. Ma, A. Bartholome, M. H. Tong, Z. Qin, Y. Yu, T. Shepherd, K. Kyeremeh, H. Deng, and D. O'Hagan, *Chem. Sci.*, 2015, **6**, 1414–1419.

15. S. O. Thomas, V. L. Singleton, J. A. Lowry, R. W. Sharpe, L. M. Pruess, J. N. Porter, J. H. Mowat, and N. Bohonos, *Antibiot. Annu.*, 1957, 716–721.

16. D. A. Schuman, R. K. Robins, and M. J. Robins, *J. Am. Chem. Soc.*, 1969, **91**, 3391.

17. J. B. Patrick and W. E. Meyer, in *Abstracts of the 156th National Meeting of the American Chemical Society', Sept 1968, Atlantic City, New Jersey, MED1-024.*, 1968.

18. G. O. Morton, J. E. Lancaster, G. E. Van Lear, W. Fulmor, and W. E. Meyer, *J. Am. Chem. Soc.*, 1969, **91**, 1535–1537.

19. I. D. Jenkins, J. P. Verheyden, and J. G. Moffatt, *J. Am. Chem. Soc.*, 1976, **98**, 3346–3357.

20. K. Fukuda, T. Tamura, Y. Segawa, Y. Mutaguchi, and K. Inagaki, *Actinomycetologica*, 2009, **23**, 51–55.

21. D. O'Hagan and D. B. Harper, *J. Fluor. Chem.*, 1999, **100**, 127–133.

22. X.-H. Xu, G.-M. Yao, Y.-M. Li, J.-H. Lu, C.-J. Lin, X. Wang, and C.-H. Kong, *J. Nat. Prod.*, 2003, **66**, 285–288.

23. D. O'Hagan and K. K. J. Chan, in *Methods in Enzymology: Natural Product Biosynthesis by Microorganisms and Plants, Part 1*, ed. D. Hopwood, Academic Press, 2012, pp. 223–224.

24. N. Jaivel, C. Uvarani, R. Rajesh, D. Velmurugan, and P. Marimuthu, *J. Nat. Prod.*, 2014, **77**, 2–8.

25. M. S. Ayoup, D. B. Cordes, A. M. Z. Slawin, and D. O'Hagan, *J. Nat. Prod.*, 2014, **77**, 1249–1251.

26. H. Aldemir, S. V. Kohlhepp, T. Gulder, and T. A. M. Gulder, *J. Nat. Prod.*, 2014, **77**, 2331–2334.

27. G. W. Gribble, *J. Chem. Educ.*, 2004, **81**, 1441–1449.

28. H. A. Wagenknecht and W. D. Woggon, *Chem. Biol.*, 1997, **4**, 367–372.

29. R. D. Libby, T. M. Beachy, and A. K. Phipps, *J. Biol. Chem.*, 1996, **271**, 21820–21827.

30. J. Littlechild, E. Garcia Rodriguez, and M. Isupov, *J. Inorg. Biochem.*, 2009, **103**, 617–621.

31. A. Butler and J. N. Carter-Franklin, *Nat. Prod. Rep.*, 2004, **21**, 180–188.

32. D. G. Fujimori and C. T. Walsh, *Curr. Opin. Chem. Biol.*, 2007, **11**, 553–560.

33. D. Galonic, E. Barr, C. Walsh, J. Bollinger Jr, and C. Krebs, *Nat. Chem. Biol.*, 2007, **3**, 113–116.

34. D. O'Hagan, C. Schaffrath, S. L. Cobb, and J. T. G. Hamilton, *Nature*, 2002, **416**, 279.

35. A. S. Eustáquio, F. Pojer, J. P. Noel, and B. S. Moore, *Nat. Chem. Biol.*, 2008, **4**, 69–74.

36. L. P. Hager, D. R. Morris, F. S. Brown, and H. Eberwein, *J. Biol. Chem.*, 1966, **241**, 1769–1777.

37. S. Keller, T. Wage, K. Hohaus, M. Hölzer, E. Eichhorn, and K.-H. van Pée, *Angew. Chem. Int. Ed.*, 2000, **39**, 2300–2302.

38. D. L. Zechel, S. P. Reid, O. Nashiru, C. Mayer, D. Stoll, D. L. Jakeman, R. A. J. Warren, and S. G. Withers, *J. Am. Chem. Soc.*, 2001, **123**, 4350–4351.

39. O. Nashiru, D. L. Zechel, D. Stoll, T. Mohammadzadeh, R. A. J. Warren, and S. G. Withers, *Angew. Chem. Int. Ed.*, 2001, **40**, 417–420.

40. C. Schaffrath, S. L. Cobb, and D. O'Hagan, *Angew. Chem. Int. Ed.*, 2002, **41**, 3913–3915.

41. C. Schaffrath, H. Deng, and D. O'Hagan, *FEBS Lett.*, 2003, **547**, 111–114.

42. C. Dong, H. Deng, M. Dorward, D. O. Hagan, and J. H. Naismith, *Acta Crystallogr.*, 2003, **D59**, 2292–2293.

43. C. Dong, F. Huang, H. Deng, C. Schaffrath, J. B. Spencer, D. O'Hagan, and J. H. Naismith, *Nature*, 2004, **427**, 561–565.

44. D. O'Hagan, R. J. M. Goss, A. Meddour, and J. Courtieu, *J. Am. Chem. Soc.*, 2003, **125**, 379–387.

45. C. D. Cadicamo, J. Courtieu, H. Deng, A. Meddour, and D. O'Hagan, *ChemBioChem*, 2004, **5**, 685–690.

46. O. S. Smart, J. G. Neduvelil, X. Wang, B. A. Wallace, and M. S. P. Sansom, *J. Mol. Graph.*, 1996, **14**, 354–360.

47. H. M. Senn, D. O'Hagan, and W. Thiel, *J. Am. Chem. Soc.*, 2005, **127**, 13643–13655.

48. X. Zhu, D. A. Robinson, A. R. McEwan, D. O'Hagan, and J. H. Naismith, *J. Am. Chem. Soc.*, 2007, **129**, 14597–14604.

49. H. Deng, L. Ma, N. Bandaranayaka, Z. Qin, G. Mann, K. Kyeremeh, Y. Yu, T. Shepherd, J. H. Naismith, and D. O'Hagan, *ChemBioChem*, 2014, **15**, 364–368.

50. D. C. Lohman, D. R. Edwards, and R. Wolfenden, *J. Am. Chem. Soc.*, 2013, **135**, 14473–14475.

51. H. Deng, S. L. Cobb, A. R. McEwan, R. P. McGlinchey, J. H. Naismith, D. O'Hagan, D. A. Robinson, and J. B. Spencer, *Angew. Chem. Int. Ed.*, 2006, **45**, 759–762.

52. K. A. Reid, J. T. G. Hamilton, R. D. Bowden, D. O'Hagan, L. Dasaradhi, M. R. Amin, and D. B. Harper, *Microbiology*, 1995, **141**, 1385–1393.

53. J. Nieschalk, J. T. G. Hamilton, C. D. Murphy, D. B. Harper, and D. O'Hagan, *Chem. Commun.*, 1997, 799–800.

54. J. T. G. Hamilton, C. D. Murphy, M. R. Amin, D. O'Hagan, and D. B. Harper, *J. Chem. Soc. Perkin Trans. 1*, 1998, 759–768.

55. S. J. Moss, C. D. Murphy, D. O'Hagan, C. Schaffrath, J. T. G. Hamilton, W. C. McRoberts, and D. B. Harper, *Chem. Commun.*, 2000, 2281–2282.

56. C. D. Murphy, S. J. Moss, and D. O'Hagan, *Appl. Environ. Microbiol.*, 2001, **67**, 4919–4921.

57. C. D. Murphy, D. O'Hagan, and C. Schaffrath, *Angew. Chem. Int. Ed.*, 2001, **40**, 4479–4481.

58. F. Huang, S. F. Haydock, D. Spiteller, T. Mironenko, T. L. Li, D. O'Hagan, P. F. Leadlay, and J. B. Spencer, *Chem. Biol.*, 2006, **13**, 475–484.

59. S. L. Cobb, H. Deng, J. T. G. Hamilton, R. P. McGlinchey, and D. O'Hagan, *Chem. Commun.*, 2004, **35**, 592.

60. H. Tamura, Y. Saito, H. Ashida, T. Inoue, Y. Kai, A. Yokota, and H. Matsumura, *Protein Sci.*, 2008, **17**, 126–135.

61. M. Onega, R. P. McGlinchey, H. Deng, J. T. G. Hamilton, and D. O'Hagan, *Bioorg. Chem.*, 2007, **35**, 375–385.

62. H. Deng, S. M. Cross, R. P. McGlinchey, J. T. G. Hamilton, and D. O'Hagan, *Chem. Biol.*, 2008, **15**, 1268–1276.

63. A. S. Eustáquio and B. S. Moore, *Angew. Chem. Int. Ed.*, 2008, **47**, 3936–3938.

64. A. S. Eustaquio, D. O'Hagan, and B. S. Moore, *J. Nat. Prod.*, 2010, **73**, 378–382.

65. Y. Wang, Z. Deng, and X. Qu, *F1000Research*, 2014, **3**, 61.

66. V. Barbe, M. Bouzon, S. Mangenot, B. Badet, J. Poulain, B. Segurens, D. Vallenet, P. Marlière, and J. Weissenbach, *J. Bacteriol.*, 2011, 193, 5055–5056.

67. L. Vera-Cabrera, R. Ortiz-Lopez, R. Elizondo-Gonzalez, A. A. Perez-Maya, and J. Ocampo-Candiani, *J. Bacteriol.*, 2012, 194, 2761–2762.

68. L. Vera-Cabrera, R. Ortiz-Lopez, R. Elizondo-Gonzalez, and J. Ocampo-Candiani, *PLoS One*, 2013, **8**, e65425.

69. *July 15th 2015; Actinoplanes genome http//www.ncbi.nlm.nih.gov/ nuccore/494682416*.

70. A. M. Weeks, N. S. Keddie, R. D. P. Wadoux, D. OHagan, and M. C. Y. Chang, *Biochemistry*, 2014, **53**, 2053–2063.

71. T. Liang, C. N. Neumann, and T. Ritter, *Angew. Chem. Int. Ed.*, 2013, **52**, 8214–8264.

72. S. Pascu and J. Dilworth, *J. Labelled Comp. Radiopharm.*, 2014, **57**, 191–194.

73. P. W. Miller, N. J. Long, R. Vilar, and A. D. Gee, *Angew. Chem. Int. Ed.*, 2008, **47**, 8998–9033.

74. K. Frey, in *Basic Neurochemistry: Molecular, Cellular and Medical Aspects. 6th edition*, eds. G. Siegel, B. Agranoff, and R. Albers, Lippincott-Raven, Philidelphia, 1999.

75. S. C. Jones, J. H. Greenberg, R. Dann, G. D. Robinson, M. Kushner, A. Alavi, and M. Reivich, *J. Cereb. Blood Flow Metab.*, 1985, **5**, 566–575.

76. H. R. Schelbert, M. E. Phelps, S. C. Huang, N. S. MacDonald, H. Hansen, C. Selin, and D. E. Kuhl, *Circulation*, 1981, **63**, 1259–1272.

77. M. Allard, E. Fouquet, D. James, and M. Szlosek-Pinaud, *Curr. Med. Chem.*, 2008, **15**, 235–277.

78. E. D. Hostetler, G. E. Terry, and H. D. Burn, *J. Label. Compd. Radiopharm.*, 2005, **48**, 629–634.

79. M. Bjorkman, H. Doi, B. Resul, M. Suzuki, R. Noyori, Y. Watanabe, and B. Langström, *J. Label. Compd. Radiopharm.*, 2002, **43**, 1327–1334.

80. D. R. Hwang, N. R. Simpson, J. Montoya, J. J. Mann, and M. Laruelle, *Nucl. Med. Biol.*, 1999, **26**, 815–819.

81. C. Rami-Mark, J. Ungersboeck, D. Haeusler, L. Nics, C. Philippe, M. Mitterhauser, M. Willeit, R. Lanzenberger, G. Karanikas, and W. Wadsak, *Appl. Radiat. Isot.*, 2013, **82**, 75–80.

82. S. Kealey, A. Gee, and P. W. Miller, *J. Label. Compd. Radiopharm.*, 2014, **57**, 195–201.

83. T. J. Wadas, E. H. Wong, G. R. Weisman, and C. J. Anderson, *Chem. Rev.*, 2010, **110**, 2858–2902.

84. P. K. E. Börjesson, Y. W. S. Jauw, R. Boellaard, R. de Bree, E. F. I. Comans, J. C. Roos, J. A. Castelijns, M. J. W. D. Vosjan, J. A. Kummer, C. R. Leemans, A. A. Lammertsma, and G. A. M. S. van Dongen, *Clin. Cancer Res.*, 2006, **12**, 2133–2140.

85. J. P. Holland, V. Divilov, N. H. Bander, P. M. Smith-Jones, S. M. Larson, and J. S. Lewis, *J. Nucl. Med.*, 2010, **51**, 1293–1300.

86. M. Pretze, P. Große-Gehling, and C. Mamat, *Molecules*, 2011, **16**, 1129–1165.

87. E. P. Gillis, K. J. Eastman, M. D. Hill, D. J. Donnelly, and N. A. Meanwell, *J. Med. Chem.*, 2015, DOI: 10.1021/acs.jmedchem.5b0025.

88. D. O'Hagan, *J. Fluor. Chem.*, 2010, **131**, 1071–1081.

89. D. Barnes-Seeman, J. Beck, and C. Springer, *Curr. Top. Med. Chem.*, 2014, **14**, 855–864.

90. D. O'Hagan, *Chem. Soc. Rev.*, 2008, **37**, 308–319.

91. B. M. Gallagher, A. Ansari, H. Atkins, V. Casella, D. R. Christman, J. S. Fowler, T. Ido, R. R. MacGregor, P. Som, C. N. Wan, A. P. Wolf, D. E. Kuhl, and M. Reivich, *J. Nucl. Med.*, 1977, **18**, 990–996.

92. H. H. Coenen, P. H. Elsinga, R. Iwata, M. R. Kilbourn, M. R. A. Pillai, M. G. R. Rajan, H. N. Wagner, and J. J. Zaknun, *Nucl. Med. Biol.*, 2010, **37**, 727–740.

93. E. K. Pauwels, E. J. Sturm, E. Bombardieri, F. J. Cleton, and M. P. Stokkel, *J. Cancer Res. Clin. Oncol.*, 2000, **126**, 549–559.

94. M. D. Farwell, D. A. Pryma, and D. A. Mankoff, *Cancer*, 2014, **120**, 3433–3445.

95. G. Blessing, H. H. Coenen, K. Franken, and S. M. Qaim, *Int. J. Radiat. Appl. Instrumentation. Part A. Appl. Radiat. Isot.*, 1986, **37**, 1135–1139.

96. S. L. Pimlott and A. Sutherland, *Chem. Soc. Rev.*, 2011, **40**, 149–162.

97. M. Tredwell and V. Gouverneur, *Angew. Chem. Int. Ed.*, 2012, **51**, 11426–11437.

98. S. Forsback, O. Eskola, M. Haaparanta, J. Bergmann, and O. Solin, *Radiochim. Acta*, 2008, **96**, 845–848.

99. S. Forsback, O. Eskola, J. Bergman, M. Haaparanta, and O. Solin, *J. Label. Compd. Radiopharm.*, 2009, **52**, 286–288.

100. H. Teare, E. G. Robins, A. Kirjavainen, S. Forsback, G. Sandford, O. Solin, S. K. Luthra, and V. Gouverneur, *Angew. Chem. Int. Ed.*, 2010, **49**, 6821–6824.

101. H. Teare, E. G. Robins, E. Arstad, S. K. Luthra, and V. Gouverneur, *Chem. Commun.*, 2007, 2330–2332.

102. F. Dolle, D. Roeda, B. Kuhnast, M. Lasne, A. Tressaud, and G. Haufe, in *Fluorine and Health (San Francisco)*, Elsevier Science: Amsterdam, 2008, pp. 3–65.

103. L. Cai, S. Lu, and V. W. Pike, *European J. Org. Chem.*, 2008, **2008**, 2853–2873.

104. K. Hamacher, H. H. Coenen, and G. Stöcklin, *J. Nucl. Med.*, 1986, **27**, 235–238.

105. Z. Li and P. S. Conti, *Adv. Drug. Del. Rev.*, 2010, **62**, 1031–1051.

106. H.-J. Machulla, A. Blocher, M. Kuntzsch, M. Piert, R. Wei, and J. R. Grierson, *J. Radioanal. Nucl. Chem.*, 2000, **243**, 843–846.

107. L.-Q. Sun, T. Mori, C. S. Dence, D. E. Ponde, M. J. Welch, T. Furukawa, Y. Yonekura, and Y. Fujibayashi, *Nucl. Med. Biol.*, 2006, **33**, 153–158.

108. D. W. Kim, D.-S. Ahn, Y.-H. Oh, S. Lee, H. S. Kil, S. J. Oh, S. J. Lee, J. S. Kim, J. S. Ryu, D. H. Moon, and D. Y. Chi, *J. Am. Chem. Soc.*, 2006, **128**, 16394–16397.

109. D. W. Kim, H.-J. Jeong, S. T. Lim, M.-H. Sohn, J. A. Katzenellenbogen, and D. Y. Chi, *J. Org. Chem.*, 2008, **73**, 957–962.

110. Y. H. Oh, D. S. Ahn, S. Y. Chung, G. H. Jeon, S. W. Park, S. J. Oh, D. W. Kim, H. S. Kil, D. Y. Chi, and S. Lee, *J. Phys. Chem. A*, 2007, **111**, 10152–10161.

111. M. R. Kilbourn, M. J. Welch, C. S. Dence, J. Tewson, H. Saji, and M. Maeda, *Int. J. Appl. Radiat. Isot.*, 1984, **35**, 591–598.

112. K. Hashizume, H. Tamakawa, N. Hashimoto, and Y. Miyake, *Appl. Radiat. Isot.*, 1997, **48**, 1179–1185.

113. R. Littich and P. J. H. Scott, *Angew. Chem. Int. Ed.*, 2012, **51**, 1106–1109.

114. A. F. Brooks, J. J. Topczewski, N. Ichiishi, M. S. Sanford, and P. J. H. Scott, *Chem. Sci.*, 2014, **5**, 4545–4553.

115. Z. Gao, Y. H. Lim, M. Tredwell, L. Li, S. Verhoog, M. Hopkinson, W. Kaluza, T. L. Collier, J. Passchier, M. Huiban, and V. Gouverneur, *Angew. Chem. Int. Ed.*, 2012, **51**, 6733–6737.

116. T. L. Ross, J. Ermert, C. Hocke, and H. H. Coenen, *J. Am. Chem. Soc.*, 2007, **129**, 8018–8025.

117. A. Shah, V. W. Pike, and D. A. Widdowson, *J. Chem. Soc. Perkin Trans. 1*, 1998, 2043–2046.

118. B. C. Lee, C. S. Dence, H. Zhou, E. E. Parent, M. J. Welch, and J. A. Katzenellenbogen, *Nucl. Med. Biol.*, 2009, **36**, 147–153.

119. B. H. Rotstein, N. A. Stephenson, N. Vasdev, and S. H. Liang, *Nat. Commun.*, 2014, **5**, 4365.

120. J. Cardinale, J. Ermert, S. Humpert, and H. H. Coenen, *RSC Adv.*, 2014, **4**, 17293–17299.

121. E. Lee, A. S. Kamlet, D. C. Powers, C. N. Neumann, G. B. Boursalian, T. Furuya, D. C. Choi, J. M. Hooker, and T. Ritter, *Science*, 2011, **334**, 639–642.

122. J. R. Brandt, E. Lee, G. B. Boursalian, and T. Ritter, *Chem. Sci.*, 2014, **5**, 169–179.

123. E. Lee, J. M. Hooker, and T. Ritter, *J. Am Chem. Soc.*, 2012, **134**, 17456–17458.

124. C. Hollingworth, A. Hazari, M. N. Hopkinson, M. Tredwell, E. Benedetto, M. Huiban, A. D. Gee, J. M. Brown, and V. Gouverneur, *Angew. Chem. Int. Ed.*, 2011, **50**, 2613–2617.

125. J. J. Topczewski, T. J. Tewson, and H. M. Nguyen, *J. Am. Chem. Soc.*, 2011, **133**, 19318–19321.

126. E. Benedetto, M. Tredwell, C. Hollingworth, T. Khotavivattana, J. M. Brown, and V. Gouverneur, *Chem. Sci.*, 2013, **4**, 89–96.

127. T. J. A. Graham, R. F. Lambert, K. Ploessl, H. F. Kung, and A. G. Doyle, *J. Am. Chem. Soc.*, 2014, **136**, 5291–5294.

128. S. T. Lee and A. M. Scott, *Semin. Nucl. Med.*, 2007, **37**, 451–461.

129. X. Huang, W. Liu, H. Ren, R. Neelamegam, J. M. Hooker, and J. T. Groves, *J. Am. Chem. Soc.*, 2014, **136**, 6842–6845.

130. M. Tredwell, S. M. Preshlock, N. J. Taylor, S. Gruber, M. Huiban, J. Passchier, J. Mercier, C. Génicot, and V. Gouverneur, *Angew. Chem. Int. Ed.*, 2014, **53**, 7751–7755.

131. N. Ichiishi, A. F. Brooks, J. J. Topczewski, M. E. Rodnick, M. S. Sanford, and P. J. H. Scott, *Org. Lett.*, 2014, **16**, 3224–3227.

132. M. Huiban, M. Tredwell, S. Mizuta, Z. Wan, X. Zhang, T. L. Collier, V. Gouverneur, and J. Passchier, *Nat. Chem.*, 2013, 8–11.

133. T. Rühl, W. Rafique, V. T. Lien, and P. J. Riss, *Chem. Commun.*, 2014, **50**, 6056–6059.

134. P. Ivashkin, G. Lemonnier, J. Cousin, V. Grégoire, D. Labar, P. Jubault, and X. Pannecoucke, *Chem. Eur. J.*, 2014, **20**, 9514–9518.

135. D. van der Born, J. K. D. M. Herscheid, R. V. A. Orru, and D. J. Vugts, *Chem. Commun.*, 2013, **49**, 4018–4020.

136. D. van der Born, C. Sewing, J. K. D. M. Herscheid, A. D. Windhorst, R. V. A. Orru, and D. J. Vugts, *Angew. Chem. Int. Ed.*, 2014, **53**, 11046–11050.

137. T. Khotavivattana, S. Verhoog, M. Tredwell, L. Pfeifer, S. Calderwood, K. Wheelhouse, T. Lee Collier, and V. Gouverneur, *Angew. Chem. Int. Ed.*, 2015, DO!:10.1002/anie.201504665.

138. P. J. Riss and F. I. Aigbirhio, *Chem. Commun.*, 2011, **47**, 11873–11875.

139. P. J. Riss, V. Ferrari, L. Brichard, P. Burke, R. Smith, and F. I. Aigbirhio, *Org. Biomol. Chem.*, 2012, **10**, 6980–6986.

140. M. V. Fawaz, A. F. Brooks, M. E. Rodnick, G. M. Carpenter, X. Shao, T. J. Desmond, P. Sherman, C. A. Quesada, B. G. Hockley, M. R. Kilbourn, R. L. Albin, K. A. Frey, and P. J. H. Scott, *ACS Chem. Neurosci.*, 2014, **5**, 718–730.

141. S. Richter and F. Wuest, *Molecules*, 2014, **19**, 20536–20556.

142. V. Tolmachev and S. Stone-Elander, *Biochim. Biophys. Acta*, 2010, **1800**, 487–510.

143. H.-J. Wester, K. Hamacher, and G. Stöcklin, *Nucl. Med. Biol.*, 1996, **23**, 365–372.

144. P. Mäding, F. Füchtner, and F. Wüst, *Appl. Radiat. Isot.*, 2005, **63**, 329–332.

145. R. Haubner, H. Wester, W. A. Weber, P. E. Tomography, C. Mang, S. I. Ziegler, S. L. Goodman, R. Senekowitsch-Schmidtke, H. Kessler, and M. Schwaiger, *Cancer Res.*, 2001, **61**, 1781–1785.

146. G. Vaidyanathan and M. Zalutsky, *Nat. Protoc.*, 2006, **4**, 1655–1661.

147. L. Lang and W. Eckleman, *Appl. Radiat. Isot.*, 1997, **48**, 169–173.

148. W. Cai, T. Olafsen, X. Zhang, Q. Cao, S. S. Gambhir, L. E. Williams, A. M. Wu, and X. Chen, *J. Nucl. Med.*, 2007, **48**, 304–310.

149. J. L. Sutcliffe-Goulden, M. J. O'Doherty, and S. S. Bansal, *Bioorg. Med. Chem. Lett.*, 2000, **10**, 1501–1503.

150. J. Marik, S. H. Hausner, L. A. Fix, M. K. J. Gagnon, and J. L. Sutcliffe, *Bioconjug. Chem.*, 2006, **17**, 1017–1021.

151. S. H. Hausner, J. Marik, M. K. J. Gagnon, and J. L. Sutcliffe, *J. Med. Chem.*, 2008, **51**, 5901–5904.

152. Y. S. Chang, J. M. Jeong, Y. S. Lee, H. W. Kim, G. B. Rai, S. J. Lee, D. S. Lee, J. K. Chung, and M. C. Lee, *Bioconjug. Chem.*, 2005, **16**, 1329–1333.

153. T. Poethko, M. Schottelius, G. Thumshirn, U. Hersel, M. Herz, G. Henriksen, H. Kessler, M. Schwaiger, and H.-J. Wester, *J. Nucl. Med.*, 2004, **45**, 892–902.

154. E. Ishikawa, Y. Hamaguchi, and S. Yoshitake, in *Enzyme Immunoassay*, eds. I. Ishikawa, T. Kawai, and K. Miyai, Igaku-Shoin, Tokyo, 1981, pp. 67–80.

155. M. Berndt, J. Pietzsch, and F. Wüest, *Nucl. Med. Biol.*, 2007, **34**, 5–15.

156. F. Wuest, M. Berndt, R. Bergmann, J. Den Van Hoff, and J. Pietzsch, *Bioconjug. Chem.*, 2008, **19**, 1202–1210.

157. B. de Bruin, B. Kuhnast, F. Hinnen, L. Yaouancq, M. Amessou, L. Johannes, A. Samson, R. Boisgard, B. Tavitian, and F. Dollé, *Bioconjug. Chem.*, 2005, **16**, 406–420.

158. O. Prante, J. Einsiedel, R. Haubner, P. Gmeiner, H. J. Wester, T. Kuwert, and S. Maschauer, *Bioconjug. Chem.*, 2007, **18**, 254–262.

159. L. Mirfeizi, L. Campbell-Verduyn, R. Dierckx, B. Feringa, and P. Elsinga, *Curr. Org. Chem.*, 2013, **17**, 2108–2118.

160. J. Marik and J. L. Sutcliffe, *Tetrahedron Lett.*, 2006, **47**, 6681–6684.

161. D. Thonon, C. Kech, J. Paris, C. Lemaire, and A. Luxen, *Bioconjug. Chem.*, 2009, **20**, 817–823.

162. M. Glaser and E. Arstad, *Bioconj. Chem.*, 2007, **18**, 989–993.

163. S. Maschauer, J. Einsiedel, R. Haubner, C. Hocke, M. Ocker, H. Hübner, T. Kuwert, P. Gmeiner, and O. Prante, *Angew. Chem. Int. Ed.*, 2010, **49**, 976–979.

164. G. J. Brewer, *Clin. Neurophysiol.*, 2010, **121**, 459–460.

165. H. L. Evans, R. L. Slade, L. Carroll, G. Smith, Q.-D. Nguyen, L. Iddon, N. Kamaly, H. Stöckmann, F. J. Leeper, E. O. Aboagye, and A. C. Spivey, *Chem. Commun.*, 2012, **48**, 991–993.

166. J. M. Baskin, J. A. Prescher, S. T. Laughlin, N. J. Agard, P. V Chang, I. A. Miller, A. Lo, J. A. Codelli, and C. R. Bertozzi, *Proc. Natl. Acad. Sci. U. S. A.*, 2007, **104**, 16793–16797.

167. J. A. Codelli, J. M. Baskin, N. J. Agard, and C. R. Bertozzi, *J. Am. Chem. Soc.*, 2008, **130**, 11486–11493.

168. R. D. Bach, *J. Am. Chem. Soc.*, 2009, **131**, 5233–5243.

169. V. Bouvet, M. Wuest, and F. Wuest, *Org. Biomol. Chem.*, 2011, **9**, 7393–7399.

170. S. Arumugam, J. Chin, R. Schirrmacher, V. V Popik, and A. P. Kostikov, *Bioorg. Med. Chem. Lett.*, 2011, **21**, 6987–6991.

171. L. S. Campbell-Verduyn, L. Mirfeizi, A. K. Schoonen, R. A. Dierckx, P. H. Elsinga, and B. L. Feringa, *Angew. Chem. Int. Ed.*, 2011, **50**, 11117–11120.

172. H. L. Kim, K. Sachin, H. J. Jeong, W. Choi, H. S. Lee, and D. W. Kim, *ACS Med. Chem. Lett.*, 2015, **6**, 402–407.

173. S. B. Lee, H. L. Kim, H.-J. Jeong, S. T. Lim, M.-H. Sohn, and D. W. Kim, *Angew. Chem. Int. Ed.*, 2013, **52**, 10549–10522.

174. M. L. Blackman, M. Royzen, and J. M. Fox, *J. Am. Chem. Soc.*, 2008, **130**, 13518–13519.

175. J. C. Knight, S. Richter, M. Wuest, J. D. Way, and F. Wuest, *Org. Biomol. Chem.*, 2013, **11**, 3817–3825.

176. X.-G. Li, A. Roivainen, J. Bergman, A. Heinonen, F. Bengel, T. Thum, and J. Knuuti, *Chem. Commun.*, 2015, **51**, 9821–9824.

177. Z. Li, H. Cai, M. Hassink, M. L. Blackman, R. C. D. Brown, P. S. Conti, and J. M. Fox, *Chem. Commun.*, 2010, **46**, 8043–8045.

178. R. Selvaraj, S. Liu, M. Hassink, C. W. Huang, L. P. Yap, R. Park, J. M. Fox, Z. Li, and P. S. Conti, *Bioorganic Med. Chem. Lett.*, 2011, **21**, 5011–5014.

179. H. Wu, S. Liang, S. Liu, Y. Pan, D. Cheng, and Y. Zhang, *Nucl. Med. Commun.*, 2013, **34**, 701–708.

180. J. C. Knight and B. Cornelissen, *Am. J. Nucl. Med. Mol. Imaging*, 2014, **4**, 96–113.

181. C. Denk, D. Svatunek, T. Filip, T. Wanek, D. Lumpi, J. Fröhlich, C. Kuntner, and H. Mikula, *Angew. Chem. Int. Ed.*, 2014, **53**, 9655–9659.

182. N. K. Devaraj, G. M. Thurber, E. J. Keliher, B. Marinelli, and R. Weissleder, *Proc. Natl. Acad. Sci.*, 2012, 109, 4762–4767.

183. J. Becaud, L. Mu, M. Karramkam, P. a Schubiger, S. M. Ametamey, K. Graham, T. Stellfeld, L. Lehmann, S. Borkowski, D. Berndorff, L. Dinkelborg, A. Srinivasan, R. Smits, and B. Koksch, *Bioconjug. Chem.*, 2009, **20**, 2254–2261.

184. U. Roehn, J. Becaud, L. Mu, A. Srinivasan, T. Stellfeld, A. Fitzner, K. Graham, L. Dinkelborg, A. P. Schubiger, and S. M. Ametamey, *J. Fluor. Chem.*, 2009, **130**, 902–912.

185. O. Jacobson, L. Zhu, Y. Ma, I. D. Weiss, X. Sun, G. Niu, D. O. Kiesewetter, and X. Chen, *Bioconjug. Chem.*, 2011, **22**, 422–428.

186. Y. Li, Z. Liu, J. Lozada, M. Q. Wong, K.-S. Lin, D. Yapp, and D. M. Perrin, *Nucl. Med. Biol.*, 2013, **40**, 959–966.

187. R. Schirrmacher, G. Bradtmöller, E. Schirrmacher, O. Thews, J. Tillmanns, T. Siessmeier, H. G. Buchholz, P. Bartenstein, B. Wängler, C. M. Niemeyer, and K. Jurkschat, *Angew. Chem. Int. Ed.*, 2006, **45**, 6047–6050.

188. C. A. D'Souza, W. J. McBride, R. M. Sharkey, L. J. Todaro, and D. M. Goldenberg, *Bioconjug. Chem.*, 2011, **22**, 1793–1803.

189. L. Iovkova, B. Wängler, E. Schirrmacher, R. Schirrmacher, G. Quandt, G. Boening, M. Schürmann, and K. Jurkschat, *Chem. Eur. J.*, 2009, **15**, 2140–2147.

190. C. Wa, B. Waser, A. Alke, L. Iovkova, H. Buchholz, S. Niedermoser, K. Jurkschat, C. Fottner, P. Bartenstein, R. Schirrmacher, and J. Reubi, *Bioconjug. Chem.*, 2010, **21**, 2289–2296.

191. J. Zhu, S. Li, C. Wängler, B. Wängler, R. Bruce Lennox, and R. Schirrmacher, *Chem. Commun.*, 2015, **51**, 12415–12418.

192. R. Ting, M. J. Adam, T. J. Ruth, and D. M. Perrin, *J. Am. Chem. Soc.*, 2005, **127**, 13094–13095.

193. W. J. McBride, C. A. D'Souza, R. M. Sharkey, H. Karacay, E. A. Rossi, C.-H. Chang, and D. M. Goldenberg, *Bioconjug. Chem.*, 2010, **21**, 1331–1340.

194. R. Ting, C. Harwig, U. auf dem Keller, S. McCormick, P. Austin, C. M. Overall, M. J. Adam, T. J. Ruth, and D. M. Perrin, *J. Am. Chem. Soc.*, 2008, **130**, 12045–12055.

195. Y. Li, J. Guo, S. Tang, L. Lang, X. Chen, and D. M. Perrin, *Am. J. Nucl. Med. Mol. Imaging*, 2013, **3**, 44–56.

196. C. A. D'Souza, W. J. McBride, R. M. Sharkey, L. J. Todaro, and D. M. Goldenberg, *Bioconjug. Chem.*, 2011, **22**, 1793–1803.

197. S. Liu, H. Liu, H. Jiang, Y. Xu, H. Zhang, and Z. Cheng, *Eur. J. Nucl. Med. Mol. Imaging*, 2011, **38**, 1732–1741.

198. W. J. McBride, C. A. D'Souza, H. Karacay, R. M. Sharkey, and D. M. Goldenberg, *Bioconjug. Chem.*, 2012, **23**, 538–547.

199. W. Wan, N. Guo, D. Pan, C. Yu, Y. Weng, S. Luo, H. Ding, Y. Xu, L. Wang, L. Lang, Q. Xie, M. Yang, and X. Chen, *J. Nucl. Med.*, 2013, **54**, 691–698.

200. M. B. Cohen, L. Spolter, C. C. Chang, N. S. MacDonald, J. Takahashi, and D. D. Bobinet, *J. Nucl. Med.*, 1974, **15**, 1192–1195.

201. M. G. Straatmann and M. J. Welch, *Radiat. Res.*, 1973, **56**, 48.

202. K. Ishiwata, T. Ido, H. Sato, R. Iwata, K. Kawashima, K. Yanai, S. Watanuki, H. Ohtomo, and K. Kogure, *Eur. J. Nucl. Med.*, 1986, **11**, 449–452.

203. A. S. Gelbard, D. S. Kaseman, K. C. Rosenspire, and A. Meister, *Int. J. Nucl. Med. Biol.*, 1985, **12**, 235–242.

204. J. R. Ropchan and J. R. Barrio, *J. Nucl. Med.*, 1984, **25**, 887–892.

205. P. Bjurling, Y. Watanabe, and B. Långström, *Int. J. Radiat. Appl. Instrumentation. Part A. Appl. Radiat. Isot.*, 1988, **39**, 627–630.

206. E. Eriks-Fluks, P. H. Elsinga, N. H. Hendrikse, E. J. F. Franssen, and W. Vaalburg, *Appl. Radiat. Isot.*, 1998, **49**, 811–813.

207. S. Kaneko, K. Ishiwata, K. Hatano, H. Omura, K. Ito, and M. Senda, *Appl. Radiat. Isot.*, 1999, **50**, 1025–1032.

208. H. Deng, S. L. Cobb, A. D. Gee, A. Lockhart, L. Martarello, R. P. McGlinchey, D. O'Hagan, and M. Onega, *Chem. Commun.*, 2006, 652–654.

209. T. Smith, University of Aberdeen, M. Onega, and D. O'Hagan, University of St Andrews, *Unpublished Results*.

210. A. Salskov, V. S. Tammisetti, J. Grierson, and H. Vesselle, *Semin. Nucl. Med.*, 2007, **37**, 429–439.

211. S. Lehel, G. Horváth, I. Boros, P. Mikecz, T. Márián, and L. Trón, *J. Radioanal. Nucl. Chem.*, 2000, **245**, 399–401.

212. S. Lehel, H. Horvath, I. Boros, T. Marian, and L. Tron, *J. Radioanal. Nuc. Chem.*, 2002, **251**, 413–416.

213. M. Winkler, J. Domarkas, L. F. Schweiger, and D. O'Hagan, *Angew. Chem. Int. Ed.*, 2008, **47**, 10141–10143.

214. C. L. Ho, M. K. Cheung, S. Chen, T. T. Cheung, Y. L. Leung, K. C. Cheng, and W. D. Yeung, *Mol. Imaging*, 2012, **11**, 229–239.

215. T. Mori, L.-Q. Sun, M. Kobayashi, Y. Kiyono, H. Okazawa, T. Furukawa, H. Kawashima, M. J. Welch, and Y. Fujibayashi, *Nucl. Med. Biol.*, 2009, **36**, 155–162.

216. J. Marik, A. Ogasawara, B. Martin-McNulty, J. Ross, J. E. Flores, H. S. Gill, J. N. Tinianow, A. N. Vanderbilt, M. Nishimura, F. Peale, C. Pastuskovas, J. M. Greve, N. van Bruggen, and S. P. Williams, *J. Nucl. Med.*, 2009, **50**, 982–990.

217. D. E. Ponde, C. S. Dence, N. Oyama, J. Kim, Y. Tai, R. Laforest, B. A. Siegel, and M. J. Welch, *J. Nucl. Med.*, 2007, **48**, 420–428.

218. J. M. Jeong, D. S. Lee, J.-K. Chung, M. C. Lee, C.-S. Koh, and S. S. Kang, *J. Label. Compd. Radiopharm.*, 1997.

219. H. Roth and R. Kuhn, *Ber. Dtsch. Chem. Ges. B*, 1933, **66**, 1274.

220. K.-R. Oxidation, in *Comprehensive Organic Name Reactions and Reagents*, John Wiley & Sons, Inc., Hoboken, NJ, USA, 2010.

221. X.-G. Li, J. Domarkas, and D. O'Hagan, *Chem. Commun.*, 2010, **46**, 7819–7821.

222. M. Onega, J. Domarkas, H. Deng, L. F. Schweiger, T. A. D. Smith, A. E. Welch, C. Plisson, A. D. Gee, and D. O'Hagan, *Chem. Commun.*, 2010, **46**, 139–141.

223. S. Dall'Angelo, N. Bandaranayaka, A. D. Windhorst, D. J. Vugts, D. van der Born, M. Onega, L. F. Schweiger, M. Zanda, and D. O'Hagan, *Nucl. Med. Biol.*, 2013, **40**, 464–470.

2. Synthesis and evaluation of an alkynyl-bearing substrate for the fluorinase

2.1. Modified fluorinase substrates

The fluorinase enzyme has found applications for positron emission tomography through the synthesis of [^{18}F]-FDA **22** and its subsequent modification, as discussed in the previous chapter.[1–3] We were interested in exploring novel ways of using the fluorinase for [^{18}F]-labelling of biomolecules through the design of modified substrates.

When the fluorinase was first discovered, the substrate scope of the enzyme was explored. Investigations showed that the fluorinase utilised chloride ion as a substrate for the synthesis of 5'-chloro-5'-deoxyadenosine **23** (ClDA) (**Scheme 1**).[4] This reaction does not proceed in the forward direction under standard conditions, i.e. incubation of the enzyme with SAM **20** and chloride, but required the presence of an L-amino acid oxidase (L-AAO). The native fluorinase-catalysed reaction of SAM **20** to FDA **22** is an equilibrium process lying in favour of FDA **22**. The synthesis of ClDA **23** is also an equilibrium process, but the equilibrium lies heavily in favour of SAM **20** and chloride ion. This equilibrium is moved in favour of ClDA **23** production by the removal of L-methionine **21** by L-AAO.

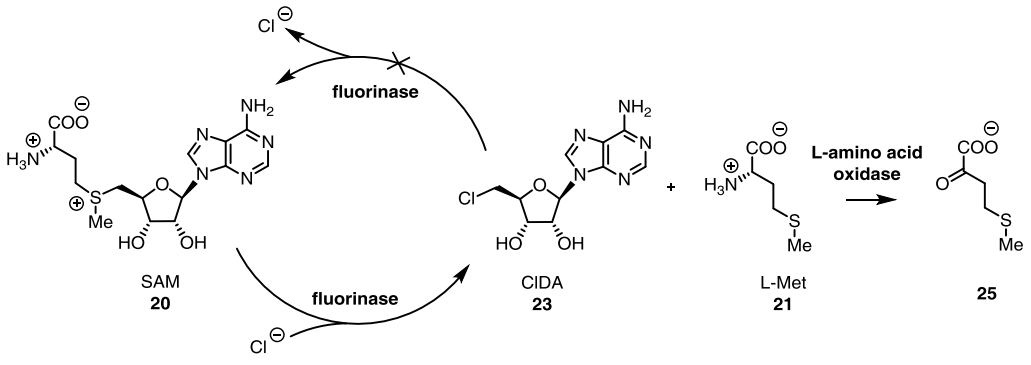

Scheme 1. Fluorinase reaction using chloride ion as the nucleophile to generate ClDA **23**, while L-methionine **21** is removed by of L-AAO, generating the corresponding α-oxo acid **25**.

The equilibrium relationship between ClDA **23**, SAM **20**, and FDA **22** led to the discovery of a fluorinase-catalysed transhalogenation reaction.[4] Incubation of ClDA **23** with the fluorinase and fluoride ion in the presence of catalytic L-methionine gave

SAM **20**, which then undergoes a fluorinase-catalysed reaction with fluoride ion in a one-pot transformation to FDA **22**, as shown in **Scheme 2**.

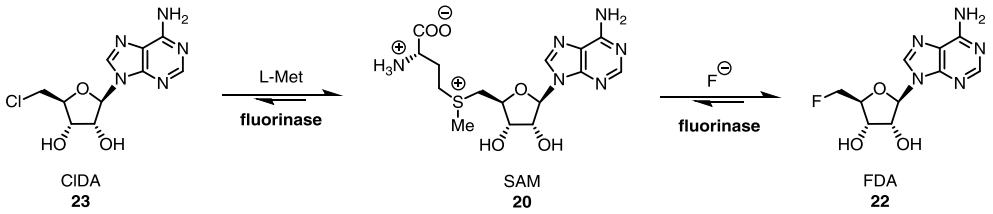

Scheme 2. Fluorinase-catalysed transhalogenation in water, where ClDA **23** reacts with L-Met to give SAM **20**, which then reacts with fluoride ion to generate FDA **22**.

The brominated analogue, 5'-bromo-5'-deoxyadenosine (BrDA) was also investigated as a substrate for the fluorinase. In the presence of fluoride ion, BrDA was converted to FDA **22**.[5] This conversion was, however, independent of the presence of L-methionine. It was hypothesised that rather than the bromine atom occupying the fluoride binding site, it was located in the sulfonium binding site (as had been observed for the chloro analogue in the active site of the fluorinase ClDA **23** co-crystal structure).[4] Bromine atom is acting as a surrogate for the sulfonium leaving group of SAM **20**. While this allows for direct conversion of BrDA to FDA **23**, the brominated substrate was not a true fluorinase substrate as no SAM **20** intermediate is involved. Bromide and iodide were also explored as substrates in the L-AAO coupled assays, but no brominated or iodinated products were observed.[5]

A range of L-methionine **21** analogues were also investigated.[5] L-Selenomethionine **161** proved an excellent substrate for the fluorinase, generating FDA **22** from ClDA **23** at 6 × the rate compared to L-methionine (**Scheme 3**).[4] L-Selenomethionine is a better nucleophile than L-methionine due to the presence of a higher energy HOMO on the chalcogen atom. It is also a better leaving group due to the larger and more polarisable selenium atom, which is able to stabilise the departing electron pair more efficiently. Other L-methionine **21** analogues were also investigated as substrates, including **162** to **166** shown in **Scheme 3**. Only D-methionine **162** generated traces of FDA **22**, while the remaining analogues showed no conversion. It has been recently reported that the *N*-methylaza-SAM analogue **167** (**Scheme 3**) is a substrate for the fluorinase with [^{18}F]fluoride, generating [^{18}F]FDA [^{18}F]-**22**.[6]

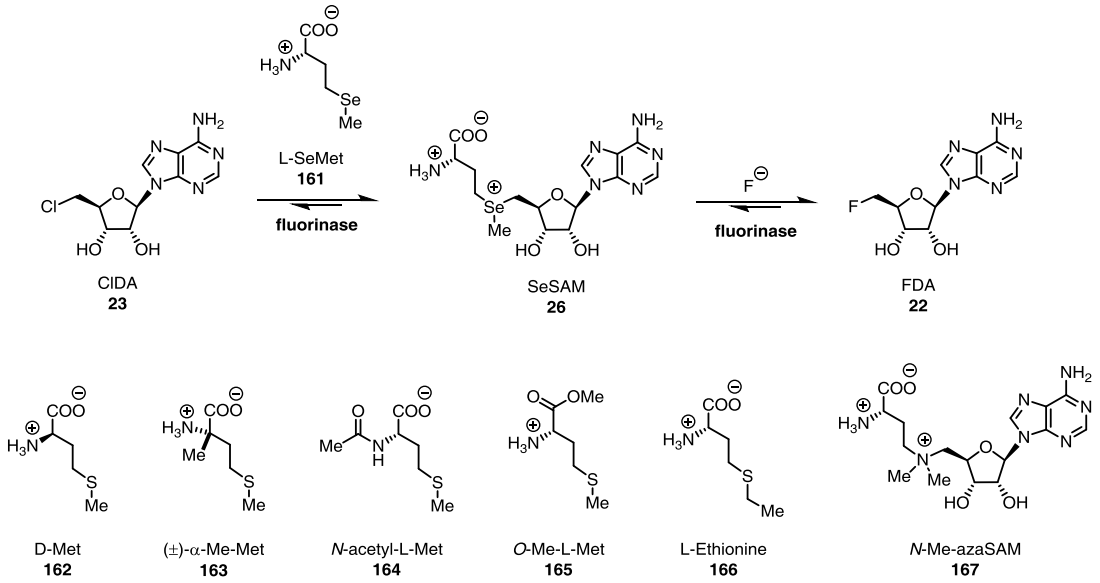

Scheme 3. A fluorinase catalysed transhalogenation in the presence of L-selenomethionine **161** led to the efficient generation of FDA **22**. L-Methionine analogues (**162** to **166**) were not substrates for the fluorinase enzyme, while **167** has been reported to generate [^{18}F]FDA [^{18}F]-**22** in the presence of fluorinase and [^{18}F]fluoride.

A number of modified nucleosides have also been explored as substrates for the fluorinase, shown in **Scheme 4**. The carbacyclic nucleoside **168** was investigated as a substrate, however it did not undergo transhalogenation, emphasising the importance of the endocyclic oxygen for catalysis.[7]

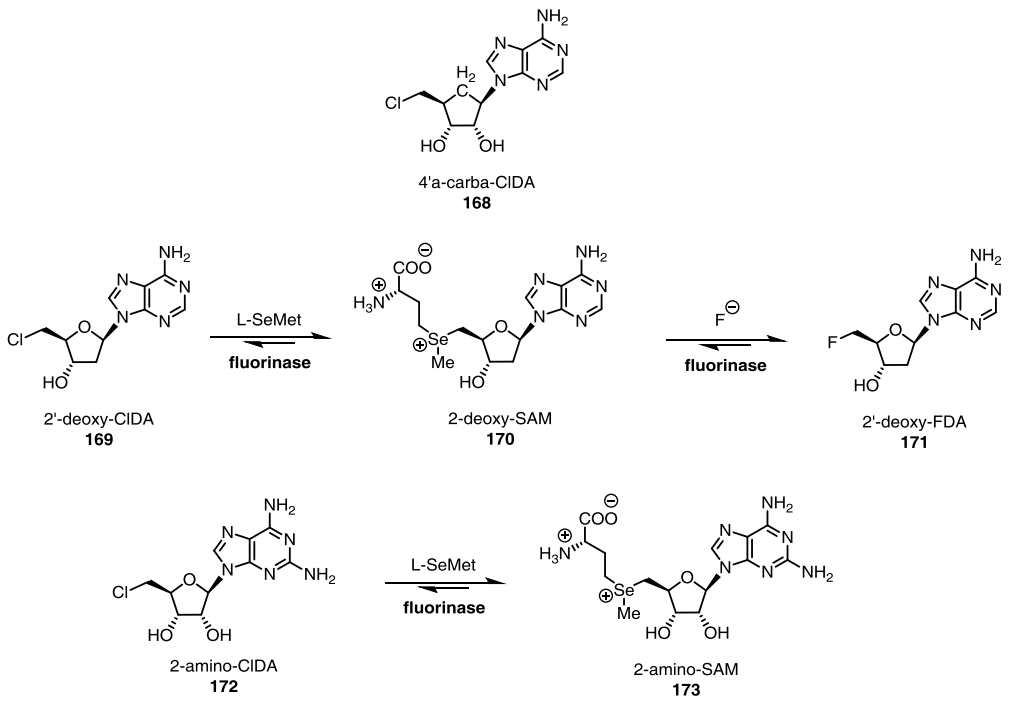

Scheme 4. Modified nucleosides explored as substrates for the fluorinase.

The 2'-deoxy **169** analogue was prepared and assessed as a substrate for fluorinase catalysed transhalogenation. 2'-Deoxy-ClDA **169** proved to be a substrate, and did generate 2'-deoxy-FDA **171**. This reaction proceeded at approximately 50% the rate of ClDA **23**.[8]

2-Amino substrate **172** was efficiently transformed into the corresponding 2-amino-SAM **173** analogue by the fluorinase.[5] Examination of the crystal structure of the fluorinase bound to SAM **20** (**Figure 1 A** and **Figure 1 B**)[9] revealed that the C-2 position of the adenine base is oriented towards the surface of the enzyme at the interface of two subunits. Plotting the inner surface of the active site (**Figure 1 C**) reveals a "hole" which aligns with the C-2 position, and it is possible that the amine substituent of **172** is accommodated in this free space.

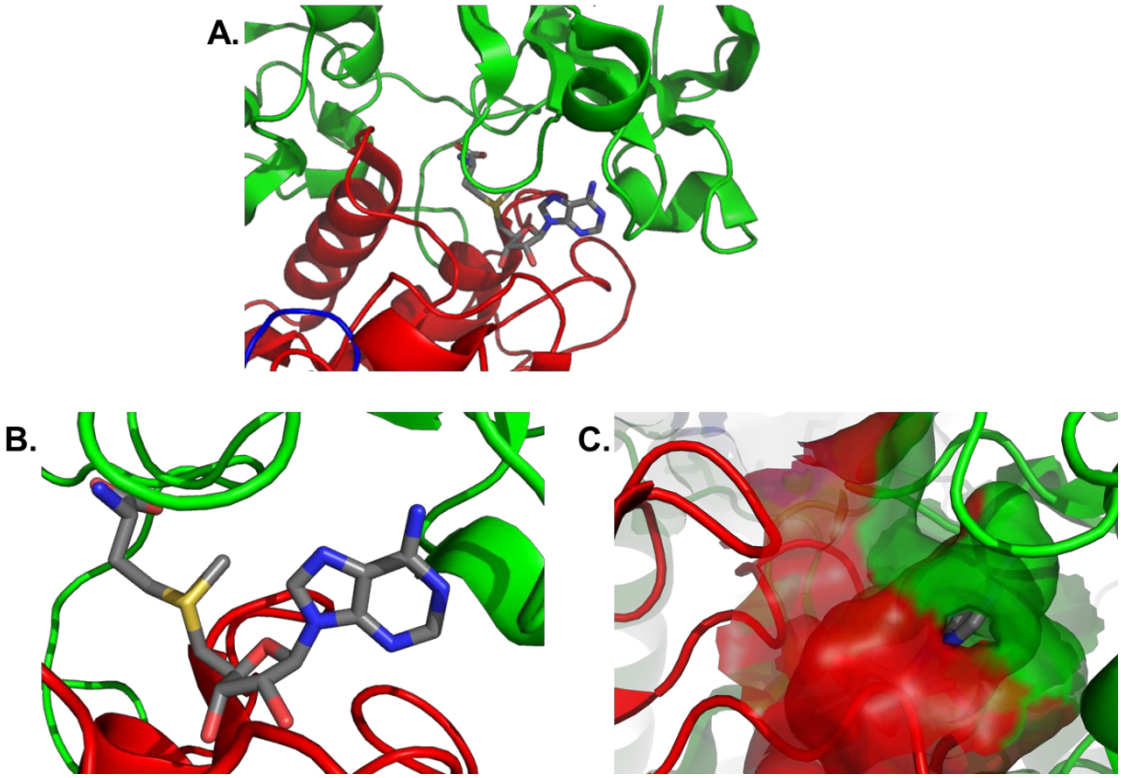

Figure 1. **A**. Crystal structure of the fluorinase bound to its native substrate, SAM **20** showing the active site located near the surface of the enzyme. **B**. A closer view of SAM **20** in the active site of the fluorinase, between two monomers of the fluorinase shown in green and red. **C**. The surface profile of the active site, showing a hole in this surface which aligns with C-2 of the adenine of SAM **20**.

We were intrigued by this apparent "hole" in the active site, and wished to further explore the C-2 position as a site of further substrate modification, where such modification to incorporate a reactive group would improve the scope of fluorinase as a biocatalyst.

Towards this end, we envisaged substituting the C-2 position of ClDA **23** with a small reactive group which would be suitable for bio-orthogonal reaction after enzymatic fluorination. An alkyne was an immediate candidate, as it is linear and offers low steric impact and was envisaged to project through the "hole" in the active site. In addition, the alkyne would be available for reaction with an appropriately substituted azide, through a copper-catalysed alkyne-azide cycloaddition (CuAAC), coupling the fluorinase to "click" chemistry, an established protocol for bioconjugations for PET appplications.[10]

2.2. Aims

Modifying the substrate of the fluorinase at C-2 of adenine with an acetylene moiety generates 5'-chloro-2-ethynyl-5'-deoxyadenosine **174** (ClDEA), which became a synthetic target. The fluorinated analogue, 5'-fluoro-2-ethynyl-5'-deoxyadenosine **176** (FDEA), was also required as a reference compound. ClDEA **174** would be investigated as a fluorinase substrate for the generation of selenoethynyl-SAM intermediate **175** (SeEAM), which was proposed to undergo fluorination in the presence fluoride to generate FDEA **176**, as shown in **Scheme 5**. Bioconjugation of the enzymatically synthesised FDEA **176** to a relevant biomolecule, such as an azide modified peptide, is clearly attractive. If successful, the goal would be to transfer this system to the PET environment for radiolabelling of peptides.

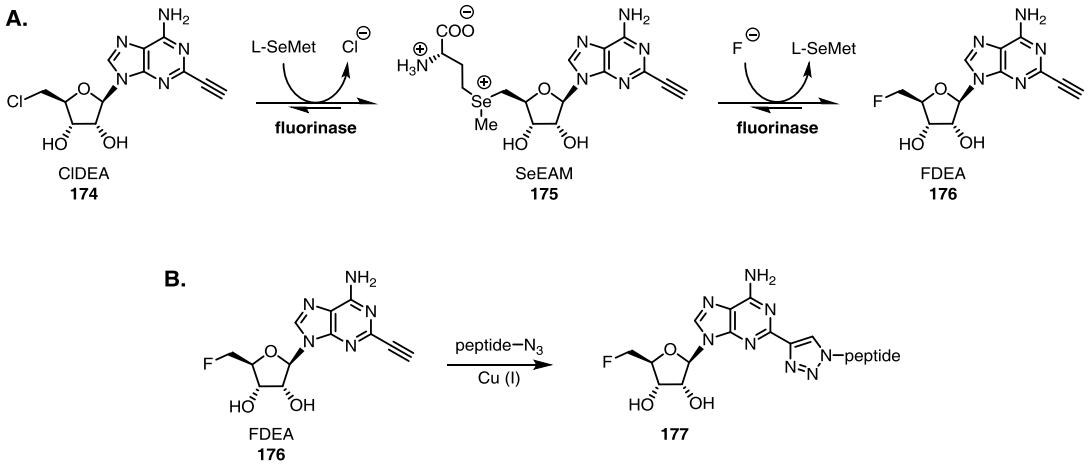

Scheme 5. **A.** ClDEA **174** will be explored as a transhalogenation substrate for the fluorinase. **B.** The resultant FDEA **176** will be explored in a CuAAC reaction with an azide-labelled peptide to generate triazole **177**.

Utilisation of [^{18}F]fluoride as a fluoride source offers a two-step radiolabelling protocol where [^{18}F]FDEA [^{18}F]-**176** acts as a prosthetic group for coupling to biomolecules of interest. Unlike most radiolabelling procedures with fluorine-18, which use heating, organic solvents and high temperatures, if successful, the synthesis of this radiolabel would take place under aqueous conditions at neutral pH, ideal for biomolecules.

2.3. Synthesis of an ethynyl substrate for the fluorinase

While both ClDEA **174** and FDEA **176** are novel compounds, the 5'-hydroxy analogue, 2-ethynyladenosine **180**, has been synthesised by two strategies. The first, reported by Matsuda *et al.*[11–13] and Nair *et al.*,[14] started from guanosine **178**, and through a series of functional group manipulations, generated iodoadenosine **179** as a key intermediate. The report utilised **179** in Sonogashira couplings with a variety of alkynes, including ethynyltrimethylsilane, which, after deprotection, furnished 2-ethynyladenosine **180**, as shown in **Scheme 6 A**.

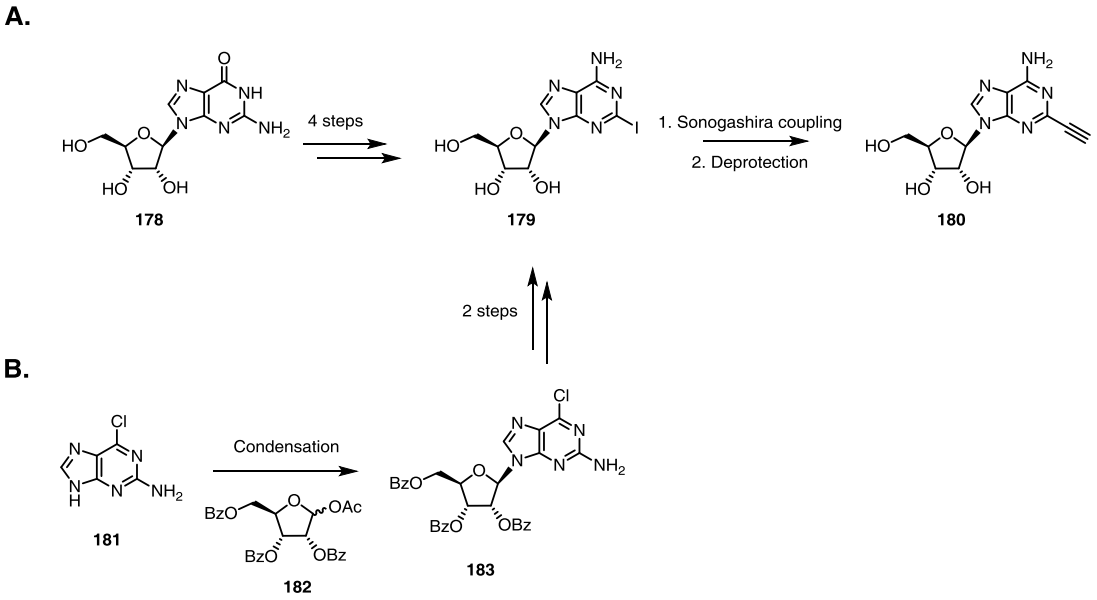

Scheme 6. Synthetic route to 2-ethynyladenosine **180** from **A.** guanosine **178** as described by Matsuda *et al.*[11–13] and Nair *et al.*[14] and **B.** from 2-amino-6-chloropurine **181** as described by Lee *et al.*[15]

Lee *et al.*[15] coupled a substituted purine **181** to ribosyl donor **182** to generate protected nucleoside **183**, which was also converted to 2-iodoadenoisine **179**, and on to 2-ethynyladenosine **180** *via* the same route as Matsuda and Nair. [11–14]

The route from guanosine described by Matsuda and Nair [11–14] avoids coupling of a ribosyl donor to the base, where generation of α- and β- anomers is possible. Therefore, synthesis of **180** from guanosine, and subsequent chlorination or fluorination would be expected to give targets ClDEA **174** and FDEA **176** respectively.

2.3.1. Synthesis of 5'-chloro-2-ethynyl-5'-deoxyadenosine (ClDEA) 174

Guanosine **178** was heated in the presence of acetic anhydride and pyridine in dimethylformamide (DMF) to furnish per-*O*-acetylated guanosine **184** (**Scheme 7**). The product was recrystallised from isopropanol to give **184** as a white powder in 85% yield.

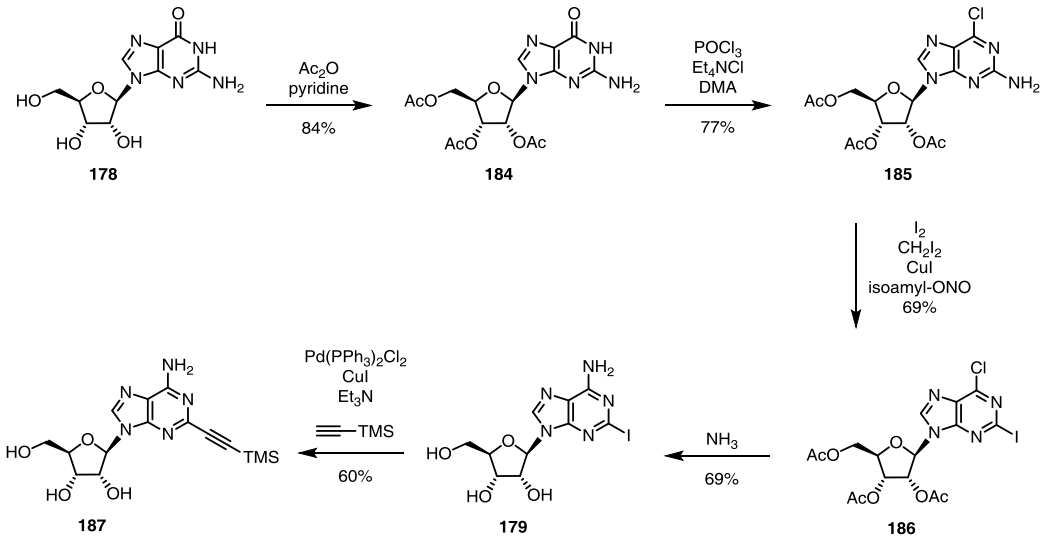

Scheme 7. Synthetic route to 2-(trimethylsilylethynyl)adenosine **187** from guanosine **178**.

Chlorination at the 6-position of the nucleoside had been reported to be poor yielding and difficult to replicate,[16] and has been investigated by Robins *et al.*[17] They determined that while the initial activation of the oxygen at C-6 of **184** was rapid, attack of chloride to form the Meisenheimer complex, and subsequent departure of oxygen was slow. They also found that the intermediate phosphorodichloridate was prone to decomposition, leading to low yields and that the addition of another chloride ion source, such as Et_4NCl, led to improved yields.

The reaction required a meticulously dry source of highly hygroscopic Et_4NCl. Thus recrystallisation of Et_4NCl from absolute ethanol followed by drying over P_2O_5 *in vacuo* afforded the dry salt. This consistently provided higher yields of the chlorinated product. The reaction yield was low when performed on any scale larger than ~1 g or when left to react for longer than 30 minutes.

The optimised reaction was carried out by heating **184** in a solution of dry acetonitrile, $POCl_3$, dry Et_4NCl and dimethylaniline (DMA) in small batches (<1 g), in parallel reactions, to furnish **185** in 77% yield.

Chlorinated nucleoside **185** was subject to diazotization in the presence of iso-amyl nitrite and copper (I) iodide in refluxing THF in a Sandmeyer-type reaction. The aryl radical formed after expulsion of N_2 is quenched *in situ* by either diiodomethane or molecular iodine, generating **186** in 69% yield.[18]

2-Iodoadenosine **179** was synthesised by heating **189** in a freshly saturated solution of ammonia in methanol in a sealed tube for 16 hours. The acetyl protecting groups are concomitantly cleaved by aminolysis during this reaction. The product was purified from the reaction mixture by recrystallisation from water to give **179** as a colourless powder in 69% yield.

The key reaction for installing the acetylene functionality involved a Sonogashira coupling of **179** to ethynyltrimethylsilane in the presence of $Pd(PPh_3)_2Cl_2$ and copper (I) iodide, as shown in **Scheme 8**. The yields for the reaction were found to be moderate, furnishing **187** in 60% yield, giving access to the desired protected acetylenic compound.

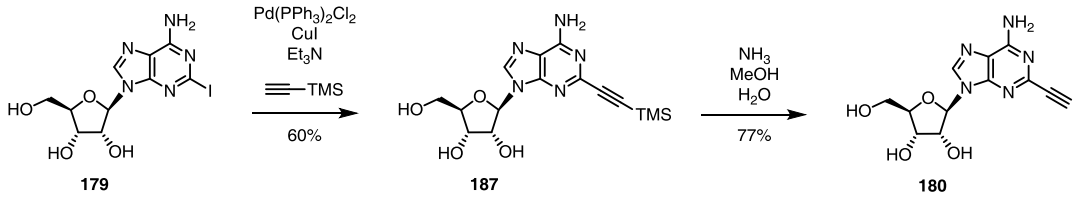

Scheme 8. Synthesis of 2-ethynyladenosine **180** from 2-iodoadenosine **179**.

Conventional silyl deprotection of **187** with TBAF in THF furnished the free acetylene **180**. The product, however, proved difficult to separate from residual tetrabutylammonium salts. A fluoride-free deprotection method was investigated using 30% methanolic ammonia solution, as reported by Lee *et al.*,[15] and this furnished **180** as a pale brown powder after purification by recrystallisation from water (77% yield).

With acetylene **180** in hand, attention turned to chlorination at the 5'-position. Robins *et al.*[19] have reported a method for the chlorination of adenosine **188** directly using thionyl chloride and pyridine in acetonitrile. The procedure generates a 2',3'-cyclic sulfite intermediate, which can be isolated and characterised, before hydrolysis with aqueous ammonia in methanol (**Scheme 9**) yields the chlorinated product. Upon trialling this reaction with adenosine **188**, it was found that the intermediate

cyclic sulfite **189** need not be isolated, and that after concentration, the crude cyclic sulfite **189** was hydrolysed directly to **23** in quantitative yield.

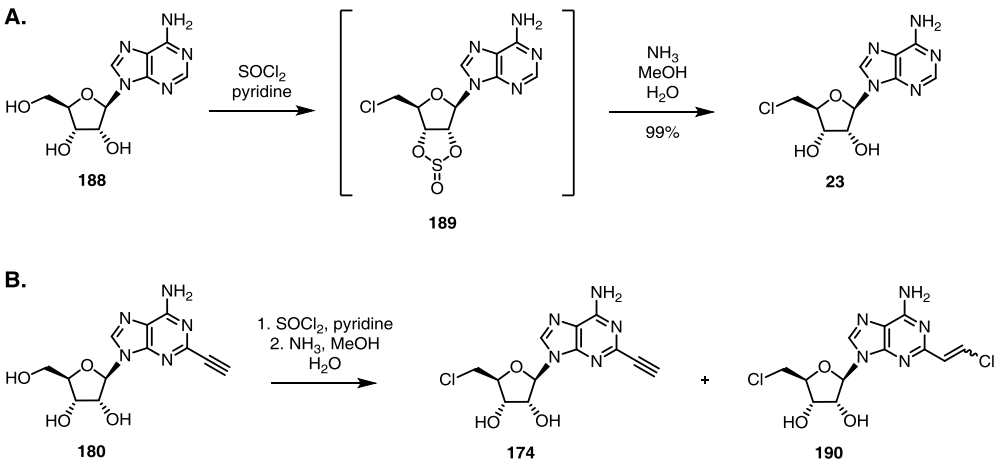

Scheme 9. **A.** Synthesis of 5'-chloro-5'-deoxyadenosine **23** via the cyclic sulfite intermediate. **B.** Chlorination of ethynyladenosine **180** gave the desired compound **174** in low yield, with an inseparable dichlorinated by-product **190**.

Repeating these reaction conditions with 2-ethynyladenosine **180** afforded a mixture of two products that could not easily be separated. LC-MS of this mixture resolved two compounds: ClDEA **174**, with a *m/z* = 310 ($[M+H]^+$); and a dichlorinated species with a *m/z* = 346 and the characteristic isotope pattern for the presence of two chlorine atoms. This mass represents the addition of HCl to **174**. Based on this mass, the lack of a signal for an associated acetylenic proton in the ^{1}H NMR spectrum, and the presence of resonances associated with a distinctive AB system at 6.72 ppm suggested **190** (**Scheme 9**) as the structure of the adduct. The substitution pattern of the alkene was not determined.

It was found that by-product **190** was not formed when the chlorination reaction was performed directly on TMS-protected acetylene **187** (**Scheme 10**). The TMS group appears to protect the alkyne from HCl addition, and is conveniently cleaved during the hydrolysis of the cyclic sulfite. In the end, this synthetic route gave ClDEA **174** in a moderate yield (47%).

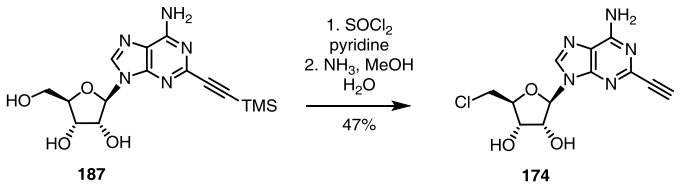

Scheme 10. Synthesis of ClDEA **174** directly from TMS-protected ethynyladenosine **187**.

Single crystal X-ray structure analysis of ClDEA **174** (**Figure 2**) revealed that the stereochemistry of the ribose ring was intact and the molecule adopted the South conformation (C2'-endo-C3'-exo) in the solid state. Interestingly, the linearity of the acetylene functionality was slightly distorted, showing a C-C≡C angle of 173.5°, likely due to crystal packing forces.

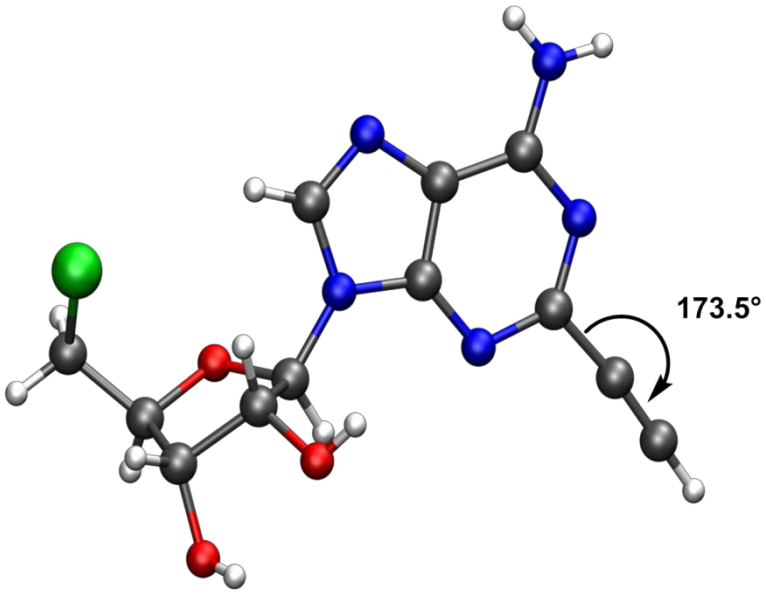

Figure 2. Single crystal X-Ray structure of ClDEA **174**. Data collected and refined by Prof. Alexandra Slawin at the University of St Andrews.

With the proposed new substrate for the fluorinase, ClDEA **174** in hand, we explored the synthesis of the anticipated product of the enzymatic transformation, FDEA **176**.

2.3.2. 5'-fluoro-2-ethynyl-5'-deoxyadenosine (FDEA) 176

Reported syntheses of 5'-fluorinated nucleosides often involve an initial activation of the 5'-position of a suitably protected nucleoside as a sulfonate ester.[20–22] Subsequent fluorination with a fluoride source such as tetrabutylammonium fluoride (TBAF) generates the fluorinated product. This approach, however, leads to the formation of cyclised by-products, where N-3 of the purine ring attacks the 5'-position, in an intramolecular substitution reaction. Aston *et al.*[23] and Spitale *et al.*[24] have reported a one-pot conversion of 5'-hydroxy compounds to 5'-fluoro compounds by the action of tosyl fluoride (TsF) and TBAF in refluxing THF. These are attractive conditions as they do not involve isolation of the sulfonate ester intermediate.

Protection of **187** as its acetonide, under the action of the 2,2-dimethoxypropane and Amberlyst 15 H^+, gave **191** (71% yield) as shown in **Scheme 11**. Fluorination of

acetonide **191** under the reported[23,24] TBAF-TsF conditions afforded fluorinated nucleoside **192** in 71% yield. During the reaction, the TMS group was cleaved by fluorolysis to generate the free alkyne. Fluorinated acetonide **192** was then hydrolysed in a 9:1 mixture of trifluoroacetic acid and water to furnish **176** (53% yield).

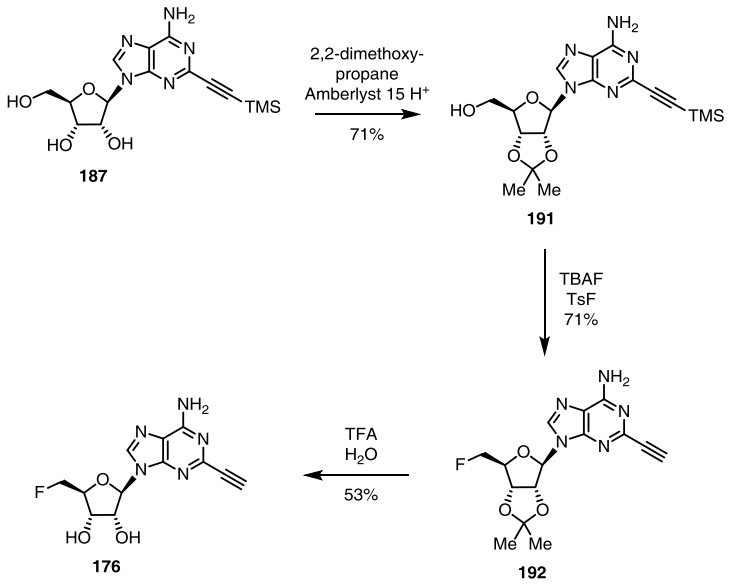

Scheme 11. Synthesis of the anticipated product of the fluorination reaction, FDEA **176**.

Single crystal X-ray structure analysis (**Figure 3**) of FDEA **176** showed that the fluorinated nucleoside adopts an almost identical conformation to ClDEA **174** in the solid state. The ribose ring was also observed in the South conformation (C2'-endo-C3'-exo) and the acetylene is marginally more distorted from linear than that of the acetylene of ClDEA **174**, with a C-C≡C angle of 171.6°.

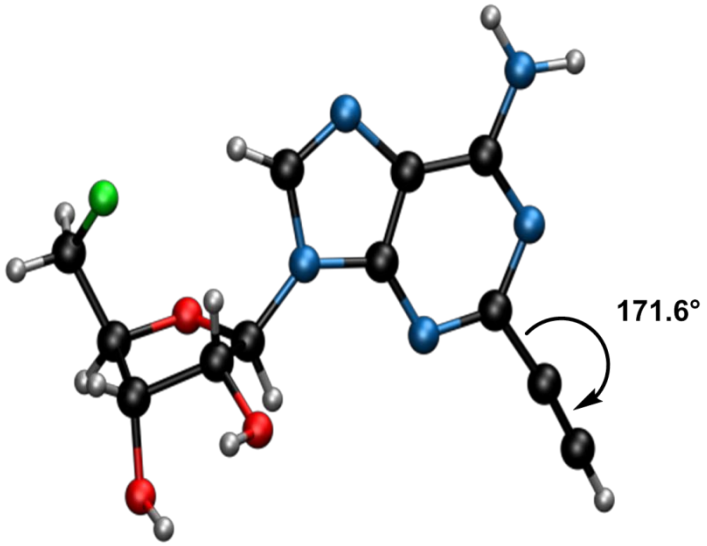

Figure 3. Single crystal X-Ray structure of FDEA **176**. Data collected and refined by Prof. Alexandra Slawin at the University of St Andrews.

With both ClDEA **174**, and FDEA **176** in hand, attention turned to over-expression and purification of the fluorinase for use in the appropriate assays.

2.4. Over-expression and purification of recombinant fluorinase

2.4.1. Fluorinase over-expression

The over-expression of a recombinant fluorinase in *Escherichia coli* using a Luria Broth (LB) and isopropyl β-D-1-thiogalactopyranoside (IPTG) based system has been reported previously.[9] This method uses *E. coli* BL21 Gold cells containing the pET-28a plasmid, into which the fluorinase gene has been cloned. This plasmid offers kanamycin resistance to the cells, while also incorporating an *N*-terminal polyHis tag onto the fluorinase.

Baffled shake flasks (2 L) containing LB media (1 L) containing kanamycin (50 μg/mL^{-1}) were inoculated with transformed *E. coli* and cultured at 37 °C until the optical density (OD_{600}) reached 0.6. Overexpression of the fluorinase was induced by addition of IPTG and the temperature was lowered to 30 °C. The cultures were incubated with shaking for 16 hours before harvesting by centrifugation.

Alternatively, the fluorinase was overexpressed using an autoinduction protocol.[25] This protocol uses a media containing a mixture of glucose, lactose and glycerol to control the *lac* operon and the induction of overexpression. During the initial stage of growth, glucose provides the primary energy source for the cells and strongly represses the activation of the *lac* operon by inhibiting lactose uptake *via* the membrane transporter lactose permease. Depletion of glucose reactivates lactose permease and lactose is transported into the cell, ceasing the repression of the *lac* operon. The cells are consequently induced to overexpress the desired protein.

In this case, autoinduction media (400 mL) containing kanamycin (100 $\mu g.mL^{-1}$) was inoculated with *E.coli* and the culture grown for 4 hours at 37 °C. The temperature was lowered to 16 °C and the cells were grown at this temperature for 48 hours. Cells were harvested by centrifugation and the same purification protocol used for the LB-IPTG method was followed.

The cells were disrupted after addition of DNAse, and the lysate clarified by centrifugation and filtration. The polyHis-tagged fluorinase was purified by affinity chromatography by trapping on a Ni^{2+} Sepharose column. Bound protein was eluted from the Ni^{2+} column using a high concentration (400 mM) imidazole buffer. SDS-PAGE analysis of samples taken throughout the purification process (**Figure 4**) showed that the elution fractions from the column contained fluorinase and were free from significant amounts of other proteins. Fractions containing the fluorinase were pooled and dialysed overnight against a low salt buffer (150 mM NaCl, 20 mM Tris-HCl pH 7.8) to remove imidazole and salt from the protein. The identity of the fluorinase was confirmed by mass spectrometry of a trypsin digest of the elution band from the SDS-PAGE gel.

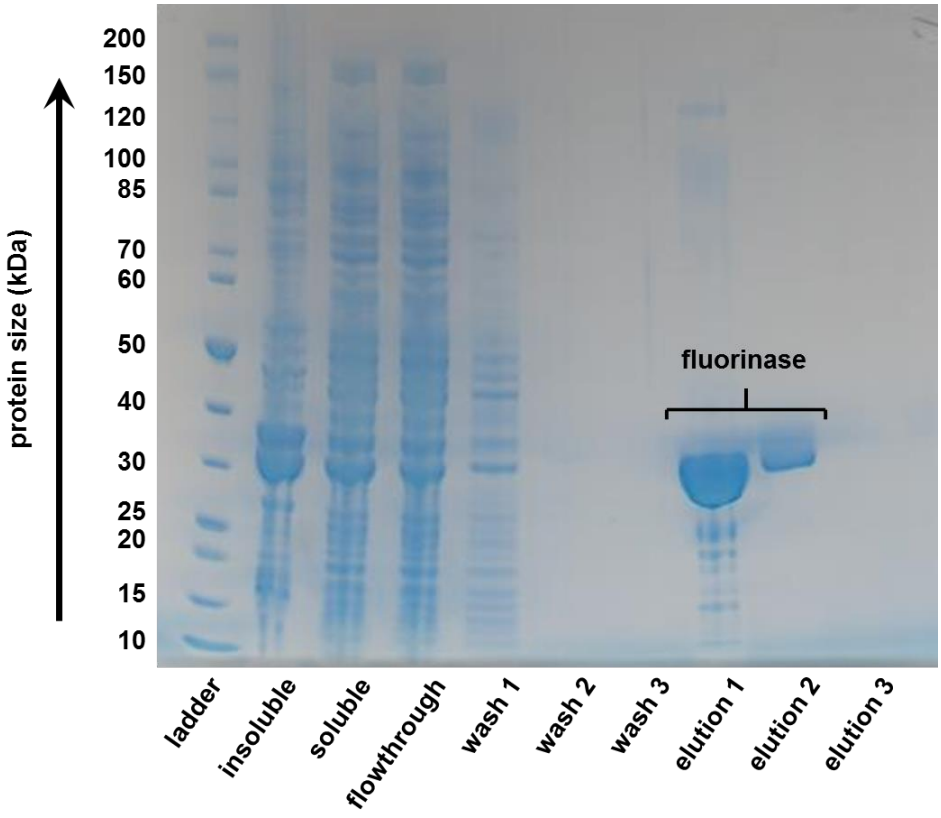

Figure 4. SDS-PAGE of the fluorinase, showing the insoluble and soluble fractions after centrifugation of the crude lysate, the flowthrough after loading of the clarified supernatant, the wash fractions (20 mM imidazole) and the elution fractions (400 mM imidazole). Some fluorinase is identified in the insoluble fraction and wash fractions, however yields of soluble enzyme were good.

Both induction methods furnish the fluorinase in high purity, however the yields for the autoinduction method tended to be higher per litre of culture. The average yield of fluorinase enzyme after the first Ni^{2+} column for the autoinduction method was 60 mg per litre of culture, while the yield for LB/IPTG induction method was 29 mg per litre of culture.

2.4.2. Removal of adenosine from the fluorinase

Recombinant fluorinase is known to co-purify with adenosine **188** (**Figure 5**) bound.[8] Previous isothermal titration calorimetry experiments had confirmed this binding, and found that adenosine **188** has a binding constant (K_a) of 12.2×10^5 M^{-1}, the same order of magnitude as FDA **22** (45.5×10^5 M^{-1}).[26] HPLC analysis of a denatured sample of the fluorinase from these preparations reveals that the protein did contain adenosine, and that **188** was not efficiently removed by dialysis.

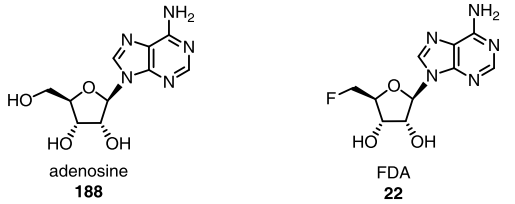

Figure 5. Comparison of adenosine **188** and the product of the fluorinase reaction, FDA **22**.

Adenosine **188** bound to the active site of the fluorinase can act as a competitive inhibitor for the enzyme. Adenosine can be removed from the enzyme by incubating the fluorinase-adenosine mixture with adenosine deaminase (ADA), an enzyme that irreversibly deaminates adenosine **188** to generate inosine **193** (**Scheme 12**).[26] Inosine **193**, unlike adenosine **188**, does not bind to the fluorinase and is readily dialysed away to give an apo-fluorinase for use in assays.

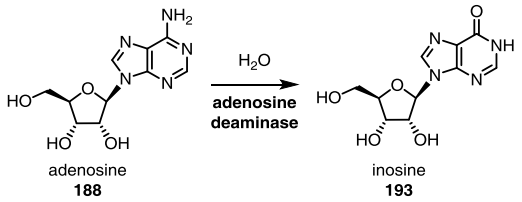

Scheme 12. Conversion of adenosine **188** to inosine **193** under the action of adenosine deaminase.

Two commercially available preparations of ADA were assessed for removal of adenosine **188**. The first, a recombinant human ADA expressed in *E. coli*, showed very low activity (reported to be less than 1 unit.mL^{-1}). Upon incubation with the fluorinase during dialysis, this preparation was found to be ineffective at removing adenosine **188** from the enzyme. The activity of the enzyme was found to vary between preparations.

A second commercial preparation of ADA, isolated directly from calf spleen, was found to be efficient at converting adenosine **188** to inosine **193**. This preparation of ADA had much higher activity (250 units.mL^{-1}) and converted 80–90% of the endogenous adenosine **188** to inosine **193**. The inosine **193** formed was removed by dialysis. A fluorinase preparation (100 to 200 mg fluorinase in 30 mL) was usually treated with 20–50 µL of this ADA preparation (equating to approx. 5 units ADA) at 4 °C overnight, while undergoing dialysis. HPLC analysis of fluorinase samples before and after ADA treatment confirmed the removal of adenosine from the fluorinase, as shown below in **Figure 6**. For crystallography and calorimetry experiments, where complete adenosine removal was required, the ADA treatment was repeated.

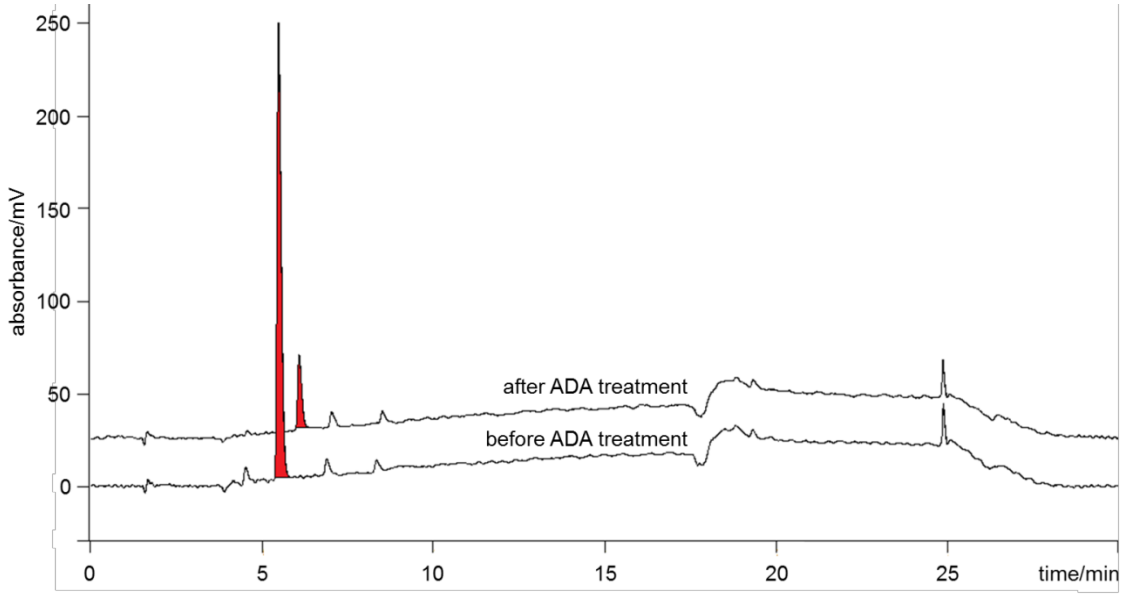

Figure 6. HPLC analysis of fluorinase samples before and after treatment by ADA. Adenosine **188** (red) has been reduced by 82% from the original isolate. Inosine is not observed as dialysis removes inosine from the sample as it is formed.

The protein solution was passed through a second Ni^{2+} column after ADA treatment to separate the two enzymes. ADA, as a preparation from calf spleen, does not bear a polyHis tag, and does not bind to the Ni^{2+} beads. The fluorinase was eluted from the column using a high-imidazole concentration (400 mM) buffer.

Although chloride is a poor substrate for the fluorinase, it is possible that chloride in the buffer could act as a (weak) competitive inhibitor for fluoride. This problem would be particularly pertinent when fluorinase is used for PET experiments where chloride ion concentration would be 6–9 orders of magnitude higher than [^{18}F]fluoride ion concentration. Consequently, chloride free buffers were used and the enzyme was dialysed into a phosphate buffer (50 mM, pH 7.8).

Post dialysis analysis showed the fluorinase as a single band on SDS-PAGE, as shown below in **Figure 7**, with no other proteins present. Concentration of the enzyme solution through a membrane-spin concentrator and storage at 4 °C, or freeze drying appropriate aliquots, furnished the fluorinase for use either in assays or for PET experiments respectively.

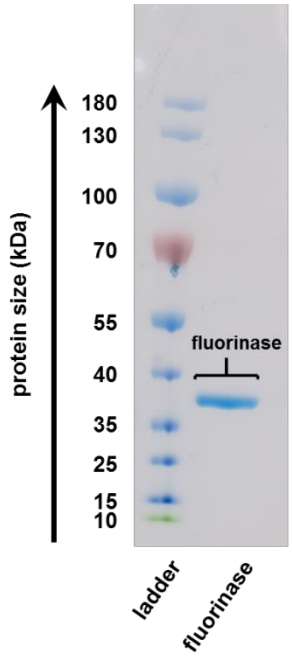

Figure 7. SDS-PAGE gel of the fluorinase post ADA treatment, after purification through a second Ni^{2+} Sepharose column to remove the adenosine deaminase. The fluorinase monomer (36.5 kDa) is a single band.

2.4.3. Cleavage of His-Tag for protein crystallisation

We also wished to prepare the fluorinase for use in crystallisation trials with the new ligands. This required cleavage of the polyHis tag from the *N*-terminus of the fluorinase. The fluorinase expressed from the pET-28a plasmid contains a thrombin cleavage site, as shown below in **Scheme 13**.

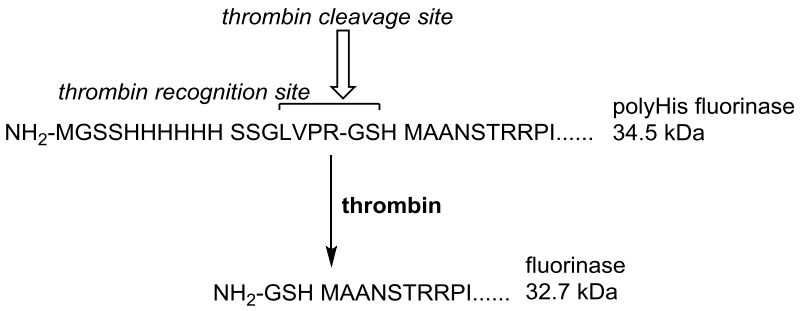

Scheme 13. Cleavage of the *N*-terminal polyHis tag from the recombinant fluorinase by thrombin to give a fluorinase which is 2 kDa smaller.

Incubation of the fluorinase with human thrombin at room temperature overnight cleaved the polyHis tag from the fluorinase, as evidenced by the SDS-PAGE shown in **Figure 8**. Since neither the fluorinase nor thrombin bore an affinity tag, the two species were separated by size exclusion chromatography (SEC). Thrombin has a molecular

weight of 33.6 kDa, while the fluorinase (monomer of 32.7 kDa) exists as a dimer of trimers with an effective mass 196 kDa. The mass difference allows for efficient separation of the fluorinase from thrombin and the cleaved polyHis tag by SEC. SEC also showed that the fluorinase exists as a monodisperse species in solution, ideal for crystallography. Pooling of fractions containing fluorinase and concentration (to 6 $mg.mL^{-1}$) using a membrane-spin concentrator gave a solution of the fluorinase, free of adenosine, and suitable for use in crystallisation trials.

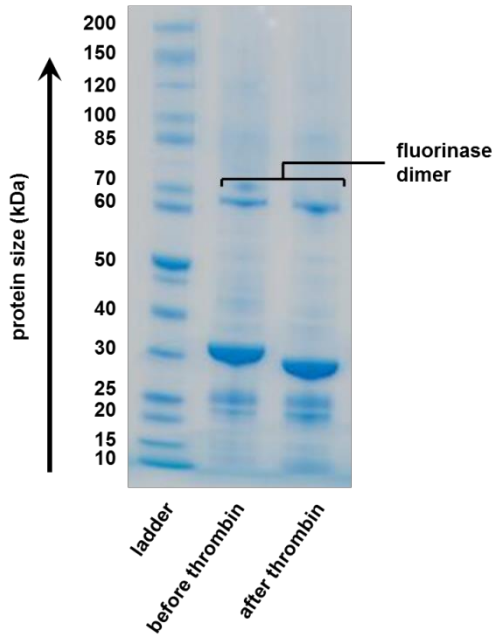

Figure 8. SDS-PAGE showing cleavage of the polyHis tag by incubation with thrombin. In some gels, a fluorinase dimer was observed, likely due to incomplete reduction of a disulfide bridge.

2.5. Evaluation of ClDEA 174 as a substrate for the fluorinase

With both the fluorinase and the candidate new substrates in hand, attention turned to investigating whether the fluorinase was able to catalyse a transhalogenation of ClDEA **174** to FDEA **176**.

2.5.1. Evaluation of ClDEA 174 as a substrate for the fluorinase

ClDEA **174** (0.2 mM), was incubated with a solution of the prepared fluorinase (5 $mg.mL^{-1}$) in phosphate buffer at pH 8, in the presence of fluoride ion (75 mM) and L-selenomethionine (0.1 mM) to assess the viability of the reaction, as illustrated below in **Scheme 14**.

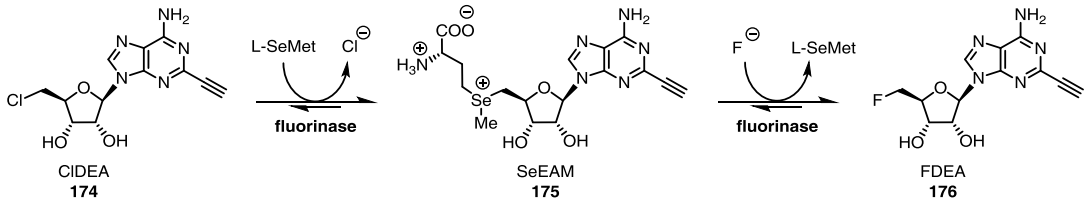

Scheme 14. Proposed fluorinase-catalysed-transhalogenation of the ethynyl-modified substrate ClDEA **174** to FDEA **176** proceeding through a selenoSAM intermediate **175**.

Reaction progress was monitored by HPLC analysis of aliquots of the reaction solution (**Figure 9**). The samples were heat-treated to 95 °C and centrifuged, to stop the reaction and precipitate the denatured fluorinase as a pellet respectively. A new peak was evident in the chromatograms at t_R = 7.8 min, which showed time dependent increase in peak area. This peak was confirmed to be FDEA **176** by comparison of retention time to that of the synthetic sample of FDEA **176**, prepared previously.

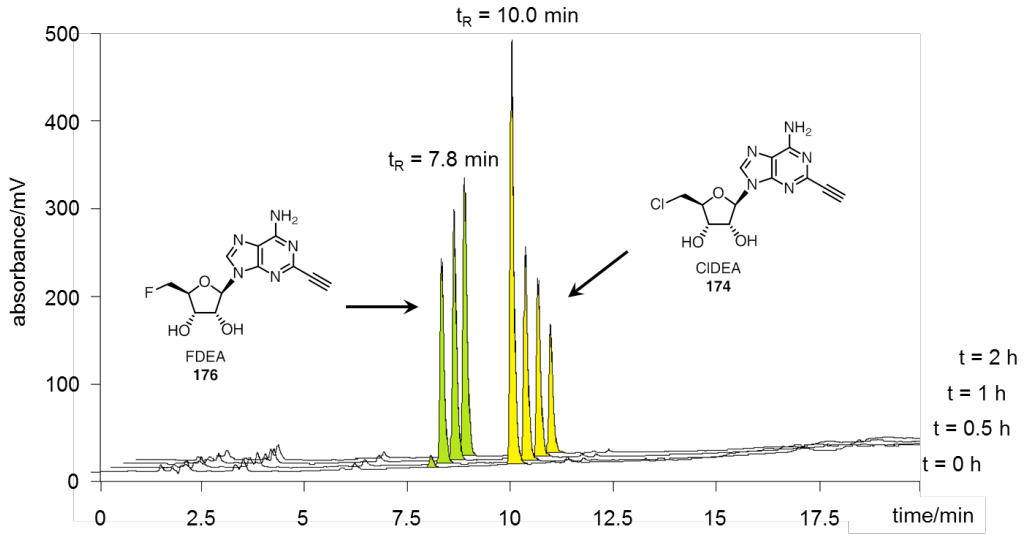

Figure 9. HPLC time course (260 nm) of incubation of ClDEA **174**, yellow, (t_R = 10.0 min) with the fluorinase, showing samples taken at t = 0, 0.5, 1 and 2 h. A new peak appeared at t_R = 7.8 min, green, identified as FDEA, **176**.

This new product was confirmed as FDEA **176** by liquid chromatography-mass spectrometry (LC-MS). The supernatant of a reaction (run for 24 h) was analysed by LC-MS (**Figure 10**) and revealed a single retained peak in the UV (**Figure 10 A**) and total ion chromatogram (**Figure 10 B**) at t_R = 14.2 min. The summed mass spectrum of this peak (**Figure 10 C**) showed a peak at *m/z* = 294, the $[M+H]^+$ ion of FDEA **176**, confirming this as the product of the transhalogenation.

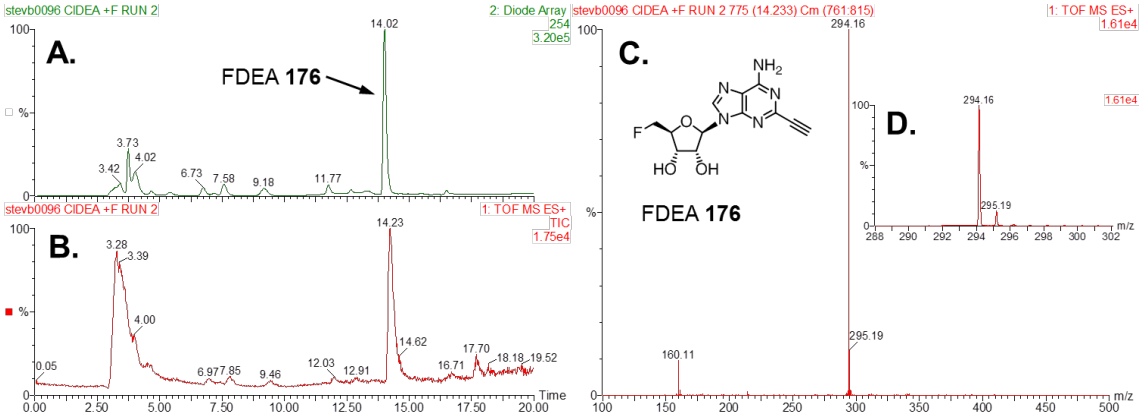

Figure 10. **A.** UV (254 nm) trace of a fluorinase-CIDEA **174** reaction mixture incubated with fluoride ion after 24 hours showing a single major peak at t_R = 14.0 min, identified as FDEA **176**. **B.** Total ion chromatogram of the reaction mixture, showing the corresponding ion peak at t_R = 14.2 min. **C.** Combined mass spectra acquired for the peak at t_R = 14.2 min showing a peak at *m/z* = 294, corresponding to FDEA **176**. **D.** Zoomed region showing the isotope pattern is as expected for FDEA **176**.

A control experiment, incubating CIDEA **174**, L-selenomethionine and fluoride ion for 24 hours without fluorinase enzyme showed only the presence of CIDEA **176**. No FDEA **176** or SeEAM **175** was observed by HPLC, confirming that the transhalogenation reaction is catalysed by the fluorinase.

Incubation of CIDEA **174** with the fluorinase in the absence of fluoride ion, but with a stoichiometric amount of L-selenomethionine showed complete consumption of CIDEA **174**. SeEAM **175** was detected, but only at low levels in the LC-MS experiments, eluting with the solvent front (**Figure 11**).

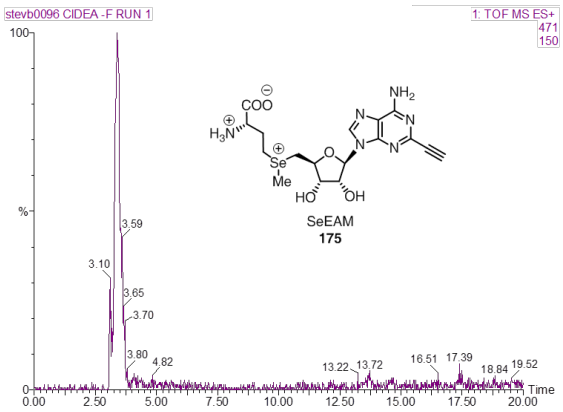

Figure 11. Ion selective chromatogram for *m/z* = 471, corresponding to the mass of SeEAM **175**, showing detection of ions of this mass eluting with the solvent front.

Three new products were detected by LC-MS (**Figure 12 A** and **B**) in this experiment. These products were derived from the breakdown of the SeEAM **175** intermediate, either during the incubation period, or during heating to precipitate the fluorinase.

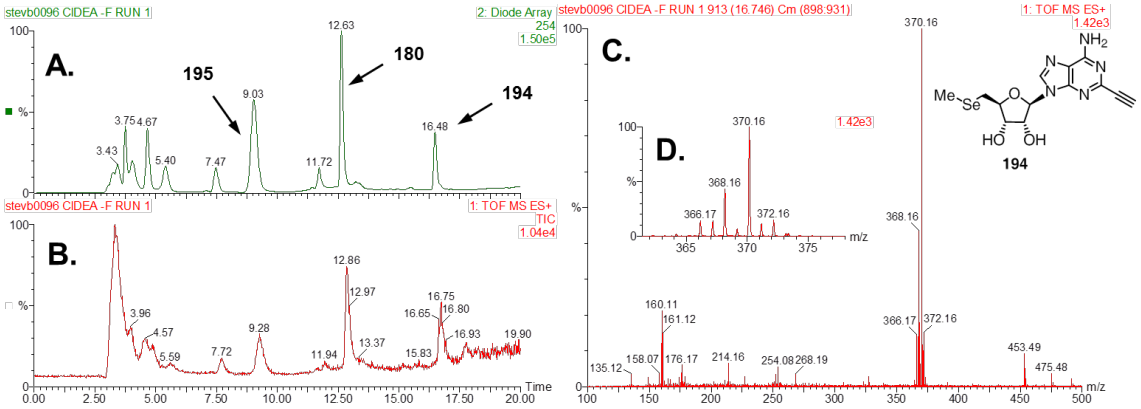

Figure 12. **A.** UV (254 nm) trace of a fluorinase-CIDEA **174** reaction mixture in the absence of fluoride ion after 24 hours showing a three major products at t_R = 9.0 min, t_R = 12.6 min and t_R = 16.4 min. **B.** Total ion chromatogram of the reaction mixture, showing the corresponding ion peaks at t_R = 9.2 min, t_R = 12.9 min and t_R = 16.8 min. **C.** Combined mass spectra acquired for the peak at t_R = 16.8 min showing a peak at *m/z* = 370, corresponding to methyl selenoether **194**. **D.** Zoomed region showing the distinctive isotope pattern expected for selenium containing **194**.

The breakdown product at t_R = 16.4 min was identified as 5'-selenomethyl-5'-deoxy-2-ethynyladenosine **194**, with *m/z* = 370 ($[M+H]^+$), showing the characteristic isotope pattern for the presence of selenium (**Figure 12 C** and **D**). *S*-Adenosylmethionine is known to break down when heated to generate the sulfur analogue of **194**, along with homoserine lactone.[27,28]

The two other major peaks in **Figure 12 A** were identified as hydrolysis products of SeEAM **175**. The peak at t_R = 9.0 min showed a mass of *m/z* = 160 (**Figure 13 A**), and corresponded to the free base **195** derived from hydrolysis at the anomeric position. The peak at t_R = 12.6 min showed a mass of *m/z* = 292 (**Figure 13 B**) and corresponded to the adenosine analogue **180** derived from hydroxide displacement at the 5'-position.

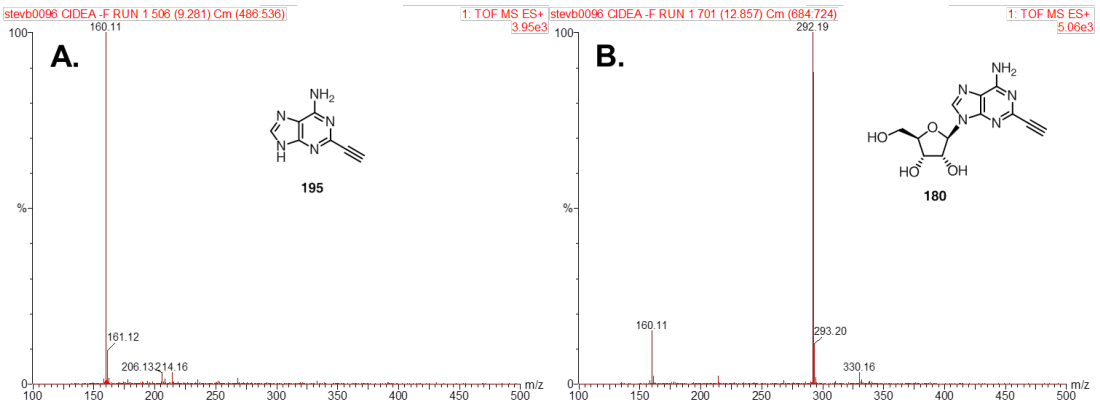

Figure 13. **A.** Combined mass spectrum of SeEAM **175** breakdown product eluting at t_R = 9.0 min, identified as free base **195**. **B.** Combined mass spectrum of SeEAM **175** breakdown product eluting at t_R = 12.3 min, identified as hydroxylated analogue **180**.

Identification of SeEAM **175** breakdown products confirmed that the transhalogenation takes place *via* an activated selenonium intermediate, as observed with other fluorinase-catalysed transhalogenations. This confirms that the transhalogenation does not take place through a direct substitution of chloride for fluoride, as observed for the brominated substrate analogue (see **Section 2.1**).

The alkyne substituent at C-2 of the nucleoside appears to be well tolerated by the fluorinase. The C-2 modified substrate, ClDEA **174** (**Figure 14**), behaves similarly to the unmodified chlorinated substrate, ClDA **23**, undergoing substitution by L-selenomethionine to generate the activated intermediate. Intermediate **175** then acts as a substrate for a subsequent fluorinase-catalysed fluorination.

ClDEA **174** is the second substrate with a modification at the C-2 position known to be well tolerated by the fluorinase (**172** was the first)[5]. The tolerance most likely arises as a result of the location of the active site near the surface of the protein, rather than being buried within the protein. C-2 adenine site is specifically oriented towards the solvent, projecting out of the active site, leaving this position open for modification.

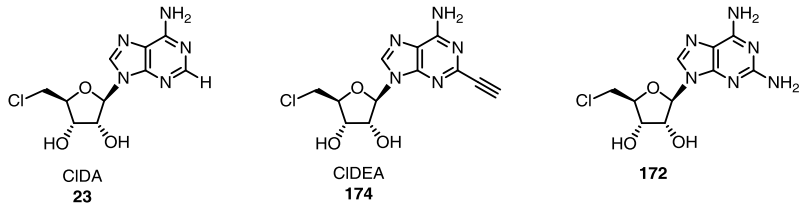

Figure 14. Substrates for the fluorinase, **174** and **172**, with substitutions at C-2 of the adenine base of unmodified **23**.

Following the qualitative analysis of ClDEA **174** as a fluorinase substrate, the kinetic behaviour of ClDEA **174** was investigated.

2.5.2. Comparison of rate of transhalogenation for ClDEA 174 and ClDA 23

The fluorinase-catalysed transhalogenation couples two independent reactions *i.e.* generation of the selenonium intermediate from the corresponding chlorinated substrate and then fluorination of the selenonium intermediate. The net transformation involves a number of distinct events; therefore a simple kinetic analysis was initially undertaken.

In this study, the rates of production of FDA **22** from ClDA **23,** and FDEA **176** from ClDEA **174** (**Scheme 15**) were determined in separate experiments. The

substrate (0.25 mM) and fluorinase (2.5 mg.mL^{-1}) were incubated at 37 °C in the presence of L-selenomethionine (0.075 mM) and potassium fluoride (50 mM) in phosphate buffer (pH 7.8, 8 mM). Aliquots of the solution were removed every 15 minutes and the concentration of FDA **22** or FDEA **176** were determined by HPLC, by comparison of peak area to those of standard curves. The results are summarised in **Figure 15**.

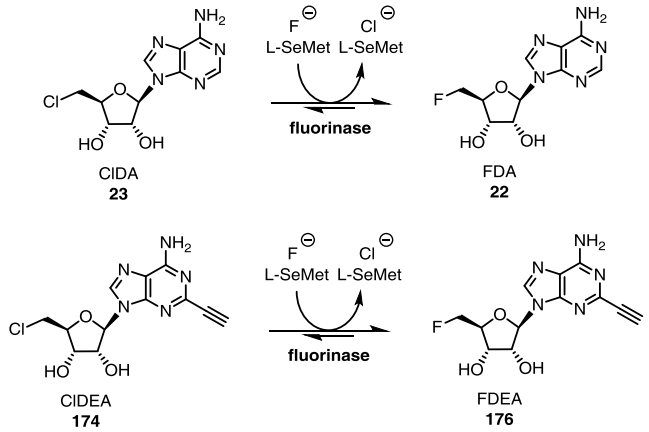

Scheme 15. Fluorinase-catalysed transhalogenations investigated for comparison of the rate of production of fluorinated products.

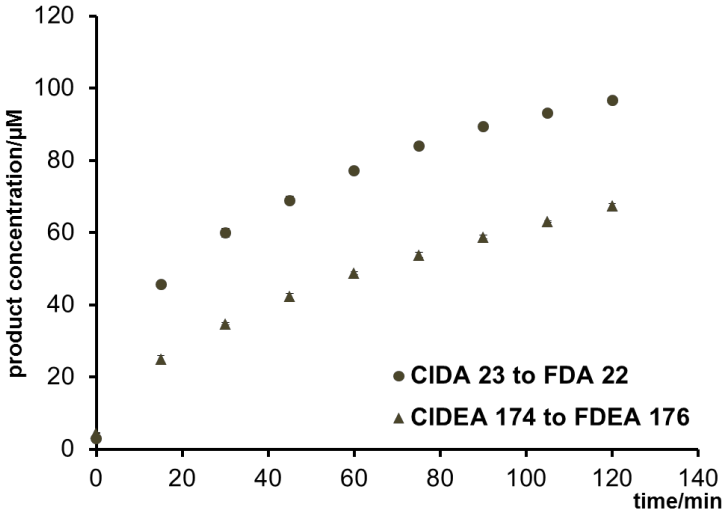

Figure 15. Graph showing the concentration of FDA **22** (●) and FDEA **176** (▲) produced by the fluorinase under identical reaction conditions. Reactions were repeated in duplicate.

FDA **22** was generated more rapidly than FDEA **176**, showing that the transhalogenation reaction on the unmodified substrate is the faster of the two reactions. FDEA **176** is produced at approximately 60% of the rate of FDA **22** throughout the duration of the experiment.

The alkyne substituent at C-2 affects the rate of transhalogenation and the nature of this effect was further explored by closer examination of the kinetic and binding parameters of this new substrate.

2.5.3. Michaelis-Menten kinetic evaluation of ClDEA 174 as a fluorinase substrate

Michaelis-Menten kinetics cannot be easily evaluated for the two step transhalogenation reaction, however, it was possible to isolate and investigate the first step in the sequence involving the displacement of chloride to generate the modified SAM intermediate, SEAM **196**, as shown in **Scheme 16**. L-Methionine rather than L-selenomethionine was used in these investigations to facilitate comparison to similar measured parameters from previous experiments.

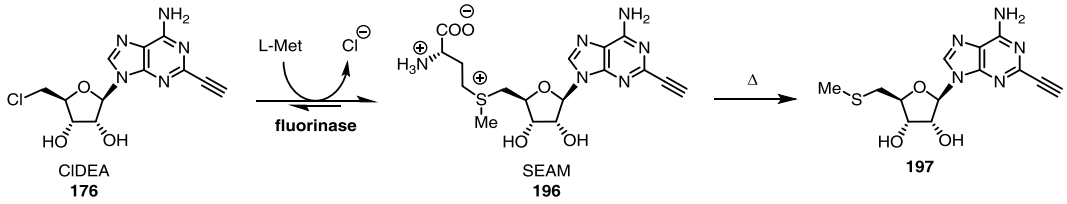

Scheme 16. First step of the fluorinase-catalysed transhalogenation reaction, showing conversion of ClDEA **176** to SEAM **196** by substitution with L-methionine. This product decomposes upon heating to give thiomethyl ether **197**.

Steady state kinetic experiments were conducted with ClDEA **176** at six different concentrations (10 μM, 25 μM, 50 μM, 100 μM, 250 μM and 500 μM). The reactions were run in the presence of saturating concentrations of L-methionine (10 mM), which had previously been reported to have a K_M of 4.5 mM in the reverse direction with FDA **22** as a substrate.[4]

Measuring the decreasing concentration of ClDEA **174** proved difficult, as quantifying small changes in area of a dominant peak is prone to large errors. As an alternative, changes in the concentration of the product SEAM **196** were measured. *S*-Adenosylmethionine is unstable and decomposes to 5'-thiomethyl-5'-deoxyadenosine upon heating.[27,28] Similarly, SEAM **196** decomposed through the same pathway, to generate the thiomethyl ether **197** (**Scheme 16**) and this could be detected by HPLC. Quantification of **197** was achieved by comparison to a standard curve for ClDEA **174**, as both bear the same 2-ethynyladenyl chromophore. The results of these experiments are illustrated in **Figure 16**.

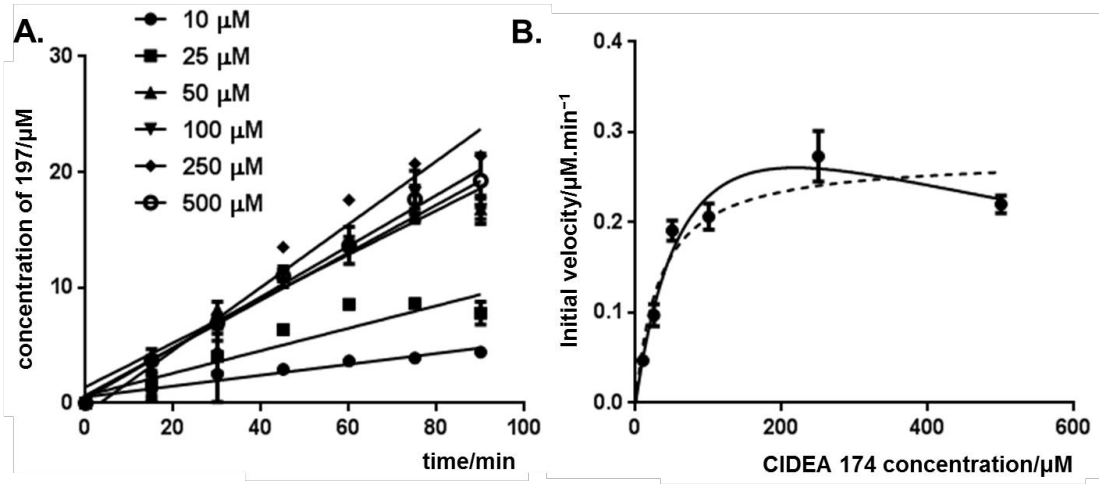

Figure 16. Steady state kinetic analysis of reaction of CIDEA **174** with L-methionine. **A.** Product concentration against time for various substrate concentrations. **B.** Michaelis-Menten plot, revealing substrate inhibition at high concentration, fitted without factoring in substrate inhibition (- - -) and factoring in substrate inhibition (—).

The data show that the fluorinase is subject to substrate inhibition at high substrate concentration. This may arise due to the way the chlorinated substrates bind in the active site. It has previously been shown in X-ray crystal structures that the CIDA **23** resides in two conformations within the active site.[4] The first has the chlorine atom bound within in the halogen binding site, as required for reaction. A second is observed where the chorine atom is rotated into the vacant sulfonium binding pocket. Observation of these two conformers in the solid state would suggest that they are of similar energy. Investigations into the binding order of the reactants have shown that L-methionine binds after the nucleoside, and that no appreciable L-methionine binding was detected by isothermal titration calorimetry in the absence of a nucleoside (such as adenosine).

In the case of substrate inhibition, binding of L-methionine and subsequent reaction is slowed as the concentration of substrate increased. More binding events would give rise to the conformer of the substrate that is not productive to binding of L-methionine, resulting in the observed inhibition at high substrate concentrations.

Fitting of the kinetic data to a model which factors in the observed substrate inhibition gives a K_M of 81.7 ± 32.5 µM, and k_{cat} of 0.062 ± 0.004 min^{-1} for CIDEA **174** as substrate. The fluorinase is reported to have a K_M for SAM **20** of between 6.5 µM and 29 µM,[26,29] while the K_M for FDA **22** in the reverse direction was previously found to be 140 µM. The modified substrate **174** has a K_M within the same order of magnitude as other known fluorinase substrates.[4,26,29] The turnover number is reflective of the

number of turnovers per active site (k_{cat}). The value of k_{cat} for ClDEA **174** is low compared to k_{cat} values for other enzymes, but is comparable to the values obtained with SAM **20** and native fluorinases from *S. cattleya* and other organisms (0.08–0.26 min^{-1}).

2.5.4. Competition experiment with ClDEA 174 and ClDA 23

Assessing the ability of the fluorinase to discriminate ClDA **23** from ClDEA **174**, provides a crude measure of affinity of the fluorinase for the novel acetylene bearing substrate ClDEA **174**. If the affinity of the modified substrate is significantly lower than that of the natural substrate, we would expect the natural substrate, ClDA **23**, to act as an effective "inhibitor" of the reaction of ClDEA **174**.[30] Therefore, the two substrates were simultaneously presented to the fluorinase, as illustrated in **Scheme 17**, in order to assess whether they were both converted to the corresponding fluorinated products, and whether turnover of ClDA **23** acted as an "inhibitor" for turnover of ClDEA **174**.

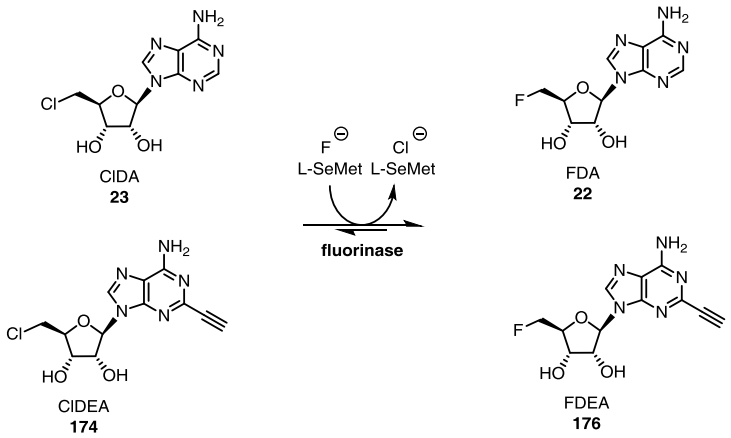

Scheme 17. Competition experiment where ClDA **23** and ClDEA **174** were simultaneously presented to the fluorinase and their conversion to products monitored.

The two substrates, each at 0.2 mM were incubated with the fluorinase (6 $mg.mL^{-1}$) in phosphate buffer (20 mM, pH 7.8) in the presence of catalytic L-selenomethionine (0.08 mM) and excess fluoride (75 mM) and the conversion to products monitored over 2 hours by HPLC, as shown in **Figure 17**.

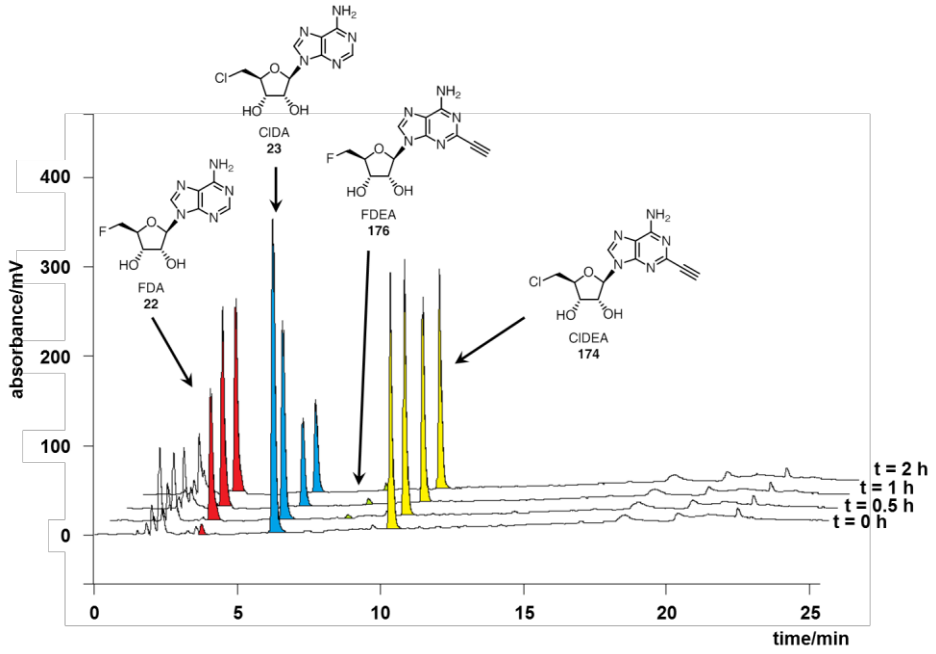

Figure 17. HPLC chromatograms of a competition experiment. The traces show conversion of ClDA **23** (blue) to FDA **22** (red), while conversion of ClDEA **174** (yellow) to FDEA **176** (green) is almost negligible.

HPLC analysis showed that there was almost no conversion of ClDEA **174** to FDEA **176**, with only traces of the acetylene-modified product observed after 2 hours. Conversely, there was approximately 70% conversion of ClDA **23** to FDA **22** during the same time period. Considering that the acetylene modified substrate is processed at approximately 60% of the rate of the unmodified substrate when investigated separately, the enzyme shows a distinct preference for the unmodified substrate in the competition experiment.

ClDA **23** outcompeted ClDEA **174** as a substrate, effectively behaving as a competitive inhibitor with a significantly higher affinity. The result is exaggerated over the two independent reactions which make up the transhalogenation. Following this result, we were interested in quantifying the affinity of the novel compounds to the fluorinase in order to determine whether this was responsible for the high selectivity observed in the competition experiment.

2.5.5. Thermodynamic characterisation of ClDEA 174 and FDEA 176 as ligands

The binding affinities of the new ligands were determined using isothermal titration calorimetry (ITC) in a series of independent experiments where the ligands (ClDA **23**, ClDEA **174**, FDA **22**, and FDEA **176**) were titrated into a solution of the fluorinase in

phosphate buffer. The raw ITC data and binding curves for ClDA **23** and ClDEA **174** are shown below in **Figure 18 A** and **B** respectively.

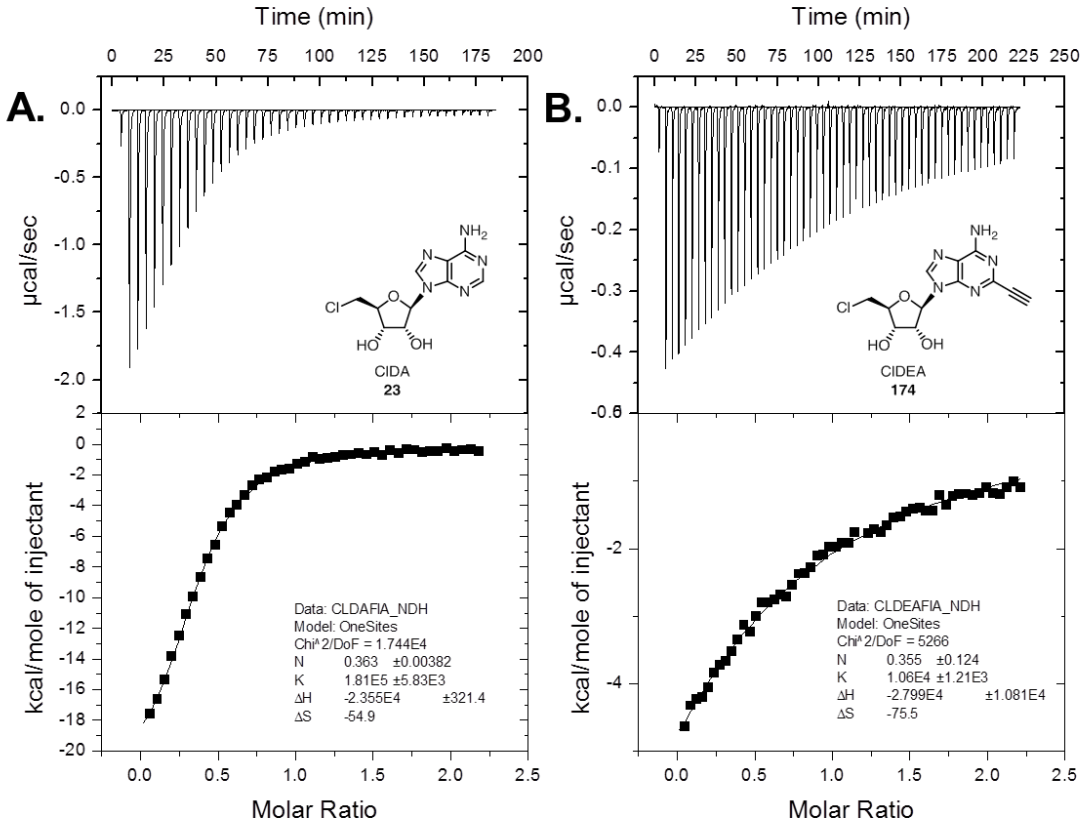

Figure 18. Isothermal titration calorimetric determination of the binding affinity of **A.** ClDA **23** (0.70 mM) into the fluorinase (53.6 µM) and **B.** ClDEA **174** (0.57 mM) into the fluorinase (53.6 µM).

The data show that ClDEA **174**, the acetylene-modified substrate has a lower binding affinity (K_a = 0.106 ± 0.012 × 10^5 M^{-1}) when compared to the unmodified substrate ClDA **23** (K_a = 1.81 ± 0.058 × 10^5 M^{-1}). There is an order of magnitude difference in the binding affinity which explains the ability of the fluorinase to effectively distinguish the two substrates in the competition experiments.

Binding of either ligand is a thermodynamically favourable process, with a large contribution from the enthalpy factor for both ligands. The calculated entropy change for both ligands is negative, indicating that binding is entropically unfavourable.

A similar study was undertaken where the two products of the reaction, FDA **22** and FDEA **176** were titrated into the fluorinase enzyme in phosphate buffer. The raw traces and peak data after integration are shown in **Figure 19 A** and **B** respectively.

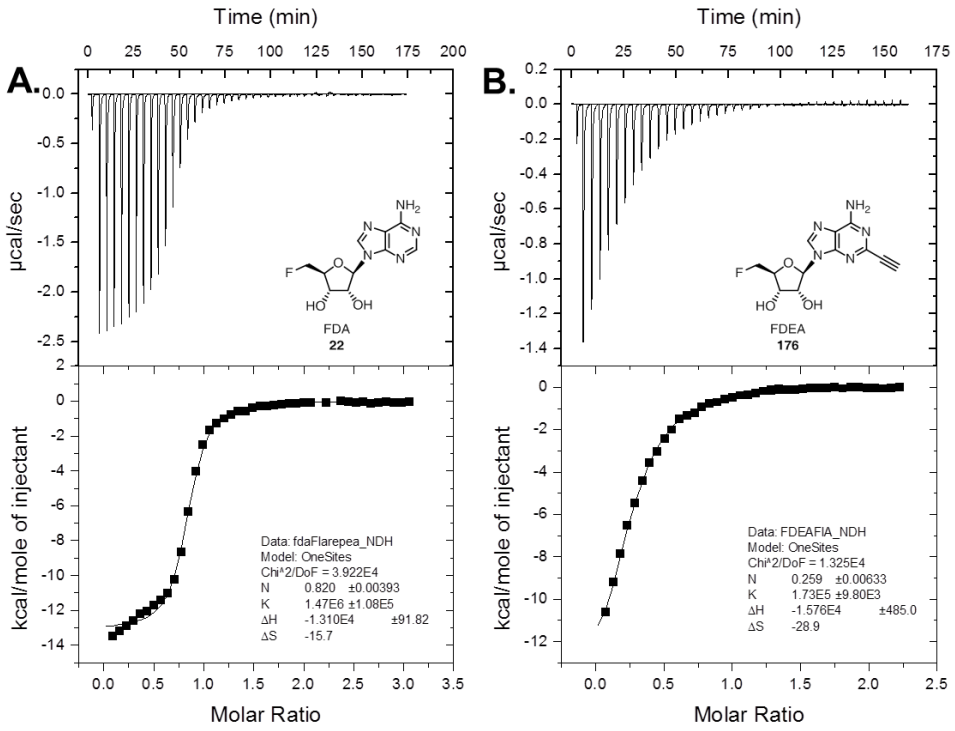

Figure 19. Isothermal titration calorimetric determination of the binding affinity of **A.** FDA **22** (1.03 mM) into the fluorinase (53.6 µM) and **B.** FDEA **176** (0.89 mM) into the fluorinase (58.8 µM).

The binding data for the fluorinated analogues show a similar trend to the chlorinated compounds. FDA **22** displays higher binding affinity (K_a = 14.7 ± 1.08 × 10^5 M^{-1}) for the fluorinase, as has been shown previously.[26] The acetylene modified FDEA **176** has a binding constant of K_a = 1.73 ± 0.09 × 10^5 M^{-1}, an order of magnitude lower than the unmodified analogue.

The presence of the acetylene lowers the affinity of the compound for the enzyme for both the chlorinated and fluorinated nucleosides. The enthalpy of binding is again similar for both compounds, while the entropy change is again negative, and is greater for the acetylenic compound FDEA **176**.

A comparison of the thermodynamic binding properties of all four compounds, as shown in **Figure 20**, reveals interesting detail about the binding of these ligands to the fluorinase. The enthalpic change (ΔH) for the chlorinated ligands is larger than for the analogous fluorinated ligands. The improved enthalpic term is compensated for by a much larger entropic penalty (-TΔS), and this entropic penalty is greater for the acetylenic compounds. The nett result is that the free energy change of binding (ΔG, directly related to K_a) is lower for the chlorinated compounds. The origin of this large

entropic penalty is unknown. While the fluorinated analogues show lower enthalpic gains upon binding, the entropic penalty is much lower, and together this results in a higher binding affinity for the fluorinated compounds.

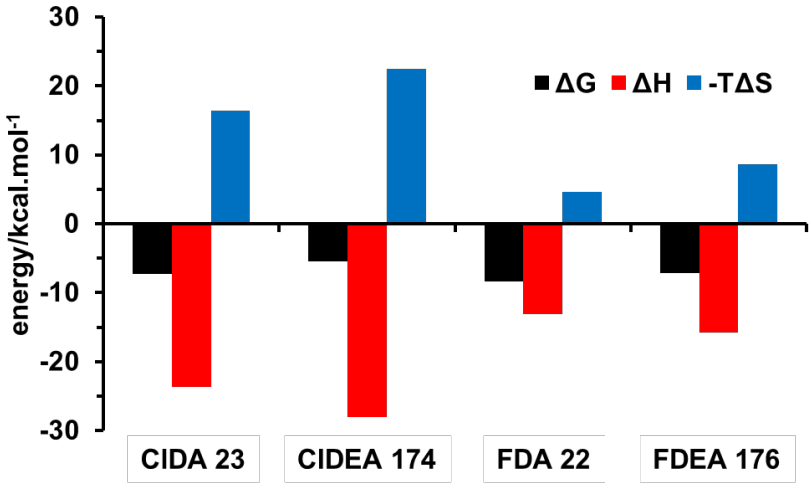

Figure 20. Comparison of the thermodynamic parameters of binding for CIDA **23**, CIDEA **174**, FDA **22** and FDEA **176**. ΔH was measured directly, while the –TΔS term was calculated using T = 298.15 K. ΔG was calculated as the sum of these two terms.

The enthalpic term for both acetylenic compounds is greater than that for the analogous unmodified substrates, evidence of increased interaction through hydrogen bonding or van der Waals interactions.[31] The only change in the compounds is the addition of the acetylene functionality, and the substitution must be partly responsible for the increased enthalpic effect. From previous crystallographic work showing the FDA **22** within the active site of the enzyme,[9] it is evident that the adenine moiety is bound between a tryptophan (Trp-50) and phenylalanine (Phe-254) residue through π-π interactions. It is possible that the presence of the electron donating triple bond may increase the strength of this interaction. The acetylenic compounds are also more hydrophobic than their unmodified analogues (as estimated by HPLC).[32] Their entry into to the relatively hydrophobic active site of the enzyme and out of aqueous solvent is also likely contributes to the favourable gain in enthalpy observed.

The entropic term for the two acetylenic compounds is also shown to be greater than their analogous unmodified compounds. This increase in entropic contribution could arise due to enhanced π-π-stacking in the active site, reducing conformational degrees of freedom for residues in the active site. The presence of the acetylene in the “hole” in

the active site may also restrict the conformational flexibility of residues which are normally free to move into or out of this gap.

Following the kinetic and thermodynamic evaluation of the novel acetylenic substrates, it was immediately attractive to investigate the structural impact of the acetylene substitution, therefore attention turned to co-crystallising these new substrates with the fluorinase.

2.5.6. Crystallographic study of FDEA 176 as a ligand

Fluorinase enzyme was overexpressed, treated with adenosine deaminase and the polyHis tag cleaved by treatment with thrombin, to give a preparation of the fluorinase suitable for X-ray crystallisation trials, as described in **Section 2.4**.

The fluorinase (6.5 $mg.mL^{-1}$) was incubated with both ClDEA **174** and FDEA **176** at 1 mM (from DMSO stock solution), at room temperature overnight, before a series of in house and commercial stochastic crystallisation screens were set up in collaboration with Dr Stephen McMahon and Prof. Jim Naismith.

Crystals were obtained under a number of conditions, with both ClDEA **174** and FDEA **176** bound, however best diffracting crystals grew from solutions with FDEA **176**, 20% PEG 3350 and 0.2 M ammonium formate. Cryoprotection of a crystal was achieved by doping the mother liquor with 20% glycerol and flash freezing in liquid nitrogen. The resultant diffraction data were collected at the DIAMOND Light Source beam I03 at 100 K. The data were solved by molecular replacement from previous fluorinase crystal structures by Dr Stephen McMahon, to generate a crystal structure of FDEA **176** bound into the active site of the fluorinase. The structure was solved to a resolution of 2.4 Å, and is shown in **Figure 21 A**.

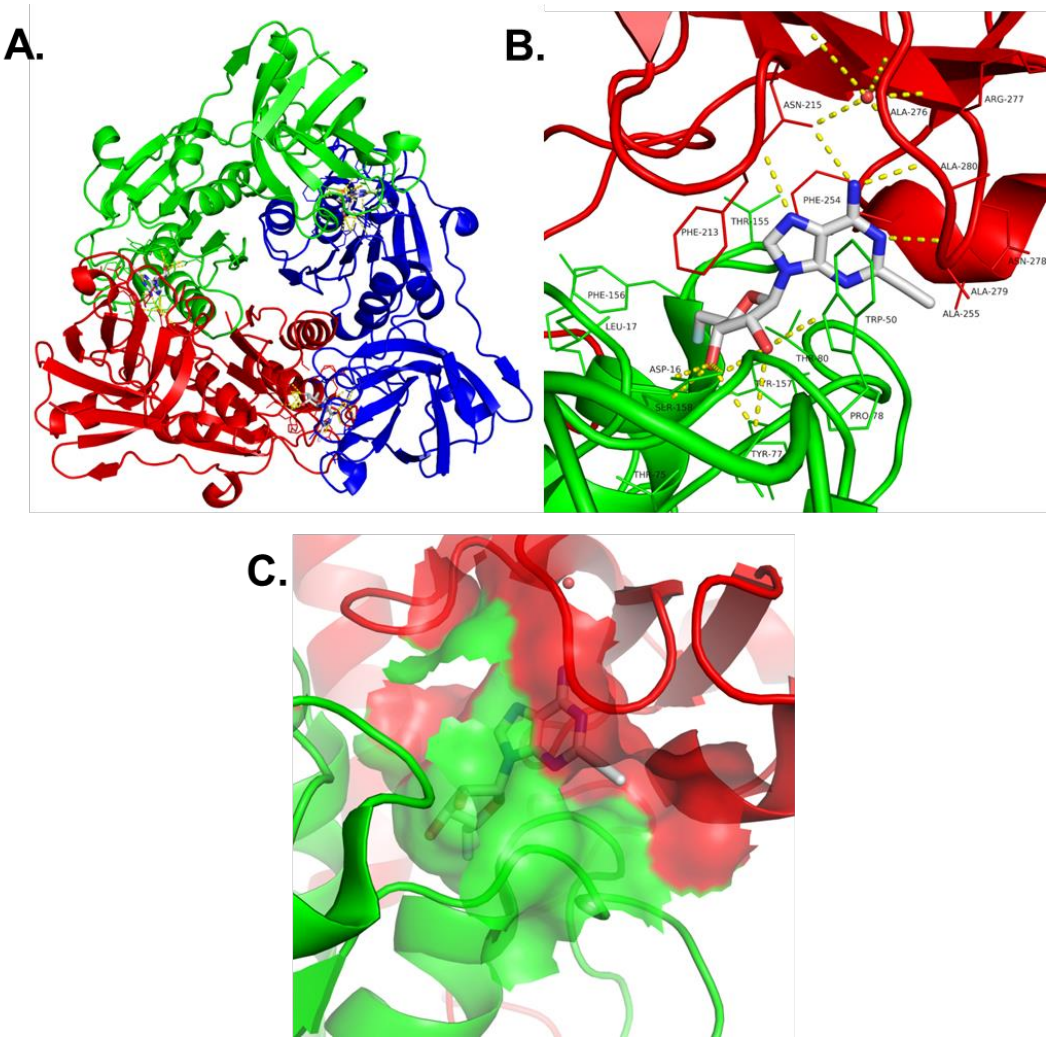

Figure 21. **A.** Crystal structure of FDEA **176** in the active site of the fluorinase, showing the trimeric structure of the enzyme with individual monomers shown in green, blue and red. **B.** Close up of one of the active sites of the fluorinase showing FDEA **176** and its interaction with surrounding residues. The alkyne projects between the two subunits as predicted. **C.** Solvent accessible surface profile of the interior of the active site, showing the hole through which the acetylene of FDEA **176** projects.

FDEA **176** binds in the active site in a manner similar to FDA **22**, showing similar contacts to active site residues as shown in **Figure 21 B**. Asp-16 forms hydrogen bonds to the 2',3'-diol system, and the proton of the amide nitrogen of Ser-158 forms a close contact with the fluorine atom in FDEA **176**. Both interactions are known to be critical for catalysis.[26] As for FDA **22**, the adenine base forms a hydrogen bonding network in the active site through a bridging water molecule to residues Ala-279, Ala-280, Asn-215 and further out of the active site. The adenine base also participates in π-π stacking interactions with Trp-50 and Phe-254. The acetylene moiety of FDEA **176** projects from the active site, out towards the solvent void as predicted by initial observations of the hole in the active site. A solvent accessible surface profile of

the active site (**Figure 21 C**) shows a gap in the active site through which the acetylene projects. The projection of the acetylene out of the active site opens up the possibility of tethering molecules of interest from the acetylene through an appropriate linker.

Direct comparison of the co-crystal structures of FDA **22** and FDEA **176** shows that the gross conformation adopted by the proteins is essentially identical, as illustrated in **Figure 22 A**. A comparison of the binding of the nucleoside within the active site (**Figure 22 B**) also reveals that they are bound in a similar orientation within the active site, with the two adenines co-planar. The ethynyl nucleoside is slightly offset to accommodate the steric impact of the acetylene.

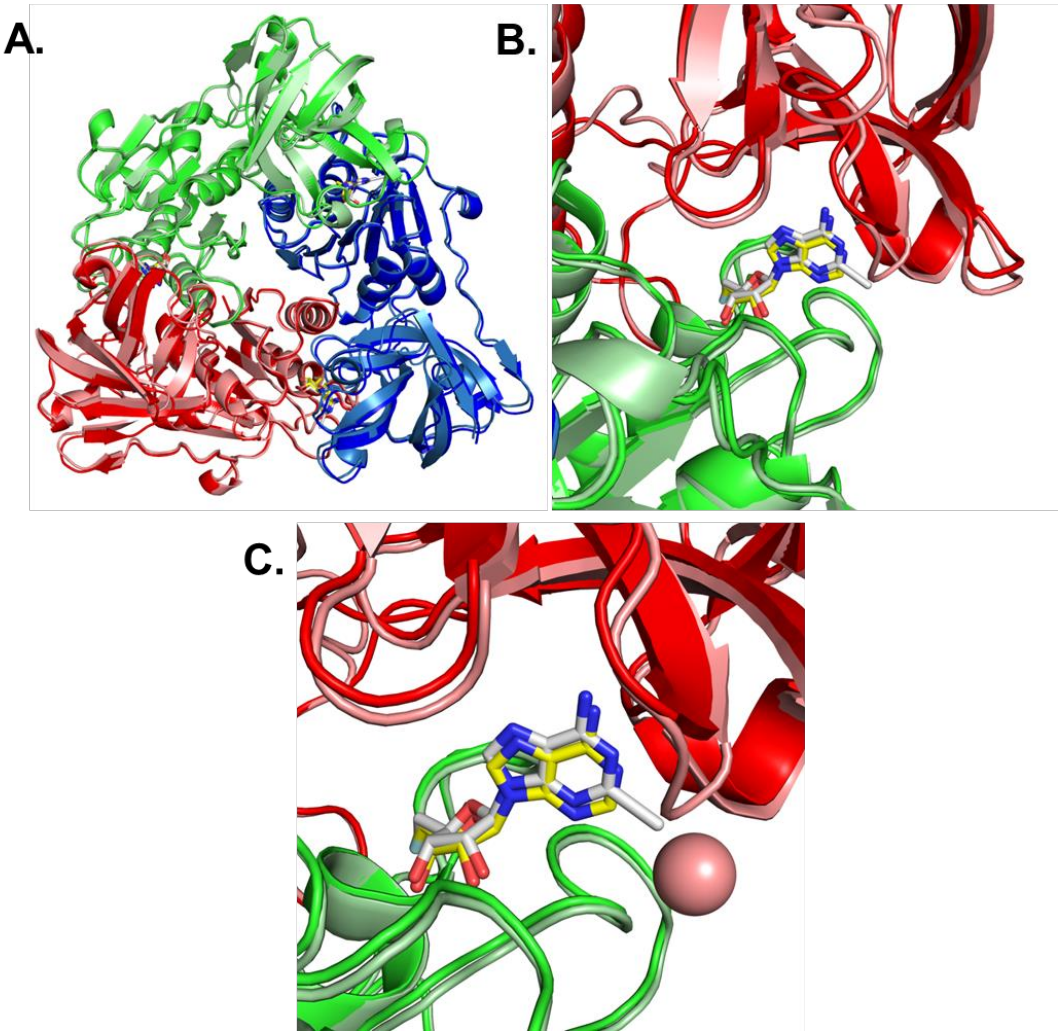

Figure 22. **A.** Overlay of the structure of fluorinase bound to FDA **22** (pastel colours) and FDEA **176** (bright colours) showing no gross conformational change. **B.** Close up of the active site of the fluorinase showing an overlay of the two ligands, FDA **22** (yellow backbone) and FDEA **176** (grey backbone). **C.** Close up of the active site showing the water molecule (pink sphere) in the cavity in the FDA **22** structure which is displaced by the alkyne in the FDEA **176** structure.

2.6. Bioconjugation of FDEA 176 to a peptide

With the goal of using the fluorinase and this modified alkyne substrate for bioconjugations, attention turned to selecting an appropriate biomolecule with which to evaluate this bioconjugation. Previous work in the St Andrews group[33] has made use of cyclic Arg-Gly-Asp-bearing peptides (cRGDs), biomarkers for cell surface proteins known as integrins, as suitable test peptides for evaluating bioconjugations for PET.

The $\alpha_V\beta_3$ integrin (the vitronectin receptor) is an important biomarker of angiogenesis, a hallmark of tumours in many cancers.[34] Binding of vitronectin to $\alpha_V\beta_3$ integrin occurs through an RGD tripeptide motif **196** (**Figure 23**) present on the surface vitronectin.[35,36] Incorporating this simple tripeptide motif into peptides has resulted in a range of analogues bearing the RGD sequence being developed as imaging biomarkers for the angiogenesis process.[37]

The most successful range of these mimics are the cyclic pentapeptide RGD-containing species, which were found to generally show an order of magnitude greater affinity to $\alpha_V\beta_3$ integrin when compared to their linear analogues.[38] The cyclic peptides were found to have highest affinity when bearing a hydrophobic residue (such as D-phenylalanine) adjacent to the Asp residue, while the final remaining residue could be substituted without loss of affinity for $\alpha_V\beta_3$ integrin.[39] Two of the most commonly utilised RGD peptides for bioconjugations contain a cysteine residue, bearing a free thiol **197** for reaction with soft electrophiles like maleimides; or a lysine residue **198** for bioconjugation to activated carboxylic acids or aldehydes.[37]

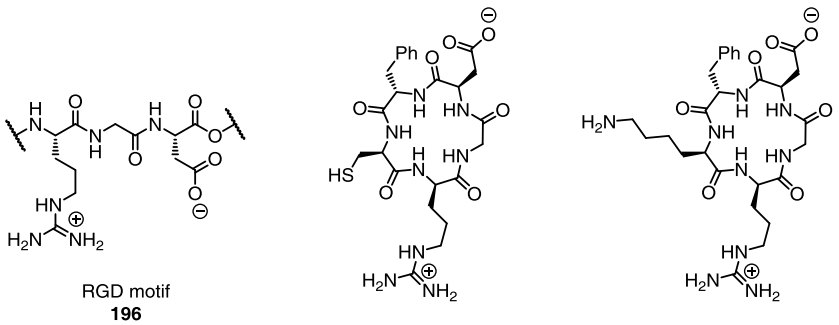

Figure 23. The RGD motif **196**, identified as the binding element of vitronectin to its receptor, $\alpha_V\beta_3$ integrin, along with two of the more commonly used cRGD peptides for bioconjugations, cysteine bearing **197** and lysine bearing **198**.

The acetylenic product of the enzymatic fluorination FDEA **176** requires an azide for bioconjugation through a copper-catalysed alkyne-azide cycloaddition (CuAAC),

therefore an azide-modified derivative of a cRGD peptide was required. A derivative of the lysine bearing peptide c(RGDfK) **197**, where the lysine ε-amine group has been modified to an azide, gives c(RGDfK[N_3])[40] **199**, as shown in **Figure 24**, which is commercially available. This RGD-peptide was investigated in a CuAAC reaction with ClDEA **174** and FDEA **176**.

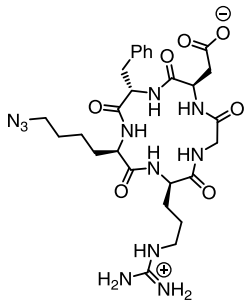

c(RGDfK[N_3])
199

Figure 24. Azide modified cRGD peptide **199** for coupling to alkynes through CuAAC reaction.

2.6.1. Preparation of synthetic samples of ClDEA-RGD 200 and FDEA-RGD 201

Prior to investigating the CuAAC reaction with enzymatically synthesised FDEA **176**, synthetic samples of the CuAAC reaction products of both ClDEA **174** and FDEA **176** with c(RGDfK[N_3]) **199** were prepared synthetically for use as reference compounds, as shown in **Scheme 18**.

The alkynes were taken up in solution in either water, or a mix of water and DMSO to obtain a homogenous solution (0.16 mM), to which the RGD peptide **199** (1.25 eq.) and a freshly prepared aqueous solution of sodium ascorbate were added.[41] Sodium ascorbate acts as an oxygen scavenger and reducing agent during the reaction. The reaction was initiated by addition of a copper source, in this case a premixed aqueous-DMSO solution of copper (II) sulfate and the ligand TBTA **202**. The copper (II) ions are reduced to copper (I) species by ascorbate, while TBTA **202** acts as a protective ligand for the active copper (I) species.[42]

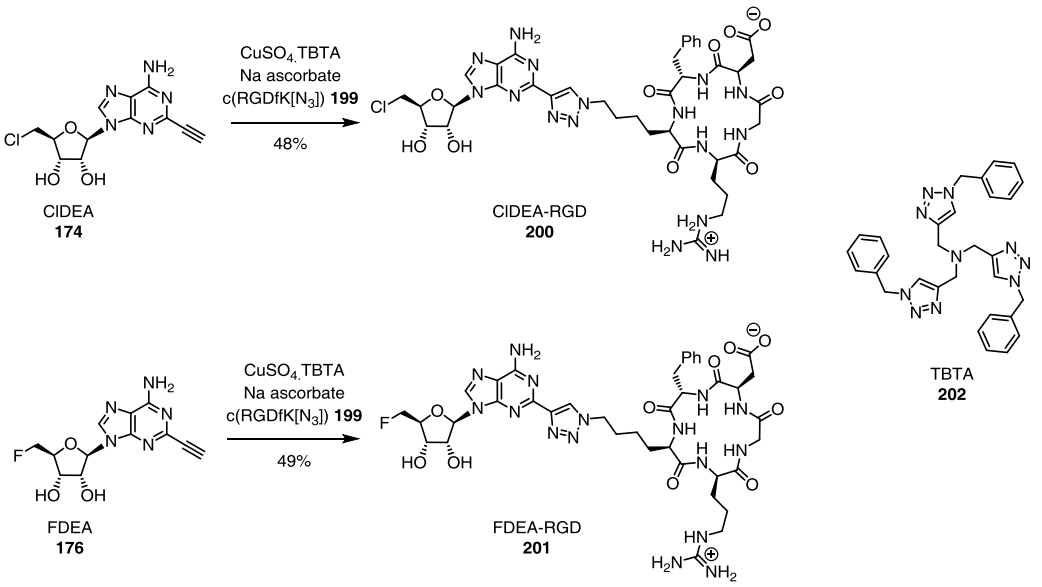

Scheme 18. Synthetic reactions to prepare standards of the anticipated products, ClDEA-RGD **200** and FDEA-RGD **201**.

The progress of the reactions was monitored by HPLC, and the starting alkynes were found to be consumed within 30 min and new products were evident. The products were trapped on a reverse phase C_{18} silica cartridge and washed with water to remove DMSO, ascorbate and copper salts. The triazoles (and residual TBTA **202**) were eluted from the cartridge using 50% acetonitrile in water, before concentration under a stream of compressed air afforded the crude product.

The triazoles were purified by semi-preparative HPLC on a reverse phase column to give ClDEA-RGD **200** in 48% yield and FDEA-RGD **201** in 49% yield.

2.6.2. Coupling the enzymatic transhalogenation with the CuAAC reaction

The coupling reaction was now explored using FDEA **176** which had been synthesised by enzymatic transhalogenation of ClDEA **174**. It was anticipated that this process will be developed for the ^{18}F-labelling of peptides, where unreacted ClDEA **174** will not be removed from the solution before "click" reaction. Therefore the "click" reaction was conducted using a crude reaction mixture directly, after precipitation and removal of the fluorinase. The solution will still contain phosphate buffer and L-selenomethionine, along with residual ClDEA **174**.

ClDEA **174** (0.2 mM, yellow, t_R = 10.0 min, **Figure 25**) was incubated with the fluorinase (5 mg.mL^{-1}) and L-selenomethionine (0.1 mM) in phosphate buffer (20 mM,

pH 7.8) and in the presence of potassium fluoride (75 mM). The reaction was monitored by HPLC from when the enzyme was added (t = 0 h) and then after 2 hours of reaction time (t = 2 h). HPLC (**Figure 25**) revealed that the reaction had proceeded to 78% completion, producing FDEA **176** (t_R = 8.1 min, green), while residual ClDEA **174** (t_R = 10.0 min, yellow) is still observed. The reaction mixture was heated to 95 °C and subsequently centrifuged, and the resultant supernatant transferred to a new vial for the CuAAC reaction.

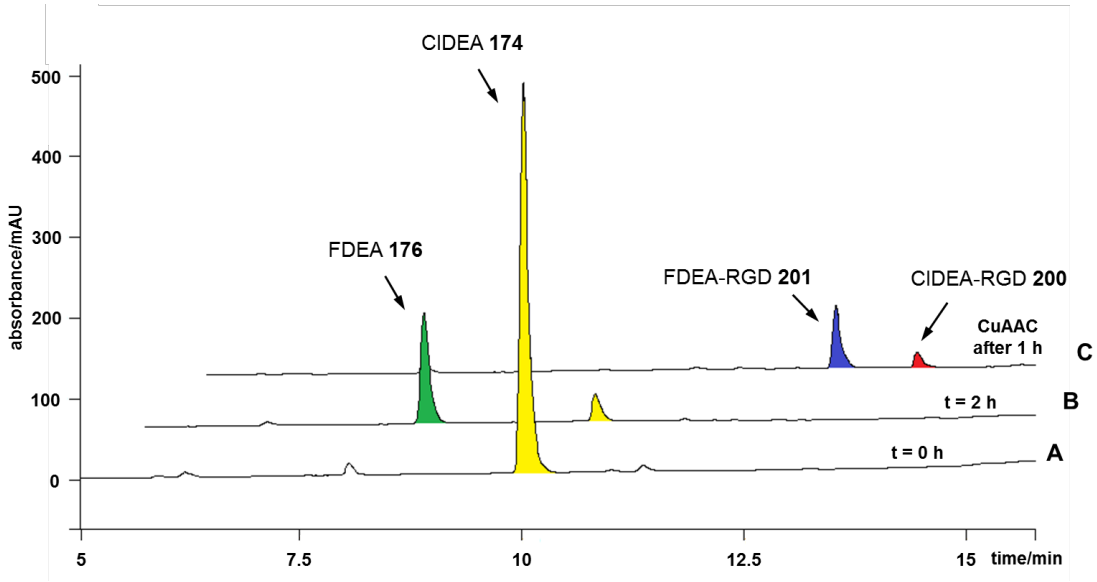

Figure 25. **A.** Fluorinase-catalysed transhalogenation of ClDEA **174** (t_R = 10.0 min, yellow) at t = 0 min. **B.** After 2 h, conversion of ClDEA **174** (t_R = 10.0 min, yellow) to FDEA **176** (t_R = 8.1 min, green) was observed to be 78% complete. **C.** Click reaction with azido peptide **199** after 1 h showing new triazole product, FDEA-RGD **201** (t_R = 11.4 min, dark blue). ClDEA-RGD **200** (t_R = 12.7 min, red) was also observed, from residual ClDEA **174** present after the transhalogenation.

A sample of the supernatant containing FDEA **176** (0.1 mM) (and residual ClDEA **174**) was added to an aqueous solution of c(RGDfK[N_3]) **199** (0.2 mM) before sodium ascorbate solution (0.5 mM) and $CuSO_4$.TBTA (1 mM) were added. The mixture was left to react for 1 h before HLPC analysis (**Figure 25**) confirmed that all of the alkyne products were consumed. Two new peaks were observed in the chromatogram, with a similar ratio to that of the starting alkynes. Comparison of the retention time of the standards, FDEA-RGD **201** and ClDEA-RGD **200**, confirmed these two new peaks were the corresponding fluoro- and chloro-triazoles, **201** and **200** respectively.

The identity of these new products was further confirmed through LC-MS. A similar CuAAC experiment was performed on an enzymatically derived mixture of FDEA **176**

and ClDEA **174**, but in this case, with only 0.5 equivalents of c(RGDfK[N_3]) **199**. The mixture was analysed by LC-MS, and the results are shown below in **Figure 26**.

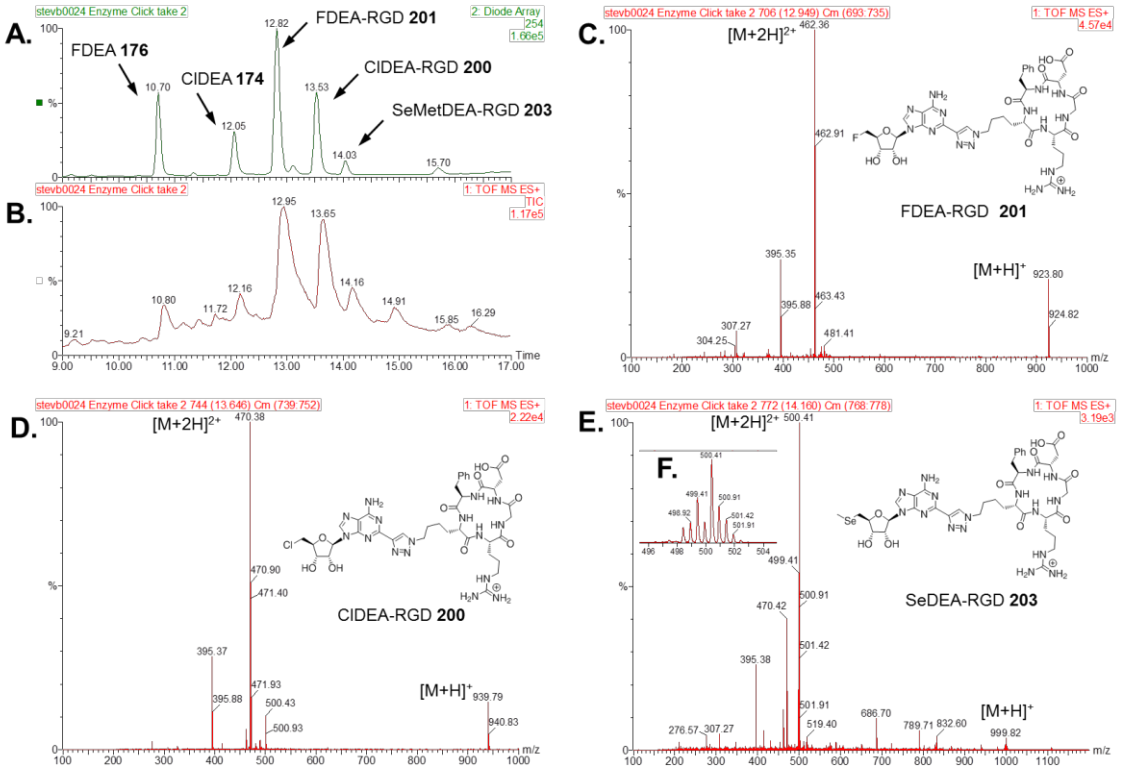

Figure 26. **A.** Portion of the LC chromatogram obtained from the CuAAC mixture, showing the identities of the major peaks, identified by their distinctive masses. **B.** Total ion chromatogram (TIC) for the same region. Peaks in the TIC were individually combined to produce a summed mass spectrum for each peak. Peaks at t_R = 10.8 min and t_R = 12.2 min were identified as FDEA **176** and ClDEA **174** respectively. **C.** Summed mass spectrum for the peak at t_R = 13.0 min, showing *m/z* = 923.8 and *m/z* = 462.4, as the singly and doubly charged species of FDEA-RGD **201**. **D.** Summed mass spectrum for the peak at t_R = 13.7 min, showing *m/z* = 939.8 and *m/z* = 470.4, as the singly and doubly charged species of ClDEA-RGD **200**. **E.** Summed mass spectrum for the peak at t_R = 14.1 min, showing *m/z* = 999.8 *m/z* = 500.4, as the singly and doubly charged species derived from the CuAAC reaction of the intermediate selenium containing alkyne and the azido RGD peptide **199**, as SeDEA-RGD **203**. **F.** Expansion of the peak at *m/z* = 500.4, showing the distinctive selenium isotope pattern.

LC-MS showed peaks corresponding to the unreacted alkynes, FDEA **176** (t_R = 10.7 min) and ClDEA **174** (t_R = 10.7 min). In addition three new peaks were observed and found by their masses to be the triazole products of the CuAAC reaction. The first new peak at t_R = 12.8 min was identified as FDEA-RGD **201** by the *m/z* peak at 923.8, corresponding to the $[M+H]^+$ species shown in **Figure 26 C**. This peak was well separated from the corresponding chloro-triazole ClDEA-RGD **200**, at t_R = 13.5 min, with *m/z* = 939.8 shown in **Figure 26 D**. The separation of this chlorinated triazole from the fluorinated triazole is important, as these two compounds need to be resolved upon preparation of the radiolabelled version of FDEA-RGD **201**.

In addition to the two expected halogenated products, a third minor peak was observed (**Figure 26 E**), found to be the triazole formed by reaction of c(RGDfK[N_3]) **199** with the selenomethyl ether by-product from the breakdown of the transhalogenation intermediate SeEAM **174**. Triazole **203** was identified both by the peak at *m/z* = 999.8 and a distinctive selenium isotope pattern (**Figure 26 F**).

The CuAAC reaction produced the desired triazole compounds efficiently, in a reaction coupled to the enzymatic transhalogenation. The next step was to demonstrate this new labelling methodology in the PET environment. However, before the synthesis was optimised with [^{18}F]fluoride, the anticipated triazole products were assessed for their affinity towards $\alpha_V\beta_3$ integrin.

2.6.3. Binding assay of FDEA-RGD 201 to $\alpha_V\beta_3$ integrin

A multitude of synthetic RGD peptide derivatives are known to maintain high affinity for $\alpha_V\beta_3$ when modified at the lysine residue.[43,44] We wished to establish that the bioconjugation to the fluoroadenosine moiety of FDEA **176** though the triazole linker was not detrimental to the binding affinity of the RGD motif.

The binding affinity of the prepared RGD construct was determined by evaluation of the binding of the peptide to immobilised $\alpha_V\beta_3$.[37] These experiments were conducted by Dr Ian Fleming at the University of Aberdeen. In an ELISA based assay, the compounds were evaluated for their ability to complete with c(RGDfK[PEG-PEG-biotin]) for binding to immobilised $\alpha_V\beta_3$, and the values compared to those of reference peptides. The results of these investigations are summarised in **Table 1**.

Table 1. IC_{50} values of selected RGD-containing peptides measured as the ability to compete with c(RGDfK[PEG-PEG-biotin]) for binding to immobilized $\alpha_V\beta_3$ integrin. Results are the average ± standard error (s.e.) from three independent experiments performed in triplicate. Q is the normalised affinity of the peptides, referenced to GRGDSPK. Measurements were performed by Dr Ian Fleming.

Compound	*IC_{50} ± s.e /μM*	*Q*
RGD	8.56 ± 2.24	4.019
GRGDSPK	2.13 ± 0.41	1.000
c(RGDfK[N_3]) **199**	0.09 ± 0.01	0.042
FDEA-RGD **201**	0.33 ± 0.03	0.155

The RGD motif itself shows only a moderate competitive ability, with an IC_{50} value of 8.56 μM, while the more standard reference peptide GRGDSPK[38] shows higher affinityy with an IC_{50} value of 2.13 μM. Unmodified azido-peptide c(RGDfK[N_3]) **199**

shows an order of magnitude greater binding affinity for $\alpha_V\beta_3$ than the linear peptides, a well-documented feature of the cyclic RGD peptides.[39] Conjugation of azido peptide **199** to the fluoroacetylene FDEA **176** results in an RGD peptide which retains high affinity. While the IC_{50} value for FDEA-RGD **201** is three times higher than that of the unmodified peptide **199**, the construct still retains an affinity approximately an order of magnitude greater than the linear reference compounds. The presence of the fluoroadenosine moiety is therefore not deleterious to the integrin affinity of the peptide, and would be expected to show similar *in vivo* binding properties to other RGD peptides, assuming the peptide is not metabolised upon administration.

2.7. Radiosynthetic evaluation of CIDEA-fluorinase system for PET

PET experiments described in this section were conducted at Imanova Ltd., based at the Hammersmith Hospital in London. Radiolabelling experiments were performed by Dr Mayca Onega, while animal studies were performed by Dr Sharon Ashworth. All of the experiments described were performed in accordance with the U.K. Animals (Scientific Procedures) Act 1986. The procedures used were approved by the Animal Ethical Review Committee of Imperial College, London.

2.7.1. Fluorinase mediated [^{19}F]fluoride labelling *vs* [^{18}F]fluoride labelling

Enzymatic assays conducted with the fluorinase enzyme using [^{19}F]fluoride are usually conduced with catalytic quantities of the enzyme (29–145 μM), and an excess of fluoride ion (20–75 mM). This ratio changes dramatically when using [^{18}F]fluoride, where the fluoride ion concentration is very much lower, and the enzyme concentration very much higher.

The amount of fluorine-18 in a sample is quantified in terms of activity, in units of Bequerel (Bq), where 1 Bq = 1 decay per second. Specific activity is the measure of the activity per mole of compound and specific activity decreases in the presence of any fluorine-19. The theoretical maximum specific activity of [^{18}F]fluoride ion is 6.4×10^7 GBq.mmol^{-1}.[45] Therefore, a 0.5 GBq sample of [^{18}F]fluoride used in a 250 μL volume reaction (average fluorinase PET experiment) has a [^{18}F]fluoride ion concentration of 31 nM. In real terms, [^{18}F]fluoride concentrations are used in the low nanomolar or picomolar range.[45] This, coupled to fluorinase concentrations of 0.5 mM (20 mg.mL^{-1}), means there is ~10^6 excess of fluoride compared to enzyme. The

fluorinase is operating under single turnover conditions. The result of this is that the fluorinase has been found to be very efficient in transforming [^{18}F]fluoride to organic fluorine-18, where reactions are rapid and incorporations high.[1,46,3,47,48]

2.7.2. Synthesis of [^{18}F]FDEA-RGD [^{18}F]-201

The reaction of the alkyne-modified substrate ClDEA **174** was explored in a transhalogenation reaction with [^{18}F]fluoride to produce [^{18}F]FDEA [^{18}F]-**176**, as illustrated in **Scheme 19**.

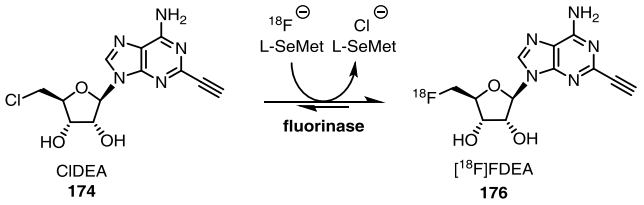

Scheme 19. Fluorinase catalysed transhalogenation reaction with [^{18}F]fluoride where the fluorinase is used to synthesise [^{18}F]FDEA [^{18}F]-**176**.

ClDEA **174** (~0.1 mg, final concentration ~1 mM) was incubated with the fluorinase (20 mg.mL^{-1}), L-selenomethionine (0.08 mM) and [^{18}F]fluoride (up to 525 MBq) for 30 minutes at 37 °C. The enzyme was denatured and precipitated by heating to 95 °C for 5 min and the reaction centrifuged at 13 000 rpm for 5 min. The supernatant was analysed by HPLC coupled to a UV- and radio- detector in series, and the resulting chromatograms are shown in **Figure 27**. In the radio-HPLC trace shown in **Figure 27 A** two peaks were evident, one with t_R = 1.7 min, which was identified as unreacted [^{18}F]fluoride, while the second, at t_R = 7.2 min represented a new product. The new product was identified as [^{18}F]FDEA [^{18}F]-**176** by spiking with a synthetic sample of [^{19}F]-**176**, which was found to co-elute. This can be seen in the UV trace shown in **Figure 27 B**. The radiochemical incorporation of [^{18}F]fluoride into [^{18}F]-**176** was found to be 69%.

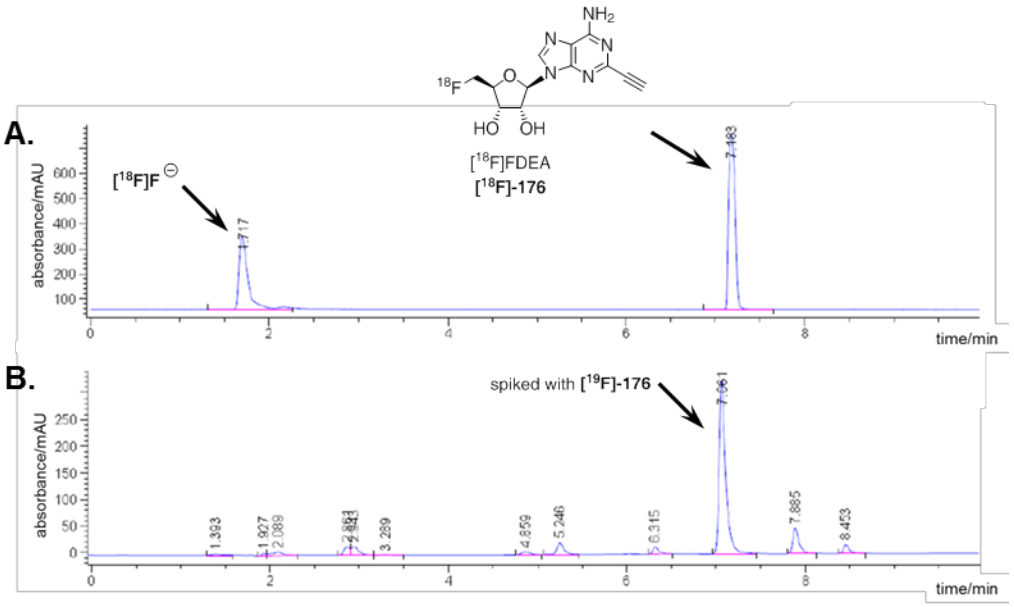

Figure 27. **A.** Radio-HPLC chromatogram of the transhalogenation mixture after 30 minutes, showing residual [^{18}F]fluoride at t_R = 1.7 min and a new product, [^{18}F]FDEA [^{18}F]-**176**, at t_R = 7.2 min. **B.** UV HPLC chromatogram after spiking this sample with FDEA **176** confirmed that the new product was [^{18}F]-**176**. Chromatograms acquired by Dr Mayca Onega at Imanova.

The crude fluorinase reaction mixture containing [^{18}F]FDEA [^{18}F]-**176** was subjected to a CuAAC reaction with the azido RGD peptide **199** as described previously in **Section 2.6.2**, and shown in **Scheme 20**. c(RGDfK[N_3]) **199** (0.3 mg) was dissolved in the supernatant after centrifugation. This was followed by addition of fresh sodium ascorbate solution and a solution of $CuSO_4$.TBTA. This mixture was incubated at room temperature for 30 min, before the crude reaction mixture assessed by radio-HPLC (**Figure 28**). Conversion to the triazole [^{18}F]-**201** (t_R = 8.8 min) was complete, and only residual excess [^{18}F]fluoride (t_R = 1.7 min) from the labelling step was still present.

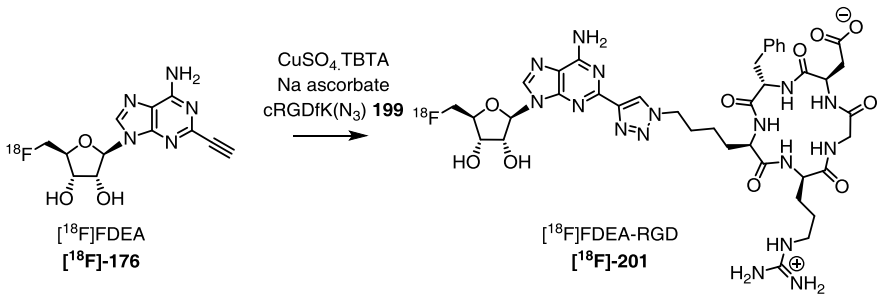

Scheme 20. CuAAC reaction between radiolabelled [^{18}F]-**176** and c(RGDfK[N_3]) **199**, to generate triazole [^{18}F]-**201**.

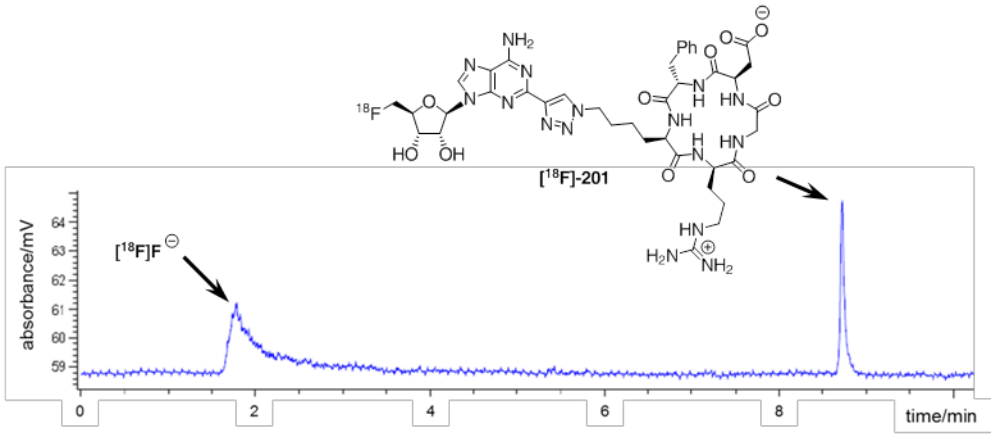

Figure 28. Radio-HPLC trace after the CuAAC reaction showing residual [^{18}F]fluoride, and the production of a new compound, [^{18}F]FDEA-RGD [^{18}F]-**201** at t_R = 8.8 min. [^{18}F]FDEA [^{18}F]-**176** (t_R = 7.2 min) is not observed.

[^{18}F]FDEA-RGD [^{18}F]-**201** was purified by semi-preparative HPLC. Fractions containing the product were collected, diluted in water and the product [^{18}F]-**201** was trapped on a C_{18} cartridge. The cartridge was washed with water to remove any acetonitrile before eluting [^{18}F]-**201** with ethanol into saline to give a solution suitable for injection. The non-decay corrected radiochemical yield for the synthesis of [^{18}F]-**201** from [^{18}F]fluoride was found to be up to 20%, delivering up to 95 MBq of the product for injection after a 2 h synthesis procedure.

After formulation, the product, [^{18}F]-**201** was analysed for its purity by UV- and radio-HPLC, as shown in **Figure 29**. The radio-HPLC trace shown in **Figure 29 A** indicates that all residual [^{18}F]fluoride has been removed from the reaction mixture, and that [^{18}F]-**201** has a high radiochemical purity. Spiking the final product with a synthetic sample of [^{19}F]-**201** (**Figure 29 B**) was consistent with the identity of the isolated tracer as [^{18}F]FDEA-RGD [^{18}F]-**201**.

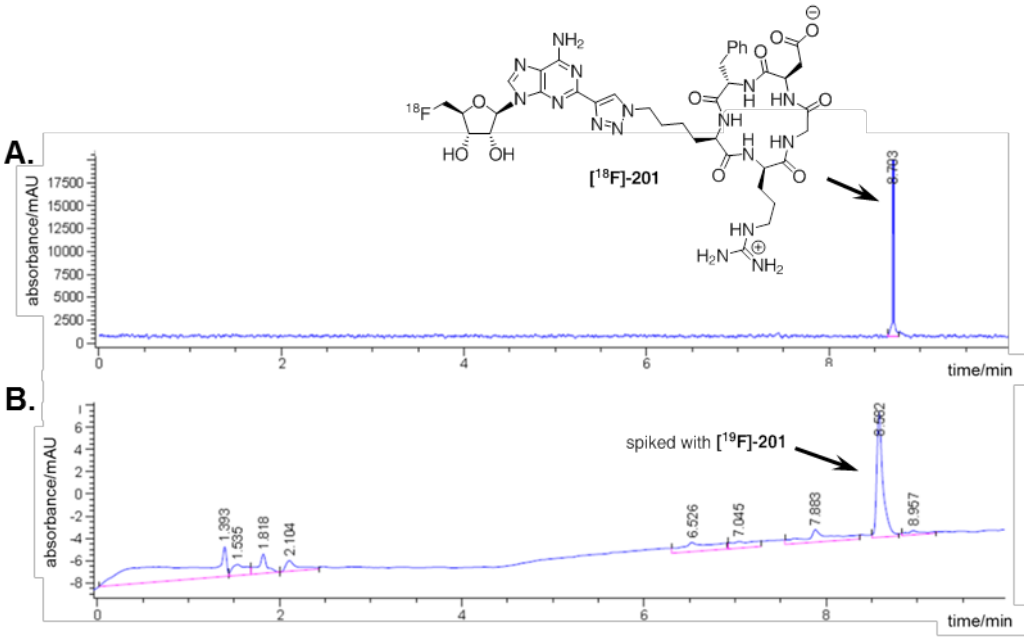

Figure 29. **A.** Radio-HPLC chromatogram of the purified triazole product [^{18}F]-**201**, a single peak at t_R = 8.8 min. **B.** UV HPLC chromatogram after spiking with FDEA-RGD **201** confirmed that the product was [^{18}F]-**201**. Chromatograms acquired by Dr Mayca Onega at Imanova.

These results illustrate that the synthetic procedure with the new fluorinase substrate works well under the conditions of a PET radiolabelling experiment. The fluorinase coupled to this novel alkyne-bearing substrate, can clearly be applied further as a tool for radiolabelling peptides. The [^{18}F]-triazole [^{18}F]-**201** synthesis was investigated in an imaging experiment in healthy rats to assess the stability of the new construct and to investigate the biodistribution of the tracer *in vivo*.

2.7.3. *In vivo* evaluation of [^{18}F]FDEA-RGD 201

One of the requirements of a good radiotracer is that it remains stable *in vivo* for the duration of the imaging experiment. Radiotracers, like other drugs, pass through normal metabolic pathways and have defined metabolic half-lives once administered. Metabolism of the tracer compromises its utility on two fronts. If the metabolism involves cleavage of the ^{18}F–C bond, the primary agent which interferes with the imaging process is [^{18}F]fluoride. [^{18}F]Fluoride that is released from the tracer into systemic circulation is absorbed by the bone due to the high affinity of fluoride for the calcium minerals.[49] Bone uptake can mask other pathologies and is an undesired quality for radiotracers. Metabolites which do still contain the fluorine-18 label will have altered pharmacokinetic properties to the parent tracer, obscuring accurate determination of its imaging profile.

[^{18}F]FDEA-RGD [^{18}F]-**201** was synthesised as described above and administered to two healthy, male Sprague-Dawley rats. For one of the rats, a dynamic PET scan was acquired over 60 min, co-registered with a CT scan for attenuation correction. Arterial blood samples were periodically drawn from both rats for metabolite monitoring. The rats were euthanased post-imaging and dissected *post mortem* and the activity accumulation in the dissected tissues assessed by gamma counting.

The summed PET-CT image of the rat is shown below in **Figure 30**. PET image scales are presented as standard uptake values (SUV = {(tissue activity/mL)/(injected activity/animal weight[g])}). The image illustrated that [^{18}F]FDEA-RGD [^{18}F]-**201** accumulated predominantly in the liver of the rat during the scan. Lower uptake was also observed in the skin and lungs, but it was clear that [^{18}F]-**201** did not cross the blood-brain barrier into the CNS.

The image also confirmed that the ^{18}F–C bond of [^{18}F]-**201** was metabolically stable *in vivo*. No uptake of radioactivity was observed in the bone in **Figure 30**, indicating that the tracer was stable to defluorination. Further information about the biodistribution of the tracer was obtained from *post mortem* gamma counting.

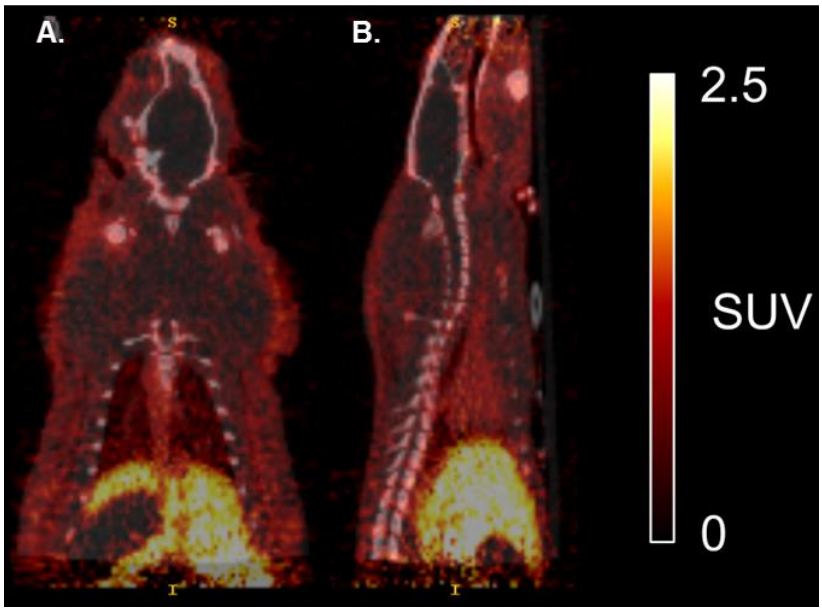

Figure 30. **A.** Coronal and **B.** sagittal fused summed PET (colour) and CT (greyscale) images (0-70 min). [^{18}F]FDEA-RGD [^{18}F]-**201** in the liver. PET image scales are presented as standard uptake values (SUV= {(tissue activity/mL)/(injected activity/animal weight[g])}). Images acquired by Dr Sharon Ashworth and Dr Mayca Onega of Imanova Ltd.

The biodistribution of activity (**Figure 31**, expressed as SUV values) showed that the tracer was excreted rapidly by the urinary system, and that after 60 min most of the activity was present in the urine, with significant levels also present in the kidneys and

bladder. Accumulation of the tracer however was observed in the liver, small and large intestines and the lungs. This is consistent with the natural biodistribution profile of $\alpha_V\beta_3$ integrin and similar accumulation has been observed in heathy controls for other radiolabelled RGD constructs.[50]

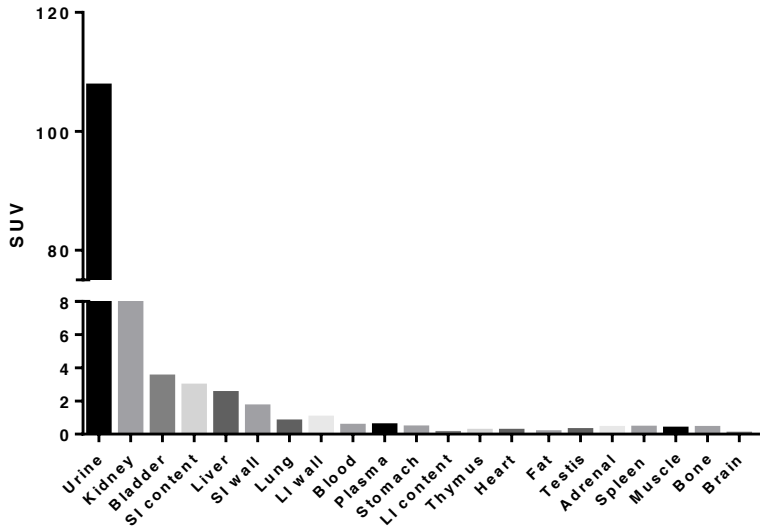

Figure 31. The mean biodistribution of radioactivity in the tissues of healthy rats (n=2) expressed as standardised uptake values (SUV) at 60 minutes injection of [^{18}F]FDEA-RGD [^{18}F]-**201**. SI = small intestine, LI = large intestine. Data collected by Dr Sharon Ashworth.

The blood plasma of the rats was analysed for the presence of radiolabelled metabolites to investigate whether the tracer is metabolised at sites other than the ^{18}F-C bond. Arterial blood samples were drawn from both rats at 5, 15, 30 and 60 min post injection and the plasma fractions extracted with acetonitrile and the extracts analysed by HPLC. Thirty fractions were collected from the HPLC over 10 min, and these fractions were analysed for their radioactivity content. In the samples from both rats at all time points, only a single peak was observed in the reconstructed chromatograms. The chromatograms for the 60 min samples are shown in **Figure 32**. The single peak was confirmed to be [^{18}F]FDEA-RGD [^{18}F]-**201** by co-elution with a synthetic standard of [^{19}F]FDEA-RGD **201**. This data confirms that in addition to demonstrating ^{18}F–C bond stability, the circulating tracer in the blood was not subject to significant metabolism at other sites and that the intact compound was successfully perfusing the tissues.

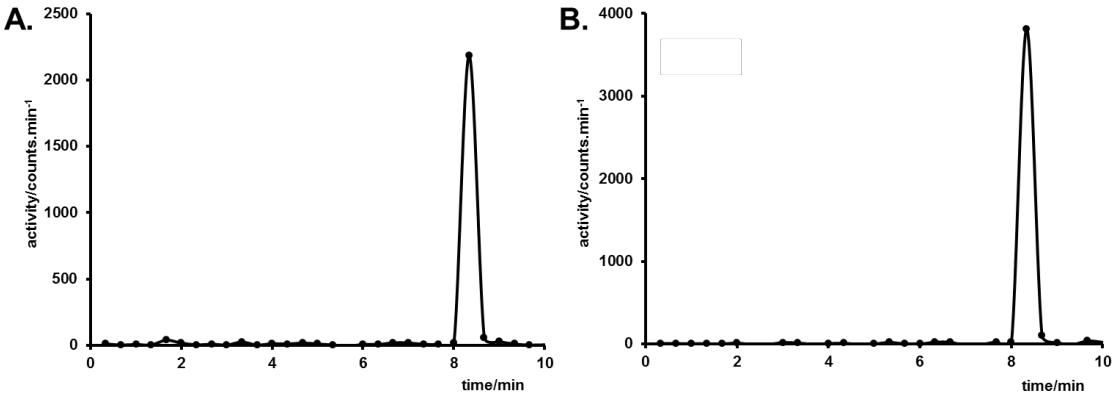

Figure 32. Reconstructed radiochromatogram of acetonitrile plasma extracts of arterial blood from **A.** rat A and **B.** rat B, taken 60 min post injection and showing a single peak, corresponding to unmetabolised [^{18}F]FDEA-RGD [^{18}F]-**201**.

The biodistribution data confirm that the compound behaves in a manner consistent with an intact RGD motif and that [^{18}F]-**201** targets organs that have naturally higher levels of expression of the $\alpha_V\beta_3$ integrin.

2.8. Conclusions

The aim of this project was to design and investigate a novel substrate for the fluorinase for application towards novel labelling strategies for positron emission tomography. Based on known protein crystal structures of the fluorinase, there was an indication that an acetylenic substrate, ClDEA **174**, may be a suitable candidate for investigation. The acetylene was expected to lie in a void projecting from the active site of the fluorinase.

Towards this end, the new substrate and its anticipated product were synthesised and the fluorinase was overexpressed for biotransformation assays. ClDEA **174** was investigated as a substrate and it was found to be a relatively good substrate for the fluorinase, undergoing a transhalogenation reaction when incubated with the enzyme.

The kinetics of this new substrate with the fluorinase were investigated and the transhalogenation reaction was found to operate at approximately 60% of the rate of the unmodified substrate. Steady state kinetic parameters, similar to those of other known fluorinase substrates were obtained. In a competition experiment, where ClDEA **174** was incubated with the fluorinase in the presence of the unmodified substrate ClDA **23**, the fluorinase catalysed the reaction only of unmodified substrate confirming that the enzyme was able to distinguish the two substrates.

The ability of the enzyme to distinguish these two substrates prompted investigation of the binding parameters of the new substrate **174** and product **176**, by comparison to ClDA **23** and FDA **22**. Isothermal titration calorimetry indicated that the acetylenic substrates bind with lower affinity than their non-modified analogues, while maintaining the trend that the fluorinated compounds show an order of magnitude higher binding affinity when compared to their chlorinated analogues.

Crystallographic investigations of FDEA **176** bound to the fluorinase showed that the acetylene occupied the pocket that was predicted when the substrate was designed.

FDEA **174** was investigated in a CuAAC reaction with and azide-bearing RGD peptide **199**, and found to undergo a rapid reaction. The addition of the fluoroacetylene moiety to the cyclic peptide did not significantly affect the binding of the motif to immobilised $\alpha_V\beta_3$ integrin, and showed a similar sub-micromolar affinity to that of the unmodified cyclic RGD peptide.

This novel biotransformation was transferred to the PET environment, and the transhalogenation experiments repeated with [^{18}F]fluoride. [^{18}F]FDEA [^{18}F]-**176** was prepared with a 69% radiochemical conversion, and this compound was reacted with c(RGDfK[N_3]) **199** in a CuAAC reaction to efficiently generate [^{18}F]FDEA-RGD [^{18}F] **201**. The "click" product was purified by HPLC and formulated to prepare a dose ready for injection into a rat. The non-corrected radiochemical yield was found to be 20% for the synthesis of [^{18}F]-**201**.

[^{18}F]FDEA-RGD [^{18}F]-**201** was injected into two rats and was found to accumulate in tissues in accordance with the natural distribution of $\alpha_V\beta_3$ integrin. The novel tracer, [^{18}F]-**201**, was found to be metabolically stable up to 60 minutes *in vivo*.

These protocols extend the application of the fluorinase as a mild and efficient ^{18}F-labelling tool beyond the natural substrate. One limitation of this approach is that it requires the availability of azide-bearing biomolecules, which are pre-functionalized prior to labelling. This can be achieved by recombinant protein expression with azide-containing amino acids[51] or by using traditional bioconjugations at lysine or cysteine to azide-bearing linkers.[52] However, it was discovered that the alkyne functionality projects out of the active site and into the solvent, and this opened up the additional possibility of extending a linker from the terminus of the acetylene to pre-tag a peptide for single step labelling. This development is discussed in the next chapter.

2.9. References

1. H. Deng, S. L. Cobb, A. D. Gee, A. Lockhart, L. Martarello, R. P. McGlinchey, D. O'Hagan, and M. Onega, *Chem. Commun.*, 2006, 652–654.

2. M. Winkler, J. Domarkas, L. F. Schweiger, and D. O'Hagan, *Angew. Chem. Int. Ed.*, 2008, **120**, 10295–10297.

3. X.-G. Li, J. Domarkas, and D. O'Hagan, *Chem. Commun.*, 2010, **46**, 7819–7821.

4. H. Deng, S. L. Cobb, A. R. McEwan, R. P. McGlinchey, J. H. Naismith, D. O'Hagan, D. A. Robinson, and J. B. Spencer, *Angew. Chem. Int. Ed.*, 2006, **45**, 759–762.

5. S. L. Cobb, University of St Andrews, *PhD Thesis*, 2006.

6. M. E. Sergeev, F. Morgia, M. R. Javed, M. Doi, and P. Y. Keng, *J. Mol. Catal. B Enzym.*, 2013, **97**, 74–79.

7. M. Coliboeuf and D. O'Hagan, University of St Andrews, *Unpublished Results*.

8. S. L. Cobb, H. Deng, A. R. McEwan, J. H. Naismith, D. O'Hagan, and D. A. Robinson, *Org. Biomol. Chem.*, 2006, **4**, 1458–1460.

9. C. Dong, F. Huang, H. Deng, C. Schaffrath, J. B. Spencer, D. O'Hagan, and J. H. Naismith, *Nature*, 2004, **427**, 561–565.

10. H. C. Kolb, M. G. Finn, and K. B. Sharpless, *Angew. Chem. Int. Ed.*, 2001, **40**, 2004–2021.

11. A. Matsuda, M. Shinozaki, M. Tadashim, H. Machida, and T. Abiru, *Chem. Pharm. Bull.*, 1985, **33**, 1766–1769.

12. A. Matsuda, M. Shinozaki, T. Yamaguchi, H. Homma, R. Nomoto, T. Miyasaka, Y. Watanabe, and T. Abiru, *J. Med. Chem.*, 1992, **35**, 241–252.

13. H. Homma, Y. Watanabe, T. Abiru, T. Murayama, Y. Nomura, and A. Matsuda, *J. Med. Chem.*, 1992, **35**, 2881–2890.

14. S. A. Adah and V. Nair, *Tetrahedron*, 1997, **53**, 6747–6754.

15. J. Lee, S. E. Kim, J. Y. Lee, S. Y. Kim, S. U. Kang, S. H. Seo, M. W. Chun, T. Kang, S. Y. Choi, and H. O. Kim, *Bioorg. Med. Chem. Lett.*, 2003, **13**, 1087–1092.

16. J. Gerster, J. Jones, and R. Robins, *J. Org. Chem.*, 1963, **28**, 945–948.

17. M. Robins and B. Uznanski, *Can. J. Chem.*, 1981, **59**, 2601–2607.

18. V. Nair and S. Richardson, *Synthesis*, 1982, 670–672.

19. M. J. Robins, F. Hansske, S. F. Wnuk, and T. Kanai, *Can. J. Chem.*, 1991, **69**, 1468–1474.

20. V. Clark, A. Todd, and J. Zussman, *J. Chem. Soc.*, 1951, 2952–2958.

21. V. Bakthavachalam, L. Lin, X. Cherian, and A. W. Czarnik, *Carbohydr. Res.*, 1987, **170**, 124–135.

22. S. Lehel, H. Horvath, I. Boros, T. Marian, and L. Tron, *J. Radioanal. Nuc. Chem.*, 2002, **251**, 413–416.

23. T. D. Ashton and P. J. Scammells, *Bioorg. Med. Chem. Lett.*, 2005, **15**, 3361–3363.

24. R. C. Spitale, M. G. Heller, A. J. Pelly, and J. E. Wedekind, *J. Org. Chem.*, 2007, **72**, 8551–8554.

25. F. W. Studier, *Protein Expr. Purif.*, 2005, **41**, 207–234.

26. X. Zhu, D. A. Robinson, A. R. McEwan, D. O'Hagan, and J. H. Naismith, *J. Am. Chem. Soc.*, 2007, **129**, 14597–14604.

27. L. W. Parks and F. Schlenk, *Arch. Biochem. Biophys.*, 1958, **75**, 291–292.

28. S. K. Shapiro and A. N. Mather, *J. Biol. Chem.*, 1958, **233**, 631–633.

29. H. Deng, L. Ma, N. Bandaranayaka, Z. Qin, G. Mann, K. Kyeremeh, Y. Yu, T. Shepherd, J. H. Naismith, and D. O'Hagan, *ChemBioChem*, 2014, **15**, 364–368.

30. S. Schäuble, A. K. Stavrum, P. Puntervoll, S. Schuster, and I. Heiland, *FEBS Lett.*, 2013, **587**, 2818–2824.

31. D. Moll, B. Zimmerman, F. Gesellchen, and F. W. Herbery, in *Proteomics in Drug Research. Volume 28 of Methods and Principles in Medicinal Chemistry*, eds. M. Hamacher, K. Marcus, K. Stühler, A. van Hall, B. Warscheid, and H. E. Meyer, John Wiley & Sons, 2006, pp. 163–165.

32. K. Dross, R. F. Rekker, G. de Vries, and R. Mannhold, *Mol. Inform.*, 1998, **17**, 549–557.

33. S. Dall'Angelo, Q. Zhang, I. N. Fleming, M. Piras, L. F. Schweiger, D. O'Hagan, and M. Zanda, *Org. Biomol. Chem.*, 2013, **11**, 4551–4558.

34. C. J. Avraamides, B. Garmy-Susini, and J. A. Varner, *Nat. Rev. Cancer*, 2008, **8**, 604–617.

35. E. Ruoslahti and M. D. Pierschbacher, *Science*, 1987, **238**, 491–497.

36. E. Ruoslahti and M. D. Pierschbacher, *Cell*, 1986, **44**, 517–518.

37. R. Haubner, H. J. Wester, U. Reuning, R. Senekowitsch-Schmidtke, B. Diefenbach, H. Kessler, G. Stöcklin, and M. Schwaiger, *J. Nucl. Med.*, 1999, **40**, 1061–1071.

38. R. Haubner, R. Gratias, B. Diefenbach, and S. Goodman, *J. Am. Chem. Soc.*, 1996, **118**, 7461–7472.

39. M. Aumailley, M. Gurrath, G. Müller, J. Calvete, R. Timpl, and H. Kessler, *FEBS Lett.*, 1991, **291**, 50–54.

40. I. Dijkgraaf, A. Y. Rijnders, A. Soede, A. C. Dechesne, G. W. van Esse, A. J. Brouwer, F. H. M. Corstens, O. C. Boerman, D. T. S. Rijkers, and R. M. J. Liskamp, *Org. Biomol. Chem.*, 2007, **5**, 935–944.

41. V. V. Rostovtsev, L. G. Green, V. V. Fokin, and K. B. Sharpless, *Angew. Chem. Int. Ed.*, 2002, **41**, 2596–2599.

42. T. R. Chan, R. Hilgraf, K. B. Sharpless, and V. V Fokin, *Org. Lett.*, 2004, **6**, 2853–2855.

43. W. Li, L. Lang, G. Niu, N. Guo, Y. Ma, D. O. Kiesewetter, B. Shen, and X. Chen, *Amino Acids*, 2012, **43**, 1349–1357.

44. S. Liu, *Bioconj. Chem.*, 2009, **20**, 2199–2213.

45. N. Mason and C. Mathis, in *Positron Emission Tomography: Basic Sciences*, eds. D. L. Bailey, D. W. Townsend, P. E. Valk, and M. N. Maisey, Springer Science & Business Media, 2006, p. 205.

46. M. Winkler, J. Domarkas, L. F. Schweiger, and D. O'Hagan, *Angew. Chem. Int. Ed.*, 2008, **47**, 10141–10143.

47. M. Onega, J. Domarkas, H. Deng, L. F. Schweiger, T. A. D. Smith, A. E. Welch, C. Plisson, A. D. Gee, and D. O'Hagan, *Chem. Commun.*, 2010, **46**, 139–141.

48. S. Dall'Angelo, N. Bandaranayaka, A. D. Windhorst, D. J. Vugts, D. van der Born, M. Onega, L. F. Schweiger, M. Zanda, and D. O'Hagan, *Nucl. Med. Biol.*, 2013, **40**, 464–470.

49. V. W. Pike, *Trends Pharmacol. Sci.*, 2009, **30**, 431–440.

50. J. Oxboel, M. Brandt-Larsen, C. Schjoeth-Eskesen, R. Myschetzky, H. H. El-Ali, J. Madsen, and A. Kjaer, *Nucl. Med. Biol.*, 2014, **41**, 259–267.

51. K. L. Kiick, E. Saxon, D. A. Tirrell, and C. R. Bertozzi, *Proc. Natl. Acad. Sci. U. S. A.*, 2002, **99**, 19–24.

52. L. N. Goswami, Z. H. Houston, S. J. Sarma, S. S. Jalisatgi, and M. F. Hawthorne, *Org. Biomol. Chem.*, 2013, **11**, 1116–1126.

3. Synthesis and evaluation of multimeric RGD substrates for the fluorinase

3.1. Extension of the fluorinase system to "last step" labelling for PET

The development of ClDEA **174**, the acetylenic substrate for the fluorinase, showed that the enzyme has a tolerance at the 2-position of the adenine base. **Chapter 2** discussed how the modification of the nucleoside substrate at this position generated a novel substrate for the enzyme. The modified substrate was employed in a fluorinase-catalysed transhalogenation reaction coupled to a CuAAC reaction for the synthesis of a novel PET radiotracer, [^{18}F]FDEA-RGD [^{18}F]-**201**, in a two-step procedure for peptide radiolabelling.

There is a need for simple, "last step" radiolabelling procedures with fluorine-18 that are conducted under conditions suitable for labelling peptides and proteins.[1] The poor nucleophilicity of aqueous [^{18}F]fluoride ion precludes direct labelling of biomolecules in buffer, and to do so requires the use of either prosthetic groups[2] or fluoride sequestering species (boron,[3] aluminium[4] or silicon[5]). Based on the substrate tolerance of the fluorinase, we were interested in exploring this enzymatic system for "last step" radiolabelling of peptides.

The 2-position of the fluorinase substrate lies close to a hole at the surface of the enzyme active site. A co-crystal structure of FDEA **176** with the fluorinase (**Figure 1 A**) showed that the acetylene at C-2 projects out of the active site of the enzyme, towards the bulk solvent. It was immediately attractive to explore tethering a peptide cargo to the acetylene through an appropriate linker.

The enzymatic approach could offer a novel protocol for "last step" fluorination of peptides. A "last step" labelling procedure using an enzyme is attractive as it avoids the use of heating, low pH, or organic solvents during the radiolabelling reaction. Harsh conditions are required for all of the other presently available "last step" labelling procedures.

Based on this hypothesis, a peptide-bearing substrate for the fluorinase was designed, as shown in **Figure 1 B**. The proposed substrate, ClDEA-TEG-RGD **204**, bears a chlorinated nucleoside for transhalogenation with fluoride, a tetraethyleneglycol (TEG) linker to extend the peptide cargo away from the surface of the enzyme, and an RGD peptide as a PET-relevant biomolecule. The acetylene of the modified substrate was preserved, extending the linker and peptide cargo out of the active site as it was suspected to be essential for maintaining activity.

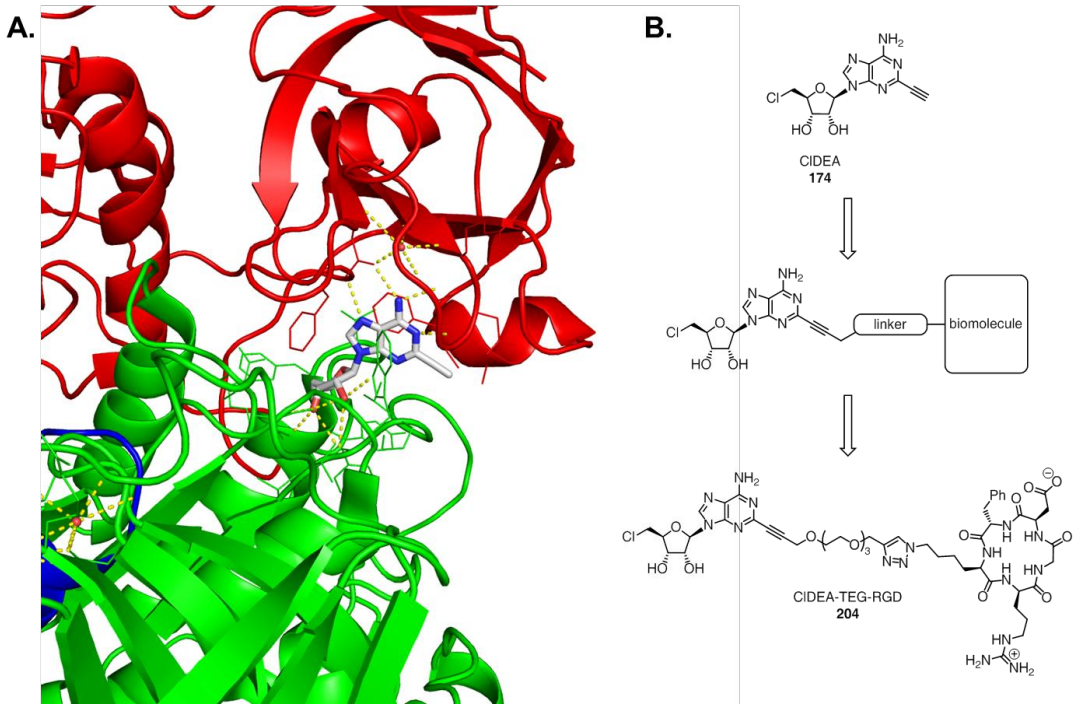

Figure 1. **A.** Co-crystal structure of the fluorinase and FDEA **174** showing the acetylene oriented out of the active site, between two subunits of the trimer. **B.** Tethering a biomolecule to the acetylene through an appropriate linker offers the potential of a "last step" biomolecule labelling for PET using the fluorinase enzyme.

3.1.1. Development of a peptide-bearing substrate for the fluorinase

ClDEA-TEG-RGD **204** was synthesised by Dr Qingzhi Zhang (St Andrews), using a similar approach to that employed in the synthesis of ClDEA **174**, described in **Chapter 2**. A Sonogashira coupling of mono-protected TEG-derivative **205** to 2-iodoadenosine **179**, followed by chlorination and silyl deprotection generated ClDEA-TEG **206** as a key intermediate. ClDEA-TEG **206** was coupled to azido-RGD peptide **199** using a CuAAC reaction, to give ClDEA-TEG-RGD **204**.

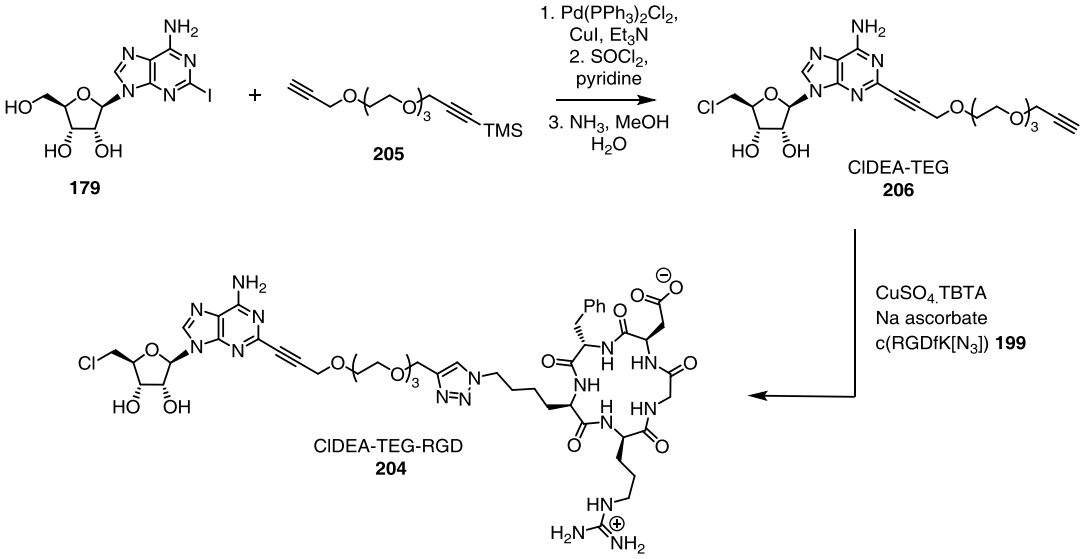

Scheme 1. Synthetic route towards ClDEA-TEG-RGD **204**, using a CuAAC reaction to tether the peptide cargo **199** to the linker-bearing nucleoside **206**. Synthesis conducted by Dr Qingzhi Zhang.

ClDEA-TEG-RGD **204** was incubated with the fluorinase in the presence of L-SeMet and fluoride in a phosphate buffer, and found to undergo enzymatic transhalogenation to rapidly generate FDEA-TEG-RGD **207**, as shown in **Figure 2**. The construct was also found to retain high affinity (0.07 μM) for immobilised $\alpha_V\beta_3$ integrin in a competition-based assay, similar to that described for FDEA-RGD **201** in **Chapter 2**.

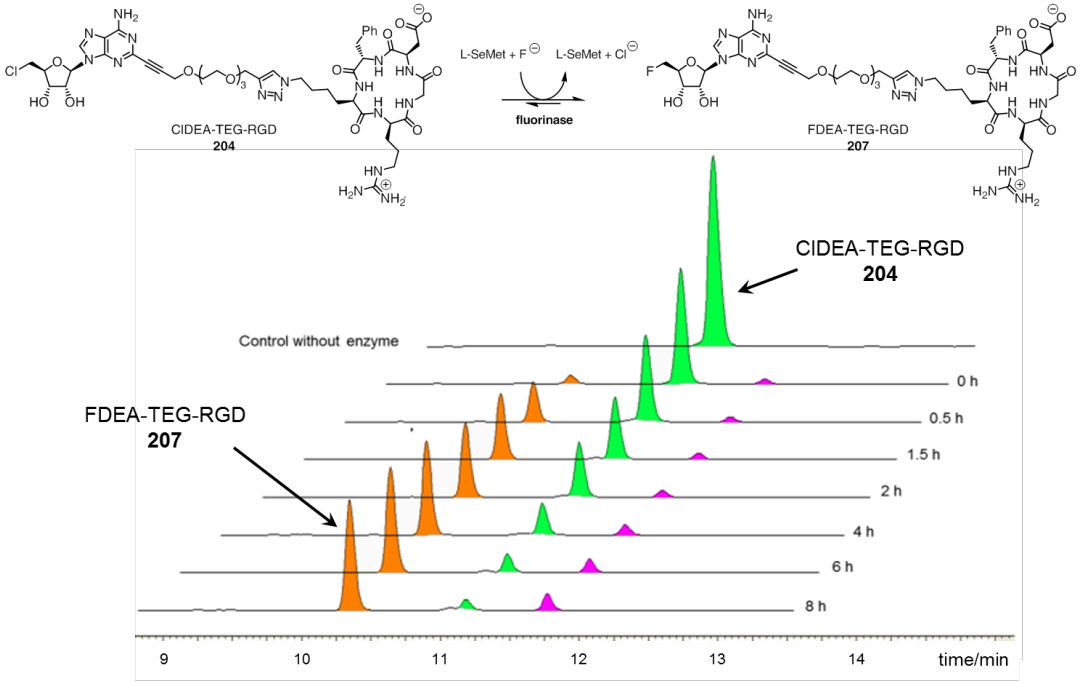

Figure 2. Fluorinase catalysed transhalogenation of ClDEA-TEG-RGD **204** to FDEA-TEG-RGD **207**, showing that the fluorinase can be applied to "last step" fluorination of peptides. Experiments conducted by Dr Qingzhi Zhang.

3.1.2. "Last step" radiolabelling of a peptide with fluorine-18

The "last step" fluorination protocol was explored under PET radiolabelling conditions at Imanova Ltd by Dr Mayca Onega. When the ClDEA-TEG-RGD **204** (0.3 mM) was incubated with the fluorinase (20 $mg.mL^{-1}$) and [^{18}F]fluoride solution, the transhalogenation reaction was found to proceed to completion within 30 minutes. No residual [^{18}F]fluoride was observed by radio-HPLC, suggesting that all [^{18}F]fluoride was incorporated into the radiolabelled product, [^{18}F]-**207**, as shown in **Figure 3 A**.

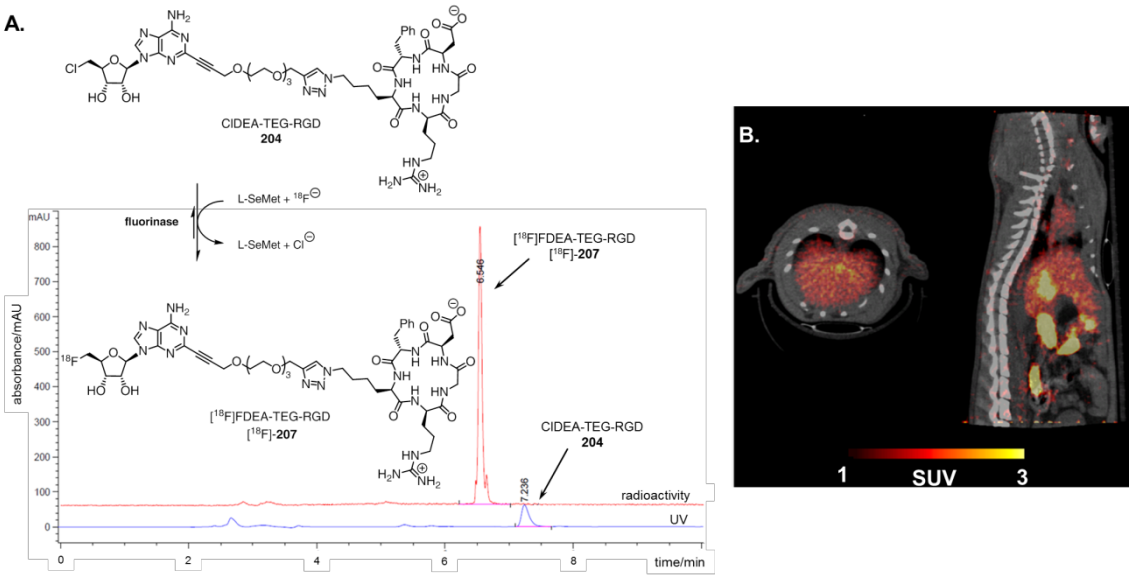

Figure 3. **A.** Radio- and UV- HPLC traces of a fluorinase-catalysed transhalogenation reaction with ClDEA-TEG-RGD **207** and [^{18}F]fluoride showing complete conversion to [^{18}F]-**207** after 30 min. No residual [^{18}F]fluoride was observed in the supernatant. **B.** Co-registered PET-CT image of a healthy rat dosed with [^{18}F]FDEA-TEG-RGD [^{18}F]-**207**. No uptake of radioactivity is seen in the bone indicating that the construct is stable to defluorination. Experiments conducted by Dr Mayca Onega and Dr Sharon Ashworth at Imanova Ltd.

The radiolabelling reaction with ClDEA-TEG-RGD **204** was repeated and the product, [^{18}F]-**207** purified by semi-preparative HPLC. Isolated [^{18}F]-**207** was formulated into sterile saline and injected into a healthy rat in order to assess if this new peptide construct was metabolised *in vivo*. The summed PET-CT image of the rat obtained post administration is shown below in **Figure 3 B**. The image revealed uptake of the RGD-construct [^{18}F]-**207** into tissues of known high expression of the $\alpha_V\beta_3$ integrin, including the kidneys and the liver.[6] Importantly, little bone uptake of radioactivity was observed, indicating that [^{18}F]-**207** is not metabolised to release [^{18}F]fluoride ion.

Blood plasma metabolite analysis revealed that the construct was metabolised at a site other than the C–^{18}F bond. A more polar radioactive metabolite was observed in blood extracts, suggesting oxidative metabolic processing of [^{18}F]-**207**. In contrast,

[^{18}F]FDEA-RGD [^{18}F]-**201**, discussed in **Chapter 2**, did not undergo metabolism after administration. The difference between these two constructs is the presence of the acetylene and TEG chain in [^{18}F]FDEA-TEG-RGD [^{18}F]-**207**, suggesting that this may be the site of metabolic processing. The most likely position for metabolism is the internal alkyne, which could be a substrate for oxidation by P450 enzymes,[7] resulting in metabolism to more polar metabolites.

The ability of the fluorinase to recognise and react with the construct **204** revealed that the substrate tolerance of the fluorinase can be exploited beyond a simple acetylene. The tolerance of a more elaborate peptide-bearing substrate opened the possibility of tethering a range of larger and more complex peptide cargos to the PEG linker.

With an appropriate substrate, the fluorinase offers novel methodology for "last step" radiolabelling of peptides, under neutral pH conditions directly from aqueous [^{18}F]fluoride. The above experiments have demonstrated that a simple peptide-linked substrate could be efficiently fluorinated by the enzyme using both high concentrations of [^{19}F]fluoride, and under low [^{18}F]fluoride concentration conditions for PET. It was therefore attractive to explore more elaborate substrates for the fluorinase enzyme, in an effort to further probe the extent of the tolerance at the C-2 position of the substrate.

Multimeric RGD peptides are well characterised[8,9] constructs employed for PET imaging using either fluorine-18 or other heavy metallic PET isotopes. We were therefore interested in exploring such constructs as potential substrates for the fluorinase enzyme.

3.2. RGD multimers in molecular imaging

Multimeric interactions play a key role in recognition events between biological ligands and receptors.[10] For such interactions, multiple weak non-covalent interactions between monovalent ligands and individual receptors are enhanced by attaching the individual ligands to a single scaffold. For such interactions, many individually weak binding interactions can give rise to a highly thermodynamically favourable association.

The increased strength of the binding interaction between a multivalent ligand and multiple receptors arises as the entropic penalty associated with binding is largely paid upon binding of the first component of the multimeric ligand. The subsequent binding of additional ligands each provides a favourable enthalpic contribution to the total free energy of the interaction, while contributing a smaller entropic penalty.[11]

An example of multimeric enhancement of binding is observed with the association of the pentameric cholera toxin (as a pentavalent receptor) to ganglioside G_{M1} on the surface of cells.[12] The total free energy change of the sequential binding of the cholera toxin to five individual oligomers of ganglioside G_{M1} in solution (first binding event shown in **Figure 4 B**) was less than the total free energy change upon binding to densely packed G_{M1} on a cell surface. On the lipid surface, the individual units of G_{M1} are no longer free to translate and rotate, and the assembly behaves more like a multivalent ligand. The binding of the pentavalent toxin to G_{M1} on the surface of a bilayer (**Figure 4 C**) was essentially irreversible. The cholera toxin- G_{M1} system was also found to exhibit positive cooperativity, where the binding of one oligomer of G_{M1} to the toxin led to a larger enthalpic gain upon binding of the second, and subsequent oligomers of G_{M1}. For such multimeric systems, cooperativity can be positive, neutral or negative, however, the nett effect of enhanced free energy of binding is still observed in truly multivalent interactions.[13]

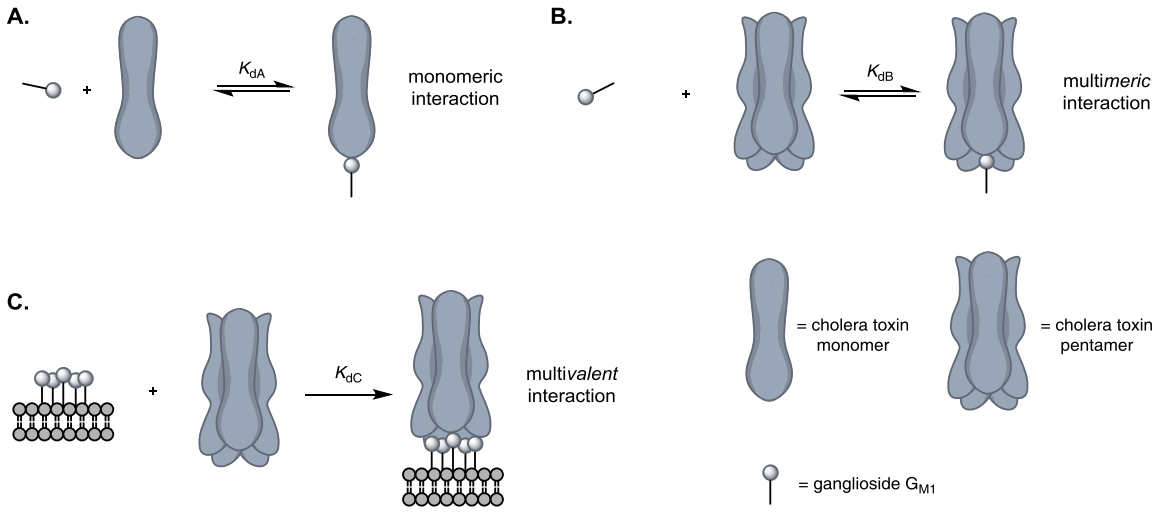

Figure 4. **A.** Binding of a monomeric ligand to a monomeric receptor. **B.** Binding of multiple monomeric ligands to a multimeric receptor. In this case, the increased affinity largely results from increased effective molarity of the receptor. **C.** An assembly of effectively pentavalent ligands binding to a pentavalent receptor in a multivalent interaction, which was found to be essentially irreversible for the cholera toxin-G_{M1} system.

The inherent increase in strength of the receptor-ligand interaction upon multimerisation, through either simple multimeric or more complex multivalent effects, is attractive within the context of molecular imaging. High affinity ligands are most desired as they show lower non-specific uptake coupled to stronger association with their target. The result of stronger binding interactions is improved signal to noise ratios (or tumour/blood ratios in the contexts of cancer), leading to improved images for use

in tumour diagnosis and monitoring.[14] The search for high affinity ligands for biological receptors has led to the development of imaging agents based on multivalent antibody fragments[15] or multivalent small peptides.[16]

The integrin proteins are a series of cell surface receptors that play a role in cellular recognition and adhesion. One such integrin, $\alpha_V\beta_3$, has been identified as a biomarker of angiogenesis, and is strongly associated with malignant tumours.[17] The ligand recognition sequence for binding to $\alpha_V\beta_3$ integrin is the arginyl-glycinyl-aspartyl (RGD) tripeptide motif. This motif has been incorporated into many monovalent molecular imaging agents, as discussed in **Chapter 2**.[18]

Cyclic RGD-containing peptides are high affinity ligands for $\alpha_V\beta_3$ integrin,[19] and multimerisation of these peptides has proved a reliable strategy for further enhancing the affinity (or avidity) of the resultant radiotracer.[8,9,14]

3.2.1. Multimeric RGD peptides based on amides

Amide couplings have been widely applied for the synthesis of multimeric RGD peptides. c(RGDfK), bearing a lysine side chain has been used as a source of the RGD peptide for such multimers. The constructs are synthesised by coupling a suitably protected cRGD peptide, bearing a free amine, to a divalent (or tetravalent) acid derivative.

The first synthesis of a radiolabelled multimeric RGD peptide was reported by Barret *et al.*[16] who synthesised technetium-99m labelled RGD-dimer [^{99m}Tc]-**208** (**Figure 5**) for use in SPECT (single photon emission computerised tomography) imaging. This assembly is based on a glutamic acid core, conjugated to the lysine residues of c(RGDfK). Subsequent coupling of the α-amine of the glutamic acid to a hydrazinonicotinic acid (HYNIC) ligand, followed by coordination to technetium-99m, gave the active dimeric RGD radiotracer [^{99m}Tc]-**208**.

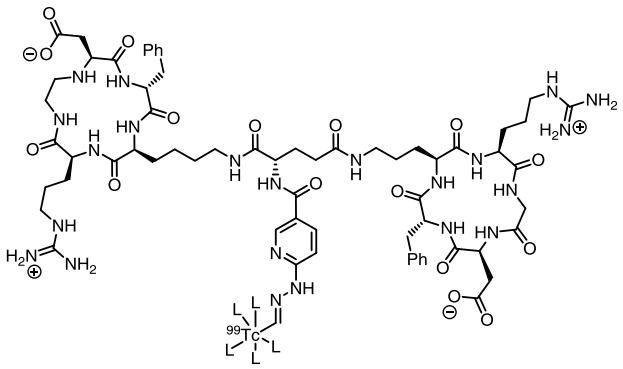

[^{99m}Tc]-**208**

Figure 5. RGD-dimer [^{99m}Tc]-**208** synthesised by Barret *et al.*[16] as the first multimeric RGD peptide for application to molecular imaging.

Janssen *et al.*[20] subsequently synthesised a monovalent analogue of [^{99m}Tc]-**208**, where the ε-amine of the lysine residue was coupled directly to the HYNIC ligand. Dimer [^{99m}Tc]-**208** exhibited a 100-fold lower IC_{50} in *in vitro* assays compared to its monomeric analogue (0.1 vs 10 nM). SPECT imaging experiments in mouse tumour models, revealed that that the dimeric RGD peptide [^{99m}Tc]-**208** showed higher tumour retention compared to the monomer. The authors suggested that this was due to the effect of the multimeric nature of [^{99m}Tc]-**208**, resulting in increased affinity $\alpha_V\beta_3$ integrin present on tumour cell surfaces.

Following these initial results, a range of multimeric RGD peptides based on amide couplings have been developed for use in both SPECT and PET imaging. Many of these investigations have attempted to optimise the linker between the RGD units to develop truly multi*valent* ligands, as opposed to multi*meric* ligands.[21] If the linker between two ligands is not sufficiently long, or is unable to access the required conformation to interact with two distant receptor sites, the multi*valent* effect is lost.[9] A tetrameric RGD peptide construct based on a central deca-peptide linker led to decreased mobility of integrins on the surface of cells, suggesting that correctly designed multimers can lead to multivalent binding events.[22]

Modification of the linkers has also been used to tune the pharmacokinetic properties of the resultant tracers. Linkers of various lengths based on polyethyleneglycol (PEG),[23] triglycinyl,[24] triaspartyl,[25] and sugar-amino acids[26] (**Figure 6**) have been used in multiple architectures in an attempt to maximise binding, promote urinary rather than gastrointestinal clearance, and also for accelerating washout of non-specific bound tracer, improving signal to noise ratios.

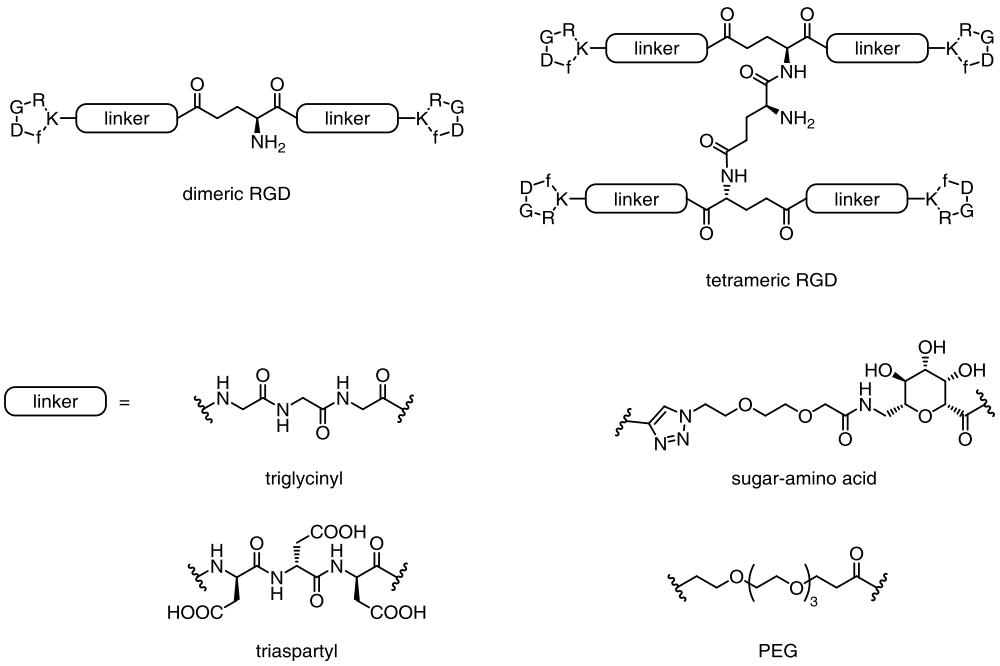

Figure 6. Dimeric and tetrameric RGD scaffolds and linkers used to identify multimers with optimal binding properties. Figure adapted from Liu.[9]

Many multimeric RGD peptides bear metal chelating groups, as co-ordination to radiometals is often the last step in the synthesis of such tracers. Fewer fluorine-18-based multivalent radiotracers have been developed, as incorporation of fluorine-18 into such scaffolds often requires a multi-step, prosthetic group-based strategy.[27–30] Two multimeric RGD compounds, synthesised using a "last step" radiofluorination protocol have been recently evaluated in humans for the first time. These aluminium chelates, [^{18}F]alfatide I [^{18}F]-**210**[31,32] and [^{18}F]alfatide II [^{18}F]-**212**[33,34] as shown in **Scheme 2**, have been prepared using a kit-like[35] form of the methodology described in **Chapter 1**.

An aluminium [^{18}F]fluoride complex is chelated by a NOTA-ligand attached to a peptide, which in both cases is a dimeric RGD peptide. These two clinical imaging candidates differ in the linker topology. Alfatide I [^{18}F]-**210** bears a thiourea-PEG linker between the radiolabel and the dimeric c(RGDfK) peptides, which are conjugated by amide bonds to a central glutamic acid core. The NOTA chelating unit of alfatide II [^{18}F]-**212** is directly attached to a glutamate core, to which two units of c(RGDfK) are conjugated through PEG linkers.

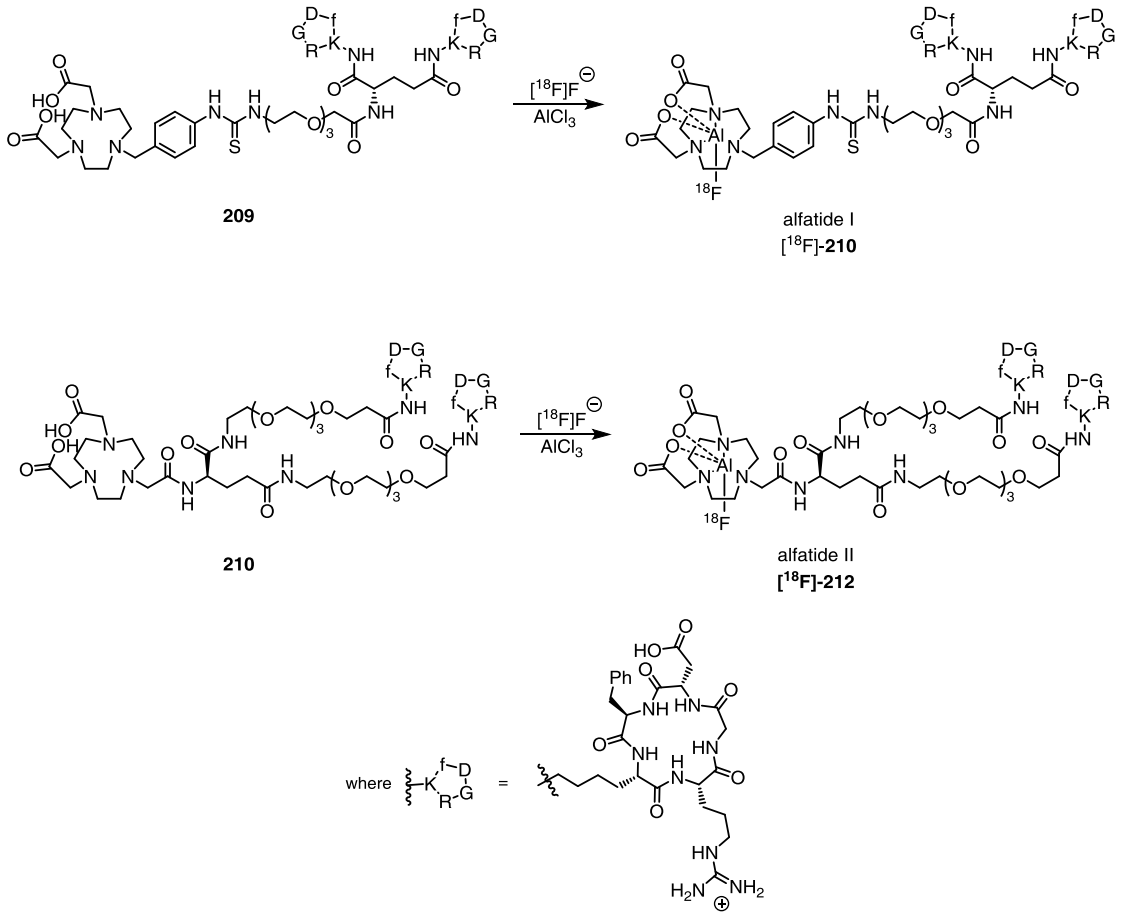

Scheme 2. Syntheses of [^{18}F]alfatide I [^{18}F]-**210** and [^{18}F]alfatide II [^{18}F]-**212** as multimeric RGD complexes, labelled with fluorine-18 using "last step" methodology.[31–34]

[^{18}F]Alfatide I [^{18}F]-**210** was evaluated for imaging of $\alpha_V\beta_3$ integrin expression in patients with lung squamous carcinoma and adenomatous carcinoma. The tracer showed excellent tumour to blood ratios, an outcome suggested to be due to the multimerisation of the RGD peptide.[31] The novel radiotracer had the ability to identify almost all tumours in the nine lung cancer patients, however in one case, additional lesions were detected using [^{18}F]FDG-based imaging, the gold standard for assessment of PET radiopharmaceuticals.

[^{18}F]Alfatide II [^{18}F]-**212** has been evaluated in patients with metastatic brain tumours which had previously been identified by MRI or CT.[34] In this case, the novel tracer proved superior to [^{18}F]FDG [^{18}F]-**35**, visualising all lesions that had been previously identified in the anatomical scans, whereas [^{18}F]FDG [^{18}F]-**35** only identified 10 of the 20 previously identified lesions. These clinical results emphasise the need for the development of novel, selective tracers to compliment the widespread use of [^{18}F]FDG [^{18}F]-**35**.

3.2.2. Multimeric RGD peptides based on triazoles

The CuAAC reaction between an alkyne and an azide-modified RGD peptide has proven to be a useful reaction for the assembly of dendrimeric peptides.[36,37] The ε-amine of the lysine residue of c(RGDfK) has been exploited for functionalisation to make the scaffold applicable to CuAAC-based "click" chemistry. Incorporation of an azide is accomplished either using a diazo-transfer reaction,[36,38,39] or alternatively by coupling the terminal amine to an azidopentanoic acid.[37]

Liskamp *et al.*[38] reported the use of the CuAAC reaction for the synthesis of indium-111 labelled di- and tetra-meric RGD peptides. Their approach began with the synthesis of a dipropargyldihydroxybenzoic ester derivative, used as the core of the dendrimeric assembly. This core was either used to generate a dimeric scaffold, or it was coupled to two further dipropargyldihydroxybenzoic ester derivatives to offer a tetrameric scaffold. The scaffolds were coupled to a protected DOTA (1,4,7,10-tetraazadodecane-*N*,*N*′,*N*″,*N*‴-tetraacetate) chelator *via* an ethylenediamine linker, to generate **213** and **215** as shown in **Scheme 3**. These dendrimeric assemblies were then coupled to c(RGDfK[N_3]) **199** using a CuAAC reaction.

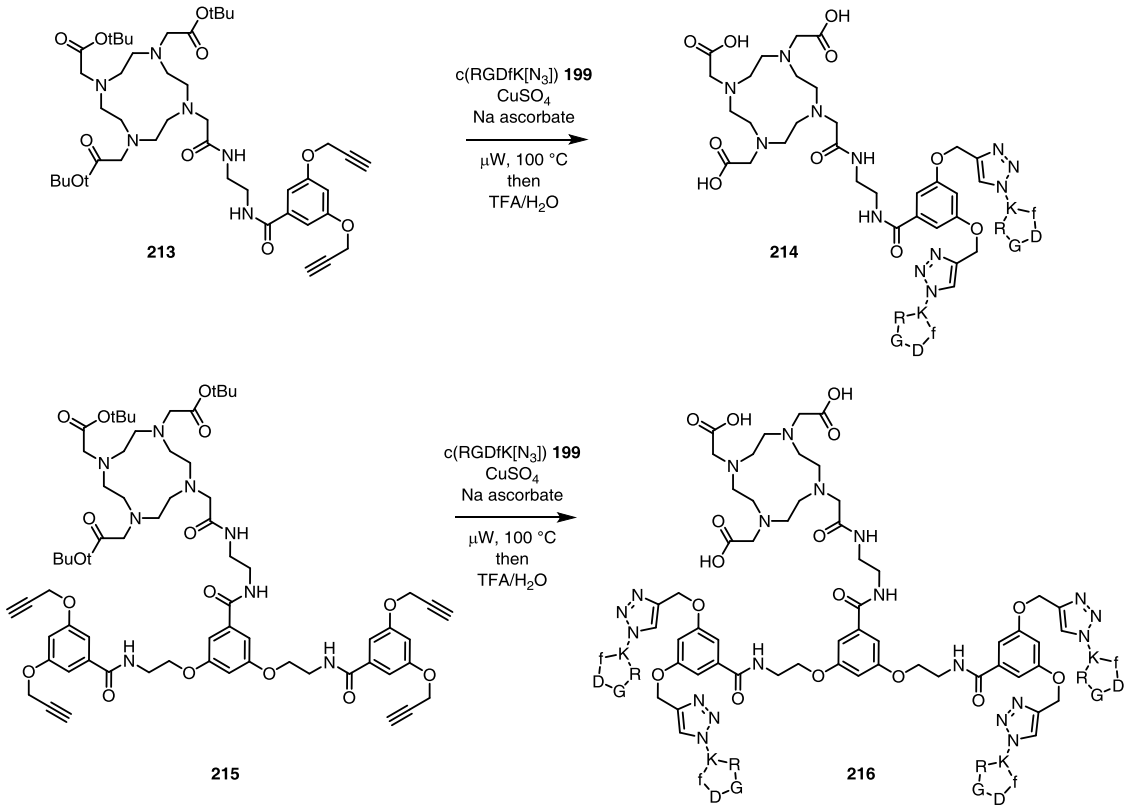

Scheme 3. Divalent **213** and tetravalent **215** dendrimeric alkynes were found to undergo efficient CuAAC reaction with c(RGDfK[N_3]) **199** under microwave conditions, generating **214** and **216**.

The CuAAC reaction between **213** or **215** and c(RGDfK[N_3]) **199**, catalysed by a $CuSO_4$-ascorbate-Cu wire system, was found to be inefficient at room temperature. The reaction proceeded rapidly (5-30 min) to generate **214** or **216** when heated by microwave irradiation in DMF/H_2O mixtures. Isolated yields for the synthesis of chelators **214** and **216** were moderate, at 11% and 36% respectively. The dendrimers **214** and **216** were subsequently labelled with ^{111}In and *in vivo* assessment revealed that the [^{111}In]-labelled tetrameric RGD dendrimer was taken up in renal cell carcinoma xenografts in mice to a higher degree than the dimeric analogue. *In vitro* assays showed that tetrameric dendrimer **216** showed lower IC_{50} values (50 nM) compared to the dimeric construct **214** (356 nM). These results illustrate the advantage of multimerisation of RGD peptides for imaging of $\alpha_V\beta_3$ integrin expression in cancers.

A similar multimerisation approach using the CuAAC reaction based on a trifunctionalised melamine core (**Scheme 4**) was reported by Reichert *et al.*[40] They synthesised a DOTA-bearing melamine derivative bearing either one or two propargyl-diethyleneglycol units. Using a similar microwave-enhanced CuAAC reaction, the coupled the alkynes to c(RGDfK[N_3]) **199** to generate monomeric and dimeric RGD constructs. They found the dimeric analogue **218** to have a higher affinity for immobilised $\alpha_V\beta_3$ integrin than its monovalent counterpart.

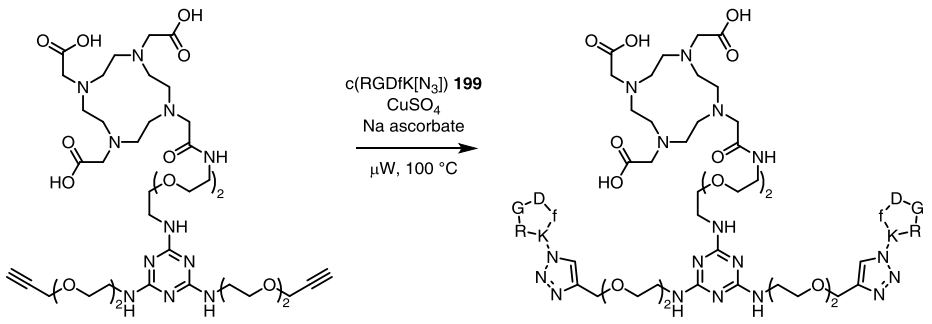

217 **218**

Scheme 4. Synthesis of a dimeric RGD peptide **218** using the CuAAC reaction, as reported by Reichart *et al.*[40]

In both reports, the CuAAC reaction was reported to require forcing conditions (microwave or conventional heating) to ensure complete reaction. Wängler *et al.*[37] have reported a failed attempt to synthesise high order polyamidoamine (PAMAM) RGD dendrimers using the CuAAC reaction. They found that the CuAAC reaction with di- and tetra- alkynyl PAMAM dendrimer scaffolds gave only mono- or di-meric triazole products, even when large excesses of an azido-modified RGD peptide were employed.

3.3. Aims

It was recently demonstrated in St Andrews (Dr. Qingzhi Zhang) that the fluorinase could be utilised to radiolabel an RGD peptide in a “last step” protocol for PET. Exploration of tethering of larger peptide cargos to the nucleoside substrate for the enzyme became an immediate objective. The set objective was now to design and synthesise multimeric RGD peptide assemblies as potential substrates for the fluorinase enzyme, as illustrated in **Figure 7**. The multimeric substrates derive from a divalent or tetravalent linker, for attachment to two or four bioactive peptides respectively.

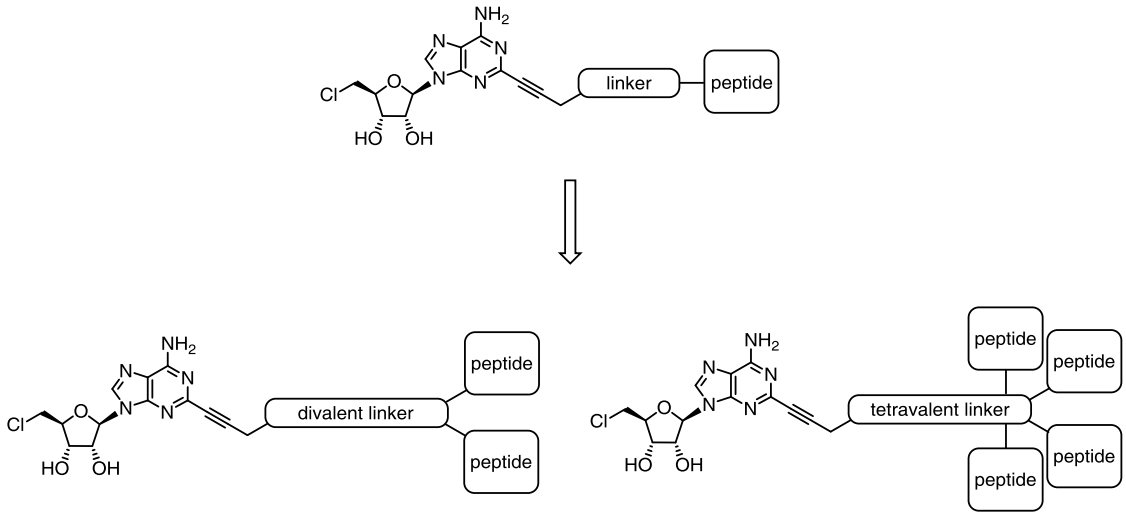

Figure 7. Extension of fluorinase substrates towards “last step” radiolabelling of multimeric peptides.

c(RGDfK[N_3]) **199** was an attractive building block for the assembly of the multimeric substrates using the CuAAC reaction. In order to utilise this RGD-azide, dimeric and tetrameric alkynes, bearing the ClDEA motif were required.

Using the dipropargyl-diphenol ether core described by Liskamp *et al.*,[38] and a PEG linker bearing an amine as the site for multimerisation, ClDEA-PEG-(C≡CH)$_2$ **219** and ClDEA-PEG-(C≡CH)$_4$ **220** in **Scheme 5** were designated as synthetic targets. The analogous 5'-fluoro compounds were also required for use as reference compounds for anticipated enzyme assays. Mono- and di-alkylation of amine **222** by aldehyde **223** under reductive amination conditions were anticipated to produce a trialkyne and penatalkyne respectively. Sonogashira coupling of the terminal, unprotected alkynes to an appropriate 2-iodoadenosine, such as **221**, was expected to furnish the desired multimeric constructs after silyl deprotection.

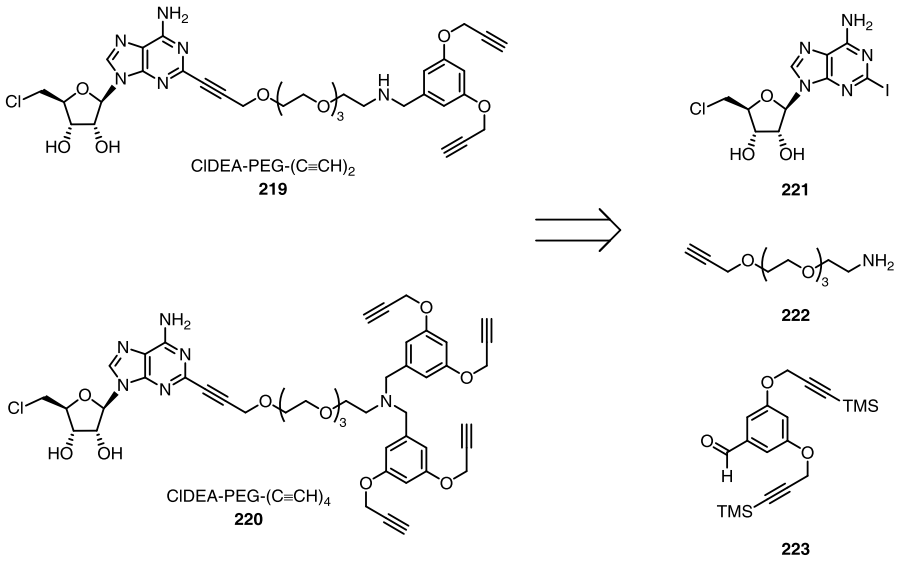

Scheme 5. Synthetic targets and retrosynthetic analysis to 5'-chloro-5'-deoxy-2-iodoadenosine **221**, a PEG linker **222**, and a protected dialkynyl aldehyde core **223**.

These di- and tetra-meric compounds would be investigated in CuAAC coupling with c(RGDfK[N_3]) **199** to generate multimeric RGD peptides **224** and **225**, as shown in **Scheme 6**. Compounds **224** and **225** are potential new substrates for the fluorinase-catalysed transhalogenation reaction. If the constructs prove successful as substrates, the goal would be to explore radiolabelling of these constructs in the PET context with [^{18}F]fluoride. It was hoped that this would provide access to a “last step” radiolabelling of larger peptides (10-20 amino acids) using the fluorinase under neutral pH, ambient, aqueous conditions.

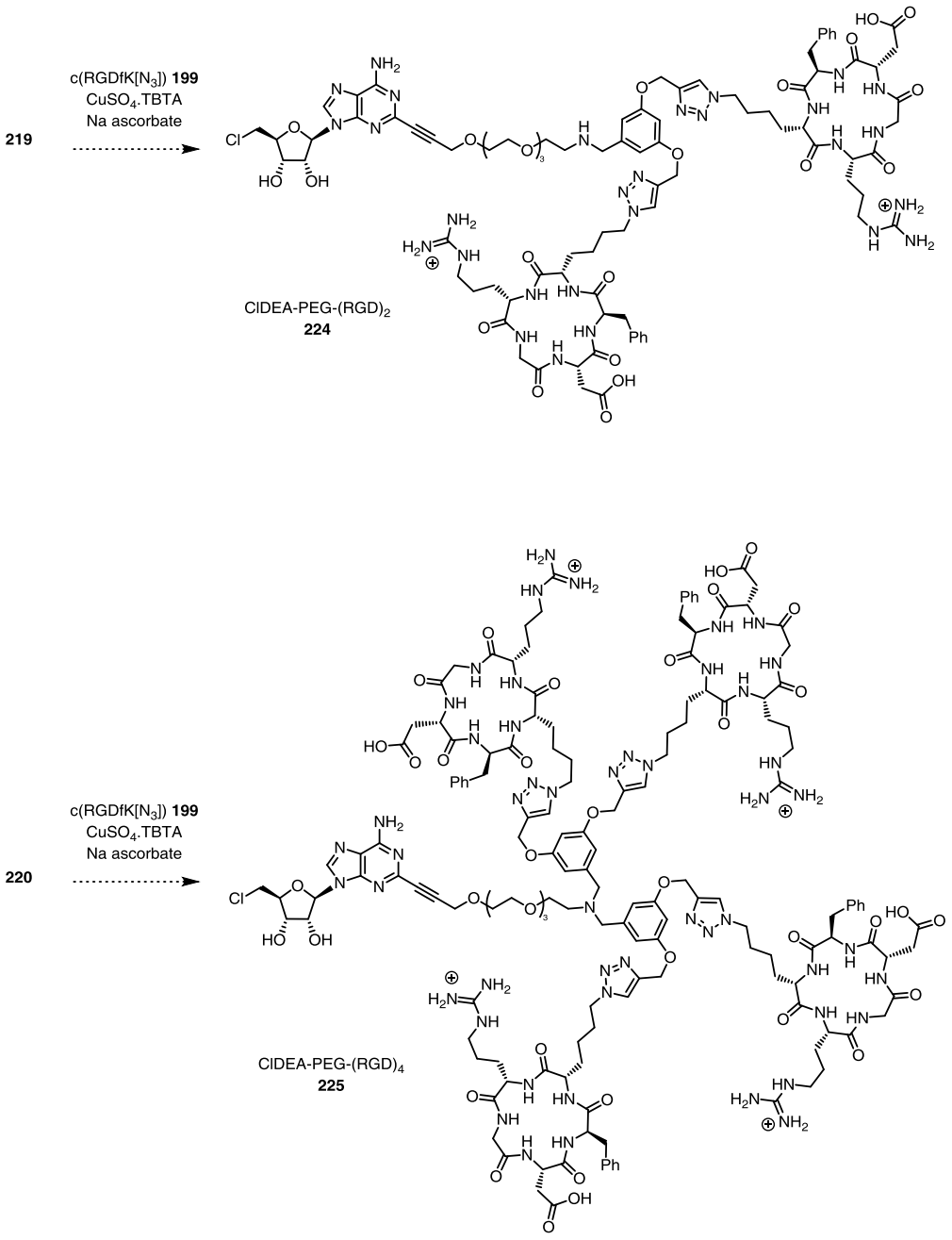

Scheme 6. CuAAC reaction of alkynes **219** and **220** with c(RGDfK[N_3]) **199** to generate ClDEA-PEG-$(RGD)_2$ **224** and ClDEA-PEG-$(RGD)_4$ **225** as potential new substrates for the fluorinase.

3.4. Synthesis of di- and tetra-alkynes for a CuAAC reaction

3.4.1. Synthesis of the alkyne fragments for Sonogashira couplings

Methyl 3,5-dihydroxybenzoate **226** was dialkylated using potassium carbonate and propargyl bromide in refluxing acetone (**Scheme 7**).[38] The resultant dialkyne **227** was purified by recrystallisation from methanol. The two acetylene functional groups were protected with silyl groups by treatment of **227** with lithium diisopropylamide (LDA), and quenching the resultant dianion with TMSCl, furnishing ester **228**.

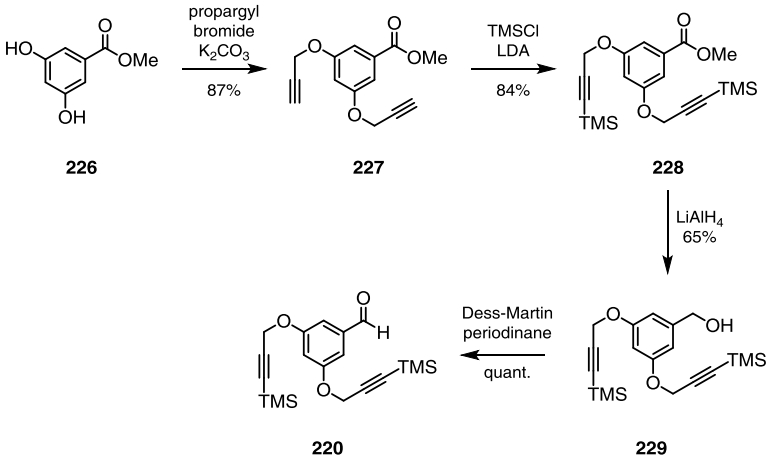

Scheme 7. Synthesis of protected aldehyde **220** for reductive amination.

Ester **228** was reduced to the corresponding benzylic alcohol **229** using lithium aluminium hydride. The resulting alcohol **229** was oxidised using Dess-Martin periodinane.[41] Quenching with sodium thiosulfate, followed by a base extraction, generated aldehyde **220** in quantitative yield without further purification.

Tetraethylene glycol **230** was treated with propargyl chloride and a dispersion of sodium hydride in mineral oil, to give the monoalkylated PEG derivative **231** shown in **Scheme 8**, along with its dialkylated analogue. Separation of these products by column chromatography allowed **231** to be purified in 47% yield, which was then converted to tosylate **232**.

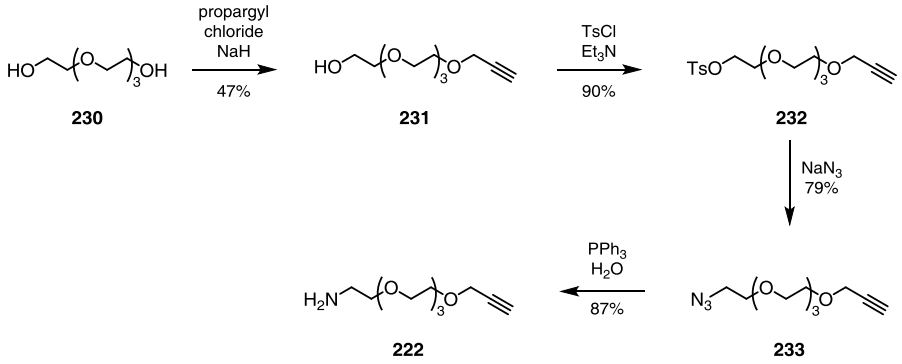

Scheme 8. Synthesis of amino-alkyne linker **222** from tetraethyleneglycol **230**.

Nucleophilic displacement of the tosyl group by azide gave **233** in good yield, and a Staudinger reduction[42] of the azide generated amine **222**. With both aldehyde **223** and amine **222** in hand, attention turned to coupling the two fragments by reductive amination.

Condensation of amine **222** with aldehyde **223** in a direct reductive amination was expected to produce predominantly the monoalkylated amine product.[43] To this end, a slight excess of amine **222** was added to a solution of the aldehyde **223** in THF, before acetic acid and sodium triacetoxyborohydride were added (**Scheme 9**). TLC analysis showed the formation of two major species, found to be the mono- and di-alkylated products **234** and **235**, respectively. As the dialkylated species **235** was also desired for the construction of the multimeric assembly, and that the mono- and di- alkylated products were easily separable by chromatography, no attempt to improve the formation of the mono-alkylated product was made. Separation of the two products by column chromatography revealed that monoalkylated product **234** had been formed in 35% yield (based on aldehyde **223**), while dialkylated product **235** was formed in 21% yield (based on aldehyde **223**).

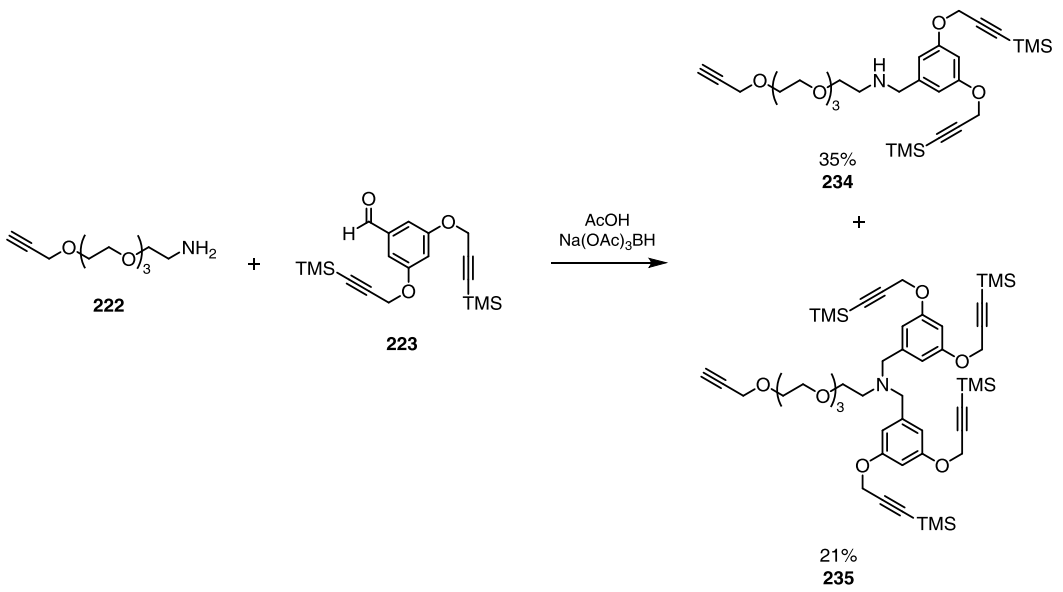

Scheme 9. Reductive amination of aldehyde **223** to generate alkynes **234** and **235**.

With the alkyne substrates for the anticipated Sonogashira reactions in hand, attention turned to the synthesis of the required iodinated coupling partners.

3.4.2. Synthesis of the iodinated fragments for Sonogashira couplings

During the chlorination of hydroxy-alkynes **180** and **236** (**Scheme 10**) described in **Chapter 2** and **Section 3.11** respectively, a by-product, the alkyne-HCl adduct, was observed. Adducts **190** and **237** are thought to arise from HCl generation during the reaction, which then adds across the triple bond. These HCl adducts were found to be difficult to separate from their alkyne analogues, therefore, an alternative to late-stage chlorination was investigated.

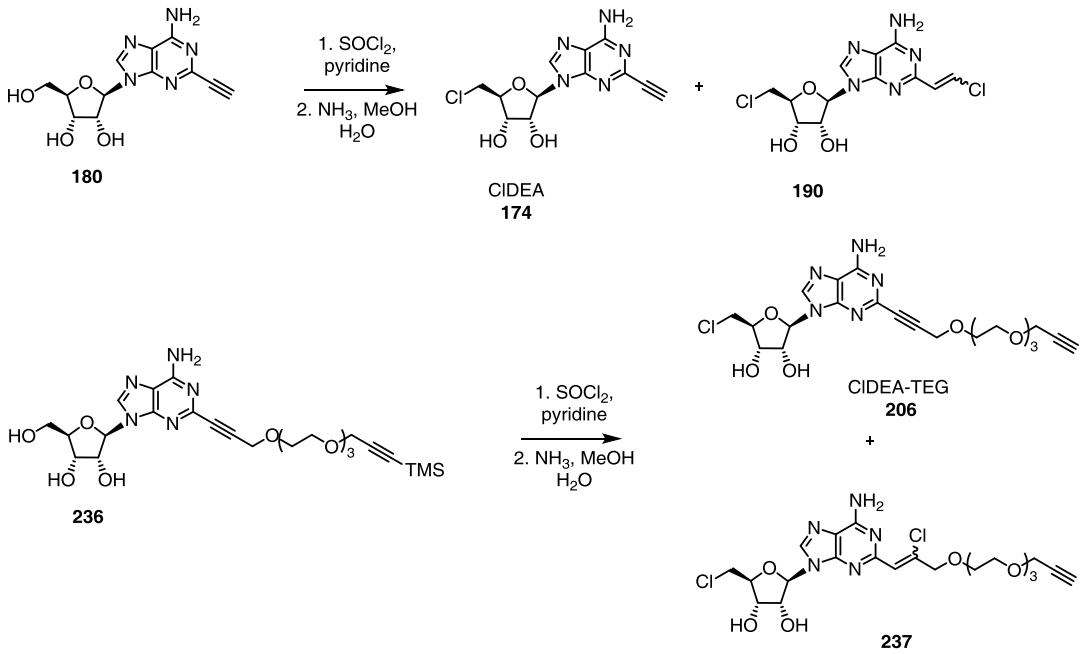

Scheme 10. Chlorination of alkynes **180** and **236** led to undesired HCl adducts **190** and **237**.

To this end, the chlorination of 2-iodoadenosine **197** prior to the Sonogashira coupling was investigated. 2-Iodoadenosine **179** was treated with thionyl chloride and pyridine in acetonitrile,[44] to generate an intermediate chlorinated cyclic sulfite. Base hydrolysis of this intermediate furnished the corresponding 5'-chloro analogue **238** in moderate yield, as shown in **Scheme 11**.

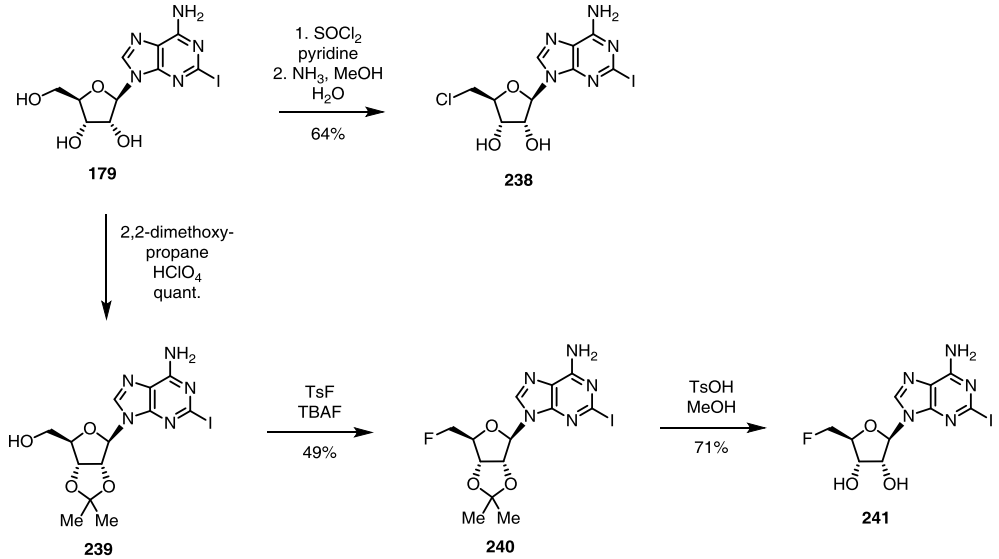

Scheme 11. Synthesis of halogenated 2-iodo coupling partners **238** and **241** for the anticipated Sonogashira coupling.

Similarly, it was envisaged that 2-iodoadenosine **179** could be fluorinated prior to the Sonogashira couplings. 2-Iodoadenosine **179** was protected as its 2',3'-acetonide derivative using 2,2-dimethoxypropane in acetone, catalysed by perchloric acid, to give acetonide **239** in quantitative yield. Acetonide **239** was then fluorinated by the action of TsF and TBAF in refluxing THF, to give **240** in moderate yield. Deprotection of **240** with TFA/water mixtures led to hydrolysis of the *N*-glycosidic bond, giving 2-iodoadenine as a decomposition product. 2-Iodoadenine was found to be difficult to separate from **241** and alternative conditions for the deprotection of **240** were investigated. Successful deprotection was achieved in good yield with catalytic anhydrous TsOH in dry MeOH.[45] Stirring at room temperature for 48 h resulted in an incomplete conversion to the free nucleoside **241**, but refluxing the reaction for 16 h led to complete deprotection to **241**. Happily, cleavage of the *N*-glycosidic bond was not observed under these conditions.

3.4.3. Sonogashira couplings towards multimeric alkynes

Sonogashira couplings[46–48] of the halogenated 2-iodonucleosides with acetylenes **234** and **235** were now investigated.

The first reactions to be investigated involved coupling of chloro-nucleoside **238** to alkynes **234** and **235**, as shown in **Scheme 12**. The conditions employed were the same as those reported for the coupling of 2-iodoadenosine **179** to TMS-acetylene described in **Chapter 2**. 5'-Chloro-5'-deoxy-2-iodoadenosine **238** was added to an excess of either **234** or **235** in dry, degassed DMF, before 10 mol% of $Pd(PPh_3)Cl_2$ and CuI were added and the mixture heated to 60 °C. TLC monitoring of both reactions revealed the formation of a number of by-products, and consumption of the starting materials was slow. Reaction progress was also difficult to monitor by ^{1}H NMR spectroscopy, as an excess of the alkyne used in each case masked the disappearance of the alkynyl proton as the product formed. Mass spectrometry of the reaction mixtures did, however, indicate that the coupled products **242** and **243** were being produced.

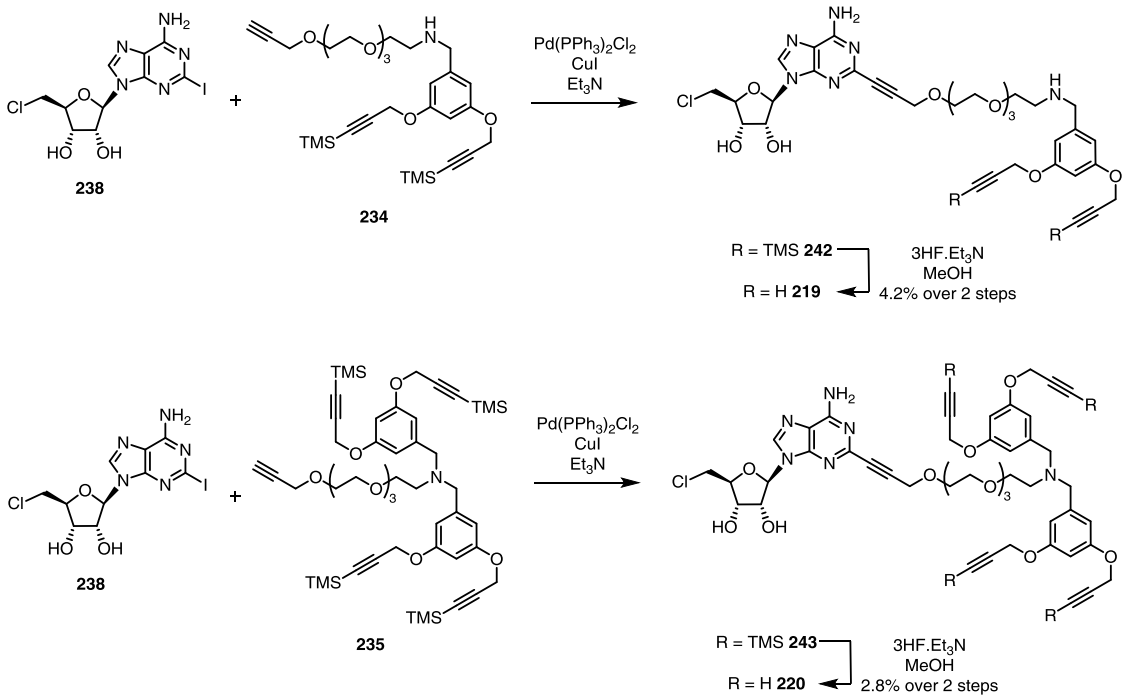

Scheme 12. Sonogashira coupling of **238** to **234** and **235**. Crude products were silyl-deprotected under the action of 3HF.Et_3N, before the products **219** and **220** were purified by semi-preparative HPLC.

While evidence from MS suggested that products were being formed in significant amounts in both cases, TLC analysis did not reveal the appearance of a major reaction product in either case.

Dimer **242** proved particularly difficult to isolate by chromatography, and required the use of extremely polar conditions (10:89:1 MeOH:acetone:1% aqueous ammonia (30%)) for elution from silica gel. Tetrameric alkyne **243** was found to require less polar conditions for elution from silica gel, but in both cases, the products obtained were not sufficiently pure, even after multiple rounds of purification by silica gel chromatography.

At this point, the crude reaction mixtures (20 mg containing **242** and 40 mg containing **243**) were subjected to fluoride-based deprotection of the silyl groups using 3HF.Et_3N in methanol. After quenching the reactions with aqueous sodium bicarbonate, the crude deprotected products **219** and **220** were passed through a plug of silica gel, eluting with MeOH:acetone:aqueous ammonia (30%) or DCM:MeOH mixtures respectively. This gave access to products **219** and **220**, each of which required further purification before use in CuAAC reactions.

The two products were each passed through a C_{18} reverse phase cartridge, before being purified by semi-preparative HPLC, to give ClDEA-PEG-$(C{\equiv}CH)_2$ **219** and

ClDEA-PEG-(C≡CH)$_4$ **220**. The yield over two steps in both cases was low, at only 4.2% and 2.8% respectively, when calculated based on **238**. Despite the low yield, the synthetic route gave access to 3–5 mg of each of the products, which was sufficient for investigation of the respective CuAAC reactions, and for the preparation of milligram quantities of multimeric RGD peptides.

Following a similar protocol to that described for the chlorinated analogues, FDEA-PEG-(C≡CH)$_2$ **245** and FDEA-PEG-(C≡CH)$_4$ **247** were prepared as shown in **Scheme 13**. Sonogashira coupling of 5'-fluoro-5'-deoxy-2-iodoadenosine **241** to alkynes **234** and **235** were performed under identical conditions, and the crude components of the product, identified using MS, were separated from the reaction mixture by passage through a plug of silica. At this stage, the mixture was subjected directly to silyl deprotection with 3HF.Et$_3$N in MeOH. After quenching with aqueous sodium bicarbonate, the mixtures were concentrated and immediately applied to a C_{18} reverse phase cartridge. The products were further purified by semi-preparative HPLC to give FDEA-PEG-(C≡CH)$_2$ **245** and FDEA-PEG-(C≡CH)$_4$ **247** in a similar yield to their chlorinated analogues, at 2.5% and 2.3% respectively.

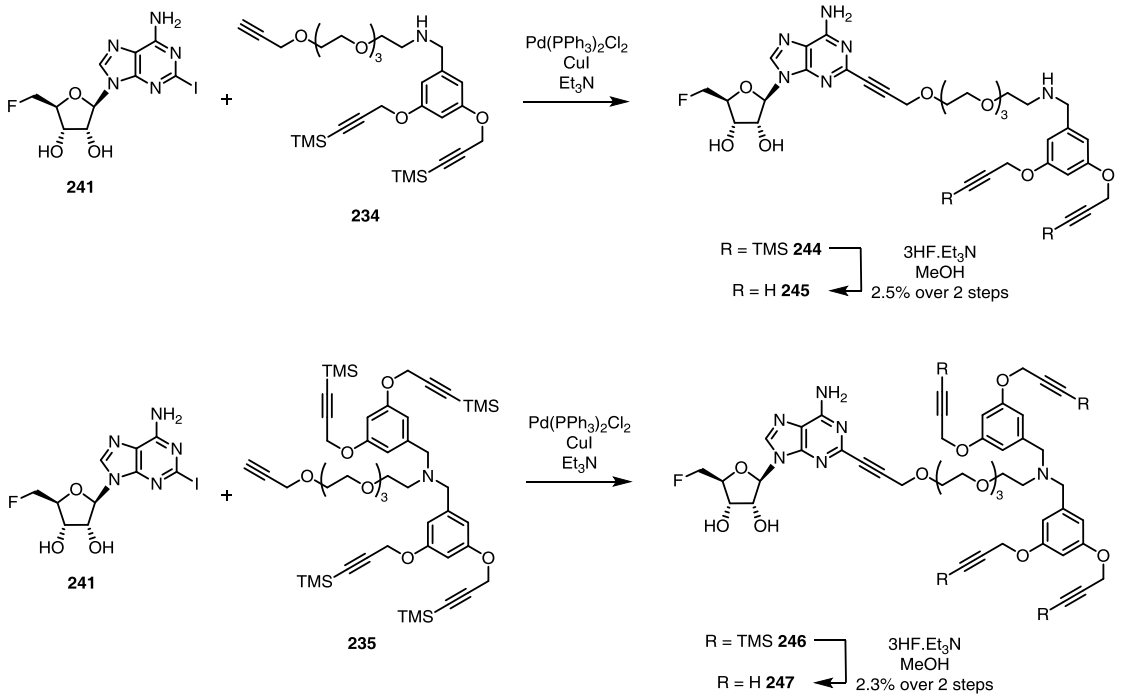

Scheme 13. Sonogashira coupling of **241** to **234** and **235** Crude products were silyl-deprotected under the action of 3HF.Et$_3$N, before the products were purified by semi-preparative HPLC.

3.4.4. Assessment of ClDEA-PEG-(C≡CH)$_2$ 219 as a fluorinase substrate

With a modified nucleoside substrate in hand, ClDEA-PEG-(C≡CH)$_2$ **219**, which was soluble in water, unlike **220**, was investigated as a substrate for fluorinase-catalysed transhalogenation. ClDEA-PEG-(C≡CH)$_2$ **219** (0.3 mM) was incubated with the fluorinase (10 mg.mL^{-1}) in the presence of fluoride (75 mM) and L-SeMet (0.5 mM), as shown in **Figure 8 A**, and the reaction progress monitored by HPLC (**Figure 8 B**).

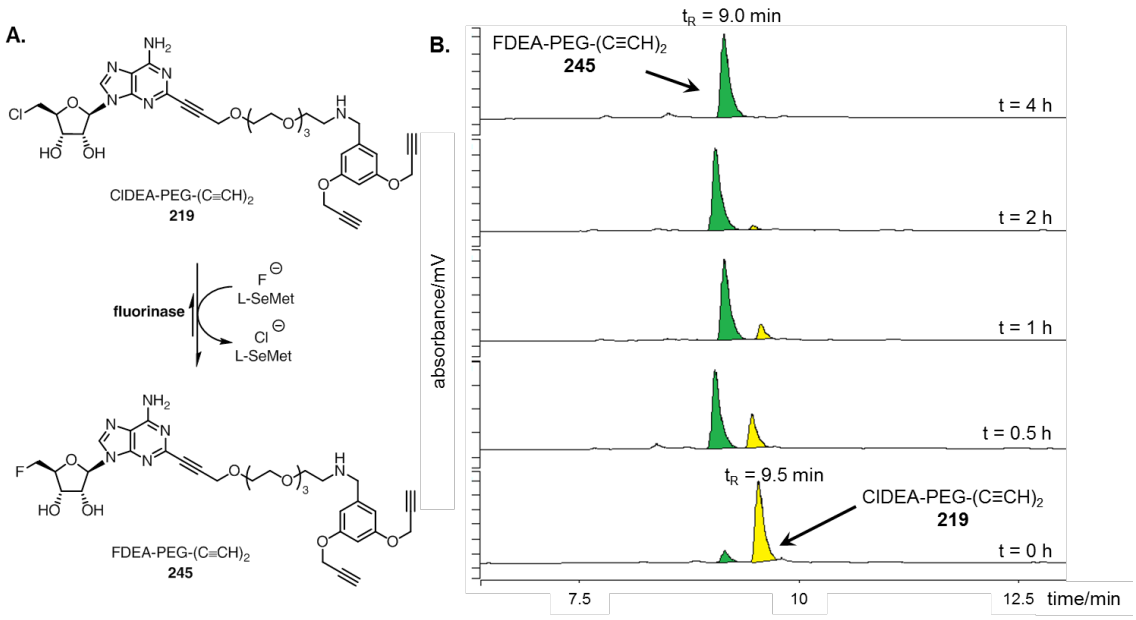

Figure 8. **A.** Fluorinase-catalysed transhalogenation of ClDEA-PEG-(C≡CH)$_2$ **219**. **B.** HPLC trace of the reaction mixture showing ClDEA-PEG-(C≡CH)$_2$ **219** (t_R = 9.5 min, yellow) at t = 0 min. After 4 hours, conversion to FDEA-PEG-(C≡CH)$_2$ **245** (t_R = 9.0 min, green) was complete.

HPLC analysis revealed that ClDEA-PEG-(C≡CH)$_2$ **219** (t_R = 9.5 min) was consumed, and a new product (t_R = 9.0 min) was steadily produced. Over a period of 4 h, the conversion to this new product was found to be complete. LC-MS analysis of the reaction mixture revealed a peak in the total ion chromatogram with t_R = 13.6 min, and whose summed mass spectrum (**Figure 9**) revealed a peak at *m/z* = 697.2 and *m/z* = 349.2. This corresponds to the $[M+H]^+$ and $[M+2H]^{2+}$ ions of FDEA-PEG-(C≡CH)$_2$ **245**, confirming that the transhalogenation reaction was successful. Control experiments in the absence of the enzyme or L-SeMet, did not show conversion to any new products, confirming the role of the fluorinase enzyme in this transformation.

The successful transhalogenation demonstrated that the new linker was well tolerated by the fluorinase. The presence of the substituted aromatic ring coupled to the amino-

PEG linker appeared to have minimal effect on the fluorinase-catalysed transhalogenation reaction.

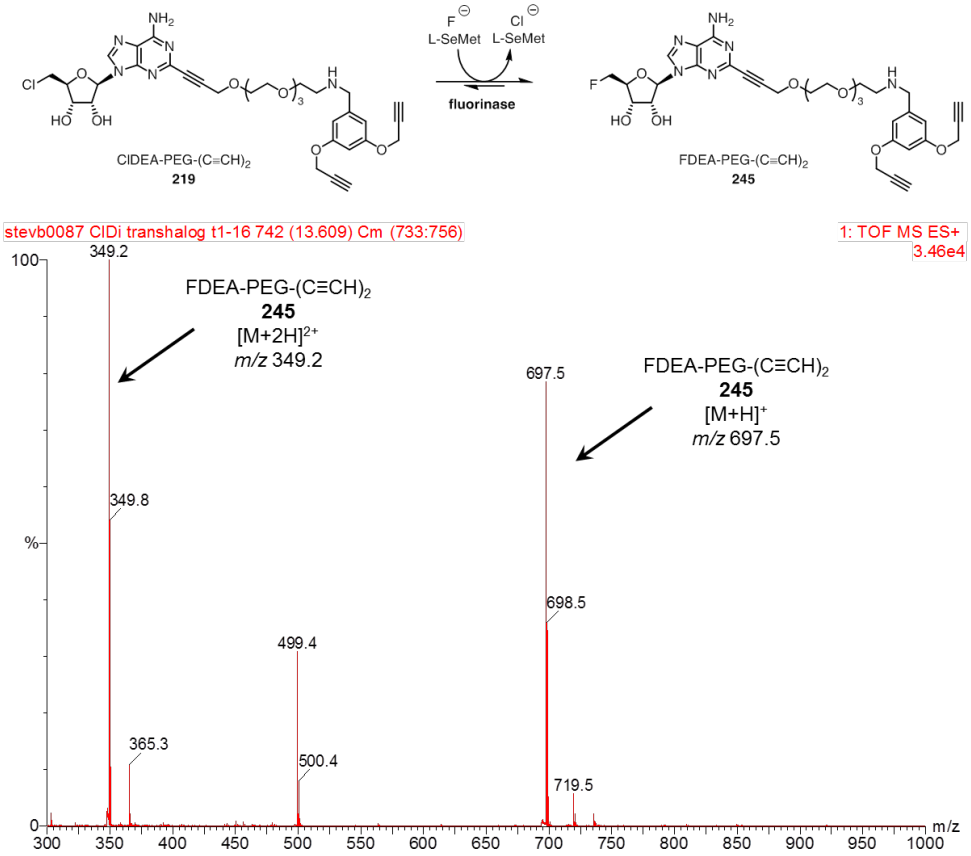

Figure 9. Summed mass spectrum of peak corresponding to the product of the transhalogenation reaction mixture after 4 h, showing $[M+H]^+$ and $[M+2H]^{2+}$ peaks of the anticipated fluorinated product, FDEA-PEG-(C≡CH)$_2$ **245**.

3.5. CuAAC reaction with c(RGDfK[N_3]) 199

With the proposed alkynes in hand, the CuAAC reaction between **219** and **220** and c(RGDfK[N_3]) **199** were explored for the generation of the multimeric RGD substrates for the fluorinase. It had been reported in the literature that the CuAAC reaction of c(RGDfK[N_3]) **199** with a variety of alkynes was slow, and required microwave heating in order to achieve good conversions.[38,40]

3.5.1. Investigation of the CuAAC reaction under microwave heating

Initial trials of the reaction were performed on an analytical scale using ClDEA-PEG-(C≡CH)$_4$ **220** as the starting alkyne, as illustrated in **Scheme 14**. With sodium ascorbate and $CuSO_4$.TBTA as the catalyst system, the CuAAC reaction of

ClDEA-PEG-$(C{\equiv}CH)_4$ **220** with c(RGDfK[N_3]) **199** was investigated. The reaction mixture was heated by microwave irradiation at 100 °C for 2 hours in DMF. HPLC analysis of the reaction mixture after 2 hours revealed a complex mixture of products. LC-MS analysis showed the presence of traces of the desired product, ClDEA-PEG-$(RGD)_4$ **225**, along with many unidentified products of lower mass. These lower molecular weight species were thought to be decomposition products. Under identical reaction conditions, but with MeOH as the solvent, only the mono-triazole product was observed by LC-MS.

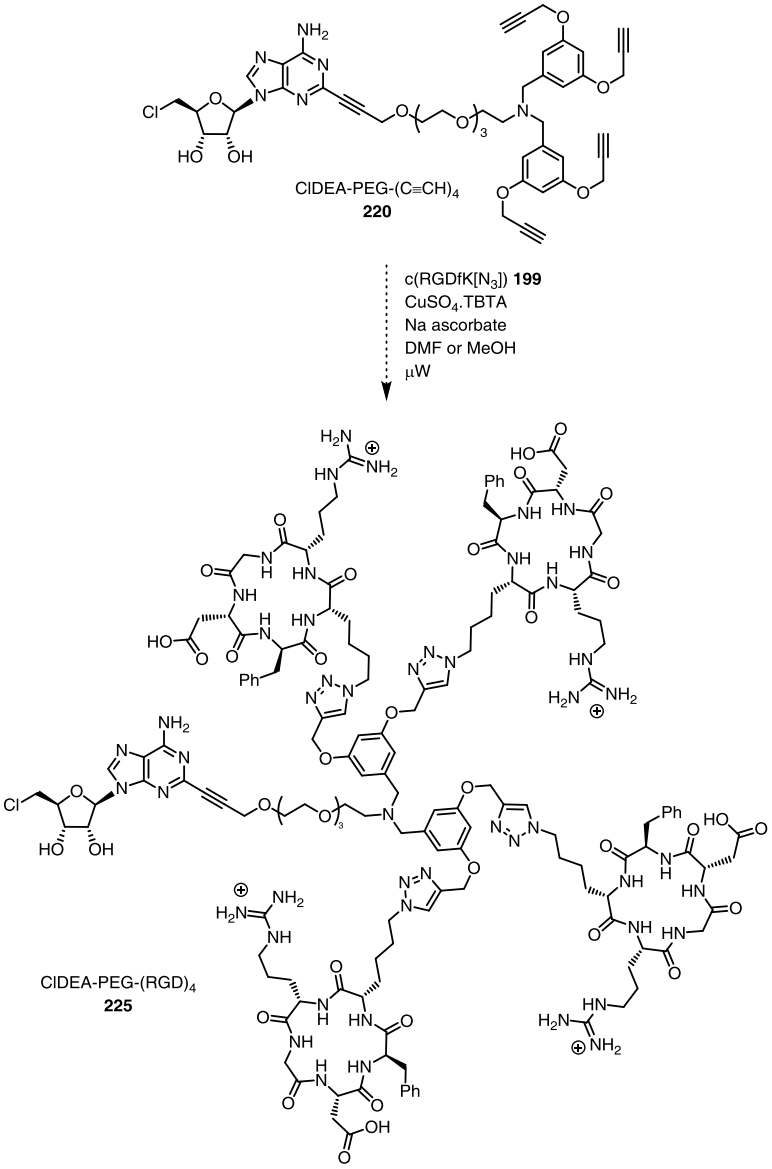

Scheme 14. Investigation of CuAAC reaction with ClDEA-PEG-$(C{\equiv}CH)_4$ **220** under microwave conditions only gave traces of the desired product **225**.

The observation of products of lower mass suggested that the tetrameric product may be unstable to the harsh microwave conditions, and that the product was perhaps decomposing. Milder conditions were therefore investigated for the CuAAC reaction.

In **Chapter 2**, the CuAAC reaction with c(RGDfK[N_3]) **199** proceeded quantitatively at room temperature in water, when fluorinase generated FDEA **176** was reacted with c(RGDfK[N_3]) **199**. These conditions were trialled on a small scale with water soluble FDEA-PEG-(C≡CH)$_2$ **245**, produced by the enzymatic transhalogenation described in **Section 3.4.4**, and illustrated below in **Figure 10 A**. Fluorinase-generated FDEA-PEG-(C≡CH)$_2$ **245** was added to a solution of c(RGDfK[N_3]) **199** in water before sodium ascorbate was added and a sample removed for HPLC analysis. After addition of $CuSO_4$.TBTA, the mixture was allowed to react for 30 min at room temperature, at which point a second sample was removed for HPLC analysis. The resultant HPLC traces are illustrated below in **Figure 10 B**.

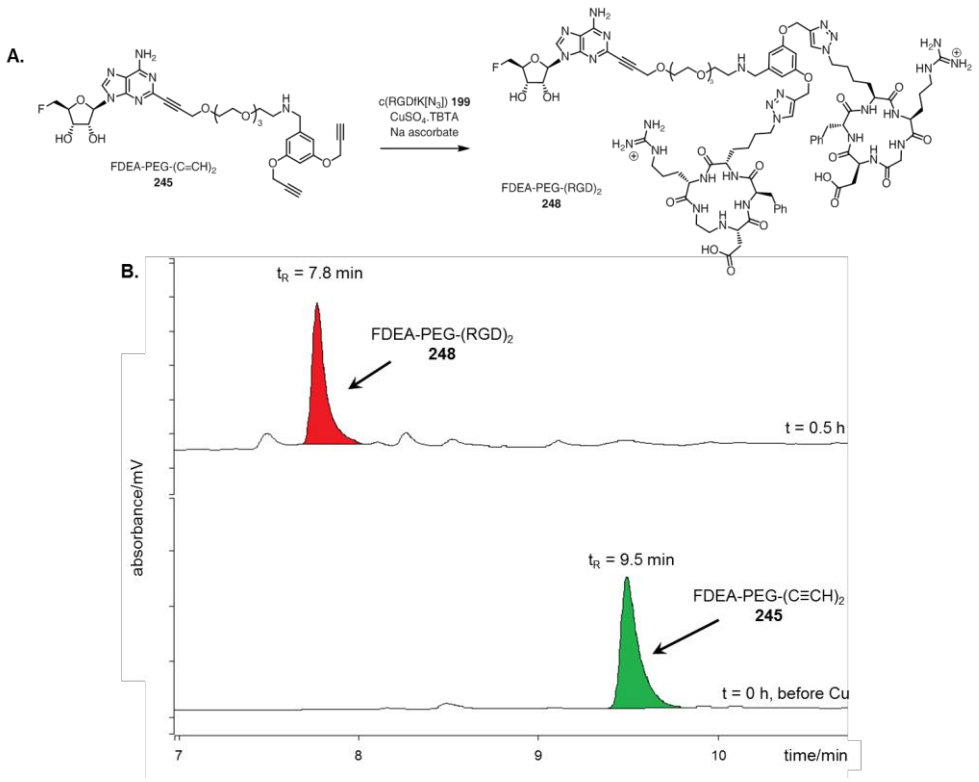

Figure 10. **A.** Fluorinase-generated FDEA-PEG-(C≡CH)$_2$ **245** was subjected to the CuAAC reaction with azido peptide **199** in water, at room temperature to generate FDEA-PEG-(RGD)$_2$ **245**. **B.** HPLC trace (260 nm) of the reaction showing FDEA-PEG-(C≡CH)$_2$ **245** (t_R = 9.5 min, green) before addition of the catalyst, and 30 min after catalyst addition showing new di-triazole product, FDEA-PEG-(RGD)$_2$ **248** (t_R = 7.8 min, red).

After 30 min, HPLC analysis revealed that all the starting alkyne **245** (t_R = 9.5 min) had been consumed, while a new product was evident at t_R = 7.8 min. Conversion

appeared complete. LC-MS analysis of the reaction mixture revealed the product as FDEA-PEG-$(RGD)_2$ **248**, showing peaks at *m/z* = 979.3, 652.8 and 489.9, and corresponding to the $[M+2H]^{2+}$, $[M+3H]^{3+}$and $[M+4H]^{4+}$ ions of **248** respectively.

3.5.2. Synthesis of ClDEA-PEG-$(RGD)_2$ 224 and FDEA-PEG-$(RGD)_2$ 248

After the success of the analytical scale CuAAC reaction under mild conditions, to produce the dimeric RGD compound **248** identical conditions were trialled on a preparative scale for the synthesis of the desired multimeric compounds.

ClDEA-PEG-$(C{\equiv}CH)_2$ **219** was taken up into water, before c(RGDfK[N_3]) **199** (1.25 eq. per alkyne) was added. Sodium ascorbate solution was added to the reaction mixture and the reaction, illustrated below in **Figure 11 A**, was initiated by addition of $CuSO_4$.TBTA. After 1.25 h the reaction was found to be complete by HPLC. Ditriazole **224** was trapped on a C_{18} reverse phase cartridge, and the product eluted with 50:50 MeCN:H_2O (2 × 5 mL) and concentrated under a stream of compressed air. The crude product was purified by semi-preparative HPLC to give 1.8 mg of ClDEA-PEG-$(RGD)_2$ **224** in 78% yield. MALDI-TOF MS (**Figure 11 B**) confirmed the identity of the isolated product, showing a diagnostic peak at *m/z* = 1971.9, corresponding to the $[M+H]^+$ ion of ClDEA-PEG-$(RGD)_2$ **224**.

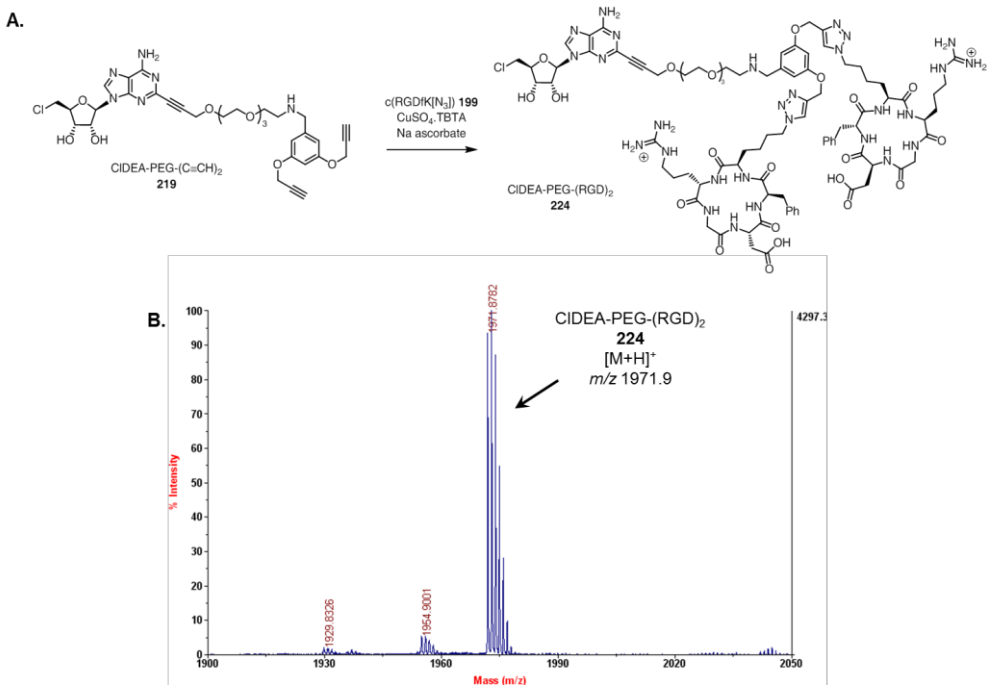

Figure 11. **A.** Preparative scale synthesis of ClDEA-PEG-$(RGD)_2$ **224**. **B.** MALDI-TOF MS spectrum of the product after purification, showing the $[M+H]^+$ ion at *m/z* = 1971.9. MALDI-TOF MS acquired by the University of St Andrews Mass Spectrometry Service.

FDEA-PEG-$(RGD)_2$ **248** was synthesised in a similar manner to that described for its chlorinated analogue as shown in **Figure 12 A**. The dialkyne **245** was taken up in a solution of 50:50 DMSO:water before addition of c(RGDfK[N_3]) **199** (1.25 eq. per alkyne), sodium ascorbate solution and $CuSO_4$.TBTA. The reaction was found to be complete after 90 min by HPLC, after which the solution was passed through a C_{18} reverse phase cartridge. The cartridge was washed with water (10 mL) to remove DMSO and residual sodium ascorbate, before the product was eluted with 50:50 MeCN:H_2O (2 × 10 mL). Crude **248** was purified by semi-preparative HPLC to yield 0.67 mg of FDEA-PEG-$(RGD)_2$ **248** (27% yield). MALDI-TOF MS (**Figure 12 B**) again confirmed the identity of FDEA-PEG-$(RGD)_2$ **248**, showing a peak at *m/z* = 1955.9, corresponding to the $[M+H]^+$ ion of FDEA-PEG-$(RGD)_2$ **248**.

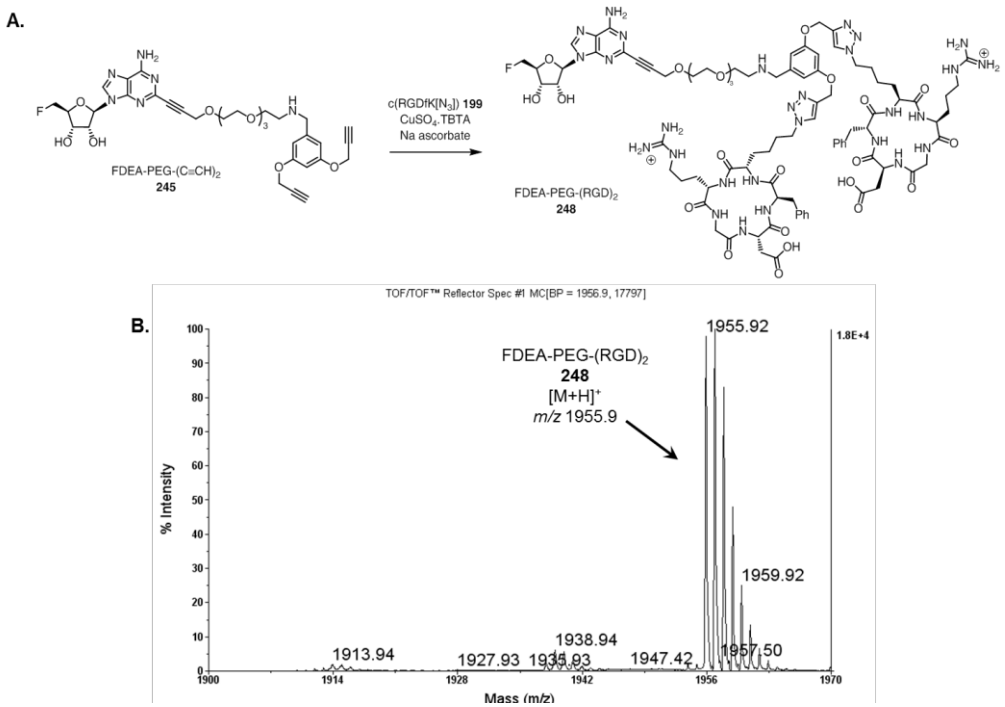

Figure 12. **A.** Preparative scale synthesis of FDEA-PEG-$(RGD)_2$ **248**. **B.** MALDI-TOF MS spectrum of the product after purification, showing the $[M+H]^+$ ion at *m/z* = 1955.9. MALDI-TOF MS acquired by the University of St Andrews Mass Spectrometry Service.

3.5.3. Synthesis of ClDEA-PEG-$(RGD)_4$ 225 and FDEA-PEG-$(RGD)_4$ 249

ClDEA-PEG-$(C{\equiv}CH)_4$ **220** was found to be poorly soluble in water, and initial CuAAC reactions carried out in water led to the production of mixtures of products. Addition of DMSO (50%) was sufficient to complete dissolution of ClDEA-PEG-$(C{\equiv}CH)_4$ **220**, allowing the reaction to proceed rapidly to completion.

For the preparative scale synthesis of ClDEA-PEG-$(RGD)_4$ **225** (**Figure 13 A**), the ClDEA-PEG-$(C{\equiv}CH)_4$ **220** was taken up into a 75:25 mixture of DMSO:water before the addition of c(RGDfK[N_3]) **199** (1.25 eq. per alkyne) in an equal volume of 25:75 mixture of DMSO:water. This gave DMSO:water (50:50) as the final reaction solvent. Sodium ascorbate solution and $CuSO_4$.TBTA were added to initiate the reaction. The reaction was followed by HPLC and found to be complete after 70 min. DMSO was removed from the sample following a similar protocol to that described above, where the product was trapped on a C_{18} reverse phase cartridge, washed with water to remove DMSO, and the product eluted with MeCN:water mixtures. Purification by semi-preparative HPLC gave 1.4 mg of ClDEA-PEG-$(RGD)_4$ **225** (70% yield). MALDI-TOF MS (**Figure 13 B**) confirmed the identity of the isolated product, showing a diagnostic peak at *m/z* = 3428.5, corresponding to the $[M+H]^+$ ion of ClDEA-PEG-$(RGD)_4$ **225**. In this sample, a peak corresponding to the loss of water (−18 Da) was also observed.

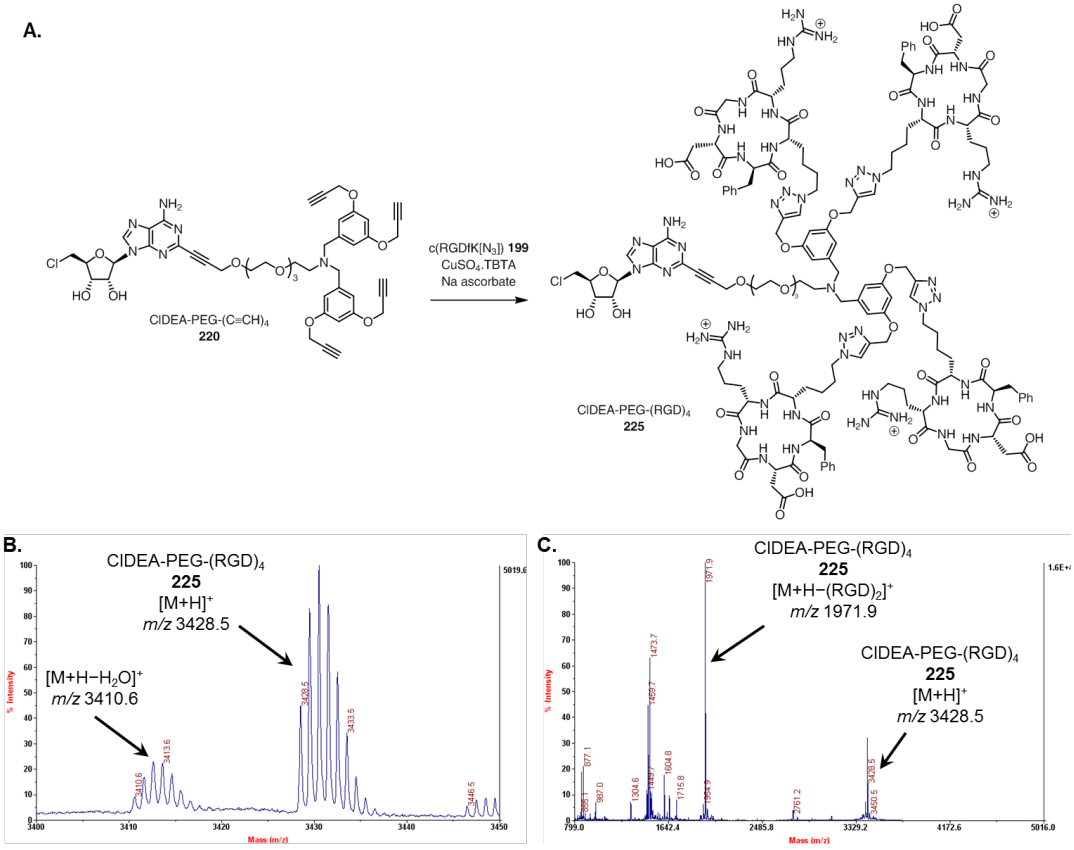

Figure 13. **A.** Preparative scale synthesis of ClDEA-PEG-$(RGD)_4$ **225**. **B.** MALDI-TOF MS spectrum of the product after purification, showing the $[M+H]^+$ ion at *m/z* = 3428.5. The ion produced by loss of water is also evident. **C.** Full MALDI-TOF MS spectrum showing the base peak (*m/z* = 1971.9) produced as a result of N–C bond cleavage. MALDI-TOF MS acquired by the University of St Andrews Mass Spectrometry Service.

The expanded MALDI-TOF MS spectrum observed for **225** (**Figure 13 C**) was found to be more complex than its dimeric analogue. The base peak in the MALDI-TOF MS spectrum for ClDEA-PEG-$(RGD)_4$ **225** was found to be at *m/z* = 1971.9, an identical mass to that of ClDEA-PEG-$(RGD)_2$ **224**. The ionisation process for this large tetrameric construct **225** appears to result in the cleavage of the N–C bond.

The fluorinated tetrameric RGD peptide **249** was synthesised in a similar manner to that described for **225**, as shown in **Figure 14**. FDEA-PEG-$(C{\equiv}CH)_4$ **247** was taken up in a mixture of DMSO:water, along with c(RGDfK[N_3]) **199** (1.25 eq. per alkyne). Sodium ascorbate solution and $CuSO_4$.TBTA were then added. The reaction was followed by HPLC and found to be complete after 90 min. A similar C_{18} reverse phase extraction protocol was used to remove DMSO, and the crude product eluted from the cartridge using an MeCN:water mixture. Purification by semi-preparative HPLC gave 0.66 mg of FDEA-PEG-$(RGD)_4$ **249** (27% yield). MALDI-TOF MS (**Figure 14 B**) confirmed the identity of FDEA-PEG-$(RGD)_4$ **249**, showing a peak at *m/z* = 3412.6, corresponding to the $[M+H]^+$ ion. A peak corresponding to the loss of water (−18 Da) was observed for this compound too. The full MALDI-TOF MS spectrum tetrameric assembly **249** (**Figure 14 C**) was more complex than that of its dimeric analogue **248**, with a species of the same mass as its dimeric analogue (*m/z* = 1955.9) forming the base peak.

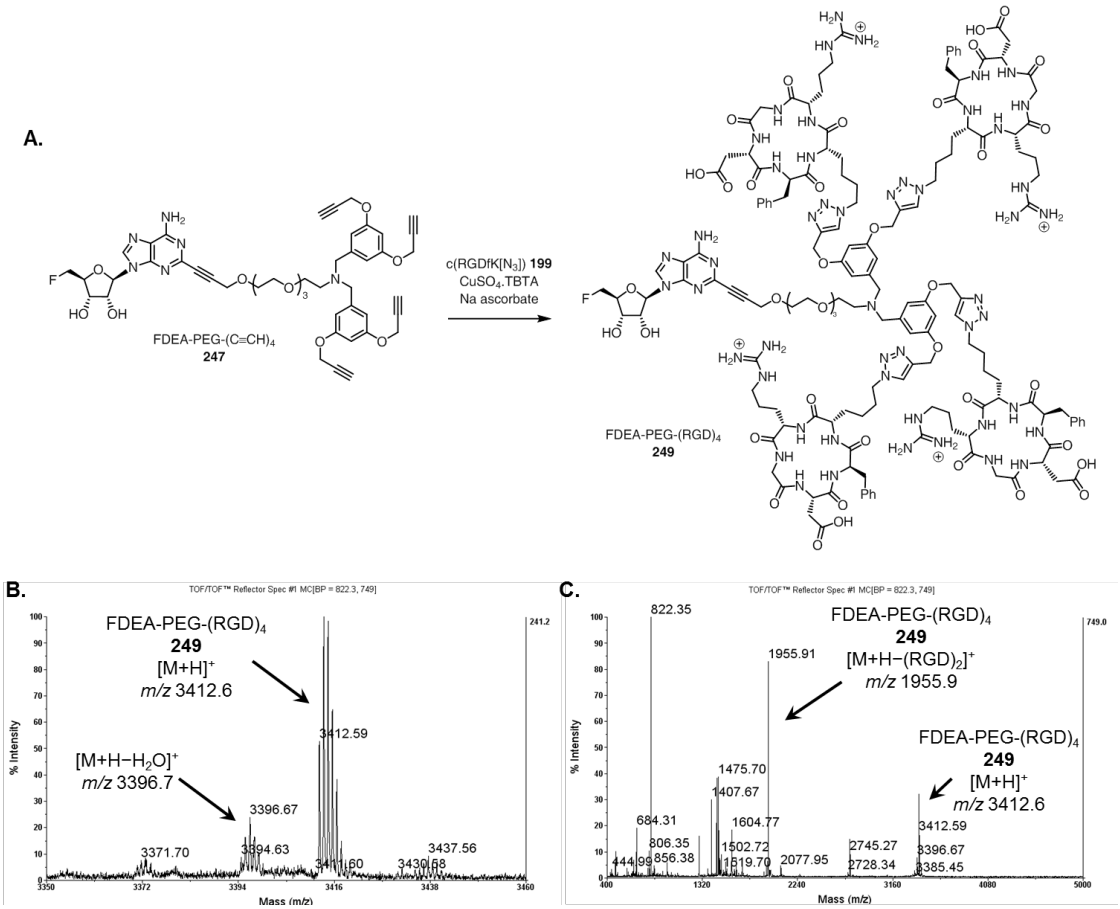

Figure 14. **A.** Preparative scale synthesis of FDEA-PEG-$(RGD)_4$ **249**. **B.** MALDI-TOF MS spectrum of the product after purification, showing the $[M+H]^+$ ion at *m/z* = 3412.6. The ion produced by loss of water is also evident. **C.** Full MALDI-TOF MS spectrum showing the peak (*m/z* = 1955.9) produced as a result of N–C bond cleavage. MALDI-TOF MS acquired by the University of St Andrews Mass Spectrometry Service.

3.6. Evaluation of multimeric RGDs as substrates for the fluorinase

With the multimeric substrates and products in hand, the fluorinase catalysed transhalogenation reactions with these peptide-modified substrates were explored.

3.6.1. Evaluation of ClDEA-PEG-$(RGD)_2$ 224 as a substrate for the fluorinase

Initial gradient-based HPLC based assays did not clearly resolve the chlorinated dimeric substrate **224** from its fluorinated analogue **248**, therefore a series of HPLC conditions were explored for separation of these two compounds. Isocratic conditions

(22 % MeCN + 0.05% TFA in water + 0.05% TFA) provided a good separation of the two species, suitable for assaying the new substrate.

ClDEA-PEG-$(RGD)_2$ **224** (40 μM) was added to a mixture of L-SeMet (75 μM) and potassium fluoride (50 mM) in a total volume of 1 mL and the reaction, shown in **Scheme 15**, was initiated by addition of the fluorinase (1 $mg.mL^{-1}$). Aliquots of the reaction mixture were removed every 30 min over 4 h. The enzyme was heat denatured and the protein removed by centrifugation, and then the clear supernatant was analysed by HPLC in order to assess conversion.

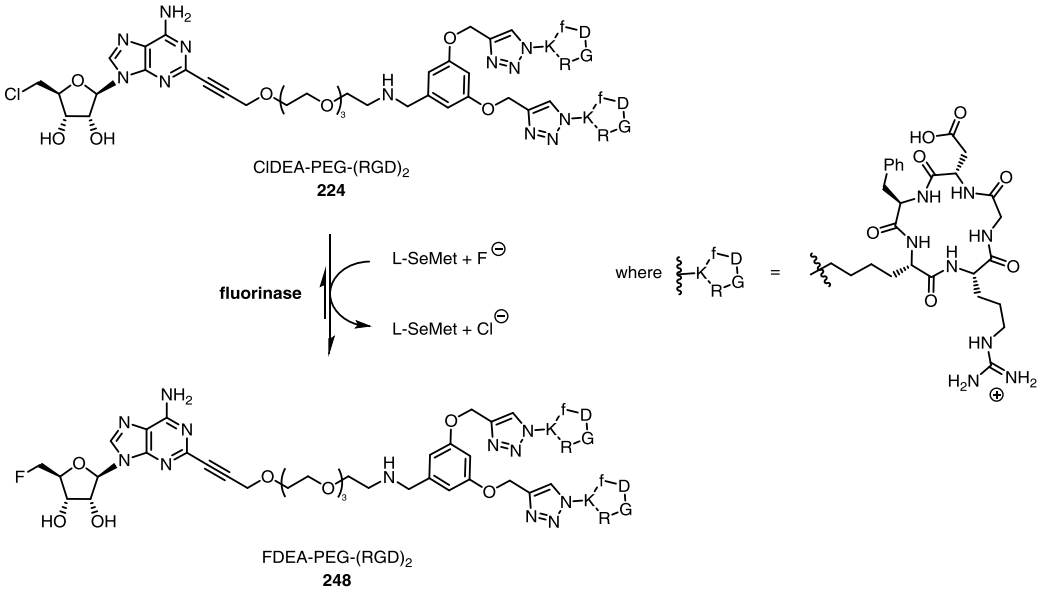

Scheme 15. Fluorinase catalysed transhalogenation of ClDEA-PEG-$(RGD)_2$ **224** to FDEA-PEG-$(RGD)_2$ **248**.

The HPLC traces, shown below in **Figure 15** showed the time-dependent appearance of a new peak at t_R = 8.2 min. This peak was identified as FDEA-PEG-$(RGD)_2$ **248** by comparison of the retention time to that of the synthetic standard of FDEA-PEG-$(RGD)_2$ **248**, synthesised as discussed in **Section 3.5.2**.

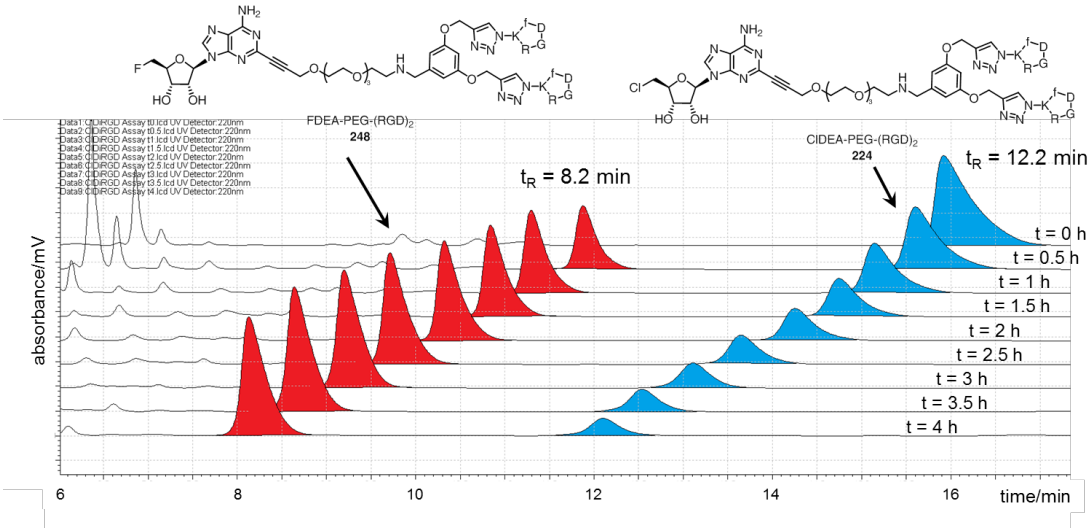

Figure 15. HPLC time course (220 nm) of incubation of ClDEA-PEG-$(RGD)_2$ **224**, blue, (t_R = 12.2 min) with the fluorinase, showing samples taken every 0.5 h over 4 h. A new peak was evident at t_R = 8.2 min, red, identified as FDEA-PEG-$(RGD)_2$ **248**.

LC-MS analysis of the reaction mixture at t = 0 h and t = 4 h confirmed that the transhalogenation had produced FDEA-PEG-$(RGD)_2$ **248**. The summed mass spectrum of the peaks corresponding to the multimeric species are shown below in **Figure 16**. In the sample taken at t = 0 h, peaks corresponding to multiply charged species of ClDEA-PEG-$(RGD)_2$ **224** are evident at *m/z* = 986.4 ($[M+2H]^{2+}$), 658.8 ($[M+3H]^{3+}$) and 494.4 ($[M+4H]^{4+}$). LC-MS analysis at t = 4 h, indicated that none of the original peaks were evident, and new peaks at *m/z* = 979.3, 652.8 and 489.9 were observed instead. The new peaks correspond to multiply charged ions of FDEA-PEG-$(RGD)_2$ **248** ($[M+2H]^{2+}$, $[M+3H]^{3+}$, and $[M+4H]^{4+}$ respectively), confirming FDEA-PEG-$(RGD)_2$ **248** as the product of the enzyme reaction.

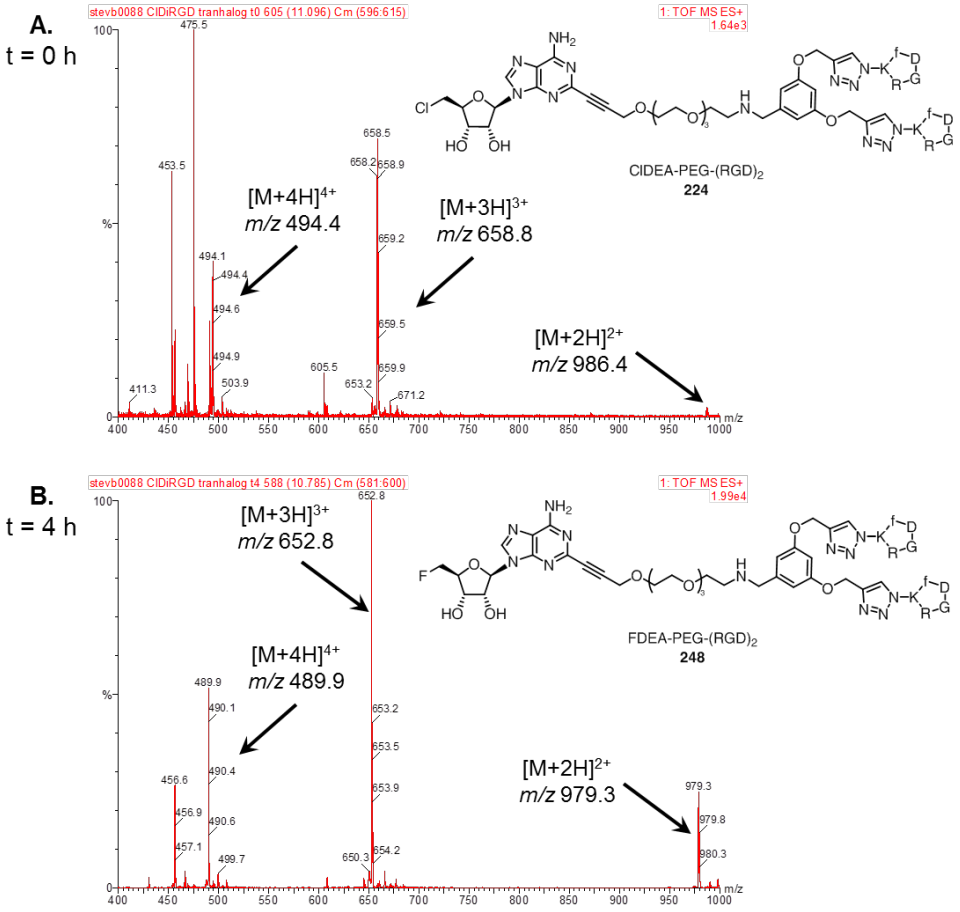

Figure 16. Summed mass spectrum (*m/z* = 400–1000) of the LC-MS peak corresponding to the tetrameric species. **A.** Sample taken at t = 0 h, showing peaks corresponding to multiply charged species of ClDEA-PEG-$(RGD)_2$ **224**. **B.** Sample taken at t = 4 h, showing peaks corresponding to multiply charged species of FDEA-PEG-$(RGD)_2$ **248**.

A series of control experiments, where the reaction was conducted in the absence of either enzyme or L-SeMet, did not result in any conversion to FDEA-PEG-$(RGD)_2$ **248**, confirming that the reaction is enzyme catalysed. In the control reaction carried out in the absence of fluoride, consumption of ClDEA-PEG-$(RGD)_2$ **224** was observed, however, no FDEA-PEG-$(RGD)_2$ **248** was detected by HPLC. This result suggests the generation of a seleno-SAM intermediate, which cannot be converted to product **248** in the absence of fluoride.

3.6.2. Evaluation of ClDEA-PEG-$(RGD)_4$ 225 as a substrate for the fluorinase

A similar HPLC-based experiment to that described in the previous section was conducted for ClDEA-PEG-$(RGD)_4$ **225** as a substrate for the enzyme, as shown in **Scheme 16**. ClDEA-PEG-$(RGD)_4$ **225** (20 μM) was added to a mixture of

L-SeMet (75 µM) and potassium fluoride (50 mM), in a total volume of 1 mL. The reaction was initiated by the addition of the fluorinase (1 $mg.mL^{-1}$) and monitored every 30 min over 4 h.

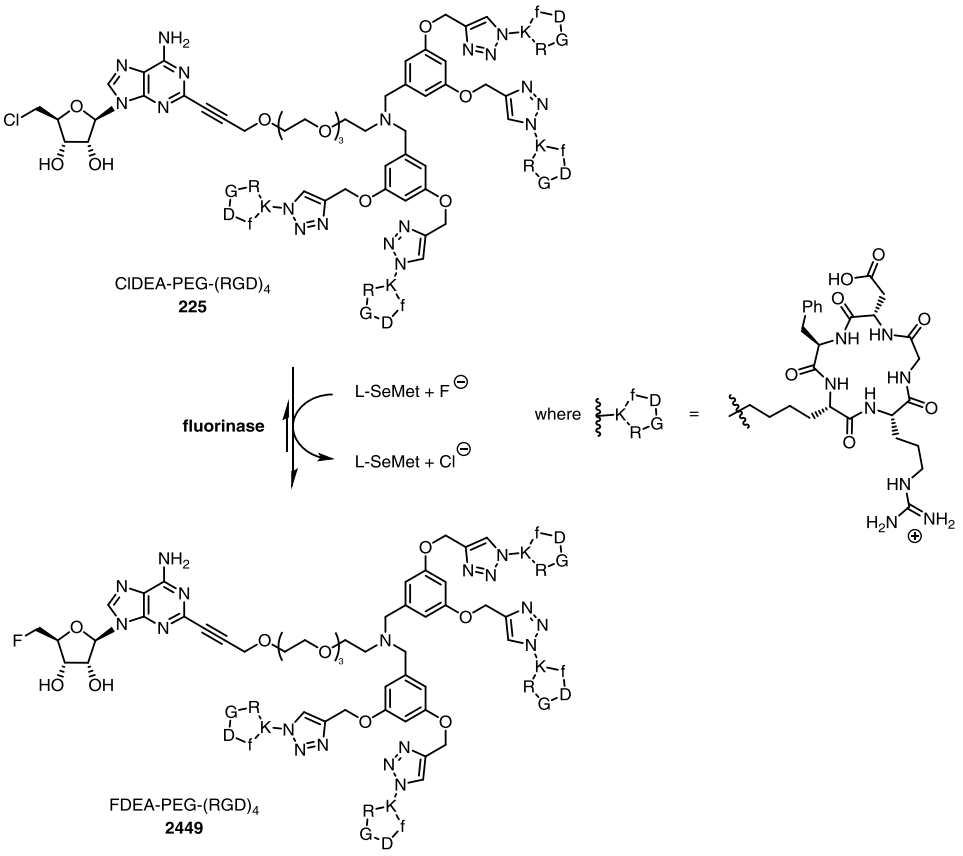

Scheme 16. Fluorinase catalysed transhalogenation of ClDEA-PEG-$(RGD)_4$ **225** to FDEA-PEG-$(RGD)_4$ **249**.

The resultant HPLC profile (**Figure 17**), obtained using isocratic conditions (24 % MeCN + 0.05% TFA in water + 0.05% TFA), showed that the chlorinated substrate **225** was consumed, while a new peak, at t_R = 9.2 min, steadily increased throughout the assay. The retention time of this new peak was identical to that of synthetic FDEA-PEG-$(RGD)_4$ **249**, and its identity was confirmed by LC-MS.

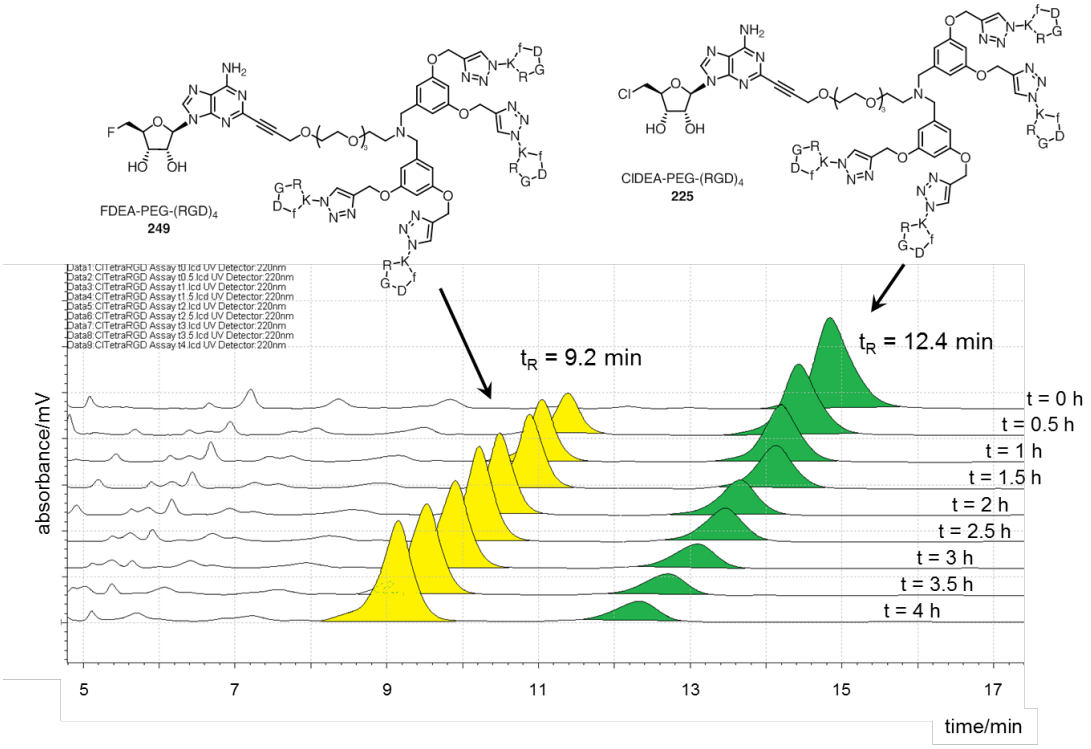

Figure 17. HPLC time course (220 nm) of incubation of ClDEA-PEG-$(RGD)_4$ **225**, green, (t_R = 12.4 min) with the fluorinase, showing samples taken every 0.5 h over 4 h. A new peak was evident at t_R = 9.2 min, yellow, identified as FDEA-PEG-$(RGD)_4$ **249**.

The summed mass spectrum of the peaks of the tetrameric species are shown below in **Figure 18**. In the sample taken at t = 0 h, peaks corresponding to multiply charged species of ClDEA-PEG-$(RGD)_4$ **225** are observed at *m/z* = 858.9 ($[M+4H]^{4+}$) and 687.2 ($[M+5H]^{5+}$). In the a sample analysed after an extended 16 h reaction time, peaks at *m/z* = 854.8 ($[M+4H]^{4+}$) and 683.8 ($[M+5H]^{5+}$) arising from FDEA-PEG-$(RGD)_4$ **249** were observed. The presence of these ions confirmed FDEA-PEG-$(RGD)_4$ **249** as the product of the enzymatic transhalogenation.

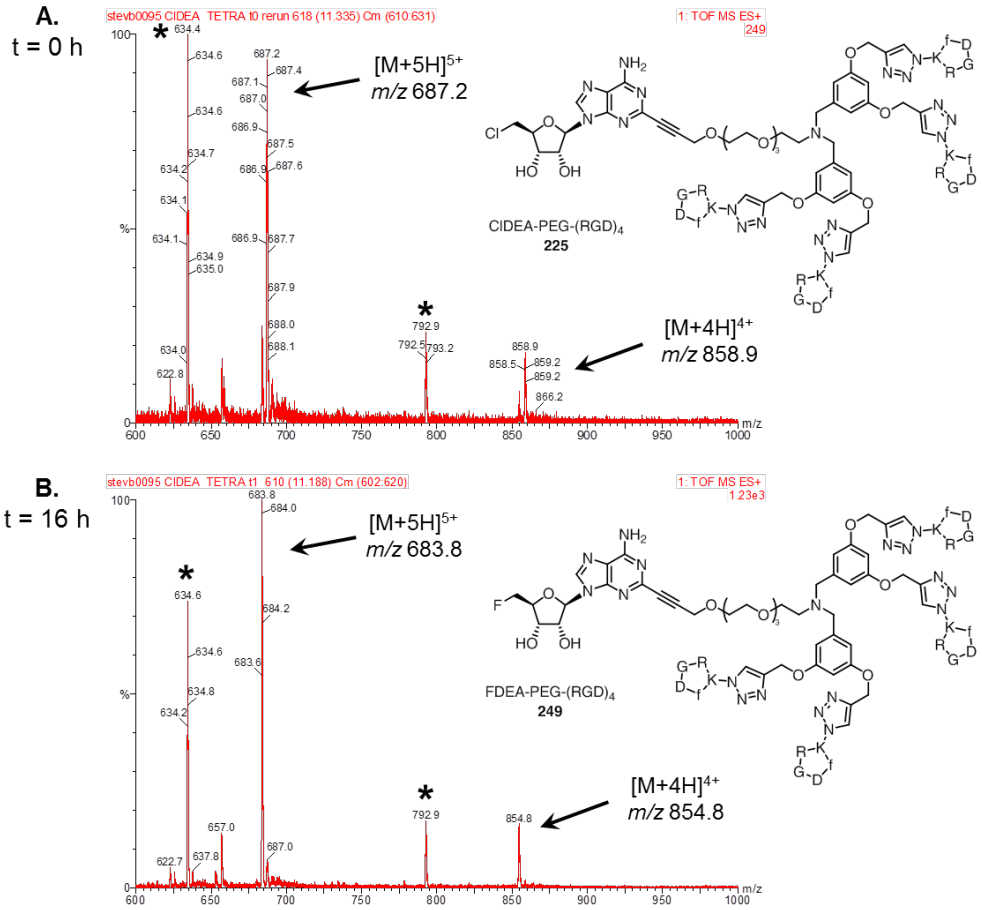

Figure 18. Summed mass spectrum (*m/z* = 600–1000) of the LC-MS peak corresponding to the tetrameric species. A. Sample taken at t = 0 h, showing peaks corresponding to multiply charged species of CIDEA-PEG-(RGD)$_4$ **225**. B. Sample taken at t = 4 h, showing peaks corresponding to multiply charged species of FDEA-PEG-(RGD)$_4$ **249**. Identical fragmentation peaks (denoted with an asterisk (*)) appear in both spectra.

Additional peaks were observed in spectra recorded at both t = 0 h and t = 16 h. These are denoted with an asterisk (*) in **Figure 18**. The peaks are identical in both spectra, suggesting the fragmentation of the parent species to produce ions which lack the halogen atom. Fragmentation of the (C-2)–C bond between the nucleoside and the acetylene to give **250**, as illustrated in **Scheme 17**, would give ions calculated to have the masses of those observed; *m/z* = 792.2 is assigned to $[M+3H+Na]^{4+}$, while the peak at *m/z* = 634.6 is assigned to $[M+4H+Na]^{5+}$.

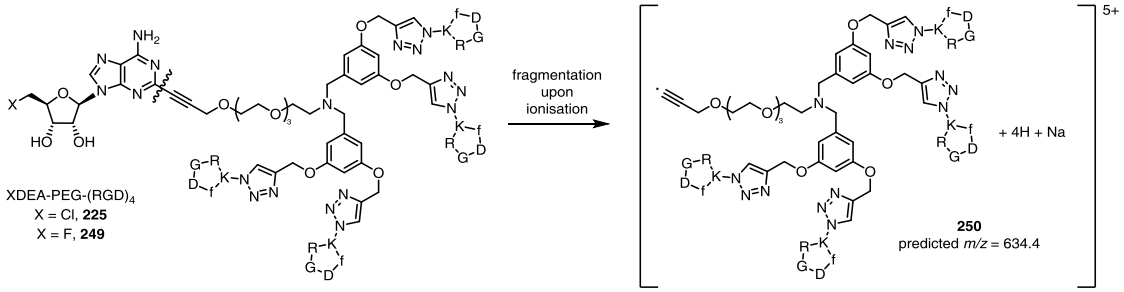

Scheme 17. Fragmentation of the halogenated tetrameric constructs **225** and **249** to ions corresponding to the observed mass (*m/z*).

The results from these two assays illustrate the successful extension of the substrate scope of the fluorinase enzyme to larger multimeric peptides. Tolerance of these multimeric substrates suggests that the C-2 position of a chlorinated nucleoside represents an ideal site for the attachment of a diverse range of peptide cargos for use in enzymatic fluorination. These constructs were shown to be efficiently fluorinated under the action of the fluorinase enzyme, using fluoride ion under aqueous, pH neutral conditions.

3.7. Binding assay of denrimeric RGDs to $\alpha_V\beta_3$ integrin

With the knowledge that the multimeric constructs were suitable substrates for the fluorinase catalysed transhalogenation, the effect of multimerisation of the RGD motif using the linkers described above on their affinity for $\alpha_V\beta_3$ integrin was explored.

The binding affinities of the FDEA-PEG-$(RGD)_2$ **248** and FDEA-PEG-$(RGD)_4$ **249** were determined by evaluating the binding of the peptide to immobilised $\alpha_V\beta_3$ integrin using the same ELISA assay described in **Chapter 2**.[18] The experiments were conducted by Dr Ian Fleming at the University of Aberdeen. The IC_{50} values for the multimers **248** and **249** are shown in **Table 1** below. The IC_{50} values for two reference peptides and two monomeric RGD peptides described previously (**201** and **207**) are included for comparison.

Table 1. IC_{50} values of selected RGD-containing peptides measured as the ability to compete with c(RGDfK[PEG-PEG-biotin]) for binding to immobilised $\alpha_V\beta_3$ integrin. Results are the average ± standard error (s.e.) from three independent experiments, each performed in triplicate. Q is the normalised affinity of the peptides, referenced to GRGDSPK. Measurements were performed by Dr Ian Fleming. [a]Affinities for these constructs were previously reported, and were measured using an identical assay.

Compound	*IC_{50} ± s.e /μM*	*Q*
RGD	8.56 ± 2.24	4.019
GRGDSPK[a]	2.13 ± 0.41	1.000
c(RGDfK[N_3]) **199**[a]	0.09 ± 0.01	0.042
FDEA-RGD **201**[a]	0.33 ± 0.03	0.155
FDEA-TEG-RGD **207**[a]	0.074 ± 0.016	0.033
FDEA-PEG-$(RGD)_2$ **248**	0.060 ± 0.013	0.027
FDEA-PEG-$(RGD)_4$ **249**	0.024 ± 0.018	0.011

The ELISA data show that the multimers have a lower IC_{50}, 60 nM and 24 nM for the dimeric **248** and tetrameric **249** constructs respectively, than the two monomeric RGD peptides described previously (**201** and **207**). The IC_{50} values measured for the multimeric constructs are also lower than the parent azido-peptide **199**. The multimeric compounds have much lower IC_{50} values compared to those of linear reference RGD-containing peptides.

The multimerisation of the RGD motif in **248** and **249** produced compounds which have better affinity to immobilised $\alpha_V\beta_3$ integrin than their monomeric analogues. The tetrameric analogue **249** has a lower IC_{50} compared to the dimeric analogue, and this difference found to be statistically significant ($p < 0.05$, Student's *t*-test). The presence of two RGD motifs in the vicinity of the receptor leads to only a marginal increase in the affinity of the construct to $\alpha_V\beta_3$ integrin. The addition of a further two RGD units to the construct (to give a tetramer) gave a compound with much higher affinity, the highest affinity observed for any fluorinase RGD-based substrate to date.

The linker between the two or four RGD units is not long, and the increased affinity is most likely due to an increased effective molarity at the binding site. Steric constraints will likely prevent multivalent binding of two RGD ligands to two individual $\alpha_V\beta_3$ integrin receptors.

Many multimeric constructs reported in the literature have IC_{50} values in the 1–100 nM range,[9] and the IC_{50} values obtained for the multimeric compounds described in this investigation are within this range. Direct comparison of the observed IC_{50} values to those in the literature is difficult, as most reports use alternate assays and different

competing peptides. The reports also do not generally report the normalisation the observed IC_{50} values to that of a reference peptide such as GRGDSPK.

3.8. Radiosynthetic evaluation of multimeric RGDs

The demonstration that large peptide assemblies of 10 or 20 amino acids are tolerated as fluorinase substrates offers an approach for mild and chemoselective fluorination of peptides for PET. As a consequence, we were interested in exploring the behaviour of the multimeric constructs upon translation to the PET environment, where the [^{18}F]fluoride ion concentration is much lower (pM to nM) than the fluoride concentration employed in the enzyme assays described above (50 mM). The fluorinase-catalysed radiolabelling of ClDEA-PEG-$(RGD)_2$ **224** and ClDEA-PEG-$(RGD)_4$ **225** was therefore explored at the University of Glasgow's radiochemistry laboratory, in collaboration with Dr Sally Pimlott and Dr Sue Champion.

3.8.1. Initial radiolabelling experiments with ClDEA-PEG-$(RGD)_2$ 224

Radiolabelling of ClDEA-PEG-$(RGD)_2$ **224** was investigated under similar conditions to the assays reported in **Section 3.6.1**, but using [^{18}F]fluoride solution rather than high concentrations of [^{19}F]fluoride. In addition, the enzyme concentration was increased from 1 mg.mL^{-1} (29 μM) to 10 mg.mL^{-1} (290 μM), as it had previously been shown that high enzyme concentrations resulted in increased incorporations of [^{18}F]fluoride.[49] Lower concentrations of the multimeric substrate were initially employed as the conditions proved successful for [^{19}F]fluoride, and the dimeric RGD substrate was not sufficiently soluble at higher concentrations used in previous fluorinase radiolabelling experiments.

To this end a solution of [^{18}F]fluoride ion (30.4 MBq) was added to a mixture of ClDEA-PEG-$(RGD)_2$ **224** (0.04 mM), L-SeMet (0.15 mM), and the fluorinase (10 mg.mL^{-1}) in a total volume of 500 μL, as shown below in **Scheme 18**. The mixture was incubated at 37 °C for 30 min, before the enzyme was precipitated by heat denaturation at 95 °C and centrifugation at 3000-4000 rpm.

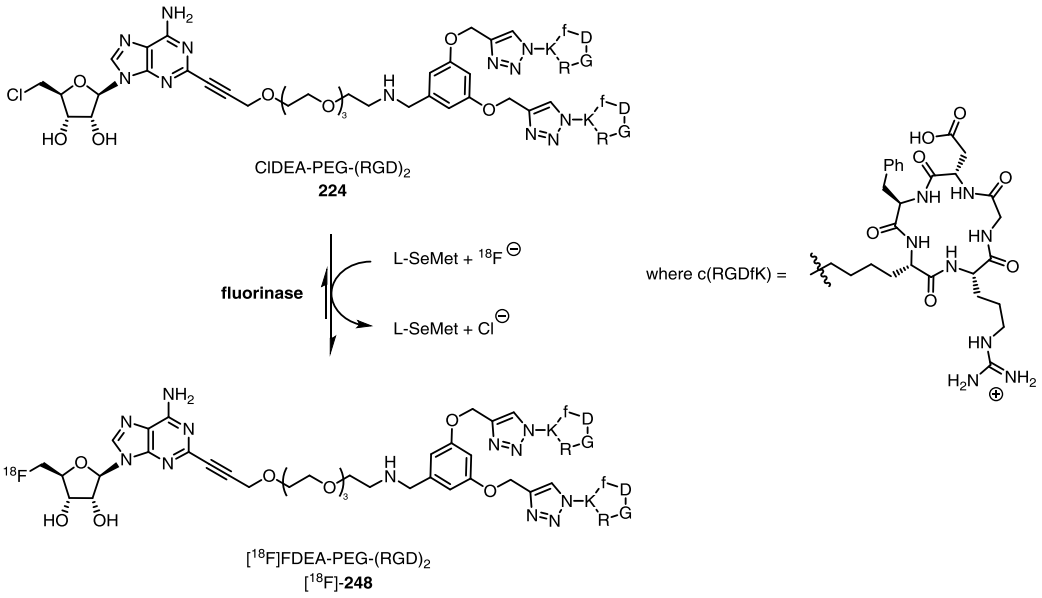

Scheme 18. Fluorinase catalysed transhalogenation reaction with ClDEA-PEG-$(RGD)_2$ **224** with [^{18}F]fluoride to produce [^{18}F]FDEA-PEG-$(RGD)_2$ [^{18}F]-**248**.

A sample of the supernatant was analysed by HPLC coupled in series to a diode array UV detector and a radioactivity detector. The resultant radio-HPLC trace is illustrated below in **Figure 19**. Unlike previous successful radiolabelling experiments with the fluorinase enzyme,[49–53] only a trace of the anticipated product [^{18}F]-**248** was observed.

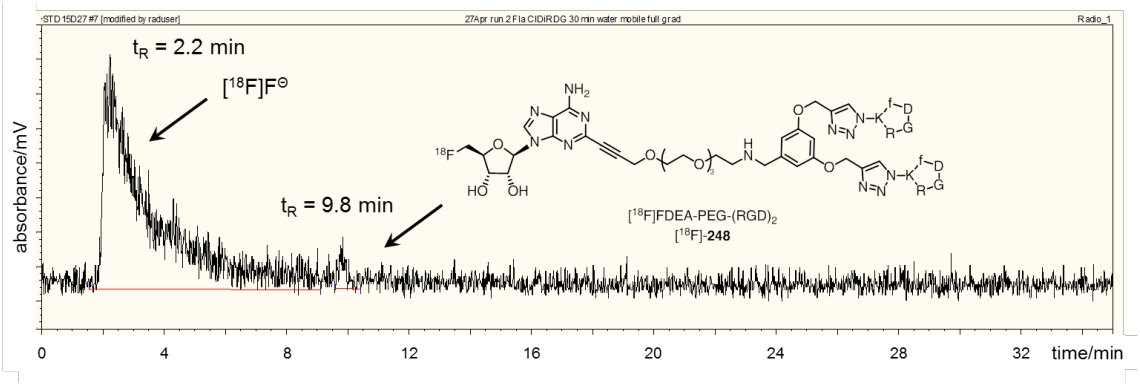

Figure 19. HPLC radioactivity trace of the reaction where ClDEA-PEG-$(RGD)_2$ **224** was incubated with the fluorinase and [^{18}F]fluoride for 30 min. [^{18}F]Fluoride is evident at the broad peak at t_R = 2.2 min, while only traces of the expected product, [^{18}F]FDEA-PEG-$(RGD)_2$ [^{18}F]-**248**, are observed at t_R = 9.8 min. Run with under gradient conditions.

[^{18}F]Fluoride ion appears as a broad, tailing peak at t_R = 2.2 min. This broad peak is due to the acidity of the mobile phase,[54] in this case 0.05% TFA in a water/MeCN mixture at pH ~2.2.[55] HF is a weak acid (pK_a = 3.17), and [^{18}F]fluoride therefore exists in an equilibrium between its protonated and deprotonated state.[54] These states interact differently with the stationary phase of the C_{18} reverse phase column resulting

in the observed broad peak. The tailing of the peak and its overlap with the peaks of the product reduced the accuracy in determining incorporation. Reported incorporations were calculated by defining the baseline at the lowest point in the valley between the two overlapping peaks.

As the incorporation of [^{18}F]fluoride was low, the activity of the enzyme was investigated. To this end, a control experiment with CIDA **23** under identical labelling conditions was performed, as shown in **Scheme 19**. The concentration of each of the components of the reaction mixture was kept constant. The supernatant of a heat-treated sample of the reaction mixture was analysed using the same HPLC conditions described above.

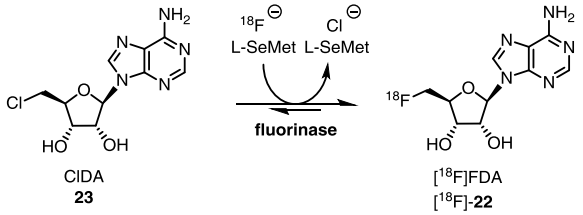

Scheme 19. Fluorinase catalysed transhalogenation reaction with CIDA **23** with [^{18}F]fluoride to produce [^{18}F]FDA [^{18}F]-**22**, used as a control experiment.

The resultant radio-chromatogram is shown below in **Figure 20**. The chromatogram reveals that under the same conditions, the reaction of CIDA **23** is also poor, and only ~10% of the [^{18}F]fluoride was converted to [^{18}F]FDA [^{18}F]-**22**, suggesting that the conditions for labelling were not optimal.

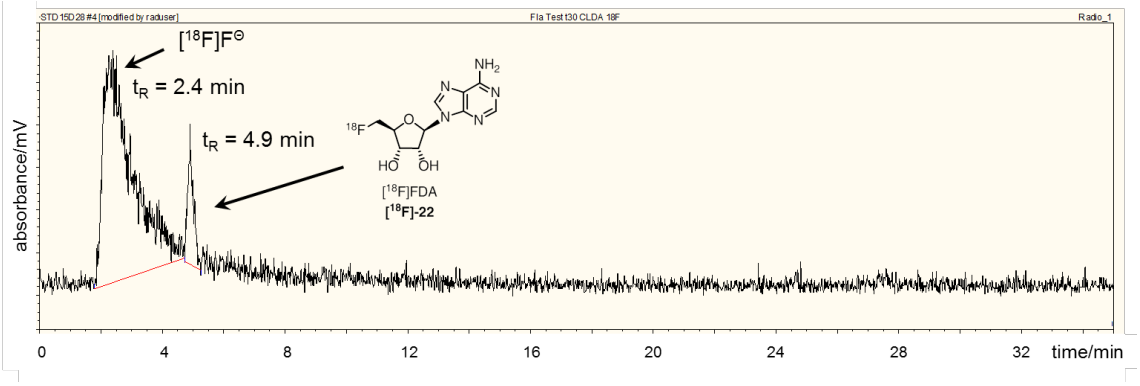

Figure 20. HPLC radioactivity trace of the reaction where CIDA **23** was incubated with the fluorinase and [^{18}F]fluoride for 30 min. [^{18}F]Fluoride is again observed as a broad peak at t_R = 2.4 min. A new peak was observed at t_R = 4.9, and identified as [^{18}F]FDA [^{18}F]-**22**.

3.8.2. Optimisation of radiolabelling conditions with ClDA 23 as a substrate

The reaction conditions employed for radiolabelling in **Chapter 2** or **Section 3.1.2** both afforded the anticipated radiolabelled products in good yield, without the need for optimisation. However, the low radiochemical incorporations observed for the multimeric substrate necessitated investigation to identify more optimal reaction conditions.

To this end, the transhalogenation reaction between ClDA **23** and [^{18}F]fluoride ion was investigated under a variety of conditions, as summarised below in **Table 2**.

Table 2. Conditions investigated for the fluorinase catalysed radiolabelling of ClDA **23** to [^{18}F]FDA [^{18}F]-**22**. Conditions changed for each experiment are highlighted in bold.

Component concentration			*radiochemical incorporation*
ClDA **23**/mM	fluorinase/mg.mL^{-1}	L-SeMet/mM	
0.04	10	0.125	10%
0.04	**10** (alt. batch)	0.125	10%
0.04	**2.8** (stoichiometric)	0.125	13%
0.04	**0.7** (catalytic)	0.125	5%
0.04	10	**0.020**	9%
0.3	**0.7**	0.125	9%
0.3	10	0.125	60%
0.3	**20**	0.125	65%
0.6	**20**	0.125	90%

Firstly, an alternative preparation of the fluorinase enzyme was investigated, but this resulted in similar radiochemical incorporations (~10%) as the original batch used. The effect of lowering the enzyme concentration to stoichiometric and catalytic levels was investigated. Surprisingly, use of stoichiometric amounts of enzyme did not significantly alter incorporation, suggesting that the ratio of enzyme to substrate may be an important factor affecting incorporation. Employing a catalytic amount of the enzyme led to a reduction in incorporation to 5%, whilst decreasing the L-SeMet concentration had no effect.

When substrate concentration was increased from 0.04 mM to 0.3 mM in the presence of catalytic enzyme (0.7 mg.mL^{-1}, 0.02 mM), the incorporation was found to recover to ~9%. The result suggested that a combination of high substrate concentration and high enzyme concentration may be necessary for high radiochemical incorporation. Repetition of the reaction at much higher enzyme concentrations (10 mg.mL^{-1}, 0.3 mM) in combination with a high substrate concentration (0.3 mM) resulted in significantly

higher radiochemical incorporations, approaching 60%. These incorporations were similar to that observed in previous, successful radiolabelling experiments. Further increasing the enzyme concentration to 20 mg.mL^{-1} only afforded a marginal increase in incorporation. However, increasing the substrate concentration to 0.6 mM, combined with 20 mg.mL^{-1} of fluorinase resulted in incorporations of approximately 90% within 30 minutes. The HPLC radio-chromatogram of this experiment is shown below in **Figure 21**, with the peak for [^{18}F]FDA [^{18}F]-**22** appearing at t_R = 5.2 min.

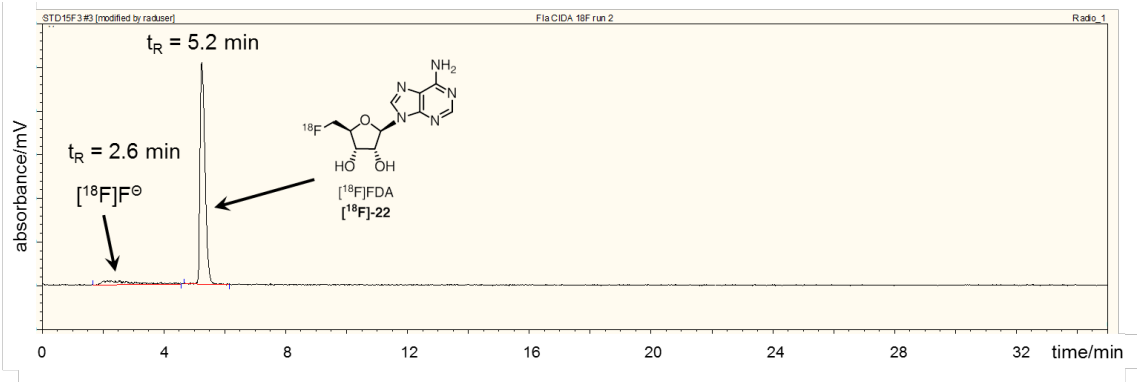

Figure 21. HPLC radioactivity trace of the reaction where CIDA **22** (0.6 mM) was incubated with the fluorinase (20 mg.mL^{-1}) and [^{18}F]fluoride for 30 min. [^{18}F]FDA [^{18}F]-**22** was observed at t_R = 5.2, with ~90% radiochemical incorporation.

These experiments suggested that a combination of high fluorinase concentration coupled to high substrate concentration is required to achieve the highest possible radiochemical incorporations. When either of these concentrations is low, a reduction in incorporation is observed. These results led us to explore the radiolabelling of the multimeric substrates under these optimised conditions.

3.8.3. Radiolabelling of ClDEA-PEG-(RGD)$_2$ 224 under optimised conditions

The optimised conditions require a substrate concentration of 0.6 mM for high radiochemical incorporations, however, the multimeric substrates ClDEA-PEG-(RGD)$_2$ **224** and ClDEA-PEG-(RGD)$_4$ **225** were found to be poorly soluble in water at this concentration. Reactions were therefore performed with a sufficient mass of substrate to give a final concentration of 0.3 mM (assuming that the compound was completely dissolved).

The radiolabelling of ClDEA-PEG-(RGD)$_2$ **224** was explored as shown in **Scheme 20**, using the conditions described above. A sample of a solution of ClDEA-PEG-(RGD)$_2$ **224** (corresponding to 0.1 mg of **224**) from a 1:1 mixture of

MeCN:water was added to a vial, and the solution concentrated to dryness under a stream of nitrogen, while heating to 95 °C. After cooling, L-SeMet (0.08 mM), and fluorinase (20 mg.mL^{-1}) were added, followed by a solution of [^{18}F]fluoride in water (380 µL) to give a final concentration of ClDEA-PEG-(RGD)$_2$ **224** of 0.3 mM. Some precipitation of the substrate was observed upon addition of aqueous [^{18}F]fluoride, suggesting that the final concentration of substrate in solution was likely lower than the desired 0.3 mM.

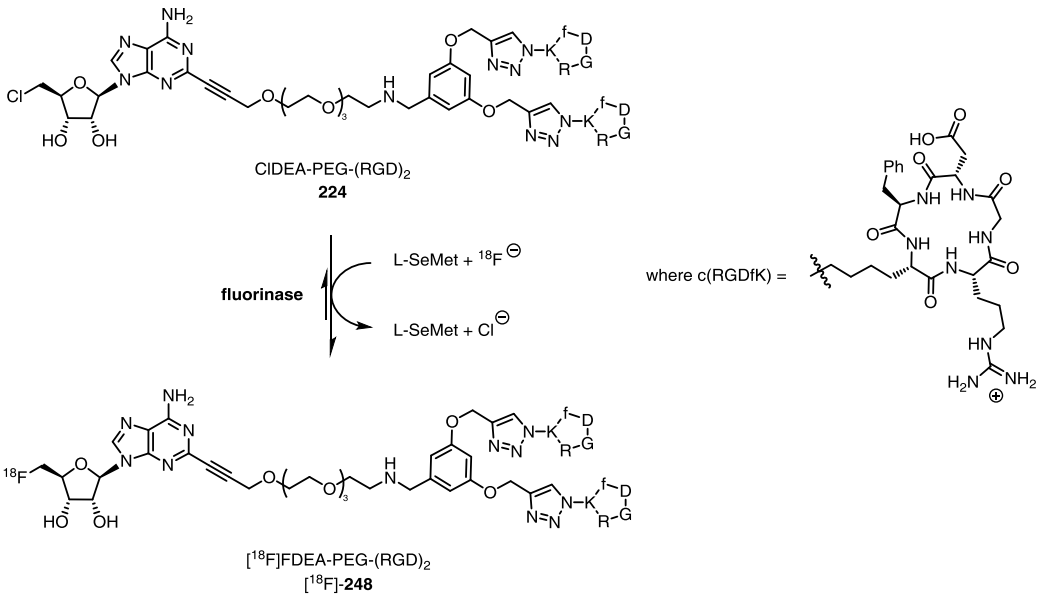

Scheme 20. Fluorinase catalysed transhalogenation reaction with ClDEA-PEG-(RGD)$_2$ **224** with [^{18}F]fluoride to produce [^{18}F]FDEA-PEG-(RGD)$_2$ [^{18}F]-**248**.

The reaction was incubated at 37 °C for 30 minutes, before the enzyme was heat denatured and the mixture centrifuged. A sample of the supernatant was analysed by HPLC, and the resultant HPLC radio-chromatogram is shown in **Figure 22**, revealed a new peak at t_R = 13.7 min, which was identified as [^{18}F]FDEA-PEG-(RGD)$_2$ [^{18}F]-**224** by spiking with a sample of [^{19}F]FDEA-PEG-(RGD)$_2$ **248**.

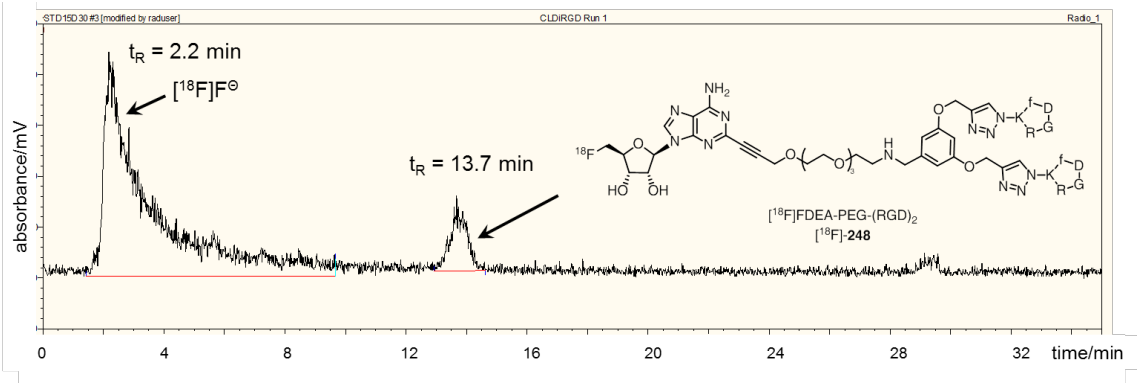

Figure 22. HPLC radioactivity trace of the reaction where ClDEA-PEG-(RGD)$_2$ **224** (0.3 mM) was incubated with the fluorinase (20 mg.mL^{-1}) and [^{18}F]fluoride for 30 min. [^{18}F]FDEA-PEG-(RGD)$_2$ [^{18}F]-**228** was observed at t_R = 13.7 min, showing 10% radiochemical incorporation. Run under isocratic HPLC conditions.

The radiochemical incorporation of [^{18}F]fluoride into [^{18}F]FDEA-PEG-(RGD)$_2$ [^{18}F]-**248** was much higher than observed in the initial experiment (shown in **Figure 19** in **Section 3.8.1**), where only traces of the desired product were observed. Radiochemical incorporations were, however, lower than those observed for the unmodified substrate ClDA **23** (60%) under similar conditions. The lower radiochemical incorporation is most likely due to the substrate ClDEA-PEG-(RGD)$_2$ **224** being poorly soluble in water and limiting substrate concentration.

A range of conditions were explored in an attempt to increase the final substrate concentration in solution. These experiments were conducted in a similar manner to those described above, but with a different preparation of ClDEA-PEG-(RGD)$_2$ **224** and fluorinase.

Three different preparations of ClDEA-PEG-(RGD)$_2$ **224** were investigated. For the first preparation, the substrate **224** was freeze-dried directly in the reaction vessel in an attempt to increase the surface area of the compound and consequently its rate of dissolution. The second attempt involved the preparation of a low concentration enzyme:**224** complex. After freeze-drying and resuspension in a smaller volume, it was hoped that **224** may be more soluble as a complex. The freeze dried compound was therefore added to a solution of the fluorinase in a large volume (1 mL, **224** concentration 0.04 mM) before the enzyme-substrate solution was freeze dried. In a third preparation, **224** was pre-dissolved in DMSO (2 µL) before the radiolabelling experiment.

In a typical experiment, the compound preparation was added to a solution of [^{18}F]fluoride (138 µL, 15.2–29.7 MBq) in water, along with the enzyme (if required) and

L-SeMet. Reactions were incubated at 37 °C for 30 min or 120 min before the enzyme was removed by heating and centrifugation. The radiochemical incorporation for each of these experiments, determined by HPLC, is summarised below in **Table 3**.

Table 3. Conditions investigated for increasing substrate concentration for the fluorinase catalysed radiolabelling of ClDEA-PEG-$(RGD)_2$ **224** to [^{18}F]FDEA-PEG-$(RGD)_2$ [^{18}F]-**248**. Conditions changed for each experiment are highlighted in bold.

Condition changed		*radiochemical incorporation*
ClDEA-PEG-$(RGD)_2$ **224** preparation	reaction time/min	
freeze dried powder	30	10%
freeze dried with enzyme	30	10%
freeze dried with enzyme	**120**	10%
pre-dissolved in DMSO (2 μL)	30	7%

The radiochemical incorporation remained ~10% in all of the experiments, suggesting that the efforts described did not significantly increase the concentration of ClDEA-PEG-$(RGD)_2$ **224** in solution. Allowing the reaction to proceed for 2 h, rather than 30 minutes did not result in any significant increased radiochemical incorporation.

These radiolabelling results indicated that ClDEA-PEG-$(RGD)_2$ **224** was a poor substrate under PET conditions, despite the good conversions observed in the "cold" experiments at high fluoride ion concentrations. This effect is most likely a combination of an inherently slower transhalogenation reaction, coupled to poor solubility of the substrate under the investigated conditions.

3.8.4. Radiolabelling of ClDEA-PEG-$(RGD)_4$ 225 under optimised conditions

The transhalogenation reaction between the tetrameric construct ClDEA-PEG-$(RGD)_4$ **225** and [^{18}F]fluoride, catalysed by the fluorinase, shown in **Scheme 21**, was also investigated under the optimised radiolabelling conditions. ClDEA-PEG-$(RGD)_4$ **225** showed very poor solubility and achieving solutions of 0.3 mM also proved difficult.

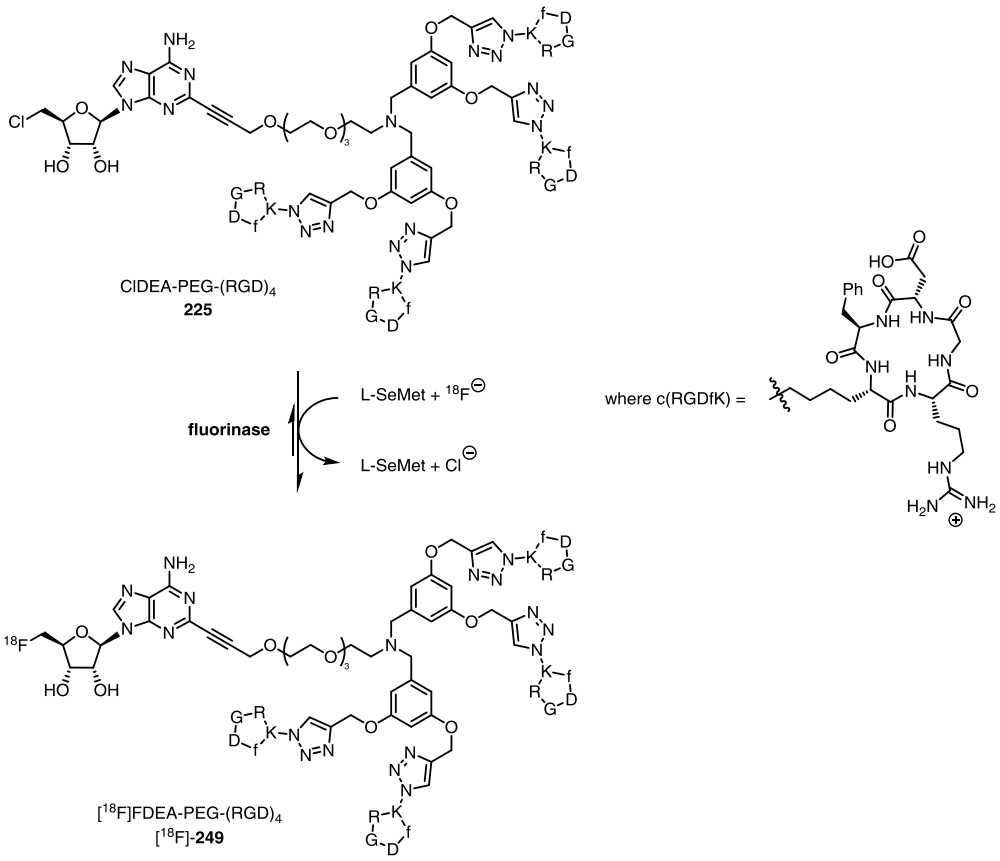

Scheme 21. Fluorinase catalysed transhalogenation reaction with ClDEA-PEG-$(RGD)_4$ **225** with [^{18}F]fluoride to produce [^{18}F]FDEA-PEG-$(RGD)_4$ [^{18}F]-**249**.

A similar investigation into increasing the concentration of the tetrameric species in solution was undertaken. Freeze-dried ClDEA-PEG-$(RGD)_4$ **225** (0.2 mg), or **225** (0.2 mg) in DMSO (2 µL) were added to L-SeMet (0.08 mM or 0.3 mM), and fluorinase (20 mg.mL^{-1}), followed addition of a solution of [^{18}F]fluoride in water (160 µL, 25.0–35.4 MBq). Alternatively, L-SeMet (0.08 mM) and [^{18}F]fluoride solution (25.1 MBq) were added to a freeze dried enzyme:**225** complex. The reactions were allowed to proceed for 30 min or 120 min at 37 °C, before the enzyme was heat denatured and the mixture centrifuged. A sample of the supernatant was analysed by HPLC in order to assess incorporation. The conditions explored are summarised in **Table 4.**

Table 4. Conditions investigated for increasing substrate concentration for the fluorinase catalysed radiolabelling of ClDEA-PEG-$(RGD)_4$ **225** to [^{18}F]FDEA-PEG-$(RGD)_4$ [^{18}F]-**249**. Conditions changed for each experiment are highlighted in bold.

Condition changed		*radiochemical incorporation*
ClDEA-PEG-$(RGD)_4$ **225** preparation	reaction time/min	
freeze dried powder	30	5%
freeze dried with enzyme	30	5%
pre-dissolved in DMSO (2 μL)	30	5%
freeze dried powder	**120**	5%
L-SeMet concentration to 0.3 mM	30	7%

For all of the explored conditions, radiochemical incorporations of [^{18}F]fluoride to generate [^{18}F]FDEA-PEG-$(RGD)_4$ [^{18}F]-**249** were found to be 5–7%, with the product observed at t_R = 10.1 min. A representative HPLC radio-chromatogram is shown in **Figure 23**, for the reaction where the enzyme and substrate were co-mixed prior to the labelling reaction. Extending the reaction time and increasing the concentration of L-SeMet had a negligible effect on the observed radiochemical incorporation.

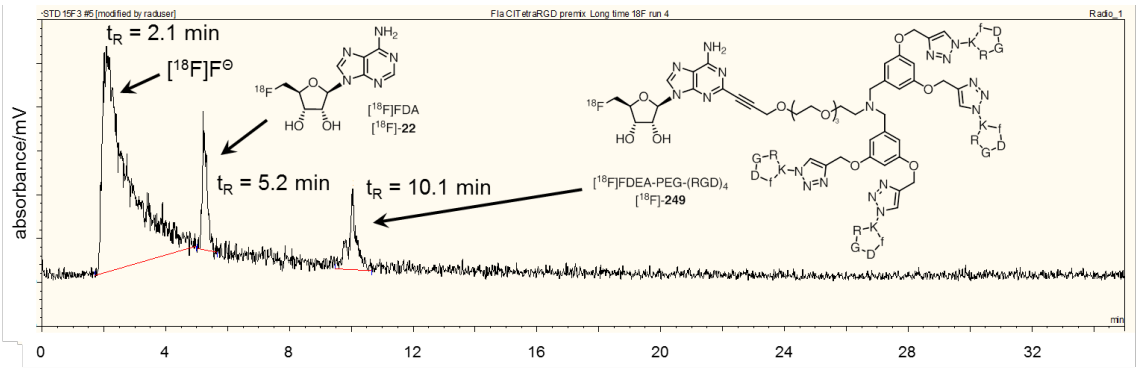

Figure 23. HPLC radioactivity trace of experiment where ClDEA-PEG-$(RGD)_4$ **225** (0.3 mM) freeze dried with the fluorinase (20 mg.mL^{-1}) prior to reaction. [^{18}F]Fluoride and L-SeMet were added and the mixture incubated for 30 min. [^{18}F]FDEA-PEG-$(RGD)_4$ [^{18}F]-**249** was observed at t_R = 10.1 min, showing 5% radiochemical incorporation. An additional peak was also observed at t_R = 5.2 min. Run under gradient conditions.

These results suggest that ClDEA-PEG-$(RGD)_4$ **225** was also a poor substrate for the fluorinase catalysed transhalogenation reaction with [^{18}F]fluoride ion. Although "cold" reactions at high fluoride ion concentration were successful, again, poor solubility of the substrate, ClDEA-PEG-$(RGD)_4$ **225**, in the aqueous reaction medium resulted in low incorporation of [^{18}F]fluoride ion.

The fluorinase is known to be a slow enzyme, even with its natural substrate *S*-adenosylmethioinine (k_{cat} = 0.06 min^{-1}).[56] It was found in **Chapter 2** that the transhalogenation rate observed with ClDEA **174**, the acetylene-modified substrate for

the enzyme, operated at approximately 60% of the rate of the unmodified substrate. Extending the logic that modification of the substrate to these more complex multimeric derivatives would suggest that the transhalogenation reaction of these multimers with fluoride would be significantly slower. The inherently slower reaction, coupled to the low solubility of ClDEA-PEG-$(RGD)_2$ **224** and ClDEA-PEG-$(RGD)_4$ **225** appears to be responsible for the low radiochemical incorporations observed during reaction with [^{18}F]fluoride.

Unlike the experiments described in the previous section for ClDEA-PEG-$(RGD)_2$ **224**, the isocratic conditions did not translate well for HPLC analysis of experiments using ClDEA-PEG-$(RGD)_4$ **225**. Consequently HPLC was conducted using a simple 5% MeCN to 95 % MeCN in water (with 0.05% TFA modifier) over a 20 minute gradient. Use of this gradient for **225** revealed the presence of an unidentified peak at t_R = 5.2 min, shown in the trace above in **Figure 23**.

The unidentified peak had the same retention time as [^{18}F]FDA [^{18}F]-**22**, the product of the optimisation reactions discussed in **Section 3.8.2**. In a control experiment, a solution of [^{18}F]fluoride ion was added to the fluorinase enzyme and L-SeMet, *without* the addition of any nucleoside substrate. After 30 min incubation at 37 °C and subsequent heat precipitation of the enzyme, the supernatant was analysed by HPLC using the same gradient conditions. The resultant radio-chromatogram (**Figure 24**) revealed the presence of a radiolabelled compound, eluting at t_R = 5.2 min. Spiking of this sample with a solution of [^{19}F]FDA **22** revealed that the peaks co-elute, suggesting that the radioactive compound was indeed [^{18}F]FDA [^{18}F]-**22**.

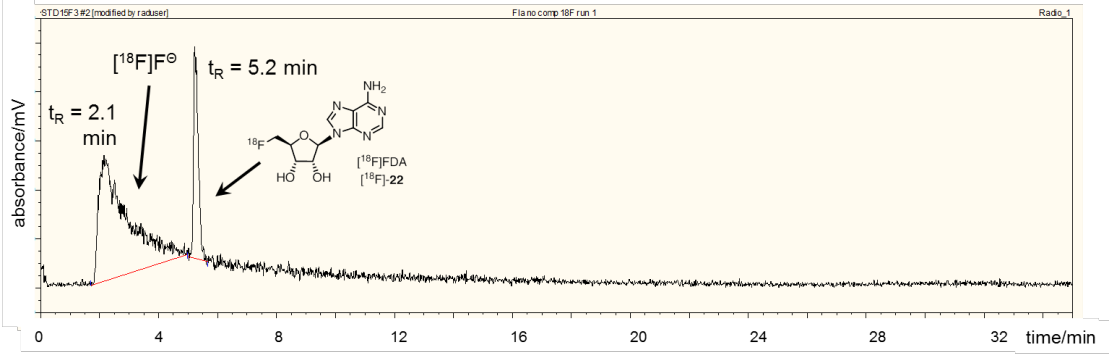

Figure 24. HPLC radioactivity trace of the control reaction where the fluorinase (20 mg.mL^{-1}) was incubated with only [^{18}F]fluoride for 30 min. [^{18}F]FDA [^{18}F]-**22** was observed at t_R = 5.2 min. Run with under gradient conditions.

The conversion of approx. 20% of [^{18}F]fluoride to [^{18}F]FDA [^{18}F]-**22** under these conditions suggested that traces of *S*-adenosylmethioinine **20** (SAM) were present in

the reaction mixture. The native fluorinase enzyme from *S. cattleya* was known to co-purify with the substrate, SAM **20**, bound to the active site.[57]

Upon incubation with [^{18}F]fluoride, the low levels of residual SAM **20** would be converted, under the action of the enzyme, to [^{18}F]FDA [^{18}F]-**22**. During previous radiolabelling experiments involving the fluorinase, with either ClDEA **174** or ClDEA-TEG-RGD **204**, the use of high substrate concentrations (0.3 mM) meant that these substrates effectively out-competed any residual SAM **20**. This may be why significant conversion to [^{18}F]FDA [^{18}F]-**22** was not observed in these experiments.

An analysis of samples from radiolabelling of both ClDEA-PEG-$(RGD)_2$ **224** and ClDEA-PEG-$(RGD)_4$ **225** under gradient conditions revealed the presence of [^{18}F]FDA [^{18}F]-**22** in both cases. This observation provided further evidence that both ClDEA-PEG-$(RGD)_2$ **224** and ClDEA-PEG-$(RGD)_4$ **225** were poorly soluble and were not present at sufficient concentration to reduce the background reaction with the residual SAM **20** in the fluorinase active site.

The study showed that ClDEA-PEG-$(RGD)_2$ **224** and ClDEA-PEG-$(RGD)_4$ **225** do undergo a fluorinase catalysed transhalogenation reaction to their corresponding [^{18}F]-fluorinated analogues, although radiochemical incorporations are low. Efforts to improve the incorporations for both substrates were unsuccessful, likely due to poor solubility of the multimeric substrates, rather than poor affinity for the fluorinase.

3.9. Conclusions

“Last step” radiolabelling using the fluorinase was extended from simple RGD constructs, to more complex multimeric RGD substrates, based on the discovery of a tolerance at the C-2 position of the substrate.

Fluorine-18 radiolabelling of such multimeric RGD peptides had been reported previously, but generally required either a prosthetic group strategy,[27–29] or required strong heating to form an aluminium [^{18}F]fluoride complex.[31,33,34] The fluorinase could offer a methodology for a “last step” radiolabelling procedure at room temperature, and under neutral pH conditions, provided that these complex substrates are tolerated by the enzyme.

Two substrates were designed, bearing two and four cyclic RGD motifs respectively. The design aimed to capitalise on the increased binding affinity that is often observed for such multimers. The chlorinated and fluorinated analogues of the dimeric and

tetrameric alkyne were synthesised using a Sonogashira coupling strategy as the key step. Using such a reaction, the nucleobase required for the fluorinase transhalogenation was coupled to the linker bearing multiple alkyne motifs, while preserving the alkyne at the C-2 position of the base. The alkyne was proposed to be critical in maintaining the correct geometry of the linker, preventing the peptide from interfering with the transhalogenation reaction.

Following the synthesis of these multimeric alkynes, the constructs were coupled to c(RGDfK[N_3]) **199** using a copper-catalysed CuAAC reaction. After purification, the reaction afforded access to dimeric and tetrameric chlorinated substrates for the fluorinase catalysed transhalogenation. The fluorinated analogues were also successfully synthesised. The new multimeric assemblies, ClDEA-PEG-$(RGD)_2$ **224** and ClDEA-PEG-$(RGD)_4$ **225**, were assessed as substrates for the fluorinase and found to undergo enzyme-catalysed transhalogenation.

The dimeric and tetrameric fluorinated products **248** and **249** were assessed for their affinity to immobilised $\alpha_V\beta_3$ integrin. The multimers showed lower IC_{50} values compared to their monomeric analogues, due to an increased effective molarity, rather than true multivalent binding.

Transfer of the transhalogenation reactions to the PET environment proved challenging. Initial radiolabelling experiments with [^{18}F]fluoride showed little conversion to radiolabelled products. The poor incorporations result led us to optimise the radiolabelling conditions with ClDA **23**. Optimisation revealed that both high substrate and high enzyme concentration were required for efficient reaction.

ClDEA-PEG-$(RGD)_2$ **224** and ClDEA-PEG-$(RGD)_4$ **225** were not sufficiently soluble under the aqueous reaction conditions, resulting in radiochemical incorporations of between 5–10%. Attempts to improve the solubility of the constructs were investigated, but found to have a negligible effect on the observed incorporations.

Extension of this system to larger peptides or proteins will depend on the extent to which such substrates dissolve in aqueous solvent while maintaining stability. Evolved proteins, such as antibodies and enzymes, should have higher water solubility. If highly soluble substrates can be developed, this methodology presents a potentially attractive approach for “last step” radiolabelling of peptides and proteins for PET.

3.10. References

1. S. Richter and F. Wuest, *Molecules*, 2014, **19**, 20536–20556.

2. P. W. Miller, N. J. Long, R. Vilar, and A. D. Gee, *Angew. Chem. Int. Ed.*, 2008, **47**, 8998–9033.

3. R. Ting, M. J. Adam, T. J. Ruth, and D. M. Perrin, *J. Am. Chem. Soc.*, 2005, **127**, 13094–13095.

4. C. A. D'Souza, W. J. McBride, R. M. Sharkey, L. J. Todaro, and D. M. Goldenberg, *Bioconjug. Chem.*, 2011, **22**, 1793–1803.

5. R. Schirrmacher, G. Bradtmöller, E. Schirrmacher, O. Thews, J. Tillmanns, T. Siessmeier, H. G. Buchholz, P. Bartenstein, B. Wängler, C. M. Niemeyer, and K. Jurkschat, *Angew. Chem. Int. Ed.*, 2006, **45**, 6047–6050.

6. J. Oxboel, M. Brandt-Larsen, C. Schjoeth-Eskesen, R. Myschetzky, H. H. El-Ali, J. Madsen, and A. Kjaer, *Nucl. Med. Biol.*, 2014, **41**, 259–267.

7. A. Mutlib, H. Chen, J. Shockcor, R. Espina, S. Chen, K. Cao, A. Du, G. Nemeth, S. Prakash, and L.-S. Gan, *Chem. Res. Toxicol.*, 2000, **13**, 775–784.

8. S. Liu, *Bioconj. Chem.*, 2009, **20**, 2199–2213.

9. S. Liu, *Bioconjug. Chem.*, 2015, DOI: 10.1021/acs.bioconjchem.5b00327.

10. M. Mammen, S.-K. Choi, and G. M. Whitesides, *Angew. Chem. Int. Ed.*, 1998, **37**, 2754–2794.

11. C. Fasting, C. A. Schalley, M. Weber, O. Seitz, S. Hecht, B. Koksch, J. Dernedde, C. Graf, E. W. Knapp, and R. Haag, *Angew. Chem. Int. Ed.*, 2012, **51**, 10472–10498.

12. A. Schön and E. Freire, *Biochemistry*, 1989, **28**, 5019–5024.

13. C. A. Hunter and H. L. Anderson, *Angew. Chem. Int. Ed.*, 2009, **48**, 7488–7499.

14. S. Liu, *Mol. Pharm.*, 2006, **3**, 472–487.

15. A. Goel, J. Baranowska-Kortylewicz, S. H. Hinrichs, J. Wisecarver, G. Pavlinkova, S. Augustine, D. Colcher, B. J. Booth, and S. K. Batra, *J. Nucl. Med.*, 2001, **42**, 1519–1527.

16. S. Liu, D. S. Edwards, M. C. Ziegler, A. R. Harris, S. J. Hemingway, and J. A. Barrett, *Bioconjug. Chem.*, 2001, **12**, 624–629.

17. C. J. Avraamides, B. Garmy-Susini, and J. A. Varner, *Nat. Rev. Cancer*, 2008, **8**, 604–617.

18. R. Haubner, H. J. Wester, U. Reuning, R. Senekowitsch-Schmidtke, B. Diefenbach, H. Kessler, G. Stöcklin, and M. Schwaiger, *J. Nucl. Med.*, 1999, **40**, 1061–1071.

19. R. Haubner, R. Gratias, B. Diefenbach, and S. Goodman, *J. Am. Chem. Soc.*, 1996, **118**, 7461–7472.

20. M. Janssen, W. J. G. Oyen, L. F. A. G. Massuger, C. Frielink, I. Dijkgraaf, D. S. Edwards, M. Radjopadhye, F. H. M. Corstens, and O. C. Boerman, *Cancer Biother. Radiopharm.*, 2002, **17**, 641–646.

21. H. Kubas, M. Schäfer, U. Bauder-Wüst, M. Eder, D. Oltmanns, U. Haberkorn, W. Mier, and M. Eisenhut, *Nucl. Med. Biol.*, 2010, **37**, 885–891.

22. L. Sancey, E. Garanger, S. Foillard, G. Schoehn, A. Hurbin, C. Albiges-Rizo, D. Boturyn, C. Souchier, A. Grichine, P. Dumy, and J.-L. Coll, *Mol. Ther.*, 2009, **17**, 837–843.

23. L. Wang, J. Shi, Y. S. Kim, S. Zhai, B. Jia, H. Zhao, Z. Liu, F. Wang, X. Chen, and S. Liu, *Mol. Pharm.*, 2009, **6**, 231–245.

24. J. Shi, L. Wang, Y. S. Kim, S. Zhai, Z. Liu, X. Chen, and S. Liu, *J. Med. Chem.*, 2008, **51**, 7980–7990.

25. Y. Yang, S. Ji, and S. Liu, *Bioconjug. Chem.*, 2014, **25**, 1720–1729.

26. Y. Zheng, S. Ji, E. Tomaselli, Y. Yang, and S. Liu, *Nucl. Med. Biol.*, 2015, **42**, 137–145.

27. G. Thumshirn, U. Hersel, S. L. Goodman, and H. Kessler, *Chem. Eur. J.*, 2003, **9**, 2717–2725.

28. T. Poethko, M. Schottelius, G. Thumshirn, U. Hersel, M. Herz, G. Henriksen, H. Kessler, M. Schwaiger, and H.-J. Wester, *J. Nucl. Med.*, 2004, **45**, 892–902.

29. C. Hultsch, M. Berndt, R. Bergmann, and F. Wuest, *Appl. Radiat. Isot.*, 2007, **65**, 818–826.

30. S. Liu, Z. Liu, K. Chen, Y. Yan, P. Watzlowik, H. J. Wester, F. T. Chin, and X. Chen, *Mol. Imaging Biol.*, 2010, **12**, 530–538.

31. W. Wan, N. Guo, D. Pan, C. Yu, Y. Weng, S. Luo, H. Ding, Y. Xu, L. Wang, L. Lang, Q. Xie, M. Yang, and X. Chen, *J. Nucl. Med.*, 2013, **54**, 691–698.

32. W. Cheng, Z. Wu, S. Liang, H. Fu, S. Wu, Y. Tang, Z. Ye, and H. Wang, *PLoS One*, 2014, **9**, e100521.

33. J. Guo, N. Guo, L. Lang, D. O. Kiesewetter, Q. Xie, Q. Li, H. S. Eden, G. Niu, and X. Chen, *J. Nucl. Med.*, 2014, **55**, 154–160.

34. C. Yu, D. Pan, B. Mi, Y. Xu, L. Lang, G. Niu, M. Yang, W. Wan, and X. Chen, *Eur. J. Nucl. Med. Mol. Imaging*, 2015, DOI: 10.1007/s00259–015–3118–2.

35. W. J. McBride, C. A. D'Souza, H. Karacay, R. M. Sharkey, and D. M. Goldenberg, *Bioconjug. Chem.*, 2012, **23**, 538–547.

36. J. A. F. Joosten, N. T. H. Tholen, F. Ait El Maate, A. J. Brouwer, G. W. van Esse, D. T. S. Rijkers, R. M. J. Liskamp, and R. J. Pieters, *European J. Org. Chem.*, 2005, 3182–3185.

37. C. Wängler, S. Maschauer, O. Prante, M. Schäfer, R. Schirrmacher, P. Bartenstein, M. Eisenhut, and B. Wängler, *ChemBioChem*, 2010, **11**, 2168–2181.

38. I. Dijkgraaf, A. Y. Rijnders, A. Soede, A. C. Dechesne, G. W. van Esse, A. J. Brouwer, F. H. M. Corstens, O. C. Boerman, D. T. S. Rijkers, and R. M. J. Liskamp, *Org. Biomol. Chem.*, 2007, **5**, 935–944.

39. J. Paleček, G. Dräger, and A. Kirschning, *Synthesis*, 2011, 653–661.

40. H. Li, H. Zhou, S. Krieger, J. J. Parry, J. J. Whittenberg, A. V Desai, B. E. Rogers, P. J. a Kenis, and D. E. Reichert, *Bioconjug. Chem.*, 2014, **25**, 761–772.

41. D. B. Dess and J. C. Martin, *J. Org. Chem.*, 1983, **48**, 4155–4156.

42. H. Staudinger and J. Meyer, *Helv. Chim. Acta*, 1919, **2**, 635–646.

43. A. F. Abdel-Magid, K. G. Carson, B. D. Harris, C. A. Maryanoff, and R. D. Shah, *J. Org. Chem.*, 1996, **61**, 3849–3862.

44. M. J. Robins, F. Hansske, S. F. Wnuk, and T. Kanai, *Can. J. Chem.*, 1991, **69**, 1468–1474.

45. V. Iaroshenko, D. Sevenard, A. Kotljarov, D. Volochnyuk, A. Tolmachev, and V. Sosnovskikh, *Synthesis*, 2009, **2009**, 731–740.

46. K. Sonogashira, Y. Tohda, and N. Hagihara, *Tetrahedron Lett.*, 1975, **16**, 4467–4470.

47. R. Chinchilla and C. Nájera, *Chem. Soc. Rev.*, 2011, **40**, 5084–5121.

48. M. Schilz and H. Plenio, *J. Org. Chem.*, 2012, **77**, 2798–2807.

49. H. Deng, S. L. Cobb, A. D. Gee, A. Lockhart, L. Martarello, R. P. McGlinchey, D. O'Hagan, and M. Onega, *Chem. Commun.*, 2006, 652–654.

50. M. Winkler, J. Domarkas, L. F. Schweiger, and D. O'Hagan, *Angew. Chem. Int. Ed.*, 2008, **47**, 10141–10143.

51. X.-G. Li, J. Domarkas, and D. O'Hagan, *Chem. Commun.*, 2010, **46**, 7819–7821.

52. M. Onega, J. Domarkas, H. Deng, L. F. Schweiger, T. A. D. Smith, A. E. Welch, C. Plisson, A. D. Gee, and D. O'Hagan, *Chem. Commun.*, 2010, **46**, 139–141.

53. S. Dall'Angelo, N. Bandaranayaka, A. D. Windhorst, D. J. Vugts, D. van der Born, M. Onega, L. F. Schweiger, M. Zanda, and D. O'Hagan, *Nucl. Med. Biol.*, 2013, **40**, 464–470.

54. D. Ory, J. Van den Brande, T. de Groot, K. Serdons, M. Bex, L. Declercq, F. Cleeren, M. Ooms, K. Van Laere, A. Verbruggen, and G. Bormans, *J. Pharm. Biomed. Anal.*, 2015, **111**, 209–214.

55. D. Farthing, L. Xi, L. Gehr, D. Sica, T. Larus, and H. T. Karnes, *Biomarkers*, 2006, **11**, 449–459.

56. X. Zhu, D. A. Robinson, A. R. McEwan, D. O'Hagan, and J. H. Naismith, *J. Am. Chem. Soc.*, 2007, **129**, 14597–14604.

57. C. Dong, F. Huang, H. Deng, C. Schaffrath, J. B. Spencer, D. O'Hagan, and J. H. Naismith, *Nature*, 2004, **427**, 561–565.

4. A difluoromethyl-bearing nucleoside substrate for the fluorinase

4.1. The difluoromethyl group

4.1.1. Applications of the difluoromethyl group

Compared to the trifluoromethyl ($R–CF_3$) group, the difluoromethyl group ($R–CF_2H$) and fluoromethyl group ($R–CH_2F$) remain comparatively unexplored in terms of their application to bioactive molecules.[1] The unique physical properties of the difluoromethyl group have led to renewed interest in the development of synthetic methods for the introduction of this motif into organic molecules. Fluorinase enzymatic synthesis results in monofluorinated natural products,[2] but no such products containing a CF_2 group have been described to date. The enzymatic synthesis of such groups remains unexplored. It became of interest to explore the fluorinase for capacity to prepare a difluoromethyl group.

The difluoromethyl group is found in a range of commercially important bioactive molecules. Such molecules include the anaesthetic isoflurane **251**,[3] anti-trypanosomal agent eflornithine **252**,[4] and penoxsulam **253**,[5] a broad leaf herbicide, illustrated below in **Figure 1**.

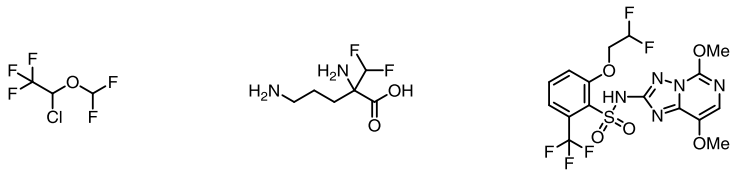

Figure 1. Structures of some commercially important molecules containing the difluoromethyl group.

The difluoromethyl group is anisotropic and possesses a hydrogen atom bonded to carbon bearing two strongly electron withdrawing fluorine substituents. As a consequence, the hydrogen atom is available as a hydrogen bond donor, although as a more lipophilic hydrogen bond donor than the more common hydrophilic O–H and N–H groups.[6]

For difluoromethyl ethers in particular, the anisotropy and inherent dipole of the difluoromethyl group allows such ethers to adopt two conformers with differing lipophilicity.[7] This property makes them attractive for use in drug discovery as molecules bearing such groups can adjust their conformation to enhance electronic interactions with a biological target.

These unique properties of the difluoromethyl group have led to its development as a bio-isostere[8] of alcohols,[9] thiols[10] and hydroxamic acids.[11] HCV NS3 protease, a drug target in the hepatitis C virus, cleaves its target at the *C*-terminus of a cysteine residue. While investigating product analogues to identify potential protease inhibitors, replacement of the cysteine thiol of a model peptide product **254**, with a difluoromethyl group gave inhibitor **255**, as shown in **Figure 2 A.** The difluoromethyl analogue **255** showed a K_i 20 times lower than its more simple methyl analogue.

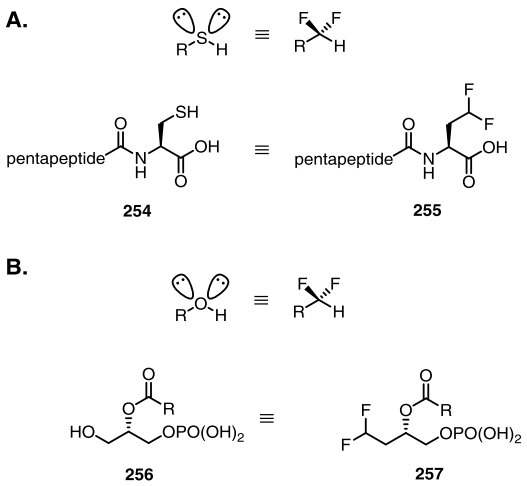

Figure 2. The difluoromethyl group acts as an effective bio-isostere of **A.** thiols and **B.** alcohols.

Similarly, replacement of the hydroxyl group in lyophosphatidic acid **256** analogues, a nuclear hormone receptor agonist, with a difluoromethyl group afforded analogue **257**, as shown in **Figure 2 B**. The novel analogue showed improved selectivity for its nuclear receptor, while also avoiding acyl migration, a problem with more conventional analogues which conserve the hydroxyl group.[10]

In both cases, the fluorine atoms were found to effectively mimic the two lone pairs present on the oxygen or sulfur atom. In addition, the difluoromethyl group proved a close match for the volume and electrostatic potential of the thiol in the hepatitis C protease inhibitor. The electropositive hydrogen atom was found to be able to mimic the proton of the thiol, and form a hydrogen bond-type interaction with the carbonyl of a lysine residue in the active site of its target.

4.1.2. Synthesis of the difluoromethyl group

The role played by the difluoromethyl group in bioactive molecules has led to renewed interest in synthetic methods for its introduction into organic molecules.[1] Traditional routes to access such motifs involve reaction of an aldehyde with sulfur tetrafluoride **258**, as shown in **Scheme 1**.[12] Sulfur tetrafluoride **258** is, however, a gas at room temperature (b.p. –38 °C), and safe handling concerns makes conducting such reactions a challenge.

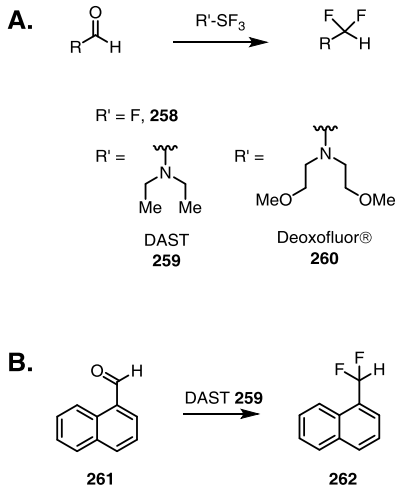

Scheme 1. **A.** Conversion of aldehydes to difluoromethyl groups using sulfur tetrafluoride **158** or reagents derived from sulfur tetrafluoride. **B.** Fluorination of 1-naphthaldehyde **261** with DAST **259** to give difluoromethylated product **262**.

In order to overcome the challenge of the reactive gas, a range of amino-sulfur trifluoride derivatives that are liquid at room temperature were developed. Such reagents include (diethylamino)sulfur trifluoride **259** (DAST)[13,14] and bis(2-methoxyethyl)aminosulfur trifluoride **260** (Deoxofluor®),[15] a more thermally stable derivative thereof. These reagents show similar reactivity to sulfur tetrafluoride, and are also capable of transforming aldehydes (such as 1-naphthaldehyde **261**) to difluoromethyl products, as shown in **Scheme 1**. α,α-Difluoroamines have also been reported to be capable of converting aldehydes to difluoromethyl groups *via* a similar transformation.[16]

In addition to the direct difluorination of carbonyl compounds, a number of methods have been developed for direct transfer of a difluoromethyl group to an appropriate substrate.[1,17] Early versions of such transformations employed nucleophilic "RCF_2^-" species, such as difluoromethyl sulfones (**265**),[18,19] sulfoxides[20] or phosphonates as a source of the nucleophilic synthon upon treatment with a base.[21] The resultant anion is

stabilised by the presence of the neighbouring electron withdrawing group. The stabilised anion reacts with a variety of electrophiles, including carbonyls, alkyl halides and cyclic sulfates to generate R-CF_2-S or R-CF_2-P species. Reductive cleavage of the CF_2-S or CF_2-P then gives a difluoromethyl group, as illustrated in **Scheme 2 A**.[22]

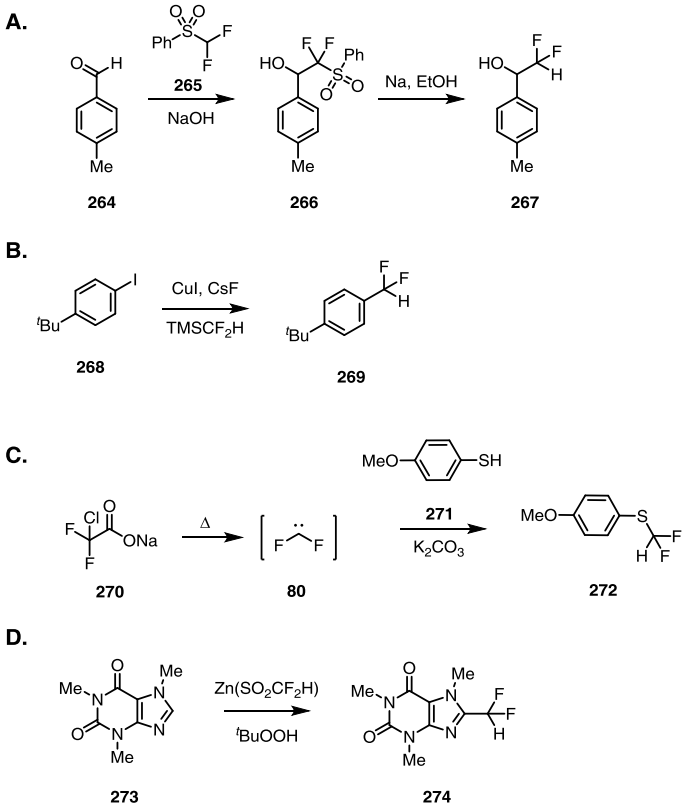

Scheme 2. **A.** Difluoromethylation using a deprotonated sulfone to generate a difluoromethyl nucleophile.[18] **B.** Difluoromethylation using a copper-mediated transfer of a CF_2H group.[23] **C.** Difluoromethylation of a thiol by difluorocarbene.[24] **D.** Difluoromethylation at unactivated C–H bonds.[25]

Trimethyltrifluoromethylsilane ($TMSCF_3$ or the Ruppert-Prakash reagent) can also be used to transfer a difluoromethyl group to acyl silanes and aldimines.[26,27] Copper-mediated nucleophilic transfer of the difluoromethyl group to an aryl iodide has also been reported, using either $TMSCF_2H$[23] (**Scheme 2 B**) or cadmium difluoromethylphosphonate[28] as the difluoromethyl source.

A more common approach for the introduction of the difluoromethyl group involves the reaction of a nucleophilic C, S, N, or O species with difluorocarbene **80**.[29] A number of reagents can be used to generate difluorocarbene **80** *in situ*, most commonly halodifluoromethanes,[1,30–33] however, these are known ozone depleting agents and more environmentally benign sources are highly desired. Such sources include sodium chlorodifluoroacetate **270** (**Scheme 2 C**),[24] diethyl bromodifluoromethyl phosphonate,[34]

and a number of metal trifluoromethide salts.[29] Difluoromethyl triflate has also been utilised as an electrophile for reaction with phenols, giving aryl difluoromethyl ethers.[35]

A radical-based approach has also been used to introduce the difluoromethyl group to alkenes and alkynes. Difluorodibromomethane or difluorobromochloromethane have been employed as sources of difluoromethyl radicals with a radical initiator such as CuCl[36] or UV light.[37] A milder radical C–H activation approach to difluorination has recently been reported by Baran *et al.*,[25] where a combination of zinc bis(difluoromethylsulfinate) and ^{t}BuOOH allows difluoromethylation at electron poor sites of *N*-heterocycles (**273**), *S*-heterocycles and enones, as shown in **Scheme 2 D**.

4.2. Aims

The recent resurgence in interest in the synthesis and application of difluoromethyl groups led us to explore a possible synthesis of the motif with the fluorinase enzyme. The fluorinase has been well characterised[2] in its ability to activate fluoride ion as a nucleophile and catalyse the formation of a C–F bond, as shown in **Scheme 3 A**. The synthesis of a difluoromethyl group by the enzyme would require the fluorinase to catalyse the reaction of fluoride with a pre-fluorinated SAM analogue **275** (FSAM), as shown in **Scheme 3 B**. Such a reaction could offer a route for the enzymatic synthesis of difluoromethylated product **276** (F_2DA).

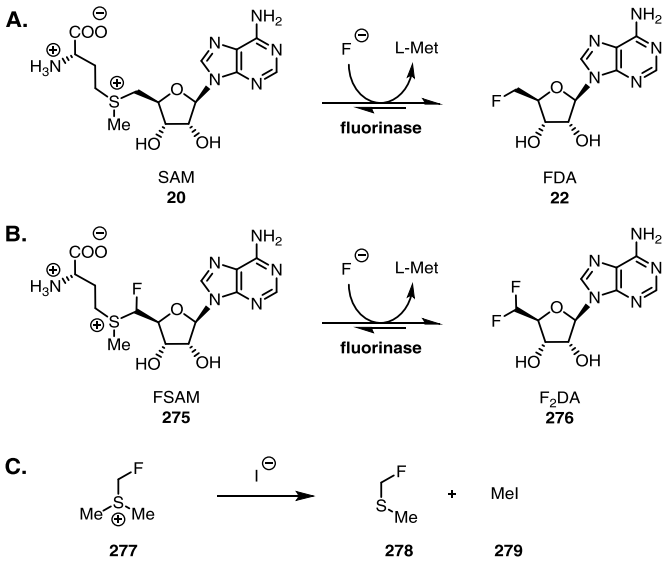

Scheme 3. **A.** Synthesis of a C–F bond by the fluorinase enzyme. **B.** Proposed enzymatic synthesis of a difluoromethyl group. **C.** α-Fluorosulfonium species reacting with iodide to generate methyl iodide.

There are no reports of any FSAM analogues, such as **275** above, bearing substituents at the 5'-position. The simplest α-fluorosulfonium species, (fluoromethyl)dimethylsulfonium (**277**) tetrafluoroborate, has been reported,[38] where its reaction at a methyl group with iodide as a nucleophile was explored, as shown in **Scheme 3 C**. In addition, the use of diaryl fluoromethylsulfonium salts as fluoroalkylating agents has also been explored. The triflate and tetrafluoroborate salts of the motif were found to be air and moisture stable, and capable of transferring a fluoromethyl group to N, O and S nucleophiles.[39] The literature reports of the α-fluorosulfonium motif suggested that FSAM **275** may be stable, however it would still be difficult to prepare this highly functionalised substrate synthetically. Without access to FSAM **275**, assessment of the proposed α-fluorosulfonium species as fluorinase substrate would be difficult.

The native reaction catalysed by the fluorinase enzyme is reversible (**Scheme 4 A**).[40] With this in mind, and the anticipated difficulty in preparing FSAM **275** synthetically, we decided to explore the proposed transformation in the reverse direction. Such a reaction would involve enzyme catalysed nucleophilic attack of L-Met at C-5' of F_2DA **276**, to generate FSAM **275**, with concomitant release of fluoride ion, as shown in **Scheme 4 B**. The reverse reaction would therefore provide a simple tool to assess the viability of the enzymatic synthesis of a difluoromethyl group.

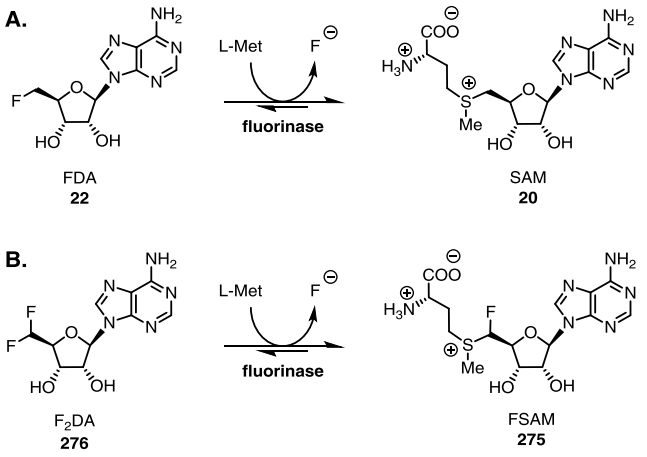

Scheme 4. **A.** Cleavage of the C–F bond of FDA **22** by the fluorinase enzyme. **B.** Proposed enzymatic transformation of F_2DA **276** to its corresponding FSAM analogue **275**.

In anticipation of exploring the reverse reaction of F_2DA **276** with the fluorinase, F_2DA **276** became a synthetic target. Investigation of F_2DA **276** as a substrate with the fluorinase would indicate whether the proposed synthesis of a difluoromethyl group by an enzymatic route was possible.

4.3. Synthesis of 5',5'-difluoro-5'-deoxyadensine 276 (F_2DA)

The synthesis of 5',5'-difluoro-5'-deoxyadensine **276** has been previously reported by Jarvi *et al.*[41,42] Fluorination of *N*,*N*-dibenzoyl-2',3'-*O*-isopropylidneadenosine-5'-aldehyde **283** with diethylaminosulfur trifluoride **259** (DAST) was the key fluorination step, as illustrated in **Scheme 5**.

The synthesis reported by Jarvi *et al.*[41,42] involved oxidation of protected adenosine **280** to the corresponding aldehyde, and trapping the resultant aldehyde as aminal **281**, using conditions described by Moffat *et al.* [43] The trapping of the aldehyde as an aminal allowed separation of the otherwise unstable aldehyde from the dicyclohexylurea oxidation by-product. Further protection, followed by hydrolysis of aminal **282** generated the aldehyde **283**, the substrate for the key difluorination step.

Aldehyde **283** was subjected to difluorination with DAST and generated **284** in 18% yield. Deprotection of the dibenzoylimide and acetonide protecting groups furnished F_2DA **276**. Despite the low yield for the fluorination reaction, the synthetic route to F_2DA **276** described by Jarvi *et al.*[41,42] was explored.

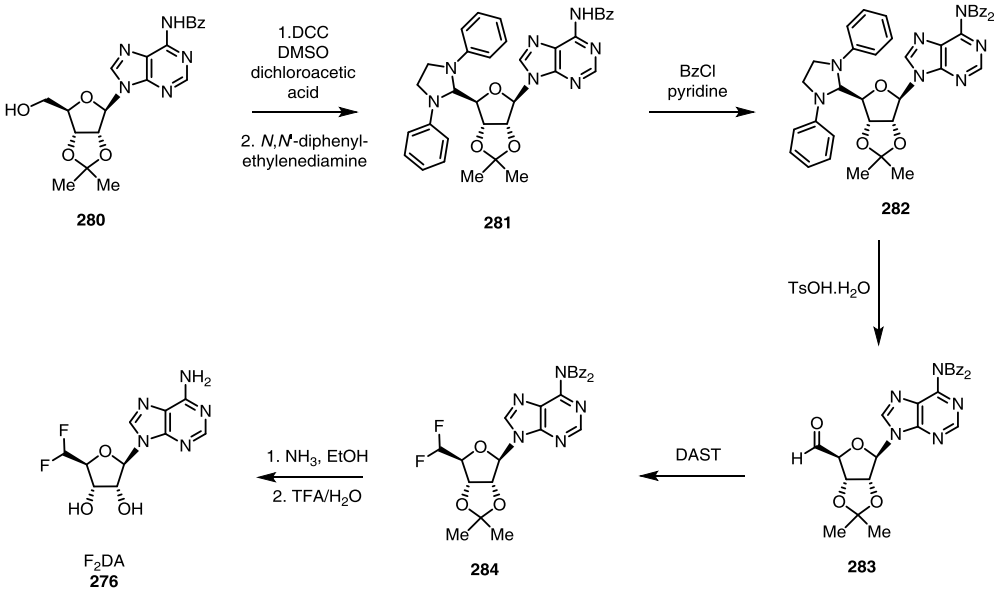

Scheme 5. Reagents employed in the synthesis of F_2DA **276** reported by Jarvi *et al.*[41,42] with difluorination by DAST as they key step.

4.3.1. Synthesis of an adenosine-5'-aldehyde

Adenosine **188** was protected as its acetonide with 2,2-dimethoxypropane in acetone, catalysed by perchloric acid, as shown in **Scheme 6**. Using a modified procedure

described by Jawalekar *et al.*,[44] the free hydroxyl group of **285** was *in situ* protected as a TMS ether, before monobenzoylation of *N*-6 with benzoyl chloride gave **280**.

Moffatt oxidation[43] of alcohol **280**, using dicyclohexylcarbodiimide (DCC) and dichloroacetic acid in DMSO, followed by precipitation of the *N*,*N*'-dicyclohexylurea by-product by addition of oxalic acid, produced a solution of aldehyde hydrate **286** in methanol. *N*,*N*'-Diphenylethylenediamine was added to this solution, upon which, crude aminal **282** precipitated. Recovery of the precipitate and further purification by chromatography afforded aminal **282** in 27% yield.

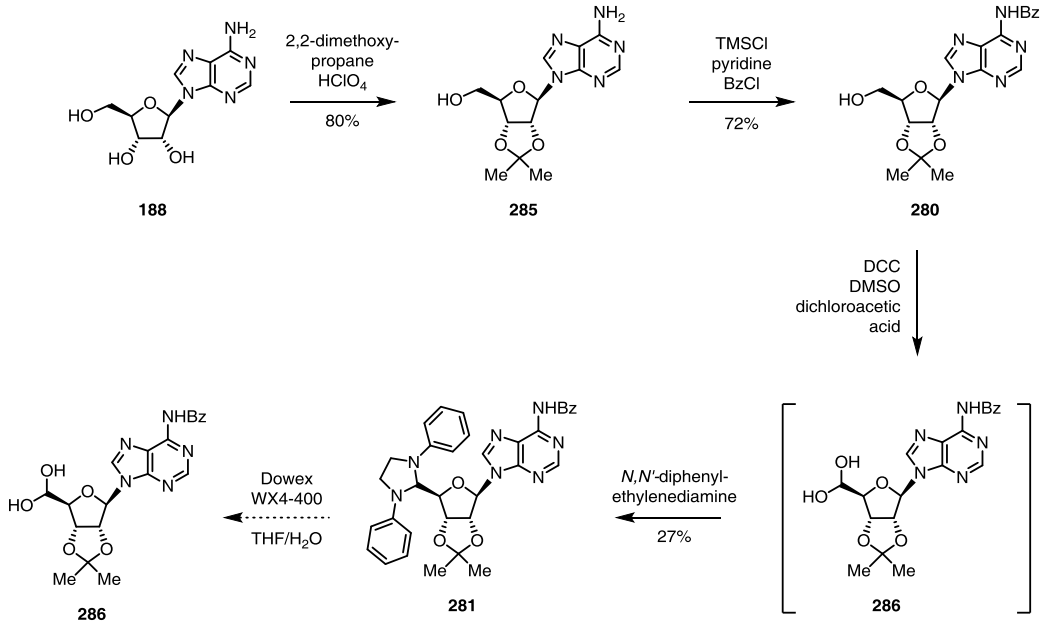

Scheme 6. Synthesis of aminal **282**, as a source of aldehyde hydrate **286**.

Unlike the procedure employed by Jarvi *et al.*,[41,42] where aminal **282** was further protected before its hydrolysis to the free aldehyde, Moffatt *et al.*[43] described the direct use of aminal **282** as a source of aldehyde hydrate **286** (and its aldehyde). In an effort to avoid an additional synthetic step, aminal **282** was subjected to acid hydrolysis using Dowex WX4-400 (an acidic resin) in aqueous THF. Trials of the reaction resulted in an inseparable mixture of products. Aldehyde hydrate **286** was identified as a component of this mixture, however, could not be separated from the other by-products.

As the yield of aminal **282** was low, and aldehyde hydrate **286** could not be isolated from the reaction mixture as a single species, alternative oxidations to give adenosine-5'-aldehyde were explored. Oxidation of both acetonide **285** and its *N*-benzoylated analogue **280** were trialled under Swern conditions, using 2-iodoxybenzoic acid (IBX) in DMSO, or employing a combination of catalytic TEMPO

with one equivalent of bis(acetoxy)iodobenzene. None of these conditions, however, afforded the corresponding aldehyde in any appreciable conversion.

As the Moffatt oxidation had been successful in generating a species at the aldehydic oxidation level, optimisation of this oxidation reaction was further explored. Inspired by the development of 1-ethyl-3-(3-dimethylaminopropyl)carbodiimide (EDCI) as a water soluble replacement for DCC in peptide couplings,[45] the use of EDCI rather than DCC may improve purification of the aldehyde product. In addition, a dibenzoylated substrate was explored as a substrate for the oxidation, anticipating that the more lipophilic substrate may facilitate product separation from the water soluble urea oxidation by-products.

To this end, acetonide **285** was dibenzoylated in excellent yield with TMSCl, and an excess of benzoyl chloride, as shown in **Scheme 7**. Oxidation of **287** under Moffatt conditions, but substituting DCC for EDCI.HCl, resulted in complete conversion of **287** to a new product. Partitioning the reaction mixture between water and ethyl acetate, followed by concentration of the organic extracts *in vacuo*, gave a mixture of aldehyde **283** and its hydrate. Azeotropic removal of water by repeated co-evaporation with toluene furnished aldehyde **283** in quantitative yield, without further purification.

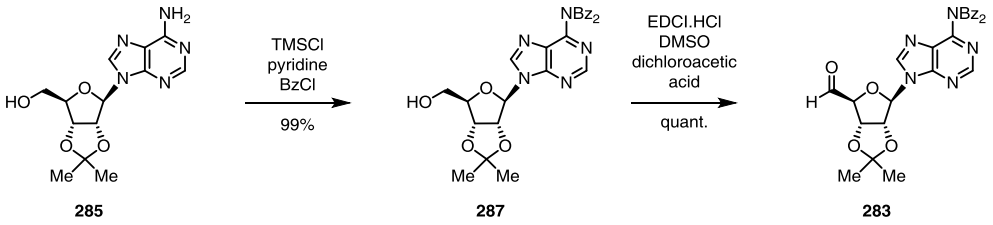

Scheme 7. Protection of acetonide **285** as imide **287**, followed by Moffatt oxidation with EDCI.HCl rather than DCC, gave aldehyde **283** in near quantitative yield over two steps.

This modified synthetic procedure gave access to protected aldehyde **283**, the required substrate for the fluorination reaction, in three steps rather than five, from adenosine. With aldehyde **283** in hand, the fluorination reaction was now explored.

4.3.2. Difluorination of adenosine-5'-aldehyde 283

The fluorination reaction was explored under the reported conditions,[41,42] by addition of DAST **259** to a solution of aldehyde **283** in DCM in room temperature in a Teflon reaction flask, as shown in **Scheme 8**. After six hours, the reaction was quenched by the addition of saturated sodium bicarbonate solution, and the crude reaction mixture analysed by $^{19}F\{^{1}H\}$NMR spectroscopy, as shown below in **Figure 3**.

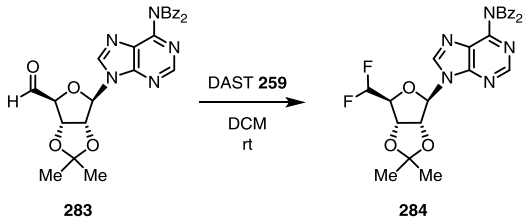

Scheme 8. Fluorination of aldehyde **283** using DAST in DCM as reported by Jarvi *et al.*[41,42]

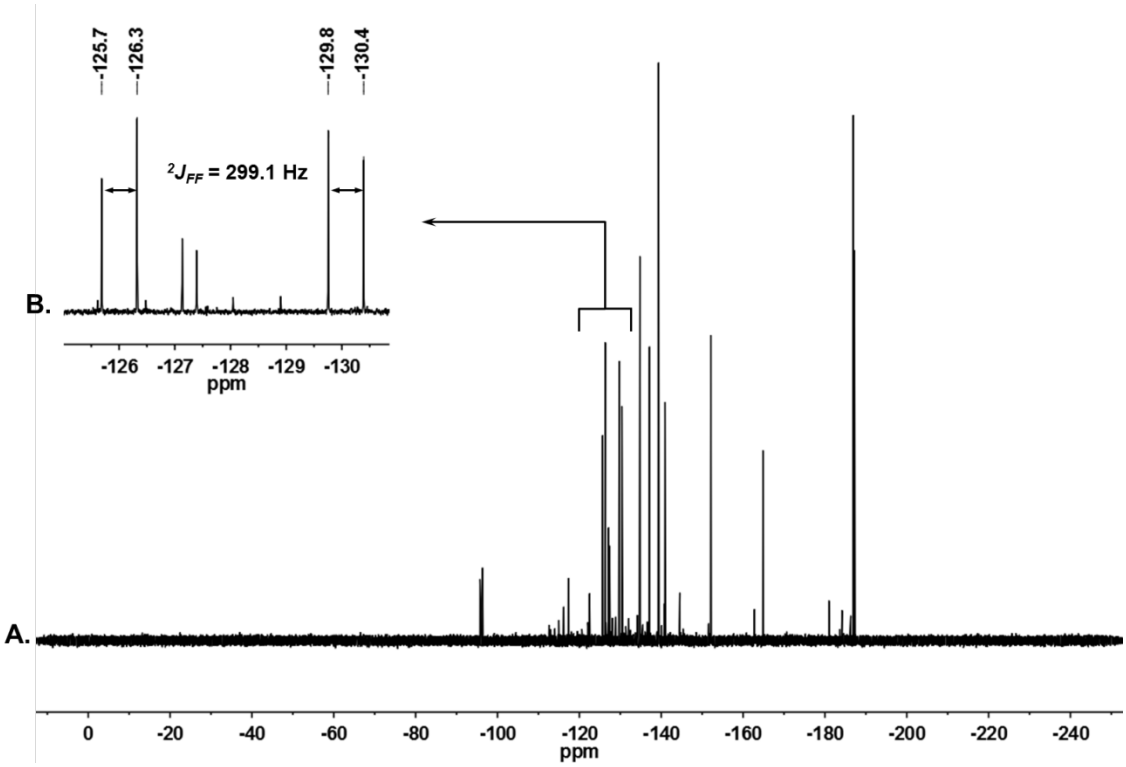

Figure 3. **A.** $^{19}F\{^1H\}$ NMR spectrum (470 MHz, $CDCl_3$) of the crude reaction mixture obtained after fluorination of aldehyde **283** with DAST, at room temperature in DCM. **B.** Expanded view of the region between −125 ppm and −131 ppm, revealing an AB system with a $^2J_{FF}$ coupling constant of 299.1 Hz.

The $^{19}F\{^1H\}$NMR spectrum of the product mixture, shown above in **Figure 3 A**, and revealed the presence of a number of fluorinated products. The chemical shifts reported for the two fluorine atoms of **284** are −65.8 ppm and −50.7 ppm,[42] or −54.8 ppm and −50.2 ppm,[41] with a $^2J_{FF}$ coupling of 299.1 Hz. Examination of this region of this spectrum did not reveal any such peaks in this region, suggesting that **284** was not present in the product mixture. However, all other difluoromethyl containing compounds reported by Jarvi *et al.*[42] have reported ^{19}F chemical shifts of between −125 ppm and −131 ppm, suggesting an error in their reporting of the ^{19}F chemical shifts for **284**. Fluorine chemical shifts for difluoromethyl groups usually appear in the −110 ppm to −145 ppm range.[46] Examination of the −110 ppm to −145 ppm region revealed an

AB spin system, as expected for **284**, with a coupling constant of 299.1 Hz, shown above in **Figure 3 B**.

The $^{19}F\{^{1}H\}$NMR spectrum (**Figure 3 A**) suggested the presence of **284** in the product mixture, but many other fluorinated products were also evident. Purification of the product proved challenging, requiring multiple rounds of chromatography, and ultimately affording only traces of **284**. As a consequence, optimisation of the fluorination of aldehyde **283** was further explored. Fluorination of **283** was carried out using a range of solvents, temperatures, and fluorination reagents, as summarised below in **Table 1**.

Table 1. Summary of fluorination conditions trialled to optimise production of **284**.

reagent	*temperature/°C*	*solvent*
DAST **259**	20	DCM
DAST **259**	−78	DCM
DAST **259**	−78	THF
DAST **259**	−78	neat
Deoxofluor® **260**	−78	THF

Product mixtures were analysed directly for the presence of **284** using $^{19}F\{^{1}H\}$NMR spectroscopy, after a sodium bicarbonate quench and extraction into ethyl acetate. The $^{19}F\{^{1}H\}$NMR spectra are shown below in **Figure 4**.

When the fluorination reaction was conducted using DAST **259** in DCM, reduction of the temperature from 20 °C to −78 °C led to a reduction in the number of fluorinated products observed in the mixture, as shown in **Figure 4 A** and **B** below. The peaks related to difluorinated product **284** (highlighted with an asterisk) were still present, though the appearance of multiple new peaks in this region suggested that a number of similar products were also being produced under these conditions. Changing the reaction solvent to THF had a significant effect on the product distribution. None of the desired product was formed, as shown in **Figure 4 C**. Conducting the reaction in neat DAST at −78 °C restored the production of **284** and reduced the formation of similar compounds (**Figure 4 D**), however, by-products were still observed, but **284** was not the major product.

Changing the fluorination reagent from DAST to Deoxofluor® (which is only available commercially as a 50% solution in THF), resulted in the formation of **284** as the major fluorinated product, as evident in the $^{19}F\{^{1}H\}$NMR spectrum of the product mixture shown in **Figure 4 E**.

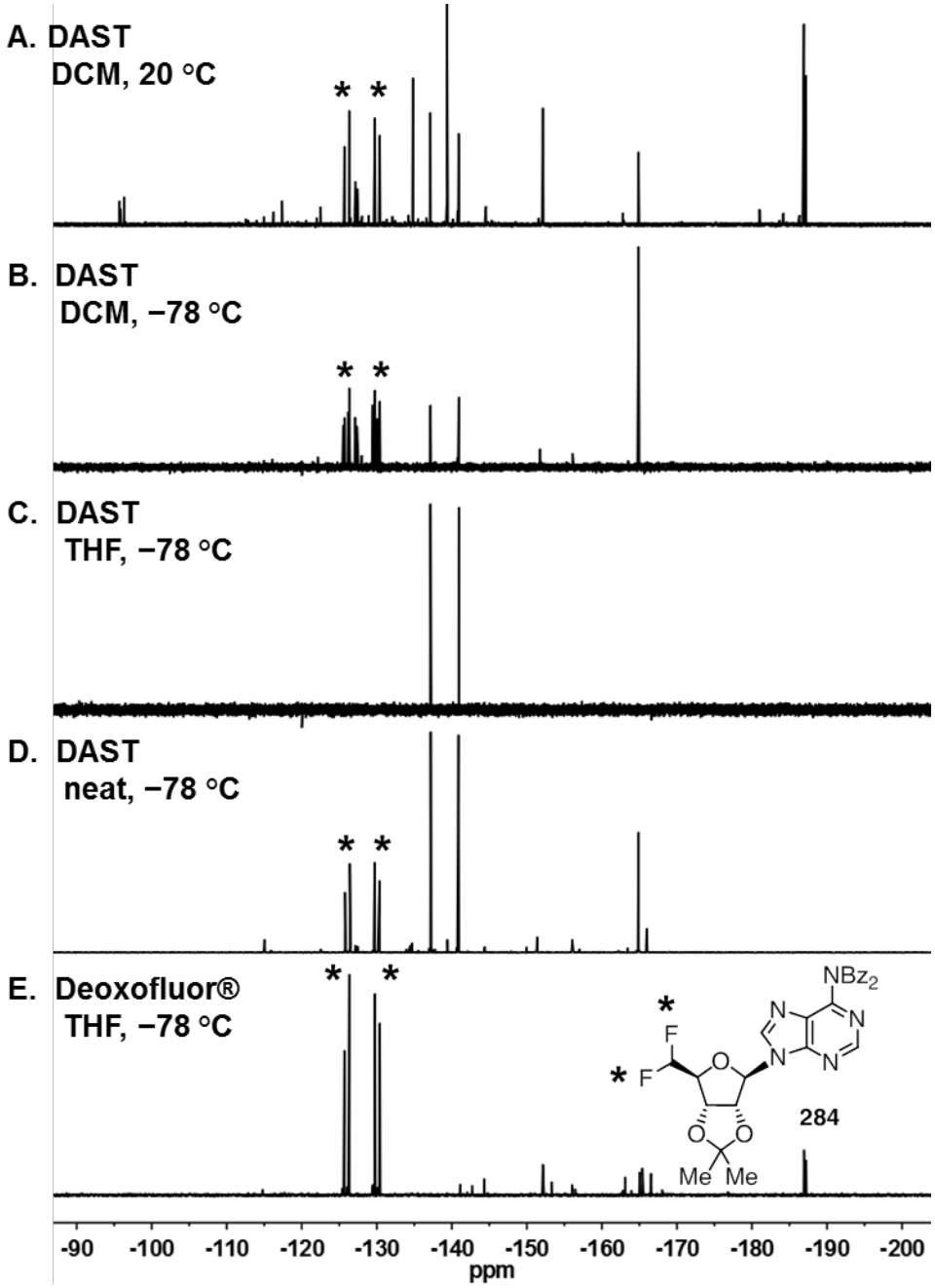

Figure 4. Partial $^{19}F\{^{1}H\}$ NMR spectra (470 MHz, $CDCl_3$) of the crude fluorination mixtures under a range of conditions. Peaks associated with the desired product, **284**, are highlighted with an asterisk.

The promising reaction using Deoxofluor® **260** in THF was repeated on larger scale, as illustrated in **Scheme 9**, and gave **284** in 10% yield after purification. The yield for the reaction is poor, however the simplicity with which aldehyde **283** is prepared meant that access to sufficient quantities (50 mg to 100 mg) of difluorinated product **284** was practical.

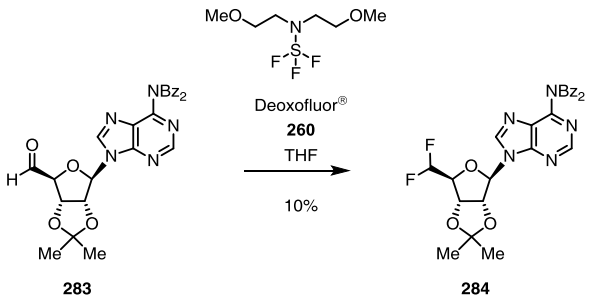

Scheme 9. Synthesis of **284** from aldehyde **283** using Deoxofluor® **260**.

As the original literature report[42] of **284** appeared to have incorrectly quoted the ^{19}F NMR chemical shifts, the data obtained from characterisation of **284** was closely examined. The coupling constants observed in the ^{19}F NMR spectrum illustrated below in **Figure 5**, $^{2}J_{FF}$ = 299.1 Hz, $^{2}J_{FH}$ = 55.1 Hz and $^{3}J_{FH}$ = 12.4 Hz and 10.1 Hz, match well with the reported values,[42] as do all the resonances in the ^{1}H NMR spectrum. The proton and fluorine spectroscopic data, combined with additional information obtained from HRMS and the ^{13}C NMR spectrum, suggested that the component isolated from the reaction was indeed **284**, and that the original reported ^{19}F chemical shifts for **284** were erroneously reported, or reported relative to a different standard.

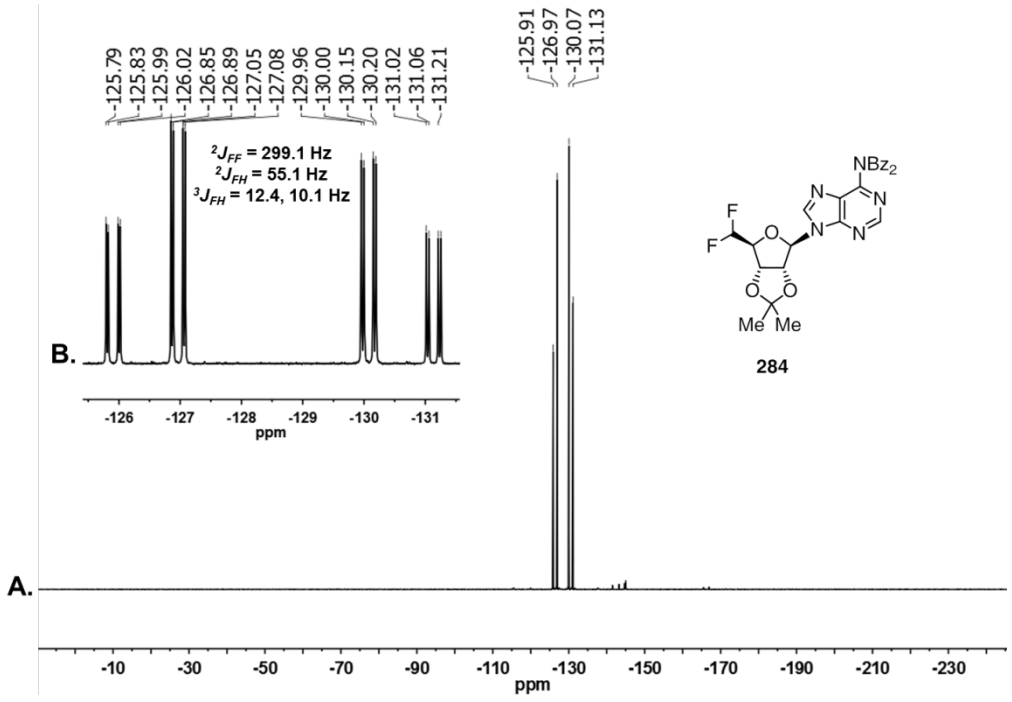

Figure 5. **A.** $^{19}F\{^{1}H\}$ NMR spectrum (282 MHz, $CDCl_3$) of **284** after purification. **B.** Partial ^{19}F NMR spectrum (282 MHz, $CDCl_3$) of the region between −125 ppm and −132 ppm, revealing two doublet of doublet of doublets (ddd), with coupling constants of $^{2}J_{FF}$ = 299.1 Hz, $^{2}J_{FH}$ = 55.1 Hz and $^{3}J_{FH}$ = 12.4 Hz and 10.1 Hz.

With protected F_2DA **284** in hand, attention turned to the two deprotection steps, as shown in **Scheme 10**. The benzoyl groups were cleaved by reaction of **284** with a freshly saturated solution of ammonia in methanol, in a sealed tube at 60 °C for 16 h. After isolation of **288**, the acetonide was cleaved using a mixture of TFA and water, to provide a sample of F_2DA **276** as a colourless powder, in good yield. All spectroscopic data for **288** and **276** agreed well with those reported in the literature.[41,42]

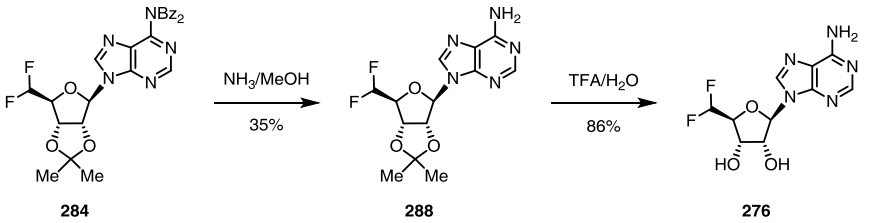

Scheme 10. Deprotection of the benzoyl groups and acetonide to give F_2DA **276**.

4.4. Investigation of F_2DA 276 binding to the fluorinase

Prior to exploring F_2DA **276** as a substrate for the fluorinase, the binding affinity of **276** to the enzyme was investigated. Using a similar approach to that described in **Chapter 2**, the binding of F_2DA **276** to the enzyme was investigated using isothermal titration calorimetry (ITC). Accordingly, a solution of F_2DA **276** in a phosphate buffer was titrated into a solution of the fluorinase in the same buffer. The binding curve obtained is illustrated below in **Figure 6 A**, and the data was fitted assuming a single binding site. The binding curve for FDA **22**, the natural substrate, with the fluorinase, described in **Chapter 2**, is shown in **Figure 6 B** for comparison.

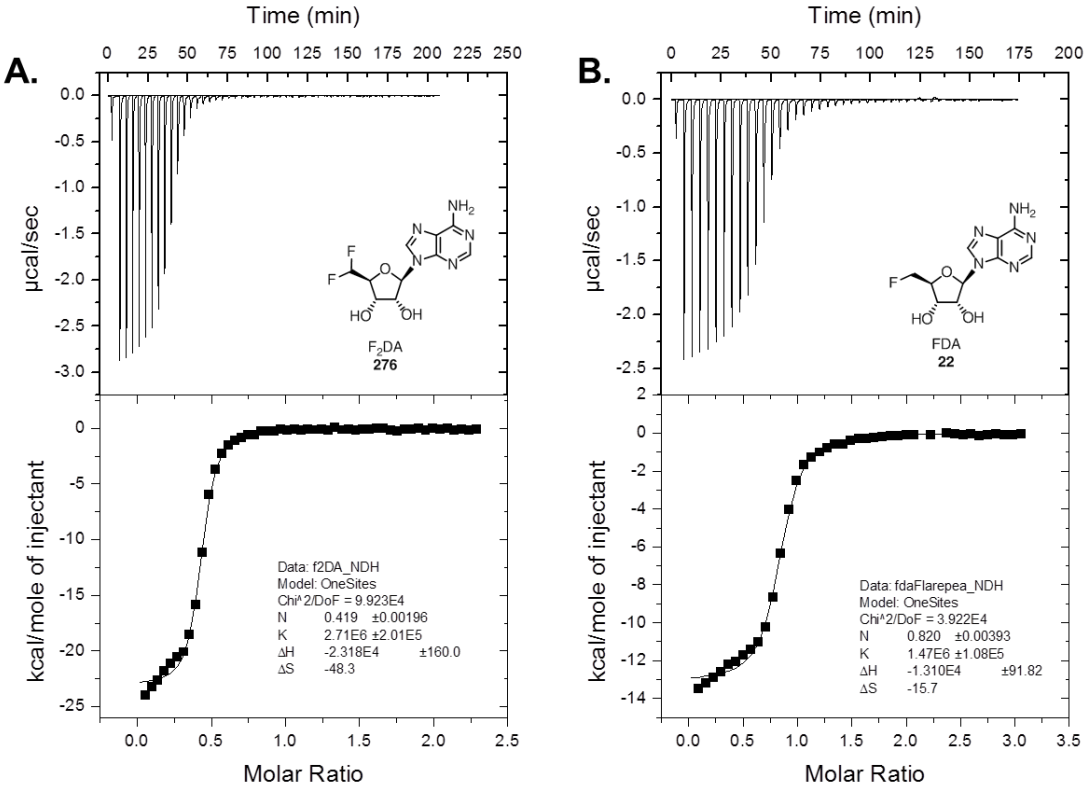

Figure 6. Isothermal titration calorimetric determination of the binding affinity of **A.** F_2DA **276** (0.72 mM) into the fluorinase (60.3 µM) and **B.** FDA **22** (1.03 mM) into the fluorinase (53.6 µM), as shown in **Chapter 2**.

The titration curve revealed that F_2DA **276** exhibited strong binding to the fluorinase. Fitting a one-site binding isotherm to the data allowed determination of the association constant (K_a) for this interaction, which was calculated as $27.1 \pm 2.01 \times 10^5$ M^{-1}. Comparison with FDA **22** revealed that F_2DA **276** has a higher affinity for the fluorinase by a factor of nearly two. The presence of the second fluorine substituent at C-5' appears to increase the affinity of the nucleoside for the enzyme.

The binding of F_2DA **276** and FDA **22** to the fluorinase show similar trends in contribution to the total free energy change for the binding event, as illustrated in **Figure 7**. Both compounds show favourable enthalpic contributions, but F_2DA **276** shows a greater exotherm upon binding. The greater enthapic contribution for F_2DA **276** is compensated for by a larger entropic penalty, which results in the similar nett free energy change to that observed for FDA **22**.

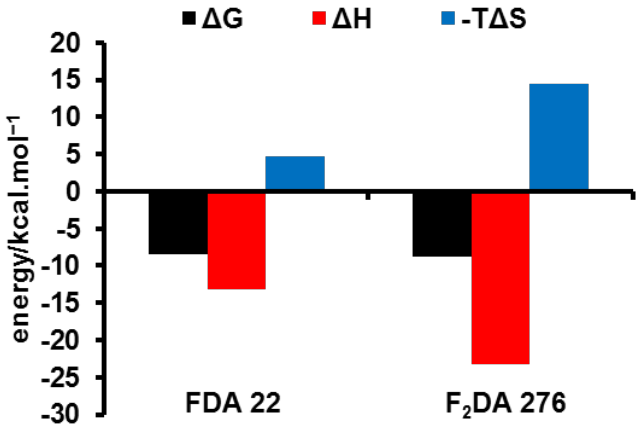

Figure 7. Comparison of the thermodynamic parameters of binding for F_2DA **276** and FDA **22**. ΔH was measured directly, while the –TΔS term was calculated using T = 298.15 K. ΔG was calculated as the sum of these two terms.

Fluorine is a poor hydrogen bond acceptor,[47] however it is possible that the introduction of the difluoromethyl group, which has known hydrogen bond donor capacity, leads to additional favourable interactions within the active site. If an additional residue in the active site were to engage in a non-classical hydrogen bond to the difluoromethyl group of F_2DA **276**, the interaction would result in increased enthalpic gain and reduce the entropy.

Further enthalpic gain likely arises from more lipophilic F_2DA **276** moving from the aqueous environment into the hydrophobic active site of the fluorinase.[48] Based on the retention time on a C_{18} reverse phase HPLC column run under identical conditions,[49] F_2DA **276** (t_R = 5.1 min) appears more lipophilic than FDA **22** (t_R = 3.8 min). The difluoromethyl group locating in the well described hydrophobic fluorine pocket may result in enthalpic gain when compared to the less lipophilic fluoromethyl group.

4.5. Evaluation of F_2DA 276 as a substrate

4.5.1. Evaluation of F_2DA 276 with L-Met 21 as a co-substrate

Confident that the candidate substrate, F_2DA **276**, binds to the enzyme, attention turned to investigating whether the fluorinase was able to catalyse substitution of one of the fluorine atoms of with L-methionine **21** (L-Met), as illustrated in **Scheme 11**.

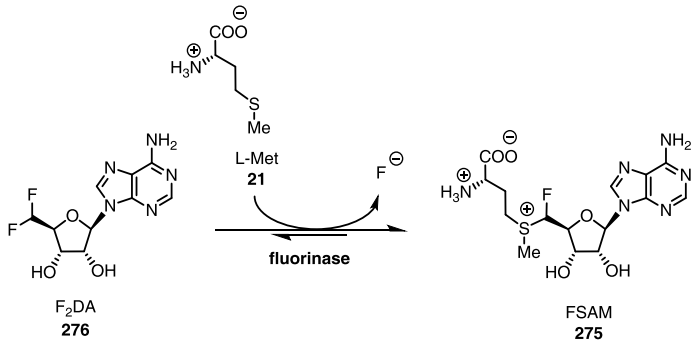

Scheme 11. Proposed substitution of F_2DA **276** with L-Met **21** to generate FSAM **275**, catalysed by the fluorinase.

To this end, F_2DA **276** (0.3 mM) and L-Met **21** (0.5 mM) were incubated with the fluorinase enzyme (2 mg.mL^{-1}) in phosphate buffer (20 mM) in a total volume of 500 µL. Reaction progress was monitored by removal of samples (100 µL) at t = 0, 1, 2, and 24 h, heat-treating the sample at 95 °C to denature the enzyme and stop any reaction. In each case, the mixture was centrifuged and precipitating the denatured fluorinase as a pellet and the cleared samples were analysed by HPLC. The results are illustrated below in **Figure 8**.

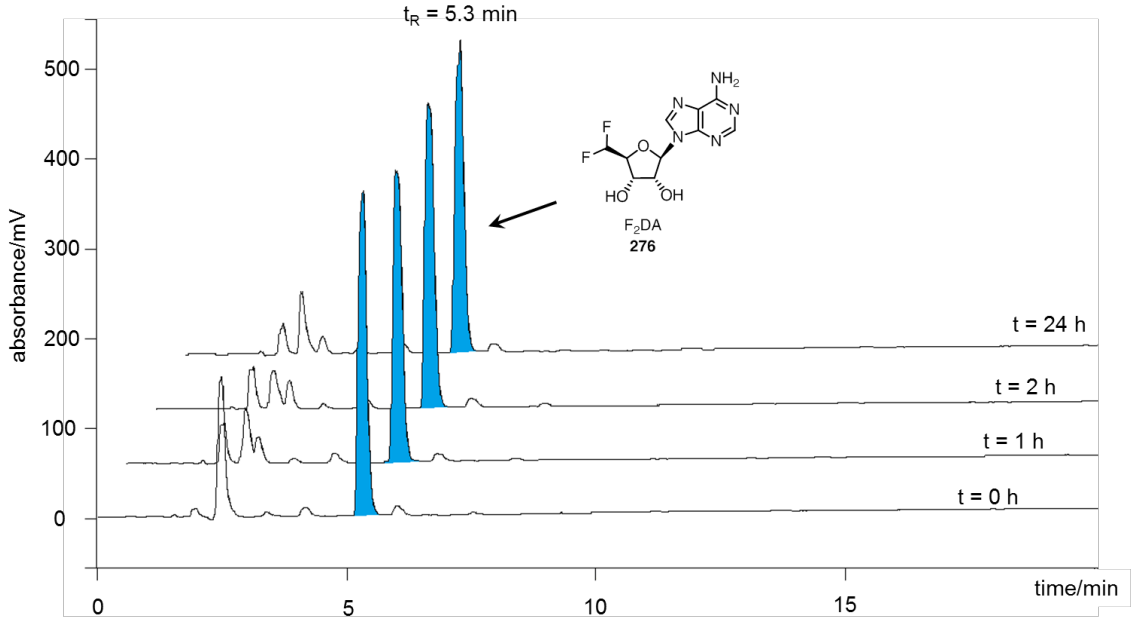

Figure 8. HPLC time course (260 nm) of incubation of F_2DA **276**, blue, (t_R = 5.3 min) with the fluorinase and L-Met **21**, showing samples taken at t = 0, 1, 2 and 24 h.

The HPLC trace did not reveal any change in the concentration of F_2DA **276** over 24 h, and there were no significant new peaks were evident in the chromatogram. This data

suggested that the fluorinase is not capable of catalysing the proposed substitution, or that the equilibrium position of the reaction heavily favours the formation of F_2DA **276**.

4.5.2. Evaluation of F_2DA 276 with L-SeMet 161 as a co-substrate

The reaction was further explored, using L-selenomethionine **161** (L-SeMet). L-SeMet **161** is a better nucleophile than L-methionine due to the presence of a higher energy HOMO on the selenium atom, and the increased polarizability of Se over S. The anticipated transformation of F_2DA **276** to FSeSAM **289** is shown below in **Scheme 12**.

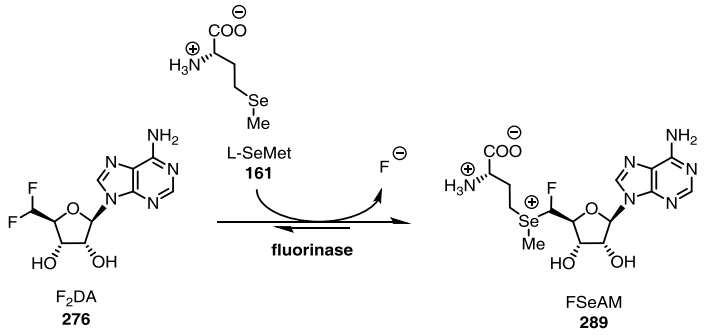

Scheme 12. Proposed substitution of F_2DA **276** with L-SeMet **161** to generate FSeAM **289**, catalysed by the fluorinase.

F_2DA **276** was incubated with L-SeMet **161** (0.1 or 0.6 mM) and fluorinase enzyme in phosphate buffer in similar experiments to those described above. Reaction progress was again monitored by HPLC at t = 0, 1, 2, and 19 h, shown below in in **Figure 9**.

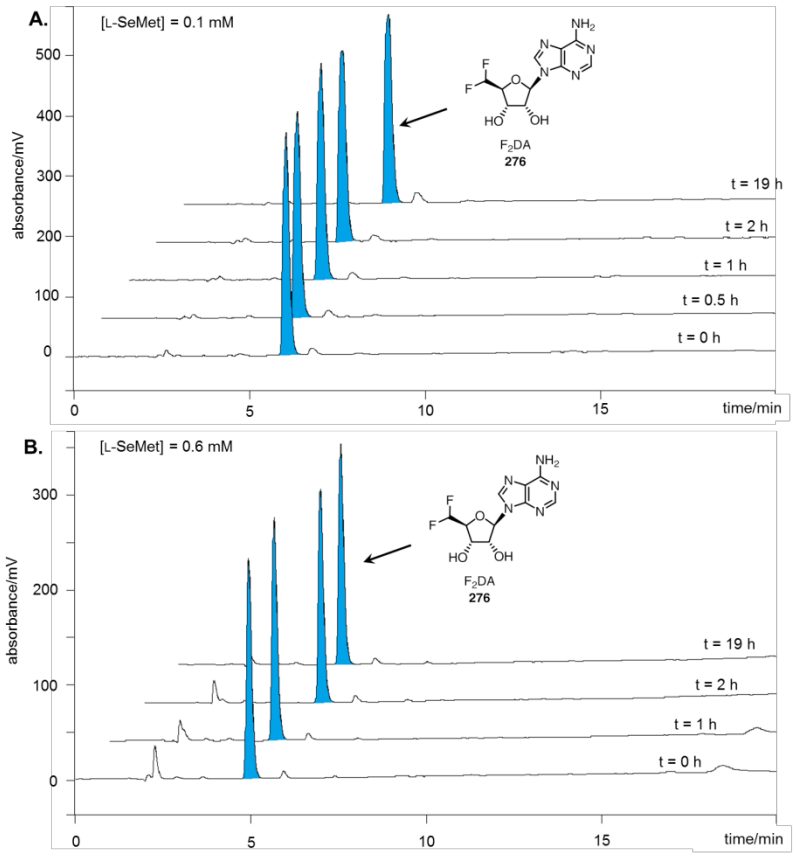

Figure 9. **A.** HPLC time course (260 nm) of incubation of F_2DA **276**, blue, with L-SeMet **161** (0.1 mM) and the fluorinase, showing samples taken at t = 0, 0.5, 1, 2 and 19 h. **B.** HPLC time course of incubation of F_2DA **276** with L-SeMet **161** (0.6 mM) and the fluorinase, showing samples taken at t = 0, 1, 2 and 19 h.

Again, there was no apparent reaction or conversion of F_2DA **276** over the duration of the experiment. This suggests an inherently inert substrate, or that the reaction equilibrium lies heavily in favour of F_2DA **276**.

The lack of any obvious reaction with either L-Met **21** or L-SeMet **161** suggested that the inherent properties of F_2DA **276**, possibly steric, electronic or a combination thereof, prevents substitution of one of the fluorine atoms at C-5'. As the fluorinase reaction is known to be reversible, the possibility that the equilibrium for this specific transformation lies far in favour of the difluorinated product also exists. Without access to a synthetic sample of FSAM **275** or its selenium analogue, distinguishing between equilibrium effects or inherent lack of reactivity is not straightforward.

4.6. Crystallography of F_2DA 276 bound to the fluorinase

To further probe the binding of F_2DA **276** to the enzyme and to try to understand the lack of reactivity, conditions were explored for the preparation of a fluorinase-F_2DA **276** co-crystal.

The fluorinase (6 mg.mL^{-1}) was incubated with F_2DA **276** at 2 mM (from 0.5 M DMSO stock solution), at 4 °C for 18 h, before a series of in house and commercial stochastic crystallisation screens were set up in collaboration with Dr Stephen McMahon and Prof. Jim Naismith.

Crystals were obtained under a range of conditions, however, the best diffracting crystals grew from 40% PEG-monomethyl ether 2K, 0.1 M sodium citrate pH 4.5, and 0.12 M ammonium tartrate. Cryoprotection of a crystal was achieved by doping the mother liquor with 20% glycerol and flash freezing in liquid nitrogen. The resultant diffraction data were collected at the European Synchrotron Radiation Facility beam ID23-1 at 100 K. The data were solved by molecular replacement from previous fluorinase crystal structures by Dr Stephen Mc Mahon, to generate a crystal structure of F_2DA **276** bound into the active site of the fluorinase. The structure was solved to a resolution of 1.8 Å, and detail of the refined structure is shown in **Figure 10**.

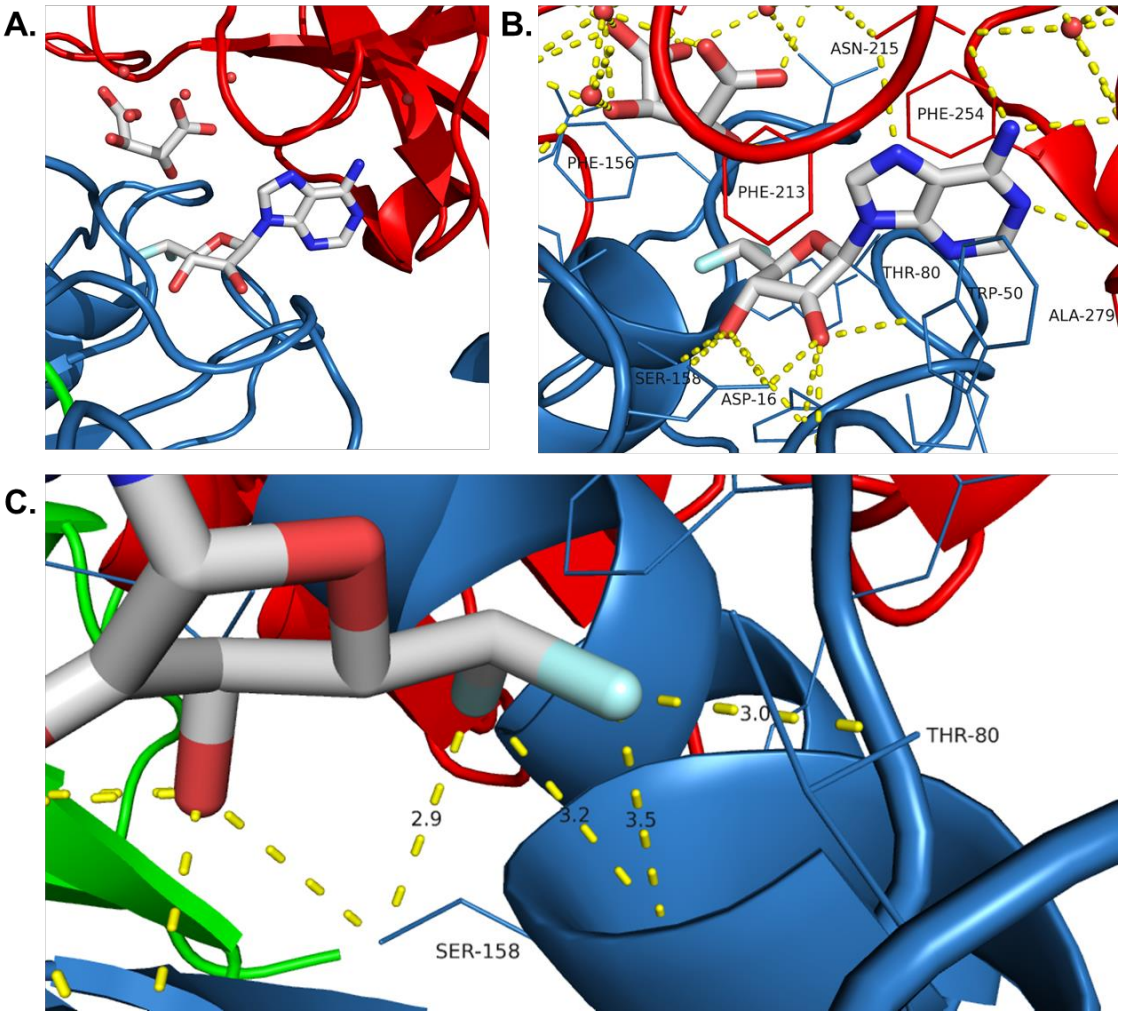

Figure 10. **A.** F_2DA **276** in the active site of the fluorinase. The two monomers of the fluorinase shown in blue and red. The structure was obtained with a molecule of tartrate bound in the active site. **B.** F_2DA **276** in the fluorinase showing interactions with surrounding residues. **C.** Close up of the difluoromethyl group, showing distances to the key residues Ser-158 (NH and OH) and Thr-80 (OH).

F_2DA **276** was located in the active site, along with a molecule of tartrate (from the crystallisation buffer), as shown in **Figure 10 A**. Examination of the structure revealed that F_2DA **276** made numerous contacts to active site residues (**Figure 10 B**), as had been observed with other nucleosides co-crystallised with the enzyme. The adenine base was found to engage in π-π stacking interactions with Phe-254 and Trp-50, while the endo- and exo-cyclic nitrogen atoms formed hydrogen bonding interactions to Ala-279 and Asn-215. The 2',3'-diol system of the ribose ring was found to participate in a hydrogen bonding interaction with Asp-16.

Examination of the difluoromethyl group (**Figure 10 C**) revealed that the fluorine atoms were located in the hydrophobic fluoride binding pocket. The interactions previously identified as important for reaction appeared conserved. One of the fluorine atoms lies

3.0 Å from the OH group of Thr-80, while the second fluorine makes contacts with the amide NH and side chain OH of Ser-158 (3.2 Å and 2.9 Å respectively). The two fluorine atoms appear to "share" the contacts usually observed with FDA **22** in the active site. The hydrogen atom of the difluoromethyl group appears to engage in a hydrogen bond with one of the hydroxyl oxygen atoms of the co-bound tartrate, but does not appear to form close contacts to any amino acid residues in the active site.

For direct comparison, the co-crystal structure of F_2DA **276** was overlaid with that of FDA **22** and L-Met **21** bound in the active site of the fluorinase (PDB code: 1RQR),[48] solved previously at St Andrews. The overlays are shown below in **Figure 11**, with the pastel coloured structure and ligands with yellow C-atoms belonging to the FDA-L-Met structure.

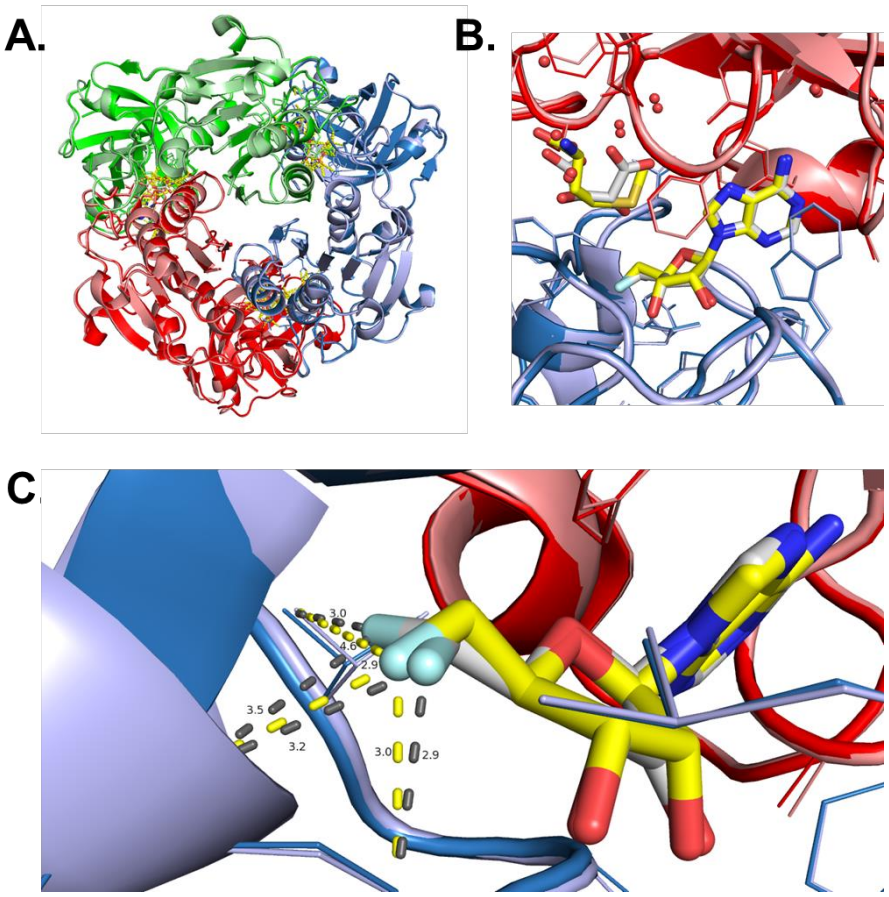

Figure 11. **A.** Overlay of the structure of fluorinase bound to FDA **22** (pastel colours) and F_2DA **276** (bright colours) showing no gross conformational change when bound to F_2DA **276**. **B.** Close up of the active site of the fluorinase showing an overlay of the two ligands, FDA **22** (yellow carbons) and F_2DA **276** (grey carbons). **C.** Close up of the active site showing orientation of the fluorine atoms of F_2DA **276** compared to the orientation of the C–F bond of FDA **22**. Distances (Å) from the fluorine atoms to key residues are shown for FDA **22** (yellow dashes) and F_2DA **276** (grey dashes).

Binding of F_2DA **276** does not result in any gross conformational change of the structure of the fluorinase, as shown in **Figure 11 A**. Upon closer examination, tartrate occupies the L-Met **21** binding site (**Figure 11 B**), adopting a similar conformation where one of the carboxylates engages in similar polar interactions to those observed for carboxylate group of L-Met **21**. The adenine bases overlay very well, as does the ribose ring. It is clear in **Figure 11 C** that the fluorine atom of FDA **22**, the natural product, lies between the two fluorine atoms of the difluoromethyl group of F_2DA **276**. The location of the two fluorine atoms and their suggested interactions with Thr-80 and Ser-158, as shown above, support the suggestion that the fluoromethyl group bridges the interactions usually engaged by the single fluorine atom of FDA **22**.

These observations suggest a possible reason why F_2DA **276** is not a substrate for the fluorinase. The C–F bond is the strongest single bond observed in organic molecules, having a bond dissociation energy, on average, of 105.4 $kJ.mol^{-1}$.[50] The fluorinase enzyme has uniquely evolved the ability to catalyse the formation, and importantly for this case, the cleavage of this bond with L-Met **21** as an incoming nucleophile. The "sharing" of key interactions between the two fluorine atoms may no longer sufficiently activate one of the fluorines for substitution by L-Met **21** or L-SeMet **161**. A second consequence of this "sharing" may be that neither of the fluorine atoms are aligned in the optimal conformation for an S_N2-type substitution with an incoming nucleophile, increasing the kinetic barrier to reaction. The addition of a second electronegative fluorine atom at C-5' is expected to increase the strength of each of the C–F bonds, due to increased positive character at carbon.[51,52] A combination of these three factors: "shared" interactions with activating residues, misaligned geometry of the C–F bond, and increased C–F bond strength, may all contribute to a lack of reactivity.

4.7. Conclusions

The difluoromethyl group was found to play an important role in a range of pharmaceuticals and agrochemicals in light of its unique physicochemical properties. In this context, we were interested in applying the fluorinase enzyme to the synthesis of difluoromethyl groups. It was proposed that the enzyme and the associated mild reaction conditions would complement existing methodology for synthesis of the $–CF_2H$ motif.

To this end, 5',5'-difluoro-5'-deoxyadenosine **276** (F_2DA) was synthesised and explored as a potential substrate for a reverse reaction with L-Met **21**. Isothermal titration

calorimetry revealed that F_2DA **276** bound to the fluorinase with a marginally larger K_a compared to that of the natural substrate, FDA **22**. Assays were conducted where F_2DA **276** was incubated with both L-Met **21**, and the more potent nucleophile, L-SeMet **161**. No reaction was observed in HPLC assays for either set of conditions, and increasing the concentration of the nucleophile also resulted in no reaction.

A co-crystal structure of the fluorinase bound to F_2DA **276** was obtained and revealed that F_2DA **276** was oriented in the active site in a nearly identical manner to FDA **22**, apart from the location of the two fluorine atoms. The two fluorine atoms were "sharing" interactions with Ser-158 and Thr-80, the two residues in the active site responsible for activating the fluorine atom for substitution. As a result, the conformation of neither of the C–F bonds matched that observed for the C–F bond in FDA **22**, suggesting that the geometry of the bond was no longer optimal for S_N2 attack by sulfur or selenium. These observations, coupled to the inherently stronger C–F bond observed in $–CF_2H$ compared to $–CFH_2$ motifs may be responsible for preventing the substitution reaction catalysed by the fluorinase.

Despite the fact that no reaction was observed with the native fluorinase, understanding the interaction of F_2DA **276** in the active site of the enzyme may, in future, allow design of active enzyme mutants. Such mutants may be able to overcome the poor substrate alignment and loss of interactions of the fluorine atom with the enzyme surface, to evolve the desired reactivity for enzymatic synthesis of a difluoromethyl group. Evolution of this defluorination activity into the enzyme, however, remains to be further investigated.

4.8. References

1. J. Hu, W. Zhang, and F. Wang, *Chem. Commun.*, 2009, 7465–7478.
2. D. O'Hagan and H. Deng, *Chem. Rev.*, 2015, **115**, 634–49.
3. R. C. Terril, 1970, US Patent no. 3535388 A.
4. J. Pepin, F. Milord, C. Guern, and P. J. Schechter, *Lancet*, 1987, **2**, 1431–1433.
5. T. C. Johnson, T. P. Martin, R. K. Mann, and M. A. Pobanz, *Bioorg. Med. Chem.*, 2009, **17**, 4230–4240.
6. J. Erickson and J. McLoughlin, *J. Org. Chem.*, 1995, **60**, 1626–1631.

7. K. Müller, *Chimia*, 2014, **68**, 356–362.

8. N. A. Meanwell, *J. Med. Chem.*, 2011, **54**, 2529–2591.

9. Y. Xu and G. D. Prestwich, *J. Org. Chem.*, 2002, **67**, 7158–7161.

10. F. Narjes, K. F. Koehler, U. Koch, B. Gerlach, S. Colarusso, C. Steinkühler, M. Brunetti, S. Altamura, R. De Francesco, and V. G. Matassa, *Bioorganic Med. Chem. Lett.*, 2002, **12**, 701–704.

11. M. A. Chowdhury, K. R. A. Abdellatif, Y. Dong, D. Das, M. R. Suresh, and E. E. Knaus, *J. Med. Chem.*, 2009, **52**, 1525–1529.

12. C.-L. J. Wang, in *Organic Reactions*, John Wiley & Sons, Inc., Hoboken, NJ, USA, 1985, pp. 319–400.

13. L. Markovskilj, V. Pashinnik, and A. Kirsanov, *Synthesis*, 1973, **1973**, 787–789.

14. W. J. Middleton, *J. Org. Chem.*, 1975, **40**, 574–578.

15. G. S. Lal, G. P. Pez, R. J. Pesaresi, and F. M. Prozonic, *Chem. Commun.*, 1999, 215–216.

16. T. Furuya, T. Fukuhara, and S. Hara, *J. Fluor. Chem.*, 2005, **126**, 721–725.

17. T. Liang, C. N. Neumann, and T. Ritter, *Angew. Chem. Int. Ed.*, 2013, **52**, 8214–8264.

18. G. P. Stahly, *J. Fluor. Chem.*, 1989, **43**, 53–66.

19. C. Ni, F. Wang, and J. Hu, *Beilstein J. Org. Chem.*, 2008, **4**.

20. L. Zhu, Y. Li, C. Ni, J. Hu, P. Beier, Y. Wang, G. K. S. Prakash, and G. A. Olah, *J. Fluor. Chem.*, 2007, **128**, 1241–1247.

21. P. Beier, A. V. Alexandrova, M. Zibinsky, and G. K. S. Prakash, *Tetrahedron*, 2008, **64**, 10977–10985.

22. G. K. S. Prakash and J. Hu, *Acc. Chem. Res.*, 2007, **40**, 921–930.

23. P. S. Fier and J. F. Hartwig, *J. Am. Chem. Soc.*, 2012, **134**, 5524–5527.

24. V. P. Mehta and M. F. Greaney, *Org. Lett.*, 2013, **15**, 5036–5039.

25. Y. Fujiwara, J. A. Dixon, R. A. Rodriguez, R. D. Baxter, D. D. Dixon, M. R. Collins, D. G. Blackmond, and P. S. Baran, *J. Am. Chem. Soc.*, 2012, **134**, 1494–1497.

26. G. K. S. Prakash, R. Krishnamurti, and G. A. Olah, *J. Am. Chem. Soc.*, 1989, **111**, 393–395.

27. G. K. S. Prakash, R. Mogi, and G. A. Olah, *Org. Lett.*, 2006, **8**, 3589–3592.

28. W. Qiu and D. J. Burton, *Tetrahedron Lett.*, 1996, **37**, 2745–2748.

29. T. Liang, C. N. Neumann, and T. Ritter, *Angew. Chem. Int. Ed.*, 2013, **52**, 8214–8264.

30. A. L. Henne and M. A. Smook, *J. Am. Chem. Soc.*, 1950, **72**, 4378–4380.

31. R. F. Clark and J. H. Simons, *J. Am. Chem. Soc.*, 1955, **77**, 6618–6618.

32. T. G. Miller and J. W. Thanassi, *J. Org. Chem.*, 1960, **25**, 2009–2012.

33. I. Rico and C. Wakselman, *Tetrahedron*, 1981, **37**, 4209–4213.

34. Y. Zafrani, G. Sod-Moriah, and Y. Segall, *Tetrahedron*, 2009, **65**, 5278–5283.

35. P. S. Fier and J. F. Hartwig, *Angew. Chem. Int. Ed.*, 2013, **52**, 2092–2095.

36. J. Gonzalez, C. J. Foti, and S. Elsheimer, *J. Org. Chem.*, 1991, **56**, 4322–4325.

37. I. Rico, D. Cantacuzene, and C. Wakselman, *Tetrahedron Lett.*, 1981, **22**, 3405–3408.

38. Y. Xu, M. Fletcher, and W. R. Dolbier, *J. Org. Chem.*, 2000, **65**, 3460–3465.

39. G. K. S. Prakash, I. Ledneczki, S. Chacko, and G. A. Olah, *Org. Lett.*, 2008, **10**, 557–560.

40. H. Deng, S. L. Cobb, A. R. McEwan, R. P. McGlinchey, J. H. Naismith, D. O'Hagan, D. A. Robinson, and J. B. Spencer, *Angew. Chem. Int. Ed.*, 2006, **45**, 759–762.

41. J. R. McCarthy, E. T. Jarvi, D. P. Matthews, M. L. Edwards, N. J. Prakash, T. L. Bowlin, S. Mehdi, P. S. Sunkara, and P. Bey, *J. Am. Chem. Soc.*, 1989, **111**, 1127–1128.

42. E. T. Jarvi, J. R. Mccarthy, S. Mehdi, D. P. Matthews, M. L. Edwards, N. J. Prakash, T. L. Bowlin, P. S. Sunkara, and P. Bey, *J. Med. Chem.*, 1991, **34**, 647–656.

43. R. S. Ranganathan, G. H. Jones, and J. G. Moffatt, *J. Org. Chem.*, 1974, **39**, 290–298.

44. A. M. Jawalekar, N. Meeuwenoord, J. G. O. Cremers, H. S. Overkleeft, G. A. van der Marel, F. P. J. T. Rutjes, and F. L. van Delft, *J. Org. Chem.*, 2008, **73**, 287–290.

45. N. Nakajima and Y. Ikada, *Bioconjug. Chem.*, 1995, **6**, 123–130.

46. W. R. Dolbier Jr, *Guide to Fluorine NMR for Organic Chemists*, John Wiley & Sons, Inc., Hoboken, NJ, USA, 2009.

47. J. A. K. Howard, V. J. Hoy, D. O'Hagan, and G. T. Smith, *Tetrahedron*, 1996, **52**, 12613–12622.

48. C. Dong, F. Huang, H. Deng, C. Schaffrath, J. B. Spencer, D. O'Hagan, and J. H. Naismith, *Nature*, 2004, **427**, 561–565.

49. K. Dross, R. F. Rekker, G. de Vries, and R. Mannhold, *Mol. Inform.*, 1998, **17**, 549–557.

50. D. O'Hagan, *Chem. Soc. Rev.*, 2008, **37**, 308–319.

51. R. D. Chambers, *Fluorine in Organic Chemistry*, CRC Press, 2004.

52. B. E. Smart, in *Molecular Structure and Energetics*, eds. J. F. Liebman and A. Greenberg, VCH Publishers, Deerfield Beach, 1986, p. 141.

5. Synthesis of [^{18}F]fluoroacetate for assessment of acetyl CoA synthetase 2 activity *in vivo*

Based on emerging evidence of the importance of acetyl CoA synthetase 2 (ACSS2) for growth and viability of a wide range of cancers, understanding and investigating ACSS2 expression and activity patterns within different cancers is an emerging area of research. We were approached by Prof. Eyal Gottlieb and Dr Zachary Schug at the Beatson Cancer Research Institute in Glasgow to collaborate in a study to investigate ACSS2 activity in colorectal cancers using PET.

They required the development of a site-specific synthesis protocol for the production of [^{18}F]fluoroacetate [^{18}F]-**1**, for use in PET imaging experiments to assess ACSS2 activity *in vivo*. Prior to discussing the optimisation of a synthetic method for production of [^{18}F]fluoroacetate for their PET imaging study, the central metabolic role played by acetyl CoA, the metabolic intermediate produced by ACSS2, and its emerging role in the growth of cancers will be discussed.

5.1. Acetyl coenzyme A

Acetyl coenzyme A **290** (acetyl CoA, **Figure 1**) is a key intermediate in general metabolism, linking a number of anabolic and catabolic biosynthetic pathways. Acetyl CoA acts as shuttle of a 2-carbon acetate unit within the cell in the form of a high energy thioester of coenzyme A **291** (CoASH, **Figure 1**). Acetyl CoA **290** is sourced from the glycolysis or β-oxidation and is used for energy production, biosynthesis of cholesterol, fatty acids and other isoprenoids, and as a source of the acetyl group in numerous acetylations.

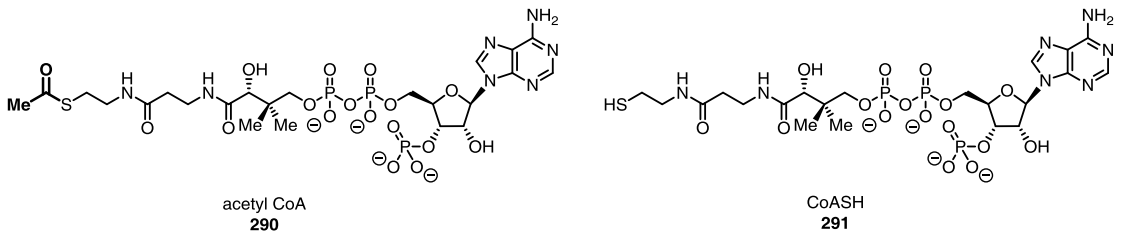

Figure 1. Structures of acetyl coenzyme A **290** and coenzyme A **291**, with the acetyl unit highlighted in bold.

5.1.1. Sources of acetyl CoA

High energy molecules, such as glucose and fatty acids, pass through the glycolysis and β-oxidation pathways, providing a source of acetyl CoA **290** which can enter the citric acid cycle and generate ATP (**Scheme 1**).

Glycolysis is the breakdown of glucose **292** into two molecules of pyruvate **293**. Pyruvate **293**, an important metabolic intermediate itself, is decarboxylated under the action of a large multi-enzyme complex (pyruvate dehydrogenase complex) to give acetyl CoA **290**, and releasing an equivalent of NADH (reduced nicotinamide adenine dinucleotide, a cellular electron shuttle) in the process.[1] The pyruvate dehydrogenase complex is localised within the mitochondrial matrix in eukaryotes and acetyl CoA **290** produced from pyruvate is predominantly utilised in the citric acid cycle within the mitochondria.[2]

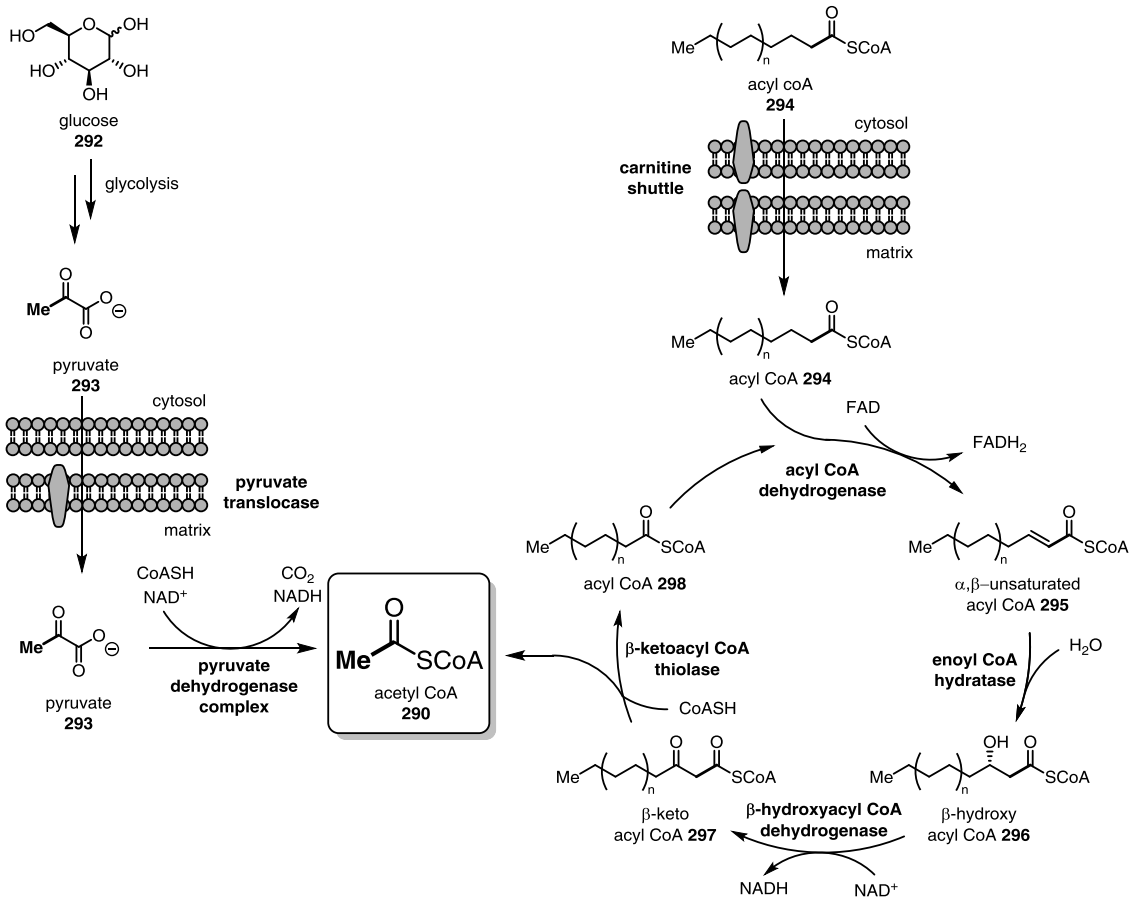

Scheme 1. Metabolic production of acetyl CoA **290** within the mitochondrial matrix. Pyruvate **293**, from glycolysis, or fatty acids from β-oxidation give acetyl CoA **290**. The bold atoms highlight the 2-C unit metabolised to acetyl CoA **290**.

β-Oxidation takes place in the mitochondrial matrix, after shuttling long chain fatty acids through the mitochondrial as acyl CoAs **294**.[3] Long chain acyl CoAs **294** are broken down in a series of steps which approximate the reverse of fatty acid biosynthesis. Oxidation by acyl CoA dehydrogenase generates an α,β-unsaturated acyl CoA **295** and an equivalent of $FADH_2$ (reduced flavin adenine dinucleotide) another cellular electron carrier.[4] The *trans*-alkene produced undergoes hydration, catalysed by enoyl CoA hydratase to generate a β-L-hydroxy CoA moiety **296**.[5] Oxidation of the hydroxyl group by β-L-hydroxyacyl CoA dehydrogenase generates a β-keto acyl CoA **297**[6] which undergoes cleavage by β-ketothiolase and CoASH to generate acetyl CoA **290** and an acyl CoA **298** which is two carbons shorter than the original fatty acid.[7] This cycle is repeated to accomplish a step-wise breakdown of the long chain fatty acid by a 2-carbon unit each cycle, to generate acetyl CoA **290** which then enters the citric acid cycle within the mitochondrion.

Both glycolysis and β-oxidation generate acetyl CoA **290** in the mitochondrial matrix, however, there is a requirement for acetyl CoA **290** in the cytosol for processes such as fatty acid biosynthesis and histone acetylation. Acetyl CoA **290** is not transported across the mitochondrial membranes directly, instead it is transported as an equivalent of citrate **300** (**Scheme 2**). When there is an abundance of citrate **300** within the mitochondrion (*e.g.* under conditions of excess dietary carbohydrates or fats), citrate **300** is transported out of the organelle by tricarboxylic acid translocase, part of the citrate shuttle system.[8] In the cytosol, citrate **300** is cleaved to oxaloacetate **299** and acetyl CoA **290** by ATP-citrate lyase, consuming an equivalent of ATP in the process.[9] This process generates a pool of cytosolic acetyl CoA **290** for use in other metabolic processes.

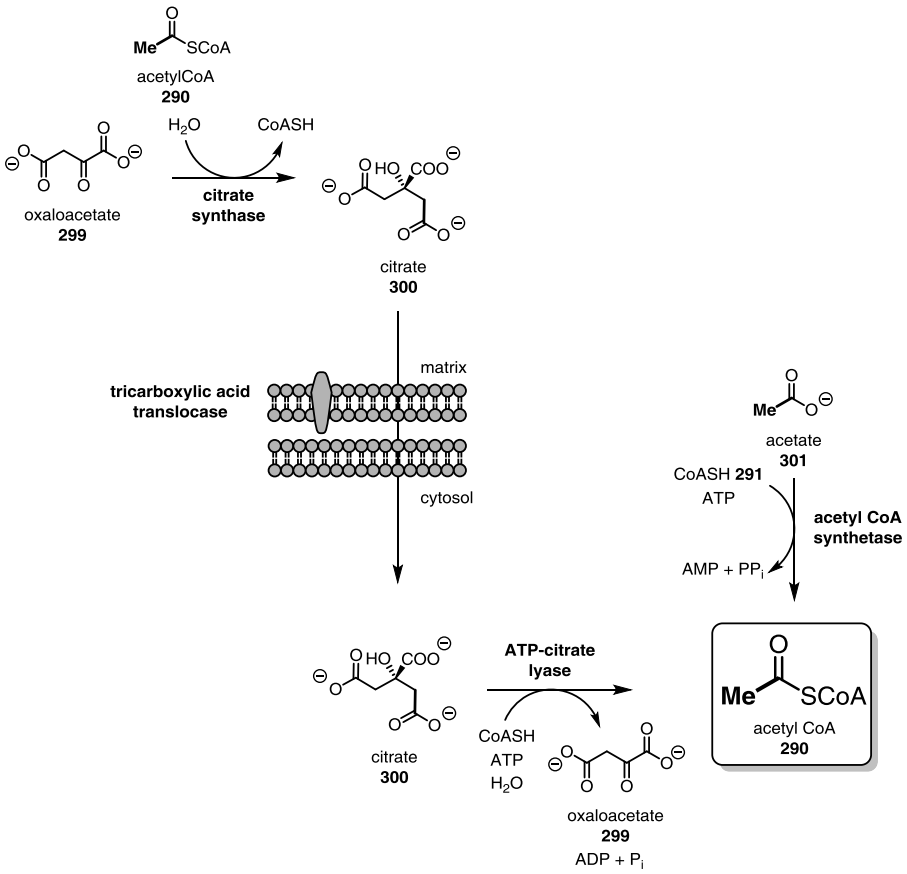

Scheme 2. Biosynthesis of cytosolic acetyl CoA. Acetyl CoA **290** is transported out of the mitochondrial matrix after condensation with oxaloacetate **399** to give citrate **300**. Citrate **300** is cleaved by ATP-citrate lyase to give cytosolic acetyl CoA **290**. Dietary acetate is condensed with co-enzyme A **291** (CoASH) to give acetyl CoA **290**. The bold atoms highlight the 2-C unit of acetyl CoA **290**.

A second source of acetyl CoA **290** within the cytosol is its direct synthesis from acetate **301** and CoASH **291** by acetyl CoA synthetase (ACSS) (**Scheme 2**).[10] Acetate **301** is primarily sourced from the gut microbiota, which ferment dietary fibre to acetate **301**. This acetate **301** is absorbed into the bloodstream.[11] Dietary ethanol is also a source of acetate **301**, by successive oxidations to acetaldehyde and acetate **301** by alcohol and acetaldehyde dehydrogenases.[12] Acetyl CoA synthetase and its role in lipid metabolism in cancer will be discussed in in **Section 5.2.**

5.1.2. Acetyl CoA as a metabolic building block

Fatty acid biosynthesis (**Scheme 3**) in the cytosol requires acetyl CoA **290** as a source of 2 carbon units. Acetyl CoA **290** is used in the initial step of fatty acid biosynthesis after condensation with an acyl carrier protein (ACP) to give acetyl ACP **303**.[13] Acetyl ACP **303** is then condensed with malonyl ACP **304** (derived from

malonyl CoA **302** and ACP)[13] to give a β-ketoacyl ACP **305**. The malonyl CoA **302** required for this elongation of the fatty acid chain is derived from carboxylation of acetyl CoA **290** with bicarbonate by acetyl CoA carboxylase.[14,15] While malonyl CoA **302** is a 3 carbon unit, it donates a 2-carbon unit to the growing acyl chain, as the condensation incorporates a decarboxylation event.

Malonyl CoA **302** is also utilised in the biosynthesis of a range secondary metabolites such as polyketides[16] and flavonoids,[17] providing 2 carbon units in a manner similar to fatty acid biosynthesis.

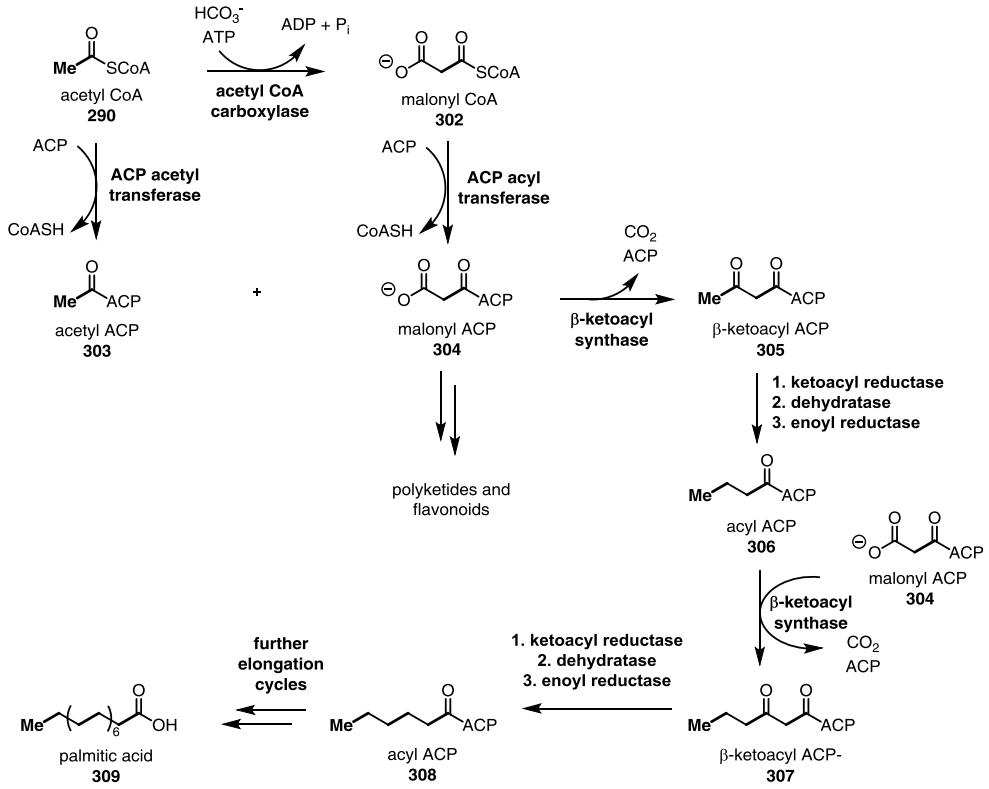

Scheme 3. Fatty acid biosynthesis using acetyl CoA **290**, and malonyl CoA **302** to give palmitic acid **309**. Malonyl CoA **302** is synthesised from acetyl CoA **290** and is used as a C-2 surrogate. The bold atoms highlight the 2-C acetyl units present in the intermediates and products.

Acetyl CoA **290** is also used for the biosynthesis of cholesterol[18] and isoprenoids,[19] *via* the mevalonate pathway (**Scheme 4**). This pathway begins with the condensation of two acetyl CoA **290** units by acetoacetyl CoA thiolase to give acetoacetyl CoA **310**.[20] A third unit of acetyl CoA is incorporated by 3-hydroxy-3-methylglutaryl CoA synthase (HMGCoA synthase) to give 3-hydroxy-3-methylglutaryl CoA **311** (HMGCoA).[21] HMGCoA is reduced by HMGCoA reductase to give mevalonate **312**.[22] Through a series of phosphorylations and a decarboxylation, mevalonate is converted to isopentenyl-5-pyrophosphate **313** (IPP), which is isomerised to dimethylallyl

pyrophosphate **314** (DMAPP). Condensation of IPP **313** and DMAPP **314** gives geranyl pyrophosphate **315** (GPP), which is condensed with another unit of IPP **313** to give farnesyl pyrophosphate **316** (FPP). FPP **316** occupies a branch point in the mevalonate pathway, from which prenylated compounds and sterols (such as cholesterol) are synthesised.[19]

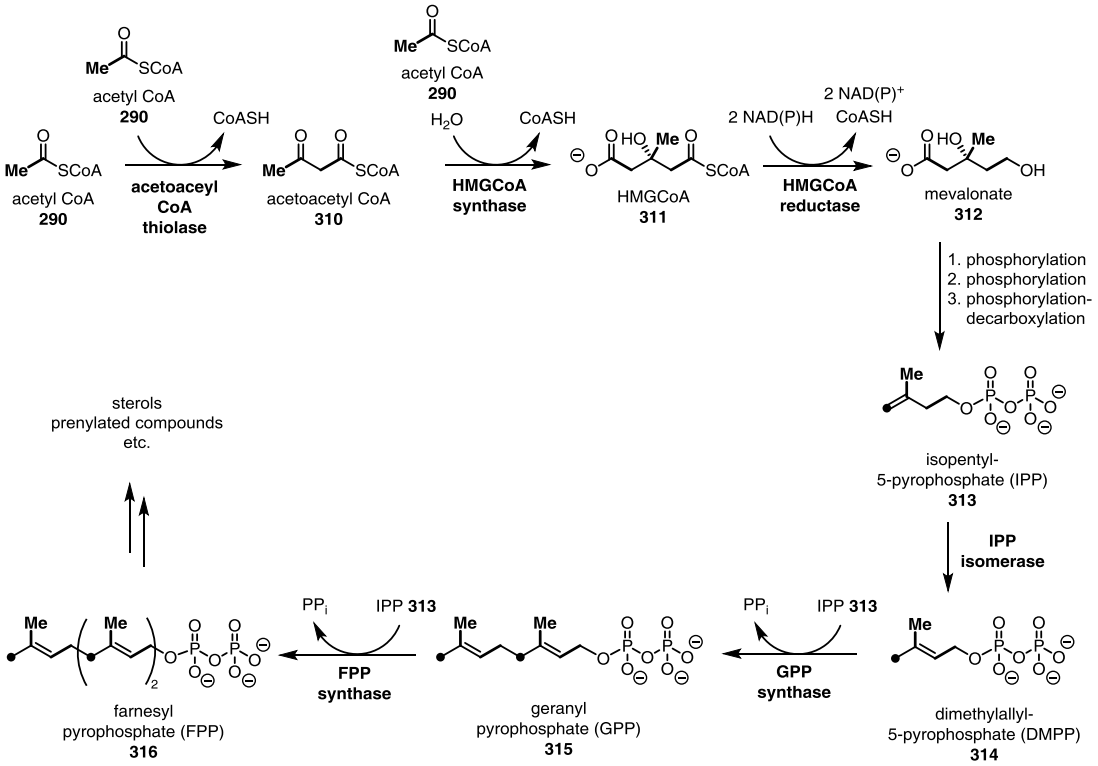

Scheme 4. The mevalonate pathway showing the utilisation of acetate units for the synthesis of HMGCoA **311**. HMGCoA **311** used to synthesise farnesyl pyrophosphate **316**, and then more complex molecules such as cholesterol. The bold atoms highlight the 2-C acetyl units present in the intermediates and products.

5.1.3. Acetyl CoA as a source of acetyl units

Acetyl CoA **290** is a source of acetate units for the post translational modification of proteins, including histones[23] and other proteins such as tubulin[24] and p53.[25] Modulation by *N*-acetylation and deacetylation of histone proteins by acetylases and deacetylases affects gene activity through conformational control of the local structure of DNA (**Scheme 5**).[26] Within eukaryotic cells, 146 base pair sections of DNA are wrapped around an assembly of eight histone proteins.[27] Acetylation of the lysine residues of these proteins, either at the *N*-terminus or within the polypeptide chain leads to a relaxation in the local structure of chromatin. This conformational change

allows access to enzymes responsible for transcription, thereby affecting gene expression.[28]

Acetylation directly affects signalling within the body through neurotransmitters but also indirectly through histone-acetylation modulated transcription of regulatory kinases.[29] Choline **317** (**Scheme 5**) is acetylated by acetyl CoA **290** under the action of choline acetyltransferase to give acetylcholine **318**,[30,31] the primary neurotransmitter of the parasympathetic nervous system.

N-Acetylated carbohydrates play an important role in cell surface stabilisation and reinforcement, as well as cell-cell recognition processes.[32,33] *N*-Acetylated amino-sugars form part of the bacterial cell wall in both Gram positive and Gram negative bacteria.[34] The peptidoglycan component of their call walls, comprised up of repeat units of *N*-acetylglucosamine (NAG) and *N*-acetylmuramic acid (NAM), linked by short peptides, provides structural rigidity and acts as a physical barrier to the environment.[35] Acetylation of these carbohydrates, such as glucose derivative **319**, proceeds under the action of *N*-acetyl transferase enzymes. In this case, glucosamine-6-phosphate *N*-acetyl transferase converts **319** to its corresponding *N*-acetyl analogue, such as *N*-acetyl-glucosamine-6-phosphate **320** (**Scheme 5**).[36]

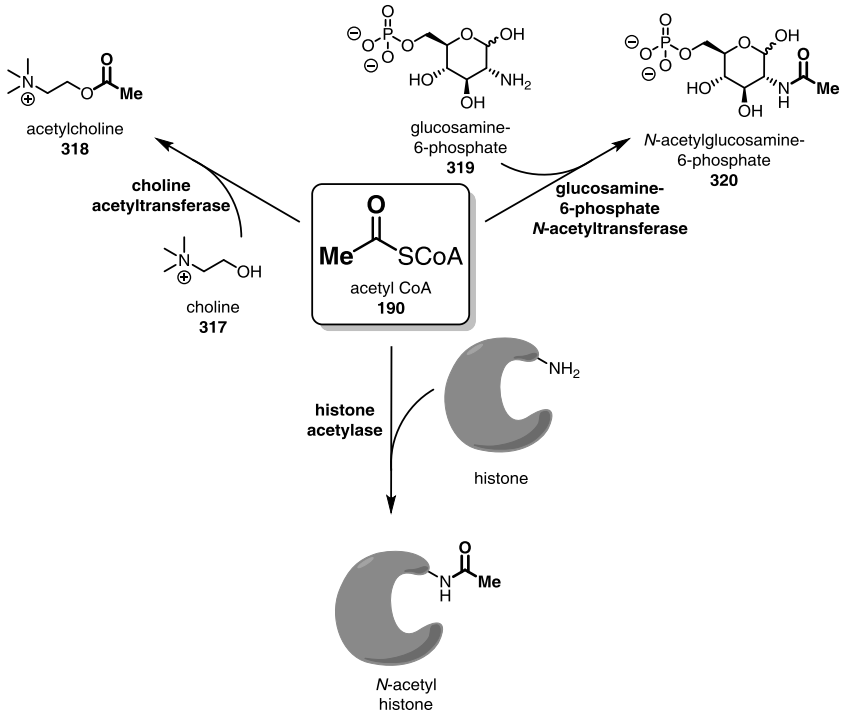

Scheme 5. Acetyl CoA **290** acts as a source of acetyl units, donating the acetyl subunit to a diverse array of biomolecules, including choline **317** for the synthesis of the neurotransmitter acetylcholine **318**, to glucosamine-6-phosphate **319** to give *N*-acetylglucosamine-6-phosphate **320**, and to histones. Acetyl units are shown in bold.

5.1.4. Other functions of acetyl CoA

Studies in *Saccharomyces cerevisiae* have shown that acetyl CoA **290** flux is intimately linked to cell growth and cell division through changes in the acetylation pattern of proteins in the cell. Specifically, acetyl CoA **290** flux is thought to be responsible for controlling the activity of acetyl transferases. A number of acetyl transferases have K_M values of the same order of magnitude as the cellular acetyl CoA **290** concentration, and their activity is therefore sensitive to the acetyl CoA **290** concentration within the cell.[37] The activity of these transferases, and therefore any downstream effects (such as gene regulation) are strongly associated with acetyl CoA **290** flux, making the understanding of mechanisms controlling the regulation of acetyl CoA **290** levels in the cell vital.

Lin *et al.*[38] showed that the acetylation of phosphoenolpyruvate carboxykinase (PCK), a key enzyme for gluconeogenesis, regulates of the activity of PCK. The authors proposed that the acetyl CoA level acts as an intracellular marker of the metabolic state of the cell, and changes in the levels of acetyl CoA **290** in the cell lead to a metabolic cascade which restores levels of glucose to those required for normal cellular function. In addition to this regulatory role, downstream changes in activity of phosphoenolpyruvate kinase led to changes in the chronological lifespan (CLS, a model system for understanding the aging process in eukaryotic cells) of the yeast cells.[39]

In a study by Tu *et al.*,[40] acetylation of components of a transcriptional coactivator complex, known as SAGA, was found to occur in response to the levels of acetyl CoA **290** within the cell. The SAGA complex itself is a histone acetyltransferase. The SAGA complex selectively acetylates histones which control the function of genes that are responsible for the growth phase induction in yeast cells, therefore acetyl CoA **290** levels in the cell reflect their metabolic state and growth stage.

5.2. Acetyl CoA Synthetase

5.2.1. Acetyl CoA synthetase genes and proteins

Acetyl CoA synthetase (ACSS) is an ATP-dependent enzyme that catalyses the ligation of acetate **301** and CoASH **291** to give acetyl CoA **290** (**Scheme 6**). Three ACSS genes (*acss1*, *acss2* and *acss3*) have been identified, two of which (*acss1* and

acss2) are known to code for acetyl CoA synthetases (ACSS1 and ACSS2) in humans.[41] ACSS3 has yet to be isolated and characterised.

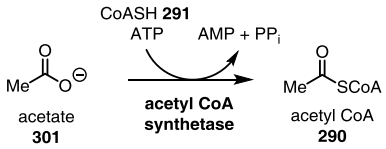

Scheme 6. Synthesis of acetyl CoA **290** by acetyl CoA synthetase.

ACSS1 is an isoform of the acetyl CoA synthetase found in the mitochondrial matrix in most tissues, but at elevated levels in the heart and skeletal muscle tissue.[42] ACSS1 is upregulated under ketogenic (starvation) conditions as a means of using acetate for energy production throughout the rest of the body. Acetate **301** is derived from hydrolysis of acetyl CoA **290** (produced by hepatic β-oxidation) under the action of acetyl CoA hydrolase (which is also upregulated under ketogenic conditions in rat models).[43] The activity of ACSS1 does not appear to vary in response to other metabolic processes.[42] ACSS1 contributes to whole body utilisation of acetate as an energy source under conditions of starvation.

The activity of the cytosolic 80 kDa human ACSS2 is intrinsically linked to the rate of lipid biosynthesis in the cells, and its activity is modulated through the action of sterol regulatory element-binding proteins (SREBPs). ACSS2 is responsible for the rate limiting step of the incorporation of acetate into fatty acids during *de novo* lipid biosynthesis.[10] Unlike ACSS1, the activity ACSS2 increases under starvation conditions highlighting the anabolic role of ACSS2, compared to the catabolic role of ACSS1. The role of ACSS2 in the biosynthesis of lipids has led to an interest in this enzyme related to cancers, where increased metabolic rates are a defining characteristic.

5.2.2. The role of ACSS2 in cancer

Fatty acid synthase (FAS), a multifunctional enzyme complex responsible for *de novo* fatty acid biosynthesis, was identified as an oncogenic antigen present in some cancers which showed poor prognosis.[44] The association of FAS with cancer has led to increased interest in lipid metabolism and its role in cancer. Radiolabelling experiments suggest that more than 90% of fatty acids in tumour cell triglycerides are derived from *de novo* fatty acid biosynthesis, under certain conditions. Understanding lipid

metabolism is thus fundamental to understanding disease origin and progression in cancer.[45]

Recent work comparing the rate of uptake of [^{14}C]acetate in four tumour cell lines relative to uptake in normal fibroblasts under normoxic conditions found that the tumour cells incorporated more of the [^{14}C]-label into the lipid fraction. Fibroblasts excrete the label predominantly as [^{14}C]CO_2.[46] Normal cells tend to utilise acetate as an energy source, channelling acetate through the citric acid cycle, while tumour cell lines appear to channel acetate towards *de novo* lipogenesis. Similarly, [^{14}C]acetate uptake is increased in prostate cancer cells under hypoxic conditions.[47] This uptake is associated with increased activity of ACSS2, whose activity has been found to be critical to the survival of these cancer cell lines.[48]

Two further studies examining the role that ACSS2 plays in the metabolic activity of cancer cells and have argued that this enzyme could in future be a novel drug target in treatment of cancers.

Tu *et al*.[49] have used gene siRNA based silencing, knockout mouse models and small molecule inhibitor screens to show that uptake and incorporation of [^{14}C]acetate is dependent on ACSS2 activity. In a large hepatic tumour model, ACSS2 knockdown resulted in a reduction in tumour burden in the liver, from 83% high tumour burden in wild type mice (*ACSS2*$^{+/+}$), to 29% high tumour burden in double knockout mice (*ACSS2*$^{-/-}$). Immunohistochemical analysis of human tumour sample microarrays showed high levels of ACSS2 expression in breast, lung and ovarian tumour sections, with little to no ACSS2 expression in normal tissues. The authors' survey of samples from patients with triple negative breast cancer showed that shorter overall survival times were associated with high expression levels of ACSS2. PET imaging with [^{11}C]acetate in the knockout models also showed increased uptake in tumours which expressed high levels of ACSS2.

Gottlieb *et al.* have observed increased *de novo* lipid biosynthesis using [^{13}C]glucose, [^{13}C]acetate and [^{14}C]acetate feeding experiments in cancer cells under metabolic stress (starvation and low oxygen perfusion). Increased *de novo* lipid biosynthesis resulted in an increased production of short chain fatty acids as detected by LC-MS/MS in lipid extracts of cell homogenates. Up to 50% labelling of the cellular acetyl-CoA pool (compared to 10% under normoxic and fed conditions) and increased sensitivity of the cells to inhibitors of fatty acid synthase was observed.[50] In these cell lines, screening of over 60 lipid metabolism gene knockouts using siRNA-mediated gene silencing

revealed the largest effect on cell growth was observed in cell lines where the *ACSS2* gene was silenced. Further analysis of reported patterns of ACSS2 expression or *ACSS2* copy number across a broad range cancer cell lines showed high expression of ACSS2 and large gene copy number gain of *ACSS2* in multiple cancers, including breast cancers (invasive ducal carcinoma and invasive lobular carcinoma) and aggressive prostate cancer treatment.

Gottlieb *et al.* further found that silencing of ACSS2 using doxycycline-induced siRNA in either in cell masses or xenograft tumour mouse models resulted in growth inhibition of the cancers.[50] Interestingly, mice that had received the knockdown treatment were found to be more viable than those which did not receive treatment and were healthier overall after reduction of ACSS2 activity. These results again strongly implicate ACSS2 as a potential drug target for cancers.

As a consequence of these promising early results into the activity of ACSS2 and its role in cancers, Prof. Eyal Gottlieb and Dr Zachary Schug at the Beatson Cancer Research Institute in Glasgow wished to further investigate this association in colorectal cancers using PET. Colorectal cancers are of relevance as free acetate **301** in the bloodstream is predominantly produced by fermentation of dietary fibre by gut bacteria. The close localisation of the tumours to the site of acetate **301** production is hypothesised to affect its metabolism in these types of tumours. Microarray data, similar to that used to identify links between ASCC2 expression in breast and prostate cancers has also revealed upregulation of ACSS2 in colorectal cancers. This upregulation was strongly associated with tumour stage, prompting further investigation into ACSS2 activity in colorectal cancers.[51]

Ideally, [^{11}C]acetate [^{11}C]-**301** would be used for this purpose, but [^{11}C]-based PET tracers were not available for use in Glasgow at the Beatson Cancer Research Institute at present. A variety of [^{18}F]-based tracers are already established at the facility, and we were approached to develop a synthesis of [^{18}F]fluoroacetate [^{18}F]-**1** as a surrogate for [^{11}C]acetate [^{11}C]-**301** for investigating ACSS2 activity *in vivo*.

5.3. Fluoroacetate

5.3.1. Fluoroacetate as a metabolic toxin

Fluoroacetate **1** is a potent toxin, found naturally in a number plant species, including *Dichapetalum cymosum*, from which fluoroacetate was initially isolated in 1943.[52,53] Fluoroacetate **1**, known commercially as "1080",[54] has found application as a vertebrate pesticide due to its high toxicity and low cost, however, the non-specificity of fluoroacetate **1** has led to increasing control measures and restrictions in the use of fluoroacetate **1** as a pesticide.[55]

The toxicity of fluoroacetate **1** arises from its incorporation into fluorocitrate **2** by the citric acid cycle enzymes (**Scheme 7**). It is firstly converted to fluoroacetyl coenzyme A **322** (fluoroacetyl CoA) by the action of acetyl CoA synthetase (ACSS). Citrate synthase then catalyses the condensation of fluoroacetyl CoA **322** and oxaloacetate **299** to produce (2*R*,3*R*)-fluorocitrate **2**.[56] (2*R*,3*R*)-Fluorocitrate **2**, the only toxic stereoisomer of fluorocitrate,[57] is then converted by aconitase to 4-hydroxy-*trans*-aconitate **324**, a product which is also a potent inhibitor of aconitase. The inhibition of aconitase shuts down the citric acid cycle, and downstream energy production ceases within cells. [58]

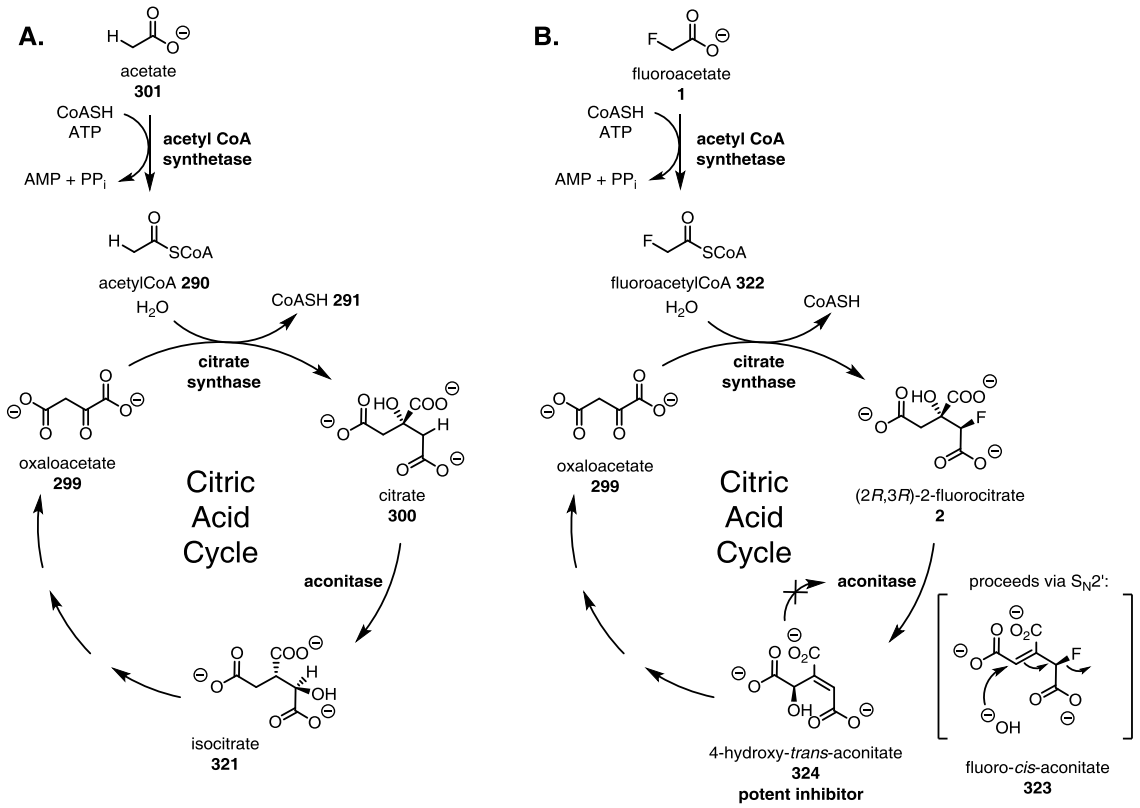

Scheme 7. **A.** Normal progression of the citric acid cycle showing condensation of acetyl CoA **290** with oxaloacetate **299** to give citrate **300** which is then converted to isocitrate **321** by aconitase. **B.** When fluoroacetate **1** enters the citric acid cycle as fluoroacetyl CoA **322**, (2*R*,3*R*)-fluorocitrate **2** is produced, which is converted to 4-hydroxy-*trans*-aconitate **324**, a potent inhibitor of aconitase.

5.3.2. Synthesis and applications of [^{18}F]fluoroacetate [^{18}F]-1

Despite fluoroacetate **1** being highly toxic (LD_{50} 0.1–5 mg.kg^{-1} in small mammals),[54] radiolabelled [^{18}F]fluoroacetate [^{18}F]-**1** has found wide scope in the literature as a tracer with applications in studying cerebral metabolism,[59,60] and imaging of prostate cancers.[61,62] The use of [^{18}F]fluoroacetate [^{18}F]-**1** arises as PET radiotracers are synthesised and administered in sub nano- and pico- molar quantities, levels well below the toxic threshold of fluoroacetate.

[^{18}F]Fluoroacetate [^{18}F]-**1** is most commonly synthesised by a S_N2 substitution of a suitably activated substrate with pre-dried [^{18}F]fluoride.[62,63] We were approached by the Beatson Institute due to previous research published by the St Andrews group where the product of the fluorinase enzyme reaction, 5′-fluoro-5′-deoxyadenosine **22** (FDA), was converted to fluoroacetate **1** *via* chromium(VI)-mediated Kuhn-Roth oxidation.[64] This procedure was successfully repeated with fluorinase generated [^{18}F]FDA [^{18}F]-**22**,

which, after Kuhn-Roth oxidation and purification, gave [^{18}F]fluoroacetate [^{18}F]-**1** in good yields, as shown in **Scheme 8**.

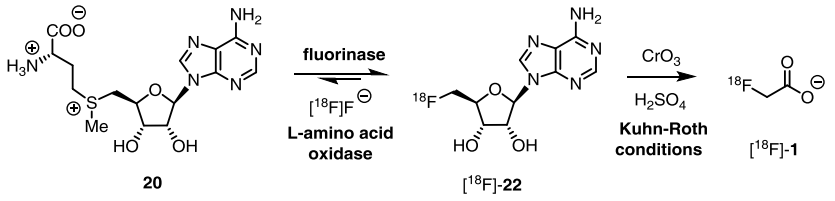

Scheme 8. Chemoenzymatic synthesis of [^{18}F]fluoroacetate [^{18}F]-**1** by an exhaustive oxidation of fluorinase-generated 5'-[^{18}F]fluoro-5'-deoxyadenosine [^{18}F]-**22**.

5.4. Aims

The reported chemoenzymatic synthesis of [^{18}F]fluoroacetate [^{18}F]-**1** using the fluorinase reported a 36 ± 11% (n = 4) decay corrected radiochemical yield (RCY). The total synthesis time was not reported, although reaction times were reported to be 1 h and 20 min respectively for the two synthetic steps. The radiochemical purity of the isolated [^{18}F]fluoroacetate [^{18}F]-**1** was found to be 96% by radio-HLPC. The [^{18}F]fluoroacetate [^{18}F]-**1** synthesised in that report was not employed in any PET imaging studies.

The aim of this project was to develop and optimise the [^{18}F]fluoroacetate [^{18}F]-**1** synthesis under site-specific conditions at the Beatson Institute in Glasgow. For this study, 50 MBq of [^{18}F]fluoroacetate [^{18}F]-**1** was required upon completion of the synthesis, starting from a maximum of 500 MBq [^{18}F]fluoride, a non-decay corrected RCY of 10%. The [^{18}F]fluoroacetate [^{18}F]-**1** was also required to be >98% radiochemically pure and to be free of chromate for formulation in sterile PBS for injection into a mouse model. We were interested in trialling this method for the production of [^{18}F]fluoroacetate [^{18}F]-**1** for imaging of breast and colorectal cancers in mice, as part of a larger study assessing metabolism of acetate **301** and ACSS2 activity in these of tumours.

In order for the synthesis to be viable, the scale and yield of the reactions needed to be addressed, along with an assessment of the purity of the final product and in a formulation suitable for injection.

5.5. Method development

5.5.1. Kuhn-Roth oxidation investigation

At the outset, the Kuhn-Roth oxidation was investigated under cold conditions, using a synthetic sample of the FDA **22**, prepared in a three-step sequence from adenosine **188**.

Adenosine **188** was protected as its 2',3'-acetonide **285** in the presence of perchloric acid, 2,2-dimethoxypropane (DMP) and acetone, in good yield as shown in Scheme **9**. Acetonide **285** was then heated in THF in the presence of tosyl fluoride (TsF) and tetrabutylammonium fluoride (TBAF) in a one-pot transformation of the 5'-alcohol to the corresponding 5-fluorinated acetonide **325** also in good yield. The acetonide **325** was then hydrolysed in a mixture of trifluoroacetic acid and water to yield the trifluoroacetate (TFA) salt of FDA **22** in moderate yield.

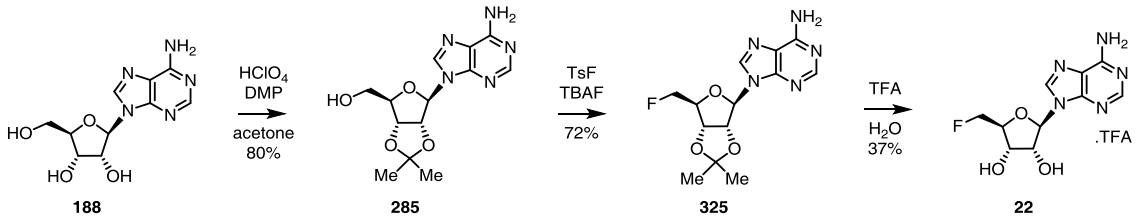

Scheme 9. Synthesis of FDA **22** from adenosine **188**.

A sample of FDA **22** was subjected to the Kuhn-Roth oxidation conditions as described by Li *et al.*[64] This chromium (VI)-mediated oxidation was expected to afford fluoroacetic acid **160**, which could be extracted from the acidic reaction mixture before being liberated as aqueous fluoroacetate **1** following base extraction, as illustrated below in **Scheme 10**.

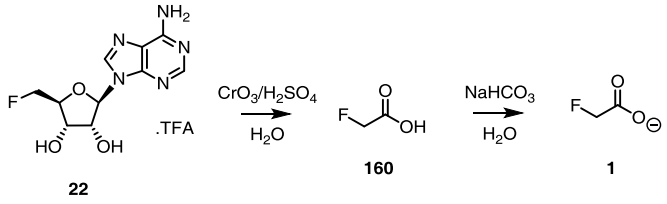

Scheme 10. Oxidation of FDA **22** to fluoroacetic acid **160**, followed by isolation as fluoroacetate **1**.

A freshly prepared solution of chromium (VI) oxide in sulfuric acid was added to a solution of FDA **22** in water and the mixture was heated to 140 °C for 10 minutes, before being cooled on ice. The mixture was carefully diluted with water, before the

aqueous phase was extracted with three portions of diethyl ether, in order to extract the newly formed fluoroacetic acid **160**. The ether extracts were combined, and extracted with aqueous sodium bicarbonate solution (8 $mg.ml^{-1}$) to liberate fluoroacetate **1** into the sodium bicarbonate solution, after separation of the two phases.

Under cold conditions, the reaction progress was monitored by ^{19}F NMR spectroscopy (**Figure 2**). In the $^{19}F\{^{1}H\}$ NMR spectrum, FDA **22** shows a resonance at −231.3 ppm (**Figure 2 A**), corresponding to the fluorine at C-5', while the peak for the trifluoroacetate counter ion appears at −75.7 ppm. After the oxidation and extraction process, the peak for FDA **22** is no longer present (**Figure 2 B**), but a new peak is present at −217.2 ppm in the $^{19}F\{^{1}H\}$ NMR spectrum. This peak appears as a triplet in the ^{19}F NMR spectrum (**Figure 2 C**), with a coupling constant of 42.8 Hz, typical for a $^{2}J_{FH}$ coupling. These data confirm that the Kuhn-Roth oxidation is efficient in converting all FDA **22** into fluoroacetate **1**, and produces no other detectable fluorinated by-products.

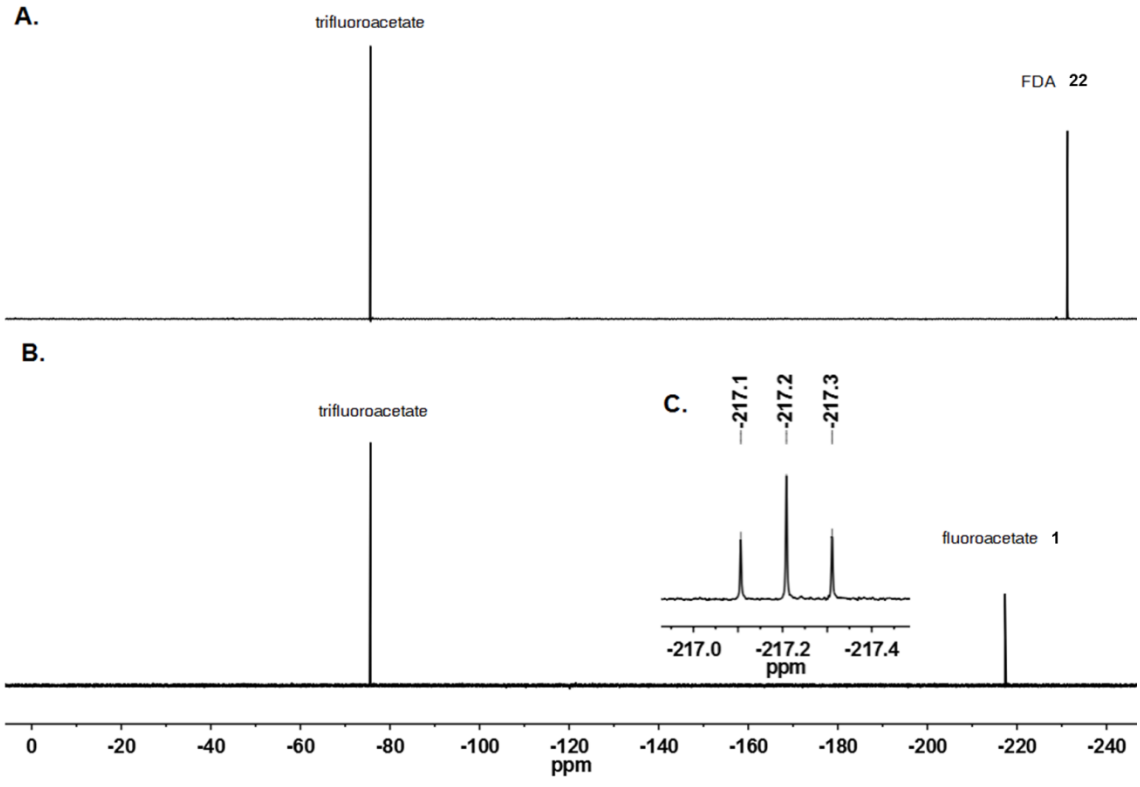

Figure 2. **A.** $^{19}F\{^{1}H\}$ NMR spectrum (470 MHz, D_2O) of the trifluoroacetate salt of FDA **22**. **B.** $^{19}F\{^{1}H\}$ NMR spectrum (470 MHz, D_2O) of the oxidation mixture after extraction, showing a single peak at 271.2 ppm. **C.** Partial ^{19}F NMR (470 MHz, D_2O) spectrum showing the fluoroacetate **1** triplet inset.

5.5.2. Enzymatic synthesis of [^{18}F]fluoroacetate [^{18}F]-1

The Kuhn-Roth oxidation was successful under "cold" conditions. The procedure was then transferred to "hot" conditions, where the fluorinase would be used to convert [^{18}F]fluoride and *S*-adenosylmethionine **20** (SAM) into [^{18}F]FDA [^{18}F]-**22**, after which oxidation would be expected to give [^{18}F]fluoroacetate [^{18}F]-**1** (**Scheme 11**).

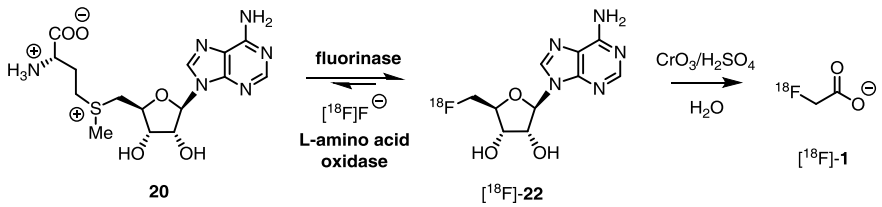

Scheme 11. [^{18}F]Fluoroacetate [^{18}F]-**1** synthesis from *S*-adenosylmethionine **20** using the fluorinase.

The fluorinase enzyme was over-expressed as described in **Chapter 2** and freeze-dried in 5 mg portions, each to be used for a single labelling experiment. Unlike conventional ^{18}F-labelling reactions, fluorinase-catalysed reactions do not require any pre-drying of the [^{18}F]fluoride ion prior to labelling. Accordingly, [^{18}F]fluoride in aqueous solution (0.3 mL, 83–269 MBq), was added to a premixed solution of the fluorinase enzyme (5 mg), SAM **20** (0.13 mg), L-AAO (L-Amino acid oxidase, 1 mg) in a total volume of 315 µL in an Eppendorf tube. L-AAO was also added to the freeze dried enzyme to oxidise any L-methionine **21** in the reaction mixture (present in commercial SAM **20** samples and produced during the fluorination reaction) to the corresponding oxo-acid **25** to shut down the reverse defluorination reaction, as shown in **Scheme 12**.

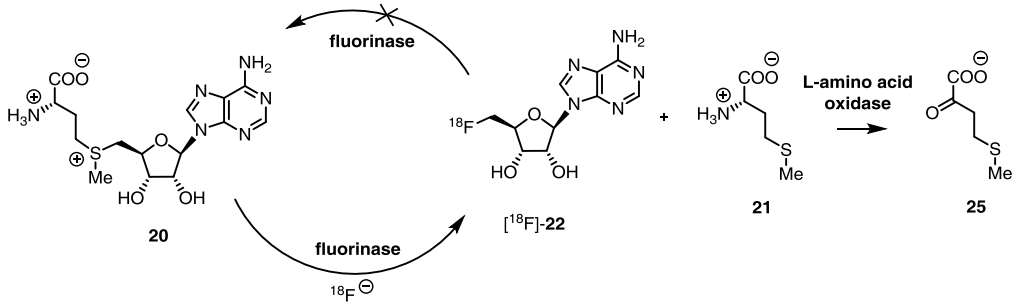

Scheme 12. L-AAO converts L-methionine **21** into the corresponding oxo-acid **25**, reducing the rate of the reverse reaction.

The reaction was allowed to proceed at 37 °C for 30 mins, before the enzyme was denatured (heating to 140 °C for 5 minutes) and centrifuged at 4500 rpm for 10 minutes. Radioactivity recovery after the centrifugation step was good, with

84% ± 4% (n = 3) of the activity recovered in the supernatant, with the remainder of the activity remaining trapped in the pellet.

An analytical sample of the supernatant was analysed by HPLC, using a hydrophilic interaction liquid chromatography (HILIC) column, with an ammonium bicarbonate/acetonitrile gradient, to assess [^{18}F]fluoride incorporation into [^{18}F]FDA [^{18}F]-**22**. This type of HILIC column is suited for the separation of highly hydrophilic compounds, such as fluoroacetate **1**. The incorporation of [^{18}F]fluoride (retention time, t_R = 19.0 min, into [^{18}F]FDA [^{18}F]-**22** (t_R = 5.6 min) was excellent (**Figure 3**), with an average incorporation of 95% ± 6% (n = 3). The identity of the two peaks was confirmed by spiking with [^{18}F]fluoride and [^{19}F]FDA **22** respectively. This result highlights the efficiency of the fluorinase in catalysing C–^{18}F bond formation, even at the low fluoride concentrations associated with PET labelling.

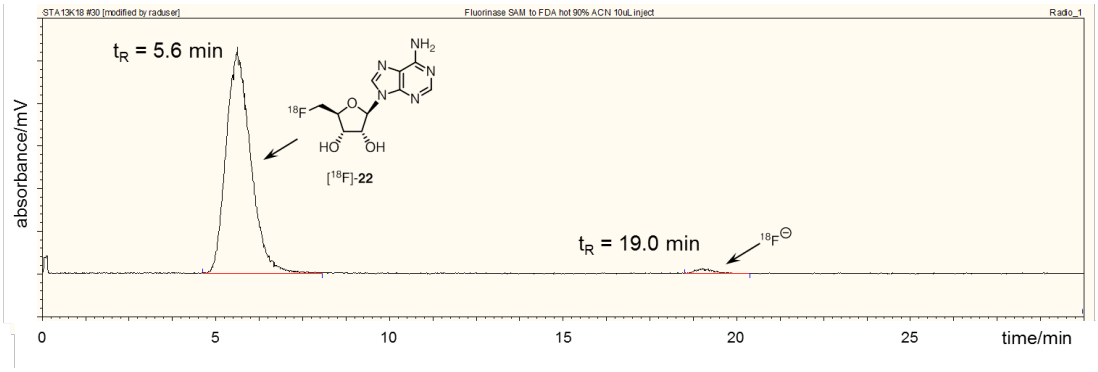

Figure 3. HILIC radio-HPLC trace of the supernatant from the enzymatic labelling reaction, showing 99% incorporation of [^{18}F]fluoride (t_R = 19.0 min) into [^{18}F]FDA [^{18}F]-**22** (t_R = 5.6 min).

The remainder of the supernatant, containing the bulk of [^{18}F]FDA [^{18}F]-**22** was added to 250 µL of a solution of chromium (VI) oxide in sulfuric acid in a sealed vial and this mixture heated to 140 °C for one hour, before being cooled on ice. The oxidation mixture was diluted with water (1 mL) and extracted into diethyl ether (5-6 × 1 mL), and the ether extracts were combined. In the strongly acidic oxidation mixture, [^{18}F]fluoroacetate [^{18}F]-**1** exists predominantly as [^{18}F]fluoroacetic acid [^{18}F]-**160**, which was previously found to extract efficiently into diethyl ether.

The extraction efficiency was investigated by measuring the activity extracted after each 1 ml ether extraction. In one experiment, the oxidation mixture was found to contain 115 MBq of activity prior to the extractions, and this extraction efficiency was determined by measuring the activity in the combined diethyl ether extracts after each extraction. The results are illustrated in **Figure 4** below. After six extractions, it was

found that 68% of the total activity was extracted, but that the total percentage activity extracted was reaching a plateau. Further extraction would likely not recover much more radioactivity, therefore 5 × 1 mL extractions were deemed to offer a reasonable recovery. Over three runs, the average extraction efficiency was found to be 74% ± 8% (n = 3).

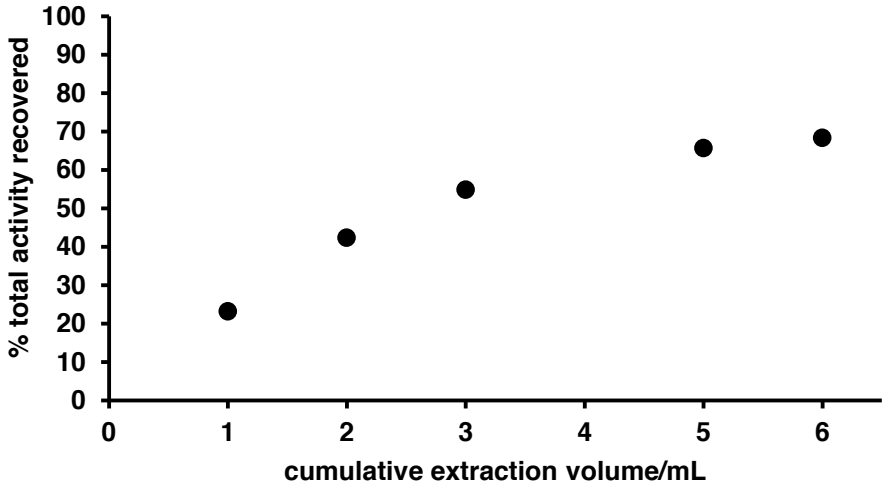

Figure 4. Extraction efficiency of diethyl ether extractions of acidic oxidation mixture, showing cumulative activity extracted after each 1 mL extraction of the acidic oxidation mixture with diethyl ether.

The ether extracts were yellow in colour, likely due to extraction of traces of aqueous Cr(VI) into the diethyl ether. The original protocol developed by Li *et al.*[64] suggested the passage of this ether extract through a Sep-Pak Si Light cartridge in order to remove adventitious chromate, sulfate or other ion contaminants. However, upon passage of the solution through a Sep-Pak Si Light cartridge, the diethyl ether eluent, which contained the bulk of the activity, remained pale yellow in colour.

An aliquot of this diethyl ether solution was extracted with sodium bicarbonate solution (0.25 mL, 8 $mg.mL^{-1}$). The basic sodium bicarbonate solution converts the [^{18}F]fluoroacetic acid [^{18}F]-**160**, which is soluble in diethyl ether, into [^{18}F]fluoroacetate [^{18}F]-**1**, which should be soluble in the aqueous sodium bicarbonate solution. The majority (61%) of the activity was isolated in the aqueous phase after the extraction with the sodium bicarbonate solution, while the remainder was found in the diethyl ether fraction. The non-decay corrected yield of isolated [^{18}F]fluoroacetate [^{18}F]-**1** was found to be 23% ± 17% (n = 2).

The sodium bicarbonate extract was analysed by HPLC, using the HILIC Fast Acid system described above, in order to assess the radiochemical purity of the final [^{18}F]fluoroacetate [^{18}F]-**1**. As can be seen from **Figure 5**, there appears a single large peak in the chromatogram at t_R = 8.4 minutes, which corresponds to [^{18}F]fluoroacetate [^{18}F]-**1**, showing a very high (>99%) radiochemical purity. A small trace of [^{18}F]fluoride was detected (t_R = 20.2 min), but accounted for less than 1% of the total activity in the final sample. Spiking the sample with 10 mM fluoroacetate **1** confirmed that the radiolabelled product was indeed [^{18}F]fluoroacetate [^{18}F]-**1**.

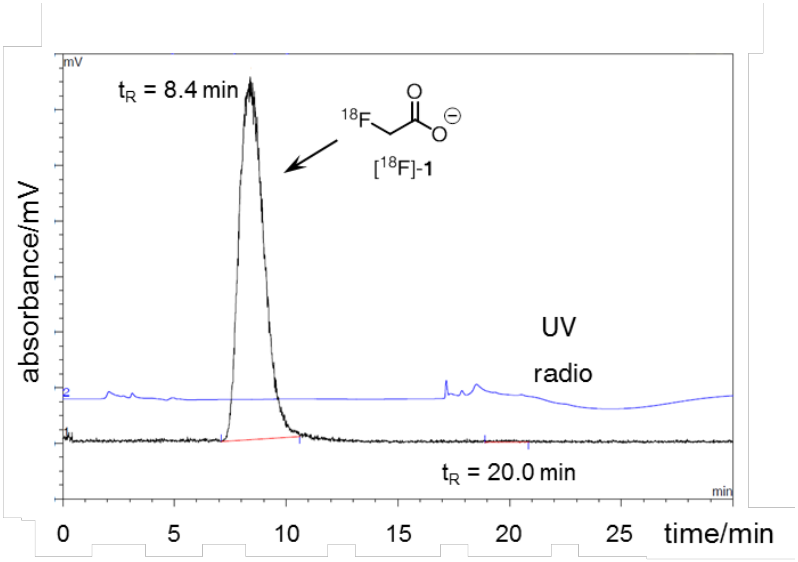

Figure 5. Radiochemical and UV chromatograms obtained after isolation of [^{18}F]fluoroacetate [^{18}F]-**1**, showing greater than 99% radiochemical purity of the final product.

In effort to remove the coloured impurity, a second aliquot of the diethyl ether containing [^{18}F]fluoroacetic acid [^{18}F]-**160** was passed through an alumina N Sep-Pak cartridge, which effectively retained the [^{18}F]fluoroacetic acid [^{18}F]-**160**. The product was eluted as [^{18}F]fluoroacetate [^{18}F]-**1** by passing 0.5 mL phosphate buffered saline (PBS) solution through the cartridge. However, this alternative solid phase extraction procedure did not prevent leakage of the yellow contaminant into the final solution.

While the radiochemical purity of the final product was high, leakage of chromate through the Sep-Pak Si Light and alumina N cartridges and the associated yellow colour of the final product was a concern. The final product was most likely contaminated with Cr(VI), and as a consequence was not ideal for *in vivo* injection into a mouse model.

In view of the fact that [^{18}F]fluoroacetate [^{18}F]-**1** was still required for the imaging study, the chemical synthesis of [^{18}F]fluoroacetate [^{18}F]-**1** by a method that does not utilise Cr(VI) was investigated.

5.5.3. Chemical synthesis of [^{18}F]fluoroacetate [^{18}F]-1

Literature syntheses of [^{18}F]fluoroacetate [^{18}F]-**1** involve an S_N2 reaction on an appropriately substituted acetate ester such as tosylate **327** or mesylate **49**, followed by hydrolysis of the fluorinated ester **328**. This is illustrated in **Scheme 13**.

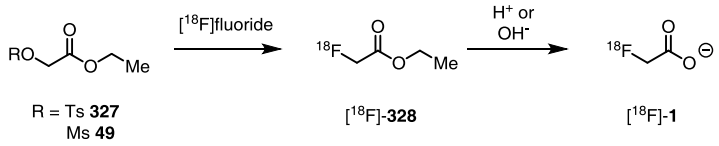

Scheme 13. [^{18}F]Fluoroacetate [^{18}F]-**1** synthesis by S_N2 substitution followed by hydrolysis, reported by Kang *et al.*[63] and Welch *et al.*[62]

Kang *et al.*[63] reported the synthesis of [^{18}F]fluoroacetate [^{18}F]-**1** from both *O*-mesyl **49** and *O*-tosyl **327** derivatives of ethyl glycolate. Incorporation of [^{18}F]fluoride was higher for ethyl *O*-mesylglycolate **49** as the substrate, in the presence of tetrabutylammonium bicarbonate in acetonitrile. Following hydrolysis of the ester with KOH, [^{18}F]fluoroacetate [^{18}F]-**1** was purified by trapping on an ion exchange resin, and elution through an alumina N cartridge (to trap residual [^{18}F]fluoride) with sodium bicarbonate solution and water to give [^{18}F]fluoroacetate [^{18}F]-**1** in 24.5% radiochemical yield (RCY).

Welch *et al.*[62] reported a synthesis from ethyl *O*-mesylglycolate **49**, using Kyrptofix 222 and potassium carbonate combination in acetonitrile. In contrast to Kang *et al.*'s method, they chose to purify the ethyl [^{18}F]fluoroacetate [^{18}F]-**328** by trapping on a Waters HLB cartridge (a reverse phase system with affinity for both lipophilic and polar molecules) and washing with water to remove unreacted [^{18}F]fluoride. Ethyl [^{18}F]fluoroacetate [^{18}F]-**328** was then eluted from the cartridge with ethanol before being hydrolysed by addition of NaOH, with concomitant ethanol removal under reduced pressure. Neutralisation and dilution into water gave a formulation of [^{18}F]fluoroacetate [^{18}F]-**1**, suitable for injection, in 55% decay corrected RCY.

Other syntheses of [^{18}F]fluoroacetate [^{18}F]-**1** have also been reported by Fujibayashi *et al.,*[65] Yeung *et al.,*[66] and Wuest *et al.*,[67] however, these involve automated synthesis platforms, suitable for working with high amounts of activity, or employ equipment not available to us in the Beatson Laboratory.

The small animal imaging facility based at the Beatson Cancer Research Institute in Glasgow requires delivery of 50 MBq of [^{18}F]fluoroacetate [^{18}F]-**1** in 0.5 mL of a sterile solution, suitable for injection. This activity and volume requirement restricts synthesis options, as the maximum activity that can be safely handled at the manual synthesis facility is 500 MBq. Both the Kang[63] and Welch[62] procedures involve delivery of high activities of [^{18}F]fluoroacetate [^{18}F]-**1** into large volumes (*e.g.* 5 mL), and delivery of activity into this volume is not suitable for this study.

This required modification of the literature methods, specifically to address the formulation into 0.5 mL. A potential solution involved combining a reported chemical synthesis with the work up and formulation procedure from the enzymatic synthesis, as this had the capability to deliver [^{18}F]fluoroacetate [^{18}F]-**1** in a small volume.

The precursor, ethyl *O*-mesylglycolate **49** was synthesised by reaction of ethyl glycolate **329** with mesyl chloride in the presence of triethylamine. The crude product was purified by distillation under reduced pressure to give ethyl *O*-mesylglycolate **49** as a colourless oil in 54% yield (**Scheme 14**). With the precursor in hand, attention turned to the synthesis of [^{18}F]fluoroacetate [^{18}F]-**1** using the more common S_N2 approach.

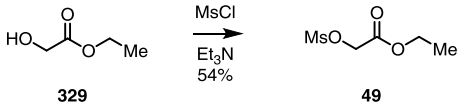

329 **49**

Scheme 14. Synthesis of ethyl *O*-mesylglycolate **329** from ethyl glycolate **49**.

[^{18}F]Fluoride is supplied as a dilute solution in water, therefore the synthesis began by azeotropic distillation and removal of the water by dilution into an acetonitrile solution of potassium carbonate and Kryptofix 222 and heating under a stream of argon. The [^{18}F]fluoride was dried further by addition and subsequent distillation of three portions of anhydrous acetonitrile to give [^{18}F]fluoride as the potassium-Kryptofix 222 salt [^{18}F]-**45**. The salt was taken up into an anhydrous acetonitrile solution of ethyl *O*-mesylglycolate **49** and heated in a sealed vial at 100 °C for 5 minutes to furnish ethyl [^{18}F]fluoroacetate [^{18}F]-**328**, as summarised in **Scheme 15**.

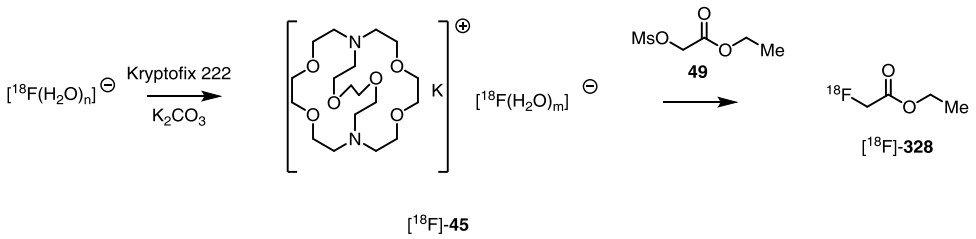

Scheme 15. Azeotropic drying of [^{18}F]fluoride, where n>m, and reaction with ethyl *O*-mesylglycolate **49** to give ethyl [^{18}F]fluoroacetate [^{18}F]-**328**.

After transfer of the reaction solution to a new vial and rinsing of the reaction vial with water, a sample of the mixture was taken for HPLC analysis using the same HILIC conditions described above. The radio-HPLC trace of this sample (**Figure 6**) showed two products (t_R = 3.46 min and t_R = 8.18 min), along with residual [^{18}F]fluoride (t_R = 18.9 min). The incorporation of [^{18}F]fluoride was generally very good (81% ± 20%, n = 8). The larger peak at t_R = 3.46 min was identified as ethyl [^{18}F]fluoroacetate [^{18}F]-**328**, while the smaller peak with t_R = 8.18 min was found to have a retention time identical to that of [^{18}F]fluoroacetate [^{18}F]-**1**. The presence of [^{18}F]fluoroacetate [^{18}F]-**1** is most probably due to the addition of water to the reaction mixture, leading to basic hydrolysis of [^{18}F]-**328** to give [^{18}F]fluoroacetate [^{18}F]-**1**.

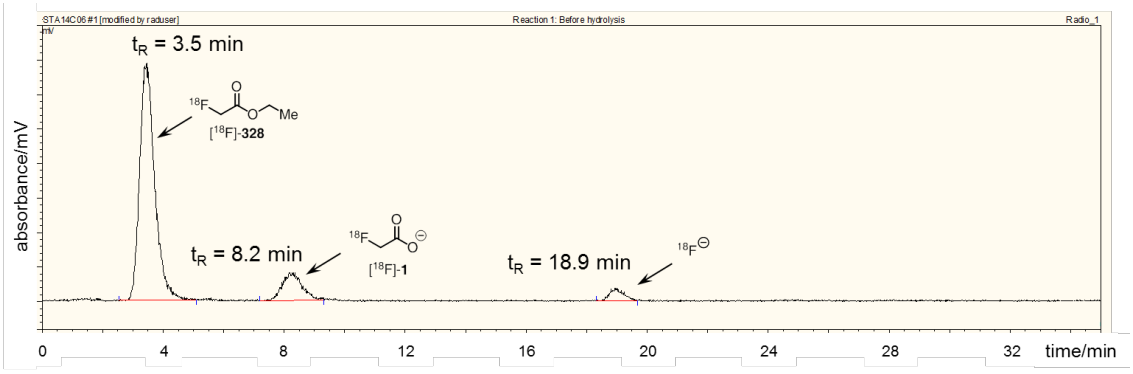

Figure 6. Radio-HPLC trace of the reaction mixture after 5 min heating and dilution with water, showing the presence of ethyl [^{18}F]fluoroacetate [^{18}F]-**328**, [^{18}F]fluoroacetate [^{18}F]-**1** produced by hydrolysis, and residual [^{18}F]fluoride.

Ester hydrolysis was completed by dilution with water and addition of 1 M NaOH solution, and the mixture warmed to 40 °C for 5 minutes. Radio-HPLC analysis (**Figure 7**) showed that all of the ethyl [^{18}F]fluoroacetate [^{18}F]-**328** had been hydrolysed to [^{18}F]fluoroacetate [^{18}F]-**1**. Residual [^{18}F]fluoride was also observed in the mixture, along with a minor unknown fluorinated product (t_R = 3.8 min).

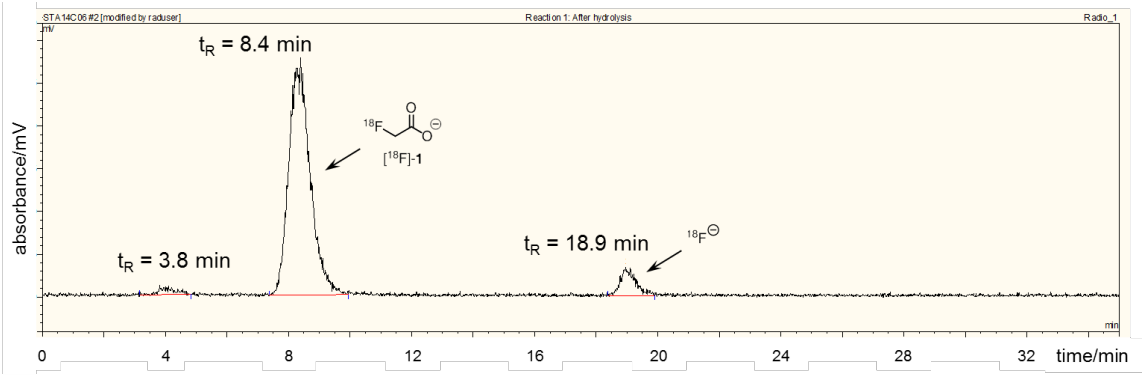

Figure 7. Radio-HPLC of the reaction mixture post-hydrolysis showing [^{18}F]fluoroacetate [^{18}F]-**1** as the predominant species, residual [^{18}F]fluoride, and an additional unknown fluorinated compound with t_R = 3.8 min.

With a crude mixture of [^{18}F]fluoroacetate [^{18}F]-**1** in hand, attention turned to its purification using the extraction protocol described in the enzymatic synthesis. The basic reaction mixture was acidified with 1 M H_2SO_4 generating [^{18}F]fluoroacetic acid [^{18}F]-**160** which was extracted into diethyl ether. Extraction efficiencies were slightly lower than those observed in the fluorinase-based synthesis (67% *vs* 74% respectively). This decrease may be due to variation in the pH of the aqueous phase between the two methods.

The ether extracts containing [^{18}F]fluoroacetic acid [^{18}F]-**160** were passed through a Si Sep-Pak cartridge to remove any residual water and associated ions from the mixture. In order to formulate and deliver the product into phosphate buffered saline (PBS), [^{18}F]fluoroacetic acid [^{18}F]-**160** was extracted directly into a small volume of PBS (pH 7.4). The PBS would convert the ether-soluble [^{18}F]fluoroacetic acid [^{18}F]-**160** (pK_a 2.59) to water soluble [^{18}F]fluoroacetate [^{18}F]-**1,** which would be extracted into the PBS.

Upon trialling this work up procedure, however, [^{18}F]fluoroacetic acid [^{18}F]-**160** was adsorbed from the diethyl ether onto the Si Sep-Pak in some experiments, rather than eluting through the cartridge as expected. This behaviour was not predictable or reproducible. The combination of traces of water in the ether extracts and the acidic nature of silica-based solid phases may result in the radiolabelled product partitioning as either [^{18}F]fluoroacetic acid [^{18}F]-**160** or [^{18}F]fluoroacetate [^{18}F]-**1**, and subsequently behaving differently on the stationary phase, depending on the exact conditions of each extraction. In cases when the [^{18}F]fluoroacetate [^{18}F]-**1** was retained on the cartridge, it was eluted simply with 0.5 mL of PBS, as required for the study. In search of a repeatable procedure, an alternative to the Si Sep-Pak was investigated.

Changing from a silica based Sep-Pak cartridge to a neutral alumina (Alumina N) Sep-Pak led to reproducible behaviour of the [^{18}F]fluoroacetate [^{18}F]-**1**, which was now consistently trapped on this type of cartridge. The [^{18}F]fluoroacetate [^{18}F]-**1** could be eluted from the Alumina N Sep-Pak with 0.5 mL PBS, through a sterile 0.22 µm filter, and into a vial for administration to the animals for the study.

Radio-HPLC of the final solution for injection (**Figure 8**) showed that the primary product was [^{18}F]fluoroacetate [^{18}F]-**1** (t_R = 8.3 min) that had been isolated in 99% ± 1% (n = 9) radiochemical purity (RCP). There was evidence of trace amounts of the unknown by-product (t_R = 4.1 min) in the final sample, however at low enough levels that the product still passed the minimum RCP requirements (>97%).

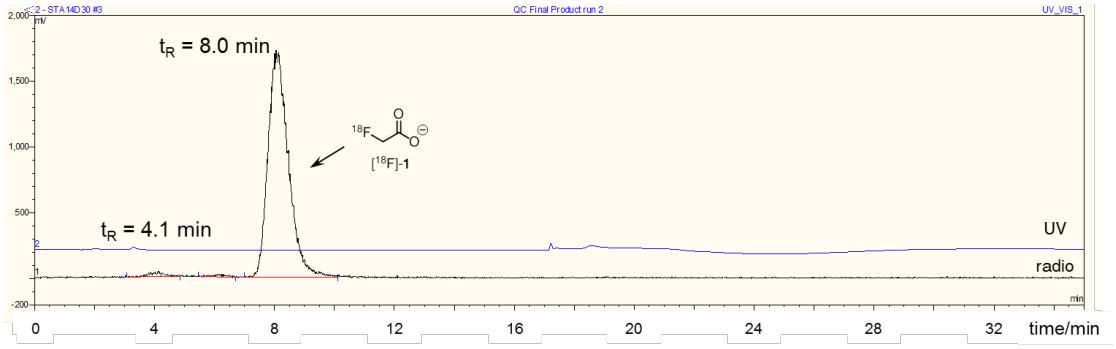

Figure 8. Radio-HPLC of [^{18}F]fluoroacetate [^{18}F]-**1**, after elution from an alumina column, showing >98% radiochemical purity for this sample. Overlay is the UV trace at 210 nm, which also shows reveals no other detectable UV active impurities.

The non-decay corrected radiochemical yield for the synthesis of [^{18}F]fluoroacetate [^{18}F]-**1** was 18% ± 7% (n=8). Considering the limitations with the amount of activity available to work with, these yields provided access to sufficient activity (33 MBq in the lowest yielding preparative experiment to 111 MBq in the highest), of [^{18}F]fluoroacetate [^{18}F]-**1**, delivered in 0.5 mL PBS, and suitable for use in tumour models in mice.

5.6. Imaging of ACSS mouse model

[^{18}F]Fluoroacetate [^{18}F]-**1** was synthesised for an imaging study aimed to investigate ACSS2 activity in tumours in knockout mouse models, and to establish if the tumours were responsive to ACSS2 gene-silencing. The imaging protocol was also intended for use as an *in vivo* pharmacodynamic biomarker for developing potential therapeutics. Towards these aims, two PET imaging investigations were undertaken.

Initially, the behaviour of [^{18}F]fluoroacetate [^{18}F]-**1** in a healthy control mouse, was contrasted with the behaviour of [^{18}F]fluoroacetate [^{18}F]-**1** in a diseased mouse (*Apc$^{Min/+}$* line, bearing 70+ small intestinal tumours and colorectal tumours).[68] These experiments were designed to establish an imaging protocol in the mice and to determine optimal imaging parameters for [^{18}F]fluoroacetate [^{18}F]-**1**. These experiments were also expected to offer information about [^{18}F]fluoroacetate [^{18}F]-**1** uptake in healthy *vs* disease models.

Following these experiments, the study would move to a breast cancer xenograft, ACSS2 knockout model to evaluate whether RNAi (RNA interference) gene silencing of ACSS2 affects uptake of [^{18}F]fluoroacetate [^{18}F]-**1** in the tumours.

Dr Zachary Schug and Dr Eyal Gottlieb, of the Beatson Institute for Cancer Research, who were leading the ACSS2 investigation provided the mice for the study, while imaging acquisitions and data analysis were conducted at the institute by Dr Gaurav Malviya and Agata Mrowinska.

5.6.1. Assessment of [^{18}F]fluoroacetate [^{18}F]-1 in healthy and *Apc$^{Min/+}$* models

[^{18}F]Fluoroacetate[^{18}F]-**1** was administered to a healthy mouse, which was imaged under dynamic scanning conditions to investigate the kinetics of tracer uptake *in vivo* and to establish optimal time points for static imaging in the disease model. The mouse was injected intravenously with [^{18}F]fluoroacetate [^{18}F]-**1** (5.41 MBq) and a 2 hour dynamic PET scan was acquired, along with a CT (computerised tomography) scan, for correcting for attenuation and providing anatomical detail.

The CT scan and PET scan snapshot from the 2 hour dynamic scan for the healthy control are shown below in **Figure 9**. The PET images (**Figure 9 A**, **B a**nd **C**) show the tracer excretion *via* the urinary system, with activity accumulating in the kidneys and bladder (largest region of activity at this time point). This mode of excretion is well established for [^{18}F]fluoroacetate [^{18}F]-**1**.[62,69] Also evident from the PET scan is activity uptake in the bone (seen as high density regions in the CT scan, **Figure 9 D**, **E** and **F**), resulting from metabolism of [^{18}F]fluoroacetate [^{18}F]-**1** to [^{18}F]fluoride, a degradation product which has high affinity for calcium present in the bone.[62]

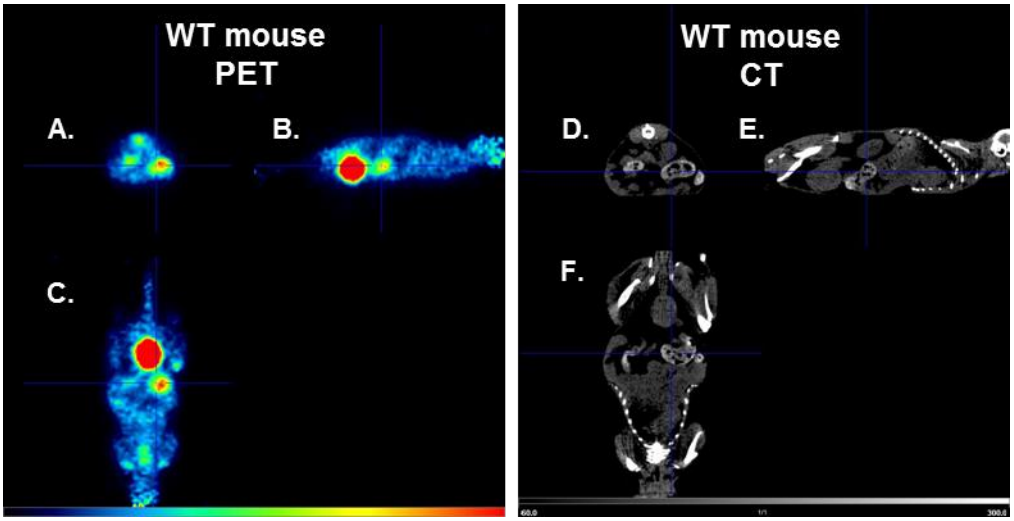

Figure 9. PET scan of a healthy mouse through the **A.** transverse, **B.** sagittal and **C.** coronal planes, and the corresponding CT images (**D.**, **E.** and **F.** respectively). The large hotspot in B and C corresponds to excretion through the bladder. The smaller hotspot (right of the bladder in B, lower right of the bladder in C) was unexpected. Bone uptake is also observed along the vertebrae, and in the fore- and hindquarters. Images acquired by Dr Gaurav Malviya and Agata Mrowinska.

Unexpectedly, a second area in the abdomen (superior to the bladder) showed increased uptake of [^{18}F]fluoroacetate [^{18}F]-**1**, and this uptake was consistently higher than the surrounding tissues throughout the duration of the PET scan. It was initially thought that this might be a tumour. The corresponding region in the CT scan and *post mortem* dissection of the mouse revealed no abnormal structures, and suggested that activity appeared to be accumulating in the cecum, the proximal region of the large intestine. In herbivores, the cecum contains large numbers of bacteria which assist in the breakdown of plant material. The broader focus of this study on ACSS2 expression in colon and breast cancers, means that non-specific uptake in the intestinal area of a healthy control, was problematic if this is repeated in the disease models.

The dynamic scan showed that optimal uptake in the caecum was 60 minutes post injection, and subsequent static imaging experiments in the disease model mice were acquired near this time point.

Two diseased *Apc*$^{Min/+}$ mice were administered with [^{18}F]fluoroacetate [^{18}F]-**1** (4.49 MBq each, one intravenously, one intraperitoneally due to poor condition of the mouse). These mice were imaged after 45 min and 90 min respectively, under static scanning conditions with 10 min PET acquisitions, followed by a CT acquisition, with the images shown in **Figure 10**. The second mouse died during the scanning period, but due to the 90 minute accumulation window, the PET data were still representative of uptake and distribution during the time the mouse was alive.

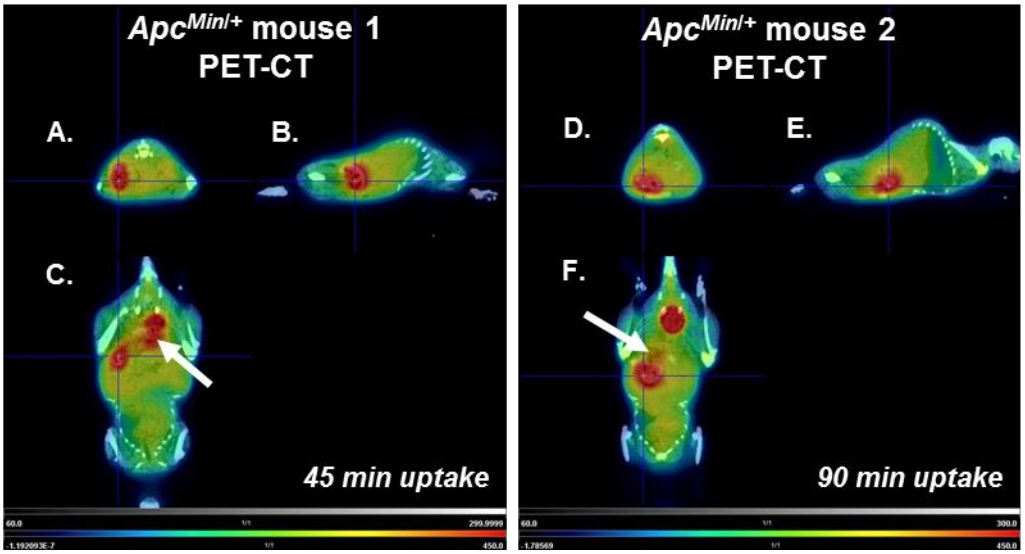

Figure 10. Overlaid PET-CT images of the two *Apc*$^{Min/+}$ mice, acquired after 45 minutes uptake (left) and 90 minutes uptake (right), through the transverse (**A**,**D**), sagittal (**B**,**E**) and coronal (**C**,**F**) planes. Evident in both scans is an area of high accumulation of tracer in the bowel region, corresponding to uptake in the caecum. Additional area of higher than background uptake (white arrows) are also observed. Images acquired by Dr Gaurav Malviya and Agata Mrowinska.

[^{18}F]Fluoroacetate [^{18}F]-**1** accumulated in the cecum of the *Apc*$^{Min/+}$ in both the 45 min and 90 min uptake mice, and uptake of activity in bone and bladder was also evident. This distribution was similar to that observed in the wild type mouse. In both scans, there appeared to be slightly increased general uptake in the bowel area (white arrows). As this model lacked large, well-defined tumours, it was difficult to assign this increased uptake specifically to the multiple small tumours in the small intestine and colon. The presence of the tracer in the caecum of the *Apc*$^{Min/+}$ was confirmed after the mice were culled by removing the small intestine and colon, and imaging these in the PET scanner (**Figure 11**).

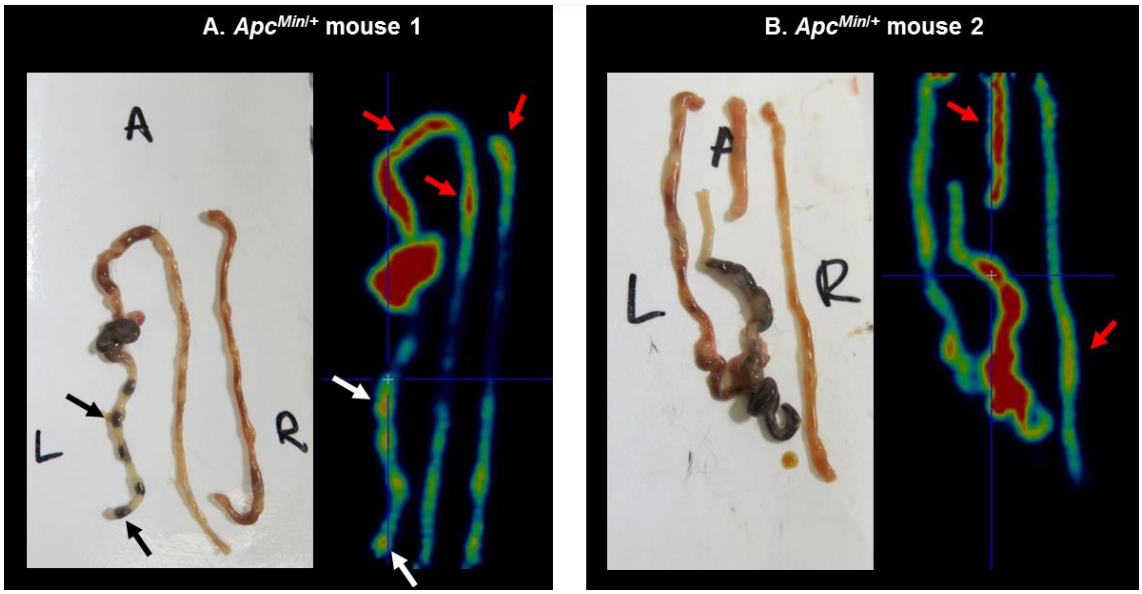

Figure 11. Image and PET scan of the small intestine and colon of the *Apc*$^{Min/+}$ mice after **A.** 45 min uptake and **B.** 90 min uptake. Both scans show high activity in the caecum, along with other areas throughout the intestine, possibly areas of tumour activity (red arrows). Activity is also observed associated with faecal pellets (black and white arrows). Images acquired by Dr Gaurav Malviya and Agata Mrowinska.

In the intestines of both *Apc*$^{Min/+}$ mice, high tracer accumulation was observed in the caecum. Biliary excretion of [^{18}F]fluoroacetate [^{18}F]-**1** has been reported previously,[69] but interestingly, high activity concentrations are observed associated with faecal pellets in the colon in the mouse which received [^{18}F]fluoroacetate [^{18}F]-**1** intravenously (black and white arrows, **Figure 11**). This region is distal from where bile enters the digestive tract and activity here is unlikely to be associated with biliary excretion. This suggests the presence of a mechanism whereby the tracer is absorbed from the blood across the lower intestinal wall and concentrated in the faecal pellets, possibly under the action of gut bacteria. Also evident from the images are other areas within the small intestine which also show high activity accumulation (red arrows, **Figure 11**). These areas do not appear to be associated with the caecum or faeces and are thought to be areas of tumour activity.

Non-tumour associated [^{18}F]fluoroacetate [^{18}F]-**1** uptake in the abdomen area is potentially problematic for investigating breast and colorectal cancers in mouse models as it would obscure the observation and quantification of uptake into areas of tumour activity. A xenograft model was therefore proposed for these investigations.

5.6.2. Xenograft breast cancer model

Breast cancer BT474 ER^+/HER^+ xenografts were proposed to investigate the difference in uptake of [^{18}F]fluoroacetate [^{18}F]-**1** in the tumours in control mice, and in mice where the ACCS2 gene was silenced in the xenograft by a doxycycline (DOX) induced siRNA system. The experiment was designed to assess the suitability of a [^{18}F]fluoroacetate-based imaging experiment for use as an *in vivo* biochemical marker for acetate consumption, reflective of ACSS2 activity, towards investigating ACSS2 as a possible therapeutic target.

The imaging time point in the xenograft study was determined by performing a dynamic PET scan in a mouse bearing a xenograft breast cancer tumour on its right flank. After injection of a 5.43 MBq dose of [^{18}F]fluoroacetate [^{18}F]-**1**, tracer uptake was monitored in the tumour over 2 hours to determine the maximum uptake time point.

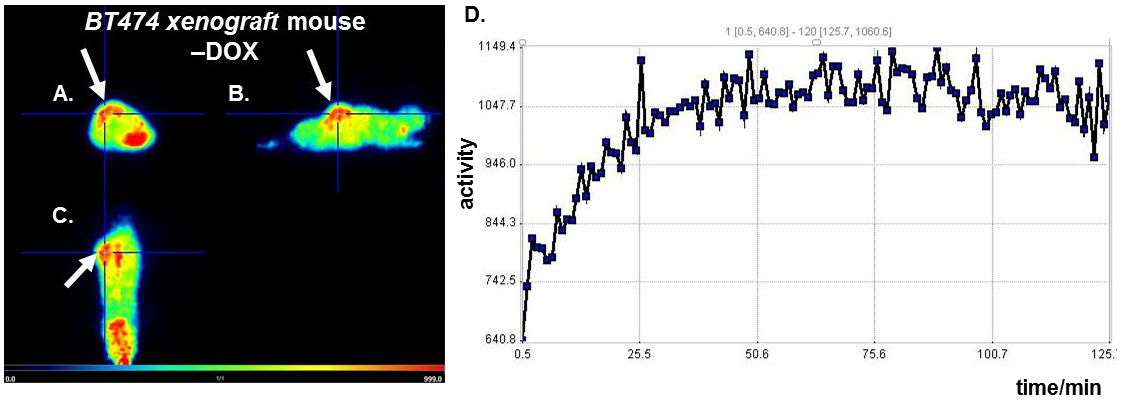

Figure 12. PET images through **A.** transverse, **B.** sagittal and **C.** coronal sections of a mouse bearing a BT474 xenograft tumour on the right flank (white arrows), showing increase uptake in the tumour. **D.** Maximal uptake curve shows steady accumulation of the tracer in the tumour region, reaching a maximum after approximately 45 min. Images and data acquired by Dr Gaurav Malviya and Agata Mrowinska.

The PET images shown in **Figure 12 A–C**, left, show increased uptake of [^{18}F]fluoroacetate [^{18}F]-**1** in the tumour, located on the upper right flank (white arrow) relative to background. Maximum uptake was observed 45 minutes post-injection (**Figure 12 D**). Subsequent static scans were therefore acquired 45 minutes post injection. [^{18}F]Fluoroacetate [^{18}F]-**1** accumulated in the caecum and bladder, as observed in the previous PET imaging experiments in the healthy and *Apc*$^{Min/+}$ mice, while defluorination and accumulation of [^{18}F]fluoride in the bone was also observed.

[^{18}F]Fluoroacetate [^{18}F]-**1** imaging was then used to determine whether doxycycline-induced (DOX) gene silencing affected acetate uptake in two groups of nude Balb/c

mice bearing xenograft tumours (BT 474 ER^+/HER^+ type) (2 per group). One group was exposed to DOX (+DOX), and the second not (−DOX). The mice were each injected with a dose of [^{18}F]fluoroacetate [^{18}F]-**1**, and imaged in the PET scanner 45 minutes post injection. DOX exposure initiates gene silencing of ACSS2 *via* RNA interference (RNAi) in this model, reducing the expression of ACSS2 within the tumour cells. Mice not exposed to DOX will have basal levels of ACSS2 expression within the tumour cells.[50]

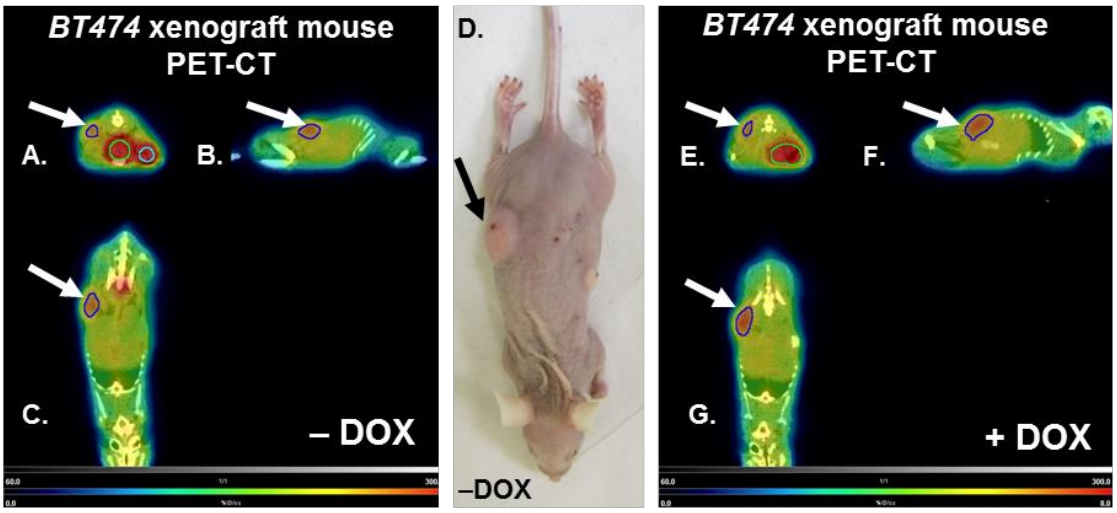

Figure 13. PET-CT image of a −DOX mouse bearing a breast cancer xenograft tumour on the right flank (white arrow), through **A.** transverse, **B.** sagittal and **C.** coronal sections. **D.** Image of the nude Balb/c mouse showing a breast cancer xenograft tumour on the right flank (black arrow). PET-CT image of a +DOX mouse with the same tumour type xenograft (white arrow), through **D.** transverse, **E.** sagittal and **F.** coronal sections. Images acquired by Dr Gaurav Malviya and Agata Mrowinska.

In both +DOX and –DOX mice, uptake of [^{18}F]fluoroacetate [^{18}F]-**1** into the xenograft tumour is observed in the PET images, as shown in **Figure 13 A–C** and **E–G**. Accumulation of [^{18}F]fluoroacetate [^{18}F]-**1** is also observed in the caecum, with excretion through the urinary system and accumulation in the bladder. Uptake is quantified by measuring the standardised uptake value (SUV, **Equation 1**), a measure of activity in a particular region (measured from the PET image) or organ of interest (from post mortem gamma counting) per unit weight of the organ at time *t*, as a function of total injected activity per unit body weight.

$$SUV = \frac{activity\ in\ organ\ at\ time\ t}{\left(\frac{total\ activity\ injected}{body\ weight}\right)} \qquad \textbf{Eq.1}$$

Maximum standard uptake value (SUV_{max}) in the tumours and caeca were calculated from the uptake maxima in regions of interest in the PET images in the –DOX and

+DOX mice after 45 minutes (**Figure 14**). The data show that average SUV_{max} for [^{18}F]fluoroacetate [^{18}F]-**1** in the caecum is higher than uptake into the tumours. The ratio of the SUV between the tumours and the heart or liver (as reference organs) shows that uptake into the tumours is marginally greater than the reference organs, by a factor of about 1.3.

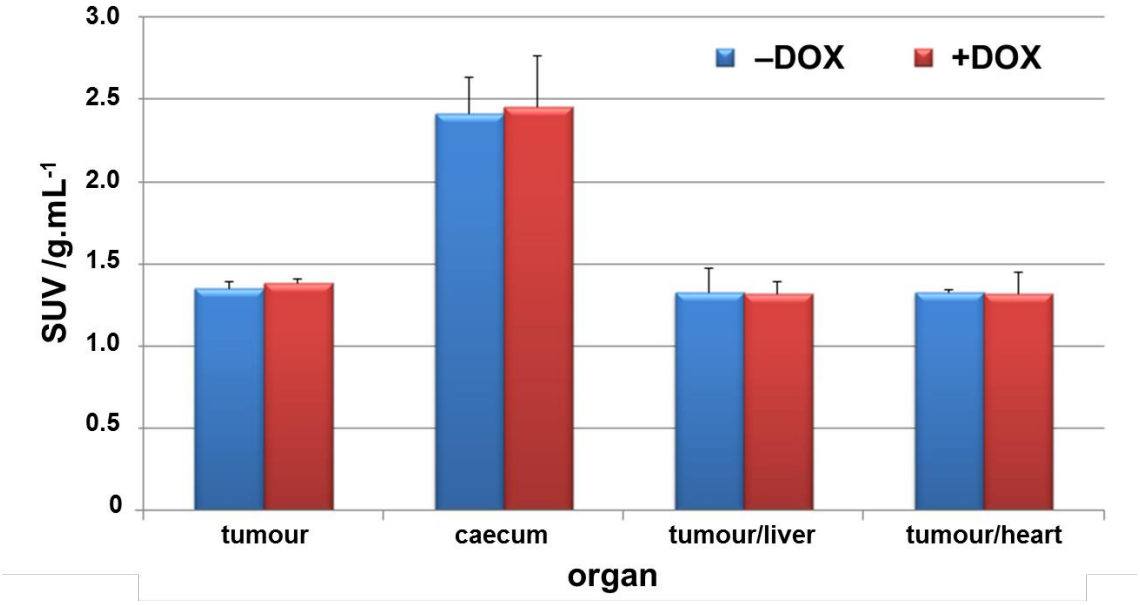

Figure 14. Maximum standard uptake values (SUV_{max}) in the tumours and caeca in the two groups of mice (–DOX and +DOX), along with ratio of SUV_{max} in the areas of interest compared to the liver and heart. Data compiled by Dr Gaurav Malviya and Agata Mrowinska.

The difference in average SUV_{max} in the tumours between the –DOX and +DOX groups is within the standard deviation of the two groups. The +DOX group, which would be expected to have lower functional ACSS2 levels in the tumour as a result of doxycycline induced gene silencing, has similar uptake of [^{18}F]fluoroacetate [^{18}F]-**1** compared to tumours from the –DOX group. At this time point (45 minutes), [^{18}F]fluoroacetate [^{18}F]-**1** uptake appears independent of ACSS2 levels within the tumour cells, suggesting that another mechanism may be operating which controls uptake and accumulation of [^{18}F]fluoroacetate [^{18}F]-**1** in the cells.

The average SUV for all organs for the –DOX and +DOX groups, assessed *post mortem*, is shown in **Figure 15**. SUV is highest in the faeces, trachea, large bowel and bone. No difference in SUV is discernible between the two groups. Faecal and large bowel uptake were observed in the PET images, however measurement of SUV shows that the activity uptake is largely associated with faecal matter, supporting the hypothesis that [^{18}F]fluoroacetate [^{18}F]-**1** is being excreted through the small intestine

and being concentrated in faecal bacteria. High SUVs in areas other than tumour represents high background uptake of [^{18}F]fluoroacetate [^{18}F]-**1**, an undesirable quality for a tracer to be used in quantifying differences in uptake in xenograft tumours.

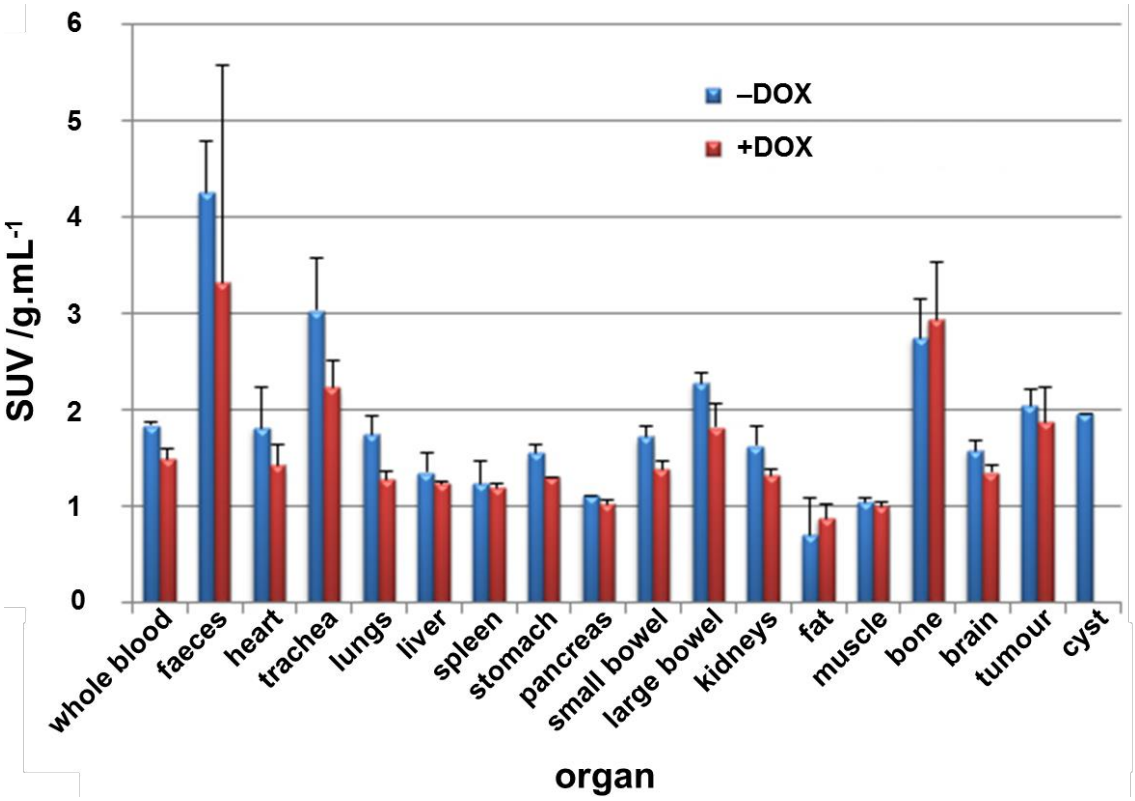

Figure 15. Average SUV in the two groups of mice (–DOX and +DOX), showing standard deviation, across multiple organs after dissection post mortem. Highest SUV appears in the faeces, bone and trachea, large bowel, followed by the tumour. One of the animals in the –DOX group had a cyst on the bladder. Data compiled by Dr Gaurav Malviya and Agata Mrowinska.

[^{18}F]Fluoroacetate [^{18}F]-**1** uptake and metabolism has been reported to be a poor model of acetate metabolism in monkey and pig studies.[69] [^{18}F]Fluoroacetate [^{18}F]-**1** showed different uptake kinetics, having a much longer residency time in the blood compared to [^{11}C]acetate [^{11}C]-**301**. This difference in behaviour may be due to differences in kinetics of transport into the cells *via* monocarboxyl transporters between [^{18}F]fluoroacetate [^{18}F]-**1** and [^{11}C]acetate [^{11}C]-**301**.

If acetate **301** and fluoroacetate **1** transport kinetics differ, rather than uptake and accumulation of the radiotracer being reflective of the rate of incorporation of [^{18}F]fluoroacetate [^{18}F]-**1** by ACSS2, uptake may be reflective simply of transport kinetics. Differences in activity of ACSS2 in the two groups of mice may be masked by transport kinetics, as this step is independent of ACSS2 activity, and consequently also DOX-induced gene silencing.

5.7. Conclusions

A chemoenzymatic method for the synthesis of [^{18}F]fluoroacetate [^{18}F]-**1** was explored based on a fluorinase enzyme catalysed fluorination of *S*-adenosylmethionine **20** with [^{18}F]fluoride. [^{18}F]Fluorodeoxyadenosine [^{18}F]-**22** (FDA), the product of this reaction was subject to Kuhn-Roth oxidation to generate [^{18}F]fluoroacetate [^{18}F]-**1**. While the enzymatic incorporations of [^{18}F]fluoride, and final radiochemical yields of [^{18}F]fluoroacetate [^{18}F]-**1** were both good, contamination of the final product with Cr(VI) species led to the investigation of an alternate chemical synthesis of [^{18}F]fluoroacetate [^{18}F]-**1**.

[^{18}F]Fluoroacetate [^{18}F]-**1** was synthesised chemically by S_N2 reaction of [^{18}F]fluoride with ethyl *O*-mesylglycolate **49**, followed by basic hydrolysis of the ester. Purification and formulation of [^{18}F]fluoroacetate [^{18}F]-**1** was then optimised to give a synthetic route to generate high radiochemical purity [^{18}F]fluoroacetate [^{18}F]-**1** (99% ± 1% (n = 9)), in good radiochemical yields (18% ± 7% (n = 8)) which was then used to investigate ACSS2 in xenograft mice models.

[^{18}F]Fluoroacetate [^{18}F]-**1** did not appear to be the optimal tracer for monitoring the physiological effect of gene silencing of ASCC2 in BT474 breast cancer xenograft models. The tracer shows low uptake in the tumour compared to reference areas such as the heart or liver. This low uptake was likely due to rate limiting transport of [^{18}F]fluoroacetate [^{18}F]-**1** into the cells, rather than being reflective of low ACSS2 activity. [^{18}F]Fluoroacetate [^{18}F]-**1** also showed significant uptake in the faeces and caecum. Significant uptake of radioactivity in the bone is a result of adventitious defluorination and release of [^{18}F]fluoride, further compromising [^{18}F]fluoroacetate [^{18}F]-**1** as a candidate radiotracer for assessing lipid metabolism *in vivo*.

Despite [^{18}F]fluoroacetate [^{18}F]-**1** being a poor tracer for comparison of ASCC2 activity in mouse models, the synthesis of this radiotracer was successfully established at the Beatson Cancer Research Institute in Glasgow. The availability of a validated synthetic method for the routine production of [^{18}F]fluoroacetate [^{18}F]-**1** means that PET tracer remains available for use in future by other research groups at the facility, should they require [^{18}F]fluoroacetate [^{18}F]-**1** for a small animal PET imaging study.

5.8. References

1. M. Koike, L. J. Reed, and W. R. Carrol, *J. Biol. Chem.*, 1960, **235**, 1924–1930.

2. C. Schnaitman and J. W. Greenawalt, *J. Cell Biol.*, 1968, **38**, 158–175.

3. J. Kerner and C. Hoppel, *Biochim. Biophys. Acta*, 2000, 1486, 1–17.

4. S. Ghisla and C. Thorpe, *Eur. J. Biochem.*, 2004, 271, 494–508.

5. G. Agnihotri and H. W. Liu, *Bioorganic Med. Chem.*, 2003, 11, 9–20.

6. S. J. Wakil, D. E. Green, S. Mii, and H. R. Mahler, *J. Biol. Chem.*, 1954, **207**, 631–638.

7. Y. Uchida, K. Izai, T. Orii, and T. Hashimoto, *J. Biol. Chem.*, 1992, **267**, 1034–1041.

8. G. V. Gnoni, P. Priore, M. J. H. Geelen, and L. Siculella, *IUBMB Life*, 2009, 61, 987–994.

9. J. A. Watson, M. Fang, and J. M. Lowenstein, *Arch. Biochem. Biophys.*, 1969, **135**, 209–217.

10. A. Luong, V. C. Hannah, M. S. Brown, and J. L. Goldstein, *J. Biol. Chem.*, 2000, **275**, 26458–26466.

11. F. J. Ballard, *Am. J. Clin. Nutr.*, 1972, **25**, 773–779.

12. S. Tsukamoto, T. Muto, T. Nagoya, M. Shimamura, M. Saito, and H. Tainaka, *Alcohol Alcohol.*, 1989, **24**, 101–108.

13. I. P. Williamson and S. J. Wakil, *J. Biol. Chem.*, 1966, **241**, 2326–2332.

14. S. J. Wakil, E. B. Titchner, and D. M. Gibson, *Biochim. Biophys. Acta*, 1958, **29**, 225–226.

15. D. M. Gibson, E. B. Titchner, and S. J. Wakil, *Biochim. Biophys. Acta*, 1958, **30**, 376–383.

16. J. Staunton and K. J. Weissman, *Nat. Prod. Rep.*, 2001, **18**, 380–416.

17. Z. L. Fowler, W. W. Gikandi, and M. A. G. Koffas, *Appl. Environ. Microbiol.*, 2009, **75**, 5831–5839.

18. L. Liscum, in *Biochemistry of Lipids, Lipoproteins and Membranes (4th ed.)*, eds. D. Vance and J. Vance, Elsevier Science B.V., 2002, pp. 409–431.

19. R. Matsumi, H. Atomi, A. J. M. Driessen, and J. van der Oost, *Res. Microbiol.*, 2011, **162**, 39–52.

20. W. Huth, R. Jonas, I. Wunderlich, and W. Seubert, *Eur. J. Biochem.*, 1975, **59**, 475–489.

21. B. Middleton and P. K. Tubbs, *Biochem. J.*, 1972, **126**, 27–34.

22. I. F. Durr and H. Rudney, *J. Biol. Chem.*, 1960, **235**, 2572–2578.

23. V. G. Allfrey, R. Faulkner, and A. E. Mirsky, *Proc. Natl. Acad. Sci. U. S. A.*, 1964, **51**, 786–794.

24. S. W. L'Hernault and J. L. Rosenbaum, *Biochemistry*, 1985, **24**, 473–478.

25. W. Gu and R. G. Roeder, *Cell*, 1997, **90**, 595–606.

26. H. Takahashi, J. M. McCaffery, R. A. Irizarry, and J. D. Boeke, *Mol. Cell*, 2006, **23**, 207–217.

27. K. Luger, A. W. Mäder, R. K. Richmond, D. F. Sargent, and T. J. Richmond, *Nature*, 1997, **389**, 251–260.

28. C. Tse, T. Sera, A. P. Wolffe, and J. C. Hansen, *Mol. Cell. Biol.*, 1998, **18**, 4629–4638.

29. M. Fu, C. Wang, J. Wang, B. T. Zafonte, M. P. Lisanti, and R. G. Pestell, *Cytokine Growth Factor Rev.*, 2002, **13**, 259–276.

30. D. Nachmansohn and A. L. Machado, *J. Neurophysiol.*, 1943, **6**, 397–403.

31. V. A. Glover and L. T. Potter, *J. Neurochem.*, 1971, **18**, 571–580.

32. R. Schauer, *Glycoconj. J.*, 2000, 17, 485–499.

33. J. Yagüe, I. Alvarez, D. Rognan, M. Ramos, J. Vázquez, and J. A. de Castro, *J. Exp. Med.*, 2000, **191**, 2083–2092.

34. W. Weidel and H. Pelzer, *Adv. Enzymol. Relat. Areas Mol. Biol.*, 1964, **26**, 193–232.

35. S. O. Meroueh, K. Z. Bencze, D. Hesek, M. Lee, J. F. Fisher, T. L. Stemmler, and S. Mobashery, *Proc. Natl. Acad. Sci. U. S. A.*, 2006, **103**, 4404–4409.

36. C. Peneff, D. Mengin-Lecreulx, and Y. Bourne, *J. Biol. Chem.*, 2001, **276**, 16328–16334.

37. F. Pietrocola, L. Galluzzi, J. M. Bravo-San Pedro, F. Madeo, and G. Kroemer, *Cell Metab.*, 2015, **21**, 805–821.

38. Y. Y. Lin, J. Y. Lu, J. Zhang, W. Walter, W. Dang, J. Wan, S. C. Tao, J. Qian, Y. Zhao, J. D. Boeke, S. L. Berger, and H. Zhu, *Cell*, 2009, **136**, 1073–1084.

39. P. Fabrizio and V. D. Longo, *Methods Mol. Biol.*, 2007, **371**, 89–95.

40. L. Cai, B. M. Sutter, B. Li, and B. P. Tu, *Mol. Cell*, 2011, **42**, 426–437.

41. P. A. Watkins, D. Maiguel, Z. Jia, and J. Pevsner, *J. Lipid Res.*, 2007, **48**, 2736–2750.

42. T. Fujino, J. Kondo, M. Ishikawa, K. Morikawa, and T. T. Yamamoto, *J. Biol. Chem.*, 2001, **276**, 11420–11426.

43. T. Matsunaga, F. Isohashi, Y. Nakanishi, and Y. Sakamoto, *Eur. J. Biochem.*, 1985, **152**, 331–336.

44. F. P. Kuhajda, K. Jenner, F. D. Wood, R. A. Hennigar, L. B. Jacobs, J. D. Dick, and G. R. Pasternack, *Proc. Natl. Acad. Sci. U. S. A.*, 1994, **91**, 6379–6383.

45. J. A. Menendez and R. Lupu, *Nat. Rev. Cancer*, 2007, **7**, 763–777.

46. Y. Yoshii, A. Waki, T. Furukawa, Y. Kiyono, T. Mori, H. Yoshii, T. Kudo, H. Okazawa, M. J. Welch, and Y. Fujibayashi, *Nucl. Med. Biol.*, 2009, **36**, 771–777.

47. T. Hara, A. Bansal, and T. DeGrado, *Nucl. Med. Biol.*, 2006, **33**, 977–984.

48. Y. Yoshii, T. Furukawa, H. Yoshii, T. Mori, Y. Kiyono, A. Waki, M. Kobayashi, T. Tsujikawa, T. Kudo, H. Okazawa, Y. Yonekura, and Y. Fujibayashi, *Cancer Sci.*, 2009, **100**, 821–827.

49. S. A. Comerford, Z. Huang, X. Du, Y. Wang, L. Cai, A. K. Witkiewicz, H. Walters, M. N. Tantawy, A. Fu, H. C. Manning, J. D. Horton, R. E. Hammer, S. L. McKnight, and B. P. Tu, *Cell*, 2014, **159**, 1591–1602.

50. Z. T. Schug, B. Peck, D. T. Jones, Q. Zhang, S. Grosskurth, I. S. Alam, L. M. Goodwin, E. Smethurst, S. Mason, K. Blyth, L. McGarry, D. James, E. Shanks, G. Kalna, R. E. Saunders, M. Jiang, M. Howell, F. Lassailly, M. Z. Thin, B. Spencer-Dene, G. Stamp, N. J. F. van den Broek, G. Mackay, V. Bulusu, J. J. Kamphorst, S. Tardito, D. Strachan, A. L. Harris, E. O. Aboagye, S. E. Critchlow, M. J. O. Wakelam, A. Schulze, and E. Gottlieb, *Cancer Cell*, 2015, **27**, 57–71.

51. Z. Schug and E. Gottlieb, Unpublished Results.

52. J. Marais, *Onderstepoort J. Vet. Sci. Anim. Ind.*, 1943, **18**, 203.

53. J. Marais, *Onderstepoort J. Vet. Sci. Anim. Ind.*, 1944, **20**, 67.

54. E. R. Kalmbach, *Science*, 1945, **102**, 232–233.

55. M. Sherley, *Anim. Welf.*, 2007, **16**, 449–458.

56. R. A. Peters, R. W. Wakelin, P. Buffa, and L. C. Thomas, *Proc. Roy. Soc. B*, 1953, **140**, 497– 507.

57. E. Kun and R. Dummel, *Methods Enzym.*, 1969, **13**, 623.

58. H. Lauble, M. C. Kennedy, M. H. Emptage, H. Beinert, and C. D. Stout, *Proc. Natl. Acad. Sci. U. S. A.*, 1996, **93**, 13699–13703.

59. F. Fonnum, A. Johnsen, and B. Hassel, *Glia*, 1997, **21**, 106–113.

60. J. Marik, A. Ogasawara, B. Martin-McNulty, J. Ross, J. E. Flores, H. S. Gill, J. N. Tinianow, A. N. Vanderbilt, M. Nishimura, F. Peale, C. Pastuskovas, J. M. Greve, N. van Bruggen, and S. P. Williams, *J. Nucl. Med.*, 2009, **50**, 982–990.

61. A. Matthies, S. Ezziddin, E.-M. Ulrich, H. Palmedo, H.-J. Biersack, H. Bender, and S. Guhlke, *Eur. J. Nucl. Med. Mol. Imaging*, 2004, **31**, 797.

62. D. E. Ponde, C. S. Dence, N. Oyama, J. Kim, Y. Tai, R. Laforest, B. A. Siegel, and M. J. Welch, *J. Nucl. Med.*, 2007, **48**, 420–428.

63. J. M. Jeong, D. S. Lee, J.-K. Chung, M. C. Lee, C.-S. Koh, and S. S. Kang, *J. Label. Compd. Radiopharm.*, 1997.

64. X.-G. Li, J. Domarkas, and D. O'Hagan, *Chem. Commun.*, 2010, **46**, 7819–7821.

65. L.-Q. Sun, T. Mori, C. S. Dence, D. E. Ponde, M. J. Welch, T. Furukawa, Y. Yonekura, and Y. Fujibayashi, *Nucl. Med. Biol.*, 2006, **33**, 153–158.

66. C. L. Ho, M. K. Cheung, S. Chen, T. T. Cheung, Y. L. Leung, K. C. Cheng, and W. D. Yeung, *Mol. Imaging*, 2012, **11**, 229–239.

67. S. Richter, R. Bergmann, J. Pietzsch, B. Beuthien-Baumann, and F. Wuest, *Curr. Radiopharm.*, 2008, **1**, 103–109.

68. A. R. Moser, H. C. Pitot, and W. F. Dove, *Science*, 1990, **247**, 322–324.

69. Ö. Lindhe, A. Sun, J. Ulin, O. Rahman, B. Långström, and J. Sörensen, *Eur. J. Nucl. Med. Mol. Imaging*, 2009, **36**, 1453–1459.

6. Experimental

6.1. General Experimental

Air and moisture sensitive reactions were carried out under an atmosphere of argon in flame-dried glassware. Room temperature (rt) refers to 18-25 °C. All evaporations and concentrations were performed under reduced pressure (*in vacuo*). All reagents (from Sigma Aldrich UK, Fluka UK, Alfa Aesar UK, Acros UK or Fisher UK) were of synthetic grade and were used without further purification, unless stated otherwise. c(RGDfK[N_3]) **199** was purchased from Peptides International, USA. When necessary, reagents were dried or purified prior to use according to standard methods.[1] Anhydrous solvents (DCM, THF, Et_2O) were obtained from MBraun MB SPS-800 solvent purification system by passage through two drying columns and dispensed under an argon atmosphere. Anhydrous MeOH and MeCN were distilled from calcium hydride in a recycling still.[1]

The course of reactions was followed by thin-layer chromatography (TLC) using aluminium plates coated with silica gel ($60F_{245}$ Merck). TLC plates were examined under UV light (254 nm and 266 nm) before being visualised with ammonium heptamolybdate, anisaldehyde-sulfuric acid, alkaline potassium permanganate or ceric sulfate-sulfuric acid and developed by heating. Column chromatography was performed on Merck Geduran silica gel 60 (250-400 mesh) under a positive pressure of compressed air eluting with solvents (reported as *v/v*) as supplied. Reverse phase column chromatography was performed using Extract Clean C_{18}-HC prepacked cartridges.

NMR spectra were recorded at 298 K on Bruker Avance 300, Avance II 400, or Avance 500. Avance III 500, or Avance III HD 500 instruments. ^{1}H and ^{13}C NMR spectra were recorded using deuterated solvent as the lock and the residual solvent signal as the internal standard. ^{19}F NMR spectra were referenced to $CFCl_3$ as an external standard. Chemical shifts are reported in parts per million (ppm) and coupling constants (*J*) are given in Hertz (Hz). The abbreviations for the multiplicity of the proton, carbon and fluorine signals are as follows: s singlet, d doublet, dd doublet of doublets, ddd doublet of doublet of doublets, t triplet, dt doublet of triplets, q quartet, m multiplet, br s broad

singlet. Compounds are numbered according to customary purine numbering. When necessary, resonances were assigned using two-dimensional experiments (COSY, HSQC, HMBC, TOCSY).

Optical rotations were measured with a Perkin Elmer 341 polarimeter in a 10.0 cm cell at the wavelength of the sodium D-line (λ = 589 nm). Specific rotations are given in implied units of 10^{-1}deg cm^2 g^{-1} and concentrations (*c*) are given in g/100 mL. High resolution electrospray ionisation mass spectra were obtained on a Micromass LCT or ThermoFisher Excalibur Orbitrap spectrometers operating in positive or negative mode, from solutions in MeOH, MeCN or water by the Mass Spectrometry Service at the University of St Andrews. MALDI MS was acquired using a 4800 MALDI TOF/TOF Analyser (ABSciex) equipped with a Nd:YAG 355 nm laser and calibrated using a mixture of peptides by Mass Spectrometry Service at the University of St Andrews.

Infrared spectra were measured on a Perkin Elmer Spectrum GX FTIR apparatus spectrometer either as KBr pellets, or as a thin film between NaCl plates, or on a Shimadzu IRAffinity-1S spectrometer with a diamond ATR attachment. Absorption maxima are given in units of wavenumbers (cm^{-1}). Melting points were recorded on an Electrothermal IA9100 melting point apparatus, or on a Griffin MPA 350.BM2.5 melting point apparatus and are uncorrected.

X-ray diffraction data were collected on a Mercury 70 diffractometer using graphite monochromated Mo-Kα radiation at 100 K by means of phi and omega scans. Structures were solved by direct methods and refined by full-matrix least squares techniques.

HPLC analyses/semi-preparations were performed using either a Shimadzu Prominence (SIL-20A HT autosampler, CL-20AT ternary pump, DGU-20A3R solvent degasser, SPD 20A UV detector and CBM-20A controller module) or a Varian Prostar (Varian 400 autosampler, Varian Prostar 230 solvent delivery system, Varian Prostar 235 UV-Vis detector) or a Dionex UltiMate 3000 system (autosampler, pump, column oven, diode array detector, and Berthold Flowstar LB513 radioactivity detector) with reverse phase or HILIC column as indicated in individual experiment.

LC-MS analysis was performed on a Waters 2795 HPLC coupled in parallel to a Waters 2996 photodiode array detector and Micromass LCT TOF mass spectrometer in ESI in positive mode using the column indicated in the individual experiment.

Activity of fluorine-18 containing samples was measured using a Capintech Amersham radioisotope calibrator ARC-120.

Samples were freeze dried from frozen solutions in water or ^{t}BuOH in water (20% *v/v*) in a Christ Alpha 1-2 LO Plus freeze drier.

Protein concentrations were measured on a NanoDrop 1000 spectrophotometer at 280 nm using an extinction coefficient of 10.42 as calculated by ExPASy ProtParam tool.[2] SDS-PAGE was run using NuPAGE 4–12% BisTris gels (Novex) in MOPS SDS running buffer. Proteins were visualised using Instant Blue Coomassie-based gel stain (Expedion).

6.2. Compound preparation for Chapter 2

6.2.1. 2′,3′,5′-Tri-*O*-acetylguanosine 184

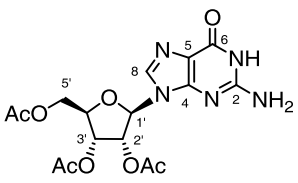

Pyridine (4.70 mL, 58.3 mmol, 5.5 eq.) and acetic anhydride (7.01 mL, 74.1 mmol, 7.0 eq.) were slowly added to a cooled (0 °C) suspension of guanosine (3.00 g, 10.6 mmol, 1.0 eq.) in DMF (40 mL). The mixture was heated to 85 °C for 2.5 h, resulting in a clear yellow solution. After cooling to rt, the volatile components were removed under reduced pressure to give an off-white powder, which was suspended in ^{i}PrOH (70 mL) and heated under reflux for 1 h. After cooling, the white solid was isolated by filtration and the residue was washed with cold Et_2O (20 mL) and dried under vacuum to afford the product **184** as a colourless amorphous powder (3.53 g, 81%): R_f = 0.20 (90:10 DCM:MeOH); $[\alpha]_D^{20}$ −26.0 (*c* 0.96, DMSO); mp 228–229 °C (^{i}PrOH); ν_{max} 3437, 3130, 1749, 1374, 1235, 1052 cm^{-1}; δ_H (400.1 MHz, d_6-DMSO): 10.74 (1 H, s, N-*H*), 7.94 (1 H, s, *H*-8), 6.54 (2 H, br s, NH_2), 5.98 (1 H, d, *J* 6.0, *H*-1′), 5.79 (1 H, dd, *J* 6.0, 6.0, *H*-2′), 5.49 (1 H, dd, *J* 6.0, 4.1, *H*-3′), 4.42-4.21 (3 H, m, *H*-4, *H*-5′a, *H*-5′b), 2.11 (3 H, s, OAc), 2.04 (3 H, s, OAc), 2.03 (3 H, s, OAc); δ_C (100.6 MHz, d_6-DMSO): 170.1, 169.4, 169.2 (CH_3C(O)), 156.6 (*C*-6), 153.9 (*C*-2), 151.9 (*C*-4), 135.6 (*C*-8), 116.8 (*C*-5), 84.4 (*C*-1′), 79.5 (*C*-4′), 72.0 (*C*-2′), 70.3 (*C*-3′), 63.1 (*C*-5′), 20.5, 20.4, 20.2 (CH_3C(O)); *m/z* (ES^+) 841 ($[2M+Na]^+$, 100%), 432 ($[M+Na]^+$, 89); HRMS (ES^+) calc. for $C_{16}H_{19}N_5O_8Na$ $[M+Na]^+$ 432.1131, found 432.1122. Data are in agreement with the literature.[3]

6.2.2. 2-Amino-6-chloro-9β-(2′,3′,5′-tri-*O*-acetyl-D-ribofuranosyl)-purine 185

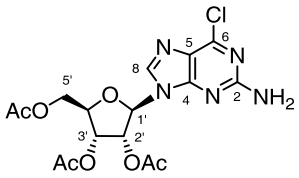

N,N-dimethylaniline (0.16 mL, 1.22 mmol, 1.0 eq.) and $POCl_3$ (0.68 mL, 7.33 mmol, 6.0 eq.) were slowly added to a solution of **184** (500 mg, 1.22 mmol, 1.0 eq.) and tetraethylammonium chloride (405 mg, 2.44 mmol, 2.0 eq.) in MeCN (20 mL). The mixture was heated to 100 °C for 25 min, before the volatile components were removed to give a yellow syrup. The syrup was reconstituted with $CHCl_3$ (20 mL) and ice water (20 mL) and stirred vigorously for 30 min. The phases were separated and the aqueous phase extracted with $CHCl_3$ (3 × 30 mL). The combined organic phases were washed with aqueous $NaHCO_3$ (5% *w/v*, 2 × 30 mL) before being dried over $MgSO_4$, filtered and concentrated. The crude product was purified by column chromatography (DCM to 95:5 DCM:MeOH) to afford the product **185** as a yellow foam (323 mg, 62%): R_f = 0.54 (90:10 DCM:MeOH); $[\alpha]_D^{20}$ −6.1 (*c* 1.04, $CHCl_3$); mp 142–143 °C (DCM); ν_{max} 3373, 3212, 1747, 1618, 1376, 1233, 1051 cm^{-1}; δ_H (400.1 MHz, $CDCl_3$): 7.87 (1 H, s, *H*-8), 6.00 (1 H, d, *J* 5.0, *H*-1′), 5.95 (1 H, dd, *J* 5.0, 5.0, *H*-2′), 5.74 (1 H, m, *H*-3′), 5.24 (2 H, br s, NH_2), 4.51-4.31 (3 H, m, *H*-4, *H*-5′a, *H*-5′b), 2.14 (3 H, s, OAc), 2.10 (3 H, s, OAc), 2.08 (3 H, s, OAc); δ_C (100.6 MHz, $CDCl_3$): 170.6, 169.7, 169.5 (CH_3C(O)), 159.2 (*C*-2), 153.2 (*C*-6), 152.1 (*C*-4), 140.8 (*C*-8), 117.2 (*C*-5) 86.8 (*C*-1′), 80.2 (*C*-4′), 72.9 (*C*-2′), 70.6 (*C*-3′), 63.1 (*C*-5′), 20.9, 20.7, 20.6 (CH_3C(O)); *m/z* (ES^+) 450 ($[M+Na]^+$, 100%); HRMS (ES^+) calc. for $C_{16}H_{18}ClN_5O_7Na$ $[M+Na]^+$ 450.0792, found 450.0796. Data are in agreement with the literature.[4]

6.2.3. 6-Chloro-2-iodo-9β-(2′,3′,5′-tri-*O*-acetyl-D-ribofuranosyl)-purine 186

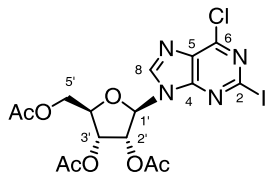

CH_2I_2 (1.57 mL, 19.5 mmol, 10 eq.) and isoamyl nitrite (0.76 mL, 5.7 mmol, 3.0 eq.) were slowly added to a suspension of **185** (811 mg, 1.90 mmol, 1.0 eq.), copper(I) iodide (379 mg, 1.99 mmol, 2.0 eq.) and iodine (481 mg, 1.90 mmol, 1.0 eq.) in THF (20 mL). The mixture was heated under reflux for 3 h, cooled to rt and filtered through a pad of celite. The filtrate was concentrated and purified by column chromatography ($CHCl_3$ to 99:1 $CHCl_3$:EtOH to 98:2 $CHCl_3$:EtOH) and the fractions containing product combined, concentrated and the resultant gum was recrystallised from EtOH (30 mL) to give the product **186** as a yellow powder (700 mg, 69%): R_f = 0.15 (99:1 $CHCl_3$:EtOH); $[\alpha]_D^{20}$ +9.0 (*c* 0.61, $CHCl_3$); mp 179–181 °C ($CHCl_3$); ν_{max} 1748, 1585, 1551, 130, 1218, 1138 cm^{-1}; δ_H (400.1 MHz, $CDCl_3$): 8.20 (1 H, s, *H*-8), 6.18 (1 H, d, *J* 5.4, *H*-1′), 5.76 (1 H, dd, *J* 5.6, 5.4, *H*-2′), 5.56 (1 H, dd, *J* 5.6, 4.4, *H*-3′), 4.47-4.34 (3 H, m, *H*-4, *H*-5′a, *H*-5′b), 2.15 (3 H, s, OAc), 2.11 (3 H, s, OAc), 2.08 (3 H, s, OAc); δ_C (125.77 MHz, $CDCl_3$): 170.3, 169.7, 169.5 (CH_3C(O)), 152.1 (*C*-6), 151.2 (*C*-4), 143.2 (*C*-8), 132.4 (*C*-2), 117.2 (*C*-5), 86.8 (*C*-1′), 81.0 (*C*-4′), 73.5 (*C*-2′), 70.7 (*C*-3′), 63.1 (*C*-5′), 21.0, 20.7, 20.6 (CH_3C(O)); *m/z* (ES^+) 561 ($[M+Na]^+$ 100%); HRMS (ES^+) calc. for $C_{16}H_{16}ClIN_4O_7Na$ $[M+Na]^+$ 560.9650, found 560.9655. Data are in agreement with the literature.[5]

6.2.4. 2-Iodoadenosine 179

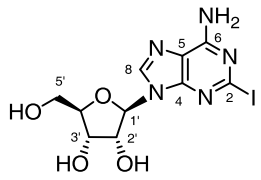

In a heavy walled tube, a suspension of **186** (1.08 g, 2.00 mmol, 1.0 eq.) in MeOH (8 mL) was cooled to 0 °C. Ammonia gas was bubbled through the solution for 1 h, before the tube was sealed and heated to 60 °C for 19 h. The vessel was cooled to rt and carefully opened, before the solution was degassed by bubbling argon through the solution for 1 h. The clear yellow solution was concentrated, and the residue recrystallised from hot water (8 mL). A second batch of crystals was obtained after concentration of the mother liquor and a second recrystallisation from hot water (4 mL). After drying under vacuum, 2-iodoadenosine **179** was obtained as colourless crystals (536 mg, 68%): R_f = 0.02 (95:5 DCM:MeOH); $[\alpha]_D^{20}$ −34.7 (*c* 0.97, DMSO); mp 139–140 °C (water); ν_{max} 3321, 3191, 2924, 1652, 1592, 1339, 1306 cm^{-1}; δ_H (400.1 MHz, d_6-DMSO): 8.30 (1 H, s, *H*-8), 7.74 (2 H, br s, NH_2), 5.80 (1 H, d, *J* 6.2, *H*-1′), 5.46 (1 H, d, *J* 6.2, C-2′ O*H*), 5.21 (1 H, d, *J* 4.9, C-3′ O*H*), 5.04 (1 H, dd, *J* 6.4, 5.1, C-5′ O*H*), 4.54-4.50 (1 H, m, *H*-2′), 4.13-4.09 (1 H, m, *H*-3′), 3.95-3.92 (1 H, m, *H*-4′), 3.64 (1 H, ddd, *J* 12.0, 5.1, 4.1, *H*-5′a), 3.54 (1 H, ddd, *J* 12.0, 6.4, 4.0, *H*-5′b); δ_C (100.6 MHz, d_6-DMSO): 155.9 (*C*-6), 149.8 (*C*-2), 139.4 (*C*-8), 120.9 (*C*-4), 119.0 (*C*-5), 87.2 (*C*-1′), 85.8 (*C*-4′), 73.6 (*C*-2′), 70.5 (*C*-3′), 61.4 (*C*-5′); *m/z* (ES^+) 416 ($[M+Na]^+$ 100%); HRMS (ES^+) calc. for $C_{10}H_{13}IN_5O_4$ $[M+H]^+$ 394.0012, found 394.0016. Data are in agreement with the literature.[5]

6.2.5. 2-(Trimethylsilylethynyl)adenosine 187

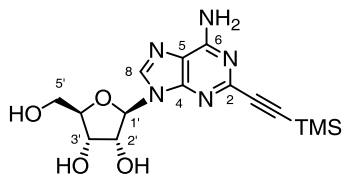

Triethylamine (0.28 mL, 2.04 mmol, 1.5 eq.) and ethynyltrimethylsilane (0.39 mL, 2.73 mmol, 2.0 eq.) were added to a suspension of $Pd(PPh_3)_2Cl_2$ (95.6 mg, 0.136 mmol, 0.1 eq.), copper(I) iodide (25.9 mg, 0.136 mmol, 0.1 eq.) and 2-iodoadenosine **179** (536 mg, 1.36 mmol, 1.0 eq.) in DMF (8 mL). The mixture was heated to 85 °C for 90 min, after which time the volatile components were removed. The residue was diluted with EtOAc (15 mL) and washed with aqueous disodium EDTA solution (10% *w/v*, 30 mL) before being dried over Na_2SO_4 and concentrated. The crude product was purified by column chromatography ($CHCl_3$ to 98:2 $CHCl_3$:MeOH to 95:5 $CHCl_3$:MeOH) to afford the product **187** as an amorphous light brown powder (296 mg, 60%): R_f = 0.13 (95:5 DCM:MeOH); $[\alpha]_D^{20}$ −40.0 (*c* 0.25, DMSO); mp 156–157 °C (DCM); ν_{max} 3332, 3260, 2958, 2920, 2169, 1653, 1590, 1335, 851 cm^{-1}; δ_H (500.0 MHz, d_6-DMSO): 8.46 (1 H, s, *H*-8), 7.52 (2 H, br s, N*H*$_2$), 5.88 (1 H, d, *J* 5.9, *H*-1′), 5.48 (1 H, d, *J* 6.2, C-2′ O*H*), 5.20 (1 H, d, *J* 4.9, C-3′ O*H*), 5.14 (1 H, dd, *J* 5.7, 5.7, C-5′ O*H*), 4.50-4.47 (1 H, m, *H*-2′), 4.13-4.11 (1 H, m, *H*-3′), 3.96-3.94 (1 H, m, *H*-4′), 3.66-3.64 (1 H, m, *H*-5′a), 3.58-3.54 (1 H, m, *H*-5′b), 0.24 (9 H, s, Si(C*H*$_3$)$_3$); δ_C (125.8 MHz, d_6-DMSO): 155.9 (*C*-6), 149.3 (*C*-4), 144.8 (*C*-2), 140.4 (*C*-8), 118.8 (*C*-5), 104.5 (*C*≡CSi), 88.7 (C≡*C*Si), 87.1 (*C*-1′), 85.7 (*C*-4′), 73.9 (*C*-2′), 70.3 (*C*-3′), 61.4 (*C*-5′), 0.36 (Si(*C*H$_3$)$_3$); *m/z* (ES^+) 386 ([M+Na]$^+$, 33%), 364 ([M+H]$^+$, 100); HRMS (ES^+) calc. for $C_{15}H_{21}N_5O_4Si$ [M+H]$^+$ 364.1436, found 364.1432. Data are in agreement with the literature.[6]

6.2.6. 2-Ethynyladenosine 180

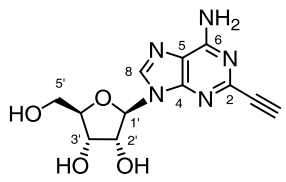

In a heavy walled tube, ammonia gas was bubbled through a solution of methanol (5 mL) for 1 h., before **187** (269 mg, 0.739 mmol, 1 eq.) was carefully added. The tube was sealed and stirred at rt for 4 h. The vessel was carefully opened, before the solution was degassed by bubbling argon through the solution for 1 h. The solution was concentrated, and the residue recrystallised from hot water (5 mL). A second batch of crystals was obtained after concentration of the mother liquor and a second recrystallisation from hot water (2 mL) to give **180** as a pale brown amorphous powder (166 mg, 77%): R_f = 0.16 (90:10, DCM:MeOH); $[\alpha]_D^{20}$ -56 (*c* 0.28, DMSO); mp 200–201 °C (dec.) (H_2O); ν_{max} 3255, 2928, 2116, 1654, 1336, 1023 cm^{-1}; δ_H (400.1 MHz, d_6-DMSO): 8.43 (1 H, s, *H*-8), 7.53 (2 H, br s, NH_2), 5.86 (1 H, d, *J* 6.1, *H*-1′), 5.47 (1 H, d, *J* 6.2, C-2′ O*H*), 5.20-5.17 (2 H, m, C-3′ O*H*, C-5′ O*H*), 4.57-4.53 (1 H, m, *H*-2′), 4.13-4.11 (1 H, m, *H*-3′), 4.02 (1H, s, C≡C*H*), 3.96-3.93 (1 H, m, *H*-4′), 3.66 (1 H, ddd, 11.9, 4.2, 4.2, *H*-5′a), 3.55 (1 H, ddd, 11.9, 6.7, 3.9, *H*-5′b); δ_C (75.5 MHz, d_6-DMSO): 155.9 (*C*-6), 149.1 (*C*-4),144.7 (*C*-2), 140.7 (*C*-8), 119.1 (*C*-5), 87.5 (*C*-1′), 85.8 (*C*-4′), 83.2 (*C*≡CH), 75.1 (C≡*C*H), 73.6 (*C*-2′), 70.5 (*C*-3′), 61.5 (*C*-5′); *m/z* (ES^+) 314 ($[M+Na]^+$, 100%); HRMS (ES^+) calc. for $C_{12}H_{13}N_5O_4Na$ $[M+Na]^+$ 314.0865, found 314.0868. Data are in agreement with the literature.[6]

6.2.7. 5′-Chloro-5′-deoxy-2-ethynyladenosine (ClDEA) 174

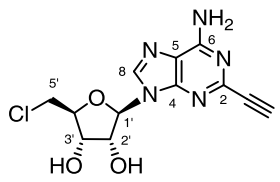

Pyridine (45 µL, 1.38 mmol, 2.0 eq.) followed by thionyl chloride (100 µL, 0.550 mmol, 5.0 eq.) were added to a solution of **187** (100 mg, 0.275 mmol, 1.0 eq.) in MeCN (6 mL) at 0 °C. The mixture was stirred for 18 h and allowed to warm to rt. The volatile components were removed, and the residue was diluted with MeOH (1.5 mL), water (0.3 mL) and aqueous ammonia solution (35% *v/v*, 0.3 mL), and the solution stirred for 3 h. After concentration, the residue was purified by column chromatography (95:5 $CHCl_3$:MeOH) to give the product **174** as a pale yellow powder (40.0 mg, 47%): R_f = 0.21 (90:10 DCM:MeOH); $[\alpha]_D^{20}$ −32.9 (*c* 0.30, DMSO); mp >285 °C (dec.) ($CHCl_3$); ν_{max} 3375, 2106, 1668, 1324, 741 cm^{-1}; δ_H (500.1 MHz, d_6-DMSO): 8.42 (1 H, s, *H*-8), 7.53 (2 H, br s, NH_2), 5.91 (1 H, d, *J* 5.7, *H*-1′), 5.62 (1 H, d, *J* 6.0, C-2′ O*H*), 5.48 (1 H, d, *J* 5.2, C-3′ O*H*), 4.72-4.68 (1 H, m, *H*-2′), 4.28-4.14 (1 H, m, *H*-3′), 4.15-4.05 (1 H, m, *H*-4′), 4.02 (1 H, s, C≡C*H*), 3.95 (1 H, dd, 11.6, 5.1, *H*-5′a), 3.86 (1 H, dd, 11.6, 6.4, *H*-5′b); δ_C (125.8 MHz, d_6-DMSO): 155.9 (*C*-6), 149.3 (*C*-2), 144.6 (*C*-4), 140.6 (*C*-8), 118.9 (*C*-5), 87.2 (*C*-1′), 83.8 (*C*-4′), 83.4 (*C*≡CH), 74.9 (C≡*C*H), 72.8 (*C*-2′), 71.3 (*C*-3′), 44.7 (*C*-5′); *m/z* (ES^+) 332 ($[M+Na]^+$, 100%); HRMS (ES^+) calc. for $C_{12}H_{12}{}^{35}ClN_5O_3Na$ $[M+Na]^+$ 332.0526, found 332.0522.

6.2.8. 2',3'-*O*-Isopropylidene-2-(trimethylsilylethynyl)adenosine 191

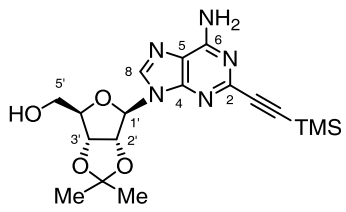

Amberlyst-15 H^+ resin (100 mg) and 2,2-dimethoxypropane (340 µL, 2.75 mmol, 10 eq.) were added to a solution of 2-(trimethylsilylethynyl)adenosine **187** (100 mg, 0.275 mmol, 1.0 eq.) in DMF (5 mL), and the mixture heated to 60 °C for 18 h. The reaction mixture was cooled to rt and filtered through a pad of celite, before being concentrated. The yellow oil was purified by column chromatography (95:5 DCM:MeOH) to give the product **191** as a pale yellow foamy solid (79 mg, 71%): R_f = 0.27 (95:5 DCM:MeOH); $[\alpha]_D^{20}$ −132.5 (*c* 0.08, $CHCl_3$); mp 177–179 °C (DCM); ν_{max} 3469, 3369, 3252, 2927, 2857, 1658, 1095, 864 cm^{-1}; δ_H (400.1 MHz, $CDCl_3$): 7.85 (1 H, s, *H*-8), 5.91 (2 H, br s, NH_2), 5.83 (1 H, d, *J* 4.8, *H*-1'), 5.75 (1 H, dd, *J* 11.5, 2.4, O*H*-5'), 5.19-5.11 (2 H, m, *H*-2', *H*-3'), 4.51 (1 H, br s, *H*-4'), 4.01-3.96 (1 H, m, *H*-5'a), 3.83-3.74 (1 H, m, *H*-5'b), 1.62 (3 H, s, C(CH_3)$_2$), 1.35 (3 H, s, C(CH_3)$_2$), 0.28 (9 H, s, Si(CH_3)$_3$); δ_C (75.5 MHz, $CDCl_3$): 155.7 (*C*-6), 148.7 (*C*-4), 145.8 (*C*-2), 141.1 (*C*-8), 120.6 (*C*-5), 114.1 (*C*(CH$_3$)$_2$), 102.4 (*C*≡C-Si), 94.1 (*C*-1'), 92.7 (C≡*C*-Si), 86.2 (*C*-4'), 83.1 (*C*-2'), 81.8 (*C*-3'), 63.4 (*C*-5'), 27.8 (C(*C*H$_3$)$_2$), 25.4 (C(*C*H$_3$)$_2$), -0.28 (Si(*C*H$_3$)$_3$)); *m/z* (ES^+) 426 ($[M+Na]^+$, 100%), 404 ($[M+H]^+$, 28); HRMS (ES^+) calc. for $C_{18}H_{25}N_5O_4SiNa$ $[M+Na]^+$ 426.1574, found 426.1569.

6.2.9. 5′-Deoxy-5'-fluoro-2',3'-*O*-isopropylidene-2-ethynyladenosine 192

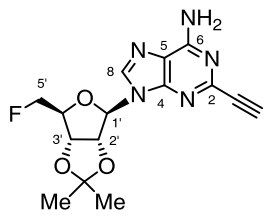

TsF (92.0 mg, 0.528 mmol, 3.0 eq.) and TBAF (1 M in THF, 1.10 mL, 1.06 mmol, 6.0 eq.) were added to a solution of **191** (71.0 mg, 0.176 mmol, 1.0 eq.) in THF (5 mL). The mixture was heated to 60 °C for 18 h, and cooled to rt. The volatile components were removed and the orange residue was purified by column chromatography (DCM to 95:5 DCM:MeOH) to give the product **192** as a yellow powder (42.0 mg, 71%): R_f = 0.37 (95:5 DCM:MeOH); $[\alpha]_D^{20}$ –22.0 (*c* 0.10, $CHCl_3$); mp 242–245 °C (DCM); ν_{max} 3319, 3244, 3165, 1161, 1593, 1360, 1213, 1082. 729, 640 cm^{-1}; δ_H (300.1 MHz, d_6-DMSO): 8.35 (1 H, s, *H*-8), 7.57 (2 H, br s, NH_2), 6.20 (1 H, d, *J* 2.2, *H*-1'), 5.39 (1 H, dd, *J* 6.2, 2.2, *H*-2'), 5.07-5.03 (1 H, m, *H*-3'), 4.77–4.48 (2 H, m, *H*-5'), 4.49-4.33 (1 H, m, *H*-4), 4.04 (1 H, s, C≡C*H*), 1.55 (3 H, s, C(CH_3)$_2$), 1.34 (3 H, s, C(CH_3)$_2$); δ_C (75.5 MHz, d_6-DMSO): 155.9 (*C*-6), 148.8 (*C*-4), 144.9 (*C*-2), 140.4 (*C*-8), 118.9 (*C*-5), 113.6 (*C*(CH$_3$)$_2$), 89.1 (*C*-1'), 84.5 (d, *J* 18.2, *C*-4'), 83.4 (*C*-2'), 83.3 (*C*≡CH), 82.8 (d, *J* 168.7, *C*-5'), 80.2 (d, *J* 6.7, *C*-3'), 75.1 (C≡*C*H), 27.0 (C(*C*H$_3$)$_2$), 25.2 (C(*C*H$_3$)$_2$); δ_F (282.3 MHz, d_6-DMSO): −227.13 (ddd, *J* 46.9, 46.7, 22.1, CH_2F); *m/z* (ES^+) 356 ([M+Na]$^+$, 100%), 334 ([M+H]$^+$, 52); HRMS (ES^+) calc. for $C_{15}H_{16}N_5O_3FNa$ [M+Na]$^+$ 356.1135, found 356.1143.

6.2.10. 5′-Deoxy-5'-fluoro-2-ethynyladenosine (FDEA) 176

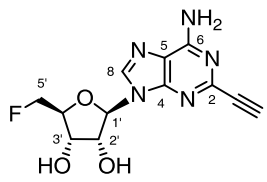

A solution of **192** (40.0 mg, 0.120 mmol) in a mixture of TFA:water (9:1 *v/v*, 5.0 mL) at 0 °C was stirred for 3 h whilst warming to rt. The volatile components were removed, and the residue co-evaporated with EtOH (3 × 10 mL) and Et_2O (10 mL) to give a brown solid. The residue was purified by column chromatography (90:10 $CHCl_3$:MeOH) to give the product **176** as a white powder (18.5 mg, 53%): R_f = 0.21 (90:10 $CHCl_3$:MeOH); $[\alpha]_D^{20}$ -46.0 (*c* 0.20, DMSO); mp 218 °C (dec.) ($CHCl_3$); ν_{max} 3179, 3210, 1660, 1592, 1332, 1125, 725 cm^{-1}; δ_H (499.9 MHz, d_6-DMSO): 8.34 (1 H, s, *H*-8), 7.54 (2 H, br s, NH_2), 5.92 (1 H, d, *J* 5.0, *H*-1'), 5.66 (1 H, d, *J* 5.7, O*H*-2'), 5.45 (1 H, d, *J* 5.4, O*H*-3'), 4.73-4.59 (2 H, m, *H*-5'), 4.57-4.54 (1 H, m, *H*-2'), 4.24-4.21 (1 H, m, *H*-3'), 4.16-4.09 (1 H, m, *H*-4), 4.02 (1 H, s, C≡C*H*); δ_C (125.7 MHz, d_6-DMSO): 155.9 (*C*-6), 149.3 (*C*-4), 144.9 (*C*-2), 140.2 (*C*-8), 118.9 (*C*-5), 87.5 (*C*-1'), 83.4 (*C*≡CH), 82.9 (d, *J* 168.3, *C*-5'), 82.5 (d, *J* 18.3, *C*-4'), 75.0 (C≡*C*H), 73.2 (*C*-2'), 69.4 (d, *J* 6.1, *C*-3'); δ_F (470.3 MHz, d_6-DMSO): −227.55 (1F, ddd, *J* 47.6, 47.6, 23.9, CH_2F); *m/z* (ES^+) 316 ($[M+Na]^+$, 100%), 294 ($[M+H]^+$, 7); HRMS (ES^+) calc. for $C_{12}H_{12}FN_5O_3Na$ $[M+Na]^+$ 316.0822, found 316.0816.

6.2.11. 5′-Chloro-5′-deoxyadenosine 23

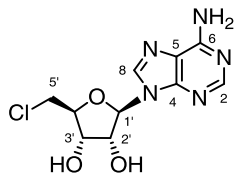

Pyridine (0.61 mL, 7.48 mmol, 2.0 eq.) and thionyl chloride (1.36 mL, 18.7 mmol, 5.0 eq.) were slowly added to a suspension of adenosine **188** (1.00 g, 3.74 mmol, 1.0 eq.) in MeCN (40 mL) at 0 °C. The mixture was stirred for 18 h, while warming to room temperature. The volatile components were removed, and the yellow residue reconstituted with MeOH (15 mL), water (5 mL) and aqueous ammonia solution (35% *v/v*, 15 mL), and the solution stirred for 3 h. After concentration, the residue was purified by recrystallisation from water to give 5′-chloro-5′-deoxyadenosine **23** as an off-white amorphous powder (1.00 g, 94%): R_f = 0.12 (90:10, DCM:MeOH); $[\alpha]_D^{20}$ -27.4 (*c* 1.1, 1 M HCl); mp 175-179 °C (water); ν_{max} 3210, 1649, 1482, 1424, 1336, 1302, 645 cm^{-1}; δ_H (300.1 MHz, d_6-DMSO): 8.35 (1H, s, *H*-8), 8.16 (1H, s, *H*-2), 7.32 (2H, br s, NH_2), 5.93 (1H, d, *J* 5.7, *H*-1'), 5.60 (1H, d, *J* 5.9, O*H*-2'), 5.47 (1H, d, *J* 5.2, O*H*-3'), 4.76 (1H, ddd, *J* 5.9, 5.7, 5.4, *H*-2'), 4.22 (1H, ddd, *J* 5.4, 5.2, 5.1, *H*-3'), 4.11-4.06 (1H, m, *H*-4'), 3.95 (1H, dd, *J* 11.6, 5.1, *H*-5'a), 3.84 (1H, dd, *J* 11.6, 6.4, *H*-5'b); δ_C (75.5 MHz, d_6-DMSO): 156.1 (*C*-6), 152.7 (*C*-2), 149.4 (*C*-4), 139.7 (*C*-8), 119.1 (*C*-5), 87.4 (*C*-1'), 83.7 (*C*-4'), 72.6 (*C*-2'), 71.3 (*C*-3'), 44.8 (*C*-5'); *m/z* (ES^+) 286 ($[M+H]^+$ 100%), Data are in agreement with literature values.[7]

6.2.12. CIDEA-RGD 200

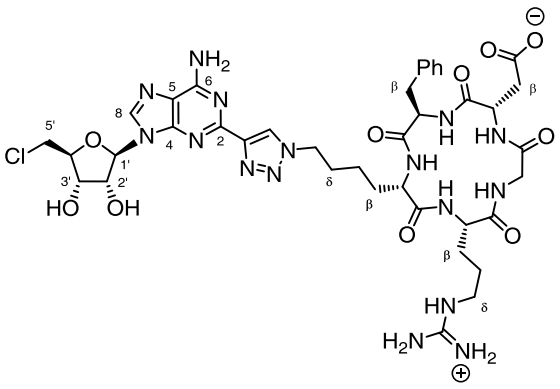

Fresh aqueous sodium ascorbate solution (20 mM, 798 µL, 10 eq.) and $CuSO_4$.TBTA solution (10 mM stock in 55% DMSO, 319 µL, 2 eq.) were added to a solution of ClDEA **174** (0.49 mg, 0.0016 mmol, 1 eq.) and c(RGDfK[N_3]) **199** (1.3 mg, 0.0020 mmol, 1.25 eq.) in water (9.5 mL), and the mixture left to react for 30 min, at which point HPLC sampling showed all the alkyne to be consumed. The reaction mixture was passed through an ExtractClean C_{18}-HC (1000 mg) cartridge (preconditioned with water), and the product eluted with 1:1 water:MeCN (2 × 10 mL). The water:MeCN fractions were combined and concentrated to dryness under a stream of air, and the crude product purified by preparative HPLC (Shimadzu Prominence, using Phenomenex Kingsorb C_{18} (250 × 10.00 mm, 5µ) column); mobile Phase: A (H_2O + 0.05% TFA), B (MeCN + 0.05% TFA); linear gradient: 20% B to 42%B in 18 min, 42% B to 95% B in 1 min; hold at 95% B for 5 min, 95% B to 20% B in 1 min, and re-equilibration at 20%B for 10 min; flow rate: 2.5 mL.min^{-1}; detection 220 nm). Fractions containing product (t_R = 10.9 min) were collected, concentrated under a stream of air, and lyophilised from a ^{t}BuOH in water (20% *v/v*) solution affording **200** (0.72 mg, 48%): δ_H (500.0 MHz, d_6-DMSO + 15% D_2O): 8.48 (1 H, s, *H*-8), 8.32 (1 H, s, triazole-*H*), 7.19–7.09 (5 H, m, D-Phe Ar*H*), 5.97 (1 H, d, *J* 5.6, *H*-1'), 4.80 (1 H, dd, *J* 5.4, 5.6, *H*-2'), 4.59 (1 H, dd, *J* 9.6, 5.5, Asp α-*H*), 4.49 (1 H, dd, *J* 7.5, 5.4, Arg α-*H*), 4.37 (2 H, t, *J* 6.8, Lys ε), 4.34–4.28 (2 H, m, Lys α-*H*, *H*-3'), 4.16–4.10 (3 H, m, *H*-4', D-Phe α-*H*, Gly α-*H*a), 3.99 (1 H, dd, *J* 11.7, 4.8, *H*-5'a), 3.92 (1 H, dd, *J* 11.7, 6.4, *H*-5'b), 3.38–3.32 (2 H, m, Gly α-*H*b, Asp β-*H*a), 3.06 (2 H, t, *J* 7.1, Arg δ-CH_2), 2.77–2.68 (1 H, m, D-Phe β-*H*a), 2.58 (1 H, dd, *J* 14.4, 9.6, Asp β-*H*b), 2.08–1.97 (1 H, m, D-Phe β-*H*b), 1.89–1.79 (2 H, m, Lys β-CH_2), 1.73–1.52 (4 H, m, Lys δ-CH_2, Arg β-CH_2), 1.50–1.33 (2 H, m, Arg δ-CH_2), 1.28–1.12 (2 H, m, Lys γ-CH_2); *m/z* (MALDI-TOF) calc. for $C_{39}H_{52}{}^{35}ClN_{16}O_{10}$ $[M+H]^+$: 939.37, found 939.37.

6.2.13. FDEA-RGD 201

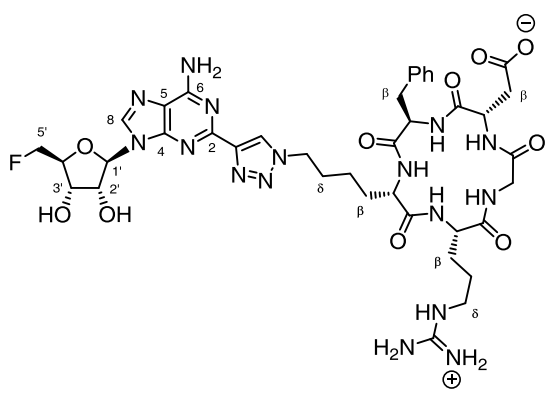

Fresh aqueous sodium ascorbate solution (20 mM, 813 µL, 10 eq.) and $CuSO_4$.TBTA solution (10 mM stock in 55% DMSO, 325 µL, 2 eq.) were added to a solution of FDEA **176** (0.48 mg, 0.0016 mmol, 1 eq.) and c(RGDfK[N_3]) **199** (1.3 mg, 0.0020 mmol, 1.25 eq.) in a mixture of DMSO (3 mL) and water (6.7 mL). The mixture was left to react at rt for 70 min, at which point HPLC sampling showed all the alkyne to be consumed. The reaction mixture diluted with water (2 mL) and was passed through an ExtractClean C_{18}-HC (1000 mg) cartridge (preconditioned with water), washed with water (10 mL), and the product eluted with 1:1 water:MeCN (2 × 10 mL). The water:MeCN fractions were combined and concentrated to dryness under a stream of air, and the crude product purified by preparative HPLC (Shimadzu Prominence, using Phenomenex Kingsorb C_{18} (250 × 10.00 mm, 5µ) column); mobile phase: A (H_2O + 0.05% TFA), B (MeCN + 0.05% TFA); linear gradient: 20% B to 42% B in 18 min, 42% B to 95% B in 1 min; hold at 95% B for 5 min, 95% B to 20% B in 1 min, and re-equilibration at 20%B for 10 min; flow rate: 2.5 mL.min^{-1}; detection 220 nm). Fractions containing product (t_R = 10.2 min) were collected, concentrated under a stream of air, and lyophilised from a ^{t}BuOH in water (20% *v/v*) solution affording **201** (0.74 mg, 49%): δ_H (500.0 MHz, d_6-DMSO + 15% D_2O): 8.48 (1 H, s, *H*-8), 8.26 (1 H, s, triazole-*H*), 7.21–7.04 (5 H, D-Phe Ar*H*), 5.99 (1 H, d, *J* 5.7, *H*-1'), 4.75–4.70 (1 H, m, ½ *H*-5a', ½ *H*-5b'), 4.67–4.61 (2 H, m, *H*-2' ½ *H*-5a', ½ *H*-5b'), 4.59 (1 H, dd, *J* 9.6, 5.5, Asp α-*H*), 4.49 (1 H, dd, *J* 7.4, 5.5, Arg α-*H*), 4.37 (2 H, t, *J* 6.9, Lys ε), 4.34–4.29 (2 H, m, Lys α-*H*, *H*-3'), 4.19–4.09 (3 H, m, *H*-4', D-Phe α-*H*, Gly α-*H*a), 3.35–3.23 (2 H, m, Gly α-*H*b, Asp β-*H*a), 3.06 (2 H, t, *J* 7.1, Arg δ-CH_2), 2.76–2.69 (1 H, m, D-Phe β-*H*a), 2.58 (1 H, dd, *J* 14.2, 9.6, Asp β-*H*b), 2.08–1.99 (1 H, m, D-Phe β-*H*b), 1.90–1.80 (2 H, m, Lys β-CH_2), 1.74–1.51 (4 H, m, Lys δ-CH_2, Arg β-CH_2), 1.49–1.32 (2 H, m, Arg δ-CH_2), 1.30–1.10 (2 H, m, Lys γ-CH_2); δ_F (470.5 MHz, d_6-DMSO + 15% D_2O): 227.01 (1 F, dt, *J* 47.4, 24.2, CH_2F); *m/z* (MALDI-TOF) calc. for $C_{39}H_{52}FN_{16}O_{10}$ $[M+H]^+$: 923.40, found 923.41.

6.3. Compound preparation for Chapter 3

6.3.1. Methyl 3,5-bis(prop-2-yn-1-yloxy)benzoate 227

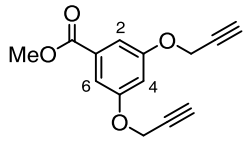

Propargyl bromide (80% *w/w* in toluene, 9.9 mL, 89.2 mmol, 3 eq.) was added to a suspension of methyl 3,5-dihydroxybenzoate (5.00 g, 29.7 mmol, 1 eq.) and K_2CO_3 (12.3 g, 89.2 mmol, 3 eq.) in acetone (50 mL), and the mixture heated under reflux for 48 h. The mixture was cooled before being filtered *in vacuo*, and the residue washed with acetone (3 × 20 mL). The combined filtrates were concentrated, and the resultant solid was dissolved in DCM and passed through a short plug of silica, eluting with DCM, and the fractions containing product concentrated *in vacuo*. The crude product was recrystallised from of MeOH to give **227** as pale yellow crystals (6.32 g, 87%): R_f = 0.61 (DCM); ν_{max} 3267, 1713, 1597, 1352, 1039, 632 cm^{-1}; mp 104–107 °C (MeOH); δ_H (500.1 MHz, $CDCl_3$): 7.29 (2 H, d, *J* 2.4, *H*-2, *H*-6), 6.81 (1 H, t, *J* 2.4, *H*-4), 4.72 (4 H, d, *J* 2.4, C*H*$_2$), 3.91 (3 H, s, OC*H*$_3$), 2.54 (2 H, t, *J* 2.4, C≡C-*H*); δ_C (125.8 MHz, $CDCl_3$): 166.6 (*C*=O), 158.6 (*C*-3, *C*-5), 132.3 (*C*-1), 109.0 (*C*-2, *C*-6), 107.5 (*C*-4), 78.1 (*C*≡C-H), 76.1 (C≡*C*-H), 56.3 (*C*H$_2$), 52.5 (O*C*H$_3$); *m/z* (ES^+) 267 ($[M+Na]^+$, 100%), 245 ($[M+H]^+$, 10); HRMS (ES^+) calc. for $C_{14}H_{12}O_4Na$ $[M+Na]^+$ 267.0628, found 267.0623. Data are in agreement with the literature.[8]

6.3.2. Methyl 3,5-bis((3-(trimethylsilyl)prop-2-yn-1-yl)oxy)benzoate 228

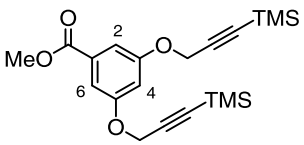

n-BuLi (2.5 M in hexanes, 21.7 mL, 54.3 mmol, 2.1 eq.) was added dropwise to a solution of diisopropylamine (8.41 mL, 59.6 mmol, 2.3 eq.) in THF (20 mL) at −78 °C. This solution was stirred for 20 min before dialkyne **227** in THF (40 mL) was added dropwise and this mixture stirred for 30 min before TMSCl (7.56 mL, 59.6 mmol, 2.3 eq.) was added slowly. This mixture was stirred for 10 min, before being allowed to warm to rt and stir for 16 h. The reaction was quenched by addition of sat. aqueous NH_4Cl (50 mL) before volatile components were removed under reduced pressure. The mixture was diluted with DCM (100 mL) and the phases separated and the aqueous phase extracted with DCM (3 × 50 mL). The combined organic phases were washed with sat. aqueous $NaHCO_3$ (50 mL) and brine (50 mL) and dried over Na_2SO_4 before being filtered and concentrated *in vacuo*. The crude product was purified by column chromatography (petroleum ether to 90:10 petroleum ether: Et_2O to 80:20 petroleum ether: Et_2O) to give **228** as a colourless oil (8.41 g, 84%): R_f = 0.49 (80:20 petroleum ether: Et_2O); ν_{max} 3147, 1720, 1651, 1595, 1045, 841, 760 cm^{-1}; δ_H (499.9 MHz, $CDCl_3$): 7.30 (2 H, d, *J* 2.4, *H*-2, *H*-6), 6.79 (1 H, t, *J* 2.4, *H*-4), 4.69 (4 H, s, CH_2), 3.90 (3 H, s, OCH_3), 0.17 (18 H, s, Si(CH_3)$_3$); δ_C (125.7 MHz, $CDCl_3$): 166.7 (*C*=O), 158.8 (*C*-3, *C*-5), 132.1 (*C*-1), 109.1 (*C*-2, *C*-6), 107.9 (*C*-4), 99.6 (*C*≡CTMS), 93.5 (C≡*C*TMS), 57.2 (CH_2), 52.4 (OCH_3), −0.18 (Si(CH_3)$_3$); *m/z* (ES^+) 799 ([2M+Na^+, 15%), 411 ([M+$Na]^+$, 100), 389 ([M+$H]^+$, 7); HRMS (ES^+) calc. for $C_{20}H_{28}O_4Si_2Na$ [M+$Na]^+$ 411.1418, found 411.1409.

6.3.3. 3,5-Bis((3-(trimethylsilyl)prop-2-yn-1-yl)oxy)benzyl alcohol 229

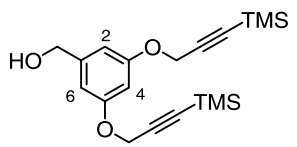

Lithium aluminium hydride (3.70 g, 97.4 mmol, 4.5 eq.) was added portion-wise to a solution of ester **228** (8.41 g, 21.6 mmol, 1 eq.) in Et_2O (100 mL) at 0 °C, and the suspension allowed to warm to rt and stirred for 3 h. The reaction was quenched after cooling the mixture to 0 °C, by the slow addition of water (3.7 mL), NaOH (2 M, 3.7 mL), and additional water (11.1 mL). The mixture stirred for 15 min before addition of $MgSO_4$, and further stirring for 15 min before the solids were removed by filtration, and the solvents removed *in vacuo.* The crude product was purified by column chromatography (67:33 petroleum ether: Et_2O) to give **229** as a colourless oil (5.06 g, 65%): R_f = 0.32 (50:50 petroleum ether: Et_2O); ν_{max} 3410, 1651, 1595, 1364, 1043, 842 cm^{-1}; δ_H (500.1 MHz, $CDCl_3$): 6.59 (2 H, d, *J* 2.3, *H*-2, *H*-6), 6.51 (1 H, t, *J* 2.3, *H*-4), 4.63 (4 H, s, ArOCH_2), 4.60 (2 H, s, HOCH_2Ar), 1.95 (1 H, br s, O*H*), 0.17 (18 H, s, Si(CH_3)$_3$); δ_C (125.8 MHz, $CDCl_3$): 159.1 (*C*-3, *C*-5), 143.5 (*C*-1), 106.3 (*C*-2, *C*-6), 101.6 (*C*-4), 100.0 (*C*≡CTMS), 93.0 (C≡*C*TMS), 65.2 (HO*C*H_2Ar), 57.0 (ArO*C*H_2), −0.2 (Si(*C*H_3)$_3$); *m/z* (ES^+) 383 ($[M+Na]^+$, 100%), 367 ($[M+H]^+$, 31); HRMS (ES^+) calc. for $C_{19}H_{28}O_3Si_2Na$ $[M+Na]^+$ 383.1469, found 383.1458. Data are in agreement with the literature.[9]

6.3.4. 3,5-Bis((3-(trimethylsilyl)prop-2-yn-1-yl)oxy)benzaldehyde 223

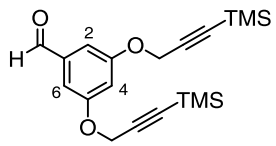

Dess-Martin periodinane (5.50 g, 13.0 mmol, 1.1 eq.) was added to a solution of alcohol **229** (4.25 g, 11.8 mmol, 1 eq.) in DCM (100 mL), and the solution stirred at rt for 1 h. The reaction was quenched by the addition of sat. aqueous $NaHCO_3$ (100 mL), followed by Et_2O (200 mL) and $Na_2S_2O_3$ (11.0 g) and the biphasic mixture stirred vigorously for 1 h. The phases were separated and the aqueous phase extracted with Et_2O (3 × 100 mL). The combined organic phases were dried over Na_2SO_4 before being filtered and concentrated *in vacuo* to give to give aldehyde **223** as a colourless oil without further purification (4.30 g, quant.): R_f = 0.86 (50:50 petroleum ether: Et_2O); ν_{max} 2959, 1703, 1595, 1292, 1252, 1157, 1059, 851 cm^{-1}; δ_H (500.1 MHz, $CDCl_3$): 9.91 (1 H, s, ArC*H*O), 7.12 (2 H, d, *J* 2.4, *H*-2), 6.86 (1 H, t, *J* 2.4, *H*-4), 4.71 (4 H, s, CH_2), 0.17 (18 H, s, Si(CH_3)$_3$); δ_C (125.8 MHz, $CDCl_3$): 191.7 (Ar*C*HO), 159.4 (*C*-3, *C*-5), 138.4 (*C*-1), 109.2 (*C*-4), 108.9 (*C*-2, *C*-6), 99.3 (C≡*C*TMS), 93.8 (*C*≡CTMS), 57.2 (*C*H_2), −0.2 (Si(*C*H_3)$_3$); *m/z* (ES^+) 413 ($[M+MeOH+Na]^+$, 100%), 381 ($[M+Na]^+$, 30), 359 ($[M+H]^+$, 5); HRMS (ES^+) calc. for $C_{19}H_{27}O_3Si_2$ $[M+H]^+$ 359.1493, found 359.1452.

6.3.5. 3,6,9,12-Tetraoxapentadec-14-yn-1-ol 231

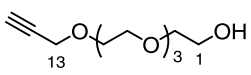

NaH (60% dispersion in mineral oil, 0.61 g, 15.3 mmol, 1.1 eq.) was added to a solution of tetraethyleneglycol (5.00 g, 25.7 mmol, 1.9 eq.) in THF (50 mL) at 0 °C. The suspension was allowed to warm to rt and stirred for 60 min, before being re-cooled to 0 °C. Propargyl chloride (0.98 mL, 14 mmol, 1.0 eq.) was added dropwise over 20 min, before the mixture was warmed to rt and stirred for 2 h. The reaction was quenched by addition of sat. aqueous NH_4Cl (10 mL), and volatile components removed *in vacuo*. The residue was diluted with DCM (100 mL) and water (30 mL) and the phases separated. The aqueous phase was extracted with DCM (3 × 50 mL). The combined organic phases were dried over Na_2SO_4 before being filtered and concentrated *in vacuo.* The crude product was purified by column chromatography (50:50 petroleum ether: acetone) to give **231** as a colourless oil (1.49 g, 47%): R_f = 0.26 (50:50 petroleum ether: acetone); ν_{max} 3394, 2875, 1716, 1250, 1105 cm^{-1}; δ_H (500.1 MHz, $CDCl_3$): 4.20 (2 H, d, *J* 2.4, C*H*$_2$C≡CH), 3.73–3.60 (16 H, m, PEG C*H*$_2$), 2.43 (1 H, t, *J* 2.4, $CH_2C{\equiv}CH$), 2.23 (1 H, br s, CH_2OH); δ_C (125.8 MHz, $CDCl_3$): 79.7 ($CH_2C{\equiv}CH$), 74.7 ($CH_2C{\equiv}CH$), 72.7 (CH_2OH), 70.8, 70.7, 70.7, 70.5, 70.5, 69.2, 61.9 (PEG CH_2), 58.5 ($CH_2C{\equiv}CH$); *m/z* (ES^+) 255 ($[M+Na]^+$, 65); HRMS (ES^+) calc. for $C_{11}H_{20}O_5Na$ $[M+Na]^+$ 255.1203, found 255.1195. Data are in agreement with the literature.[10]

6.3.6. 3,6,9,12-Tetraoxapentadec-14-yn-1-yl tosylate 232

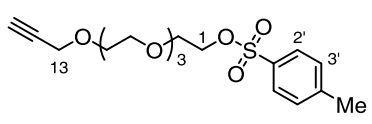

Tosyl chloride (1.46 g, 7.65 mmol, 1.2 eq.) was added to a solution of alcohol **231** (1.48 g, 6.41 mmol, 1 eq.) and Et_3N (2.66 mL, 19.1 mmol, 3 eq.) in DCM (20 mL) at 0 °C, and the solution stirred at rt for 18 h. The reaction was quenched by addition of sat. aqueous NH_4Cl (50 mL) and DCM (50 mL), the phases separated and the aqueous phase extracted with DCM (4 × 50 mL). The combined organic phases were washed with aqueous HCl solution (1 M, 50 mL), followed by brine (50mL), and dried over Na_2SO_4 before being filtered and concentrated *in vacuo*. The crude product was purified by column chromatography (DCM to 98:2 DCM: MeOH to 95:5 DCM: MeOH) to give **232** as a pale yellow oil (2.22 g, 90%): R_f = 0.71 (95:5 DCM: MeOH); ν_{max} 2870, 1456, 1352, 1175, 1096, 920, 664, 556 cm^{-1}; δ_H (500.1 MHz, $CDCl_3$): 7.81–7.78 (2 H, m, *H*-2', *H*-6'), 7.35–7.26 (2 H, m, *H*-3', *H*-5'), 4.19 (2 H, d, *J* 2.4, C*H*$_2$C≡CH), 4.17–4.14 (2 H, m, PEG C*H*$_2$), 3.70–3.61 (10 H, m, PEG C*H*$_2$), 3.59–3.57 (4 H, m, PEG C*H*$_2$), 2.45 (3 H, s, C4'-C*H*$_3$), 2.42 (1 H, t, *J* 2.4, $CH_2C{\equiv}CH$); δ_C (125.8 MHz, $CDCl_3$): 144.9 (*C*-1'), 133.1 (*C*-4'), 130.0 (*C*-3', *C*-5'), 128.1 (*C*-2', *C*-6'), 79.8 ($CH_2C{\equiv}CH$), 74.7 ($CH_2C{\equiv}CH$), 70.9, 70.7, 70.7, 70.7, 70.5, 70.5, 69.4, 69.3, 68.1 (PEG CH_2), 58.4 ($CH_2C{\equiv}CH$), 21.8 (C4'-CH_3); *m/z* (ES^+) 409 ($[M+Na]^+$, 83%), 425 ($[M+Na]^+$, 100). Data are in agreement with the literature.[10]

6.3.7. 1-Azido-3,6,9,12-tetraoxapentadec-14-yne 233

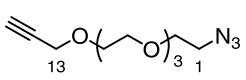

NaN_3 (0.441 g, 7.87 mmol, 2.5 eq.) was added to a solution of tosylate **232** (1.00 g, 2.71 mmol, 1 eq.) in DMF (5 mL), and the solution stirred at 50 °C for 18 h. DMF was removed *in vacuo*, and the residue was purified by column chromatography (50:50 petroleum ether: Et_2O) to give the azide **233** as a colourless oil (552 mg, 79%): R_f = 0.13 (50:50 petroleum ether: Et_2O); ν_{max} 2866, 1456, 1350, 1096, 839, 775 cm^{-1}; δ_H (500.1 MHz, $CDCl_3$): 4.20 (2 H, d, *J* 2.4, CH_2C≡CH), 3.73–3.60 (14 H, m, PEG CH_2), 3.41–3.36 (2 H, m, CH_2N_3), 2.42 (1 H, t, *J* 2.4, $CH_2C{\equiv}CH$); δ_C (125.8 MHz, $CDCl_3$): 79.8 ($CH_2C{\equiv}CH$), 74.6 ($CH_2C{\equiv}CH$), 70.8, 70.8, 70.8, 70.8, 70.6, 70.2, 69.3 (PEG CH_2), 58.6 ($CH_2C{\equiv}CH$), 50.8 (CH_2N_3); *m/z* (ES^+) 537 ($[2M+Na]^+$, 52%), 280 ($[M+Na]^+$, 27), 258 ($[M+H]^+$, 100); HRMS (ES^+) calc. for $C_{11}H_{20}N_3O_4$ $[M+H]^+$ 258.1448, found 258.1452. Data are in agreement with the literature.[11]

6.3.8. 1-Amino-3,6,9,12-tetraoxapentadec-14-yne 222

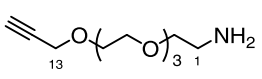

PPh_3 (2.13 g, 8.12 mmol, 1.2 eq.) and water (0.12 mL, 6.76 mmol, 1 eq.) were added to a solution of azide **233** (1.74 g, 6.76 mmol, 1 eq.) in THF (15 mL), and the solution stirred at rt for 72 h. All volatiles were removed *in vacuo*, and the residue was purified by column chromatography (DCM to 95:5 DCM: MeOH to 90:10 DCM: MeOH to 89:10:1 DCM: MeOH: Et_3N) to give the amine **222** as a colourless oil (1.36 g, 87%): R_f = 0.13 (89:10:1 DCM: MeOH: Et_3N); ν_{max} 2872, 1668, 1350, 1109, 947 cm^{-1}; δ_H (500.1 MHz, $CDCl_3$): 4.19 (2 H, d, *J* 2.4, C*H*$_2$C≡CH), 3.71–3.61 (12 H, m, PEG C*H*$_2$), 3.51 (2 H, t, *J* 5.3, C*H*$_2$CH$_2$NH$_2$), 2.86 (2 H, t, *J* 5.3, CH$_2$C*H*$_2$NH$_2$), 2.42 (1 H, t, *J* 2.4, CH$_2$C≡C*H*), 1.78 (2 H, br s, N*H*$_2$); δ_C (125.8 MHz, $CDCl_3$): 79.7 (CH$_2$*C*≡CH), 74.7 (CH$_2$C≡*C*H), 73.4, 70.7, 70.7, 70.7, 70.5, 70.4, 69.2 (PEG *C*H$_2$), 58.5 (*C*H$_2$C≡CH), 41.9 (*C*H$_2$NH$_2$); *m/z* (ES^+) 254 ($[M+Na]^+$, 62%), 232 ($[M+H]^+$, 100). Data are in agreement with the literature.[11]

6.3.9. *N*-(3',5'-bis((3-(trimethylsilyl)prop-2-yn-1-yl)oxy)benzyl)-3,6,9,12-tetraoxapentadec-14-yn-1-amine 234

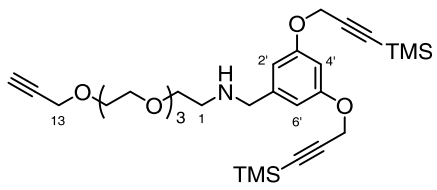

Acetic acid (0.60 mL, 10.6 mmol, 2 eq.) and $NaB(OAc)_3H$ (4.50 g, 21.22 mmol, 4 eq.) were slowly added to a solution of aldehyde **223** (1.90 g, 5.31 mmol, 1 eq.) and amine **222** (1.35 g, 5.84 mmol, 1.1 eq.) in THF (10 mL), and the mixture stirred at rt for 18 h. The mixture was diluted with Et_2O (50 mL) and quenched by careful addition of sat. aqueous $NaHCO_3$ (50 mL), before the phases were separated and the aqueous phase extracted with Et_2O (3 × 50 mL). The combined organic phases were dried over Na_2SO_4 before being filtered and concentrated *in vacuo* The crude product was purified by column chromatography (DCM to 97:3 DCM: MeOH to 95:5 DCM: MeOH) to give **234** as a colourless oil (1.09 g, 35%): R_f = 0.44 (90:10 DCM: MeOH); ν_{max} 2870, 1597, 1456, 1252, 1152, 1105, 1061, 854 cm^{-1}; δ_H (499.9 MHz, $CDCl_3$): 6.57 (2 H, d, *J* 2.2, *H*-2', *H*-6'), 6.47 (1 H, t, *J* 2.2, *H*-4'), 4.62 (4 H, s, C*H*$_2$C≡CSi), 4.17 (2 H, d, *J* 2.4 C*H*$_2$C≡CH), 3.73 (2 H, bs, NHC*H*$_2$Ar), 3.68–3.57 (14 H, m, PEG C*H*$_2$), 2.77 (2 H, t, *J* 5.1, C*H*$_2$NHCH$_2$Ar), 2.41 (1 H, t, *J* 2.4, CH$_2$C≡C*H*), 2.23 (1 H, br s, N*H*), 0.16 (18 H, s, Si(C*H*$_3$)$_3$); δ_C (125.7 MHz, $CDCl_3$): 159.0 (*C*-3', *C*-5'), 142.7 (*C*-1'), 107.7 (*C*-2', *C*-6'), 101.0 (*C*-4'), 100.1 (2 × CH$_2$*C*≡CSi), 92.7 (2 × CH$_2$C≡*C*Si), 79.7 (CH$_2$*C*≡CH), 74.7 (CH$_2$C≡*C*H), 70.7, 70.7, 70.6, 70.6, 70.5, 70.4, 69.2 (PEG *C*H$_2$), 58.5 (*C*H$_2$C≡CH), 56.9 (2 × *C*H$_2$C≡CSi), 58.8 (NH*C*H$_2$Ar), 48.6 (*C*H$_2$NHCH$_2$Ar), −0.17 (Si(*C*H$_3$)$_3$); *m/z* (ESI^+) 574 ($[M+H]^+$, 100%); HRMS (ESI^+) calc. for $C_{30}H_{48}NO_6Si_2$ $[M+H]^+$ 574.3015, found 574.3003.

6.3.10. *N,N*-bis(3',5'-bis((3-(trimethylsilyl)prop-2-yn-1-yl)oxy)benzyl)-3,6,9,12-tetraoxapentadec-14-yn-1-amine 235

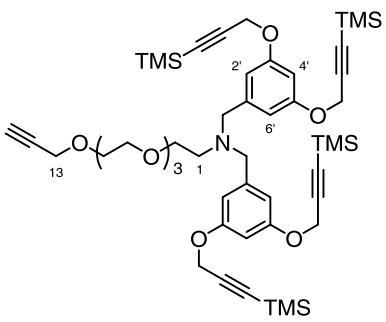

Acetic acid (0.60 mL, 10.6 mmol, 2 eq.) and $NaB(OAc)_3H$ (4.50 g, 21.22 mmol, 4 eq.) were slowly added to a solution of aldehyde **233** (1.90 g, 5.31 mmol, 1 eq.) and amine **222** (1.35 g, 5.84 mmol, 1.1 eq.) in THF (10 mL), and the mixture was stirred at rt for 18 h. The mixture was diluted with Et_2O (50 mL) and quenched by careful addition of sat. aqueous $NaHCO_3$ (50 mL), before the phases were separated and the aqueous phase extracted with Et_2O (3 × 50 mL). The combined organic phases were dried over Na_2SO_4 before being filtered and concentrated *in vacuo*. The crude product was purified by column chromatography (DCM to 97:3 DCM: MeOH to 95:5 DCM: MeOH) to give **235** as a colourless oil (500 mg, 21%): R_f = 0.85 (90:10 DCM: MeOH); ν_{max} 2959, 1597, 1456, 1361, 1252, 1153, 1061, 856, 762 cm^{-1}; δ_H (300.1 MHz, $CDCl_3$): 6.62 (4 H, d, *J* 2.3, *H*-2', *H*-6'), 6.47 (2 H, t, *J* 2.4, *H*-4'), 4.63 (8 H, s, C*H*$_2$C≡CSi), 4.18 (2 H, d, *J* 2.4 C*H*$_2$C≡CH), 3.69–3.52 (18 H, m, PEG C*H*$_2$, $CH_2N(CH_2Ar)_2$), 2.67 (2 H, t, *J* 6.1, C*H*$_2$N($CH_2Ar)_2$), 2.41 (1 H, t, *J* 2.4, $CH_2C{\equiv}CH$), 0.17 (36 H, s, $Si(CH_3)_3$); δ_C (75.5 MHz, $CDCl_3$): 158.9 (*C*-3', *C*-5'), 142.4 (*C*-1'), 108.3 (*C*-2', *C*-6'), 100.8 (*C*-4'), 100.2 (4 × $CH_2C{\equiv}CSi$), 92.7 (4 × $CH_2C{\equiv}CSi$), 79.8 ($CH_2C{\equiv}CH$), 74.7 ($CH_2C{\equiv}CH$), 70.7, 70.7, 70.7, 70.5, 70.5, 70.1, 69.2 (PEG CH_2), 59.1 ($CH_2N(CH_2Ar)_2$), 58.2 ($CH_2C{\equiv}CH$), 57.0 (4 × $CH_2C{\equiv}CSi$), 52.9 ($CH_2N(CH_2Ar)_2$), −0.11 ($Si(CH_3)_3$); *m/z* (ES^+) calc. isotope pattern for $C_{49}H_{74}NO_8Si_4$ $[M+H]^+$ 916.4 (100%), 917.4 (53), 918.4 (13), 919.4 (10), found 916.5 (100%), 917.5 (53), 918.5 (14), 919.5 (8).

6.3.11. 5'-Chloro-5'-deoxy-2-iodoadenosine 238

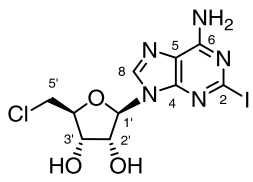

Pyridine (103 μL, 1.27 mmol, 2.0 eq.) and thionyl chloride (103 μL, 1.91 mmol, 3.0 eq.) were slowly added to a suspension of **179** (250 mg, 0.363 mmol, 1.0 eq.) in MeCN (12 mL) at 0 °C. The mixture was stirred at 0 °C for 4 h, warmed to rt and stirred for a further 18 h. The volatile components were removed, and the residue was diluted with MeOH:water:aqueous ammonia solution (35% *v/v*) (10:2:1, 10 mL) and the solution stirred for 2 h. After concentration, the residue was purified by column chromatography (95:5 DCM:MeOH to 90:10 DCM:MeOH) to afford the product **238** as a white foam (167 mg, 64%): R_f = 0.47 (20:80 petroleum ether:acetone); $[\alpha]_D^{20}$ -6.3 (*c* 0.51, MeOH); mp 127–130 °C (DCM); ν_{max} 3155, 1637, 1589, 1650, 1288, 1049, 656 cm^{-1}; δ_H (500.1 MHz, d_4-MeOD): 8.15 (1 H, s, *H*-8), 5.95 (1 H, d, *J* 5.1, *H*-1′), 4.77 (1 H, dd, *J* 5.2, 5.1, *H*-2′), 4.39 (1 H, dd, *J* 5.2, 4.2, *H*-3′), 4.27-4.24 (1 H, m, *H*-4′), 3.95 (1 H, dd, 11.8, 5.3, *H*-5′a), 3.85 (1 H, dd, 11.8, 5.2, *H*-5′b); δ_C (125.8 MHz, d_4-MeOD): 155.7 (*C*-6), 149.6 (*C*-4), 139.7 (*C*-8), 119.3 (*C*-5), 119.1 (*C*-2), 89.1 (*C*-1′), 84.1 (*C*-4′), 73.4 (*C*-2′), 71.4 (*C*-3′), 43.6 (*C*-5′); *m/z* (ES^+) 434 ($[M+Na]^+$ 60%), 412 ($[M+H]^+$, 24); HRMS (ES^+) calc. for $C_{10}H_{11}{}^{35}ClN_5O_3INa$ $[M+Na]^+$ 433.9487, found 433.9477.

6.3.12. 2',3'-*O*-Isopropylidene-2-iodoadenosine 239

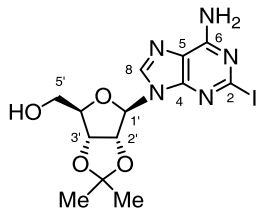

2,2-Dimethoxypropane (1.55 mL, 12.7 mmol, 10 eq.) and perchloric acid (70% *v/v* in water, 75 µL, 0.839 mmol, 0.67 eq.) were slowly added to a suspension of **179** (500 mg, 1.27 mmol, 1.0 eq.) in acetone (15 mL) at 0 °C. The mixture was allowed to slowly warm to rt, and stirred for a further 18 h. The reaction was quenched by addition of sat. aqueous $NaHCO_3$ solution (1 mL) and concentrated *in vacuo*. The residue was adsorbed onto silica and purified by column chromatography (20:80 petroleum ether:acetone) to give the product **239** as a white foam (550 mg, quant.): R_f = 0.56 (20:80 petroleum ether:acetone); $[\alpha]_D^{20}$ −19.2 (*c* 1.26, MeOH); mp 131–135 °C (petroleum ether:acetone); ν_{max} 3192, 1638, 1589, 1570, 1209, 1070, 849, 823 cm^{-1}; δ_H (500.1 MHz, $CDCl_3$): 7.73 (1 H, s, *H*-8), 6.08 (2 H, br s, NH_2), 5.79 (1 H, d, *J* 5.3, *H*-1'), 5.36 (1 H, dd, *J* 11.8, 1.9, C-5' O*H*), 5.18 (1 H, dd, *J* 5.7, 5.3, *H*-2'), 5.11 (1 H, dd, *J* 5.7, 1.4, *H*-2'), 4.52 (1 H, ddd, *J* 1.8, 1.7, 1.4, *H*-4'), 3.99 (1 H, m, *H*-5'a), 3.82 (1 H, m, *H*-5'b), 1.63 (3 H, s, $C(CH_3)_2$), 1.38 (3 H, s, $C(CH_3)_2$); δ_C (125.8 MHz, $CDCl_3$): 155.5 (*C*-6), 149.2 (*C*-4), 140.3 (*C*-8), 121.0 (*C*-5), 119.4 (*C*-2), 114.3 ($C(CH_3)_2$), 94.2 (*C*-1'), 86.1 (*C*-4'), 82.8 (*C*-2'), 81.7 (*C*-3'), 63.5 (*C*-5'), 27.8 ($C(CH_3)_2$), 25.4 ($C(CH_3)_2$); *m/z* (ES^+) 456 ($[M+Na]^+$ 100%), 434 ($[M+H]^+$, 23); HRMS (ES^+) calc. for $C_{13}H_{16}N_5O_4INa$ $[M+Na]^+$ 456.1039, found 456.1031.

6.3.13. 5'-Fluoro-5'-deoxy-2',3'-*O*-isopropylidene-2-iodoadenosine 240

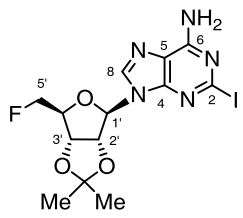

TsF (442 mg, 2.54 mmol, 2.0 eq.) and TBAF (1 M in THF, 5.08 mL, 5.08 mmol, 4.0 eq.) were added to a solution of **239** (550 mg, 1.27 mmol, 1.0 eq.) in THF (16 mL). The mixture was heated to 60 °C for 18 h, and cooled to rt. The volatile components were removed and the orange residue was purified by column chromatography (80:20 petroleum ether:acetone to 70:30 petroleum ether:acetone to 60:40 petroleum ether:acetone) to give the product **240** as a white foam (270 mg, 49%): R_f = 0.79 (50:50 petroleum ether:acetone); $[\alpha]_D^{20}$ −7.2 (*c* 1.06, MeOH); mp 88–90 °C (petroleum ether:acetone); ν_{max} 3169, 1636, 1587, 1568, 1204, 1072, 1009, 870, 754, 656 cm^{-1}; δ_H (500.1 MHz, $CDCl_3$): 7.81 (1 H, s, *H*-8), 6.14 (1 H, d, *J* 2.1, *H*-1'), 6.05 (2 H, br s, NH_2), 5.25-5.23 (1 H, m, *H*-2'), 5.07 (1 H, dd, *J* 6.2, 3.5, *H*-3'), 4.68 (1 H, ddd, *J* 46.9, 10.3, 3.6, *H*-5'a), 4.63 (1 H, ddd, *J* 47.0, 10.3, 5.2, *H*-5'b), 4.53-4.46 (1 H, m, *H*-4'), 1.63 (3 H, s, C(CH_3)$_2$), 1.40 (3 H, s, C(CH_3)$_2$); δ_C (125.8 MHz, $CDCl_3$): 155.2 (*C*-6), 149.6 (*C*-4), 139.2 (*C*-8, d, *J* 3.5), 119.8 (*C*-5, *C*-2), 114.8 (*C*(CH_3)$_2$), 90.5 (*C*-1'), 85.9 (*C*-4', d, *J* 19.3), 84.6 (*C*-2'), 82.9 (*C*-5', d, *J* 171.6), 80.7 (*C*-3', d, *J* 7.0), 27.2 (C(*C*H_3)$_2$), 25.4 (C(*C*H_3)$_2$); δ_F (470.3 MHz, $CDCl_3$): −227.93 (ddd, *J* 47.0, 46.9, 22.7, CH_2*F*); *m/z* (ES^+) 458 ($[M+Na]^+$ 100%), 436 ($[M+H]^+$ 37); HRMS (ES^+) calc. for $C_{13}H_{15}N_5O_3FINa$ $[M+Na]^+$ 458.0096, found 458.0086.

6.3.14. 5'-Fluoro-5'-deoxy-2-iodoadenosine 241

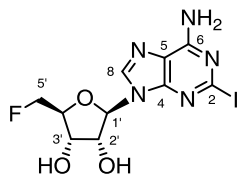

Anhydrous TsOH (16.0 mg, 0.0930 mmol, 0.15 eq.) was added to a solution of **240** (270 mg, 0.620 mmol) in MeOH (10 mL), and the mixture was heated to reflux for 48 h, before being concentrated The residue was adsorbed onto silica and purified by column chromatography (50:50 petroleum ether:acetone) to give the product **241** as a white powder (245 mg, 71%): R_f = 0.0.23 (50:50 petroleum ether:acetone); $[\alpha]_D^{20}$ −23.8 (*c* 0.32, DMSO); ν_{max} 3144, 2181, 1639, 1298, 1074, 912, 752, 656 cm^{-1}; mp 210 °C (decomp.) (petroleum ether:acetone);. δ_H (500.1 MHz, d_4-MeOD): 8.09 (1 H, s, *H*-8), 8.00 (2 H, br s, NH_2), 5.99 (1 H, d, *J* 4.2, *H*-1'), 4.74 (1 H, ddd, *J* 48.0, 10.6, 2.8, *H*-5'a), 4.68 (1 H, ddd, *J* 47.4, 10.6, 3.8, *H*-5'b), 4.57-4.55 (1 H, m, *H*-2'), 4.39 (1 H, dd, *J* 5.2, 5.2, *H*-3'), 4.27-4.17 (1 H, m, *H*-4'); δ_C (125.8 MHz, d_4-MeOD): 155.7 (*C*-6), 149.5 (*C*-2), 138.9 (*C*-8, d, *J* 4.5), 119.4 (*C*-5), 119.2 (*C*-2), 89.0 (*C*-1'), 83.1 (*C*-4', d, *J* 18.7), 82.1 (*C*-5', d, *J*, 170.5), 74.2 (*C*-2'), 69.6 (*C*-3', d, *J* 5.3); δ_F (470.3 MHz, d_4-MeOD): −232.1 (ddd, *J* 48.0, 47.4, 26.8, CH_2F); *m/z* (ES^+) 418 ($[M+Na]^+$ 100%), 396 ($[M+H]^+$ 12); HRMS (ES^+) calc. for $C_{10}H_{11}FIN_5O_3Na$ $[M+Na]^+$ 417.9784, found 417.9774.

6.3.15. ClDEA-PEG-(C≡CH)$_2$ 219

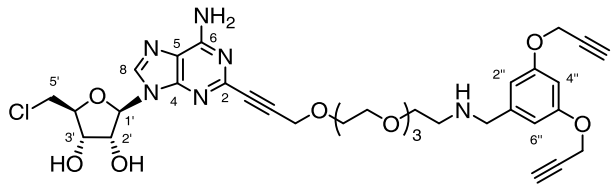

$Pd(PPh_3)_2Cl_2$ (6.8 mg, 0.0097 mmol, 0.1 eq.), copper(I) iodide (1.9 mg, 0.0097 mmol, 0.1 eq.) and triethylamine (68 µL, 0.49 mmol, 5 eq.) were added to a solution of iodo compound **238** (40 mg, 0.097 mmol, 1.0 eq.) and alkyne **234** (112 mg, 0.194 mmol, 2.0 eq.) in degassed DMF (5 mL). The mixture was heated to 80 °C for 48 h, after which time the volatile components were removed *in vacuo*. The residue was partly purified by column chromatography (50:50 petroleum ether:acetone to 40:60 petroleum ether:acetone to 80:20 petroleum ether:acetone to 80:20 EtOAc:acetone to 10:90 MeOH:acetone to 10:89:1 MeOH:acetone:1% aqueous ammonia (30%)) to afford fractions containing the coupled product (identified by ESMS). After concentration, the fractions were further purified by column chromatography (acetone to 5:95 MeOH:acetone to 10:90 MeOH:acetone) to afford the crude coupled product (20 mg) which was used directly, without further purification.

The crude product (20 mg) was dissolved in MeOH (10 mL) and 3HF.Et_3N (200 µL) was added and the mixture stirred for 18 h. The reaction was quenched by addition of sat. aqueous $NaHCO_3$ (2 mL) and the mixture concentrated under reduced pressure. The mixture was partly purified by column chromatography (99:1 acetone:aqueous ammonia (30%) to 5:94:1 MeOH:acetone:aqueous ammonia (30%) to 10:89:1 MeOH:acetone: aqueous ammonia (30%)). Fractions containing product were combined and concentrated. The residue was dissolved in MeCN: water (20:80) and purified by semi-preparative HPLC on the Shimadzu system (Phenomenex Kingsorb C_{18} (250 × 10.00 mm, 5µ); mobile Phase: A (H_2O + 0.05% TFA), B (MeCN + 0.05% TFA); linear gradient: 20% B at 0 min to 70% B at 18 min, to 95% B at 19 min, to 20% B at 24 min, to 20% B at 30 min; flow rate: 2.5 mL.min^{-1}; detection 220 nm. Fractions containing product (t_R = 16.7 min) were concentrated under a stream of compressed air, and lyophilised from a solution of ^{t}BuOH in water (20% *v/v*) affording **219** as a white solid (3.4 mg, 4.2% over two steps): δ_H (500.1 MHz, 1:1 D_2O:*d*$_3$-MeCN): 8.78 (1 H, s, *H*-8), 7.15 (2 H, d, *J* 2.2, *H*-2''), 7.08 (1 H, t, *J* 2.2, *H*-4''), 6.43 (1 H, d, *J* 4.9, *H*-1'), 5.20 (4 H, d, *J* 2.3, OC*H*$_2$C≡CH), 5.11 (1 H, dd, *J* 5.0, 4.9, H-2'), 4.87 (2 H, s, ArC≡CC*H*$_2$PEG), 5.84 (1 H, dd, *J* 5.0, 5.0, *H*-3'), 4.77 (1 H, *H*-4', under HDO peak, observed in 2D), 4.61 (2 H, s, PEGCH$_2$NHC*H*$_2$Ar), 4.40 (1 H, dd, *J* 12.2, 3.9, *H*-5'a), 4.34 (1 H, dd, *J* 12.2, 5.0, *H*-5'b), 4.22–4.08 (14 H, m, PEG-C*H*$_2$), 3.63 (2 H, t, *J* 5.0,

PEGC*H*$_2$NHCH$_2$Ar), 3.44 (2 H, t, *J* 2.3 CH$_2$C≡C*H*); δ_C (125.8 MHz, 1:1 D$_2$O:*d*$_3$-MeCN): 158.4 (*C*-3'', *C*-5''), 154.4 (*C*-6), 148.7 (*C*-4), 143.8 (*C*-2), 140.5 (*C*-8), 132.8 (*C*-1''), 118.3 (*C*-5, observed in 2D), 109.1 (*C*-2'', *C*-6''), 102.1 (*C*-4''), 87.6 (*C*-1'), 83.4 (Ar*C*≡CCH$_2$PEG), 83.0 (*C*-4'), 82.9 (2 × C≡*C*H), 78.0 (2 × C≡*C*H), 76.5 (*C*-2'), 73.4 (*C*-3'), 70.5, 69.5, 69.4, 69.3, 69.2, 69.2, 68.9, 64.8 (PEG-*C*H$_2$), 68.7 (ArC≡*C*CH$_2$PEG), 57.8 (ArC≡C*C*H$_2$PEG), 55.6 (2 × O*C*H$_2$C≡CH), 50.0 (PEG*C*H$_2$NHCH$_2$Ar), 46.0 (PEGCH$_2$NH*C*H$_2$Ar), 44.7 (*C*-5'); *m/z* (ES$^+$) calc. isotope pattern for $C_{34}H_{43}ClN_6O_9$ $[M+H]^+$ 713.3 (100), 714.3 (36), 715.3 (32), 716.3 (12), found 713.3 (40), 714.3 (100), 715.3 (87), 716.3 (28); HRMS (ES$^+$) calc. for $C_{34}H_{43}{}^{35}ClN_6O_9$ $[M+H]^+$ 714.2755, found 714.2749.

6.3.16. CIDEA-PEG-(C≡CH)$_4$ 220

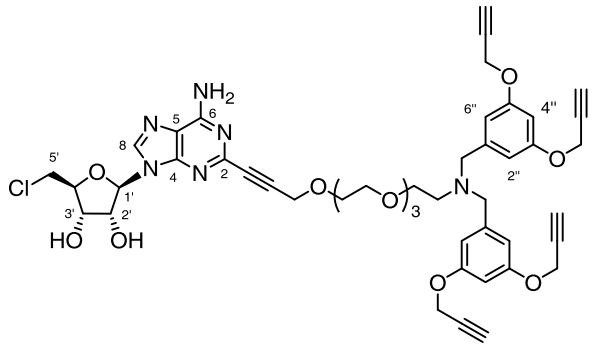

$Pd(PPh_3)_2Cl_2$ (13 mg, 0.018 mmol, 0.1 eq.), copper(I) iodide (3.5 mg, 0.018 mmol, 0.1 eq.) and triethylamine (129 µL, 0.923 mmol, 5 eq.) were added to a solution of iodo compound **238** (76 mg, 0.185 mmol, 1.0 eq.), alkyne **235** (338 mg, 0.369 mmol, 2.0 eq.) and PPh_3 (24 mg, 0.092 mmol, 0.5 eq.) in degassed DMF (5 mL). The mixture was heated to 57 °C for 48 h, after which time the volatile components were removed *in vacuo*. The residue was partly purified by column chromatography (Et_2O to 70:30 Et_2O:acetone) to afford fractions containing the coupled product (identified by ESMS). The compound was taken up into toluene (50 mL) and NaS_2O_7 solution (20% *w/v*, 50 mL) and the mixture heated to 60 °C for 1 h. After cooling, the phases were separated and the aqueous phase extracted with toluene (3 × 20 mL), and the organic phases combined, dried over Na_2SO_4 and concentrated. The product was further purified by column chromatography (90:10 petroleum ether:acetone to 70:30 petroleum ether:acetone to 60:40 petroleum ether:acetone) to afford the crude coupled product (40 mg), which was used directly in the next step, without further purification.

The crude product (40 mg) was dissolved in MeOH (15 mL) and 3HF.Et_3N (250 µL) was added and the mixture stirred for 20 h. The reaction was quenched by addition of sat. aqueous $NaHCO_3$ (4 mL) and the mixture concentrated under reduced pressure. The mixture was partly purified by column chromatography (DCM to 92.5:7.5 DCM:MeOH). Fractions containing product were combined and concentrated. The residue was dissolved in MeCN: water (20:80) and purified by semi-preparative HPLC on the Shimadzu system (Phenomenex Kingsorb C_{18} (250 × 10.00 mm, 5µ); mobile Phase: A (H_2O + 0.05% TFA), B (MeCN + 0.05% TFA); linear gradient: 20% B at 0 min to 70% B at 20 min, to 95% B at 21 min; to 95% B at 25 min, B to 5% B at 26 min, to 5% B at 35 min; flow rate: 2.5 mL.min^{-1}; detection 220 nm. Fractions containing product (t_R = 18.7 min) were concentrated under a stream of compressed air, and lyophilised from a solution of ^{t}BuOH in water (20% *v/v*) affording **220** as a white solid (5.3 mg, 2.8% over two steps): δ_H (499.9 MHz, d_4-MeOD): 8.31 (1 H, s, *H*-8), 6.69 (4 H, d, *J* 2.3, *H*-2'', *H*-6''), 6.47 (2 H, t, *J* 2.3, *H*-4''), 6.00 (1 H, d, *J* 4.9, *H*-1'), 4.74 (1 H, dd, *J* 5.0, 4.9, *H*-2'), 4.70 (8 H, d, *J* 2.4, OCH_2C≡CH), 4.42 (2 H, s, ArC≡CCH_2PEG),

4.39 (1 H, dd, *J* 5.0, 4.9, *H*-3'), 4.27 (1 H, m, *H*-4'), 3.97 (1 H, dd, *J* 11.9, 4.9, *H*-5'a), 3.86 (1 H, dd, *J* 11.9, 4.9, *H*-5'b), 3.75-3.55 (18 H, m, PEG-CH_2, PEGCH_2N(CH_2Ar)$_2$), 2.95 (4 H, t, *J* 2.4, CH_2C≡C*H*), 2.66 (2 H, t, *J* 5.8, PEGCH_2N(CH_2Ar)$_2$); δ_C (125.7 MHz, MeOD): 158.7 (2 × *C*-3'', 2 × *C*-5''), 152.0 (*C*-6), 150.1 (*C*-4, observed in 2D), 146.2 (*C*-2), 142.2 (2 × *C*-1''), 140.5 (*C*-8), 119.8 (*C*-5, observed in 2D), 107.9 (2 × *C*-2'', 2 × *C*-6''), 100.6 (2 × *C*-4''), 86.0 (Ar*C*≡CCH_2PEG, observed in 2D), 82.3 (ArC≡*C*CH_2PEG, observed in 2D), 88.9 (*C*-1'), 83.8 (*C*-4'), 79.3 (4 × *C*≡CH, observed in 2D), 78.5 (*C*-2'), 75.5 (4 × C≡*C*H), 73.6 (*C*-3'), 71.2, 70.3, 70.2, 70.2, 70.0, 70.0, 69.5, 69.1 (PEG-*C*H_2), 58.6 (2 × PEGCH_2N(*C*H_2Ar)$_2$), 58.0 (ArC≡C*C*H_2PEG), 55.6 (4 × O*C*H_2C≡CH), 52.6 (PEG*C*H_2N(CH_2Ar)$_2$), 43.8 (*C*-5'); *m/z* (ES^+) calc. isotope pattern for $C_{47}H_{52}ClN_6O_{11}$ $[M+H]^+$ 911.3 (100), 912.3 (51), 913.3 (32), 914.3 (16), 915.3 (4); found 911.3 (100), 912.3 (56), 913.3 (38), 914.3 (17), 915.3 (5). HRMS (ES^+) calc. for $C_{47}H_{52}{}^{35}ClN_6O_{11}$ $[M+H]^+$ 911.3377, found 911.3358.

6.3.17. FDEA-PEG-(C≡CH)$_2$ 245

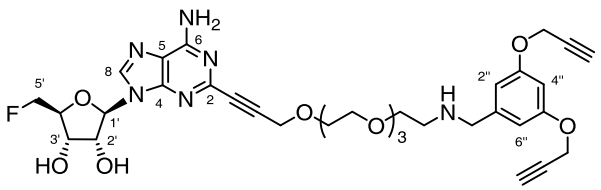

$Pd(PPh_3)_2Cl_2$ (15.4 mg, 0.022 mmol, 0.1 eq.), copper(I) iodide (4.2 mg, 0.022 mmol, 0.1 eq.) and triethylamine (150 µL, 1.10 mmol, 5 eq.) were added to a solution of iodo compound **241** (87 mg, 0.22 mmol, 1.0 eq.) and alkyne **234** (101 mg, 0.176 mmol, 0.8 eq.) in degassed DMF (4 mL). The mixture was heated to 60 °C for 48 h, after which time the volatile components were removed *in vacuo*. The resulting residue was partly purified by column chromatography (50:49:1 Et_2O:acetone:Et_3N to 20:79:1 Et_2O:acetone:Et_3N to 99:1 acetone:Et_3N to 70:20:10 EtOAc:isopropanol:water) to afford fractions containing the coupled product (identified by MS), which were combined and concentrated.

The crude product was dissolved in MeOH (20 mL) and 3HF.Et_3N (800 µL) was added and the mixture stirred overnight. The reaction was quenched by addition of sat. aqueous $NaHCO_3$ (20 mL) and the mixture concentrated under reduced pressure. The aqueous mixture was loaded onto a reverse phase cartridge (1000 mg Extract Clean C_{18}-HC, preconditioned with water), washed with water (10 mL), and the product eluted with water: MeCN (50:50) (2 × 10 mL). The eluted fractions were combined and concentrated. The residue was dissolved in MeCN: water (20:80) and purified by semi-preparitive HPLC on the Shimadzu system (Phenomenex Luna C_{18} (250 × 10.00 mm, 5µ); mobile Phase: A (H_2O + 0.05% TFA), B (MeCN + 0.05% TFA); linear gradient: 20% B at 0 min to 56% B at 13 min, to 95% B at 14 min; to 95% B at 19 min, B to 20% B at 20 min, to 20% B at 30 min; flow rate: 2.5 mL.min^{-1}; detection 220 nm. Fractions containing product (t_R = 13.8 min) were concentrated under a stream of compressed air, and lyophilised from a solution of ^{t}BuOH in water (20% *v/v*) affording **245** as a white solid (5.3 mg, 2.5% over two steps): δ_H (500.0 MHz, d_4-MeOD): 8.26 (1 H, s, *H*-8), 6.73 (2 H, d, *J* 2.3, *H*-2'', *H*-6''), 6.69 (1 H, t, *J* 2.3, *H*-4''), 6.04 (1 H, d, *J* 4.4, *H*-1'), 4.82-4.61 (6 H, m, OC*H*$_2$C≡CH, H-5'), 4.54 (1 H, m, H-2'), 4.43 (2 H, s, ArC≡CC*H*$_2$PEG), 4.39 (1 H, dd, *J* 5.2, 5.2, *H*-3'), 4.29-4.17 (3 H, m, PEGCH$_2$NHC*H*$_2$Ar, *H*-4'), 3.83-3,57 (14 H, m, PEG-C*H*$_2$), 3.28 (2 H, t, *J* 5.1, PEGC*H*$_2$NHCH$_2$Ar), 3.00 (2 H, t, *J* 2.4 CH$_2$C≡C*H*); δ_C (125.8 MHz, d_4-MeOD): 160.7 (*C*-3'', *C*-5''), 156.9 (*C*-6), 150.6 (*C*-4), 146.6 (*C*-2), 141.3 (d, *J* 4.9, *C*-8), 134.5 (*C*-1''), 120.0 (*C*-5), 110.6 (*C*-2''), 103.8 (*C*-4''), 90.0 (*C*-1'), 85.9 (Ar*C*≡CCH$_2$PEG), 84.6 (d, *J* 18.2, *C*-4'), 83.6 (d, *J* 163.8, *C*-5'), 82.9 (ArC≡*C*CH$_2$PEG), 79.4 (*C*≡CH), 77.4 (C≡*C*H), 75.9 (*C*-2'), 71.6, 71.5, 71.4, 71.3, 71.1

(PEG-*C*H_2), 73.4 (d, *J* 4.9, *C*-3'), 70.6, 66.6 (PEG-*C*H_2), 59.4 (ArC≡C*C*H_2PEG), 56.9 (O*C*H_2C≡CH), 51.9 (PEGCH_2NH*C*H_2Ar), 47.9 (PEG*C*H_2NHCH_2Ar); δ_F (470.5 MHz, d_4-MeOD): −232.48 (1F, ddd, *J* 47.8, 47.8, 28.4, CH_2F); *m/z* (ES^+) 697 ($[M+H]^+$ 100%); HRMS (ES^+) calc. for $C_{34}H_{42}FN_6O_9$ $[M+H]^+$ 697.2992, found 697.2984.

6.3.18. FDEA-PEG-(C≡CH)$_4$ 247

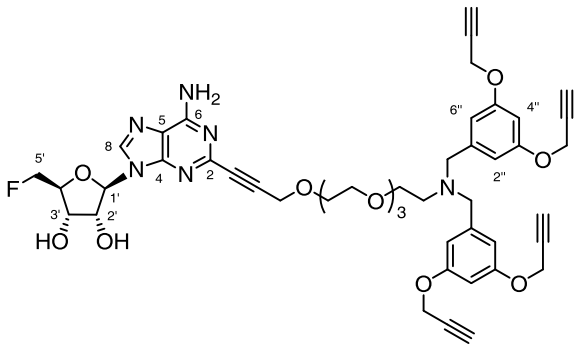

$Pd(PPh_3)_2Cl_2$ (15.4 mg, 0.022 mmol, 0.1 eq.), copper(I) iodide (4.2 mg, 0.022 mmol, 0.1 eq.) and triethylamine (150 µL, 1.10 mmol, 5 eq.) were added to a solution of iodo compound **241** (87 mg, 0.22 mmol, 1.0 eq.) and alkyne **235** (403 mg, 0.440 mmol, 2 eq.) in degassed DMF (4 mL). The mixture was heated to 60 °C for 48 h, after which time the volatile components were removed *in vacuo*. The residue was partly purified by column chromatography (50:49:1 Et_2O:acetone:Et_3N to 99:1 acetone:Et_3N) to afford fractions containing the coupled product (identified by ESMS), which were combined and concentrated.

The crude product was dissolved in MeOH (20 mL) and 3HF.Et_3N (800 µL) was added and the mixture stirred for 18 h. The reaction was quenched by addition of sat. aqueous $NaHCO_3$ (20 mL) and the mixture concentrated under reduced pressure. The aqueous mixture was loaded onto a reverse phase cartridge (1000 mg Extract Clean C_{18}-HC, preconditioned with water), washed with water (10 mL), and the product eluted with water: MeCN (50:50) (2 × 10 mL) and MeCN (2 × 10 mL). The water:MeCN and MeCN fractions were combined and concentrated. The residue was dissolved in MeCN: water (33:66) and purified by semi-preparative HPLC on the Shimadzu system (Phenomenex Luna C_{18} (250 × 10.00 mm, 5µ); mobile Phase: A (H_2O + 0.05% TFA), B (MeCN + 0.05% TFA); linear gradient: 33% B at 0 min to 70% B at 13 min, to 95% B at 14 min; to 95% B at 95 min, B to 33% B at 20 min, to 33% B at 30 min; flow rate: 2.5 mL.min^{-1}; detection 220 nm. Fractions containing product (t_R = 13.3 min) were concentrated under a stream of compressed air, and lyophilised from a solution of ^{t}BuOH in water (20% *v/v*) affording **247** as a white solid (5.4 mg, 2.3% over two steps): δ_H (500.1 MHz, d_4-MeOD): 8.23 (1 H, s, *H*-8), 6.95–6.57 (6 H, m, *H*-2'', *H*-4''), 6.02 (1 H, d, *J* 4.2, *H*-1'), 4.80-4.62 (14 H, m, OCH_2C≡CH, PEGCH_2N(CH_2Ar)$_2$, H-5'), 4.53 (1 H, dd, *J* 4.6, 4.6 *H*-2'), 4.39-4.37 (3 H, m, ArC≡CCH_2PEG, *H*-3'), 4.26-4.11 (1 H, m, *H*-4'), 3.76-3.62 (14 H, m, PEG-CH_2), 3.31 (2 H, under solvent peak, PEGCH_2N(CH_2Ar)$_2$), 2.99 (4 H, t, *J* 2.3 CH_2C≡C*H*); δ_F (470.3 MHz, d_4-MeOD): −232.61 (1 F, ddd, *J* 47.6, 47.6, 27.9 Hz), CH_2F); *m/z* (ES$^+$) calc. isotope pattern for $C_{47}H_{52}FN_6O_{11}$ $[M+H]^+$ 895.4 (100), 896.4 (53), 897.4 (16), 898.4 (2); found 895.4 (100),

896.4 (52), 897.4 (13), 898.4 (2); HRMS (ES^+) calc. for $C_{47}H_{52}FN_6O_{11}$ $[M+H]^+$ 895.3673, found 895.3660.

6.3.19. ClDEA-PEG-(RGD)$_2$ 224

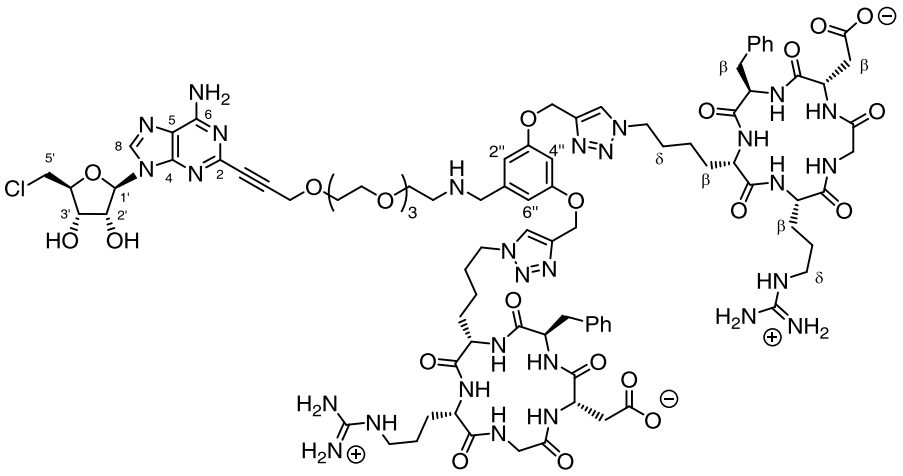

A suspension of ClDEA-PEG-(C≡CH)$_2$ **219** (0.72 mg, 1.0 μmol, 1 eq.) and c(RGDfK[N_3]) **199** (1.60 mg, 2.53 μmol, 2.5 eq.) in water (6.05 mL) was sonicated until homogenous. To this solution, aqueous sodium ascorbate (507 μL, 20 mM, 10 eq.), followed by $CuSO_4$-TBTA complex (203 μL, 10 mM in 55:45 DMSO: water) were added, and the reaction allowed to proceed for 75 min at rt, when HPLC analysis showed reaction to be complete. The reaction mixture was loaded onto a reverse phase cartridge (1000 mg Extract Clean C_{18}-HC, preconditioned with water), washed with water (5 mL), and the product eluted with water: MeCN (50:50) (2 × 5 mL). The eluted fractions were combined and solvents removed under reduced pressure. The residue was dissolved in MeCN: water (20:80) and purified by semi-preparative HPLC on the Shimadzu system (Phenomenex Kingsorb C_{18} (250 × 10.00 mm, 5μ); mobile Phase: A (H_2O + 0.05% TFA), B (MeCN + 0.05% TFA); linear gradient: 20% B at 0 min to 70% B at 20 min, to 95% B at 21 min; to 95% B at 25 min, B to 5% B at 26 min, to 5% B at 35 min; flow rate: 2.5 mL.min^{-1}; detection 220 nm, Fractions containing product (t_R = 10.4 min) were concentrated under a stream of compressed air, and lyophilised from a solution of ^{t}BuOH in water (20% *v/v*) affording **224** as a white solid (1.8 mg, 78%): δ_H (500.1 MHz, D_2O): 8.23 (1 H, s, *H*-8), 7.88 (2 H, s, triazole-*H*), 7.02–6.92 (10 H, m, D-Phe Ar*H*), 6.63 (2 H, br s, *H*-2", *H*-6"), 6.57 (1 H, br s, *H*-4"), 5.93 (1 H, d, *J* 4.7, *H*-1'), 5.15 (4 H, br s, ArO-C*H*$_2$-triazole), 4.68–4.65 (3 H, m, Asp α-*H*, *H*-2'), 4.47–4.40 (3 H, m, D-Phe α-*H, H*-3'), 4.35–4.31 (5 H, m, *H*-4', Arg α-*H*, AdoC≡CC*H*$_2$O), 4.28–4.20 (4 H, m, Lys ε-C*H*$_2$), 4.18–4.13 (4 H, m, CH_2NHCH_2Ar, Gly α-*H*a), 3.72–3.43 (16 H, m, Lys α-*H*, PEG C*H*$_2$), 3.44 (2 H, d, *J* 14.7, Gly α-*H*b), 3.18–3.09 (6 H, m, C*H*$_2$NHCH_2Ar, Arg δ-C*H*$_2$), 2.96 (2 H, dd, *J* 13.0, 5.8, D-Phe β-*H*a), 2.78 (2 H, dd, *J* 13.0, 11.0, D-Phe β-*H*b), 2.69–2.61 (2 H, m, Asp β-*H*a), 2.56–2.47 (2

H, m, Asp β-*H*b), 1.84–1.77 (2 H, m, Arg β-*H*a), 1.67–1.57 (6 H, m, Lys δ-C*H*$_2$, Arg β-*H*b), 1.50–1.37 (8 H, m, Lys β-C*H*$_2$, Arg δ-*H*b), 0.69–0.57 (4 H, m, Lys γ-C*H*$_2$); *m/z* (MALDI) calc. for $C_{88}H_{120}{}^{35}ClN_{28}O_{23}$ $[M+H]^+$: 1971.9, found 1971.9.

6.3.20. ClDEA-PEG-(RGD)$_4$ 225

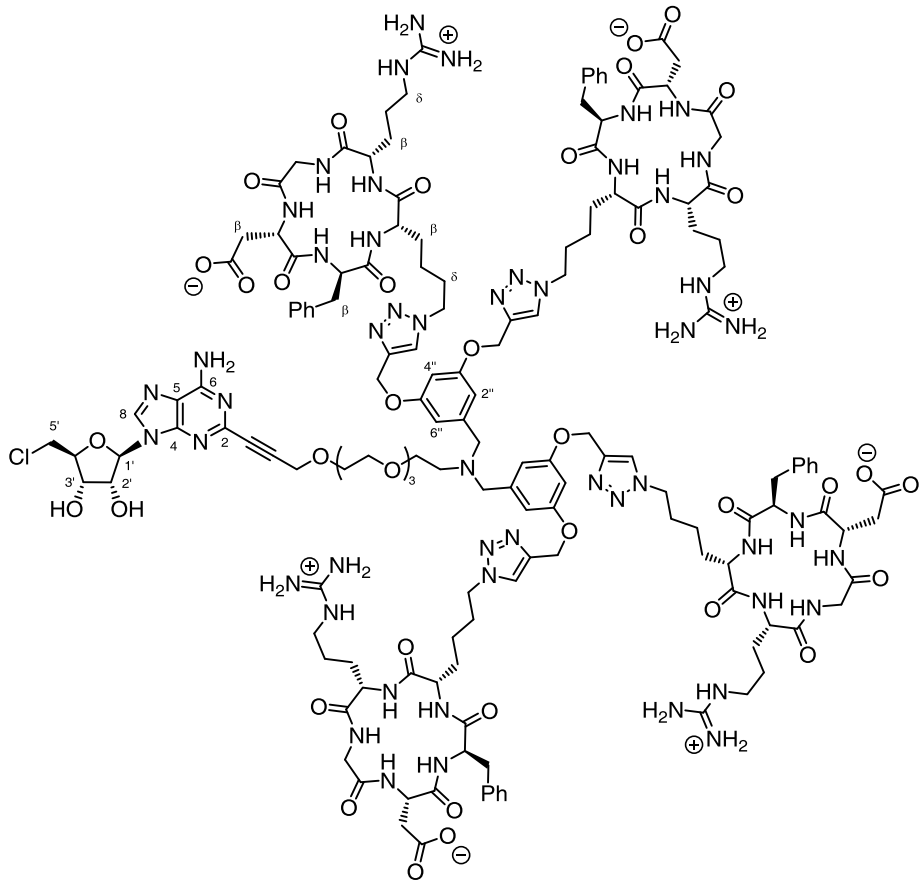

Fresh aqueous sodium ascorbate (291 µL, 20 mM, 10 eq.), followed by $CuSO_4$-TBTA complex (117 µL, 10 mM in 55:45 DMSO: water) were added to a solution of ClDEA-PEG-(C≡CH)$_4$ **220** (0.67 mg, 0.58 µmol, 1 eq.) in DMSO: water (75:25, 1.5 mL) and a solution of c(RGDfK[N_3]) **119** (1.83 mg, 2.91 µmol, 5 eq.) in DMSO: water (75:25, 1.5 mL). The reaction was allowed to proceed for 70 min at rt, when HPLC analysis showed reaction to be complete. The reaction mixture was diluted with water (4 mL) and loaded onto a reverse phase cartridge (1000 mg Extract Clean C_{18}-HC, preconditioned with water), washed with water (10 mL), and the product eluted with water: MeCN (50:50) (2 × 5 mL) and water: MeCN (25:75) (1 × 5 mL). The eluted fractions were combined and excess MeCN removed under a stream of compressed air to give a cloudy, aqueous solution. MeCN (200 µL) was added until the solution became clear and this mixture purified by semi-preparative HPLC on the Shimadzu system (Phenomenex Kingsorb C_{18} (250 × 10.00 mm, 5µ); mobile Phase: A (H_2O + 0.05% TFA), B (MeCN + 0.05% TFA); linear gradient: 5% B to 50% B at 10 min, to 95% B at 11 min; to 95% B at 14 min, to 5% B at 15 min, to 5% B at 25 min; flow rate: 2.5 mL.min^{-1}; detection 220 nm, t_R = 12.1–12.6 min). Fractions containing product

(t_R = 10.2 min) were concentrated under a stream of compressed air, and lyophilised from a solution of ^{t}BuOH in water (20% *v/v*) affording **225** as a white solid (1.4 mg, 70%): δ_H (500.1 MHz, 10% d_3-MeCN in D_2O): 8.44 (1 H, s, *H*-8), 8.13 (4 H, s, triazole-*H*), 7.26–7.15 (20 H, m, D-Phe Ar*H*), 6.82 (6 H, br s, *H*-2'', *H*-4'', *H*-6''), 6.06 (1 H, d, *J* 4.6, *H*-1'), 5.31 (8 H, br s, ArO-CH_2-triazole), 4.85 (4 H, t, *J* 7.4, Asp α-*H*), 4.79 (1 H, *H*-2', overlapped by HOD, observed in 2D), 4.77 (4 H, dd, *J* 10.0, 6.1, D-Phe α-*H*), 4.53 (1 H, t, *J* 5.1, *H*-3'), 4.47–4.38 (19 H, m, *H*-4', Lys ε-CH_2, Arg α-*H*, $CH_2N(CH_2Ar)_2$, AdoC≡CCH_2O), 4.32 (4 H, d, *J* 15.0, Gly α-*H*a), 4.02 (1 H, dd, *J* 12.2, 3.6, *H*-5'a), 3.98 (1 H, dd, *J* 12.2, 4.9, *H*-5'b), 3.94 (4 H, dd, *J* 11.0, 4.0 Lys α-*H*), 3.82–3.66 (14 H, m, PEG CH_2), 3.60 (4 H, d, *J* 15.0, Gly α-*H*b), 3.33–3.25 (10 H, m, C$H_2N(CH_2Ar)_2$, Arg δ-CH_2), 3.09 (4 H, dd, *J* 13.2, 6.1, D-Phe β-*H*a), 2.98 (4 H, dd, *J* 13.2, 10.0, D-Phe β-*H*b), 2.93 (4 H, dd, *J* 16.6, 7.4, Asp β-*H*a), 2.77 (4 H, dd, *J* 16.6, 7.4, Asp β-*H*b), 2.01–1.94 (4 H, m, Arg β-*H*a), 1.85–1.72 (16 H, m, Lys β-CH_2, Arg β-*H*b, Arg γ-*H*a), 1.66–1.56 (12 H, m, Lys δ-CH_2, Arg γ-*H*b), 0.97–0.92 (8 H, m, Lys γ-CH_2); *m/z* (MALDI) calc. for $C_{155}H_{208}{}^{35}ClN_{50}O_{39}$ $[M+H]^+$: 3428.6, found 3428.5.

6.3.21. FDEA-PEG-(RGD)$_2$ 248

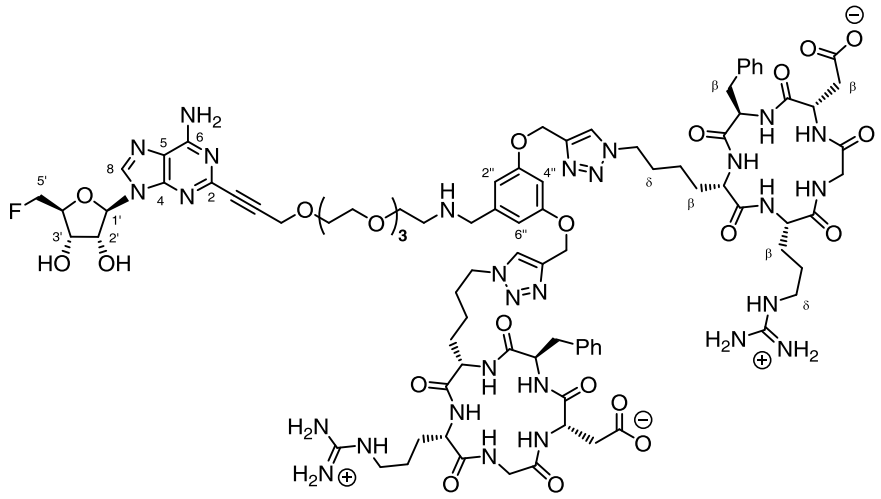

Fresh aqueous sodium ascorbate (541 µL, 20mM, 10 eq.), followed by $CuSO_4$-TBTA complex (216 µL, 10 mM in 55:45 DMSO: water) were added to a solution of FDEA-PEG-(C≡CH)$_2$ **245** (1.0 mg, 1.08 µmol, 1 eq.) and c(RGDfK[N_3]) **199** (1.7 mg, 7.70 µmol, 2.5 eq.) in DMSO: water (50:50, 6.5 mL). The reaction was allowed to proceed for 70 min at rt, when HPLC analysis showed reaction to be complete. The reaction mixture was loaded onto a reverse phase cartridge (1000 mg Extract Clean C_{18}-HC, preconditioned with water), washed with water (10 mL), and the product eluted with water: MeCN (50:50) (2 × 10 mL) and MeCN (1 × 10 mL). The water: MeCN fractions were dried under a stream of compressed air. The residue was suspended in MeCN:H_2O (20:80) and this mixture purified by semi-preparative HPLC on the Shimadzu system (Phenomenex Kingsorb C_{18} (250 × 10.00 mm, 5µ); mobile Phase: A (H_2O + 0.05% TFA), B (MeCN + 0.05% TFA); linear gradient: 20% B to 42% B at 8 min, 42% B to 95% B at 9 min; 95% B at 14 min, 95% B to 20% B at 15 min, 20% B at 25 min; flow rate: 2.5 mL.min^{-1}; detection 220 nm. Fractions containing product (t_R = 10.0 min) were concentrated under a stream of compressed air, and lyophilised from a solution of ^{t}BuOH in water (20% *v/v*) affording **248** as a white solid (0.67 mg, 27%): *m/z* (MALDI) calc. for $C_{88}H_{120}FN_{23}O_{23}$ $[M+H]^+$: 1955.9, found 1955.9.

6.3.22. FDEA-PEG-(RGD)$_4$ 249

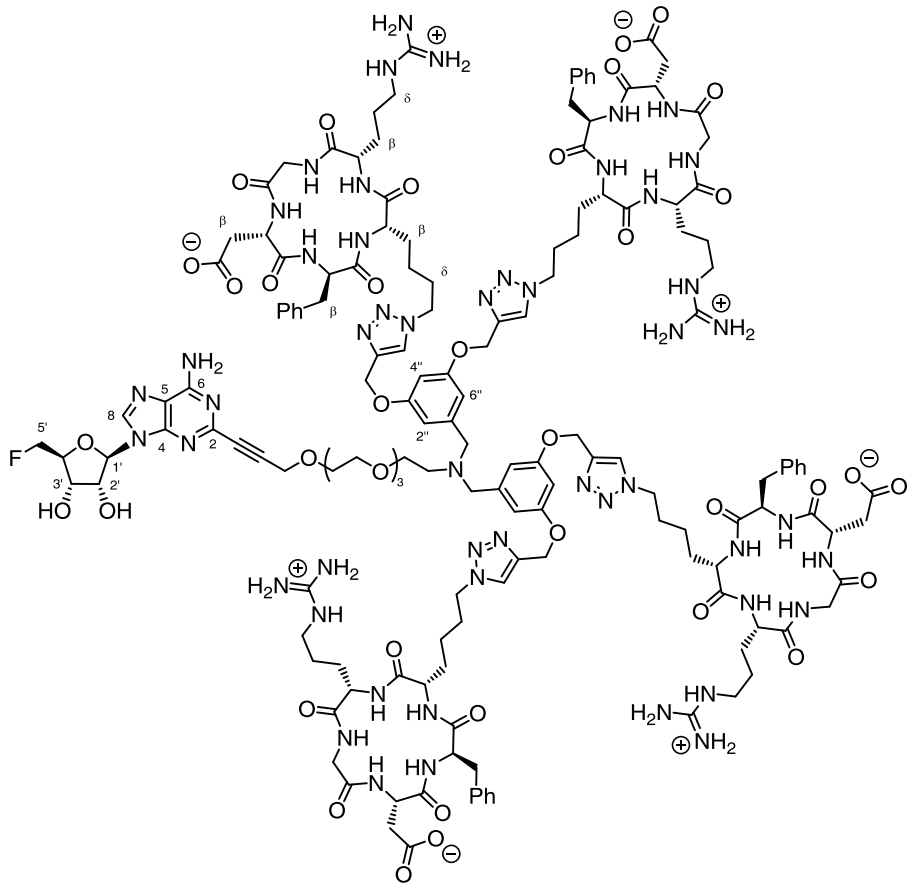

Fresh aqueous sodium ascorbate (262 µL, 20mM, 10 eq.), followed by $CuSO_4$-TBTA complex (145 µL, 10 mM in 55:45 DMSO:water) were added to a solution of FDEA-PEG-(C≡CH)$_4$ **247** (0.75 mg, 0.72 µmol, 1 eq.) and c(RGDfK[N_3]) **199** (2.28 mg, 3.62 µmol, 5 eq.) in DMSO: water (50:50, 4.3 mL). The reaction was allowed to proceed for 90 min at rt, when HPLC analysis showed reaction to be complete. The reaction mixture was loaded onto a reverse phase cartridge (1000 mg Extract Clean C_{18}-HC, preconditioned with water), washed with water (10 mL), and the product eluted with water: MeCN (50:50) (2 × 10 mL) and MeCN (1 × 10 mL). The water: MeCN and MeCN fractions were dried a stream of compressed air. The residue was suspended in MeCN:H_2O (20:80) and this mixture purified by semi-preparative HPLC on the Shimadzu system (Phenomenex Kingsorb C_{18} (250 × 10.00 mm, 5µ); mobile Phase: A (H_2O + 0.05% TFA), B (MeCN + 0.05% TFA); linear gradient: 20% B to 42% B at 18 min, 42% B to 95% B at 19 min; 95% B at 24 min, 95% B to 20% B at 25 min, 20% B at 35 min; flow rate: 2.5 mL.min^{-1}; detection 220 nm. Fractions containing product (t_R = 13.3 min) were concentrated under a stream of compressed air, and lyophilised

from a solution of ^{t}BuOH in water (20% *v/v*) affording **249** as a white solid (0.66 mg, 27%): $C_{155}H_{208}FN_{50}O_{39}$ $[M+H]^{+}$: 3412.6, found 3412.6.

6.4. Compound preparation for Chapter 4

6.4.1. 2',3'-*O*-Isopropylideneadenosine 285

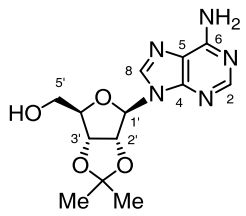

2,2-Dimethoxypropane (45.8 mL, 374 mmol, 10 eq.) and perchloric acid (70% in water, 3.54 mL, 24.7 mmol, 0.67 eq.) were slowly added to a suspension of adenosine **188** (10.0 g, 37.4 mmol, 1.0 eq.) in acetone (200 mL) at 0 °C. The mixture was allowed to slowly warm to rt, and stirred for a further 18 h. The reaction was quenched by addition of aqueous ammonia (30%, 20 mL) and concentrated. The residue was taken up into DCM (150 mL) and water water (100 mL) was added. The phases were separated and the aqueous phase washed with EtOAc (3 × 100 mL) before the organic phases were combined, dried over Na_2SO_4, and concentrated to a white powder. The powder was suspended in Et_2O (200 mL), and filtered before being washed with further Et_2O (3 × 100 mL) to give **285** as a white powder (9.16 g, 80%.). R_f = 0.21 (95:5 DCM:MeOH); $[\alpha]_D^{20}$ -65.3 (*c* 0.42, DMSO); mp 218-220 °C (DCM); ν_{max} 3721, 3110, 1687, 1605, 1208, 1085, 715 cm^{-1}; δ_H (300.0 MHz, d_6-DMSO): 8.34 (1 H, s, *H*-8), 8.15 (1 H, s, *H*-2), 7.36 (2 H, br s, NH_2), 6.12 (1 H, d, *J* 3.1, *H*-1'), 5.34 (1 H, dd, *J* 6.2, 3.1, *H*-2'), 5.25 (1 H, dd, *J* 6.0, 5.1, *C*-5' O*H*), 4.69 (1 H, dd, *J* 6.2, 2.5, *H*-3'), 4.23-4.19 (1 H, m, *H*-4'), 3.60-3.47 (1 H, m, *H*-5'a, *H*-5'b), 1.54 (3 H, s, $C(CH_3)_2$), 1.32 (3 H, s, $C(CH_3)_2$); δ_C (125.8 MHz, $CDCl_3$): 156.2 (*C*-6), 152.7 (*C*-2), 148.8 (*C*-4), 139.7 (*C*-8), 119.1 (*C*-5), 113.1 ($C(CH_3)_2$), 89.6 (*C*-1'), 86.4 (*C*-4'), 83.2 (*C*-2'), 81.4 (*C*-3'), 61.6 (*C*-5'), 27.1 ($C(CH_3)_2$), 25.2 ($C(CH_3)_2$); *m/z* (ES^+) 308 ($[M+H]^+$,100%), 330 ($[M+Na]^+$, 29).

6.4.2. *N*-Benzoyl-2',3'-*O*-isopropylideneadenosine 280

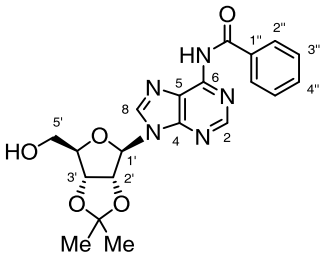

A suspension of 2',3'-*O*-isopropylideneadenosine **285** (1.53 g, 4.98 mmol, 1.0 eq.) in dry pyridine (5 mL) was concentrated to dryness *in vacuo*, before being re-suspended in dry pyridine (20 mL). To this suspension, TMSCl (3.20 mL, 15.2 mmol, 3.0 eq.) was slowly added and the mixture stirred for 30 min and BzCl (0.75 mL, 6.4 mmol, 1.3 eq.) was added and the mixture stirred for a further 3 h. The reaction was cooled to 0 °C and quenched by the careful addition of water (5 mL). Aqueous ammonia (35%, 10 mL) was added, and the mixture stirred for 30 min before being concentrated under reduced pressure. The residue was purified by column chromatography (DCM to 95:5 DCM:MeOH), and fractions containing product were combined and concentrated to dryness, before the residue was recrystallised from MeOH to give the product **280** as a white foamy solid (1.48 g, 72%): R_f = 0.17 (95:5 DCM:MeOH); $[\alpha]_D^{20}$ -93.5 (*c* 1.09, $CHCl_3$); mp 135–138 °C (MeOH); ν_{max} 3348, 1708, 1605, 1591, 1462, 1327, 1256, 1211, 1056, 702 cm^{-1}; δ_H (500.1 MHz, $CDCl_3$): 9.08 (1 H, br s, N*H*), 8.79 (1 H, s, *H*-2), 8.07 (1 H, s, *H*-8), 8.03–8.01 (2 H, m, *H*-2''), 7.64-7.60 (1 H, m, *H*-4''), 7.55-7.52 (2 H, m, *H*-3''), 5.94 (1 H, d, *J* 5.1, *H*-1′), 5.79-5.76 (1 H, m, 5'-O*H*), 5.23 (1 H, dd, *J* 5.7, 5.1, *H*-2′), 5.12 (1 H, dd, *J* 5.7, 1.4, *H*-3′), 4.56-4.55 (1 H, m, *H*-4'), 4.01-3.98 (1 H, m, *H*-5'a), 3.84-3.79 (1 H, m, *H*-5'b), 1.66 (3 H, s, $C(CH_3)_2$), 1.39 (3 H, s, $C(CH_3)_2$); δ_C (125.8 MHz, $CDCl_3$): 164.9 (*C*=O), 152.7 (*C*-4), 150.5 (*C*-2), 149.8 (*C*-6), 142.6 (*C*-8), 133.3 (*C*-4''), 133.1 (*C*-1''), 129.1 (*C*-2''), 128.2 (*C*-3''), 122.4 (*C*-5'), 114.4 ($C(CH_3)_2$), 94.6 (*C*-1′), 87.1 (*C*-4′), 83.8 (*C*-2′), 81.9 (*C*-3′), 63.2 (*C*-5′), 27.6, 25.3 ($C(CH_3)_2$); *m/z* (ES^+) 845 ($[2M+Na]^+$, 100%), 434 ($[M+Na]^+$, 64), 412 ($[M+H]^+$, 64). Data are in agreement with the literature.[12]

6.4.1. *N*-Benzoyl-5'-deoxy-2',3'-*O*-isopropylidene-5',5'-(*N*',*N*''-diphenylethylenediamino)adenosine 282

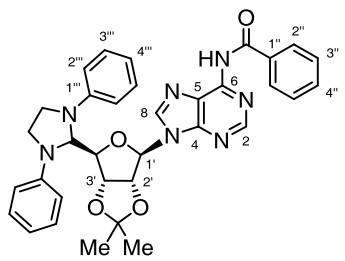

N,*N*'-dicyclohexylcarbodiimide (150 mg, 0.729 mmol, 3 eq.) and dichloroacetic acid (10 µL, 0.122, 0.5 eq.) were added to a solution of alcohol **280** (100 mg, 0.243 mmol, 1.0 eq.) in dry DMSO (1 mL). The mixture was stirred at rt for 90 min, before oxalic acid solution (62 mg in 0.2 mL MeOH) was added, the mixture stirred for a further 30 min before being filtered and the solids washed with cold MeOH. To the filtrate, *N*,*N*'-diphenylethylenediamine (59 mg, 0.280 mmol, 1.15 eq.) was added, and the mixture stirred for 30 min, before being cooled to 4 °C, upon which a white solid precipitated from the solution. The solids were collected by filtration, further purified by column chromatography (DCM to 95:5 DCM:MeOH), followed by a second round of column chromatography (DCM to 90:0 DCM:MeOH), to give the product **282** as a white solid (40 mg, 27%): R_f = 0.19 (95:5 DCM:MeOH); $[\alpha]_D^{20}$ +23.0 (*c* 1.13, $CHCl_3$); ν_{max} 3335, 1709, 1599, 1501, 1076, 749, 512 cm^{-1}; mp 132–135 °C (decomp.); δ_H (500.1 MHz, d_6-acetone): 8.60 (1 H, s, *H*-8), 8.19 (1 H, s, *H*-2), 8.15-8.13 (2 H, m, *H*-2''), 7.67-7.64 (1 H, m, *H*-4''), 7.59-7.55 (2 H, m, *H*-3''), 7.16-7.09 (4 H, m, *H*-3'''), 6.88-6.87 (2 H, m, *H*-2a'''), 6.73-6.67 (4 H, m, *H*-2b''', *H*-4'''), 6.29 (1 H, d, *J* 2.2, *H*-1′), 5.87 (1 H, d, *J* 3.5, *H*-5′), 5.45 (1 H, dd, *J* 6.4, 2.2, *H*-2′), 5.36 (1 H, dd, *J* 6.4, 4.6, *H*-3′), 4.63 (1 H, dd, *J* 4.6, 3.5, *H*-4'), 3.76-3.72 (1 H, m, CH_2a), 3.67-3.63 (1 H, m, CH_2b), 3.60-3.57 (2 H, m, CH_2c,d) 1.43 (3 H, s, C(CH_3)$_2$), 1.31 (3 H, s, C(CH_3)$_2$); δ_C (125.8 MHz, d_6-acetone): 165.7 (*C*=O), 152.7 (*C*-4), 152.6 (*C*-2), 151.1 (*C*-6), 147.9, 147.8 (*C*-1'''), 143.6 (*C*-8), 135.0 (*C*-1''), 133.2 (*C*-4''), 129.8, 129.7 (*C*-3'''), 129.4 (*C*-3''), 129.2 (*C*-2''), 122.6 (*C*-5'), 118.1, 118.5 (*C*-4'''), 114.6, 114.2 (*C*-2'''), 113.2 (*C*(CH$_3$)$_2$), 89.2 (*C*-1′), 80.1 (*C*-4′), 84.5 (*C*-2′), 81.4 (*C*-3′), 74.3 (*C*-5′), 48.2, 47.3 (*C*H$_2$), 27.6, 25.8 (C(*C*H$_3$)$_2$); *m/z* (ES$^+$) 626 ([M+Na]$^+$, 100%), 604 ([M+H]$^+$, 41); Data in agreement with literature values.[12]

6.4.2. *N*,*N*-Dibenzoyl-2',3'-*O*-isopropylideneadenosine 287

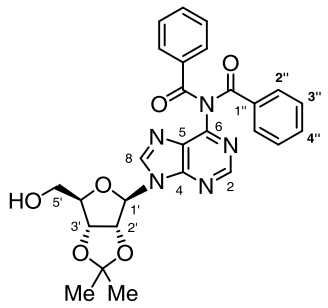

TMSCl (2.50 mL, 19.7 mmol, 3.0 eq.) was slowly added to a suspension of 2',3'-*O*-isopropylideneadenosine **285** (2.00 g, 6.50 mmol, 1.0 eq.) in dry pyridine (20 mL) at 0 °C, and the mixture allowed to warm to rt while stirring for 1.5 h. The mixture was again cooled to 0 °C and BzCl (1.66 mL, 14.3 mmol, 2.2 eq.) added and the mixture allowed to warm to rt while stirring for 2.5 h. The reaction was cooled to 0 °C and quenched by the careful addition of water (5 mL). The reaction mixture was diluted with $CHCl_3$ (50 mL) and water (50 mL) and the phases separated. The organic phase was washed with H_2SO_4 (1 M, 50 mL), sat. aqueous $NaHCO_3$ (50 mL), sat. aqueous $CuSO_4$ (50 mL), H_2SO_4 (1 M, 50 mL) and water (50 mL). The organic phase was dried over Na_2SO_4 and concentrated to a white powder. The residue was purified by column chromatography (DCM to 99:1 DCM:MeOH) to give the product **287** as a white foamy solid (3.32 g, 99%): R_f = 0.07 (99:1 DCM:MeOH); $[\alpha]_D^{20}$ -70.9 (*c* 0.60, $CHCl_3$); ν_{max} 2988, 1699, 1599, 1578, 1236, 1074, 829, 694, 640 cm^{-1}; mp 129-133 °C; δ_H (500.1 MHz, $CDCl_3$): 8.63 (1 H, s, *H*-2), 8.24 (1 H, s, *H*-8), 7.86-7.83 (4 H, m, *H*-2''), 7.51-7.48 (2 H, m, *H*-4''), 7.38-7.34 (4 H, m, *H*-3''), 5.94 (1 H, d, *J* 4.5, *H*-1′), 5.21 (1 H, dd, *J* 6.0, 4.5, *H*-2′), 5.09 (1 H, dd, *J* 6.0, 1.4, *H*-3′), 4.57-4.53 (1 H, m, *H*-4'), 3.97 (1 H, dd, *J* 12.7, 1.7, *H*-5'a), 3.79 (1 H, dd, *J* 12.7, 2.1, *H*-5'b), 1.65 (3 H, s, $C(CH_3)_2$), 1.38 (3 H, s, $C(CH_3)_2$); δ_C (125.8 MHz, $CDCl_3$): 172.2 (*C*=O), 152.6 (*C*-4), 152.0 (*C*-2), 151.7 (*C*-6), 144.5 (*C*-8), 133.9 (*C*-1''), 133.3 (*C*-4''), 129.6 (*C*-2''), 129.0 (*C*-3'', *C*-5), 114.4 ($C(CH_3)_2$), 94.3 (*C*-1′), 86.6 (*C*-4′), 83.4 (*C*-2′), 81.7 (*C*-3′), 63.3 (*C*-5′), 27.7, 25.3 ($C(CH_3)_2$); *m/z* (ES^+) 554 ($[M+K]^+$, 100%), 538 ($[M+Na]^+$, 59). Data are in agreement with the literature.[13]

6.4.3. *N,N*-Dibenzoyl-2',3'-*O*-isopropylideneadenosine-5'-aldehyde 283

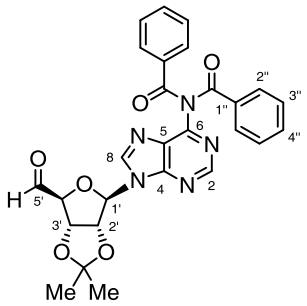

Dichloroacetic acid (120 µL, 1.45 mmol, 0.5 eq.) was added dropwise to a cooled solution of **287** (1.50 g, 2.91 mmol, 1.0 eq.) and EDCI.HCl (1.34 g, 6.98 mmol, 3.4 eq.) in DMSO (8 mL). The reaction mixture was stirred at room temperature for 3 h, before being quenched by addition of water (15 mL) and EtOAc (15 mL) and the mixture stirred vigorously for 15 min. The resultant phases were separated and the aqueous phase extracted with EtOAc (2 × 15 mL) and the combined organic phases washed with brine (20 mL). The organic phase was dried over Na_2SO_4 and concentrated to a colourless oil. The residue was co-evaporated with toluene (5 × 25 mL) to give the product **283** as a white foam (1.49 g, quant), which was used directly without further purification. R_f = 0.65 (95:5 DCM:MeOH); $[\alpha]_D^{20}$ -11.5 (*c* 1.11, $CHCl_3$); mp 110–113 °C (DCM); ν_{max} 2358, 1697, 1599, 1578, 1449, 1236, 1072, 694, 640 cm^{-1}; δ_H (500.1 MHz, $CDCl_3$): 9.35 (1 H, s, *H*-5'), 8.53 (1 H, s, *H*-2), 8.17 (1 H, s, *H*-8), 7.87-7.83 (4 H, m, *H*-2''), 7.51-7.48 (2 H, m, *H*-4''), 7.38-7.34 (4 H, m, *H*-3''), 6.27 (1 H, br s, *H*-1′), 5.52 (1 H, dd, *J* 6.2, 1.9, *H*-3′), 5.34 (1 H, d, *J* 6.2, *H*-2′), 4.71 (1 H, d, *J* 1.9, *H*-4'), 1.61 (3 H, s, C(CH_3)$_2$), 1.41 (3 H, s, C(CH_3)$_2$); δ_C (125.8 MHz, $CDCl_3$): 199.4 (*C*-5′), 172.3 (*C*=O), 152.5 (*C*-4), 152.3 (*C*-2), 151.6 (*C*-6), 144.3 (*C*-8), 134.0 (*C*-1''), 133.3 (*C*-4''), 129.6 (*C*-2''), 128.9 (*C*-3''), 125.4 (*C*-5), 114.4 (*C*$(CH_3)_2$), 93.2 (*C*-4′), 92.5 (*C*-1′), 84.7 (*C*-2′), 83.4 (*C*-3′), 26.7, 25.1 (C(*C*H_3)$_2$); *m/z* (ES^+) 536 ($[M+Na]^+$, 42%) ; HRMS (ES^+) calc. for $C_{27}H_{23}N_5O_6Na$ $[M+Na]^+$ 536.1541, found 536.1534. Data are in agreement with the literature.[14]

6.4.4. *N,N*-Dibenzoyl-5',5'-difluoro-5'-deoxy-2',3'-*O*-isopropylideneadenosine 284

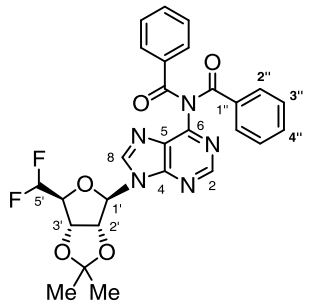

Deoxofluor® (50% in THF, 4.5 mL, 10.6 mmol, 4.0 eq.) was slowly added to a solution of aldehyde **283** (1.36 g, 2.64 mmol, 1.0 eq.) at −78 °C in a Teflon flask, and the mixture stirred while warming to rt for 16 h. The reaction was quenched by careful dropwise addition of sat. aqueous $NaHCO_3$ (50 mL) and the mixture diluted with EtOAc (80 mL). The phases were separated and the aqueous phase extracted with EtOAc (3 × 30 mL) before the combined organic phases were washed with brine (50 mL). The organic phase was dried over $MgSO_4$ and concentrated. The residue was purified by column chromatography (50:50 cyclohexane:EtOAc) to give the crude product **284**, which was further purified by column chromatography (80:20 cyclohexane:EtOAc to 70:30 cyclohexane:EtOAc) to give the product as a yellow foam (138 mg, 10%): R_f = 0.16 (70:30 cyclohexane:EtOAc); $[\alpha]_D^{20}$ -20.0 (*c* 0.21, $CHCl_3$); mp 101–105 °C (DCM); ν_{max} 2988, 1699, 1599, 1559, 1236, 1211, 694 cm^{-1}; δ_H (300.6 MHz, $CDCl_3$): 8.67 (1 H, s, *H*-2), 8.16 (1 H, s, *H*-8), 7.87-7.83 (4 H, m, *H*-2''), 7.52-7.45 (2 H, m, *H*-4''), 7.39-7.32 (4 H, m, *H*-3''), 6.28 (1 H, br s, *H*-1′), 5.97 (1 H, td, *J* 55.1, 4.5, *H*-5′), 5.39 (1 H, dd, *J* 6.1, 2.0, *H*-2′), 5.27 (1 H, dd, *J* 6.1, 2.9 *H*-3'), 4.47 (1 H, dddd. *J* 12.6, 10.1, 4.5, 2.9, *H*-4′), 1.64 (3 H, s, $C(CH_3)_2$), 1.41 (3 H, s, $C(CH_3)_2$); δ_C (125.8 MHz, $CDCl_3$): 172.3 (*C*=O), 152.5 (*C*-2), 152.4 (*C*-6), 152.3 (*C*-4), 143.6 (*C*-8), 134.1 (*C*-1''), 133.2 (*C*-4''), 129.6 (*C*-2''), 128.9 (*C*-3''), 127.9 (*C*-5), 115.3 ($C(CH_3)_2$), 113.7 (t, *J* 244.3, *C*-5'), 91.6 (*C*-1′), 85.9 (t, *J* 26.2, *C*-4′), 84.3 (*C*-2′), 80.0 (t, *J* 3.7, *C*-3'), 27.1, 25.3 ($C(CH_3)_2$); δ_F (282.3 MHz, $CDCl_3$): –130.60 (1 F, ddd, *J* 299.1, 55.1, 12.6, CHF_2), –126.44 (1 F, ddd, *J* 299.1, 55.1, 10.1, CHF_2); *m/z* (ES^+) 1093 ($[2M+Na]^+$, 52%), 558 ($[M+Na]^+$, 100), 536 ($[M+H]^+$, 15); HRMS (ES^+) calc. for $C_{27}H_{23}N_5O_5F_2Na$ $[M+Na]^+$ 558.1565, found 558.1549. All data are in agreement with the literature,[14] except for the ^{19}F NMR chemical shifts. The discrepancy is discussed in **Section 4.3.2.**

6.4.5. 5',5'-Difluoro-5'-deoxy-2',3'-*O*-isopropylideneadenosine 288

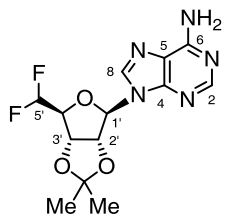

In a heavy walled tube, a solution of **284** (57 mg, 0.11 mmol, 1.0 eq.) in MeOH (5 mL) was cooled to 0 °C. Ammonia gas was bubbled through the solution for 1 h, before the tube was sealed and heated to 60 °C for 19 h. The vessel was cooled to rt and carefully opened, before the solution was degassed by bubbling argon through the solution for 2 h before being concentrated. The residue was purified by column chromatography (DCM to 99:2 DCM:MeOH to 97:3 DCM:MeOH) to give the product **288** as a white foam (35 mg, 45%): R_f = 0.56 (90:10 DCM:MeOH); mp 160-161 °C (DCM); δ_H (500.1 MHz, $CDCl_3$): 8.34 (1 H, s, *H*-2), 7.87 (1 H, s, *H*-8), 6.19 (1 H, br s, *H*-1′), 6.01 (2 H, br s, NH_2), 6.00 (1 H, td, *J* 55.5, 6.0, *H*-5′), 5.43-5.41 (1 H, m, *H*-2′), 5.36-5.24 (1 H, m, *H*-3'), 4.44-4.39 (1 H, m, *H*-4′), 1.63 (3 H, s, C(CH_3)$_2$), 1.41 (3 H, s, C(CH_3)$_2$); δ_C (125.8 MHz, $CDCl_3$): 155.9 (*C*-6), 155.3 (*C*-2), 149.2 (*C*-4), 139.8 (*C*-8), 120.4 (*C*-5), 114.4 (t, *J* 124.5, *C*-5'), 112.0 (*C*(CH$_3$)$_2$), 91.6 (*C*-1′), 86.6 (dd, *J* 28.8, 24.4, *C*-4′), 84.5 (*C*-2′), 80.7 (t, *J* 5.7, *C*-3'), 27.1, 25.3 (C(*C*H$_3$)$_2$); δ_F (470.4 MHz, $CDCl_3$): –129.62 (1 F, ddd, *J* 299.5, 55.5, 9.7, CHF_2), –125.32 (1 F, ddd, *J* 299.5, 55.5, 10.8, CHF_2); *m/z* (ES^+) 350 ($[M+Na]^+$, 35%), 328 ($[M+H]^+$, 100); HRMS (ES^+) calc. for $C_{13}H_{16}N_5O_3F_2$ $[M+H]^+$ 328.1216, found 328.1214. Data are in agreement with the literature.[14]

6.4.6. 5',5'-Difluoro-5'-deoxyadenosine (F_2DA) 276

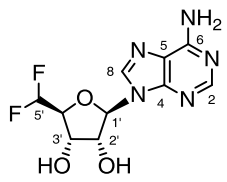

A solution of **288** (16 mg, 0.048 mmol) in a mixture of TFA:water (9:1 *v/v*, 1.0 mL) at 0 °C was stirred for 3 h whilst warming to rt. The volatile components were removed, and the residue co-evaporated with toluene (3 × 10 mL). The mixture was taken up into MeOH (1 mL) and neutralised by addition of NaOH (2 M, 2 drops) before being concentrated *in vacuo*. The residue was purified by column chromatography (90:10 $CHCl_3$:MeOH) to give the product **276** as a white powder (14 mg, 86%): R_f = 0.18 (90:10 DCM:MeOH); mp 189–190 °C ($CHCl_3$); δ_H (500.1 MHz, d_6-DMSO): 8.32 (1 H, s, *H*-8), 8.16 (1 H, s, *H*-2), 7.35 (2 H, br s, NH_2), 6.31 (1 H, td, *J* 55.0, 4.8, *H*-5′), 5.98 (1 H, d, *J* 6.2, *H*-1′), 5.71 (1 H, d, *J* 6.3, 2'-O*H*), 5.67 (1 H, d, *J* 5.1, 3'-O*H*), 4.77 (1 H, ddd, *J* 6.3, 6.2, 5.9, *H*-2′), 4.38-4.36 (1 H, m, *H*-3'), 4.10-4.04 (1 H, m, *H*-4′); δ_C (125.8 MHz, d_6-DMSO): 156.1 (*C*-6), 152.8 (*C*-2), 149.6 (*C*-4), 139.5 (*C*-8), 119.1 (*C*-5), 113.8 (*C*-5', observed in 2D), 87.6 (*C*-1′), 82.2 (*C*-4′, observed in 2D), 72.5 (*C*-2′), 69.3 (*C*-3'); δ_F (470.5 MHz, d_6-DMSO): –127.98 (1 F, ddd, *J* 291.1, 55.0, 9.9, CHF_2), –126.97 (1 F, ddd, *J* 299.5, 55.0, 12.8, CHF_2); *m/z* (ES^+) 310 ($[M+Na]^+$ 5%), 288 ($[M+H]^+$ 100); HRMS (ES^+) calc. for $C_{10}H_{12}N_5O_3F_2$ $[M+H]^+$ 288.0903, found 288.0896. Data are in agreement with the literature.[14]

6.5. Compound preparation for Chapter 5

6.5.1. 5'-Fluoro-5'-deoxy-2',3'-*O*-isopropylideneadenosine 325

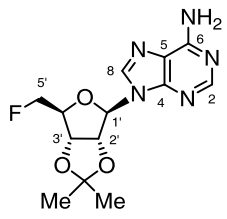

TsF (0.851 g, 4.88 mmol, 1.5 eq.) and TBAF (1 M in THF, 9.77 mL, 9.77 mmol, 3.0 eq.) were added to a solution of acetonide **285** (1.00 g, 3.26 mmol, 1.0 eq.) in THF (100 mL). The mixture was heated to 60 °C for 18 h, and cooled to rt. The volatile components were removed and the orange residue was purified by column chromatography (50:50 petroleum ether:acetone) to give the product **325** as a white powder (790 mg, 78%): R_f = 0.21 (50:50 petroleum ether:acetone); $[\alpha]_D^{20}$ -60.7 (*c* 0.42, DMSO); mp 144-146 °C (petroleum ether:acetone); ν_{max} 3301, 3149, 1681, 1604, 1076, 850, 721 cm^{-1}; δ_H (500.1 MHz, $CDCl_3$): 8.36 (1 H, s, *H*-2), 7.94 (1 H, s, *H*-8), 6.20 (1 H, d, *J* 2.2, *H*-1'), 5.72 (2 H, br s, NH_2), 5.38-5.36 (1 H, m, *H*-2'), 5.10 (1 H, dd, *J* 6.3, 3.1, *H*-3'), 4.73-4.48 (3 H, m, *H*-5'a, *H*-5'b, *H*-4'), 1.64 (3 H, s, $C(CH_3)_2$), 1.40 (3 H, s, $C(CH_3)_2$); δ_C (125.8 MHz, $CDCl_3$): 155.6 (*C*-6), 153.4 (*C*-2), 149.6 (*C*-4), 139.4 (*C*-8), 120.3 (*C*-5), 114.8 ($C(CH_3)_2$), 90.1 (*C*-1'), 85.7 (*C*-4', d, *J* 19.3), 84.7 (*C*-2'), 83.0 (*C*-5', d, *J*, 171.9), 80.9 (*C*-3', d, *J*, 6.7), 27.3 ($C(CH_3)_2$), 25.5 ($C(CH_3)_2$); δ_F (376.4 MHz, $CDCl_3$): −230.13 (ddd, *J* 46.9, 46.9, 27.9, CH_2F); *m/z* (ES^+) 332 ($[M+Na]^+$, 27%),310 ($[M+H]^+$, 37); HRMS (ES^+) calc. for $C_{13}H_{17}N_5O_3F$ $[M+H]^+$ 310.10, found 310.1303.

6.5.2. 5'-Fluoro-5'-deoxyadenosine 22

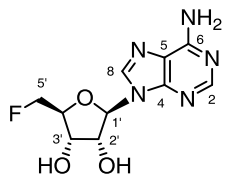

A solution of **325** (710 mg, 0.120 mmol) in a mixture of TFA:water (9:1 *v/v*, 5.0 mL) at 0 °C was stirred for 18 h whilst warming to rt. The volatile components were removed, and the residue co-evaporated with EtOH (3 × 10 mL) and Et_2O (10 mL) to give a syrup. The residue was neutralised with NaOH (2 M) and concentrated before being purified by column chromatography (90:10 DCM:MeOH) to give the crude product. The crude product was recrystallised from water, before being freeze dried to yield **22** a white powder (230 mg, 37%): R_f = 0.27 (90:10 DCM:MeOH); $[\alpha]_D^{20}$ -61.1 (*c* 0.80, DMSO); mp 164-168 °C (water); ν_{max} 3310, 3158, 1679, 1652, 1209, 723 cm^{-1};. δ_H (500.1 MHz, D_2O): 8.27 (1 H, s, *H*-2), 8.19 (1 H, s, *H*-8), 6.09 (1 H, d, *J* 5.0, *H*-1'), 4.81-4.68 (1 H, m, *H*-5'a, under D_2O peak), 4.71-4.68 (2 H, m, *H*-5'b, *H*-3'), 4.50 (1 H, dd, *J* 5.0, 5.0, *H*-2'), 4.36 (1 H, ddt, *J* 30.3, 5.1, 2.8, *H*-4'); δ_C (125.8 MHz, D_2O): 155.4 (*C*-6), 152.7 (*C*-2), 148.8 (*C*-4), 139.5 (*C*-8, d, *J* 4.2), 118.6 (*C*-5), 87.4 (*C*-1'), 83.1 (*C*-4'), 82.4 (*C*-5', d, *J* 148.8), 73.8 (*C*-2'), 69.4 (*C*-3', d, *J* 5.0); δ_F (282.3 MHz, D_2O): −231.9 (ddd, *J* 47.2, 47.2, 30.3, CH_2F); *m/z* (ES^+) 270 ($[M+H]^+$, 100%), 292 ($[M+Na]^+$, 31); HRMS (ES^+) calc. for $C_{10}H_{13}FN_5O_3$ $[M+H]^+$ 270.0997, found 270.0989.

6.5.3. Ethyl *O*-mesylglycolate 49

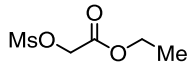

Triethylamine (3.4 mL, 53 mmol, 2.2 eq.) was slowly added to a solution of ethyl glycolate (2.3 mL, 24 mmol, 1.0 eq.) and mesyl chloride (1.6 mL, 21 mmol, 0.88 eq.) in DCM (20 mL) at 0 °C. The mixture was allowed to warm to room temperature and stirred for 1 h, before being quenched by addition of aqueous hydrochloric acid (1 M, 50 mL). The phases were separated and the organic phase washed with water (3 × 50 mL) before being dried over anhydrous Na_2SO_4 and concentrated. The resultant oil was purified by distillation under reduced pressure and ethyl *O*-mesylglycolate **49** was collected at 105 °C (1.8 torr) as a colourless oil (2.05 g, 54%): ν_{max} 1755, 1352, 1170, 1047, 804, 524 cm^{-1}; δ_H (500.1 MHz, $CDCl_3$): 4.76 (2 H, s, C*H*$_2$OSO$_2$CH$_3$), 4.27 (2 H, q, *J* 7.1, C*H*$_2$CH$_3$), 3.21 (3 H, s, SO$_2$C*H*$_3$), 1.31 (3 H, t, *J* 7.1, CH$_2$C*H*$_3$); δ_C (125.8 MHz, $CDCl_3$): 166.9 (*C*O), 64.9 (*C*H$_2$OSO$_2$CH$_3$), 62.1 (*C*H$_2$CH$_3$), 39.1 (SO$_2$*C*H$_3$), 14.1 (CH$_2$*C*H$_3$); *m/z* (ES$^+$) 205 ([M+Na]$^+$ 100%); HRMS (ES$^+$) calc. for $C_5H_{10}O_5SNa$ [M+Na]$^+$ 205.0141, found 205.0136. Data are in agreement with the literature.[15]

6.6. Fluorinase overexpression and purification

E. coli BL21 (DE3) Gold cells bearing the pET-28a(+)-flA[16] vector were grown while shaking (180 rpm) in autoinduction medium (4 × 400 mL in 2 L flasks) or in Luria Broth (4 × 1000 mL in 2 L flasks) containing kanamycin (100 μg.mL^{-1}) at 37 °C overnight. In protocols where Luria Broth was used, optical density (OD_{600}) was measured periodically and expression was induced when OD_{600} reached 0.6 by addition of IPTG to a final concentration of 0.5 mM.

After 48 h (autoinduction) or 18 h (Luria Broth + IPTG), cells were harvested by centrifugation (4500 rpm, 20 min), and the cell pellet resuspended in lysis buffer (100–300 mL, 150 mM NaCl, 20 mM TRIS pH8, 20 mM imidazole), before protease inhibitor cocktail (1 × Complete Mini, EDTA-free, Roche), and bovine pancreatic DNAse (Sigma, 5 mg) were added. The cells were lysed using a cell disruptor (Constant Systems) at 30 kPSI. The lysate was centrifuged (20 000 rpm, 20 min) and the resulting pellet discarded before the supernatant was filtered (0.45 μm). The recombinant protein was purified from the lysate by passing the supernatant though a Ni^{2+} affinity column (Ni-NTA Agarose, Qiagen or Ni Sepharose 6 Fast Flow, GE, 5-7 mL bed volume) which was pre-equilibrated with the lysis buffer. The bound protein was washed (3 × 15 mL, 20 mM TRIS pH 8, 20 mM imidazole, 500 mM NaCl) before being eluted (3 × 15 mL, 20 mM TRIS pH 8, 400 mM imidazole, 500 mM NaCl). Fractions containing the desired fluorinase were pooled.

Adenosine deaminase (ADA) suspension (50 μL calf spleen ADA type XI, Sigma Aldrich) was added to the fractions containing fluorinase, and the mixture dialysed against buffer (20 mM TRIS pH 8 and 150 mM NaCl, or 20 mM phosphate buffer pH 7.8 and 150 mM NaCl, 7 L) overnight. The non-His-tagged ADA enzyme was separated from the fluorinase by passing the supernatant though a Ni^{2+} affinity column (Ni-NTA Agarose, Qiagen or Ni Sepharose 6 Fast Flow, GE, 5-7 mL bed volume) which was pre-equilibrated with the dialysis buffer. The bound protein was washed (2 × 15 mL, 20 mM TRIS pH 8, 20 mM imidazole, 500 mM NaCl) before being eluted (2 × 15 mL, 20 mM TRIS pH 8, 500 mM imidazole, 500 mM NaCl).and the resultant eluate dialysed against buffer (50 mM phosphate buffer pH 7.8, 7 L) overnight. The solution was concentrated by centrifugation (Amicon Ultra-15, 10 000 kDa cutoff) to give recombinant fluorinase (5-20 mg.mL^{-1}).

Adenosine **188** removal was monitored by HPLC of samples of fluorinase which had been adjusted to the same protein concentration, denatured by heating at 95°C for

5 min, before being clarified by centrifugation (13 000 rpm, 10 min). Samples of the supernatant (60 µL) were removed for analysis by HPLC.

HPLC analysis was performed on a Varian Prostar system using a Kingsorb 3µm C_{18} (150 mm × 4.6 mm) column and a guard cartridge. Mobile phase: 0.05% TFA in water (solvent A) and 0.05% TFA in MeCN (solvent B); Linear gradient: 0% solvent B for to 30% of solvent B in 15 min, from 30% to 95% of solvent B in 2 min and finally 95% solvent B to flush the column; Flow rate: 1 $mL.min^{-1}$; Detection: 260 nm; Injection volume: 20 µL.

Where freeze dried fluorinase was used, the enzyme solution was aliquotted into portions (5 mg or 10 mg, based on fluorinase), before being lyophilised, and stored at −78 °C until needed.

For X-ray crystallography, the deaminated fluorinase was subject to His-Tag removal by dialysis in the presence thrombin (10 units, from human plasma, Roche) against buffer (20 mM TRIS pH 8, 150 mM NaCl, 5 L). Gel filtration (10mM Tris-HCl pH 7 and 30mM NaCl) through a Superdex S-200 (HR16/60) column (Pharmacia Biotech) afforded fluorinase free of thrombin and the His-Tag. The solution was concentrated by centrifugation (Amicon Ultra-15, 10 000 kDa cutoff) to give His-Tag free recombinant fluorinase (6.5 $mg.mL^{-1}$)

6.7. Enzymatic Assays for Chapter 2

6.7.1. ClDEA 174 to FDEA 176

In a total reaction volume of 800 µL, recombinant fluorinase (5 $mg.mL^{-1}$) was incubated with phosphate buffer pH 7.8 (20 mM), ClDEA **174** (0.2 mM), L-SeMet (0.1 mM) and KF (75 mM) at 37 °C. Samples (100 µL) were periodically removed, denatured by heating at 95°C for 3 min, before being clarified by centrifugation (13 000 rpm, 10 min). Samples of the supernatant (60 µL) were removed for analysis by HPLC. Control experiments without enzyme, L-SeMet and fluoride were also performed and showed no formation of FDEA **176**. In the control without fluoride, conversion of ClDEA **174** to methyl selenoether **194** was observed.

HPLC analysis was performed on a Varian Prostar system using a Kinetix 5µm XB-C_{18} 100A (150 mm × 4.6 mm) column and a guard cartridge. Mobile phase: 0.05% TFA in water (solvent A) and 0.05% TFA in MeCN (solvent B); Linear gradient: 5% solvent B

for 2 min, then from 5% to 25% of solvent B in 10 min, from 25% to 50% of solvent B in 3 min and finally 95% solvent B to flush the column; Flow rate: 1 mL.min^{-1}; Detection: 260 nm; Injection volume: 20 µL. For LC-MS analysis, the same column and the linear gradient, where TFA was replaced with formic acid, were employed with a flow rate of 0.5 mL.min^{-1}.

6.7.2. ClDEA 174 and ClDA 23 rate comparison experiments

For kinetic comparison of ClDA **23** and CLDEA **174**, separate reactions with the two substrates were performed in duplicate.

In a total reaction volume of 1000 µL, recombinant fluorinase (2.5 mg.mL^{-1}, in phosphate buffer) was incubated with ClDA **23** (0.25 mM) or ClDEA **174** (0.25 mM), L-SeMet (0.075 mM) and KF (50 mM) at 37 °C. Samples (100 µL) were removed every 15 min for 2 h, denatured by heating at 95°C for 3 min, before being clarified by centrifugation (13 000 rpm, 10 min). Samples of the supernatant (60 µL) were removed for analysis by HPLC.

Concentration of the products, FDA **20** and FDEA **176** were determined by comparison of HPLC peak area to those of standard curves.

HPLC analysis for both sets of experiments was performed on a Varian Prostar system using a Kinetix 5µm XB-C_{18} 100A (150 mm × 4.6 mm) column and a guard cartridge. Mobile phase: 0.05% TFA in water (solvent A) and 0.05% TFA in MeCN (solvent B); Linear gradient: 5% solvent B for 2 min, then from 5% to 25% of solvent B in 10 min, from 25% to 50% of solvent B in 3 min and finally 95% solvent B to flush the column; Flow rate: 1 mL.min^{-1}; Detection: 260 nm; Injection volume: 20 µL.

6.7.3. Michaelis-Menten investigation of ClDEA 174

For Michaelis Menten kinetics, ClDEA **174** was incubated with the fluorinase at 10 µM, 25 µM, 50 µM, 100 µM, 250 µM and 500 µM, in duplicate.

In a total reaction volume of 600 µL, recombinant fluorinase (0.15 mg.mL^{-1}) and phosphate buffer (pH 7.8, 20 mM) was incubated with ClDEA **174** (at the appropriate concentration) and L-Met (10 mM) at 37 °C. Samples (100 µL) were removed every 15 min for 1.5 h, denatured by heating at 95°C for 5 min, before being clarified by centrifugation (13 000 rpm, 10 min). Samples of the supernatant (60 µL) were removed for analysis by HPLC.

HPLC analysis for both sets of experiments was performed on a Varian Prostar system a Kinetix 5µm XB-C_{18} 100A (150 mm × 4.6 mm) column and a guard cartridge. Mobile phase: 0.05% TFA in water (solvent A) and 0.05% TFA in MeCN (solvent B); Linear gradient: 5% solvent B for 2 min, then from 5% to 25% of solvent B in 10 min, from 25% to 50% of solvent B in 3 min and finally 95% solvent B to flush the column; Flow rate: 1 $mL.min^{-1}$; Detection: 260 nm; Injection volume: 20 µL.

Concentration of the methyl thioether product **197** in each sample was determined by comparison of HPLC peak area to those of a standard curve of ClDEA **174**. Kinetic data were analysed using GraphPad Prism software, and kinetic constants fitted both with and without the effect of substrate inhibition.

6.7.4. ClDEA 174 and ClDA 23 competition experiments

For the competition experiment, both substrates were added to the same final concentration (0.2 mM).

In a total reaction volume of 1000 µL, recombinant fluorinase (6 $mg.mL^{-1}$, in phosphate buffer) was incubated with ClDA **23** (0.2 mM) and ClDEA **074** (0.2 mM), L-SeMet (0.08 mM) and KF (75 mM) at 37 °C. Samples (100 µL) were removed, denatured by heating at 95°C for 3 min, before being clarified by centrifugation (13 000 rpm, 10 min). Samples of the supernatant (60 µL) were removed for analysis by HPLC.

HPLC analysis for both sets of experiments was performed on a Varian Prostar system a Kinetix 5µm XB-C_{18} 100A (150 mm × 4.6 mm) column and a guard cartridge. Mobile phase: 0.05% TFA in water (solvent A) and 0.05% TFA in MeCN (solvent B); Linear gradient: 5% solvent B for 2 min, then from 5% to 25% of solvent B in 10 min, from 25% to 50% of solvent B in 3 min and finally 95% solvent B to flush the column; Flow rate: 1 $mL.min^{-1}$; Detection: 260 nm; Injection volume: 20 µL.

6.7.5. Enzymatic production and click reaction of FDEA 174 with c(RGDfK[N_3]) 199

In a total volume of 300 µL in water, ClDEA **174** (0.2 mM), L-SeMet (0.1 mM), potassium fluoride (75 mM), phosphate buffer (20 mM) and fluorinase (5 $mg.mL^{-1}$) were combined left to react at 37°C for 2 h. The mixture was heated to 95°C for 5 min, and centrifuged at 13 000 rpm for 10 min. Supernatant was used for the subsequent click reaction.

Enzymatically produced FDEA **176** (0.1 mM) and c(RGDfK[N_3]) **199** (0.2 mM) and fresh sodium ascorbate solution (0.5 mM) was added to water (23 µL) ("t = 0 min" sample removed (50 µL) and analysed by HPLC) before $CuSO_4$.TBTA solution (1.0 mM) and the mixture left to react for 70 min. A "t = 70 min" sample removed (50 µL) and analysed by HPLC.

HPLC analysis was performed on a using the Varian instrument, Varian Prostar system a Kinetix 5µm XB-C_{18} 100A (150 mm × 4.6 mm) column and a guard cartridge; mobile phase: A (H_2O + 0.05% TFA), B (MeCN + 0.05% TFA); linear gradient: 5% B for 2 min, 5% to 25% B in 10 min, 25% to 50% B in 6 min, 50% B to 95% B in 2 min; hold at 95% B for 3 min, 95% B to 5% B in 2 min, and re-equilibration at 95% B for 10 min; flow rate: 1 mL.min^{-1}; detection 220 and 254 nm); injection volume: 20 µL.

6.7.6. LC-MS of Click Reaction with 0.5 eq. of c(RGDfK[N_3]) 199

An enzymatic mixture of FDEA **176** (with residual ClDEA **174**) (0.2 mM) and c(RGDfK[N_3]) **199** (0.1 mM) and fresh sodium ascorbate solution (0.075 mM) was added to water (158 µL) before $CuSO_4$.TBTA solution (0.075 mM) was added and the mixture left to react for 15 h to go to completion. A sample (50 µL + 100 µL water) was analysed by LC-MS.

LC-MS analysis was performed on a using the Waters/Micromass instrument, using Phenomenex Kinetix 5µm XB-C_{18} 100A (150 mm × 4.6 mm) column and a guard cartridge; mobile phase: A (H_2O + 0.05% TFA), B (MeCN + 0.05% TFA); linear gradient: 5% B for 2 min, 5% to 25% B in 10 min, 25% to 50% B in 6 min, 50% B to 95% B in 2 min; hold at 95% B for 3 min, 95% B to 5% B in 2 min, and re-equilibration at 95% B for 10 min; flow rate: 1 mL.min^{-1}; detection 220 and 254 nm); injection volume: 20 µL.; mobile phase: A (H_2O + 0.1% formic acid), B (MeCN + 0.1% formic acid); linear gradient: 5% B for 2 min, 5% to 25% B in 10 min, 25% to 50% B in 6 min, 50% B to 95% B in 2 min; hold at 95% B for 3 min, 95% B to 5% B in 2 min, and re-equilibration at 95% B for 10 min; flow rate: 0.5 mL.min^{-1}; injection volume: 50 µL.

6.7.7. Synthesis of [^{18}F]FDEA [^{18}F]-176 and [^{18}F]FDEA-RGD [^{18}F]-201

Synthesis of [^{18}F]FDEA [^{18}F]-**176** and [^{18}F]FDEA-RGD [^{18}F]-**201** were performed by Dr. Mayca Onega at Imanova Ltd at Hammersmith Hospital, London.

6.7.8. *In vivo* evaluation of [^{18}F]FDEA-RGD [^{18}F]-201

The experiments conducted for this section were performed in accordance with the U.K. Animals (Scientific Procedures) Act 1986. The procedures used in the present study are approved by the Animal Ethical Review Committee of Imperial College.

Dosing of the rats, metabolite analysis and *post mortem* gamma counting were conducted by Dr Sharon Ashworth, while imaging acquisitions and data analysis conducted by both Dr. Mayca Onega and Dr Sharon Ashworth at Imanova Ltd at Hammersmith Hospital, London.

6.8. Enzymatic experiments for Chapter 3

6.8.1. ClDEA-PEG-(C≡CH)$_2$ 219 to FDEA-PEG-(C≡CH)$_2$ 245

In a total reaction volume of 1000 µL, recombinant fluorinase (10 mg.mL^{-1}) was incubated with ClDEA-PEG-(C≡CH)$_2$ **219** (0.3 mM), L-SeMet (0.5 mM) and KF (75 mM) at 37 °C. Samples (100 µL) were periodically removed, denatured by heating at 95°C for 3 min, before being clarified by centrifugation (13 000 rpm, 10 min). Samples of the supernatant (100 µL) were removed for analysis by HPLC. Control experiments without enzyme, L-SeMet and fluoride were also performed and showed no formation of FDEA-PEG-(C≡CH)$_2$ **245**. In the control without fluoride, conversion of ClDEA-PEG-(C≡CH)$_2$ **245** to SeEAM-PEG-(C≡CH)$_2$ was observed.

HPLC analysis was performed on a Varian Prostar system using a Kinetix 5µm XB-C$_{18}$ 100A (150 mm × 4.6 mm) column and a guard cartridge. Mobile phase: 0.05% TFA in water (solvent A) and 0.05% TFA in MeCN (solvent B); Linear gradient: 5% solvent B to 95% solvent B over 20 min, 95% solvent B for 4 min then to 5% solvent B in 1 min and hold for 10 min to re-equilibrate the column; Flow rate: 1 mL.min^{-1}; Detection: 260 nm; Injection volume: 20 µL.

6.8.2. ClDEA-PEG-(RGD)$_2$ 224 to FDEA-PEG-(RGD)$_2$ 248

In a total reaction volume of 1000 µL, recombinant fluorinase (1 mg.mL^{-1}) was incubated with ClDEA-PEG-(RGD)$_2$ **224** (0.04 mM), L-SeMet (0.075 mM) and KF (50 mM) at 37 °C. Samples (100 µL) were periodically removed, denatured by heating at 95°C for 3 min, before being clarified by centrifugation (13 000 rpm, 10 min). Samples of the supernatant (100 µL) were removed for analysis by HPLC. Control

experiments without enzyme, L-SeMet and fluoride were also performed and showed no formation of FDEA-PEG-$(RGD)_2$ **248**. In the control without fluoride, conversion of ClDEA-PEG-$(RGD)_2$ **224** to SeEAM-PEG-$(RGD)_2$ was observed.

HPLC analysis was performed on a Shimadzu Prominence system using a Kinetix 5µm XB-C_{18} 100A (150 mm × 4.6 mm) column and a guard cartridge. Mobile phase: 0.05% TFA in water (solvent A) and 0.05% TFA in MeCN (solvent B); Isocratic: 22% solvent B for 20 min, then from 22% to 95% of solvent B in 1 min, hold at 95% B for 2 min, and back to 22% B for 7 min to re-equilibrate the column. Flow rate: 1 $mL.min^{-1}$; Detection: 220 nm; Injection volume: 20 µL.

6.8.3. ClDEA-PEG-$(RGD)_4$ 225 to FDEA-PEG-$(RGD)_4$ 249

In a total reaction volume of 1000 µL, recombinant fluorinase (1 $mg.mL^{-1}$) was incubated with ClDEA-PEG-$(RGD)_4$ **225** (0.02 mM), L-SeMet (0.075 mM) and KF (50 mM) at 37 °C. Samples (100 µL) were periodically removed, denatured by heating at 95°C for 3 min, before being clarified by centrifugation (13 000 rpm, 10 min). Samples of the supernatant (100 µL) were removed for analysis by HPLC. Control experiments without enzyme, L-SeMet and fluoride were also performed and showed no formation of FDEA-PEG-$(RGD)_4$ **249**. In the control without fluoride, conversion of ClDEA-PEG-$(RGD)_4$ **225** to SeEAM-PEG-$(RGD)_4$ was observed.

HPLC analysis was performed on a Shimadzu Prominence system using a Kinetix 5µm XB-C_{18} 100A (150 mm × 4.6 mm) column and a guard cartridge. Mobile phase: 0.05% TFA in water (solvent A) and 0.05% TFA in MeCN (solvent B); Isocratic: 24% solvent B for 20 min, then from 22% to 95% of solvent B in 1 min, hold at 95% B for 2 min, and back to 24% B for 7 min to re-equilibrate the column. Flow rate: 1 $mL.min^{-1}$; Detection: 220 nm; Injection volume: 20 µL.

6.8.4. ClDA 23 to [^{18}F]FDA [^{18}F]-22

A standard experiment for the synthesis of [^{18}F]FDA [^{18}F]-**22** is described below. In experiments to determine optimal incorporation conditions, each factor was changed as described in **Table 1**. Concentrations shown are final concentrations.

To a solution of ClDA **23** (0.04 mM, 20 µL), L-SeMet (0.075 mM, 38 µL) and fluorinase (5 mg, freeze dried), a solution of [^{18}F]fluoride in water (200 µL, 56.1 MBq) was added and the final volume made up to 500 µL with water. The mixture was incubated at 37 °C for 30 min before the enzyme was denatured by heating the sample to 100 °C for

5 min. The sample was centrifuged (3000-4000 rpm) for 5 min before a sample of the supernatant was analysed using the Dionex HPLC system.

Table 1. Conditions investigated for optimization of incorporation of [^{18}F]fluoride to [^{18}F]FDA [^{18}F]-**22**. Conditions changed are shown in bold. All reactions performed in a total volume of 500 µL.

Component final concentration		
ClDA **23**/mM	fluorinase/mg.mL^{-1}	L-SeMet/mM
0.04	10	0.125
0.04	**10** (alt. batch)	0.125
0.04	**2.8** (stoichiometric)	0.125
0.04	**0.7** (catalytic)	0.125
0.04	10	**0.020**
0.3	**0.7**	0.125
0.3	10	0.125
0.3	**20**	0.125
0.6	**20**	0.125

6.8.5. ClDEA-PEG-(RGD)$_2$ 224 to [^{18}F]FDEA-PEG-(RGD)$_2$ [^{18}F]-248

A standard experiment for the synthesis of [^{18}F]-**248** is described below. In experiments to determine optimal incorporation conditions, each factor was changed as described in **Table 2**. Final concentrations of each component were used according to the optimised conditions described above, were the substrate was used at 0.3 mM, L-SeMet at 0.08 mM and fluorinase at 20 mg.mL^{-1}.

To ClDEA-PEG-(RGD)$_2$ **224** (0.1 mg) and fluorinase (2.88 mg), L-SeMet (6 µL, 2 mM) was added, followed by a solution of [^{18}F]fluoride in water (138 µL, 42.4 MBq). The mixture was incubated at 37 °C for 30 min before the enzyme was denatured by heating the sample to 100 °C for 5 min. The sample was centrifuged (3000-4000 rpm) for 5 min before a sample of the supernatant was analysed by HPLC.

Analysis was performed on a Dionex system using a Kinetix 5µm XB-C$_{18}$ 100A (150 mm × 4.6 mm) column and a guard cartridge. Mobile phase: 0.05% TFA in water (solvent A) and 0.05% TFA in MeCN (solvent B); Isocratic: 22% solvent B for 20 min, then from 22% to 95% of solvent B in 1 min, hold at 95% B for 2 min, and back to 22% B for 7 min to re-equilibrate the column. An alternate gradient was also used in some experiments: Linear gradient: 5% solvent B to 95% solvent B over 20 min, 95% solvent B for 4 min then to 5% solvent B in 1 min and hold for 10 min to re-equilibrate the column; Flow rate: 1 mL.min^{-1}; Detection: 220 nm; Injection volume: 10-50 µL.

Table 2. Conditions investigated for optimization of incorporation of [^{18}F]fluoride to [^{18}F]-**248**. Conditions changed are shown in bold.

Condition changed	
224 preparation	reaction time (min)
freeze dried powder	30
freeze dried with enzyme	30
pre-dissolved in DMSO (2*μ*L)	30
freeze dried with enzyme	**120**

6.8.6. ClDEA-PEG-(RGD)$_4$ 225 to [^{18}F]FDEA-PEG-(RGD)$_4$ [^{18}F]-249

A standard experiment for the synthesis of [^{18}F]-**249** is described below. In experiments to determine optimal incorporation conditions, each factor was changed as described in **Table 3**. Final concentrations of each component were used according to the optimised conditions described above, were the substrate was used at 0.3 mM, L-SeMet at 0.08 mM and fluorinase at 20 mg.mL^{-1}.

To ClDEA-PEG-(RGD)$_4$ **225** (0.2 mg) and fluorinase (3.34 mg), L-SeMet (7 μL, 2 mM) was added, followed by a solution of [^{18}F]fluoride in water (160 μL, 34.4 MBq). The mixture was incubated at 37 °C for 30 min before the enzyme was denatured by heating the sample to 100 °C for 5 min. The sample was centrifuged (3000-4000 rpm) for 5 min before a sample of the supernatant was analysed by HPLC.

Analysis was performed on a Dionex system using a Kinetix 5μm XB-C$_{18}$ 100A (150 mm × 4.6 mm) column and a guard cartridge. Mobile phase: 0.05% TFA in water (solvent A) and 0.05% TFA in MeCN (solvent B); Linear gradient: 5% solvent B to 95% solvent B over 20 min, 95% solvent B for 4 min then to 5% solvent B in 1 min and hold for 10 min to re-equilibrate the column; Flow rate: 1 mL.min^{-1}; Detection: 220 nm; Injection volume: 10-50 μL.

Table 3. Conditions investigated for optimization of incorporation of [^{18}F]fluoride to [^{18}F]-**249**. Conditions changed are shown in bold.

Condition changed	
225 preparation	reaction time (min)
freeze dried powder	30
freeze dried with enzyme	30
pre-dissolved in DMSO (2*μ*L)	30
freeze dried powder	**120**

6.9. Enzymatic Experiments for Chapter 4

6.9.1. F_2DA 276 with L-Met 21

In a total volume of 500 µL in water, F_2DA **276** (0.3 mM), L-Met (0.5 mM), phosphate buffer (20 mM) and fluorinase (2 mg.mL^{-1}) were combined left to react at 37°C for 24 h. Samples were removed at t = 0 h, t = 1 h, t = 2 h, and t = 24 h. The samples were heated to 95°C for 5 min, and centrifuged at 13 000 rpm for 10 min. Supernatant was then analysed by HPLC.

HPLC analysis was performed on a Varian Prostar system using a Kinetix 5µm XB-C_{18} 100A (150 mm × 4.6 mm) column and a guard cartridge. Mobile phase: 0.05% TFA in water (solvent A) and 0.05% TFA in MeCN (solvent B); Linear gradient: 5% solvent B for 2 min, then from 5% to 25% of solvent B in 10 min, from 25% to 50% of solvent B in 3 min and finally 95% solvent B to flush the column; Flow rate: 1 mL.min^{-1}; Detection: 260 nm; Injection volume: 20 µL.

6.9.2. F_2DA 276 with L-SeMet 161

In a total volume of 500 µL in water, F_2DA **276** (0.3 mM), L-SeMet (0.1 or 0.6 mM), phosphate buffer (20 mM) and fluorinase (1, 2 or 5 mg.mL^{-1}) were combined left to react at 37°C for 19 h. Samples were removed at t = 0 h, t = 1 h, t = 2 h, and t = 24 h. The samples were heated to 95°C for 5 min, and centrifuged at 13 000 rpm for 10 min. Supernatant was then analysed by HPLC.

HPLC analysis was performed on a Varian Prostar system using a Kinetix 5µm XB-C_{18} 100A (150 mm × 4.6 mm) column and a guard cartridge. Mobile phase: 0.05% TFA in water (solvent A) and 0.05% TFA in MeCN (solvent B); Linear gradient: 5% solvent B for 2 min, then from 5% to 25% of solvent B in 10 min, from 25% to 50% of solvent B in 3 min and finally 95% solvent B to flush the column; Flow rate: 1 mL.min^{-1}; Detection: 260 nm; Injection volume: 20 µL.

6.10. Synthesis of [^{18}F]FAc [^{18}F]-1 for Chapter 5

6.10.1. Enzymatic synthesis of [^{18}F]FAc [^{18}F]-1

To a solution of SAM **20** (20 mM, 20 µL), L-amino acid oxidase (1 mg) and fluorinase (5 mg, freeze dried), a solution of [^{18}F]fluoride in water (300 µL, 83-269 MBq) was

added and the mixture vortexed before being incubated at 37 °C for 30 min. The enzyme was denatured by heating the sample to 140 °C for 5 min, before the sample was centrifuged (3000-4000 rpm) for 5 min. The supernatant was transferred to a new vial containing CrO_3/H_2SO_4 (prepared by adding 1 g CrO_3 to 3 mL 33% H_2SO_4, 250 µL) and the mixture heated to 140 °C for 20 min. The mixture was cooled on ice, and water added (1 mL) before the aqueous phase was extracted with Et_2O (5 × 1 mL). The ether extracts were combined and passed through a Si Sep-Pak Light, and the cartridge washed with further Et_2O (1 mL). The ether was extracted with sodium carbonate solution (8 $mg.mL^{-1}$, 500 µL) to give a solution of [^{18}F]fluoroacetate [^{18}F]-**1** (23% non-decay corrected radiochemical yield, n=2).

HPLC analysis was performed on the Dionex system using a ZIC-pHILIC, 5 µm PEEK (150 mm × 2.1 mm) column and a guard cartridge. Mobile phase: 50 mM ammonium bicarbonate (solvent A) and MeCN (solvent B); Linear gradient: 90% solvent B for 3 min, then from 90% to 20% of solvent B in 0.5 min, 20% solvent B for 4.5 min, then to 90% solvent B in 0.5 min, and hold for 26.5 min to re-equilibrate the column; Flow rate: 0.2 $mL.min^{-1}$; Injection volume: 10-50 µL.

6.10.2. Chemical synthesis of [^{18}F]FAc [^{18}F]-1

A solution of Kryptofix 222/K_2CO_3 (250 µL, prepared by adding K_2CO_3 (12 mg) in water (0.5 mL) to Kryptofix 222 (100 mg) in MeCN (2 mL)) was added to a solution of [^{18}F]fluoride (49-553 MBq) in [^{18}O]H_2O in a Wheaton v-vial. The vial was sealed, and the fluoride ion dried at 100 °C under a stream of argon by azeotropic distillation by addition of MeCN (3 × 500 µL). The argon stream was removed and ethyl *O*-mesylglycolate **49** (1.3-1.5 mg) in MeCN (300 µL) was added to the dried ^{18}F-fluoride ion, and the mixture gently shaken before being heated to 100 °C for 5 min. The vial was cooled in water (20 °C) for 5 min. The solution was transferred to a new vial and the original v-vial rinsed with water (300 µL) and this too added to the new vial. Additional water (700 µL), and NaOH solution (1.0 M, 200 µL) was added to the new vial and the mixture incubated at 40 °C for 5 min. Et_2O (1 mL) was added, and the mixture shaken, the phases allowed to separate, and the aqueous phase transferred to a new vial and H_2SO_4 (1 M, 1 mL) was added. The acidified mixture was extracted with Et_2O (5 × 1 mL) and the ether extracts combined before being loaded onto an Alumina-N Sep-Pak. The Sep-Pak was washed with Et_2O (0.5 mL), followed by air (2 mL). The Sep-Pak was attached to a PBS-treated sterile 0.22 µm filter, and [^{18}F]fluoroacetate [^{18}F]-**1** was eluted into a sealed Wheaton v-vial from the Sep-Pak with phosphate

buffered saline (0.5 mL, pH 7.5), and the Sep-Pak and filter blown dry with air (1 mL). Argon was bubbled through the [^{18}F]fluoroacetate-saline solution which was heated to 100 °C for 5 min. This gave [^{18}F]fluoroacetate [^{18}F]-**1** (10-103 MBq, 6-26% RCY) in phosphate buffered saline, shown to be >99% radiochemically pure by HPLC (retention time 8.10 min).

HPLC analysis was performed on the Dionex system using a ZIC-pHILIC, 5 µm PEEK (150 mm × 2.1 mm) column and a guard cartridge. Mobile phase: 50 mM ammonium bicarbonate (solvent A) and MeCN (solvent B); Linear gradient: 90% solvent B for 3 min, then from 90% to 20% of solvent B in 0.5 min, 20% solvent B for 4.5 min, then to 90% solvent B in 0.5 min, and hold for 26.5 min to re-equilibrate the column; Flow rate: 0.2 mL.min^{-1}; Injection volume: 10-50 µL.

6.10.3. *In vivo* evaluation of [^{18}F]FAc [^{18}F]-1

Dr Zachary Schug and Dr Eyal Gottlieb, of the Beatson Institute for Cancer Research, who were leading the ACSS2 investigation, provided the mice for the study, while imaging acquisitions and data analysis were conducted at the institute by Dr Gaurav Malviya and Agata Mrowinska.

6.11. Miscellaneous

6.11.1. Preparation of 10 mM $CuSO_4$.TBTA (55% DMSO solution)

Copper (II) sulfate pentahydrate (50 mg) was dissolved in water (10 mL), and to this, a solution of TBTA **202** (tris[(1-benzyl-1H-1,2,3-triazol-4-yl)methyl]amine,[17] Sigma Aldrich) (116 mg) in DMSO (11 mL) was added. The solution was well mixed to generate the complex, which was stored at room temperature until use.

6.11.2. Isothermal titration calorimetry

Isothermal titration calorimetry experiments were performed using a VP-ITC (microCal). The fluorinase was dialysed into phosphate buffer (20 mM, pH 7.8, 5 L) twice prior to titration. The final dialysis buffer also used for instrument equilibration. Pre-weighed, freeze-dried compounds for titration were dissolved in dialysis buffer to make solutions of ~1 mM. Solutions were degassed at 25 °C prior to titration of into a solution of fluorinase (~ 60 µM in 1.4 mL) at 25 °C. The first injection was 2 µL, followed by

multiple 10 µL injections. Data were analysed by MicroCal Origin software using a single binding site model.

6.11.3. X-Ray crystallography of the fluorinase and FDEA 176 and F_2DA 276

Purified fluorinase was concentrated to 6.5 mg ml^{-1} and incubated with 1 mM FDEA **176** (from 0.5 M stock in DMSO) at room temperature overnight prior to the setting of crystallization trials. Crystal trials were set with an Art Robbins Gryphon at protein/ligand to precipitant ratios of 1:1, 2:1 and 1:2 using in-house stochastic screens alongside commercially available crystallization screens. Crystals were obtained in several conditions but those diffracting the best grew from 20% PEG 3350, 0.2 M ammonium formate.

Purified fluorinase was concentrated to 6.5 mg ml^{-1} and incubated with 2 mM F_2DA **276** (from 0.5 M stock in DMSO) at room temperature overnight prior to the setting of crystallization trials. Crystal trials were set with an Art Robbins Gryphon at protein/ligand to precipitant ratios of 1:1, 2:1 and 1:2 using in-house stochastic screens alongside commercially available crystallization screens. Crystals were obtained in several conditions but those diffracting the best grew from 40% PEG-MME (2K), 0.1 M sodium citrate pH 4.5 and 0.12 M ammonium tartrate.

X-ray data was collected at the DIAMOND light source (for the FDEA-fluorinase structure) or at the European Synchrotron Radiation Facility (for the F_2DA-fluorinase structure). Analysis and refinement were performed by Dr Stephen McMahon and Prof. Jim Naismith at the University of St Andrews.

6.11.4. Evaluation of RGD compound affinity to $\alpha_V\beta_3$

Binding affinity of cold bioconjugates was determined by Dr. Ian Fleming at the University of Aberdeen. Binding affinity of compounds to purified $\alpha_V\beta_3$ integrin was determined by ELISA as described in Zanda *et al.*[18]

6.12. References

1. D. D. Perrins and W. L. F. Armarego, *Purification of laboratory chemicals. 3rd Ed.*, Pergamon Press, Oxford.

2. E. Gasteiger, C. Hoogland, A. Gattiker, S. Duvaud, M. R. Wilkins, R. D. Appel, and A. Bairoch, <http://web.expasy.org/protparam/>.

3. M. Robins and B. Uznanski, *Can. J. Chem.*, 1981, **59**, 2601–2607.

4. I. M. Buck, A. Eleuteri, and C. B. Reese, *Tetrahedron*, 1994, **50**, 9195–9206.

5. A. Matsuda, M. Shinozaki, M. Tadashim, H. Machida, and T. Abiru, *Chem. Pharm. Bull.*, 1985, **33**, 1766–1769.

6. A. Matsuda, M. Shinozaki, T. Yamaguchi, H. Homma, R. Nomoto, T. Miyasaka, Y. Watanabe, and T. Abiru, *J. Med. Chem.*, 1992, **35**, 241–252.

7. J. Verheyden and J. G. Moffatt, *J. Org. Chem.*, 1972, **37**, 2289–2299.

8. I. Dijkgraaf, A. Y. Rijnders, A. Soede, A. C. Dechesne, G. W. van Esse, A. J. Brouwer, F. H. M. Corstens, O. C. Boerman, D. T. S. Rijkers, and R. M. J. Liskamp, *Org. Biomol. Chem.*, 2007, **5**, 935–44.

9. G. Bergamini, P. Ceroni, P. Fabbrizi, and S. Cicchi, *Chem. Commun.*, 2011, **47**, 12780.

10. C. J. Serpell, R. Chall, A. L. Thompson, and P. D. Beer, *Dalt. Trans.*, 2011, **40**, 12052.

11. F. Tran, A. V Odell, G. E. Ward, and N. J. Westwood, *Molecules*, 2013, **18**, 11639–11657.

12. R. S. Ranganathan, G. H. Jones, and J. G. Moffatt, *J. Org. Chem.*, 1974, **39**, 290–298.

13. V. M. Vrudhula, F. Kappler, C. Afshar, S. L. Ginell, L. Lessinger, and A. Hampton, *J. Med. Chem.*, 1989, **32**, 885–890.

14. E. T. Jarvi, J. R. Mccarthy, S. Mehdi, D. P. Matthews, M. L. Edwards, N. J. Prakash, T. L. Bowlin, P. S. Sunkara, and P. Bey, *J. Med. Chem.*, 1991, **34**, 647–656.

15. J. M. Jeong, D. S. Lee, J.-K. Chung, M. C. Lee, C.-S. Koh, and S. S. Kang, *J. Label. Compd. Radiopharm.*, 1997.

16. C. Dong, F. Huang, H. Deng, C. Schaffrath, J. B. Spencer, D. O'Hagan, and J. H. Naismith, *Nature*, 2004, **427**, 561–565.

17. T. R. Chan, R. Hilgraf, K. B. Sharpless, and V. V Fokin, *Org. Lett.*, 2004, **6**, 2853–2855.

18. M. Piras, I. Fleming, W. Harrison, and M. Zanda, *Synlett*, 2012, **23**, 2899–2902.

EXPLORING THE SUBSTRATE SCOPE OF THE FLUORINASE FROM STREPTOMYCES CATTLEYA FOR APPLICATIONS TO POSITRON EMISSION TOMOGRAPHY

Stephen Thompson

A Thesis Submitted for the Degree of PhD
at the
University of St Andrews

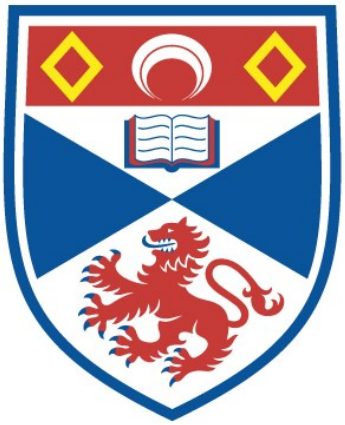

2015